

PLASMA DIAGNOSTICS PACKAGE

FINAL SCIENCE REPORT

Volume 2

SPACELAB 2 SECTION

PART A

NASA/MSFC Contract No. NAS8-32807



(NASA-CR-183698) PLASMA DIAGNOSTICS
PACKAGE. VOLUME 2: SPACELAB 2 SECTION, PART
A Final Science Report (Iowa Univ.) 488 p
CSCL 201

N89-26722

Unclas
0146664

G3/75

Department of Physics and Astronomy
THE UNIVERSITY OF IOWA

Iowa City, Iowa 52242

**PLASMA DIAGNOSTICS PACKAGE
FINAL SCIENCE REPORT**

Volume 2

SPACELAB 2 SECTION

PART A

NASA/MSFC Contract No. NAS8-32807

**Compiled by
J. S. Pickett
L. A. Frank
W. S. Kurth**

**Department of Physics and Astronomy
University of Iowa
Iowa City, Iowa 52242**

June, 1988

I. INTRODUCTION

This volume (2), which consists of two parts (A and B), of the Plasma Diagnostics Package (PDP) Final Science Report contains a summary of all of the data reduction and scientific analyses which were performed using PDP data obtained on STS-51F as a part of the Spacelab 2 (SL-2) payload. This work was performed under NASA/Marshall Space Flight Center Contract No. NAS8-32807 with the University of Iowa during the period of launch, July 29, 1985, through June 30, 1988. During this period the primary data reduction effort consisted of processing summary plots of the data received by 12 of the 14 instruments located on the PDP and submitting these data to the National Space Science Data Center (NSSDC).

The scientific analyses during the performance period consisted of follow-up studies of shuttle orbiter environment and orbiter/ionosphere interactions and various plasma particle and wave studies which dealt with data taken when the PDP was on the Remote Manipulator System (RMS) arm and when the PDP was in free flight. Of particular interest during the RMS operations and free flight were the orbiter wake studies and joint studies of beam/plasma interactions with the SL-2 Fast Pulse Electron Generator (FPEG) of the Vehicle Charging and Potential Investigation (VCAP). Internal reports, published papers and presentations which involve PDP/SL-2 data are listed in Sections III and IV. In addition, three Master's and three Ph.D. theses were written using PDP instrumentation data. These theses are listed and copies are included in Volume 2, Part B. A PDP/SL-2 scientific results meeting was held at the University of Iowa on June 10, 1986. This meeting was attended by most of the PDP and VCAP investigators and provided a forum for discussing and comparing the various results, particularly with regard to the PDP free flight.

II. SUMMARY OF DATA PROCESSED

During the period July 29, 1985 through June 30, 1988, the University of Iowa generated 10-minute color survey slides for all of the times when the PDP was turned on during the SL-2 flight, July 29, 1985 to August 6, 1985. These slides contain 15 panels of data representing the output from 12 of the instruments mounted on the PDP structure. Two sets of slides, together with a Data User's Guide, were submitted to NSSDC on June 13, 1988. In addition, 70 mm black and white wideband analog film for certain specified portions of the SL-2 flight was generated showing high time and frequency resolution of the electric and magnetic noise signals (0-30 kHz) received by the wideband analog receiver mounted on the PDP. This film, together with a Data User's Guide, was submitted to NSSDC on June 16, 1988.

III. INTERNAL REPORTS

A list of University of Iowa internally-generated reports, which contain PDP/SL-2 data, is given below. None of the internal reports was published, but each is on file in the PDP Project Office in the Department of Physics and Astronomy.

KUSR Final Engineering Report (Ku-Band/S-Band Receiver) for the PDP on Spacelab, G. B. Murphy, presented to the Aerospace Corporation, El Segundo, California, April, 1985.

Plasma Diagnostics Package (PDP) 90-Day Summary Science Report, L. A. Frank, W. S. Kurth, et al., Required Report under Marshall Space Flight Center Contract NAS8-32807, Huntsville, Alabama, November, 1985.

Plasma Diagnostics Package/Spacelab-2 Data User's Guide, compiled by J. S. Pickett, University of Iowa, Iowa City, Iowa, January, 1986.

Flight Thermal Report PDP/SL-2, M. E. Kerl, Engineering Report No. ER-07-86.006, University of Iowa, Iowa City, Iowa, June, 1986.

Measurements of Plasma Density and Turbulence Near the Shuttle Orbiter, A. Tribble, N. D'Angelo, G. Murphy, and J. Pickett, January, 1987.

IV. PUBLICATIONS

A list of publications and oral presentations, which contain PDP/SL-2 data, is given below. Copies of the publications are included in the remainder of this volume.

A. LIST OF PUBLICATIONS IN REFEREED JOURNALS

- Whistler-Mode Radiation from the Spacelab 2 Electron Beam, D. A. Gurnett, W. S. Kurth, J. T. Steinberg, P. M. Banks, R. I. Bush, and W. J. Raitt, Geophys. Res. Lett., **13**, 225-228, 1986.
- Thermal Ion Perturbations Observed in the Vicinity of the Space Shuttle, J. M. Grebowsky, H. A. Taylor, Jr., M. W. Pharo, III, and N. Reese, Planet. Space Sci., **35**, 501-513, 1987.
- Electromagnetic Fields from Pulsed Electron Beam Experiments in Space: Spacelab-2 Results, R. I. Bush, G. D. Reeves, P. M. Banks, T. Neubert, P. R. Williamson, W. J. Raitt, and D. A. Gurnett, Geophys. Res. Lett., **14**, 1015-1018, 1987.
- The Emissions of Broadband Electrostatic Noise in the Near Vicinity of the Shuttle Orbiter, K. S. Hwang, N. H. Stone, K. H. Wright, Jr., and U. Samir, Planet. Space Sci., **35**, 1373-1379, 1987.
- Thermal Ion Complexities Observed within the Spacelab 2 Bay, J. M. Grebowsky, H. A. Taylor, Jr., M. W. Pharo, III, and N. Reese, Planet. Space Sci., **35**, 1463-1469, 1987.
- An Analysis of Whistler - Mode Radiation from the Spacelab 2 Electron Beam, W. M. Farrell, D. A. Gurnett, P. M. Banks, R. I. Bush, and W. J. Raitt, J. Geophys. Res., **93**, 153-161, 1988.
- Double Probe Potential Measurements Near the Spacelab-2 Electron Beam, J. T. Steinberg, D. A. Gurnett, P. M. Banks and W. J. Raitt, J. Geophys. Res., submitted, July, 1987, resubmitted April, 1988.
- Coherent Cerenkov Radiation from the Spacelab-2 Electron Beam, W. M. Farrell, D. A. Gurnett, C. K. Goertz, J. Geophys. Res., submitted October, 1987, resubmitted May, 1988.
- The Plasma Wake of the Shuttle Orbiter, G. B. Murphy, D. L. Reasoner, A. Tribble, N. D'Angelo, J. S. Pickett, W. S. Kurth, J. Geophys. Res., submitted December, 1987, resubmitted May, 1988.
- The Polar Code Wake Model: Comparison With In-Situ Observations, G. Murphy, I. Katz, J. Geophys. Res., submitted December, 1987, resubmitted May, 1988.
- Orbiter Environment at S- and K_u-Band Frequencies, G. B. Murphy and W. D. Cutler, J. of Spacecraft and Rockets, **25**, 81-87, 1988.

- Exposed High-Voltage Source Effect on the Potential of an Ionospheric Satellite, A. C. Tribble, N. D'Angelo, G. B. Murphy, J. S. Pickett, and J. T. Steinberg, J. of Spacecraft and Rockets, 25, 64-69, 1988.
- The Gaseous Environment of the Shuttle Early in the Spacelab 2 Mission, J. S. Pickett, G. B. Murphy and W. S. Kurth, J. of Spacecraft and Rockets, 25, No. 2, 1988.
- Pulsed Electron Beam Emission in Space, T. Neubert, J. G. Hawkins, G. D. Reeves, P. M. Banks, R. I. Bush, P. R. Williamson, D. A. Gurnett, and W. J. Raitt, Journal of Geomagnetism and Geoelectricity, submitted, February, 1988.
- Plasma Wave Turbulence Around the Shuttle: Results from the Spacelab-2 Flight, D. A. Gurnett, W. S. Kurth, J. T. Steinberg, and S. D. Shawhan, Geophys. Res. Lett., submitted April, 1988.
- On the Expansion of Ionospheric Plasma into the Near-Wake of the Shuttle Orbiter, N. H. Stone, K. H. Wright, Jr., U. Samir, and K. S. Hwang, Geophys. Res. Lett., submitted April, 1988.
- VLF Wave Emissions by Pulsed and DC Electron Beams in Space 1: Spacelab-2 Observations, G. D. Reeves, P. M. Banks, T. Neubert, R. I. Bush, P. R. Williamson, A. C. Fraser-Smith, D. A. Gurnett, and W. J. Raitt, J. Geophys. Res., submitted April, 1988.
- VLF Wave Emissions by Pulsed and DC Electron Beams in Space 2: Analysis of Spacelab-2 Results, G. D. Reeves, P. M. Banks, T. Neubert, K. J. Harker, and D. A. Gurnett, J. Geophys. Res., submitted April, 1988.
- Hot Ion Plasmas from the Cloud of Neutral Gases Surrounding the Orbiter, W. R. Paterson and L. A. Frank, J. Geophys. Res., in preparation, 1988.
- The Spacelab 2 Plasma Diagnostics Package, W. S. Kurth and L. A. Frank, J. Spacecraft and Rockets, in preparation, 1988.

B. LIST OF PUBLICATIONS IN PROCEEDINGS

- A Review of the Findings of the Plasma Diagnostic Package and Associated Laboratory Experiments: Implications of Large Body/Plasma Interactions for Future Space Technology, Gerald B. Murphy and Karl E. Lonngren, Proceedings of the Workshop on Space Technology Plasma Issues in 2001, Jet Propulsion Laboratory, Pasadena, CA, September 24-26, 1986.
- Contaminant Ions and Waves in the Space Station Environment, G. B. Murphy, Space Station Contamination Workshop Proceedings, OSSA/NASA, Hilton Head, SC, October 29-30, 1987.

C. LIST OF ORAL PRESENTATIONS

Plasma Diagnostics Package (PDP) 90-Day Summary Science Report, L. A. Frank, W. S. Kurth, et al., presented at 90-Day Spacelab-2 Science Meeting, Marshall Space Flight Center, Huntsville, Alabama, November 14-15, 1985.

The Gaseous Environment of the Space Shuttle, J. S. Pickett, G. B. Murphy, W. S. Kurth, presented at AIAA Shuttle Environment and Operations II Meeting, American Institute of Aeronautics and Astronautics, Houston, Texas, November 13-15, 1985.

Electromagnetic Environment of the Orbiter at S and Ku-Band Frequencies, G. B. Murphy, W. D. Cutler, presented at AIAA Shuttle Environment and Operations II Meeting, American Institute of Aeronautics and Astronautics, Houston, Texas, November 13-15, 1985.

Plasma Waves Observed Near the Shuttle During the SL-2 Mission, D. A. Gurnett, J. Steinberg, W. Kurth, P. Banks, R. Bush, presented at the 1985 Fall AGU Meeting, American Geophysical Union, San Francisco, California, December 9-13, 1985.

Electric Field Measurements Near the Shuttle During the SL-2 Mission, J. Steinberg, D. Gurnett, R. Bush, J. Raitt, presented at the 1985 Fall AGU Meeting, American Geophysical Union, San Francisco, California, December 9-13, 1985.

Charged Particle Distributions Measured in the Vicinity of the Space Shuttle, W. R. Paterson, L. A. Frank, P. M. Banks, presented at the 1985 Fall AGU Meeting, American Geophysical Union, San Francisco, California, December 9-13, 1985.

Plasma Densities and Temperatures Near the Shuttle Orbiter, A. C. Tribble, J. S. Pickett, N. D'Angelo, G. B. Murphy, presented at the 1985 Fall AGU Meeting, American Geophysical Union, San Francisco, California, December 9-13, 1985.

Results from the Plasma Diagnostics Package, L. A. Frank, D. A. Gurnett, N. D'Angelo, J. M. Grebowsky, D. L. Reasoner, N. H. Stone, presented at the AIAA 24th Aerospace Sciences Meeting, American Institute of Aeronautics and Astronautics, Reno, Nevada, January 6-9, 1986.

Velocity Distributions of Plasmas Associated with Electron Beam Injections During the SL-2 Mission, L. A. Frank, W. R. Paterson, P. M. Banks, R. I. Bush, W. J. Raitt, presented at the 1986 National Radio Science Meeting, International Union of Radio Science, Boulder, Colorado, January 13-16, 1986.

Short Wavelength Electrostatic Noise Observed in the Vicinity of the Shuttle During the SL-2 Mission, D. A. Gurnett, J. T. Steinberg, W. S. Kurth, presented at the 1986 National Radio Science Meeting, International Union of Radio Science, Boulder, Colorado, January 13-16, 1986.

Wave Emissions from the SL-2 Electron Beam: Similarities to the Aurora, D. A. Gurnett, W. S. Kurth, J. T. Steinberg, T. Neubert, R. Bush and P. Banks, presented at the 1986 National Radio Science Meeting, International Union of Radio Science, Boulder, Colorado, January 13-16, 1986.

- Electromagnetic Environment of the Orbiter at S and KU-Band Frequencies, G. B. Murphy and W. D. Cutler, presented to the Aerospace Corporation, Los Angeles, CA, April 8, 1986.
- Conditions for the Emission of Broadband Electrostatic Waves Near the Shuttle Orbiter, K. S. Hwang, N. H. Wright, Jr., U. Samir, paper presented at the 1986 Spring AGU Meeting, American Geophysical Union, Baltimore, Maryland, May 19-23, 1986.
- A Preliminary View of the Orbiter Plasma Wake from Spacelab 2, K. H. Wright, Jr., N. H. Stone, K. S. Hwang, U. Samir, paper presented at the 1986 Spring AGU Meeting, American Geophysical Union, Baltimore, Maryland, May 19-23, 1986.
- Electric Fields Associated with the SL-2 Electron Beam, J. T. Steinberg, D. A. Gurnett, P. M. Banks, presented at the 1986 Spring AGU Meeting, American Geophysical Union, Baltimore, Maryland, May 19-23, 1986.
- Measurements of the Power and Efficiency of Whistler-Mode Radiation from the Spacelab-2 Electron Beam, W. M. Farrell, D. A. Gurnett, P. M. Banks, presented at the 1986 Spring AGU Meeting, American Geophysical Union, Baltimore, Maryland, May 19-23, 1986.
- Spatial Extent of Thermal Plasma Contaminants in the Vicinity of the Space Shuttle During the SL-2 Mission, J. M. Grebowsky, H. A. Taylor, Jr., M. W. Pharo III, N. T. Reese, presented at the 1986 Spring AGU Meeting, American Geophysical Union, Baltimore, Maryland, May 19-23, 1986.
- A Study of the Space Shuttle's Wake Using the Plasma Diagnostics Package, W. S. Kurth, L. A. Frank, N. D'Angelo, J. M. Grebowsky, D. A. Gurnett, G. B. Murphy, D. L. Reasoner, N. H. Stone, presented at XXVI COSPAR 86, Toulouse, France, June 30-July 12, 1986.
- Comparison Between In-situ and Ground-based Plasma Interactions, N. H. Stone, presented at the Workshop on Space Technology Plasma Issues in 2001, Jet Propulsion Laboratory, Pasadena, California, September 24-26, 1986.
- Overview of Discoveries from PDP Spacelab Plasma Experiments -- New and Unanswered Questions, G. B. Murphy, presented at the Workshop on Space Technology Plasma Issues in 2001, Jet Propulsion Laboratory, Pasadena, California, September 24-26, 1986.
- Electron and Ion Distributions Associated with the Electron Beam and the Neutral Gas Envelope of the Orbiter, W. R. Paterson and L. A. Frank, presented at Spacelab 2 Scientific Results Meeting, Annapolis, Maryland, October 20-22, 1986.
- Plasma Turbulence and Spacecraft Charging Near the Shuttle Orbiter, A. Tribble and N. D'Angelo, presented at Spacelab 2 Scientific Results Meeting, Annapolis, Maryland, October 20-22, 1986.
- Neutral Pressure Results from SL-2, J. Pickett, presented at Spacelab 2 Scientific Results Meeting, Annapolis, Maryland, October 20-22, 1986.
- Some Spatial and Temporal Complexities in the Shuttle's Thermal Ion Envelope, J. Grebowsky, presented at Spacelab 2 Scientific Results Meeting, Annapolis, Maryland, October 20-22, 1986.

- Assessment of Ku-Band and S-Band Orbiter Electromagnetic Interference, G. Murphy, and W. Cutler, presented at Spacelab 2 Scientific Results Meeting, Annapolis, Maryland, October 20-22, 1986.
- Electrostatic Noise Induced by Gas Clouds Around the Shuttle, D. Gurnett, presented at Spacelab 2 Scientific Results Meeting, Annapolis, Maryland, October 20-22, 1986.
- Whistler Mode Radiation from the Electron Beam, W. Farrell and D. Gurnett, presented at Spacelab 2 Scientific Results Meeting, Annapolis, Maryland, October 20-22, 1986.
- Double Probe Electric Field Measurements Near the Electron Beam, J. Steinberg and D. Gurnett, presented at Spacelab 2 Scientific Results Meeting, Annapolis, Maryland, October 20-22, 1986.
- The Large Scale Wake Structure of the Shuttle Orbiter, G. B. Murphy, I. Katz, D. L. Reasoner, N. D'Angelo, J. S. Pickett, W. S. Kurth, presented at the 1986 Fall AGU Meeting, American Geophysical Union, San Francisco, California, December 8-12, 1986.
- The Effect of the Earth's Magnetic Field on Plasma Turbulence Near the Shuttle Orbiter, A. C. Tribble, N. D'Angelo, G. B. Murphy, J. S. Pickett, presented at the 1986 Fall AGU Meeting, American Geophysical Union, San Francisco, California, December 8-12, 1986.
- Possible Wave Generation Mechanisms of the Whistler Mode Signal from the SL-2 Electron Beam, W. M. Farrell, D. A. Gurnett, S. Machida, presented at the 1986 Fall AGU Meeting, American Geophysical Union, San Francisco, California, December 8-12, 1986.
- Ambient Ion Perturbations Induced by an Electron Gun on the Shuttle Orbiter, D. L. Reasoner and R. I. Bush, presented at the 1986 Fall AGU Meeting, American Geophysical Union, San Francisco, California, December 8-12, 1986.
- An Analysis of the Electrostatic Noise Observed Around the Shuttle During the SL-2 Mission, D. A. Gurnett, T. Z. Ma, and A. M. Persoon, presented at the 1987 Spring AGU Meeting, American Geophysical Union, Baltimore, Maryland, May 18-22, 1987.
- Electric Field Measurements Near the Space Shuttle at Times of Shuttle Thruster Operation, J. T. Steinberg, D. A. Gurnett, presented at the 1987 Spring AGU Meeting, American Geophysical Union, Baltimore, Maryland, May 18-22, 1987.
- Effect of an Exposed High-Voltage Source on the Potential of an Ionospheric Satellite Released from the Shuttle Orbiter, A. C. Tribble, N. D'Angelo, G. B. Murphy, J. S. Pickett, and J. T. Steinberg, presented at the 1987 Spring AGU Meeting, American Geophysical Union, Baltimore, Maryland, May 18-22, 1987.
- Shuttle/Plasma Interactions and Subsattellites, G. B. Murphy, presented at the Space Physics Briefing for Astronaut Corps, Johnson Space Center, Houston, Texas, September 9, 1987.
- Plasma Wave Emissions from the SL-2 Electron Beam, D. A. Gurnett, presented (invited) at the Active Experiments Workshop, Kyoto, Japan, October 19-20, 1987.

The Secondary Electron Beams and Plasma Waves Associated with Electron Beam Injection in Space, L. A. Frank, D. A. Gurnett, M. Ashour-Abdalla, W. R. Paterson, W. S. Kurth, N. Omid, P. M. Banks and W. J. Raitt, presented at Twenty-Ninth Annual Meeting, American Physical Society, Division of Plasma Physics, Princeton, New Jersey, November 2-6, 1987.

The Plasma Wake of the Shuttle Orbiter, presented (invited) as a seminar at Jet Propulsion Laboratory, Pasadena, California, November 12, 1987.

Positive Ion Effects Associated with Spacelab 2 Vernier Engine Firings, J. M. Grebowsky and A. C. Schaefer, presented at the 1987 Fall AGU Meeting, American Geophysical Union, San Francisco, California, December 6-11, 1987.

A Comparison of the Plasma Wake of the Shuttle Orbiter to the Wake of a Smaller Ionospheric Satellite, A. Tribble, N. D'Angelo, and G. Murphy, presented at the 1987 Fall AGU Meeting, American Geophysical Union, San Francisco, California, December 6-11, 1987.

Observations and Modeling of Ion Pickup in the Vicinity of the Orbiter, W. R. Paterson, L. A. Frank, presented at the 1987 Fall AGU Meeting, American Geophysical Union, San Francisco, California, December 6-11, 1987.

Coherent Cerenkov Radiation from the Spacelab-2 Electron Beam, W. M. Farrell, D. A. Gurnett and C. K. Goertz, presented at the 1987 Fall AGU Meeting, American Geophysical Union, San Francisco, California, December 6-11, 1987.

Quasi-Static Electric Field Measurements Near the Space Shuttle at Times of Shuttle Thruster Operation, J. T. Steinberg, D. A. Gurnett, C. K. Goertz, presented at the 1988 National Radio Science Meeting, International Union of Radio Science, Boulder, Colorado, January 5-8, 1988.

Coherent Cerenkov Radiation from the Spacelab-2 Electron Beam, W. M. Farrell, D. A. Gurnett, C. K. Goertz, presented at the 1988 National Radio Science Meeting, International Union of Radio Science, Boulder, Colorado, January 5-8, 1988.

Plasma Observations in the Vicinity of the Shuttle, L. A. Frank, W. R. Paterson, P. M. Banks, R. I. Bush, W. J. Raitt, presented at the 1988 National Radio Science Meeting, International Union of Radio Science, Boulder, Colorado, January 5-8, 1988.

Electron Distributions Observed from Electron Beam Injections During the Spacelab-2 Mission, W. R. Paterson, L. A. Frank, M. Ashour-Abdalla, D. Schriver, N. Omid, P. M. Banks, and W. J. Raitt, presented at the 1988 Spring AGU Meeting, Baltimore, Maryland, May 16-20, 1988.

D. PDP/SL-2 PUBLICATIONS

WHISTLER-MODE RADIATION FROM THE SPACELAB 2 ELECTRON BEAM

D. A. Gurnett¹, W. S. Kurth¹, J. T. Steinberg¹, P. M. Banks², R. I. Bush² and W. J. Raitt³

¹Department of Physics and Astronomy, University of Iowa, Iowa City, Iowa 52242

²Department of Electrical Engineering, Stanford University, Stanford, California 94305

³Center for Atmospheric and Space Science, Utah State University, Logan, Utah 84322

Abstract. During the Spacelab 2 mission the Plasma Diagnostics Package (PDP) performed a fly-around of the shuttle at distances of up to 300 meters while an electron beam was being ejected from the shuttle. We discuss a magnetic conjunction of the shuttle and the PDP while the electron gun was operating in a steady (DC) mode. During this conjunction, the PDP detected a clear funnel-shaped emission that is believed to be caused by whistler-mode emission from the beam. Ray-path calculations show that the shape of the funnel can be accounted for by whistler-mode waves propagating near the resonance cone. Because the beam and waves are propagating in the same direction, the radiation must be produced by a Landau, $\omega/k_{\parallel} = v_p$, interaction with the beam. Other types of waves generated by the beam are also described.

I. Introduction

During the recent Spacelab 2 flight, which was launched on July 29, 1985, a spacecraft called the Plasma Diagnostics Package (PDP) was released from the shuttle to survey the plasma environment around the shuttle. Among the various investigations performed was a study of the effects produced by an electron beam ejected from the shuttle. This paper describes the plasma waves observed during a magnetic conjunction between the PDP and the shuttle while the electron gun was being operated. As will be shown, the plasma-wave emissions observed are remarkably similar to emissions detected by spacecraft flying through auroral electron beams.

The PDP was designed and constructed at The University of Iowa and is a reflight of the spacecraft previously flown on the STS-3 flight [Shawhan et al., 1984]. The PDP included instrumentation from The University of Iowa, Goddard Space Flight Center, and Marshall Space Flight Center. For a description of the spacecraft and instruments, see Shawhan [1982]. The electron gun on the shuttle is part of the Vehicle Charging and Potential (VCAP) experiment which was provided by Stanford University and Utah State University. For a description of the VCAP instrumentation, see Raitt et al. [1982].

The Spacelab 2 mission was flown in a nearly circular low-inclination orbit with a nominal altitude of about 325 km and an inclination of 49.5°. The PDP was in free flight around the shuttle from 0010 to 0620 UT on August 1, 1985. During this roughly 6-hour interval the shuttle performed two complete fly-arounds of the PDP. These fly-arounds included four magnetic

conjunctions in which the shuttle was targeted to intersect the magnetic field line passing through the PDP. During the first two conjunctions the electron gun was off so that the PDP could monitor disturbances produced in the ionosphere by the shuttle. During the third conjunction, which is discussed here, the gun was operated in a steady (DC) mode to simulate a natural aurora, and during the fourth conjunction the gun was operated in a pulsed mode.

II. Observations

The trajectory of the shuttle relative to the PDP during the third conjunction is shown in Figure 1. The coordinate system used in this diagram is the so-called local-vertical, local-horizontal system. The +z axis is directed toward the center of the earth, the x axis is in the orbital plane, and the y axis completes the usual right-handed coordinate system. Time is shown by the tick marks along the trajectory. A complete fly-around takes one orbit, or about 92 minutes. The magnetic conjunction of interest occurred at 0334:12 UT. The magnetic field at the time of the conjunction is shown in Figure 1 projected onto the x-z plane. The (x,y,z) coordinates of the shuttle at this time are (-53, 89, -188) meters, and the separation distance is 216 meters. Calculations based on a model magnetic field indicate that the magnetic field line through the shuttle came within 10 meters of the PDP.

A spectrogram of the plasma wave electric field intensities during a 30-minute period around the magnetic conjunction is shown in Figure 2. These measurements are from the 3.89 meter double-sphere electric antenna on the PDP. The frequency range extends from 31 Hz to 17.8 MHz and the dynamic range extends from about

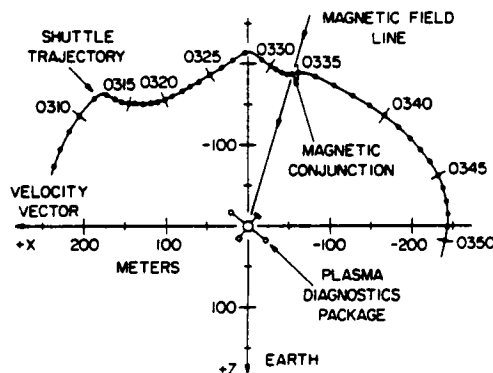


Fig. 1. The trajectory of the shuttle relative to the PDP during the third magnetic conjunction. The electron beam was ejected downward, toward the PDP.

Copyright 1986 by the American Geophysical Union.

Paper number 5L6773.
0094/8276/86/005L-6773\$03.00

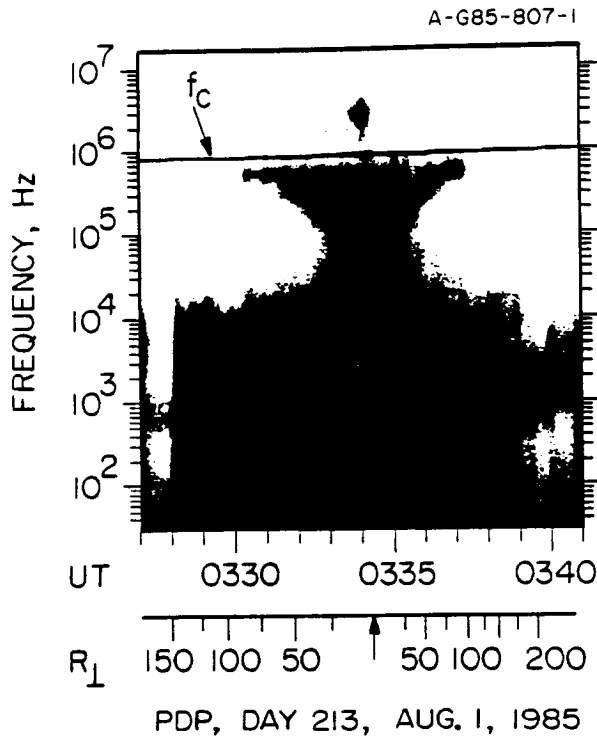


Fig. 2. A spectrogram of the plasma wave electric field intensities during the third magnetic conjunction.

10^{-14} to 10^{-6} volts 2 m $^{-2}$ Hz $^{-1}$. The perpendicular distance, R_1 , in meters, from the PDP to the magnetic field line through the shuttle is shown at the bottom of the spectrogram. The electron gun was turned on in the steady (DC) mode with a beam energy of 1 keV and current of 50 mA at 0330:00 UT and stayed on until 0337:40 UT. During this period the shuttle was oriented such that the electron beam was ejected downward toward the PDP, as shown in Figure 1.

The intense nearly symmetric emission centered on about 0334:05 UT in Figure 2 is produced by the electron beam. At low frequencies the spectrum is characterized by a very intense broadband emission from about 0333:20 UT to 0334:20 UT. Another type of low frequency noise can be seen extending from about 0328 to 0339. This noise is produced by an interaction of the shuttle with the ionosphere and is not related to the electron beam. At higher frequencies a very well defined funnel-shaped feature can be seen extending up to about 1 MHz, spreading out at higher frequencies. The upper cutoff of the funnel-shaped emission is just below the electron cyclotron frequency, which is shown by the solid line labelled f_c in Figure 2. The onset and termination of the funnel at 0330:00 UT and 0337:40 UT correspond to the start and stop times of the electron gun operation. At even higher frequencies an intense narrowband emission can be seen at about 3.1 MHz, lasting for about 30 seconds, from 0333:45 to 0334:15 UT. From a preliminary comparison with the electron density [N. D'Angelo, personal communication], it is believed that this narrowband emission is at either the electron plasma frequency, f_p , or the upper hybrid resonance frequency, $f_{UHR} = (f_c^2 + f_p^2)^{1/2}$. For $f_p \sim 3.1$ MHz

and $f_c \sim 1$ MHz, both of these frequencies are nearly the same, so it is difficult to be sure which is the relevant frequency.

Representative plots of the electric and magnetic field spectra are shown in Figure 3. To minimize antenna orientation effects, the intensities have been averaged over 30 seconds, which includes several spacecraft rotations. Both the electric and magnetic antennas are perpendicular to the spacecraft spin axis. The spectrum at 0334:00 UT shows the intensities near the beam, and the spectrum at 0335:00 UT shows the intensities away from the beam. Near the beam both the electric and magnetic intensities are above the instrument noise level over the entire frequency range measured. The narrowband emission near the plasma frequency is clearly evident. The electric field strength of this emission is about 2.8 mV/m. Although this emission is most likely an electrostatic wave, the electrostatic/electromagnetic character cannot be clearly established because no magnetic field measurements are available in this frequency range. Near the beam, at 0334:00 UT it is difficult to distinguish the funnel-shaped emission above about 10 kHz from the intense low frequency noise below 10 kHz. Both types of emissions have a magnetic field component. The electric field strength of the low frequency noise, integrated from 31 Hz to 10 kHz, is about 150 mV/m, and the magnetic field strength integrated over the same frequency range, is about 0.17 nT. As a crude indication of the electrostatic/electromagnetic character of this noise one can compute the magnetic to electric field ratio, cB/E , and compare this ratio to the expected index of refraction for an electromagnetic wave. The cB/E

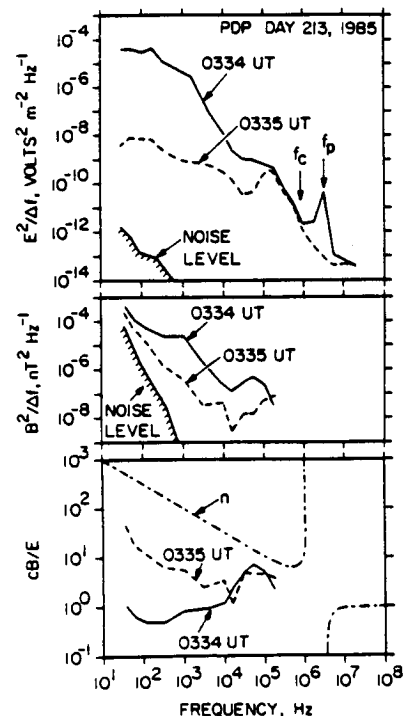


Fig. 3. Electric and magnetic spectra, $E^2/\Delta f$ and $B^2/\Delta f$, and the magnetic to electric field ratio, cB/E , averaged over 30-sec. intervals near the magnetic conjunction, 0334:00, and shortly after the magnetic conjunction, 0335:00 UT.

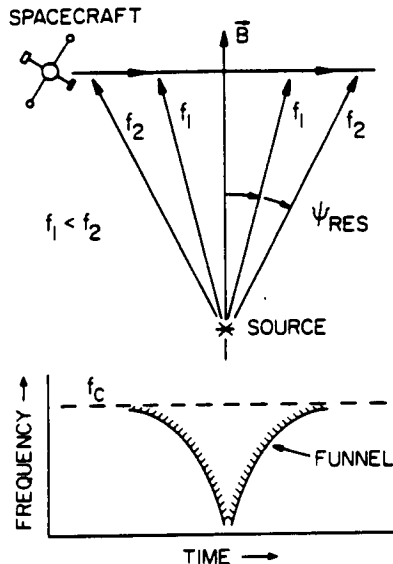


Fig. 4. A schematic illustration showing the ray paths of whistler-mode radiation from a point source for wave normal angles near the resonance cone. The ray path angle ϕ increases with increasing frequency, thereby producing a funnel-shaped feature as the spacecraft crosses the source field line.

ratio is shown in the bottom panel of Figure 3. The cB/E ratio of the low frequency noise varies from 3.0 to 30, less than would be expected for a purely electromagnetic mode of propagation. For reference the index of refraction, n , for parallel propagation is shown in Figure 3. The field strength of the funnel-shaped emission is best determined in the region away from the beam, at 0335:00 UT, where it can be clearly distinguished from the low-frequency noise. The broadband electric and magnetic field strengths, integrated over the emission bandwidth, are 7.5 mVolts/m and 0.1 nT. Again the cB/E ratio is less than would be expected for parallel propagation.

III. Interpretation

The plasma wave emissions from the SL-2 electron beam bear a close similarity to waves observed in the earth's auroral zones. The most remarkable similarity is the funnel-shaped emissions. Very similar funnel-shaped emissions have been observed on a variety of polar orbiting spacecraft and have been called V-shape hiss, saucers and funnels [Gurnett, 1966; Smith, 1969; Mosier and Gurnett, 1969; Gurnett and Frank, 1972; James, 1976; Gurnett et al., 1983]. These emissions are a special case of a general class of emissions known as auroral hiss [Helliwell, 1965]. It is widely believed that this noise is whistler-mode radiation produced by electron beams associated with the aurora [Gurnett, 1966; Hartz, 1971; Hoffman and Laaspere, 1972; Gurnett and Frank, 1972].

The funnel-shaped spectral feature has a simple explanation based on the propagation of whistler-mode waves near the resonance cone. For wave normal angles near the resonance cone the ray propagates at an angle ϕ_{RES} with respect to the magnetic field, as illustrated in Figure 4. The angle ϕ_{RES} is given by

$$\tan^2 \phi_{RES} = -\frac{S}{P} = \frac{f^2}{f_c^2 - f^2}, \quad (1)$$

where S and P are defined by Stix [1962]. The approximation is valid in the high density limit, where the wave frequency and electron cyclotron frequency are much less than the electron plasma frequency. Equation 1 shows that at low frequencies the ray path is almost exactly along the magnetic field. As the frequency increases the ray angle increases, approaching perpendicular as the wave frequency approaches the cyclotron frequency. Propagation ceases at frequencies above the cyclotron frequency. For a spatially localized line source, this frequency dependence produces a funnel-shaped frequency-time variation as the spacecraft crosses the source, as illustrated in Figure 4. The fact that the funnel is filled in indicates that the source is an extended (line) source. The sharply defined outer boundary indicates that the source starts at a well-defined point. The starting point is the electron gun in the case of the SL-2 electron beam, and the acceleration region in the case of the aurora.

To verify that the funnel-shaped emission observed by the PDP is caused by whistler-mode radiation near the resonance cone we have computed the limiting ray paths from the electron beam and compared the boundaries with the observed shape of the funnel. The results of these calculations are shown in Figure 5. The cross-hatched region shows the outline of the funnel, and the solid lines show the boundaries from the ray path computations. Because the distances involved are small compared to the spatial scale lengths in the ionosphere, the ray paths were assumed to be straight lines. The finite size of the beam was included, assuming a beam diameter of 5.2 meters. The actual equations for S and P were used, including electrons but no ions. The electron cyclotron frequency and magnetic field direction were obtained from a multipole expansion of the earth's magnetic field. The computations are relatively insensitive to the electron plasma frequency. To provide a realistic value, $f_p =$

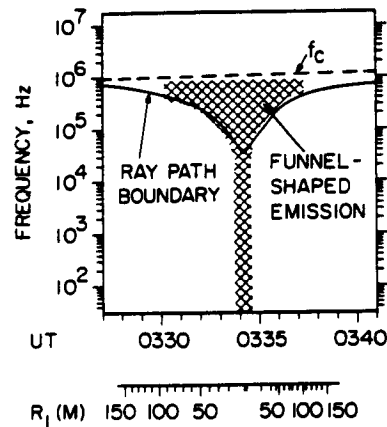


Fig. 5. A comparison of the computed ray path boundaries with the observed shape of the funnel-shaped emission. The close agreement indicates that the radiation is produced by whistler mode waves propagating near the resonance cone.

3.1 MHz was used. As can be seen from Figure 5, the ray path computations are in good agreement with the observations.

The whistler-mode interpretation of the funnel-shaped emission is also consistent with the observed magnetic to electric field ratio. For whistler-mode waves propagating near the resonance cone the electric field is stronger than for parallel propagation. This explains why the cB/E ratio is smaller than for parallel propagation. The observed ratios, $cB/E \sim 1$ to 10 , are also consistent with the magnetic to electric field ratios measured for whistler-mode auroral hiss [Gurnett and Frank, 1972]. The existence of an easily detectable magnetic field also rules out the possibility that the noise could be an electrostatic electron acoustic mode, as has been suggested by Tokar and Gary [1984]. Also, there is no evidence of waves propagating in the direction opposite the beam. Therefore, the radiation can be entirely attributed to the Landau resonance at $\omega/k_{\parallel} = v_b$.

Although the funnel-shaped emission is almost certainly whistler-mode radiation, the mode responsible for the more intense noise at lower frequencies has not been established. Although this noise appears to be a simple extension of the whistler-mode noise to lower frequencies there are several problems with attributing this noise to the whistler mode. First, at low frequencies, below the lower hybrid frequency, which should be around 5.8 kHz, the whistler mode no longer has a resonance cone. Quasi-electrostatic propagation along the resonance cone is no longer possible. Second, at low frequencies the wavelength of the whistler mode becomes very large for all directions of propagation, much larger than the spatial thickness of the region of low frequency electrostatic noise, which is not more than a few tens of meters in diameter. Evidently this intense low-frequency noise is caused by a local beam-generated instability. For a discussion of possible beam instabilities that could account for this noise, see Grandel [1982]. It is interesting to note that this noise has a spectrum similar to the broadband electrostatic noise observed by Gurnett and Frank [1977] along the auroral field lines.

Acknowledgements. The research at the University of Iowa was supported by NASA through contract NAS8-32807, and grants NGL-16-001-043 and NGL-16-001-002, and by the Office of Naval Research through grant N00014-85-K-0404. The research at Stanford University was supported by contract NAS8-36011 and grant NAGW-235. The research at Utah State University was supported by subcontract PR3936 with Stanford University.

References

- Grandel, B., Artificial Particle Beams in Space Plasma Studies, Plenum, N. York, 1982.
- Gurnett, D. A., A satellite study of VLF hiss, J. Geophys. Res., **71**, 5599-5615, 1966.
- Gurnett, D. A., and L. A. Frank, VLF hiss and related plasma observations in the polar magnetosphere, J. Geophys. Res., **77**, 172-190, 1972.
- Gurnett, D. A., and L. A. Frank, A region of intense plasma wave turbulence on auroral field lines, J. Geophys. Res., **82**, 1031-1050, 1977.
- Gurnett, D. A., S. D. Shawhan and R. R. Shaw, Auroral hiss, z-mode radiation, and auroral kilometric radiation in the polar magnetosphere: DE 1 observations, J. Geophys. Res., **88**, 329-340, 1983.
- Hartz, T. R., Particle precipitation patterns, The Radiating Atmosphere, 1970, ed. by B. McCormac, 222, Von Nostrand Reinhold, N. York, 1971.
- Helliwell, R. A., Whistlers and Related Ionospheric Phenomena, Stanford University Press, Stanford, 207, 1965.
- Hoffman, R. A., and T. Laaspere, Comparison of very-low-frequency auroral hiss with precipitating low-energy electrons by the use of simultaneous data from two OGO 4 experiments, J. Geophys. Res., **77**, 640-650, 1972.
- James, H. G., VLF saucers, J. Geophys. Res., **81**, 501-514, 1976.
- Mosier, S. R., and D. A. Gurnett, VLF measurements of the Poynting flux along the geomagnetic field with the Injun 5 satellite, J. Geophys. Res., **74**, 5675-5687, 1969.
- Raitt, W. J., P. M. Banks, W. F. Denig, and H. R. Anderson, Transient effect in beam-plasma interactions in a space simulation chamber stimulated by a fast pulse electron gun, Artificial Particle Beams in Space Plasma Studies, ed. by B. Grandel, 405-418, Plenum, N. York, 1982.
- Shawhan, S. D., Description of the plasma diagnostics package (PDP) for the OSS-1 shuttle mission and JSC chamber test in conjunction with the fast pulse electron gun (FPEG), Artificial Particle Beams in Space Plasma Studies, ed. B. Grandel, 419-430, Plenum, N. York, 1982.
- Shawhan, S. D., G. B. Murphy, P. M. Banks, P. R. Williamson and W. J. Raitt, Wave emissions from dc and modulated electron beams on STS-3, Radio Science, **19**, 471-486, 1984.
- Smith, R. L., VLF observations of auroral beams as sources of a class of emission, Nature, **224**, 351-352, 1969.
- Stix, T. H., The Theory of Plasma Waves, McGraw-Hill, N. York, 10, 1962.
- Tokar, R. L., and S. P. Gary, Electrostatic hiss and the beam driven electron acoustic instability in the dayside polar cusp, Geophys. Res. Lett., **11**, 1180-1183, 1984.

(Received December 4, 1985
Accepted December 23, 1985)

THERMAL ION PERTURBATIONS OBSERVED IN THE VICINITY OF THE SPACE SHUTTLE

J. M. GREBOWSKY, H. A. TAYLOR, JR. and M. W. PHARO, III

Laboratory for Atmospheres, NASA Goddard Space Flight Center, Greenbelt, MD 20771, U.S.A.

and

N. REESE

Physics Department, University of Maryland, College Park, MD 20742, U.S.A.

(Received in final form 11 September 1986)

Abstract - During the Spacelab-2 Shuttle mission the University of Iowa Plasma Diagnostic Package (PDP) probed the plasma environment of the Space Shuttle by maneuvers at the end of the extended Remote Manipulator System (RMS) arm. Also the PDP was operated as a free flying satellite which remained in the vicinity of the Shuttle as the Shuttle was maneuvered about it. During this portion of the mission, the Bennett thermal ion mass spectrometer on the PDP measured some distinctive effects of the large and gaseous emitting Shuttle upon the ambient thermal plasma environment. Within the open cargo bay when thrusters were not firing there was typically an absence of measurable thermal ions when the bay was in the wake of the spacecraft. Just above the top of the bay when traces of ions are detected in the wake the dominant ion was the contaminant water. When the PDP was released in the wake of the Shuttle and moved away, the spin modulation of the ion flux into the spectrometer was initially different for the O^+ and H_2O^+ ions. The O^+ ions were streaming into the spectrometer from the spacecraft velocity direction whereas the water ions were flowing from a direction as much as 77° from this. The concentration of water ions in the near wake decreased with increasing distance, becoming less than the predominant ion O^+ at wake distances of the order of 30 m. However, traces of contaminant ions were present as far as the maximum distance of several hundred meters explored by the free-flying PDP. The neutral gases from the Shuttle extend in all directions as was shown by the presence of water ions, not only in the immediate vicinity of the Shuttle and in its wake but also even several hundred meters upstream. The presence of contaminant NO and O_2^+ ions brings into question whether reliable ambient ion measurements can be made from the Shuttle.

INTRODUCTION

Thermal ion composition measurements in the vicinity of the Space Shuttle have shown that the Shuttle may have a significant impact on the ambient ionosphere. This is most obvious in the persistent presence of H_2O^+ ions in its near vicinity (e.g. Narcisi *et al.*, 1983; Grebowsky *et al.*, 1983). Previous measurements of ion composition near the Shuttle have been restricted primarily to observations at fixed positions within or near the open Shuttle bay. The ion measurements considered by Narcisi *et al.* (1983), for example, were made on the mission STS-4 from a bay position in which the ion spectrometer looked basically horizontally over the right wing, whereas those described by Grebowsky *et al.* (1983) were taken on the STS-3 mission predominantly within the bay with the ion spectrometer facing the port wall of the bay. In the latter experiment, which was one instrument on the Plasma Diagnostic Package (PDP), use of the Remote Manipulator System (RMS) arm was also made to

take measurements in the vicinity of the bay up to a 15 m distance. Those observations showed that the water released from the Shuttle (e.g. by thruster firings, outgassing, water dumps and cabin leakage) readily results in the production of positive water molecule ions, primarily through charge exchange with ambient O^+ ions. The spatial extent of this disturbance however could not be determined from the limited positions of these earlier experiments.

The large releases of water during water dumps and during thruster firings lead to local depletions of the ambient ionospheric O^+ concentration (Narcisi *et al.*, 1983; Pickett *et al.*, 1985). Narcisi *et al.* (1983) pointed out that, nevertheless, it is still typically possible to measure accurately ambient ions when Shuttle-borne ion spectrometers are in a ram configuration. Although this is possibly true for the major ion O^+ , caution needs to be exercised regarding minor ambient ions. For example, although most of the contaminant ions observed (e.g. H_2O^+ , OH^+ , H_3O^+) are of definite Shuttle origin, the source of

molecular ions such as NO^+ and O_2^+ in the vicinity of the Shuttle may be ambiguous. The latter ions are not only present in the *F*-region but by the same chemical reactions which produce them in the ambient plasma they are also produced from the neutral NO , N_2 and O_2 of Shuttle origin which, particularly during thruster firings, have concentrations greatly exceeding their ambient counterparts (Wulf and von Zahn, 1986). Hence it is still not resolved whether reliable ambient thermal ion concentration measurements can be made from the vicinity of any large gas-emitting structure like the Space Shuttle.

In addition to the chemical production of contaminant ions via interaction with the ambient plasma, Hunton *et al.* (1983) have pointed out that the dynamics of the contaminants themselves are complicated, with evidence for both drifting and stationary components of water ions in the Shuttle frame of reference. Further, Stone *et al.* (1983, 1986) have described the existence of localized streams of ions flowing from different directions near the Shuttle. The source of these streams has yet to be isolated. Their presence however demonstrates that, apart from interest in determining the contaminating impact of the Shuttle on the external environment, the Shuttle's interaction with the ambient plasma enables an exploration of new plasma processes.

The most dramatic effects in the thermal plasma distribution are anticipated downstream in the wake of the Shuttle and it is in this region that the extent of the Shuttle's influence on the plasma environment should be greatest. It is known that the plasma wake near the Shuttle is a deep void of detectable plasma (e.g. Raitt *et al.*, 1984), but its spatial extent and structure have not been measured in much detail. This paper will explore some of the wake features as well as contaminant ion distributions using Bennett RF ion mass spectrometer measurements from the University of Iowa PDP flown on the Spacelab-2 (SL-2) mission. During part of this flight the PDP was flown free of the Shuttle to sample different regions out to separation distances of several hundred meters, permitting for the first time a sampling of the spatial extent of the Shuttle's perturbation.

ORBITAL FEATURES

The Spacelab-2 Shuttle mission (STS-51F) on which the Plasma Diagnostic Package was flown went into orbit on 29 July 1985. The orbit had an inclination of 49.5° , a period of $1\frac{1}{2}$ h, and was circularized eventually at a mean altitude of 310 km. It reached poleward to magnetic latitudes of the order of 60° ,

i.e. near the main midlatitude ionospheric trough (see the review by Morfett and Quegan, 1983, for an overview of this feature). The phase of the orbit was such that the most poleward latitudes were traversed near the terminators—the high latitudes of the southern winter hemisphere near dawn and those of the northern summer near dusk. The PDP was released as a free flying satellite on the second day of the mission and after a 6 h period was picked up by the Shuttle via the RMS arm for eventual return to Earth on 6 August 1985.

CHARACTERISTICS OF THE ION SPECTROMETER

The Bennett RF ion mass spectrometer flown was not designed for this particular mission but was a test instrument previously developed for flight on a sounding rocket. To scan through the ion mass range from below 1 to 70 amu, the RF frequency applied to the sensor grids was swept, rather than the dc acceleration voltage as has been usual in space applications (e.g. Brinton *et al.*, 1973). The restricted telemetry requirements of the mission were approached by using internal logic circuits to pick all the resonant mass current peaks detected during each sweep of the RF. The amplitude of the peak current and its frequency (which defines the ion amu) were then digitized for telemetry. Although the peak detector resolved the mass to a small fraction of an amu, digitization of the resonant peak frequency (or equivalently the amu) for telemetry was performed using an algorithm that provided high mass resolution at the low mass end of the spectrum, a nominal resolution of the order of 0.5 amu near the water-oxygen masses, a resolution of 1.5 amu near the important 30 amu region and in the high mass range above 40 amu a resolution greater than 3 amu. These resolutions were considered sufficient for resolving the most significant masses anticipated before launch.

Some difficulty occurred in positively resolving several ion species due to the fact that the RF sections of Bennett spectrometers function by resonantly selecting incoming ions, not on the basis of their mass but by their incoming velocity (e.g. see Bennett, 1950). By providing a fixed accelerating electrical potential near the entrance to the tube (in this instance, 80 V) each incoming positive ion received its own unique mass discriminating velocity that could be resonantly selected in the following RF stages. This feature of the spectrometer is also an asset in that it can be used to determine the incoming energy of ions due to drift or satellite charge.

The ion spectrometer flown on the SL-2 mission

was calibrated in the laboratory to provide a frequency-mass relationship under conditions of no net energy into the entrance of the spectrometer. If an ion enters the spectrometer with a nonvanishing energy E , then its telemetry mass (i.e. the amu from the calibration identified by the frequency of the current peak), TM , will be $TM = E(\text{eV})/112$ amu lower than the actual mass. In the vicinity of the Shuttle, complex changes in flow dynamics and the production of ions stationary with respect to the vehicle may occur such that different ion mass species blend into only one resolvable resonant current peak. For example, the measurement of an ion at 30 amu could be a non-streaming 30 amu ion or a 32 amu ion with approximately 7 eV of ram energy. Also, high plasma turbulence levels have been detected in the vicinity of the Space Shuttle (Siskin *et al.*, 1984). The presence of such plasma irregularities would broaden adjacent ion current peaks and reduce the resolution of the spectrometer. A noticeable feature during parts of the SL-2 mission is an inability of the spectrometer to resolve 30 from 32 amu ions on some of the sensitivity levels (see below) employed, presumably due to a combination of the foregoing factors.

The spectrometer employed four distinct sensitivity modes, obtained by stepping a retarding voltage (V_r) on a grid just in front of the current collector plate. A laboratory calibration curve showing the response of the spectrometer (using Ne^+ as the source) to changes in this retarding voltage is shown in Fig. 1. The four levels of sensitivity used during flight are indicated on the voltage axis. The lowest sensitivity mode (level 1) has maximum resolution of mass whereas level 4 has the highest sensitivity. As the incoming ion energy increases, the effective collector retarding voltage decreases by the same amount. The calibration curve also indicates the presence of harmonically generated ion peaks in the RF stages. These vary proportionally with the resonant ion current at a fixed V_r . The observed ratio of the harmonic amplitude to that of the fundamental ion can also be used to determine the relative variation of the fundamental currents, thus providing an estimate of incoming ion energies. For the SL-2 mission spectrometer each retarding potential was held fixed for approximately 2.4 s, while the RF was swept to sample the complete mass range of ions from below 1 to 70 amu. All four steps were cycled resulting in a repetition of a given sensitivity level every 9.6 s.

The conversion of collected ion currents to incoming ion concentrations requires that the incoming ion energy and flow direction be known. In usual satellite missions the spectrometer points in the ram direction and the spacecraft potential is well

behaved, allowing an uncomplicated conversion to concentrations. Under the conditions existing during the Shuttle mission under consideration this was not the case. Therefore, only the raw collected ion currents will be presented here and the sensitivity level used in the plots will be selected on the basis of what features are to be emphasized and which level best depicts them. The dynamic current range of the collector was 2×10^{-13} – 2×10^{-8} A.

PRE-RELEASE AND NEAR WAKE STRUCTURE

Although the major focus of the discussion is to be ion measurements made when the PDP was physically separated from the Shuttle, observations made while extended on the RMS arm just before release will be used to provide a relative reference for the ion environment observed further away. Figure 2 depicts measurements of the major ions detected during a 30 min period encompassing the PDP release from the Shuttle (which took place at 01:00 G.M.T. on day 213, i.e. 1 August 1985). During the beginning of the interval, the Shuttle was flying in the "airplane" mode, i.e. nose pointing into the orbit direction and belly towards the Earth. The PDP was held by the RMS arm approximately 10 m out beyond the port side with the ion spectrometer orifice directed into the Shuttle ram direction. This PDP location was maintained until approximately 23:47 G.M.T. when the PDP was moved to its deployment position a few meters above the circular envelope of the bay and over the nose-tail symmetry axis of the Shuttle—the spectrometer still pointing into ram. The dominant ion throughout this period was O^+ with minor species NO^+ and O_2^+ present in concentrations comparable to one another and indistinguishable in the sensitivity mode under consideration. In addition, there was a background of water species ions H_2O^+ and H_3O^+ with similar concentrations.

The energy response of the O^+ collected current when the instrument was positioned over the bay is consistent with an energy of only slightly more than the ambient O^+ flow energy (~ 5 eV) with respect to the Shuttle. However, during the measurements on the side of the bay, much higher energies were indicated requiring more than 5 V of negative spacecraft charge in addition to the ram flow energy. Such variations in spacecraft potential are not unexpected in the light of earlier STS-3 observations (e.g. Shawhan and Murphy, 1983), which showed that the PDP potential variation is complex, varying in response to thruster firings and to the motion of the Orbiter and PDP with respect to the Earth's magnetic field. The

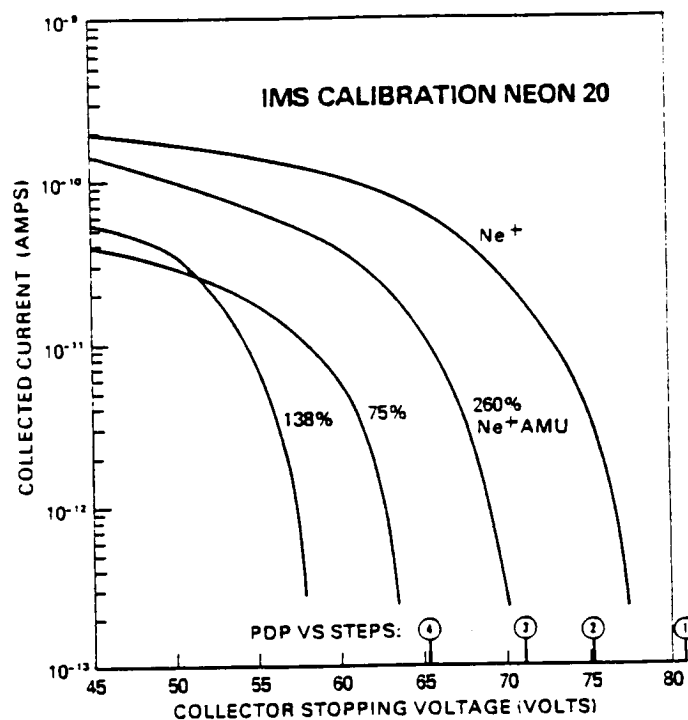


FIG. 1. LABORATORY CALIBRATION CURVE FOR AN IONIZED Ne SOURCE.

The four voltage levels indicated were the values stepped through on the SL-2 instrument. In addition to the fundamental peak, harmonics of the fundamental ion are generated at apparent masses that are fixed percentages of the fundamental mass. In flight the effective stopping voltage is the sum of the V_s level of the instrument plus the incident ion energy in electronvolts. The Ne^+ calibration curves typify the response for other masses.

NO^+ , O_2^+ current peak-frequency response to incoming energy is consistent with this behavior, taking into account the proportionately higher ram energy associated with the larger masses. However, the water species (H_2O^+ , H_3O^+) measurements show no evidence of ram flow energy, confirming the observation of Hunton and Calo (1983) that the water ion distributions near the Shuttle can have nonconvecting components as might be expected for a dense scattering medium and/or a localized ion source. The water species ion telemetry mass and current collection efficiency are only responding to spacecraft charge. For example, the Xs in Fig. 2 which denote a one-telemetry-count higher mass than the +s for H_3O^+ begin consistently near 23:47 G.M.T., indicating a drop in the magnitude of the PDP's negative potential by several volts.

As was inferred by Narcisi *et al.* (1983), a first glance at the pre-release data would give the impression that under proper conditions (corresponding to an unoccluded ram view for the spectrometer) ionospheric features can seemingly be measured from the

Shuttle. However, the plasma environment always shows traces of the spacecraft's presence. For example, characteristically, as seen in Fig. 2, there is a background level of water ions and also H_3O^+ of comparable concentration in the near vicinity of the vehicle. The presence of the latter ion (which requires water-water ion collisions) and the absence of net motion indicates (as was pointed out by Hunton and Calo, 1983) that a dense cloud of water occurred in the vicinity of the Shuttle. In addition, the Shuttle's Reaction Control System thrusters sporadically fire to maintain attitude. These deposit concentrated streams of gases that have a further impact on the local plasma environment. The enhancement of the water ion concentrations near 23:45 G.M.T. for example occurred simultaneously with a sequence of such firings.

In addition to water products, NO , N_2 and O_2 are also released in the engine firings and are apparently always present near the Shuttle in quantities exceeding their counterparts in the ambient atmosphere (Wulf and von Zahn, 1986). These readily interact with the

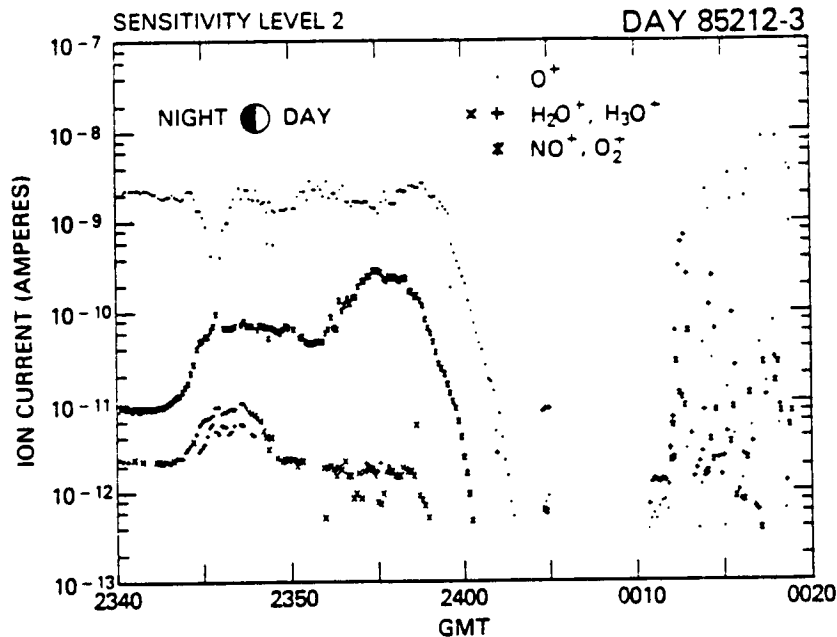


FIG. 2. ION MEASUREMENTS BEFORE, DURING AND AFTER RELEASE.

Release took place near 00:10 G.M.T. The complex behavior after release is due to the spin modulation of the collected ion current with consecutive current measurements made at different attack angles. Before release the PDP was on the extended RMS arm over the port side until ~23:47 G.M.T. whereupon it was repositioned over the bay—during this period the Shuttle flew in the "airplane" configuration. All currents dropped off when the Shuttle reorientated for the release and the PDP entered its wake.

ambient F -region O^+ to produce NO^+ and O_2^+ . This leads one to suspect that ambient plasma variations are not being observed near 23:45 G.M.T. even though the spectrometer had the ideal ram look direction. As the water ion currents peaked the heavy molecules followed suit, while a sharp trough developed for O^+ . The trough in O^+ may be interpretable in terms of an ionospheric hole produced by charge exchange of the flowing O^+ with a cloud of water molecules (e.g. Mendillo and Forbes, 1978)—the charge exchange rate of O^+ with H_2O occurring orders of magnitude faster than the normal ambient O^+ chemical loss rate. Similarly, the rise in heavy molecular ion concentrations at the same time can be attributed to the Shuttle's emissions. In fact, a reduction in the concentration of O^+ would also result due to losses of O^+ via atom-ion interchange with contaminant N_2 and O_2 —a process which enhances NO^+ and O_2^+ production. The rates of these reactions increase with increases in the relative velocities of the interacting ion and neutrals (McFarland *et al.*, 1973) and were recognized by Banks *et al.* (1974) to play a significant role in modifying the Earth's high latitude ion composition. At the 8 km s^{-1} velocity of the Shuttle this loss

scheme for O^+ could play an important role in the production of the observed NO^+ and O_2^+ . These contaminant ions are particularly troublesome with respect to ambient ion composition measurements in the F -region since ambient NO^+ and O_2^+ can at times be quite low and irregular in concentration, making it difficult to discriminate them from contaminants. A word of caution is necessary on this interpretation of the pre-release measurements. An alternative explanation of the NO^+ , O_2^+ ion variation could be offered in terms of a complex stormtime midlatitude ionosphere structure being traversed coincidentally—this phase of the observations took place during a magnetically active period with a K_p index of 5⁺ (Coffey, 1985).

Just before release with the PDP held fixed in its position over the bay, the Shuttle changed its attitude from the "airplane" configuration, maneuvering so its tail was directed toward the Earth and its bay into the downstream direction. This attitude change beginning just prior to 24:00 G.M.T. is seen in Fig. 2 as a parallel complete dropout of the measurable ions as the PDP moved into the Shuttle's wake. The wake of the Shuttle in its near vicinity was very deep as has

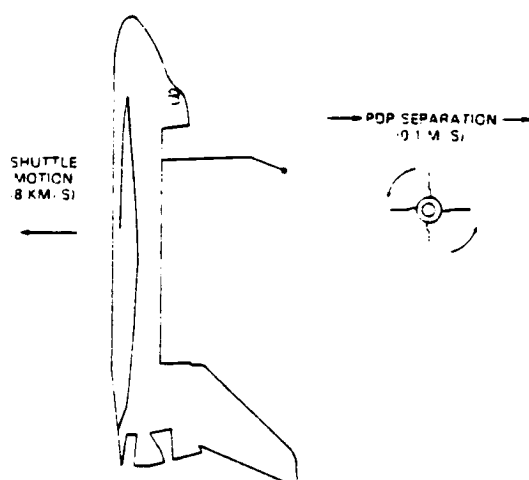


FIG. 3. THE RELATIVE POSITION OF THE PDP WITH RESPECT TO THE SHUTTLE DURING RELEASE.

The Shuttle's tail was directed to the Earth, its belly in the ram direction. The PDP was released and separated down the wake. At release the spectrometer was pointing upward. Its location in the spin equator of the satellite enabled it to sample the ram flux of ions once each spin revolution.

been previously noted and expected for such a large vehicle (e.g. Samir *et al.*, 1986). The only ions that get into the near wake are those scattered into the wake in association with thruster firings such as the spikes of ion current detected near 00:05 G.M.T.

PDP RELEASE AND THERMAL IONS DOWN THE WAKE

The detailed processes by which plasma enters the wake of the Shuttle are not fully established. Some of the energetics involved are evident in the ion measurements made when the PDP was released. Figure 2 includes some of the observations post-release and, if examined closely, will reveal water to be the dominant ion seen initially after release. Apart from this and the presence of O^+ and molecular ions, the complexity of the spin modulation of the current flux into the spectrometer obscures in the figure the thermal ion measurements after release. An expanded time scale will be used to see more closely the spin response. First, however, some general description of the release is needed.

Figure 3 schematically depicts the attitude configuration of the Shuttle and the PDP at release. The Shuttle's tail was directed toward the Earth while its belly was facing into the direction of motion. When the PDP was released from the RMS the Shuttle moved forward of the PDP while maintaining the PDP along the projection of the Shuttle anti-velocity

vector. The PDP therefore moved down the Shuttle wake. The ion spectrometer at the time of release was pointing upward in the nose direction of the Shuttle. A momentum wheel in the satellite was used to spin-up the satellite into a stable configuration with the spin axis directed perpendicular to the orbit plane as seen in Fig. 3. The spectrometer was located on the spin equator of the PDP so that it sampled the ram direction on each spin. The full-up spin period was near 13 s which was attained 1 h 15 min after release. The relative separation of the PDP and Shuttle took place at a rate of 0.1 m s^{-1} until establishing initial station, keeping at a distance of 90 m. Only the early part of the separation will be considered here in detail since it shows the most pronounced Shuttle-related behavior.

The measurements of the two main ions O^+ and H_2O^+ as well as H^+ from all sensitivity levels during the first two spin cycles after release are combined in Fig. 3. As discussed earlier, the spectrometer sampled the same sensitivity level approximately every 9 s. Initially this was short compared to the spin period and one sensitivity level provided fair coverage of the angle of attack variation of the current flux into the instrument. As the spin rate increased however, reasonable angular resolution could be approached only by combining the measurements of all sensitivity levels. To do this the collected current of a given ion species in sensitivity modes one-three were multiplied by constant factors so that the resultant current variation smoothly blended in to the fourth level variation through the first few spin cycles. That is, the currents in accordance with the calibration efficiencies (e.g., Fig. 1) were approximately normalized to one level. This superposition for the first 10 min of free flight is shown for three of the prime ions present. The solid curve for O^+ and the dashed curve for H^+ consist of line segments connecting the actual normalized data points and are not smoothed curves.

Initially after release at 00:10 G.M.T. at a range of 6.4 m (measured from the Shuttle center of mass, which is located approximately 3 m from the top of the circular, 4.6 m diameter payload bay envelope) water was the dominant ion detected. During this period the aperture of the spectrometer was slowly turning from its initial upward direction towards the Shuttle as the PDP spun up. Just before 00:12 G.M.T. by using its Reaction Control System thrusters the Shuttle began to increase its distance from the PDP. The range indicated in the figure is based on a model (Pickett and Murphy, personal communication) using pre-mission planning since the Shuttle's range radar did not lock on to the PDP until the very end of the period plotted in Fig. 4. A definite spin modulation

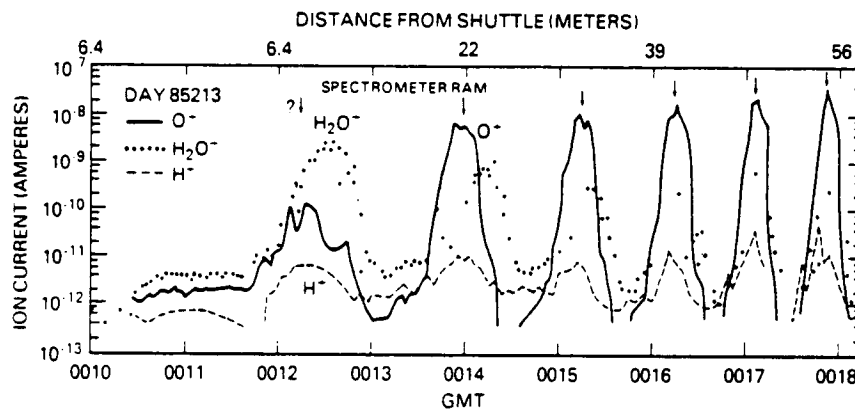


FIG. 4. SPIN MODULATION OF ION CURRENTS AFTER RELEASE. Current profiles for three ions detected on release show the existence of flow enhancements of the collected current fluxes. The water ions are streaming into the wake of the shuttle from a different direction than the flowing ambient ions O^+ and H^+ .

of the collected ion fluxes was observed, indicating plasma streams in the wake.

O^+ exhibited a maximum number flux into the spectrometer from the ram direction even during the first spin close to the bay. The precise orientation of the PDP throughout the first spin cycle was not specified in the ancillary data base so the first ram point was only a guess estimated on the basis of the known starting orientation of the PDP and the first known attitude near 12:30 G.M.T. This location is consistent with the H^+ modulation which was not characterized by an irregular spin envelope during this period. What is particularly interesting is that the water ions also show spin modulation—evidence that H_2O^+ is also streaming into the Shuttle wake. Further, H_2O^+ was not moving from the spacecraft ram direction as was O^+ , but rather from a direction downward (i.e. tailward) of it. In sequence the angles from the ram direction for the first three water ion current peaks were approximately 63° , 77° and 48° , respectively. After the third spin the spin rate had increased to a value such that the angular separation between individual ion measurements became too large to fully resolve the H_2O^+ angle of attack variation. Further, the average amplitude of the H_2O^+ currents decreased with increasing distance and thruster pulses of water ions became dominant over the background fluxes, introducing irregularities in the spin response. However, a skewing of the flow angle is still apparent in the tendency of the water ion currents to dominate over those of O^+ as the spectrometer turns into the PDP wake direction but not when it emerges from the wake. The variation of H^+ which is ambient, with no apparent dominant

source of Shuttle origin, parallels the spin angle variation of the O^+ with proportionately larger currents in the wake of the PDP due to its lighter mass (e.g. Samir *et al.*, 1986).

The deflection of water ions from the ram direction could be related to spacecraft electric fields as considered by Stone *et al.* (1983, 1986). Also, the water ions are initially produced stationary in the Shuttle frame of reference (i.e. no momentum is transferred in the O^+ , H_2O charge exchange reaction as pointed out by Narcisi *et al.*, 1983). Pickup of these ions by the ambient magnetic field with gyration velocities corresponding to the Shuttle motion perpendicular to the local magnetic field would produce cycloidal motions in the Shuttle-PDP frame of reference. This would lead to contaminant ion streamlines in the wake that differ from those of the ambient ions which have small gyration velocities compared to their drift speed. Regardless of the source, in retrospect it seems natural that contaminant ions produced on the ram side of the shuttle would stream into the wake at a different angle than ambient ions. Even if the acceleration processes in the wake were the same for both ion species their different initial velocity states would lead to different average trajectories.

The relatively low irregular amplitude of the O^+ current on the first spin cycle could reflect the passage of the O^+ through dense patches of water which charged transferred with the ambient O^+ partially depleting it and/or a turbulent plasma divergence into the bay from the sides of the Shuttle (the spectrometer sampled flow variations only in the plane of the Shuttle ram and nose-to-tail symmetry axes). In addition to the dominant flowing component of

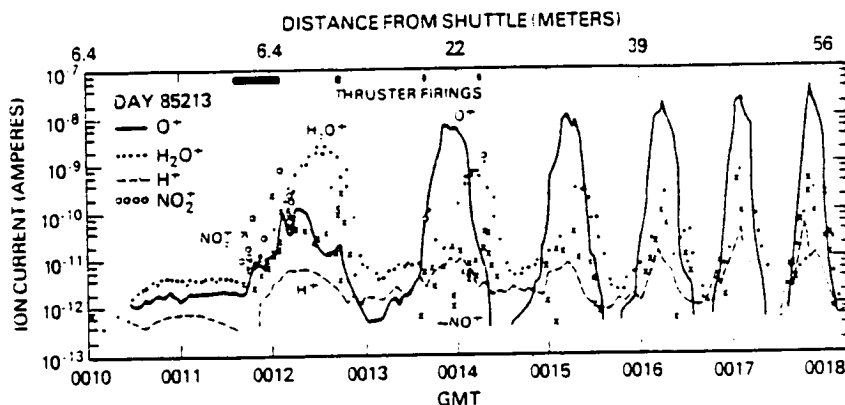


FIG. 5. PRESENCE OF THRUSTER PERTURBATIONS.

Superimposed on the previous figure are molecular ion measurements for NO^+ , O_2^+ and for an ion with a mass in the range 44–47 amu. The NO^+ shows a tendency for a spin modulation characteristic of a streaming ambient plasma but is very structured. Discrete enhancements of ions correspond to periods with thruster firings.

H_2O^+ there is also a significant thermalized or scattered background component of this ion whose presence is seen by the dominance of H_2O^+ in the wake of the spinning PDP. This component was most prominent near the Shuttle and gradually decreased with increasing separation distance until it was no longer detected. This velocity distribution is consistent with the observations of Hunton and Calo (1983). The presence of ion scattering close to the Shuttle is also hinted at by the presence of measurable O^+ in the PDP wake during the first spin cycle which disappears with increasing separation distance.

In addition to the usually prominent contaminant ion H_2O^+ , thruster firings produce intense localized enhancements of other contaminant ions—particularly in the near vicinity of the Shuttle. Some of these were clearly seen in the release measurements. Figure 5 shows the release data again but with the inclusion of the measurements of molecular ions with atomic masses in the range 30–32 amu and ions with masses in the range from approximately 44 to 47 amu. The lower mass range which consisted of O_2^+ and NO^+ was merged from all four sensitivity levels as was done in the previous plot. Significant perturbations exist in these ions, however, and the fit is not very smooth.

The very heavy ions had to be treated differently since an instrumental harmonic of H_2O^+ exists within this same mass range which could overwhelm the detection of an incoming ion with low concentrations. Since the harmonic amplitude never exceeds the fundamental, the real presence of such ions is established by plotting the measured currents in the high

mass range for only those currents which exceed that of H_2O^+ on the same sweep. These very heavy ions were present at discrete times during the first two spin cycles and occurred in coincidence with spike-like enhancements in H_2O^+ and NO^+ . Each of these distinctive perturbations arose with sequence firings. The 30–32 amu ions have previously been established as thruster ion contaminants (Grebowsky *et al.*, 1983; Narcisi *et al.*, 1983), but the high mass ion has not. Although the spectrometer mass resolution is broad at this mass range and doesn't pinpoint the ion precisely, neutrals in this mass range have been measured to be emitted during thruster firings (Wulf and von Zahn, 1986). One possibility is that the ion detected is NO_2^+ whose neutral molecule counterpart is spontaneously produced from the nitrogen tetroxide (N_2O_4) oxidizer used in the Reaction Control System thrusters. CO_2^+ is also a possibility but the telemetry mass counts tend to lay on the high mass end of the range indicating a mass higher than 44.

PDP RETRIEVAL

Another view of the near wake was provided during the retrieval of the PDP after the free flight period with a different PDP attitude. Figure 6 shows the major ions detected as the PDP was spun down and the Shuttle moved towards it for pickup. Spindown started just before the time period plotted. As was the case upon release, the PDP was positioned in the wake of the Shuttle throughout retrieval and pickup. The completion of the PDP spin down is evident in the figure by the cessation of the spin modulation of

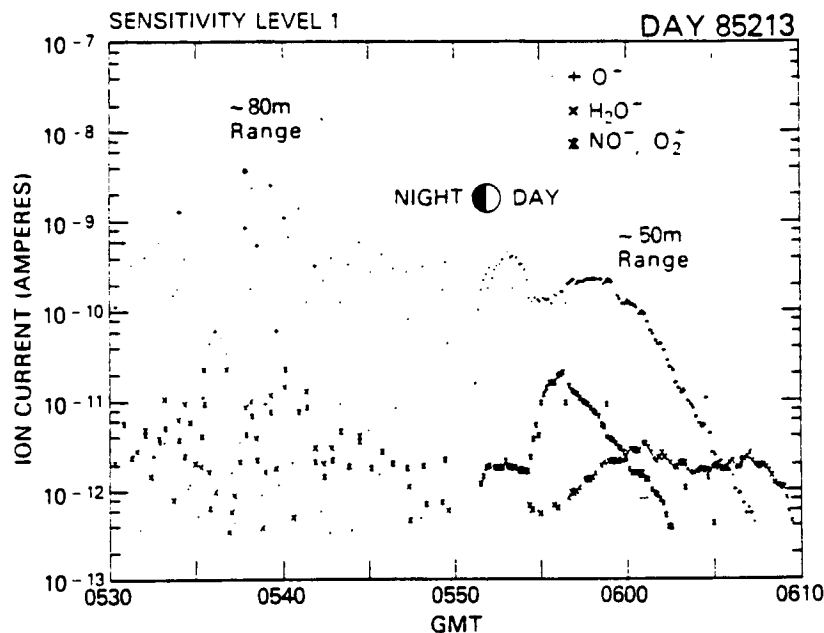


FIG. 6. SPINDOWN AND RETRIEVAL.

At the end of the free flight period time the PDP was again positioned in the wake of the Shuttle. The measurements shown began with the PDP at a range of 80 m. Water and the molecular ions are present in the spin measurements. Spindown started at 05:27 G.M.T. and was complete at 05:52. The spectrometer orifice was directed nearly into the ram direction during the spindown recovery phase. As was seen during the PDP release, water became the dominant ion before the ion currents vanished at closest approach.

Actual grapple by the RMS occurred at 06:20 G.M.T.

the currents. The Shuttle radar did not track the PDP within the 50 m range as the Shuttle approached the subsatellite for pickup. Hence, the movement in towards the bay from the 50 m range can only be discussed qualitatively.

At the 80 m range, at which spindown started, water was typically present as a minor species ion as was NO^+ . (In the approach sequence there was no evidence in the measurements of O_2^+ —the only ion detected in this mass range had a consistent telemetry mass corresponding to a 30 amu ion moving at Shuttle speed.) As the two vehicles moved into daylight the PDP stopped spinning with the spectrometer orifice near the direction of forward motion. Shortly thereafter the magnitude of the ambient(?) molecular currents began to decrease in parallel with that of O^+ as the PDP approached the Shuttle bay. On the other hand, the H_2O^+ flux increased and remained steady, becoming dominant on close approach and then, as was the case at release, no detectable ions were present at closest approach in the wake. The energy of the water ions from the spectrometer response was 5–6 eV and indicative of a flowing plasma near the bay. On the basis of the previously discussed release data,

it is possible that the onset of the reduction of ambient ion currents and the enhancement of water in the vicinity of the bay may not be totally representative of concentration variations in the Shuttle wake but rather a change in direction of the ions flowing into the wake relative to the spectrometer orifice. This is hinted at by the increase in the O^+ telemetry mass during recovery—in the figure, +s indicate a one-telemetry-mass count higher than the dots for O^+ and correspond to a lower incident ion energy. In any case, both the release and recovery data are consistent in that they both detect the strongest wake effects inward of approximately 50 m.

FLY AROUND WATER OBSERVATIONS

Two orbits were flown in which the Shuttle maneuvered far from and around the PDP. A schematic of the first such orbit is shown in Fig. 7. The Shuttle velocity vector is toward the left while the Earth is in the downward direction. Initially the PDP was in the wake of the Shuttle (the approximate boundaries of which are indicated by the Shuttle's Mach angle). The

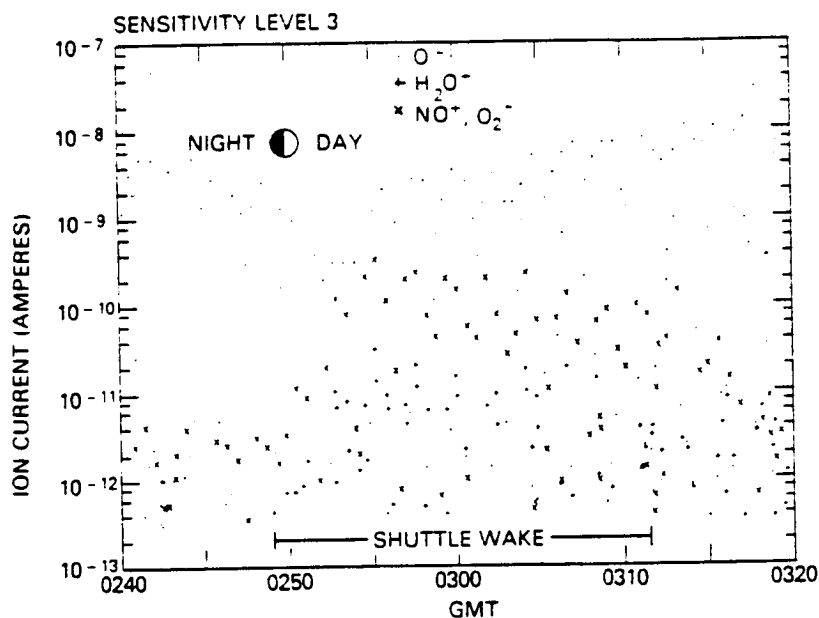


FIG. 8. PASSAGE INTO THE WAKE.

At a range of approximately 230 m behind the Shuttle, passage into the wake appears to be associated with enhancements of the water and heavier molecular ions. Due to the phasing of this crossing with passage into daylight and to highest winter magnetic latitudes the NO^+ (O_2^+) enhancements may reflect ambient ionosphere variations.

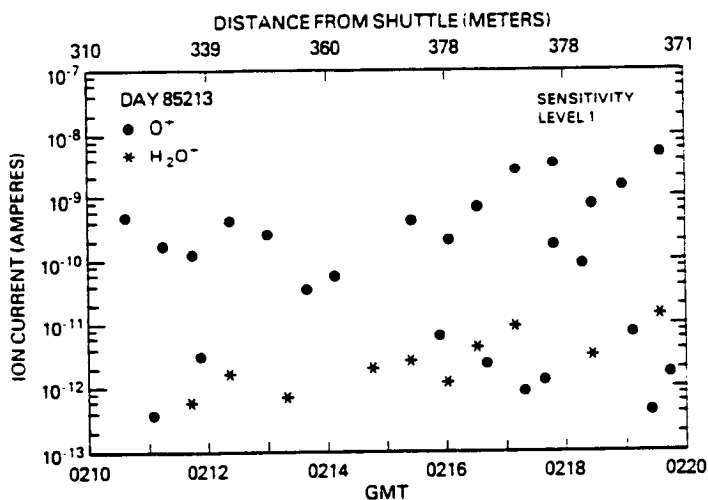


FIG. 9. MEASUREMENTS FAR IN FRONT OF THE SHUTTLE.

Water ions are not restricted to the near vicinity of the Shuttle or its wake. They were even detected upstream at a range of nearly 400 m from the Shuttle. During this period the component of the PDP's range projected onto the vehicle orbital direction was ~300 m upstream.

emissions have an impact on the thermal ion composition measurements out to separation distances of several hundred meters and are not just confined to the vehicle's wake. This is perhaps not unexpected since ambient neutral mean free paths at the Shuttle's altitude are of the order of kilometers. With such long mean free paths neutral molecules of Shuttle origin are not impeded from expanding in all directions to beyond the separation distances attained by the PDP.

Some discussion is warranted regarding the possibility that outgassing of the PDP itself might provide enough neutral water to account for the water ions detected far in front of the Shuttle. The earlier discussed pre-release, release and capture observations showed that H_2O^+ distributions detected from the PDP in the near vicinity of the Shuttle varied in response to changes in the interaction between the ambient plasma and the Shuttle's own water emissions. The ram currents of H_2O^+ relative to O^+ during those times were comparable to and sometimes even less than those observed during the free flight phase. Hence, since PDP outgassing effects from the ions were not evident in the near vicinity of the Shuttle, it does not appear likely that such PDP emissions were responsible for the H_2O^+ occurrences observed far in front of the Shuttle.

SUMMARY AND CONCLUSIONS

A survey of some of the thermal ion characteristics in the vicinity of the Space Shuttle made by a Bennett RF spectrometer as part of the Plasma Diagnostic Package (PDP) flown on the Spacelab 2 mission has been presented with emphasis on the Shuttle's extended wake. The near wake within and in near proximity to the open payload bay was found as on previous missions to be void of detectable ions except during Reaction Control System Thruster firings. In the latter instances short pulses of enhanced ion fluxes of predominantly NO^+ , O_2^+ and H_2O^+ were detected. A very heavy ion was also detected during the firings which has been tentatively identified as NO_2^+ . Such ions have their neutral molecule counterparts in the products of the monomethyl hydrazine and nitrogen tetroxide reactions (Wulf and von Zahn, 1986).

During release from the Shuttle as a free flying satellite the PDP was slowly spun up as it moved away down the wake of the Shuttle. The spin modulation of the ion fluxes into the ion spectrometer indicated the presence of multiple plasma streams analogous to those studied by Stone *et al.* (1983, 1986). The two streams were composed of different ions, O^+ and H_2O^+ separated in direction by as much as 77° , with O^+ , of apparently ambient origin, detected with

a motion in the Shuttle anti-ram direction. The spectrometer orifice was in the PDP spin plane and sampled ion fluxes essentially in the plane of the Shuttle nose-tail symmetry line and velocity vector. Given a local source for the H_2O^+ production in the vicinity of the Shuttle, which is initially produced stationary in the Shuttle frame of reference, electric fields whether of sheath origin or the convection electric field associated with cross magnetic field motion (including magnetic field pickup of the water ions) will produce a different flow pattern in the wake from that of O^+ .

Clear evidence of prominent wake plasma concentration reductions and/or two-stream effects were seen out to 50 m from the Shuttle on release of the PDP. This was also seen on the retrieval of the PDP in the wake after free flight. Inward during retrieval at the 50 m range, distinct reductions began in the ambient ion currents collected and the corresponding water ion currents became enhanced. Just outside the detectable plasma void of the Shuttle wake, as observed on both the release and retrieval, H_2O^+ was dominant.

During the free flight phase the satellite was flown across the wake of the Shuttle at a distance of several hundred meters. The ion measurements indicated enhancements of H_2O^+ and NO^+ (O_2^+) at these large distances. Although the H_2O^+ ions are of definite Shuttle origin, because the wake entrance took place at the most poleward latitudes and just after sunrise the NO^+ (O_2^+) ion variations may just reflect these inputs to the gas-plasma environment rather than a distinct far wake effect. The effects of the Shuttle on the ambient plasma are not restricted to its near vicinity or plasma wake. Water ions were also detected several hundred meters upstream of the Shuttle. This indicates that the gaseous emissions expand far in all directions and couple to the ionosphere beyond the 400 m distance sampled by the PDP. The further introduction of N_2 and O_2 gases along with H_2O may make the near environment of the Shuttle a most unsuitable place for making accurate ambient ion concentration measurements—both because of increased loss rates of ambient O^+ and the production of molecular ions that exist in the ionosphere.

REFERENCES

- Banks, P. M., Schunk, R. W. and Raitt, W. J. (1974) NO^+ and O^+ in the high latitude *F*-region. *Geophys. Res. Lett.* **1**, 239.
- Bennett, W. H. (1950) Radiofrequency mass spectrometer. *J. appl.* **21**, 143.
- Brinton, H. C., Grebowsky, J. M. and Brace, L. H. (1978) The high latitude *F*-region at 300 km: thermal plasma observations from AE-C. *J. Geophys.* **5**, 791.

- Brinton, H. C., Scott, L. R., Pharo, M. W., III and Coulson, J. T. (1973) The Bennett ion-mass spectrometer on *Atmosphere Explorer-C* and -E. 8, 323.
- Coiffy, H. E. (1985) Geomagnetic and solar data. *J. geophys. Res.* 90, 12343.
- Grebowsky, J. M., Pharo, M. W., III, Taylor, H. A., Jr. and Eberstein, I. J. (1983) Measured thermal ion environment of STS-3. AIAA-83-2597, AIAA Shuttle Environment and Operations Meeting, Oct. 31–Nov. 3 1983, Washington, DC.
- Hunton, D. E. and Calo, J. M. (1983) Low energy ions in the Shuttle environment: evidence for strong ambient-contaminant interactions. *Planet Space Sci.* 33, 945.
- McFurland, M., Albritton, D. L., Fehsenfeld, F. C., Ferguson, E. E. and Schmeltekopf, A. L. (1973) Flow-drift technique for ion mobility and ion-molecule reaction rate constant measurements II: positive ion reactions of N^+ , O^+ and N_2^+ with O_2 and O^+ with N_2 from thermal to ~ 2 eV. *J. chem. Phys.* 59, 6620.
- Mendillo, M. and Forbes, J. M. (1978). Artificially created holes in the ionosphere. *J. geophys. Res.* 83, 151.
- Moffett, R. J. and Quegan, S. (1983) The mid-latitude trough in the electron concentration of the ionospheric F-layer: a review of observations and modeling. *J. atmos. terr. Phys.* 45, 315.
- Narcisi, R. S., Trzcinski, E., Federico, G., Wlodyka, L. and Delorey, D. (1983) The gaseous and plasma environment around Space Shuttle. AIAA-83-2659, AIAA Shuttle Environment and Operations Meeting, Oct. 31–Nov. 3 1983, Washington, D.C.
- Pickett, J. S., Murphy, G. R., Kurth, W. S., Goertz, C. K. and Shawhan, S. D. (1985) Effects of chemical releases by the STS-3 orbiter on the ionosphere. *J. geophys. Res.* 90, 3487.
- Raitt, W. J., Siskind, D. E., Banks, P. M., and Williamson, P. R. (1984) Measurements of the thermal plasma environment of the Space. 32, 457.
- Samir, U., Stone, N. H. and Wright, K. H., Jr. (1986) On plasma disturbances caused by the motion of the Space Shuttle and small satellites: a. 91, 277.
- Shawhan, S. D. and Murphy, G. B. (1983) Plasma Diagnostics Package assessment of the STS-3 Orbiter environment and systems for science. AIAA-83-0253, AIAA 21st Aerospace Sciences Meeting, Reno, Nevada, Jan. 10–13 1983.
- Stone, N. H., Samir, U., Wright, K. H., Jr., Reasoner, D. L. and Shawhan, S. D. (1983) Multiple ion streams in the near vicinity of the Space Shuttle. 10, 1215.
- Stone, N. H., Wright, K. H., Jr., Hwang, K. S., Samir, U., Murphy, G. B. and Shawhan, S. D. (1986) Further observations of Space Shuttle plasma-electrodynamic effects from OSS-1 STS-3. *Geophys. Res. Lett.* 13, 217.
- Wulf, E. and von Zahn, U. (1986) The shuttle environment: effects of thruster firings on gas density and composition in the payload bay. *J. geophys. Res.* 91, 3270.

ELECTROMAGNETIC FIELDS FROM PULSED ELECTRON BEAM EXPERIMENTS
IN SPACE: SPACELAB-2 RESULTS

R. I. Bush, G. D. Reeves, P. M. Banks, T. Neubert, and P. R. Williamson

STAR Laboratory, Department of Electrical Engineering Stanford University, Stanford, CA 94305

W. J. Raitt

Center for Atmospheric and Space Sciences, Utah State University, Logan, Utah 84322

D. A. Gurnett

Department of Physics and Astronomy, University of Iowa, Iowa City, Iowa 52242

Abstract. During the Spacelab-2 mission a small satellite carrying various plasma diagnostic instruments was released from the shuttle to co-orbit at distances up to 300 m. During a magnetic conjunction of the shuttle and the satellite an electron beam modulated at 1.22 kHz was emitted from the shuttle during a 7 min period. The spatial structure of the electromagnetic fields generated by the beam was observed from the satellite out to a distance of 153 m perpendicular to the beam. Electromagnetic radiation at the fundamental and the harmonics of the modulation frequency was observed as well as broad-banded electrostatic noise. The magnetic field amplitude of the strongest harmonics were comparable to the amplitude of simultaneously observed whistlers, while the electric field amplitudes were estimated to 1-10 mV/m. The observations are related to theories for radiation from pulsed electron beams.

1. Introduction

This paper presents new results about the spectrum, intensity, and polarization of electromagnetic wave fields generated by launching a pulsed electron beam into the ionosphere from the space shuttle. Previous experiments with rockets [Cartwright and Kellogg, 1974; Winckler, 1980; Holzworth and Koons, 1981; Winckler et al., 1985] have successfully detected electron beam-produced waves in the VLF and ELF portions of the radio spectrum for brief intervals limited by the rocket trajectory. Earlier measurements by the research groups involved in the present experiments have been made from the shuttle with the OSS-1 mission of STS-3 in March, 1982 [Reeves et al., 1987]. Using plasma diagnostic instruments described later, it was found that electron bursts of various duration and pulsing frequency would generate strong ELF and VLF signals, both at the fundamental pulsing frequency and at various harmonics. Peculiar satellite lines were also found to surround the higher frequency signals up to the limit of observations at 30 kHz. Satellite lines are emissions separated in frequency from the harmonic spectral lines generated by the pulsed electron beam. The separation ranged from 100 Hz to 1 kHz. Most commonly satellite lines appeared as single subsidiary lines, which were higher in frequency than their primaries. However, since the electron source, the Fast Pulse Electron Generator (FPEG), and the instruments of the Plasma Diagnostic Package (PDP) were virtually co-located within the shuttle payload bay, the question of the extent to which these observations represented waves in the ambient plasma medium could not be answered.

The Spacelab-2 mission, flown in the period of July 25 through August 2, 1985, provided a unique opportunity both to

repeat the earlier payload bay electron beam experiments and, during two orbital periods, to investigate the behavior of beam associated phenomena with the PDP flying as a co-orbiting, free-flying, satellite. During the course of this fly-around care was taken to permit the PDP and shuttle to have two magnetic conjunctions per orbit. At these times the FPEG in the shuttle payload bay was programmed to fire various sequences with the beam pointed in the direction of the PDP. During the first complete orbit, no FPEG firings were undertaken in order that the PDP could assess the background environment associated with the motion of the Orbiter through the ionospheric plasma. On the second orbit, the first magnetic conjunction was obtained with the PDP above the Orbiter and the FPEG firing a continuous (DC) beam. Results from this experiment have been reported by Gurnett et al. [1986], showing the FPEG beam emits copious broad band whistler noise in the VLF, LF and MF bands and that this emission is similar to that found in conjunction with auroral electron beams.

The results presented here were obtained in connection with the fourth magnetic conjunction when the PDP was below the Orbiter at a distance of about 200 m, and the Orbiter payload bay was pointed towards the earth. A sequence emitting an electron beam square-wave modulated at 1.22 kHz began while the PDP was within a few meters of the actual conjunction point and continued for a period of about 7 minutes. During this time the PDP moved 153 meters perpendicular to the magnetic field as seen in the shuttle rest frame. As discussed below, the experiment was highly successful in generating VLF signals of substantial amplitude, both at the fundamental pulsing frequency and at the harmonics.

The PDP was supplied by the University of Iowa. It carried various plasma diagnostic instruments, including an electric dipole antenna and a magnetic search coil, which were connected alternately for 51.2 s to a wave receiver with a 10 kHz bandwidth. When connected, the wave receiver scanned a 30 kHz frequency range by selecting 10 kHz bands as: 0-10 kHz (25.6 s), 10-20 kHz (12.8 s), and 20-30 kHz (12.8 s). In addition, an ELF band at 0.1-1.0 kHz was continuously monitored by the same antennas. Both receiver outputs were controlled by an Automatic Gain Control (AGC) system, which ensured a 100 dB dynamic range and a roughly constant output level. The output in the ELF and VLF bands was telemetered in analog form, and the 10 kHz VLF band was later digitized at 25 kHz. For a description of the PDP and the instruments, see Shawhan [1984]. The FPEG was part of the Vehicle Charging and Potential (VCAP) experiment supplied by Stanford University and Utah State University. It emitted square-wave modulated electron beams with 100 mA beam current and 1 keV energy. The rise time of the accelerator potential was extremely small, of the order of 10^{-7} s. During the fourth flux-tube connection the beam was pulsed at 1.22 kHz, with the beam on time equal to its off time (50 % duty cycle). For a description of the VCAP instrumentation, see Banks et al. [1987].

Copyright 1987 by the American Geophysical Union.

Paper number 7L6636.

0094-8276/87/007L-6636\$03.00

2. Observations

The shuttle was launched into an almost circular orbit with a nominal altitude of 325 km and an inclination of 49.5°. The trajectory of the PDP relative to the shuttle during the fourth magnetic conjunction is shown in Figure 1. The vertical axis is the distance to the PDP measured along the earth's magnetic field, and the horizontal axis the distance perpendicular to the field. The pulsed beam sequence started at approximately 04:11 UT and lasted for about 7 min. The shuttle attitude was adjusted so that the electron beam was emitted towards the PDP. Thus the beam pitch angle varied from about 3° to 49° during the sequence.

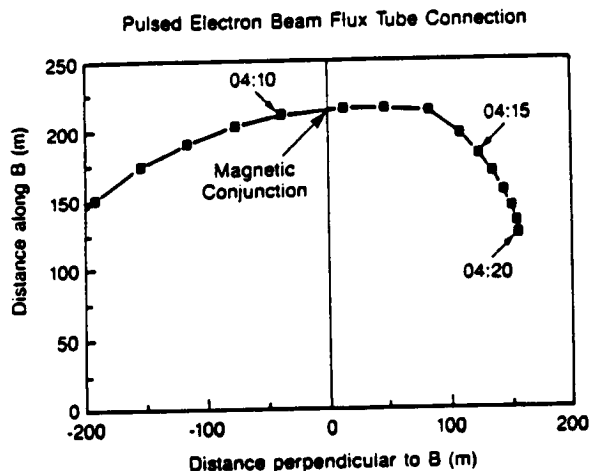


Fig. 1. The trajectory of the PDP relative to the shuttle during the fourth flux-tube connection. The beam was directed towards the PDP.

The conjunction occurred during nighttime. The ambient electron density estimated from the Langmuir probe on the PDP was $3 \times 10^4 \text{ cm}^{-3}$ [Hawkins et al., 1987], which corresponds to an electron plasma frequency, f_{pe} , of about 1.1 MHz. The electron gyrofrequency, f_{ce} , varied from 560 kHz to 600 kHz,

and the lower hybrid frequency, f_{LH} , from 2.9 kHz to 3.0 kHz, assuming the ion population consisted of O^+ .

An example of the magnetic fields observed in the 1-10 kHz range is shown in Figure 2 as function of time. The intensity of the signals is color-coded showing the fundamental and the odd harmonics of the 1.22 kHz pulsing frequency as horizontal lines. During the time interval shown the distance of the PDP perpendicular to the beam increased from about 111 m to 117 m. In addition to the emissions at the odd harmonics, weaker emissions at the even harmonics are also present as well as natural noise in the form of whistler activity. The two most pronounced whistlers are seen at 16-17 s and at the end of the frame. Note that these whistlers reach amplitudes that are comparable to the amplitude of the strongest harmonics.

The PDP was spinning with a spin period of 13 s. Both the magnetic and the electric sensors measured a component of the fields perpendicular to the spin axis. This induces a modulation of the amplitude of the measured fields with a period of 6.5 s. The modulation is very noticeable in Figure 2 for the odd harmonics, especially for harmonic numbers 5 and 7. An interesting point is that the spin modulation of the harmonics are not in phase. We expect an analysis of the amplitude modulation to give us important clues as to the polarization of the fields.

Figure 3 shows the electric fields 51.2 s later, when the electric sensor was connected to the receiver and the PDP was at a distance of 124-127 m from the beam. The strongest emissions are at the second and the third harmonics, which are spin modulated 180° out of phase. The amplitude of the harmonics has been estimated using a pre-flight calibration of the receiver and the AGC. The estimate agrees with values obtained independently from a filter bank wave experiment. We find that the amplitude of the strongest harmonics vary from about 10 mV/m close to the beam to about 1 mV/m at the maximum distance from the beam.

In addition to radiation at harmonic frequencies, the pulsed beam generated broad-banded electrostatic noise seen as the blue background in Figure 3. The noise is present at least up to the electron gyrofrequency with an intensity that decreases with frequency. The level is about 50 dB above the natural noise level in the 0-10 kHz band at closest approach to the beam. Broad-banded electrostatic noise is commonly observed in connection with DC electron beam emissions [Neubert et al., 1986]. The intensity and the frequency characteristics were

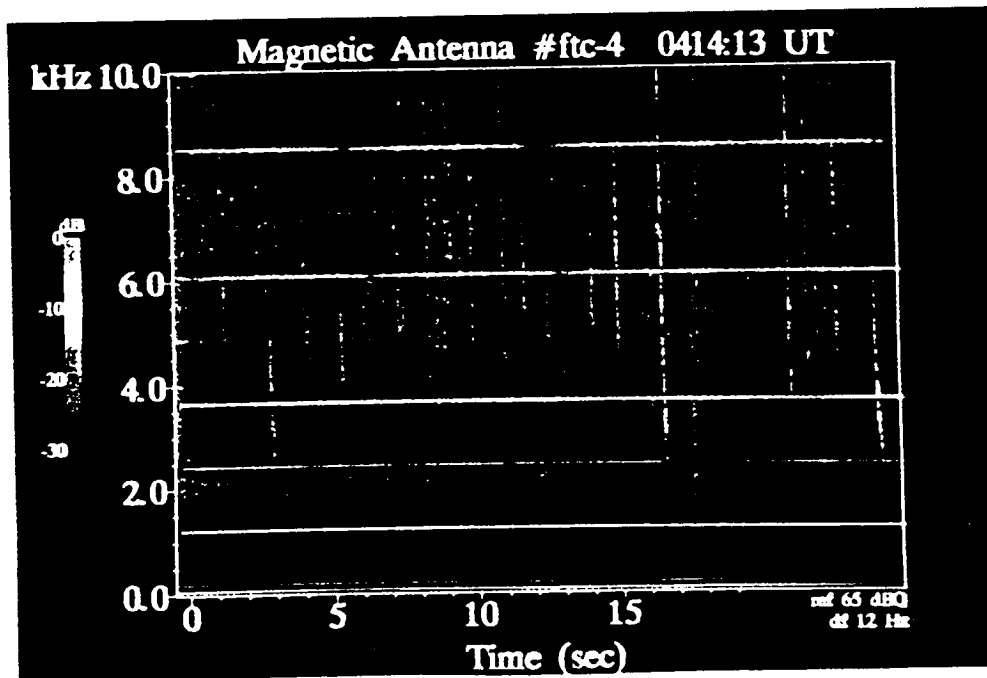


Fig. 2. The magnetic fields in the frequency range 0-10 kHz as a function of time. The perpendicular distance from the beam increased from about 111 m to 117 m.

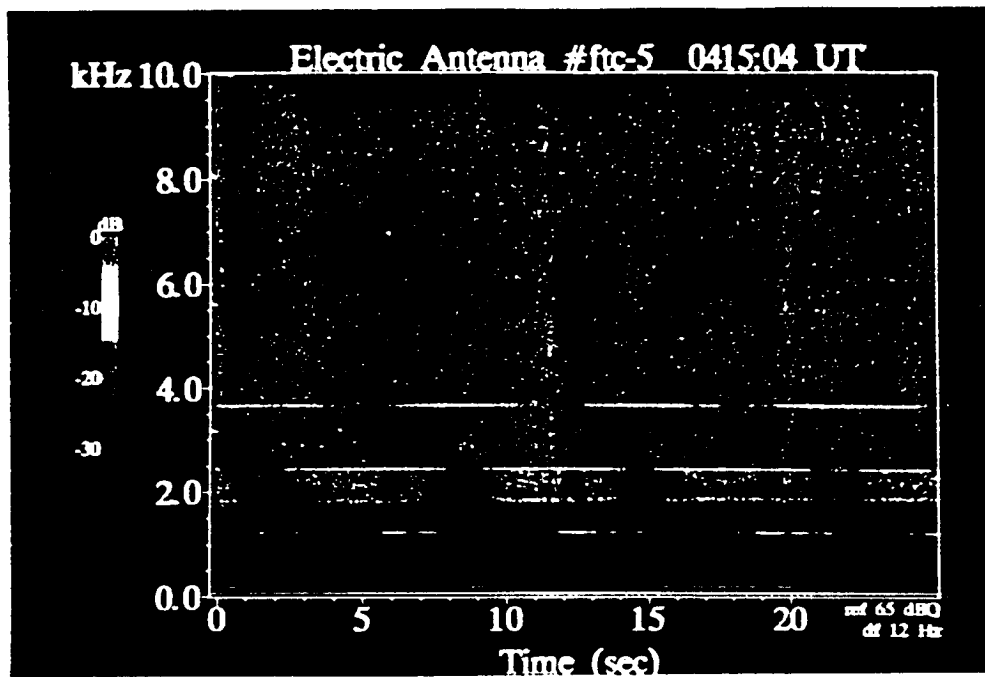


Fig. 3. The electric fields in the frequency range 0-10 kHz as a function of time. The perpendicular distance from the beam increased from about 124 m to 127 m.

comparable to that seen during the earlier DC beam firing at the third flux-tube connection [Gurnett et al., 1987]

Harmonics in the electric signal are detectable mainly below the third harmonic, except when very close to the beam. The apparent lack of emissions at the higher harmonics could be caused by the high level of broad-banded electrostatic noise, which inhibits the detection of lower amplitude harmonics.

As shown in Figure 3, a narrow-band emission is also present at a frequency of about 1.5 times the beam pulsing frequency, and with it, a band of noise extending up to the second harmonic. The noise is spin modulated and has a noticeable magnetic component as seen in Figure 2. The lower hybrid frequency induces a cutoff in the natural electromagnetic noise as whistler waves with large wave normal angles are reflected at this frequency. This effect is seen in Figure 2 at about 3 kHz. The spin-modulated noise between 1.5 and 2 times the pulsing frequency is presumably beam-generated and is at frequencies below f_{LH} . This indicates that the noise is propagated in the Alfvén mode. We note here that electromagnetic noise of a similar nature, were observed earlier during the fly-around when the electron beam was modulated at about 100 Hz. During this period, the position of the PDP was about 200 m from the shuttle along the magnetic field, and 60-90 m perpendicular to the field.

3. Discussion

The theory of Harker and Banks [1987] predicts the coherent contribution of the field intensities generated by a square wave modulated beam emitted at arbitrary pitch angles in a cold magnetized plasma. It is assumed that the beam electrons radiate coherently and that the beam retains an ideal helical structure from the exit of the beam accelerator and to infinity, while processes that destroy the ideal beam coherence are simulated by assuming that the current is exponentially decaying with distance along the magnetic field with the scale length $1/\beta$, also called the coherence scale length. The theory is applicable in both the near- and far-field regions, where an observation point is in the far-field region if the distance from the beam is much larger than a perpendicular wavelength.

We have determined some of the characteristics of the wave-predicted by the theory for the experimental conditions of the pulsed flux-tube connection. They are summarized along with a comparison with observations in the following points:

1) From the assumption of an exponentially decaying but perfectly square-wave modulated source current, it follows that the predicted electric and magnetic fields are generated at the odd harmonics of the modulation frequency as found by a Fourier transform of a square wave function with a 50 % duty cycle. While the radiation is electromagnetic in nature, detailed expressions of the amplitudes have so far only been derived for the electric field components. This renders a closer comparison with theory difficult, since the electrostatic noise generated simultaneously is of significant intensity as compared to the coherent radiation at the odd harmonics. However, from the magnetic field data we conclude that electromagnetic fields were predominantly generated at the odd harmonics of the beam modulation frequency as predicted.

2) The fields are generated through a Cherenkov resonance ($s = 0$) given by the resonance condition:

$$sf_{ce} + k_{\parallel}v_{\parallel} - f = 0 \quad (1)$$

where f , k , and v are the wave frequency, the wave normal, and the beam electron velocity, and the subscript \parallel stands for the component parallel to the earth's magnetic field. The field intensities generated through a cyclotron resonance ($s = 1$) and anomalous cyclotron resonance ($s = -1$) are several orders of magnitude lower than the contribution from the Cherenkov resonance.

The perpendicular 'wave-lengths' of the fields generated through Cherenkov resonance at 1-30 kHz are typically larger than a few hundred meters, which brings the observations during the fly-around within the near-field region.

3) With the difficulty mentioned in point 1) in mind, we attempt in the following to compare the variation with radial distance of the electric field amplitudes to the theoretical predictions. Solving the cold plasma dispersion relation for the perpendicular component of the wave normal, k_{\perp} , with k_{\parallel} given by (1) and $s = 0$ gives two physically acceptable solutions for k_{\perp} . The one (root 1) is real for frequencies above f_{LH} and corresponds to a propagating whistler mode wave with the wave normal close to the resonance cone. Below f_{LH} this root becomes imaginary and corresponds to an evanescent wave. Root 2 is real in the full 30 kHz frequency range. Below f_{LH} it corresponds to a fast Alfvén wave, while above f_{LH} to a whistler wave. The theory finds that the fields corresponding to root

1 are the strongest in the near vicinity. However, the electric component of the evanescent field below f_{LH} is strongly damped with radial distance from the beam, typically about 1 dB/m, leaving the weaker component from root 2 at larger distances.

At increasing distances from the beam, a cutoff at frequencies below about 2 kHz is developed in the broad-banded noise, which is followed by a decrease in the amplitude of the fundamental relative to the higher harmonics. We thus find the same trend in the data as predicted by theory. However, this qualitative agreement exists only when a very large beam coherence length is assumed, and is destroyed when the coherence length is of the order of, or smaller than a parallel wave length. The parallel wavelength was for the experimental conditions about 10 km.

4) With the assumption of an infinite coherence length, the predicted amplitudes of the harmonics are about two orders of magnitude above the observed amplitudes, which reached levels of 1-10 mV/m. The inclusion of a finite coherence length brings the predictions closer to the observations when close to the beam, but create problems at larger distances as mentioned above.

5) The theory predicts the radial component of the electric emissions to be the dominant component at all the observed odd harmonic frequencies, and at all distances from the beam covered by the PDP. This has as a consequence that the fields are almost linearly polarized in the radial direction. A spin modulation is thus in general expected, although we yet have to confirm the specific polarization. Note, however, that the observation of a spin modulation at the first harmonic (Figure 3), which is out of phase with the modulation of the third harmonic, is not in accordance with the theory.

In conclusion we find that the theory of Harker and Banks [1987] qualitatively describes the frequency characteristics of the coherent electromagnetic radiation as seen in the magnetic field data. The observations of weaker, but noticeable, even harmonics indicate that the current source is not perfectly square-wave modulated, even though the rise time of the accelerating potential of the FPEG gun is of the order of 10^{-7} s. Even harmonics were also present in data obtained with the PDP located in the shuttle cargo bay, in close proximity to the FPEG. We suggest that radiation at even harmonic frequencies is either generated by the return current, or caused by a degradation of the electron beam coherence.

The FPEG beam density is about $7 \times 10^6 \text{ cm}^{-3}$ at 10 cm from the nozzle [Hawkins et al., 1987], which is at least two orders of magnitude larger than the ambient ionospheric density. Computer simulations for such overdense beams show that electrostatic potentials of the order of the beam energy are created at the so-called stagnation point [Pritchett and Winglee, 1987], which for the conditions of the fly-around would be formed at a distance of some meters from the nozzle. The formation of a stagnation point drastically alters the beam structure by accelerating and reflecting beam electrons. However, as mentioned by Pritchett and Winglee [1987], the conditions for beam experiments performed from the space shuttle differs from the assumptions of the computer simulations. First, the shuttle moves through the ionosphere with a considerable velocity (7.7 km/s) and second, the surface of the return current collection is largely outside of the beam column and the collecting area is large (40 m^2) as compared to the beam cross section. Both these effects are likely to reduce the charge build-up at the stagnation point, and the observations detailed above suggest that the beam escapes the shuttle, largely retaining its square-wave modulated structure (coherence in $v_{||}$). This does not imply, however, that the helical structure is conserved as assumed in the theory of Harker and Banks [1987]. The observation of field intensities, which are orders of magnitude lower than those

predicted for infinite coherence length, and the problem of including a finite coherence length, could point towards the beam losing its helical structure almost immediately (incoherence in $v_{||}$).

Finally we point out that the observed electric field amplitudes of 1-10 mV/m are of a magnitude where non-linear wave-particle and wave-wave interactions can become important [Neubert, 1982]. The possibility that the narrow-banded electrostatic emissions at 1.5 and 2 times the modulation frequency may be the result of such processes should be considered.

Acknowledgments. The authors thank W. C. Burgess and J. W. Yarbrough for their help with the spectral analysis and the digitization of the wide-band analog data. The work done at Stanford was sponsored by NASA under contracts NGR-235 and NAG5-476. The Space Physics Analysis Network (SPAN) was used in the preparation of this report.

References

- Banks, P. M., W. J. Raitt, A. B. White, R. I. Bush, and P. R. Williamson, Results from the vehicle charging and potential experiment on STS-3, *J. Spacecr.*, 24, 1986.
- Cartwright, D. G., and P. J. Kellogg, Observations of radiation from an electron beam artificially injected into the ionosphere, *J. Geophys. Res.*, 79, 1439, 1974.
- Gurnett, D. A., W. S. Kurth, J. T. Steinberg, P. M. Banks, R. I. Bush, and W. J. Raitt, Whistler-mode radiation from the spacelab-2 electron beam, *G. Res. Lett.*, 13, 225, 1986.
- Harker, K. J., and P. M. Banks, Near fields in the vicinity of pulsed electron beams in space, *Planet. Space Sci.*, 35, 11, 1987.
- Hawkins, J. G., P. M. Banks, R. I. Bush, P. R. Williamson, and W. J. Raitt, Charging of the shuttle orbiter during electron beam emission experiments on Spacelab-2, submitted to *Geophys. Res.*, 1987.
- Holzworth, R. H., and H. C. Koons, VLF emissions from a modulated electron beam in the auroral ionosphere, *J. Geophys. Res.*, 86, 853, 1981.
- Neubert, T., Stimulated scattering of whistler waves by ion acoustic waves in the magnetosphere, *Physica Scripta*, 26, 239, 1982.
- Neubert, T., W. W. L. Taylor, L. R. O. Storey, N. Kawashima, W. T. Roberts, D. L. Reasoner, P. M. Banks, D. A. Gurnett, R. L. Williams, and J. L. Burch, Waves generated during electron beam emissions from the space shuttle, *J. Geophys. Res.*, 91, 11321, 1986.
- Pritchett, P. L., and R. M. Winglee, The plasma environment during particle beam injection into space plasmas: 1. Electron beams, Submitted to *J. Geophys. Res.*, 1987.
- Reeves, G. D., P. M. Banks, A. C. Fraser-Smith, T. Neubert, R. I. Bush, D. A. Gurnett, and W. J. Raitt, VLF wave stimulation by pulsed electron beams injected from the space shuttle, submitted to *J. Geophys. Res.*, 1987.
- Shawhan, S. D., G. B. Murphy, P. M. Banks, P. R. Williamson, and W. J. Raitt, Wave emissions from dc and modulated electron beams on STS-3, *Radio Science*, 19, 471, 1984.
- Winckler, J. R., K. N. Erickson, Y. Abe, J. E. Steffen, and P. R. Malcolm, ELF wave production by an electron beam emitting rocket system and its suppression on auroral field lines: evidence for Alfvén and drift waves, *Geophys. Res. Lett.*, 12, 457, 1985.

(Received July 27, 1987;
accepted August 17, 1987.)

THE EMISSIONS OF BROADBAND ELECTROSTATIC NOISE IN THE NEAR VICINITY OF THE SHUTTLE ORBITER

K. S. HWANG

NRC, Space Science Laboratory, NASA Marshall Space Flight Center, Huntsville, AL 35812, U.S.A.

N. H. STONE

Space Science Laboratory, NASA Marshall Space Flight Center, Huntsville, AL 35812, U.S.A.

K. H. WRIGHT, Jr.

Physics Department, The University of Alabama in Huntsville, Huntsville, AL 35899, U.S.A.

and

U. SAMIR

Tel-Aviv University, Ramat-Aviv, Israel, and Space Physics Research Laboratory,
The University of Michigan, Ann Arbor, MI 48109, U.S.A.

(Received in final form 16 April 1987)

Abstract—Measurements of the Space Shuttle environment from the *STS-3* and *Spacelab 2* missions indicate the presence of oblique ion streams and broadband electrostatic noise. A two-dimensional theoretical model is applied to study a possible causal relationship between the ion streams and the broadband noise; especially in terms of the ion acoustic wave and ion-ion wave modes. This model predicts the generation of waves with frequencies ranging from the ion cyclotron frequency up to values greater than the ion plasma frequency, with the maximum growth rate occurring in the 10 kHz range. These results are consistent with the observational data from the *STS-3* mission. The model also shows that these two wave modes can co-exist only when the wave vectors of the two wave modes are nearly perpendicular. The parametric dependence of the wave instabilities on the plasma parameters, e.g. N_b/N_e , T_e/T_i , and the inclination of the wave propagation vector, is also studied.

INTRODUCTION

Wave-particle interactions resulting from the acceleration of ions in a collisionless plasma are of fundamental significance in space plasma physics. Previous observations from the *IMP 7* satellite (Sarf *et al.*, 1974) and the *IMP 8* satellite (Gurnett *et al.*, 1976) indicate that field-aligned streams are associated with a continuum of electrostatic ion waves, ranging from 10 Hz up to several kilohertz in the Earth's magnetospheric region. Recent theoretical treatments of ion stream-background plasma interactions (Grabbe and Eastman, 1984; Omid, 1985; Akimoto and Omid, 1986; Ashour-Abdalla and Okuda, 1986) also predict the occurrence of broadband electrostatic noise with wave vectors in every direction and with the most intense wave occurring in a direction nearly perpendicular to the field-aligned current. This behavior is consistent with the *IMP 8* observations (Gurnett *et al.*, 1976).

More recently, measurements from the *STS-3* and *Spacelab 2* Space Shuttle missions have also revealed the existence of high inclination secondary ion streams in the Orbiter's near environment (Stone *et al.*, 1983,

1986). The current density of these ion streams can be a significant fraction of the ram current density,* and it is thought that these ion streams may be associated with broadband electrostatic noise, ranging from 30 Hz up to 178 kHz, that was observed on the same missions (Shawhan *et al.*, 1984; Murphy *et al.*, 1983). In addition, electron-ambient ion temperature ratios as high as 6 were reported by Raitt *et al.*, (1984) and Siskind *et al.*, (1984) based on electron and ion measurements made near the Orbiter during the *STS-3* mission. The electrons may have been heated by wave-particle interactions to higher than normal temperatures (ambient ionospheric T_e/T_i ratios are usually in the range of 1 to 2). A very preliminary analysis of the Differential Ion Flux Probe (DIFP) measure-

* In Stone *et al.* (1983), a value of 0.08 is given for the secondary-to-ram current ratio, as measured by the Differential Ion Flux Probe at a particular time. The ion current density in space can be calculated from the given value of collected instrument current by using the instrument characteristic, which includes angular effects on sensitivity. When this factor is included, the current density ratio is ~ 0.3 for the particular data in Stone *et al.* (1983). At other times, the ratio was found to be as high as ~ 0.7 .

ments indicates that the temperature of ions in the beam is in the range of a few hundred Kelvins. Although such low temperatures are abnormal for the ionospheric plasma, they may not be unreasonable for ions created within the Orbiter's neutral gas cloud. Outgassing products from the Orbiter would be expected to be in the range of 300 K. The evidence of wave growth during the STS-3 mission also suggests that the ion beam temperature was much lower than the background ion temperature (Ashour-Abdalla and Okuda, 1986). Although a more detailed analysis is needed to verify the above results, we can assume that the beam ion temperature is less than, or equal to, the ambient ionospheric temperature. Although the source and mechanisms for the oblique ion streams are still under study, the possible generation of broadband noise has similarities to several existing one-dimensional models that were developed to explain the observation of electrostatic ion waves in the ionospheric and magnetotail regions (Kintner *et al.*, 1981; Akimoto and Omid, 1986; Grabbe and Eastman, 1984).

We have developed a two-dimensional theoretical model that describes the injection of an oblique ion beam into a background plasma and is directly applicable to the beam-plasma interaction that appears to have occurred in the environmental plasma of the Orbiter. While the model requires $T_e/T_i \gg 1$ for any significant wave growth to occur, as noted above, ratios as high as $T_e/T_i = 6$ were observed at the Orbiter (Raith *et al.*, 1984; Siskind *et al.*, 1984). While the heating of the electrons probably results from wave-particle interactions, we note that the neutral gas cloud produced by the Orbiter is very extensive and apparently interacts with the ambient plasma; e.g. a significant disturbance of the ions was observed as far as 10 m upstream during the STS-3 mission (Stone *et al.*, 1986) and during the *Spacelab-2* mission Orbiter outgassing products were observed several hundred meters upstream. It appears, therefore, that the neutral gas cloud is sufficiently extensive that if the oblique ion beams begin dumping free energy into the environment in the region of its upstream boundary, a sufficient interactive growth of broadband noise and electron heating could occur to explain the wave and particle observations prior to the Orbiter-mounted instruments passing through the region: i.e. the free energy of the beams would create electrostatic waves that would initially be Landau damped because $T_e \approx T_i$ in the ambient ionosphere, but would, in this process, begin heating the electrons. As the electrons heat up, the instability created by the beam would begin to grow and a more efficient dumping of beam free-energy would occur and so on. The main objective

of this paper is to show the feasibility of the predicted relationship between the broadband electrostatic noise and the secondary ion streams. This will be done by using the particle data obtained from the STS-3 mission in the theoretical model and comparing the characteristics of the predicted plasma instabilities and oscillations with the broadband noise observations from STS-3.

THEORETICAL DERIVATION

The physical situation under which the measurements of the Shuttle's particle and field environment in space were obtained is described in Stone *et al.* (1983, 1986) and Shawhan *et al.* (1984). In developing an appropriate model, we make a transformation from the Orbiter coordinate system to a new system in which the geomagnetic field is aligned with the z axis and the relative drift velocity, V_d , of the secondary ion stream (with respect to the ambient plasma) lies in the y - z plane. The background electrons and ions are represented by local Maxwellian distribution functions, whereas the beam ions are represented by a drifting Maxwellian distribution function (Fig. 1). The wave frequency in this study is much higher than the ion cyclotron frequency but smaller than the electron cyclotron frequency, therefore it is reasonable to assume that the background electrons are magnetized while the background and stream ions are non-magnetized. We also assume quasi-neutrality. Therefore, the total number density of background and stream ions is equal to the electron number density.

The derived generalized linear dispersion relation is essentially similar to several previous papers (for example, Grabbe and Eastman, 1984; Hudson and Roth, 1984; Omid, 1985); this equation was obtained by using the usual method of integration along unperturbed trajectories. For perturbations of the type $\exp(ik \cdot r - i\omega t)$, the collisionless Vlasov-Maxwell equations yield the following dispersion relation:

$$D(k, \omega) = 1 + \frac{1}{k^2 \lambda_e^2} \left\{ 1 + \sum_n \Gamma_n(k_\perp^2 \rho_n^2) \frac{\omega}{k_z V_{Te}} \right. \\ \times Z\left(\frac{\omega - n\Omega_e}{k_z V_{Te}}\right) \left. \right\} + \frac{1}{k^2 \lambda_i^2} \left\{ 1 + \frac{\omega}{k V_{Ti}} Z\left(\frac{\omega}{k V_{Ti}}\right) \right. \\ \left. + \frac{1}{k^2 \lambda_b^2} \left\{ 1 + \frac{(\omega - k \cdot V_d)}{k V_{Tb}} Z\left(\frac{\omega - k \cdot V_d}{k V_{Tb}}\right) \right\} \right\} \quad (1)$$

where $D(k, \omega) = D_r(k, \omega) + iD_i(k, \omega)$, $\lambda_j = V_{Tj}/\sqrt{2\omega_{pj}}$ is the j th species' Debye length, $\omega_{pj} = (4\pi N_j e^2/M_j)^{1/2}$

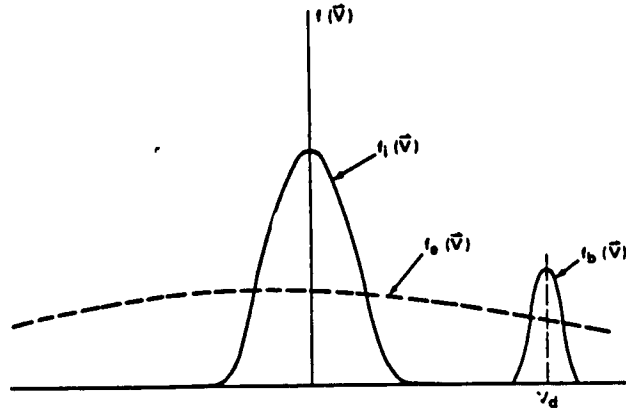


FIG. 1. THE SECONDARY ION STREAM VELOCITY DISTRIBUTION FUNCTION IN THE AMBIENT CHARGED PARTICLES' REFERENCE FRAME.

is the plasma frequency, $\rho_j = V_{Tj}/\Omega_j$ is species' gyro-radius, $\Omega_j = eB/M_jC$ is the cyclotron frequency of the j th constituent, $\Gamma_q(v_j) = e^{-v_j^2} I_q(v_j)$, $I_q(v_j)$ is the modified Bessel function of order q , and $Z(\eta) = Z_r(\eta) + iZ_i(\eta)$ is the plasma dispersion function (Fried and Conte, 1961). The wave frequency, ω , is complex (i.e. $\omega = \omega_r + i\omega_i$) with a positive growth rate. By assuming that $\omega_i \ll \omega_r$, equation (1) yields the linear frequency ω_r and growth rate ω_i , where ω_r satisfies $D_r(k, \omega_r) = 0$ and the wave growth rate is given by:

$$\omega_i = \frac{-D_i(k, \omega_r)}{\partial D_r(k, \omega_r) / \partial \omega_r} \quad (2)$$

RESULTS AND DISCUSSIONS

The properties of electrostatic ion waves can be determined by the propagation characteristics of the wave in the ω_r - k plane under equation (1). Atomic oxygen ions (O^+) are used as the ion species in this analysis, in accord with the observations from the Plasma Diagnostics Package (PDP) instruments (Grebowsky *et al.*, 1983; Murphy *et al.*, 1983). Since the frequency is measured by the moving wave instruments, the actual frequency is related to the measured frequency by $\omega' = \omega - \mathbf{k} \cdot \mathbf{V}_s$, where V_s is the shuttle velocity. The results from the model corresponding to the observed range of plasma conditions (i.e. $N_e = 3.0 \times 10^6 \text{ cm}^{-3}$, $V_{ds} = 1.8 \times 10^5 \text{ cm s}^{-1}$ and $V_{ds} = 1.1 \times 10^6 \text{ cm s}^{-1}$, $T_d/T_i = 2$, $T_i/T_e = 7.5$ and $N_b/N_e = 0.5$) are given in Fig. 2. These results show that waves may be generated with frequencies ranging from 50 Hz up to several hundred kilohertz, and that

the maximum growth rate occurs at frequencies in the range of 10 KHz, which is consistent with the observational data from STS-3.

The angle, θ , between the wave propagation vector and the ion beam is a parameter in these calculations and the results indicate that two types of wave modes may occur, i.e. the ion acoustic and the ion-ion modes. When $\theta < 60^\circ$, the phase velocity is much greater than the background ion thermal velocity and the mechanism for wave generation is mainly due to the electron-ion beam interaction which produces ion acoustic waves. However, when $\theta > 60^\circ$, the phase velocity is closer to the ion thermal velocity. In this case, a fluid type instability may occur (Tidman, 1967), and the wave may be produced by an instability resulting from the ion-ion interaction. The wave growth rate of this mode increases abruptly and reaches a maximum at $\theta \approx 77^\circ$. As the ratio of N_b/N_e is increased to 1, only the ion acoustic wave exists. However, as shown in Fig. 3, where $N_b/N_e = 1$, the ion acoustic mode disappears when the wave propagation vector is nearly perpendicular to the ion beam ($\theta \geq 70^\circ$). Since the ion-ion mode vanishes for $N_b/N_e = 1$, Fig. 3 shows the characteristics of the pure ion acoustic wave mode.

Figure 4 shows the dependence of the maximum wave growth rate on the angle between the wave vector and the ion stream for several values of the temperature ratio, T_d/T_i . The plasma conditions are, otherwise, the same as those used for Fig. 2. When the T_d/T_i ratio is small (< 1.3), the ion acoustic and ion-ion waves are restricted to very narrow areas at nearly parallel ($\theta = 0^\circ$) and nearly perpendicular ($\theta \approx 76^\circ$) directions, respectively (see Fig. 4). The

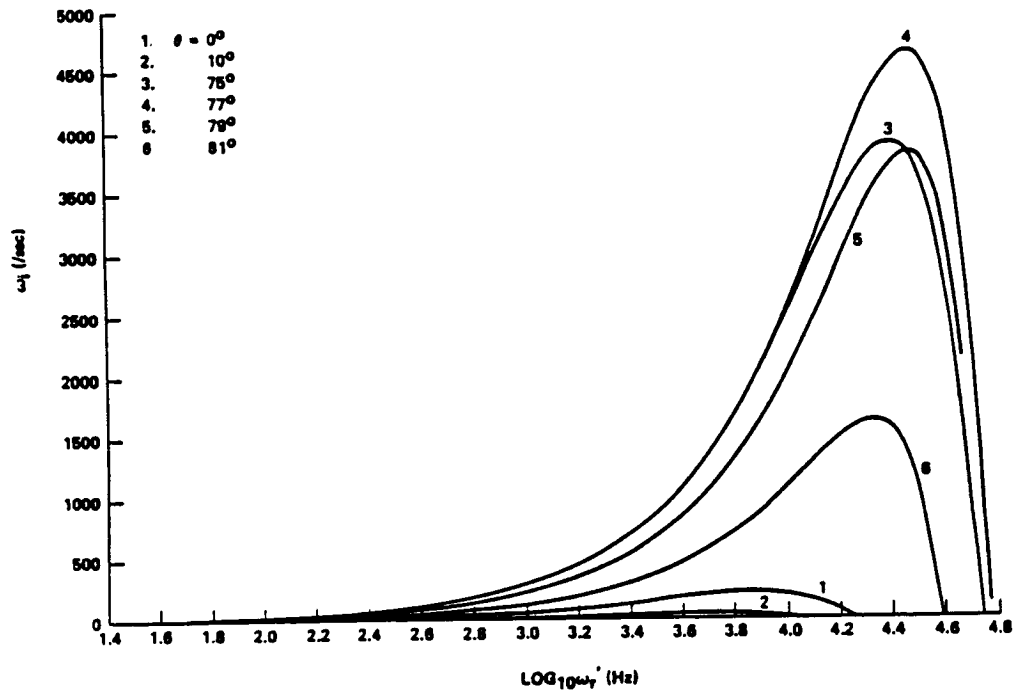


FIG. 2. THE GROWTH RATE, ω_i , AS A FUNCTION OF MEASURED FREQUENCY, ω_r' , AT $N_e = 3.0 \times 10^6 \text{ cm}^{-3}$, $V_{dr} = 1.8 \times 10^3 \text{ cm s}^{-1}$, $V_{dr} = 1.1 \times 10^6 \text{ cm s}^{-1}$, $T_d/T_i = 2$, $T_i/T_e = 7.5$ AND $N_d/N_e = 0.5$, USING $\theta = \cos^{-1}(k \cdot V_d)$ AS A PARAMETER.

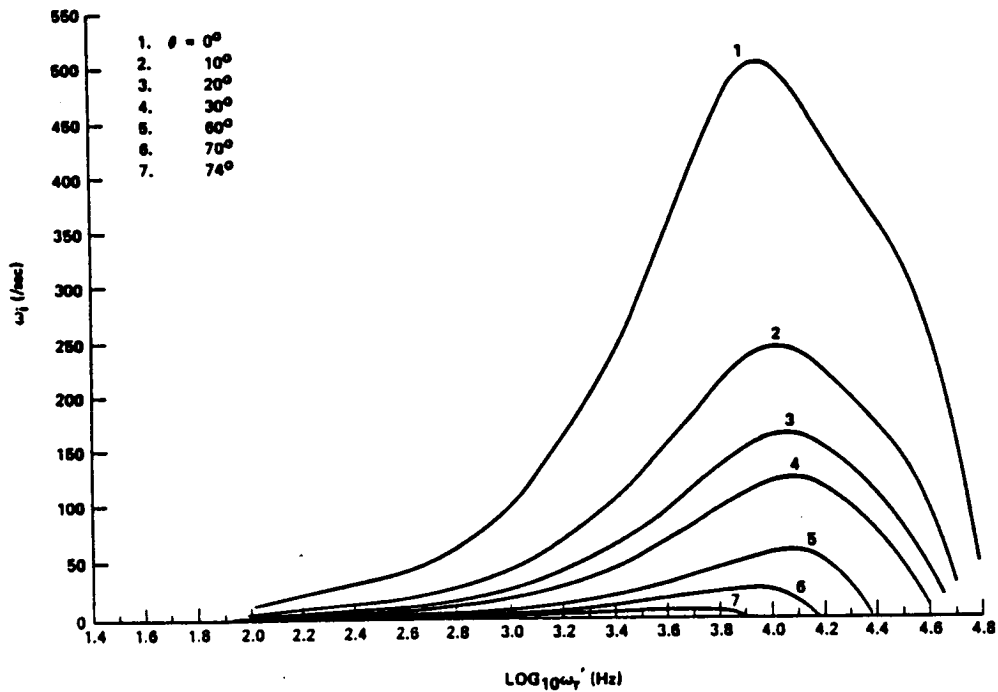


FIG. 3. THE GROWTH RATE, ω_i , AS A FUNCTION OF MEASURED FREQUENCY, ω_r' , FOR ELECTROSTATIC ION ACOUSTIC WAVES AT $N_d/N_e = 1$, THE OTHER PARAMETERS ARE THE SAME AS IN FIG. 2.

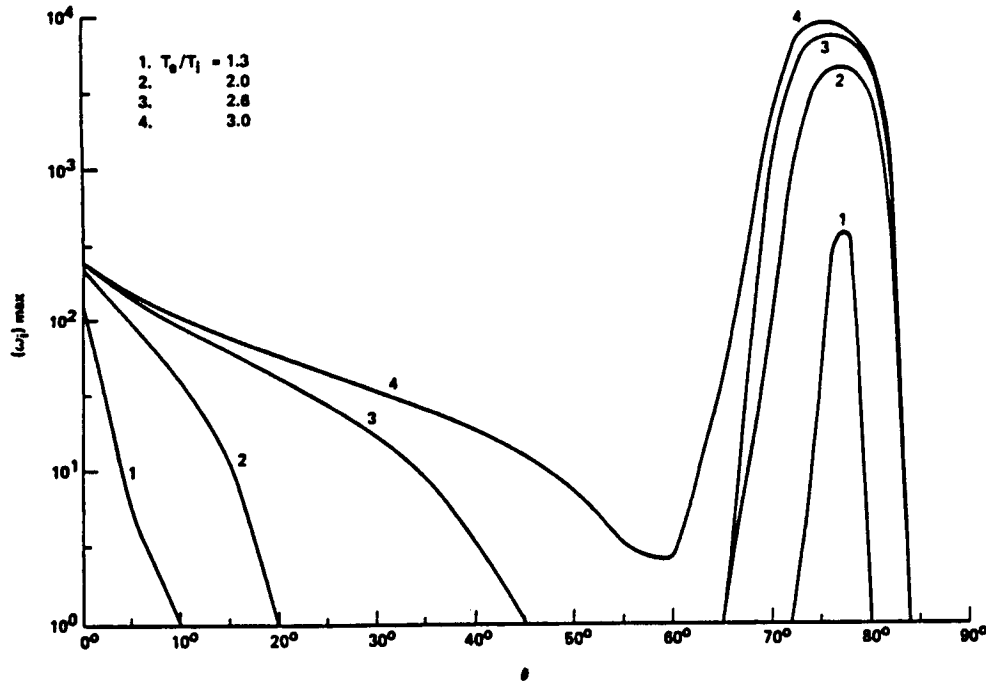


FIG. 4. THE MAXIMUM GROWTH RATE OF ELECTROSTATIC ION WAVES VS THE ANGLES BETWEEN THE WAVE VECTOR AND THE ION STREAM, θ , USING T_e/T_i AS A PARAMETER. THE OTHER PARAMETERS ARE THE SAME AS IN FIG. 2.

wave growth rate of both wave modes is small and comparable. As T_e/T_i increases, the electron damping is gradually decreased and the interaction between the electrons and beam ions increases. Therefore, the wave growth rate for the ion acoustic mode increases and spreads over a wider angular range. When the T_e/T_i ratio increases high enough such that the electron damping can be neglected, the ion acoustic wave begins to saturate in the parallel direction. At the same time, the ion-ion wave instabilities greatly enhance the wave amplitude in the nearly perpendicular direction. The results indicate that these two wave modes can only co-exist when the wave vectors of the two modes are nearly perpendicular. The ion-ion wave growth rate increases much faster than the ion acoustic wave mode as T_e/T_i increases. This result indicates that the ion-ion instability heats the beam ions more than the ion acoustic instability. The higher the electron-ion temperature ratio, the lower the instability threshold in the transition region. This is to be expected from the observed STS-3 thermal environment.

The maximum growth rate vs beam ion-electron number density ratio is presented in Fig. 5. The results show that for parallel propagation ($\theta = 0^\circ$), the wave growth rate monotonically increases with number

density ratio for the ion acoustic mode. However, when the angle between the wave vector and the ion stream increases, the number density ratio at which the maximum growth rate occurs is between 0.3 and 0.8, depending on the value of θ . This is consistent with the results calculated by Omidi (1985). Again, we notice that the wave growth rate is much larger for the ion-ion wave mode than for the ion acoustic wave mode, except at higher N_b/N_e ratios (> 0.9). The results also show that these two wave instabilities cannot grow immediately (see Fig. 5) at $N_b/N_e = 0$ without a critical value of N_b/N_e being reached, as Akimoto and Omidi (1986) suggested.

CONCLUSIONS

The Space Shuttle, with its environmental gas cloud, acts as a natural laboratory for the study of wave-particle interactions. The analysis and possible understanding of the interactions can be obtained through the use of *in situ* measurements coupled with theoretical analysis and numerical simulation. In this paper, we have studied the parametric behavior of the wave spectrum of broadband electrostatic noise in a magneto plasma with a superimposed drifting ion

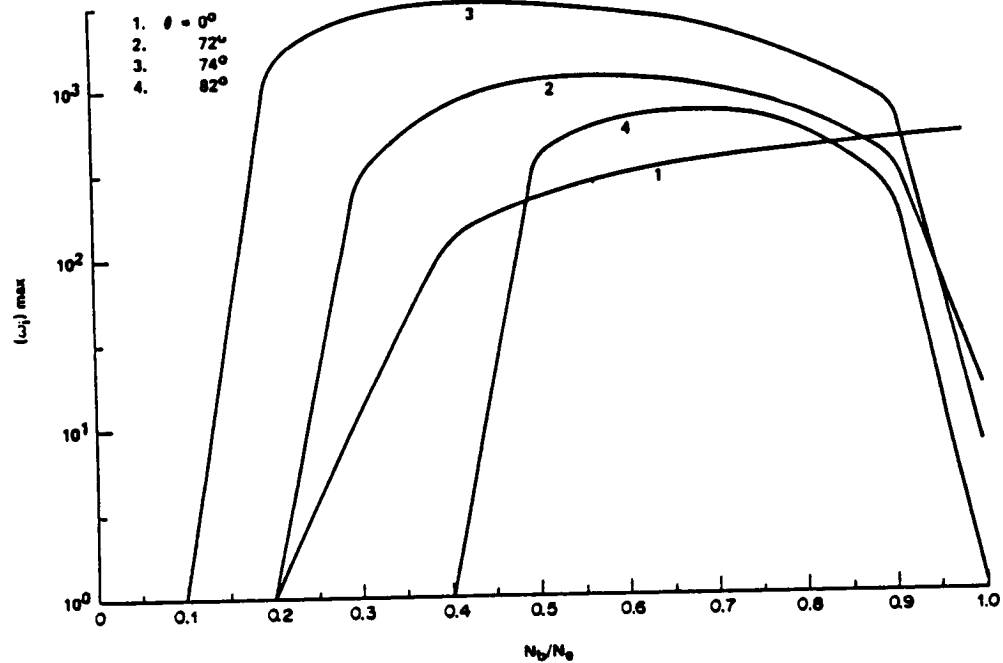


FIG. 5. THE MAXIMUM GROWTH RATE VS. N_e/N_0 , USING θ AS A PARAMETER. THE OTHER PARAMETERS ARE THE SAME AS IN FIG. 2.

stream. The drifting ions are considered to be the source free energy for the waves, leading to the growth of an instability.

This linearized two-dimensional theory predicts the generation of waves over a broad band of frequencies, ranging from above the ion plasma frequency down to the ion cyclotron frequency, in agreement with the available *in situ* observations from the STS-3 mission. The instability derived in this manner produces ion acoustic wave and ion-ion wave emissions over a wide frequency range which corresponds to the observed frequency range for a reasonable choice of the plasma parameters. As we have shown earlier, the growth rate of the ion-ion wave mode is usually greater than the ion acoustic wave mode, except at higher ion beam-electron number density ratios or at lower electron-ion temperature ratios. Thus, in general, the ion-ion wave instability heats the beam ions more than the ion acoustic instability does.

During the IMP 8 mission, Gurnett *et al.* (1976) found that the broadband electrostatic noise was generated over most wave vector directions with the most intense waves occurring in the direction nearly perpendicular to an observed field-aligned current. The theoretical analysis by Omidi (1985) was shown to be

consistent with the observations. The generation of electrostatic waves by the ion streams in the Orbiter's environmental plasma is similar in some aspects to wave-particle interactions observed in the Earth's geomagnetotail. This phenomena therefore provides an example of how processes that occur in natural space plasma phenomena, can be created and studied in more detail in the ionosphere. Although the measurements from the STS-3 mission are unable to specify the direction at which the maximum growth rate occurred, we do predict results for the STS-3 missions similar to those for IMP 8. During the Spacelab 2 mission, the PDP was spinning while in free flight and, therefore, the wave vector can be determined. The results of these measurements, when available, will provide a more viable test for the present model.

In conclusion, we note that simulation calculations by Ashour-Abdalla and Okuda (1986) predict electron heating to occur in a similar plasma model. Although, theoretically, the wave instability could heat the electron population (Davidson *et al.*, 1970) which, in turn, could ionize the neutral gas cloud, the evaluation of the possible connection between the broadband noise, electron heating, and neutral particle ionization will re-

quire a careful consideration of electric field strengths and the efficiency of coupling with the electrons as well as wave growth rates. The present study has concentrated on the generation of ion acoustic and ion-ion waves. The authors are aware that other important ion wave modes, i.e. the electrostatic ion cyclotron and ion Bernstein waves, have received no attention at this point in the analysis. According to the observations, waves can also occur with the maximum growth rate at a lower frequency near the N th order of the ion cyclotron frequency range. A detailed study of this equally important wave mode will be presented elsewhere. However, the present model, although incomplete, is adequate to show that the free energy associated with the high inclination ion streams is sufficient to ignite ion acoustic and/or ion-ion wave instabilities that are capable of producing the observed broadband noise signature.

Acknowledgements—The authors would like to thank D. Gurnett and G. Murphy of the University of Iowa for supplying the wave data from PDP/STS-3 measurements. We would also like to thank Wayne Thompson of Boeing Computer Support Services (now at Sparta, Inc.) for reduction of the DIFP data. K.S.H. acknowledges support from the National Research Council under their resident Research Associateship program. K.H.W. acknowledges support from NASA grant NAG8-058. U.S. acknowledges support from NASA grant NGR 23-005-320.

REFERENCES

- Akimoto, K. and Omid, N. (1986) The generation of broadband electrostatic noise by an ion beam in the magnetotail. *Geophys. Res. Lett.* **13**, 97.
- Ashour-Abdalla, M. and Okuda, H. (1986) Theory and simulations of broadband electrostatic noise in the geomagnetic tail. *J. geophys. Res.* **91**, 6833.
- Davidson, R., Krall, N., Papadopoulos, K. and Shanny, R. (1970) Electron heating by electron-ion beam instabilities. *Phys. Res. Lett.* **24**, 579.
- Fried, B. and Conte, S. (1961) *The Plasma Dispersion Function*. Academic Press, New York.
- Grabbe, C. L. and Eastman, T. E. (1984) Generation of broadband electrostatic noise by ion beam instabilities in the magnetotail. *J. geophys. Res.* **89**, 3865.
- Grebowsky, J. M., Pharo, M. M., III, Taylor, H. A. and Eberstein, I. J. (1983) Measured thermal ion environment of STS-3. AIAA Shuttle Environment and Operations Meeting, 31 October–3 November 1983, Washington, DC. Paper No. AIAA-83-2597.
- Gurnett, D., Frank, L. A. and Lepping, R. (1976) Plasma in the distant magnetotail. *J. geophys. Res.* **81**, 6059.
- Hudson, M. K. and Roth, I. (1984) Thermal fluctuations from an artificial ion beam injection into the ionosphere. *J. geophys. Res.* **89**, 9812.
- Kintner, P. M., Kelley, M. C., Holmgren, G. and Bostrom, R. (1981) The observation and production of ion acoustic waves during the Trigger experiment. *J. geophys. Res.* **85**, 5071.
- Murphy, G. B., Shawhan, S. D., Frank, L. A., D'Angelo, N., Gurnett, D. A., Grebowsky, J. M., Reasoner, D. L. and Stone, N. H. (1983) Interactions of the Space Shuttle Orbiter with the ionospheric plasma. Proc. 17th ESLAB Symp. on Spacecraft Plasma Interactions and their Influence on Field and Particle Measurements, Noordwijk, The Netherlands. Eur. Space Agency, ESA SP-198, pp. 73–78.
- Omid, N. (1985) Broadband electrostatic noise produced by ion beams in the Earth's magnetotail. *J. geophys. Res.* **90**, 12330.
- Raitt, W. J., Siskind, D. E., Banks, P. M. and Williamson, P. R. (1984) Measurements of the thermal plasma environment of the Space Shuttle. *Planet. Space Sci.* **32**, 457.
- Scarf, F., Frank, L., Ackerson, K. and Lepping, R. (1974) Plasma wave turbulence at distant crossings of the plasma sheet boundaries and neutral sheet. *Geophys. Res. Lett.* **1**, 189.
- Shawhan, S. D., Murphy, G. B. and Picket, J. S. (1984) Plasma Diagnostics Package assessments of the STS-3 Orbiter plasma environment. *J. Spacecraft Rockets* **21**, 387.
- Siskind, D. E., Raitt, W. J., Banks, P. M. and Williamson, P. R. (1984) Interactions between the orbiting Space Shuttle and the ionosphere. *Planet. Space Sci.* **32**, 881.
- Stone, N. H., Samir, U., Wright, K. H., Jr., Reasoner, D. L. and Shawhan, S. D. (1983) Multiple ion streams in the near vicinity of the Space Shuttle. *Geophys. Res. Lett.* **10**, 125.
- Stone, N. H., Wright, K. H., Jr., Hwang, K. S., Samir, U., Murphy, G. B. and Shawhan, S. D. (1986) Further observations of space shuttle plasma-electrodynamic effects from OSS-1/STS-3. *Geophys. Res. Lett.* **13**, 217.
- Tidman, D. A. (1967) Turbulent shock waves in plasma. *Physics Fluids* **10**, 547.

THERMAL ION COMPLEXITIES OBSERVED WITHIN THE SPACELAB 2 BAY

J. M. GREBOWSKY, H. A. TAYLOR, JR. and M. W. PHARO, III

Laboratory for Atmospheres, NASA/Goddard Space Flight Center, Greenbelt, MD 20771, U.S.A.

and

N. REESE

Physics Department, University of Maryland, College Park, MD 20742, U.S.A.

(Received 24 July 1987)

Abstract—Examples of prominent thermal ion composition variations characteristic of the Shuttle environment as observed from within the open cargo bay on the Spacelab 2 mission are discussed. Although the prominent ionization source is the inflow of the ambient plasma (in particular O^+), water ions of Shuttle origin were present throughout the mission, and there was evidence for a local source of molecular ions NO^+ and/or O_2^+ which also exist in the ionosphere. Bursts in the fluxes of these contaminant species were frequently observed coincident with thruster firings while O^+ depletions or enhancements could occur depending on the scattering geometry. These effects bring into question whether reliable ambient thermal ion measurements can be made from the vicinity of such vehicles. The presence of significant inflows of contaminant ions into the bay within the Shuttle wake also indicates that Shuttle emissions play a significant role in the evolution of its wake structure.

INTRODUCTION

The University of Iowa Plasma Diagnostic Package (PDP) activities on the Spacelab 2 (SL-2) mission were planned to explore the properties of the plasma and fields within a wide range of regions about the Shuttle. This was done by taking measurements not only from its secured position within the open cargo bay but also at various locations from the Remote Manipulator System (RMS) arm and as a free-flying satellite. One of the instruments on the PDP was a Bennett RF ion mass spectrometer which measured effects of the Shuttle's gaseous emissions and structural geometry on the ambient thermal ions. A detailed knowledge of this interaction is needed to determine what type of reliable ambient plasma measurements can be made near large, gas emitting space structures. It is also needed in order to determine the extent of the control one can have over plasma science experiments using such vehicles as large experimental laboratories moving through an extensive magneto-plasma. In this paper ion mass spectrometer observations made within the SL-2 bay will be used to pinpoint the more prominent ways in which thermal ion measurements are affected by the Shuttle. Observations made on the RMS just prior to release and after capture, as well as some of the free flying measurements, have already been considered (Grebowsky *et al.*, 1987).

SPECTROMETER CHARACTERISTICS

The ion mass spectrometer flown on the PDP was of the Bennett RF genre (Bennett, 1950). Thermal ion spectrometers flown on satellites to make ambient ion measurements are usually oriented to look into the vehicle ram direction. On the Space Shuttle many experiments compete for optimum orientations. As a result the look direction of spectrometers fixed within the bay is necessarily often facing in a non-ideal direction for measurements of ambient ions. However, such orientations can prove interesting from the viewpoint of observing Shuttle perturbations. Due to the complex attitude variations of the Shuttle and the positioning of the PDP in the midst of a complex payload bay configuration a routine conversion of collected ion currents into corresponding number densities was not feasible. Hence only the raw ion currents collected, which are dependent on the number flux of ion species entering normal to the aperture, are considered here.

The ion spectrometer on the SL-2 mission had a less effective mass resolution than that of similar instruments flown on other satellite missions (such as *OGO*, *Atmosphere Explorer*, and *Pioneer Venus* spacecraft). Since the RF section of Bennett spectrometers sorts ions on the basis of their axial velocity (Bennett, 1950), the instrument is responsive to tur-

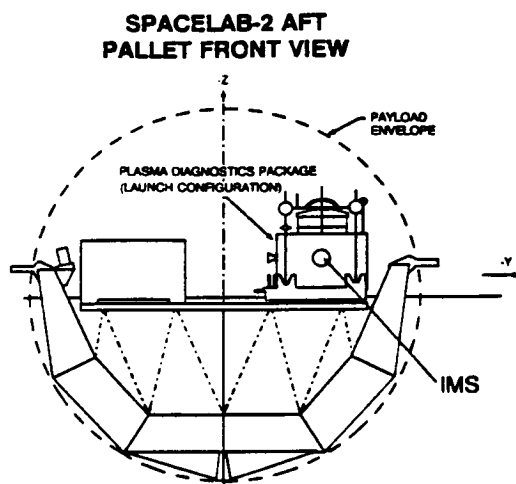


FIG. 1. THE LOCATION OF THE PLASMA DIAGNOSTIC PACKAGE (PDP) WAS ON THE PORTSIDE IN THE AFT PALLET OF THE SL-2 PAYLOAD.

The view depicted is from the front of the bay. The location of the ion mass spectrometer (IMS) on the PDP is such that within the bay it is looking directly forward parallel to the Shuttle x axis (along the nose-tail line).

bulent and multi-energy ion flows near the Shuttle, features which were prominent on earlier missions (Stone *et al.*, 1983; Raitt *et al.*, 1984; Hunton and Calo, 1983; Pickett *et al.*, 1985). As a result, masses such as 17 amu, which have been detected, and minor ionospheric ions with a mass within 1 or 2 amu of a more dominant one were not always unambiguously detected during the mission even when they were expected. As a consequence of this, subsequent SL-2 plots will refer to the molecular ion species NO^+ and H_2O^+ only with the understanding that the presence of adjacent mass ions cannot be ruled out.

SURROUNDINGS OF IMS AND SL-2

The launch position of the PDP was on the port side of the aft pallet (Fig. 1) with the ion mass spectrometer (IMS) looking forward. The ramming ambient plasma had an unoccluded, although oblique, flow component into the spectrometer only when the Shuttle was flying with its nose forward and down slightly. With regards to adjacent structures, the PDP has no large obstruction on the port side between it and the port bulkhead. However, on the starboard side just forward of the PDP is an X-ray telescope which extends above the PDP toward the payload bay envelope. Hence a distinct port-aft difference is expected in the incoming ion fluxes detected by the spectrometer.

In the absence of simultaneous ambient ion observations in a region unperturbed by the Shuttle, previous satellite observations must be used to describe its immediate ion environment. For this purpose *Atmosphere Explorer C* and *E*, which flew for extensive periods at SL-2 altitudes in the vicinity of 300 km, will be used. A measure of the range of variations in the ion composition that could occur along a typical orbit of SL-2 was obtained by sorting out all the thermal ion concentration measurements made by the Bennett RF Ion Mass Spectrometers on both satellites. All ion data obtained within a band of altitudes about that of SL-2 and within a latitude window that straddled a typical SL-2 orbital track in magnetic latitude and local time were plotted along the orbit (Fig. 2). From these observations the most prominent ions anticipated along the SL-2 orbit were O^+ and the molecular NO^+ and O_2^+ (the latter is not plotted but its concentrations and variability were similar to NO^+). During the daytime the ambient O^+ variation should have been relatively smoothly varying along the Shuttle's orbit on the SL-2 mission, but precipitous changes and irregularities in the ambient concentrations could be expected at night. Other ambient ions observed in the *AE* sort included N_2^+ , N^+ , H^+ and He^+ . These ions were detected at times throughout the SL-2 mission but will not be considered here.

OBSERVATIONS IN BAY

An example of ion measurements within the bay early in the mission which displayed the most prominent features of the interplay between the Shuttle and the ambient ionosphere is shown in Fig. 3. These data were taken only a few hours after turn on of the PDP instruments following the Spacelab launch (on 29 July 1985 at 21:00 G.M.T.). As depicted in the plot, the Shuttle's attitude was being reconfigured for an orbit-circularizing Orbital Maneuvering System (OMS) burn. The Shuttle's altitude rose from 222 km at the beginning of the interval plotted to 319 km at 03:23 G.M.T. when a 47 s duration OMS burn took place. During the attitude change the orientation of the Shuttle with respect to the orbital plane was particularly useful for highlighting general ram-wake ion behavior. It was essentially flipped about its y axis (i.e. it pitched over along the orbit with its wings directed, within a few degrees, perpendicular to the orbit plane).

The most obvious characteristic of the ion fluxes collected within the bay during this period was the overall absence of significant ionization when the bay (and the IMS) were facing into the wake of the moving vehicle. The observed ram-to-wake drop in the total

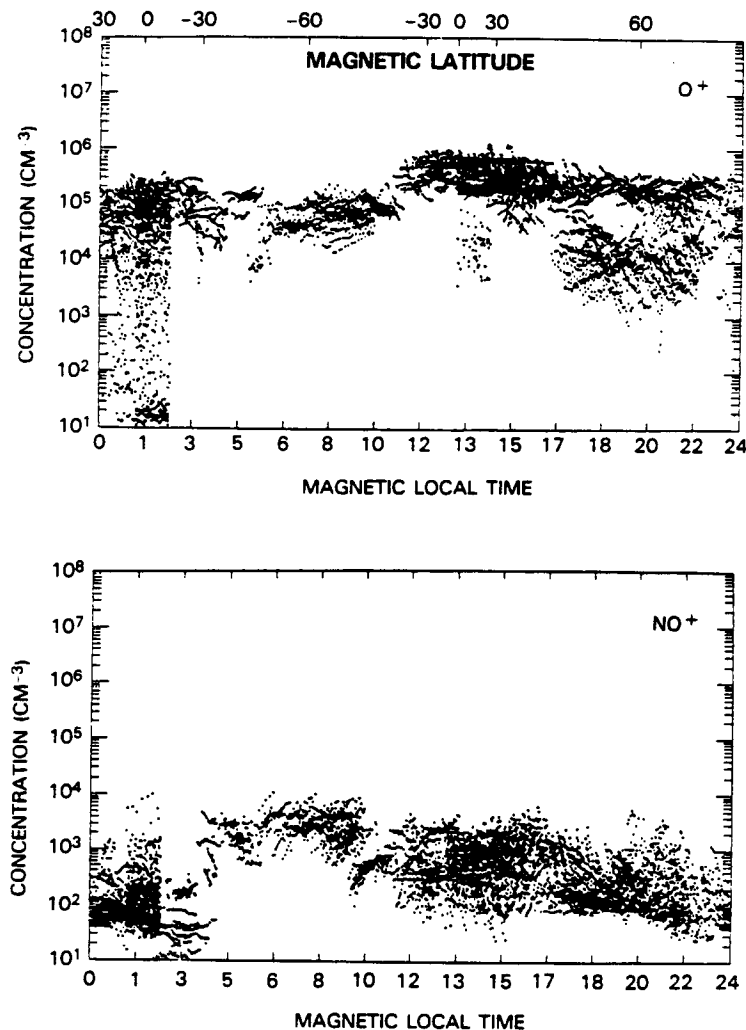


FIG. 2. O^+ and NO^+ concentrations made by the BENNETT RF ION MASS SPECTROMETERS ON *Atmosphere Explorers C and E* FROM 1973 THROUGH 1979 TYPIFY THE SL-2 AMBIENT ENVIRONMENT.

The data were selected from within a $\pm 10^\circ$ latitude window about a SL-2 orbital track in magnetic local time and latitude. Measurements were restricted to 270–330 km altitudes and to 30 day intervals about day 212 and about day 31 with the signs of the latter latitudes reversed to agree with the latitude–season dependence of the SL-2 orbit

ion flux by at least 4 orders of magnitude is typical of that expected and previously observed for the fluxes in the vicinity of such a large vehicle (Raitt *et al.*, 1984; Siskind *et al.*, 1984; Samir *et al.*, 1986). In addition to this gross effect, the collected currents of inflowing ambient ions will increase as the ions ram more directly into the spectrometer. The latter behavior is indeed apparent in the O^+ current in Fig. 3, which increases with decreasing angle of attack of the spectrometer into the ram direction until shadowing of the incoming plasma flow by the forward Shuttle cabin begins. The NO^+ ions followed a similar

response when the IMS attack angles were smaller than approximately 45° . However, when the Shuttle bay was first turning into the ram direction and the IMS angle of attack was near 90° , the NO^+ current was large relative to that of O^+ . This is not the expected response for an ambient flowing ion since it is well established (Samir, 1970) that the rate of decrease of collected currents in a flowing plasma with increasing angle of attack is faster the heavier the ion species. Since the bay was oriented into the velocity direction at this time, this indicates the presence of a Shuttle derived source of NO^+ ions. This is consistent

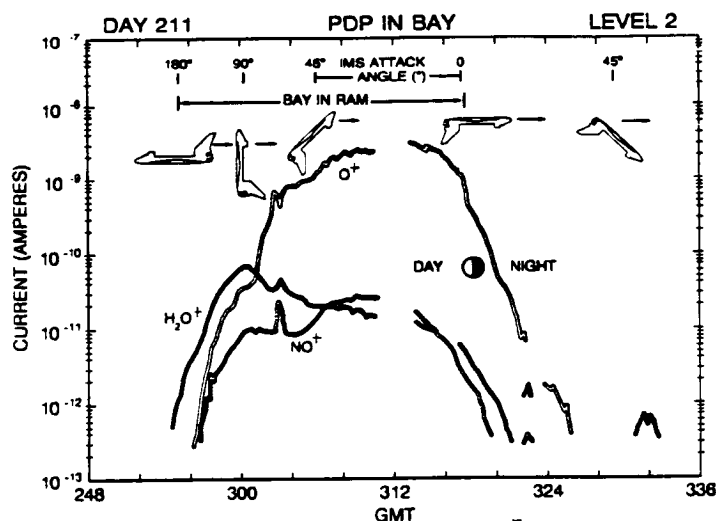


FIG. 3. ION MEASUREMENTS FROM AN ORBIT EARLY IN THE MISSION FROM THE PARKED PDP POSITION WITH THE BAY ARE SHOWN.

The Shuttle was flipping in preparation for an OMS burn near 03:23 G.M.T. The attitude variation provided a relatively simple geometry for discerning angle of attack variations of the ambient collected currents into the spectrometer and the different behavior of contaminant ions produced in the Shuttle environment.

with the observed variation of the contaminant ion H_2O^+ which peaks in the same region and whose current does not track the IMS attack angle but rather the angle of the bay into ram. Although there were undoubtedly ambient ion concentration variations along the orbit it is evident that the dominant effect on the in-bay distributions is the Shuttle attitude.

The effects of thruster firings during this sequence of measurements were most evident near 03:03 and 03:23 G.M.T. as short-lived enhancements in the molecular ion current densities—the first occurring during a Reaction Control System sequence of firings and the latter during the OMS system burn. Concentration enhancements of these molecular ion species are commonly observed in the vicinity of the Shuttle in association with engine firings (Narcisi *et al.*, 1983; Grebowsky *et al.*, 1983) and are consistent with the ionization of their neutral counterparts that has been observed (Wulf and von Zahn, 1986) to be emitted by the thrusters which employ the reaction between monomethyl hydrazine and nitrogen tetroxide. Observations of ambient O^+ ion flux depletions near the Shuttle during firings, such as occurs near 03:03 G.M.T. in Fig. 3, were observed on the earlier STS-4 mission. This is not unexpected since the O^+ loss rate through charge exchange with water molecules is very rapid compared to the nominal ambient O^+ chemical loss rate (e.g. Mendillo and Forbes, 1978). However, over the entire SL-2 mission O^+

depletions during engine burns were not always or even typically observed when the PDP was secured in the bay. This is partially due to the fact that most firings are short in duration (usually less than a second) compared to the sweep period (2.3 s) of the IMS through all masses. Ion scattering plays a part also as will be evident in the next example orbit.

Many of the orbits with the PDP parked in the bay are characterized, as in Fig. 3, by a generally totally depleted plasma wake behind the Shuttle. However, ions can get into this strongly depleted wake as is evidenced by the trace level enhancement of the water ion flux near 03:32 G.M.T., which occurred when the Shuttle velocity was at an angle of 135° from the outward bay normal. Such ion flux enhancements in the wake are sometimes coincident with thruster firings. These enhancements would be the result of the momentary scattering of thruster ions into the wake or the pickup of locally produced ions by the ambient magnetic field, which causes them to gyrate into the wake. However, the isolated wake event in Fig. 3 is much longer in duration than the vernier engine firings that took place at that time. It is more likely, therefore, that it results from a discrete stream of plasma directed into the near wake—perhaps one of the multiple streams that have previously been observed from measurements on the RMS (Stone *et al.*, 1983).

The ion flux behavior seen on the orbit depicted in Fig. 3 is one of the least complicated examples

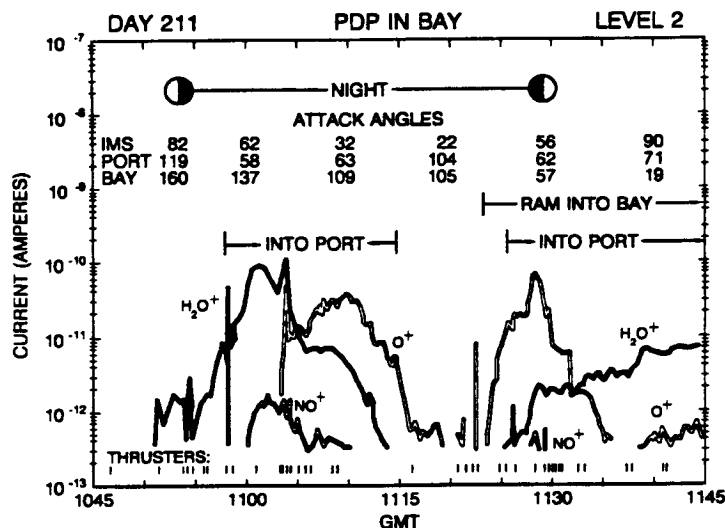


FIG. 4. THESE DATA WERE OBTAINED ON AN ORBIT IN WHICH THE ATTITUDE WAS BEING CONTROLLED TO TEST THE IPS.

Frequent vernier thruster firings were needed to maintain the attitude. The angles of the Shuttle velocity vector with respect to vectors out of the IMS, bay and port side are listed.

obtained from within the bay during the SL-2 mission. A later orbit example shown in Fig. 4 provides a glimpse of more complicated in-bay ion behavior resulting from ambient ion and Shuttle interaction processes. In this circumstance the attitude of the Shuttle was dictated by another experiment—it was an orbit dedicated to verification flight testing of the Shuttle's Instrument Pointing System. The spectrometer was looking into the forward direction of the Shuttle's motion at all times until approximately 5 min before the end of the period plotted, but the bay was exposed to the ram direction only subsequent to 11:22 G.M.T. Also, the component of the motion in the port-aft direction changed twice during the period.

The observations near and after dawn when the bay and IMS aperture were angled toward the ram direction show the expected drop off of the ambient O^+ with increasing IMS attack angle and the overall buildup of the H_2O^+ fluxes with increasing exposure of the bay to the ram direction. What was not observed was the usual absence of ion fluxes in the wake of the Shuttle. Enhanced fluxes of ambient O^+ were detected when the bay was facing as much as 110° from the ram direction. The water ion fluxes peaked even further into the wake. The shift between the O^+ and H_2O^+ maximum currents in the wake implies different average flow directions for the contaminant and ambient ions streaming around the

Shuttle. The behavior of the NO^+ follows the contaminant profile in the wake also. Hence the Shuttle's plasma wake differs significantly from ground-based experimental and theoretically studied wakes in that ions produced from Shuttle emissions play a significant role in wake filling processes. Further, the obvious reduction in currents when the Shuttle was moving towards its starboard direction (between 11:16 and 11:26 G.M.T.) indicates that plasma shadows produced by in-bay structures further complicate the near plasma wake.

There was a relatively large number of vernier thruster firings during the period displayed in Fig. 4 as well as the detection of comparatively low undisturbed ion current magnitudes. These two factors account for the increased number of distinctive thruster ion current spikes observed in the molecular ions compared to the previously discussed data sample. Another feature worth noting is the presence of, at times, spike-like enhancements in the O^+ current during firings. O^+ is not expected to be emitted from the thruster chambers, nor will it be enhanced in concentration by the chemical interaction of the neutral thruster effluents with ambient ions since the ambient O^+ provides the charge. One possibility is that ambient O^+ trajectories are momentarily perturbed by electric field changes induced by the firings—e.g. the PDP electric potential on the STS-3 mission was found to change during thruster firings (Pickett *et al.*, 1985).

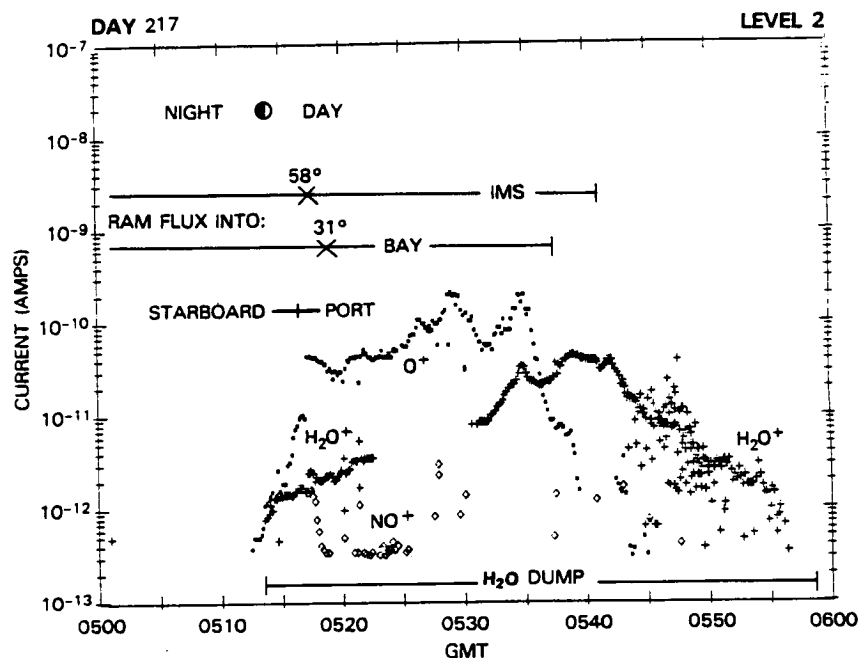


FIG. 5. AN EXAMPLE OF ION MEASUREMENTS DURING A WATER DUMP SHOWS AN ENHANCEMENT OF WATER IONS THROUGHOUT THE DUMP.

The attitude is schematically indicated by the time intervals in which the incoming ambient ram velocity had a component into the IMS, the bay and portside. The crosses denote minimum angles—the angles increase monotonically away from these points. H_2O^+ ions were also detected amidst the irregularly varying H_2O^+ ion fluxes in the wake.

Another is that ambient ion scattering by the thruster gases will produce short-term scattering effects as has been observed for the neutral gases (Wulf and von Zahn, 1986).

The effects of ion-neutral scattering processes and the filling in of the Shuttle wake are most vividly seen during water dumps. Figure 5 shows an orbital segment of observations within the bay during a period of water release on the next-to-last day of the Spacelab 2 mission. The varying attitude of the Shuttle is roughly indicated by the intervals when the incoming ram velocity was directed into the bay, the portside, and the IMS. The minimum angles of attack occurred at the points marked by crosses and increased monotonically away from these points. The actual attitude of the Shuttle was prescribed by an X-Ray Telescope star cluster tracking.

The usual enhancement of the O^+ flux when unobstructed ambient flow enters the IMS is evident once the PDP emerged from the plasma shadow of the starboard payload instruments near 05:15 G.M.T. The NO^+ current maximized near the minimum unobstructed IMS attack angle as expected for ambient incidence. The H_2O^+ currents increased with the

onset of the water dump and were detected far towards the anti-ram direction of the Shuttle until the bay was 140° from ram and the water dump terminated. During the dump there was a mixture of 18 and 19 amu ions detected in the wake with very irregular flux variations. The 19 amu ions are presumably H_2O^+ ions resulting from collisions between water ions and a dense cloud of neutral water molecules (Hunton and Calo, 1983). The flux irregularities are consistent with the production of plasma turbulence by such water releases (e.g. Pickett *et al.*, 1985). Thruster firings produced the usual isolated spike-like enhancements of the NO^+ currents. Thruster enhancements of water ion fluxes, however, were not detectable within the much more dense contaminant ion cloud resulting from the water dump.

COMMENTS

Thermal ion measurements made within the Shuttle's open cargo bay show vividly the sources of plasma variability in the near Shuttle ion environment. Measurements of ambient plasma variations in the near vicinity of such structures are obviously going

to be compromised. Measurements made under different attitude configurations are useful for understanding the plasmadynamic interactions between a large vehicle and a flowing plasma at parametric scale sizes unattainable in the laboratory. In the case of the Shuttle, however, locally generated ion species play a significant role in this interaction as is evidenced by the dominance of water ions in its wake. Finally, measurements made within the open bay envelope are dominated, to a great extent, by the payload configurations resulting in a unique ion environment for each individual Shuttle mission.

REFERENCES

- Bennett, W. H. (1950) Radiofrequency mass spectrometer. *J. appl. Phys.* **21**, 143.
- Grebowsky, J. M., Pharo, M. W., III, Taylor, H. A., Jr. and Eberstein, I. J. (1983) Measured thermal ion environment of STS-3. AIAA-83-2597, AIAA Shuttle Environment and Operations Meeting, 31 Oct.-3 Nov. 1983, Washington, DC.
- Grebowsky, J. M., Taylor, H. A., Jr., Pharo, M. W., III and N. Reese (1987) Thermal ion perturbations observed in the vicinity of the Space Shuttle. *Planet. Space Sci.* **35**, 501.
- Hunton, D. E. and Calo, J. M. (1983) Low energy ions in the Shuttle environment: evidence for strong ambient-contaminant interactions. *Planet. Space Sci.* **33**, 945.
- Mendillo, M. and Forbes, J. M. (1978) Artificially created holes in the ionosphere. *J. geophys. Res.* **83**, 151.
- Narcisi, R. S., Trzcinski, E., Federico, G., Wlodyka, L. and Delorey, D. (1983) The gaseous and plasma environment around Space Shuttle AIAA-83-2659, AIAA Shuttle Environment and Operations Meeting, 31 Oct.-3 Nov. 1983, Washington, DC.
- Pickett, J. S., Murphy, G. R., Kurth, W. S., Goertz, C. K. and Shawhan, S. D. (1985) Effects of chemical releases by the STS-3 orbiter on the ionosphere. *J. geophys. Res.* **90**, 3487.
- Raitt, W. J., Siskind, D. E., Banks, P. M. and Williamson, P. R. (1984) Measurements of the thermal plasma environment of the Space Shuttle. *Planet. Space Sci.* **32**, 457.
- Samir, U. (1970) A possible explanation of an order of magnitude discrepancy in electron wake measurements. *J. geophys. Res.* **75**, 855.
- Samir, U., Stone, N. H. and Wright, K. H., Jr. (1986) On plasma disturbances caused by the motion of the Space Shuttle and small satellites: a comparison of *in situ* observations. *J. geophys. Res.* **91**, 277.
- Siskind, D. E., Raitt, W. J., Banks, P. M. and Williamson, P. R. (1984) Interactions between the orbiting Space Shuttle and the ionosphere. *Planet. Space Sci.* **32**, 881.
- Stone, N. H., Samir, U., Wright, K. H., Jr., Reasoner, D. L. and Shawhan, S. D. (1983) Multiple ion streams in the vicinity of the Space Shuttle. *Geophys. Res. Lett.* **10**, 1215.
- Wulf, E. and von Zahn, U. (1986) The shuttle environment: effects of thruster firings on gas density and composition in the payload bay. *J. geophys. Res.* **91**, 3270.

An Analysis of Whistler Mode Radiation From the Spacelab 2 Electron Beam

W. M. FARRELL AND D. A. GURNETT

Department of Physics and Astronomy, University of Iowa, Iowa City

P. M. BANKS AND R. I. BUSH

STAR Laboratory, Stanford University, Stanford, California

W. J. RAITT

Center for Atmospheric and Space Sciences, Utah State University, Logan

During the shuttle's Spacelab 2 mission the University of Iowa's plasma diagnostics package (PDP) was released from the shuttle to free fly. At times during this free flight when the PDP was magnetically connected to the shuttle, Stanford's fast-pulsed electron generator, located in the shuttle cargo bay, ejected a 1-keV, 50-mA electron beam. The plasma wave instrument on board the PDP detected intense whistler mode radiation during these beam ejections. This paper presents a study of a whistler mode emission detected during one particular continuous electron beam firing. Calculations indicate that the beam radiated approximately 1.6 mW in the whistler mode as the beam traversed the 200 m from the shuttle to the PDP. The emissivity also decreased by about a factor of 10 over this same distance. The measured wave powers are 10^7 greater than wave powers expected from incoherent Cerenkov radiation, verifying that the radiation is generated by a coherent process. Estimates of the emissivity based on measured electric field intensities in the beam indicate that the whistler mode noise is produced by radiation from electron bunches created by an electrostatic beam-plasma instability.

INTRODUCTION

In this paper we describe an electron beam experiment performed on the Spacelab 2 (SL 2) mission. The Spacelab 2 flight, which was launched on July 29, 1985, included an electron accelerator called the fast-pulsed electron generator (FPEG) from Stanford University and a spacecraft called the plasma diagnostics package (PDP) from the University of Iowa. During a 6-hour period on August 1, 1985, the PDP was released from the shuttle to investigate plasma effects in the vicinity of the shuttle. During the PDP free flight, the shuttle was maneuvered so that the PDP passed near magnetic field lines connected to the shuttle. Four such magnetic conjunctions were achieved. During one of these magnetic conjunctions a 1-keV, 50-mA electron beam was continuously ejected from the shuttle so that radiation effects could be monitored as the PDP passed near the magnetic field line carrying the beam. Plate 1 shows a frequency versus time spectrogram from the PDP plasma wave instrument during this electron beam event. The funnel-shaped signal extending from the electron cyclotron frequency f_c down to approximately 30 kHz is whistler mode radiation from the electron beam. This whistler mode radiation was first described by Gurnett *et al.* [1986]. Our objectives in this paper will be to determine the total radiated power from the beam and compare it with the power predicted by various whistler mode radiation mechanisms.

Whistler mode emissions are known to be produced by both artificial and natural electron beams. Some of the early observations of emissions from artificial electron beams were

made in the early 1970s by the University of Minnesota group using the Echo rocket experiments [Cartwright and Kellogg, 1974; Kellogg *et al.*, 1976; Monson *et al.*, 1976; Winckler, 1980]. Observations of beam-generated emissions were also made on the joint Franco-Soviet Artificial Radiation and Auroras Between Kerguelen and the Soviet Union (ARAKS) beam experiments [Dechambre *et al.*, 1980]. The first space shuttle electron beam experiment was performed in March 1982 as part of the Space Transportation System 3 (STS 3) mission. On this flight the PDP was carried on the shuttle remote manipulator arm, and the FPEG was used to produce an artificial electron beam. During electron gun firings a possible whistler mode signal was detected from the electron beam [Shawhan *et al.*, 1984]. In December 1983 the Phenomenon Induced by Charged Particle Beams (PICPAB) experiment was carried as part of the Spacelab 1 mission. The PICPAB experiment was specifically designed to investigate radiation from electron beams injected in the ionosphere. As in the other previous experiments, whistler mode signals were again detected when the electron gun was fired [Beghin *et al.*, 1984].

Whistler mode radiation is also produced in the auroral zone in association with the field-aligned electron beams that are responsible for the aurora [Gurnett, 1966]. This radiation is usually called auroral hiss. Both upward and downward propagating auroral hiss has been observed [Mosier and Gurnett, 1969]. The downward propagating auroral hiss is associated with downward moving electron beams with characteristic energies of a few hundred electron volts [Gurnett, 1966; Hartz, 1969; Gurnett and Frank, 1972; Laaspere and Hoffman, 1976]. The upward propagating auroral hiss often has a V-shaped spectrum called a "saucer" [Smith, 1969; Mosier and Gurnett, 1969; James, 1976] or a "funnel" [Gurnett *et al.*, 1983]. Upward propagating auroral hiss has been observed in association with upward moving field-aligned elec-

ORIGINAL PAGE
 FROM THE WHITE PHOTOGRAPH

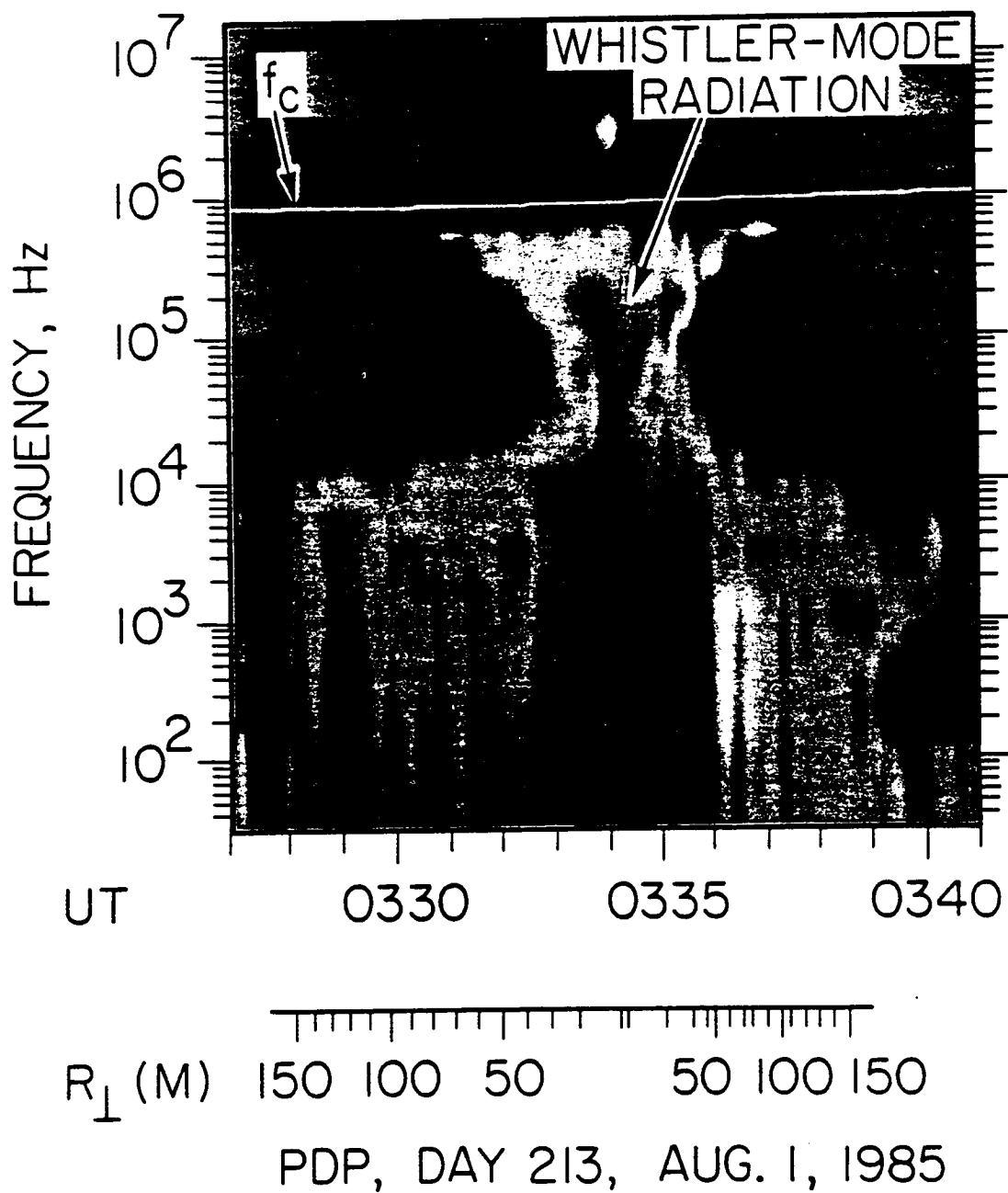


Plate 1. A frequency versus time spectrogram from the PDP plasma wave instrument showing intense emissions during a dc electron gun firing. The funnel-shaped structure that extends from the electron cyclotron frequency f_c to about 30 kHz is whistler mode radiation from the beam.

electron beams [Lin et al., 1984]. The characteristic frequency-time shape of the saucer or funnel is a propagation effect that occurs for whistler mode waves propagating near the resonance cone. Gurnett et al. [1986], in their initial analysis of the Spacelab 2 results, showed that a similar wave propagation effect was observed for the whistler mode signals generated by the SL 2 electron beam.

ELECTRIC FIELD POLARIZATION

To confirm that the radiation from the Spacelab 2 electron beam is propagating in the whistler mode, we compare the electric field polarization with the polarization expected for the whistler mode. The whistler mode has a polarization that depends on the wave frequency f , the wave normal angle θ , the cyclotron frequency f_c , and the plasma frequency f_p . Using cold plasma theory [Stix, 1962], the electric field and index of refraction vectors can be calculated as a function of f, θ, f_c , and f_p . For the whistler mode the index of refraction varies strongly as a function of the wave normal direction. This variation can be represented by an index of refraction surface, $n(\theta)$, which is a surface that is defined by the loci of index of refraction vectors at different wave normal angles. Figure 1 shows the index of refraction surface for the whistler mode. At a limiting wave normal angle, known as the resonance cone angle θ_{res} , the index of refraction goes to infinity. The resonance cone angle is given by $\tan^2 \theta_{res} = -P/S$, where $P = 1 - f_p^2/f^2$ and $S = 1 - f_p^2/(f^2 - f_c^2)$. As the wave normal approaches the resonance cone, the electric field \mathbf{E} becomes linearly polarized with \mathbf{E} parallel to \mathbf{n} . In this limit the electric field is quasi-electrostatic and the group velocity \mathbf{v}_g is perpendicular to \mathbf{E} and \mathbf{n} (see Figure 1).

In a previous paper [Gurnett et al., 1986] the funnel-shaped frequency versus time pattern of the radiation from the SL 2 electron beam was explained as a frequency dependent propagation effect for whistler mode emissions from the electron beam. Figure 2 is a sketch demonstrating how this effect works. Consider, first, a point source of whistler mode radiation, with the radiation propagating near the resonance cone. As the wave frequency increases, the resonance cone angle decreases, and the ray path direction \mathbf{v}_g becomes increasingly oblique to the magnetic field, approaching 90° as the frequency approaches the electron cyclotron frequency. Typical ray paths for a whistler mode emission propagating near the resonance cone are shown in the figure. As a spacecraft approaches the source, emissions near the gyrofrequency are detected first, since their ray paths are almost perpendicular to

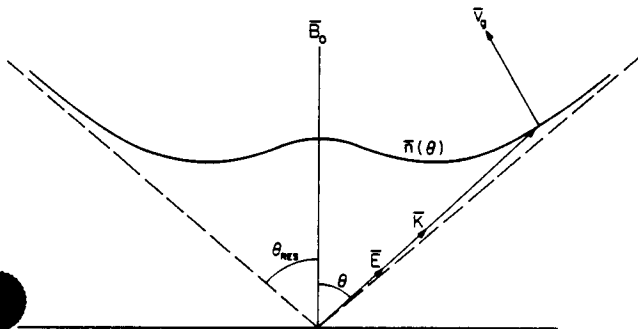


Fig. 1. The index of refraction surface for the whistler mode and the associated \mathbf{E} , \mathbf{k} , and \mathbf{v}_g vectors for propagation near the resonance cone ($\theta \approx \theta_{res}$). For propagation near the resonance cone, \mathbf{k} and \mathbf{E} are parallel and nearly perpendicular to \mathbf{v}_g . In this limit, \mathbf{E} is linearly polarized and quasi-electrostatic.

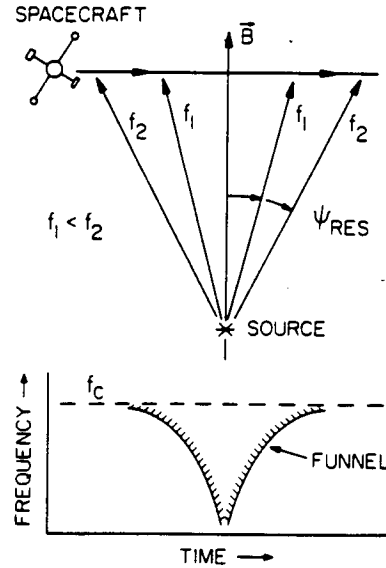


Fig. 2. The whistler mode ray paths from a point source radiator. Note that a passing spacecraft will detect radiation near the gyrofrequency first, then detect lower frequency emissions as it nears the source. A well-defined frequency versus time funnel-shaped spectrum results from this spacecraft/source encounter.

the beam. Progressively lower frequencies are then detected as the distance between the spacecraft and source decreases. This frequency dependent propagation effect creates a funnel-shaped emission pattern on a frequency versus time spectrogram. By comparing a modeled emission pattern using cold plasma theory to the funnel-shaped pattern shown in Plate 1, Gurnett et al. [1986] have confirmed that the whistler mode emission from the SL 2 electron beam is propagating upward from the shuttle near the resonance cone. The distinct funnel boundary is defined by the waves that propagate directly from the beam origin, the shuttle. The funnel on the spectrogram appears filled in, since the radiation is being emitted by a line source extending upward from the shuttle rather than a point source. Since the waves are upward propagating, $\mathbf{k} \cdot \mathbf{v}_g > 0$, where \mathbf{v}_g is the beam velocity vector.

In order to provide further confirmation that the radiation from the SL 2 electron beam is propagating near the resonance cone, an additional test was performed. This test compares model electric field directions in the PDP spin plane to their actual directions as measured by the PDP plasma wave instrument. To perform this test, a computer program was developed that calculates the angle ϕ between the projection of a model electric field onto the spin plane and a fixed reference direction. The fixed reference direction selected was the spin plane projection of the spacecraft-Sun vector. To compute ϕ , the group velocity was assumed to be directed from a point on the beam toward the PDP with the electric field vector \mathbf{E} at an angle θ_{res} relative to the beam. This field geometry is the expected configuration for an upward propagating whistler mode wave near the resonance cone. Figure 3 shows the corresponding geometry of \mathbf{E} , \mathbf{v}_g , and \mathbf{k} .

The electric field directions in the spin plane calculated using the model described above are compared to the measured electric field directions found from spin modulation maximums in the receiver data. The spin modulation maximums occur when the PDP electric antennas are aligned with the measured electric field in the spin plane, thus allowing a direct determination of this measured electric field direction.

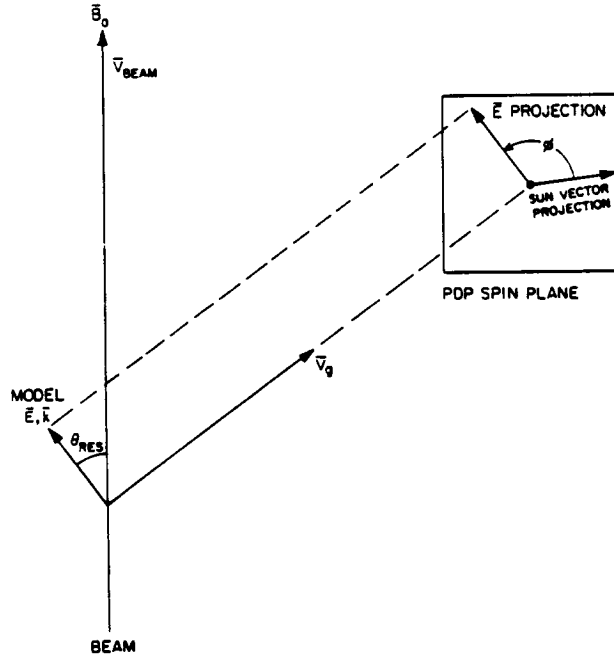


Fig. 3. The ray path and E , k , and v_b vectors used to confirm the electric field polarization. The assumed electric field is projected into the PDP spin plane, and the angle relative to the projection of the Sun vector is calculated. The projected electric field direction can then be compared to the measured directions calculated from spin modulation maximums in the electric field intensity (see Figure 4).

Figure 4 shows the results of this comparison at four frequencies: 562, 311, 178, and 100 kHz. This figure shows the phase angle ϕ between the projected electric field and the Sun vector as a function of time. The dots represent the modeled electric field directions computed assuming a resonance cone propagation scheme, while the crosses represent the measured electric field directions. The close agreement between the computed and measured electric field directions provides strong confirmation that the waves are propagating near the resonance cone and in the beam direction (i.e., $k \cdot v_b > 0$), as indicated in Figure 3.

EMITTED POWER

In this section we estimate the total power radiated from the beam in the whistler mode. By comparing the radiated power to the total power in the beam, the efficiency of the wave-beam interaction can be estimated and compared with various generation mechanisms. The power emitted from the beam in the whistler mode can be estimated by integrating the Poynting flux over a surface surrounding the beam. An inherent difficulty with this calculation is the determination of the phase and magnitude of the electric and magnetic fields in the Poynting flux, $S = E \times H$. Since three axis measurements are not available and since phase measurements were not made, the Poynting vector cannot be determined directly. Computing the Poynting flux from the electric field alone is complicated by the fact that near the resonance cone the whistler mode is quasi-electrostatic and the ratio of the electromagnetic to electrostatic components is an exceedingly sensitive function of the wave normal angle. To compute the wave normal angle, we assume that the radiation is produced by the Landau resonance, i.e., $\omega/k_{\parallel} = v_b$. Since the beam velocity is known, this condition gives a well-defined value for the wave normal direction. The fact that the radiation is propagating in

the same direction as the beam ($k \cdot v_b > 0$) provides a strong indication that the Landau resonance is involved. For example, the $s = -1$ cyclotron resonance produces radiation propagating in the opposite direction of the beam. Also, as will be discussed later, the Landau resonance gives the best agreement with the measured electric to magnetic field ratios.

To carry out the Poynting vector calculation we note that E lies almost entirely in the plane defined by n and the geomagnetic field (see Figure 3). The electrostatic and electromagnetic components of E are given by $E_0 \cos \Delta\theta$ and $E_0 \sin \Delta\theta$, respectively, where $\Delta\theta$ is the angle between E and n and E_0 is the amplitude of the total electric field. The angle $\Delta\theta$ is determined by the Landau resonance condition and cold plasma theory. The Landau resonance condition specifies the component of n parallel to the geomagnetic field, i.e.,

$$n_{\parallel} = n \cos \theta = c/v_b \quad (1)$$

where c is the speed of light. For a 1-keV electron beam moving parallel to the magnetic field, n_{\parallel} is approximately 15.9. A program was written that solves equation (1-20) of Stix [1962] for the magnitude and directions of n and E . Equation (1-20) of Stix is

$$\begin{pmatrix} S - n^2 \cos^2 \theta & -iD & n^2 \cos \theta \sin \theta \\ iD & S - n^2 & 0 \\ n^2 \cos \theta \sin \theta & 0 & P - n^2 \sin^2 \theta \end{pmatrix} \begin{pmatrix} E_x \\ E_y \\ E_z \end{pmatrix} = 0 \quad (2)$$

where

$$S = \frac{1}{2}(R + L) \quad (3)$$

$$D = \frac{1}{2}(R - L) \quad (4)$$

$$R = 1 - \sum_k \frac{\omega_{pk}^2}{\omega} \left(\frac{\omega}{\omega + \epsilon_k \omega_{ck}} \right) \quad (5)$$

$$L = 1 - \sum_k \frac{\omega_{pk}^2}{\omega} \left(\frac{\omega}{\omega - \epsilon_k \omega_{ck}} \right) \quad (6)$$

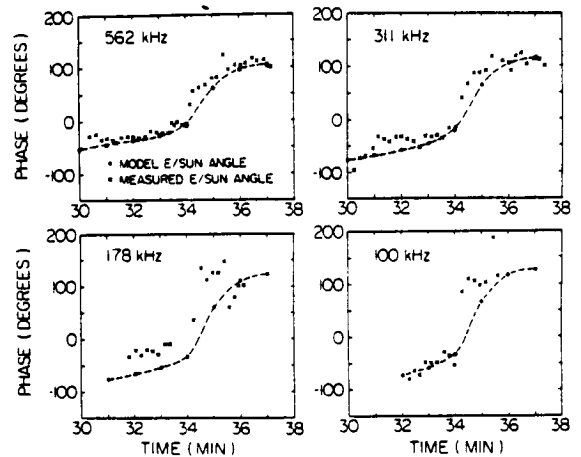


Fig. 4. The relative directions of the computed and measured electric field vectors in the PDP spin plane for the 562-, 311-, 178-, and 100-kHz frequency channels. The dots represent the computed electric field directions assuming that the wave vector is near the resonance cone with $k \cdot v_b > 0$, and the crosses represent measured electric field directions. The close agreement between the measured and modeled directions indicates that the whistler mode radiation is propagating near the resonance cone in the same direction as the beam.

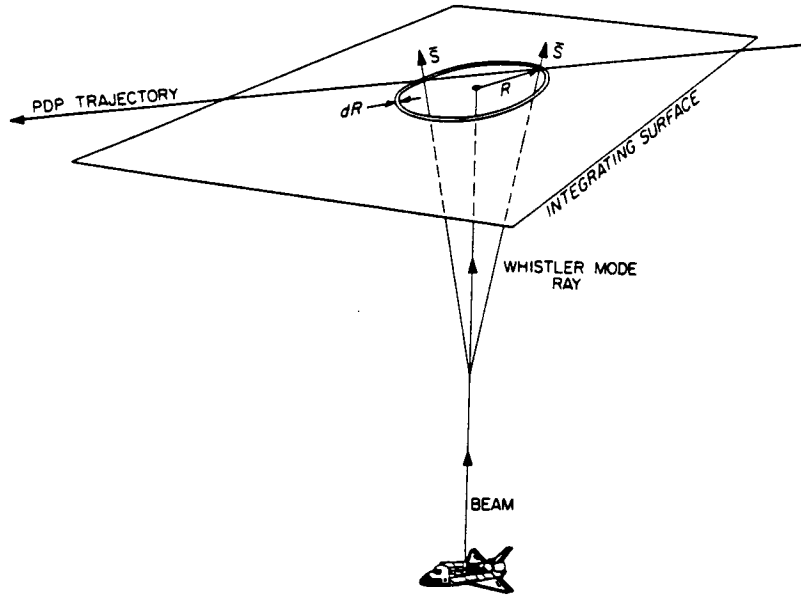


Fig. 5. The integration surface used to calculate the power emitted from the beam in the whistler mode. At closest approach, the PDP passed within 3 m of the beam at a distance of about 200 m from the shuttle.

$$P = 1 - \sum_k \frac{\omega_{pk}^2}{\omega^2} \quad (7)$$

The quantities ω_{pk} and ω_{ck} are the plasma and cyclotron frequencies for species k , while ϵ_k is the sign of the charge of species k . Using this program, we can calculate n and $\Delta\theta$ at a particular wave frequency consistent with $n_{||}$. Since $\Delta\theta$ is now determined, the electrostatic and electromagnetic components of E can be calculated. The calculated $\Delta\theta$ values are small, typically ranging from 0.06° to 1.1° from 31.1 to 562 kHz, and indicate that the wave is nearly electrostatic. It is easy to show that the magnitude of the Poynting vector is given by

$$|S| = \frac{nE_0^2}{2} \left(\frac{\epsilon_0}{\mu_0} \right)^{1/2} (A^2 + B^2)^{1/2} \quad (8)$$

where $A = 1 - \cos^2 \Delta\theta$ and $B = \sin \Delta\theta \cos \Delta\theta$. In the derivation of (8), Faraday's law, $\mathbf{n} \times \mathbf{E} = c\mathbf{B}$, was used to eliminate the magnetic field in the $\mathbf{E} \times \mathbf{H}$ term. Consequently, $|S|$ is dependent only on n and E , which are well-defined quantities. Note that as θ approaches the resonance cone angle, n and E become parallel and $|S|$ goes to zero. This behavior near θ_{res} is similar to an expression derived by Mosier and Gurnett [1971] in their paper addressing Poynting flux measurements of VLF hiss emissions.

Figure 5 shows the PDP trajectory relative to the beam. As can be seen, the PDP trajectory was nearly perpendicular to the beam. At closest approach, it passed within about 3 m of the beam at a distance of roughly 200 m from the shuttle. To compute the total radiated power, the Poynting flux is integrated over an imaginary surface perpendicular to the beam that includes the PDP trajectory. Assuming that the sampled intensities along this trajectory are constant around an annular ring of the area dA , centered on the beam, we can obtain the radiated power from the beam segment by evaluating the integral $P = \int S_{||} 2\pi R dR$, where $S_{||}$ is the field-aligned component of the Poynting vector and R is the perpendicular distance from the beam to the PDP. Note that the evaluation of this integral will yield two values for the radiated power: one

value from the inbound pass where the limits of integration extend from $R = \infty$ to $R \cong 0$ and one value from the outbound pass where the limits of the integration now extend from $R \cong 0$ to $R = -\infty$. Figure 6 shows the average power spectral density from these two passes as a function of frequency. The error bars shown in the figure represent the standard deviations of the power values. Note that the power spectral density dP/df is of the order of 10^{-9} W/Hz in the frequency range extending from 30 kHz to 1 MHz. The total emitted power in the 200-m beam segment from the shuttle to the PDP is found to be $P = 1.6$ mW. On the assumption that the power is emitted uniformly along the beam, the radiated power per unit length, dP/dl , is approximately 8×10^{-6} W/m. Since the total power of the beam was 50 W, the beam converted approximately 3.2×10^{-5} of its power to whistler mode radiation in the first 200 m. If the beam dissipated energy only via the whistler mode, the beam would only prop-

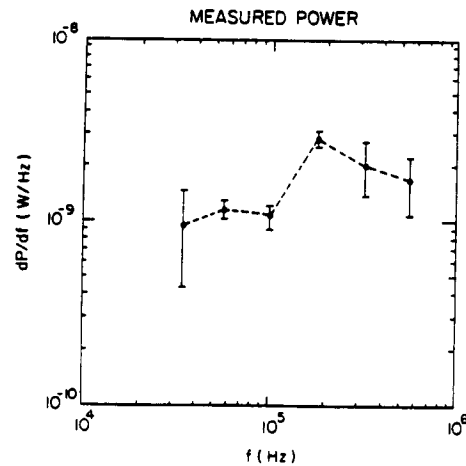


Fig. 6. The calculated power spectral density from the beam in the whistler mode is shown as a function of frequency.

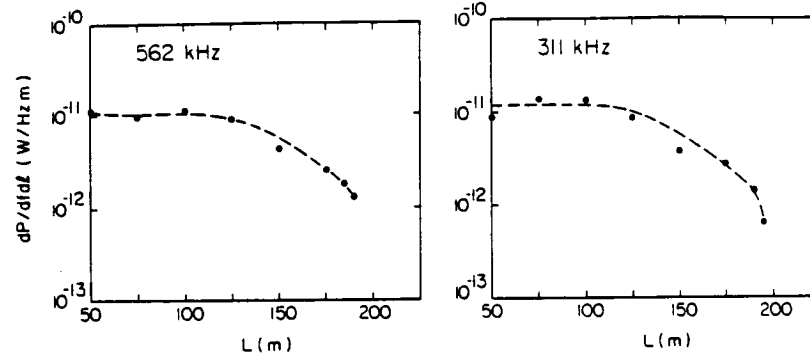


Fig. 7. The linear emissivity, dP/dL , is shown as a function of the distance L along the beam for the 562-kHz and 311-kHz frequency channels. Note that the emissivity starts to decrease rapidly beyond about 100 m.

agate approximately 6000 km before all of the beam energy would be converted to radiation.

The linear emissivity of the whistler mode radiation, dP/dL , from different locations along the beam can also be calculated. To calculate the linear emissivity, a knowledge of a signal's exact source location from the beam is required; however, by using the ray path, the source of the signal at a particular point along the PDP trajectory can be located. The power radiated from an infinitesimal beam radiation source, dl , is $P = \int S_{\perp} 2\pi R dl$, where S_{\perp} is the perpendicular component of the Poynting vector measured at the perpendicular distance R from the beam and corresponds to the Poynting flux emitted from a cylinder of radius R and length dl , surrounding the beam. The linear emissivity from this source, dP/dL , is then obtained by using the differential form of the power integral. The calculated linear emissivity of the whistler mode waves is shown in Figure 7. Note that the emissivity drops by a factor of 10 from 100 to 200 m along the beam. This decrease in emissivity indicates that the efficiency of whistler mode generation decreases with increasing distance along the beam and that the generation mechanism is capable of dynamic changes in tens of meters. If the emissivity continues to drop at the rate observed between 100 to 200 m, the radiation would be undetectable by the PDP at source distances more than about 1 km from the shuttle. This result may explain why Dynamics Explorer 1 (DE-1), which was magnetically connected to the shuttle during a gun firing on the STS 3 mission, did not see beam-generated whistler mode radiation in the vicinity of the streaming electrons [Inan et al., 1984]. From the SL 2 measurements it appears that strong whistler mode emissions are probably generated only in close proximity to the source of the beam.

As mentioned earlier, the electric and magnetic field measurements also provide further evidence that the whistler mode waves are generated via a Landau resonance process. This argument involves a comparison of computed and measured cB/E ratios. Assuming a specific resonance condition and using the solution of equation (1-20) of Stix [1962], we can compute a unique value for n and $\Delta\theta$. Faraday's law can then be used to obtain the relationship

$$\mathbf{n} \times \mathbf{E} = c\mathbf{B} \quad (9)$$

where \mathbf{E} is in the electric component and \mathbf{B} is in the magnetic component of the whistler mode waves. For the assumed field geometry, (9) can be rewritten as

$$nE_0 \sin \Delta\theta = cB_0$$

or

$$cB_0/E_0 = n \sin \Delta\theta \quad (10)$$

Using (10), we can compute $n \sin \Delta\theta$ for various resonance conditions and compare this ratio with the measured cB/E ratio. The spectrum analyzer used with the PDP search coil can only provide measurements up to 178 kHz; therefore, the magnetic to electric field ratio can only be obtained in the 56-kHz, 100-kHz, and 178-kHz frequency channels. Also, the measured values of B at high frequencies using the search coil are highly uncertain because of inaccuracies in the calibration of the instrument. The preflight calibration was performed by placing a calibration coil in the search coil and surrounding the system in a μ metal can. A problem arises at high frequencies (> 10 kHz), where frequency dependent capacitances and inductances affect the current and the expected value of B from the calibration coils. Unfortunately, postflight calibrations under more ideal conditions (specifically, without the μ metal can) have failed to reproduce the preflight calibrations. Our current best estimates are that B (and cB/E) are accurate only to within a factor of 2-4 at high frequencies. The range of measured cB/E values lies between 1.3 and 15.3. Assuming a Landau resonance, $n \sin \Delta\theta$ is computed to be 0.54, 0.52, and 0.54 for 56, 100, and 178 kHz, respectively. Note that these values lie just outside the range of measured cB/E values and fall in the range when considering the factor of 2-4 uncertainty in the calibrations. For an $s = +1$ cyclotron resonance, however, $n \sin \Delta\theta$ is computed to be between 0.05 and 0.08 for 56, 100, and 178 kHz. These values are about a factor of 20 smaller than the lowest measured cB/E value. Similar computed values are obtained for the $s = -1$ cyclotron resonance. These comparisons show that the measured cB/E ratio is closest to those expected for a Landau resonance.

INCOHERENT GENERATION MECHANISMS

From the power measurements alone it is not clear whether the beam-generated whistler mode radiation detected by the PDP during the SL 2 mission results from a coherent or incoherent generation process. A coherent mechanism involves large numbers of particles acting together to generate the emitted waves. The total power from a coherent source goes as N^2 , where N is the number of particles in coherence. Common coherent sources are plasma instabilities, lasers, and radio antennas. Incoherent mechanisms involve particles that are radiating independently. The power from the individual radiators must be added to get the total power emitted; thus

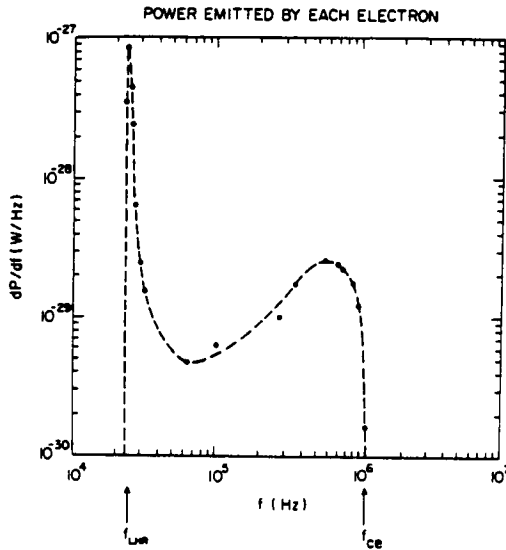


Fig. 8. The power spectra from a single electron radiating via Cerenkov processes are shown in a plasma environment similar to that surrounding the SL 2 beam. These calculations assume the wave/beam interaction is by a Landau resonance process and that the particle pitch angle is 10° . This power calculation is based on formulas derived by Mansfield [1967].

the total power is proportional to N , the number of radiators. A common incoherent source is an incandescent light bulb. This section and the next describe possible incoherent and coherent mechanisms for generating whistler mode radiation.

One possible incoherent mechanism involves Cerenkov radiation. Cerenkov radiation occurs when charged particles move with velocities greater than the phase speed of the wave in the medium. The whistler mode waves from the SL 2 electron beam are propagating near the resonance cone with large index of refractions, typically $n \sim 30$ –500. The phase speed of the wave is then much less than the speed of the 1-keV electron beam. Since the beam electrons are moving faster than the phase velocity of the whistler mode, Cerenkov radiation should be produced.

The measured whistler mode power from the beam will now be compared to the calculated power from Cerenkov radiation, assuming that the beam electrons are incoherent radiators. Our calculations are similar to those performed by Jorgensen [1968] and Taylor and Shawhan [1974], who both calculated the power from this process and compared it to the radiated powers from VLF hiss. Mansfield [1967] derived an equation that gives the power spectral density radiated from a single electron moving through an ambient ionized gas with a speed greater than the wave phase speed. For an incoherent mechanism the total power radiated from the beam is the power radiated from each electron $(dP/df)_e$, added up over all the electrons in a given beam volume N_e : $(dP/df)_{\text{total}} = N_e(dP/df)_e$. Using Mansfield's formula, we can calculate the radiated power from each beam electron, as is shown in Figure 8. In obtaining this result, we assume that the radiation is produced via a Landau resonance. We also assume, for this calculation, that the pitch angle of the electrons is 10° . The actual pitch angles varied from 0° to 20° ; however, the results are relatively insensitive to pitch angles in this range. From Figure 8 it can be seen that the most intense radiation occurs between the electron cyclotron frequency and the lower hybrid frequency f_{LHR} . Outside this range the power drops by a factor of 10^4 . Note that this frequency range corresponds rather well

to the frequency range of the radiation observed by the PDP. Multiplying the power from each electron by the number of electrons in the first 200-m segment of the beam (3×10^{12} particles) yields $(dP/df)_{\text{total}} \sim 10^{-16}$ W/Hz in the frequency range from f_e to f_{LHR} . These power spectral densities are much lower than the measured power spectral densities, by about a factor of 10^7 (compare with Figure 6, where $dP/df \sim 10^{-9}$ W/Hz). Therefore an incoherent process cannot account for the measured wave powers. Some coherent wave process must be involved. In Taylor and Shawhan's [1974] analyses of the generation of VLF hiss emissions by auroral electron beams, the calculated powers for the incoherent Cerenkov process were found to be a factor of 10^2 – 10^3 lower than those measured, again indicating a coherent process.

COHERENT GENERATION MECHANISMS

As concluded in the previous section, some coherent process must be involved in the whistler mode wave generation from the SL 2 electron beam. Coherent processes can be divided into two classes: direct and indirect. Direct mechanisms involve the direct conversion of energy from an unstable particle distribution to electromagnetic radiation, whereas indirect mechanisms involve the intermediate generation of one or more electrostatic modes which are coupled to the escaping electromagnetic radiation. This section will discuss possible direct and indirect mechanisms that may explain the whistler mode radiation.

Since an unstable electron distribution is present in the beam, the escaping electromagnetic radiation may result from direct conversion of the beam energy to electromagnetic radiation. Such a mechanism has been proposed by Maggs [1976] for the generation of auroral hiss. In his model, incoherent Cerenkov radiation produced by an auroral electron beam is directly amplified via a whistler mode plasma instability within the beam. It seems reasonable that this wave generation mechanism could be applied to the whistler mode waves emitted from the SL 2 electron beam; however, a problem arises in doing so. Unlike auroral beams the path length for wave growth in the SL 2 beam is very short, only 2–3 electron cyclotron radii (6–9 m). Using the Landau resonance condition and the fact that the emission is propagating near the resonance cone, we can derive an expression for the wavelength of the whistler mode radiation,

$$\lambda \cong (V_e/f) \cos \theta_{\text{res}} \quad (11)$$

which for the nominal parameters has a value of about 20 m. This wavelength is greater than the path length, which completely invalidates any mechanism involving exponential growth. Even if that were not the case, for typical whistler mode group velocities of 10^7 m/s the amount of time the wave spends in the beam is so short, only about 10^{-6} s, that unreasonably high growth rates ($\gamma > \omega_c \cong 10^6 \text{ s}^{-1}$) would be required to generate the radiation. No whistler mode instability is known that can produce such large growth rates from realistic electron distribution functions. These same conclusions were also reached by Jones and Kellogg [1973] in their paper addressing the growth rates of whistler mode radiation from artificially created electron beams.

Next we consider mechanisms involving the intermediate generation of electrostatic waves in the beam. Any density perturbation or bunch created by an electrostatic wave in the beam is capable of emitting coherent Cerenkov radiation. The radiated power from this process will have a frequency spectrum similar to that of a single radiating electron; however,

the wave power will be much greater, since the emitted power goes as N^2 , where N is the number of electrons in a bunch. Coherent Cerenkov radiation from a bunched beam has been considered previously by Bell [1968].

Beam-plasma instabilities are known to be capable of creating intense electrostatic waves and density perturbations in the beam. We estimate the number of coherently bunched electrons required to account for the observed whistler mode radiation. The total power emitted from the electron bunches in the beam is $(dP/df)_{\text{total}} = (dP/df)_e (\Delta N)^2 \alpha$, where $(dP/df)_e$ is the power radiated by each electron, ΔN is the typical number of electrons in a bunch, and α is the number of bunches in the 200-m segment of the beam. Beam-plasma instabilities are known to create an electrostatic wave near the local electron plasma frequency (3 MHz). Such an emission is, in fact, observed near 3 MHz [see Gurnett et al., 1986]. The corresponding wavelength is $V_{\text{be}}/f_p \approx 7$ m, which is assumed to be the approximate length of each bunch. This wavelength can then be used to calculate α , the number of bunches in the first 200 m of the beam. This number is $\alpha \approx 29$. Since the radiated power from the 200-m beam segment, $(dP/df)_{\text{total}}$, is about 10^{-9} W/Hz, $(dP/df)_e$ is about 10^{-29} W/Hz, and $\alpha \approx 29$, each bunch must contain about $\Delta N = 2 \times 10^9$ electrons in order to account for the observed radiated power.

Next we estimate the required electric field strength for the electrostatic wave in the beam that forms the bunches. Assuming that the beam diameter is about 2 cyclotron radii, we can estimate the electron number density in the bunch using the formula,

$$\Delta n = \Delta N / \pi r_c^2 \Delta L \quad (12)$$

where ΔL is the bunch length and r_c is the cyclotron radius (2 to 3 m). The required number density is found to be about $\Delta n = 1 \times 10^7$ electrons/m³. Note that the fractional density perturbation in the beam $\Delta n/n_0$ is only about 0.01; thus a relatively small perturbation can account for the measured whistler mode power. Poisson's equation can be used to determine the magnitude of the self-consistent electric field needed to generate this density perturbation:

$$\Delta E / \Delta L = e \Delta n / \epsilon_0 \quad (13)$$

From (13) we estimate that an electric field of the order of 1–2 V/m is needed to create the required coherence in the beam electrons.

Although the PDP did not fly directly through the beam during free flight, when the PDP was on the remote manipulator arm, it did provide measurements in the beam. During these times, intense field-aligned electric field signals near f_{pe} were measured with amplitudes greater than 0.3 V/m, sufficiently large to saturate the receiver. This value is within a factor of 10 of the required amplitudes needed for radiative coherence of the beam electrons. The good agreement between the calculated and measured electrostatic field strengths strongly suggests that electron bunches generated by a beam-plasma instability can account for the observed whistler mode power.

CONCLUSIONS

Like auroral hiss the whistler mode radiation from the SL 2 electron beam was found to be propagating near the resonance cone in the same direction as the beam. This conclusion was reached by comparing the measured and modeled electric field polarizations in the PDP spin plane. The total whistler

mode power radiated by the beam between the shuttle and the PDP was estimated to be 1.6 mW. This represents a conversion of about 3.2×10^{-5} of the beam power to whistler mode radiation in a path length of 200 m. The linear emissivity was also observed to decrease with increasing distance along the beam, thereby indicating that most of the whistler mode radiation is generated relatively close to the source of the beam.

The mechanism that best explains the radiated power and frequency range of the whistler mode radiation is Cerenkov radiation from coherently radiating electron bunches in the beam. The bunches are most likely created by an electrostatic instability in the beam. The estimated electric field amplitudes required to create the bunching are consistent with the field strength of electrostatic noise measured in the beam.

Future work includes calculating the radiated power from a model electron beam obtained from a particle simulation. The calculated power can then be compared to the measured whistler mode power to confirm that coherent radiation from electron bunches generates the signal.

Acknowledgments. We are grateful to Bill Kurth and John Steinberg for their helpful comments concerning this work. We would also like to thank Terry Averkamp for his valuable input on data analysis and John Birkbeck for a fine drafting job. Part of this research was funded by NASA Graduate Student Researchers Training grant NGT-50034. The research at the University of Iowa was also supported by NASA through contract NAS8-32807 and grants NGL 16-001-002 and NGL 16-001-043 and by the Office of Naval Research through contract N00014-85-K-0404. The research at Stanford University was supported by NASA through grant NAGW-235.

The Editor thanks R. H. Holzworth and P. L. Pritchett for their assistance in evaluating this paper.

REFERENCES

- Beghin, C., J. P. Lebreton, B. N. Maehlum, J. Troim, P. Ingsoy, and J. L. Michau, Phenomena induced by charged particle beams, *Science*, **225**, 188, 1984.
- Bell, T. F., Artificial production of VLF hiss, *J. Geophys. Res.*, **73**, 4409, 1968.
- Cartwright, D. G., and P. J. Kellogg, Observations of radiation from an electron beam artificially injected into the ionosphere, *J. Geophys. Res.*, **79**, 1439, 1974.
- Dechambre, M., Yu. V. Kushnerevsky, J. Lavergnat, R. Pellat, S. A. Pulinet, and V. V. Seleger, Waves observed by the ARAKS experiment: The whistler mode, *Ann. Geophys.*, **36**, 351, 1980.
- Gurnett, D. A., A satellite study of VLF hiss, *J. Geophys. Res.*, **71**, 5599, 1966.
- Gurnett, D. A., and L. A. Frank, VLF hiss and related plasma observations in the polar magnetosphere, *J. Geophys. Res.*, **77**, 172, 1972.
- Gurnett, D. A., S. D. Shawhan, and R. R. Shaw, Auroral hiss, Z mode radiation, and auroral kilometric radiation in the polar magnetosphere: DE 1 observations, *J. Geophys. Res.*, **88**, 329, 1983.
- Gurnett, D. A., W. S. Kurth, J. T. Steinberg, P. M. Banks, R. I. Bush, and W. J. Raitt, Whistler-mode radiation from the Spacelab-2 electron beam, *Geophys. Res. Lett.*, **13**, 225, 1986.
- Hartz, T. R., Radio noise levels within and above the ionosphere, *Proc. IEEE*, **57**, 1042, 1969.
- Inan, U. S., M. Pon, P. M. Banks, P. R. Williamson, W. J. Raitt, and S. D. Shawhan, Modulated beam injection from the space shuttle during magnetic conjunction of STS 3 with the DE 1 satellite, *Radio Sci.*, **19**, 487, 1984.
- James, H. G., VLF saucers, *J. Geophys. Res.*, **81**, 501–514, 1976.
- Jones, T. W., and P. J. Kellogg, Plasma waves artificially induced in the ionosphere, *J. Geophys. Res.*, **78**, 2166, 1973.
- Jorgensen, T. S., Interpretation of auroral hiss measured on OGO 2 and at Byrd Station in terms of incoherent Cerenkov radiation, *J. Geophys. Res.*, **73**, 1055, 1968.
- Kellogg, P. J., D. G. Cartwright, R. A. Hendrickson, S. J. Monson, and J. R. Winckler, The University of Minnesota Electron Echo experiment, *Space Res.*, **XVI**, 589, 1976.
- Laaspere, T., and R. A. Hoffman, New results on the correlation between low-energy electrons and auroral hiss, *J. Geophys. Res.*, **81**, 524, 1976.

- Lin, C. S., J. L. Burch, S. D. Shawhan, and D. A. Gurnett, Correlation of auroral hiss and upward electron beams near the polar cusp, *J. Geophys. Res.*, **89**, 925, 1984.
- Maggs, J. E., Coherent generation of VLF hiss, *J. Geophys. Res.*, **81**, 1707, 1976.
- Mansfield, V. N., Radiation from a charged particle spiraling in a cold magnetoplasma, *Astrophys. J.*, **147**, 672, 1967.
- Monson, S. J., P. J. Kellogg, and D. G. Cartwright, Whistler mode plasma waves observed on Electron Echo 2, *J. Geophys. Res.*, **81**, 2193, 1976.
- Mosier, S. R., and D. A. Gurnett, VLF measurements of the Poynting flux along the geomagnetic field with Injun 5 satellite, *J. Geophys. Res.*, **74**, 5675, 1969.
- Mosier, S. R., and D. A. Gurnett, Theory of the Injun 5 very low frequency Poynting flux measurements, *J. Geophys. Res.*, **76**, 972, 1971.
- Shawhan, S. D., G. B. Murphy, P. M. Banks, P. R. Williamson, and W. J. Raitt, Wave emissions from dc and modulated electron beams on STS 3, *Radio Sci.*, **19**(2), 471, 1984.
- Smith, R. L., VLF observations of auroral beams as sources of a class of emissions, *Nature*, **224**, 351, 1969.
- Stix, T. H., *The Theory of Plasma Waves*, McGraw-Hill, New York, 1962.
- Taylor, W. W. L., and S. D. Shawhan, A test of incoherent Cerenkov radiation for VLF hiss and other magnetospheric emissions, *J. Geophys. Res.*, **79**, 105, 1974.
- Winckler, J. R., The application of artificial electron beams to magnetospheric research, *Rev. Geophys.*, **18**(13), 659, 1980.
- P. M. Banks and R. I. Bush, STAR Laboratory, Stanford University, Stanford, CA 94305.
- W. M. Farrell and D. A. Gurnett, Department of Physics and Astronomy, University of Iowa, Iowa City, IA 52242.
- W. J. Raitt, Center for Atmospheric and Space Sciences, Utah State University, Logan, UT 84322.

(Received February 27, 1987;
revised July 23, 1987;
accepted September 2, 1987.)

U. of Iowa 87-24

DOUBLE PROBE POTENTIAL MEASUREMENTS
NEAR THE SPACELAB-2 ELECTRON BEAM

by

J. T. Steinberg¹, D. A. Gurnett¹

P. M. Banks², and W. J. Raitt³

July 1987

Revised April 1988

Submitted to Journal of Geophysical Research

¹Dept. of Physics and Astronomy, The University of Iowa, Iowa City, IA 52242

²STAR Laboratory, Stanford University, Stanford, CA 94305

³Center for Atmospheric and Space Sciences, Utah State University, Logan, UT 84322

I. ABSTRACT

As part of the Spacelab-2 mission the Plasma Diagnostics Package (PDP) was released from the shuttle as a free flying satellite. The PDP carried a quasi-static electric field instrument which made differential voltage measurements between 2 floating probes. At various times during the free flight, an electron beam was ejected from the shuttle. Large differential voltages between the double probes were recorded in association with the electron beam. However, analysis indicates that these large signals are probably not caused by ambient electric fields. Instead they can be explained by considering three effects: shadowing of the probes from streaming electrons by the PDP chassis, crossing of the PDP wake by the probes, and spatial gradients in the fluxes of energetic electrons reaching the probes. Plasma measurements on the PDP show that energetic electrons exist in a region 20m wide and up to at least 170 m downstream from the electron beam. At 80 or more meters downstream from the beam, the double probe measurements show that the energetic electron flux is opposite to the injection direction, as would be expected for a secondary returning electron beam produced by scattering of the primary electron beam.

I. INTRODUCTION

As part of the Spacelab-2 mission, a spacecraft called the Plasma Diagnostics Package (PDP) was released from the shuttle to survey the plasma environment around the orbiter. At various times, an electron beam was ejected from the shuttle so that the effects produced in the plasma might be studied. In this paper we report on efforts to measure the quasi-static electric fields in the plasma with the PDP, focusing on those times when the electron beam generator was operating. The PDP, a scientific instrument package containing 14 instruments, was designed and constructed at the University of Iowa, and is described by Shawhan et al. [1982]. The electron beam generator, flown as part of the Vehicle Charging and Potential (VCAP) experiment provided by Stanford University and Utah State University, is described by Banks et al. [1987]. The PDP and the electron beam generator were previously flown on the STS-3 flight [Shawhan et al., 1984].

Prior to the shuttle flights, a number of electron beam experiments were performed in plasma chambers and from rockets. Using the same PDP and the same electron beam generator later flown onboard Spacelab-2, quasi-static electric fields of the order of a few volts/m were measured within a few meters of the beam in a large plasma chamber at Johnson Space Flight Center [Shawhan, 1982]. Denig [1982]

questioned the reliability of these measurements because of the possibility of differential charging on the measuring probes, and because the fields seemed too large to be sustained in the given apparatus. Kellogg et al. [1982] also reported measuring fields of a few volts/m in a similar chamber test. Measurements of the quasi-static electric fields have also been reported in association with electron beams emitted from rockets in the ionosphere. In the Polar 5 experiment, fields of the order of 0.1 volts/m were detected over 100 meters away from the beam source [Jacobsen and Maynard, 1978]. During the Echo 6 experiment, Winckler and Erickson [1986] measured fields of the order of 0.2 volts/m at a distance of 40 meters from the flux tube on which the beam was expected to be centered. All the measurements mentioned here involved differential voltage measurements on floating probes. Considering the chamber and rocket experiments, we expected on the Spacelab-2 mission to detect fields on the order of 1 volt/m associated with the electron beam.

The Spacelab-2 mission was launched into a nearly circular orbit, of inclination 49.5° , at a nominal altitude of 325 km. The PDP was in free flight roughly 6 hours, during which the shuttle performed 2 complete fly-arounds of the PDP. During the fly-around the shuttle was maneuvered to regions upstream and downstream of the PDP. The fly-around included four magnetic conjunctions in which the shuttle was targeted to pass through the magnetic field line passing through the PDP. The electron beam generator was operated at various times throughout the free flight, both in a steady (DC) mode, and in a

pulsed mode. During several of these times large signals were detected by the quasi-static electric field instrument. The purpose of this paper is to describe the large signals associated with the electron beam firings and to determine the origin of these signals.

II. INSTRUMENTATION

The PDP quasi-static electric field instrument made potential measurements on two floating probes. These floating probes consisted of conducting spheres mounted on insulated booms on opposite sides of the spacecraft. The sphere-to-sphere separation was 3.89 meters, and the diameter of the spheres was 10.2 cm. A diagram of the PDP, showing the dimensions of the main chassis and the locations of spherical probes 1 and 2, is presented in Figure 1. Two types of measurements were made: the differential voltage, V_{diff} , between the two probes was measured at both a high gain and a low gain, and the average potential, V_{ave} , of the two probes relative to the PDP chassis was measured. The following relations describe the two measurements:

$$V_{\text{diff}} = V_2 - V_1$$

$$V_{\text{ave}} = (V_2 + V_1)/2$$

where V_1 and V_2 are respectively the potentials of sphere 1 and sphere 2 relative to the PDP chassis. Typically, the differential voltage divided by the antenna length is interpreted as a measurement of the electric field. The basic instrument parameters and dynamic ranges are given in Table 1. Since the floating potential of an object in a

plasma is dependent on the surface materials, it is also important to describe the surface properties of the spacecraft and spheres. The PDP chassis was covered with a teflon-coated fiberglass cloth which in turn was covered with an aluminum mesh to provide a uniform conducting surface. Potential measurements were referenced to the aluminum mesh. The spherical antenna probes were coated with a conducting graphite-epoxy paint.

After release from the shuttle, the PDP was made to spin by the action of an inertia wheel within the PDP. When spinning at its maximum rate, the spacecraft had a spin period of 13.1 seconds. The spin axis was oriented approximately perpendicular to the orbital plane. Thus, the spacecraft velocity vector lay approximately in the PDP spin plane.

The electron beam generator was mounted in the shuttle payload bay. A beam was produced as electrons emitted from a heated tungsten wire filament were accelerated through a 1 kilovolt potential. The generator operated at beam currents of either 50 ma or 100 ma, producing either a steady or a pulsed beam. The beam was pulsed at frequencies up to 800 kHz.

III. OBSERVATIONS

During most of the free flight, the V_{diff} signals were of the order of the induced potential due to the orbital motion of the spacecraft, $|(\vec{V} \times \vec{B}) \cdot \vec{L}|$, where \vec{V} is the spacecraft velocity and \vec{L} is a vector pointing from sphere 2 to sphere 1. These signals were typically 0.4 and 0.8 volts. The V_{ave} signal was usually between zero and a few volts positive. That is, the PDP normally floated at a slightly lower potential than the antenna probes. The V_{ave} signal also showed a periodic variation synchronous with the spacecraft spin period. The periodic variation was found to be related to the operation of the PDP Low Energy Proton and Electron Differential Energy Analyzer (Lepedea) [Tribble et al., 1987]. The Lepedea utilized a current collecting plate whose voltage jumped to +2 kilovolts every 1.6 seconds. The plate collected a large thermal electron current, and the PDP potential decreased by several volts, recovering to its initial value within 1.0 seconds. The V_{ave} signal was spin modulated because the degree of charging of the spacecraft was less when the Lepedea aperture faced the spacecraft wake, than when the aperture faced the ram direction. For the V_{diff} measurement, a large negative potential on the PDP was equivalent to a large positive common mode signal on the probes. Because of limitations in the common mode rejection, the V_{diff} signal was disturbed whenever the

PDP potential exceeded several volts negative. The magnitude of the instrument output due to the common mode signal was generally much less than $|(\nabla \times \mathbf{B}) \cdot \mathbf{L}|$. Thus, the common mode signal was large enough to make the interpretation of the measurements difficult when the difference between the V_{diff} and $|(\nabla \times \mathbf{B}) \cdot \mathbf{L}|$ was small. However, for V_{diff} signals larger than $|(\nabla \times \mathbf{B}) \cdot \mathbf{L}|$, the common mode rejection problem was not important.

At five times during the free flight when the electron beam generator was operating, V_{diff} signals were recorded that were significantly larger than $|(\nabla \times \mathbf{B}) \cdot \mathbf{L}|$. The signals for these events are shown in Figure 2, and the events are numbered 1 through 5. At no other times during the PDP free flight were signals this large recorded. Of these 5 events, the beam was operated in a steady mode for 3 events, and in a pulsed mode for 2 events. The beam injection pitch angle varied widely among these events. Table 2 lists the beam operation mode, injection pitch angle, beam current, and several other important parameters regarding these 5 events.

The basic periodicity of the V_{diff} signals in Figure 2 is due to the spinning of the spacecraft. In addition to the overall variation at the spin period, the signals have a number of unusual features. During event 1 the instrument saturates. Thus, the difference voltage on the probes is greater than 8 volts, which corresponds to an inferred electric field strength in the spin plane greater than 2 volts/m. Event 2 has a "spiky" character, and events 3, 4, and 5 all show a "double peak" character. At the end of event 3 (around 00:49),

there is an apparent higher frequency structure to the signal. This structure is associated with the pulsing of the electron beam. Note that as long as the beam pulse frequency is much greater than the V_{diff} sample rate, then no effect of the pulsing should be apparent in the V_{diff} signal. Such is the case for event 2, where the beam was pulsed at 1.2 kHz. However, during event 3 the beam pulse frequency was lowered in steps from 600 Hz down to frequencies near the V_{diff} sample frequency of 20 Hz. The apparent higher frequency structure is the result of a beating effect that occurs between the beam pulse rate and the V_{diff} sample rate.

In order to understand the origin of the large signals, the phase angle of the spinning PDP was investigated. Arrows are plotted in Figure 2 at the top of the graph to indicate the times when the electric antenna was aligned with the spacecraft velocity vector. Recall that the velocity vector lay approximately in the PDP spin plane. Arrows are plotted in Figure 2 at the bottom of the graph to indicate times when the antenna was aligned with the magnetic field projected onto the spin plane. In general, the magnetic field vector did not lie exactly in the spin plane, but made an angle of between 10° and 24° with the spin plane. The angle for each event is given in Table 2. Inspection of Figure 2 reveals that for cases 2, 3, 4, and 5 a voltage peak occurs when the antenna is aligned with the spacecraft velocity vector, and for cases 3, 4, and 5 a second peak occurs when the antenna is aligned parallel to the magnetic field projected onto the spin plane.

Figure 3 shows the trajectory of the PDP in a plane perpendicular to the magnetic field during all times that the electron beam generator was operating. The direction V_{\perp} indicated in the figure is along the component of the velocity perpendicular to \vec{B} . The origin represents the position of the magnetic field line on which the electron beam should be centered. The beam is assumed to lie on a magnetic field line which intersects the electron beam generator, and the field is determined from a multipole model of the Earth's magnetic field. Although shown in Figure 3 only as a point, the beam will have a cyclotron motion about the magnetic field. The injection pitch angles are listed in Table 2. The pitch angles vary over a large range, but are relatively small (less than 10°) for events 1 and 2, and large (greater than 30°) for events 3, 4 and 5. The beam also has some spreading due to beam divergence, space charge repulsion of the beam electrons, and beam instability. The actual width of the beam is unknown, however previous beam experiments indicate that the cyclotron radius of a beam electron with pitch angle 90° is a reasonable approximation for the beam radius. For a 1 keV electron in a magnetic field of 0.25 - 0.5 gauss, the cyclotron radius is approximately 2-4 meters.

The trajectories during the 5 large events are shown in Figure 3 as solid segments, and the trajectories during times when the beam generator was operating, but the measured differential voltage was small (i.e. less than $|(\vec{V} \times \vec{B}) \cdot \vec{L}|$), are shown by the dashed lines. During events 1 and 2, the length of time the electron beam generator

was turned on was longer than the length of time large signals were recorded, indicating that the spatial region over which large signals occur is limited. For each of events 3, 4, and 5, large signals were recorded for the entire period the beam generator was on. Note that events 1 through 5 occur at times when the PDP was in a region downstream of the flux tube carrying the electron beam. Except briefly during event 1, the perpendicular distance from the PDP to the flux tube of the electron beam was much greater than the 2 to 4 meter predicted beam radius, so that the PDP was well outside of the region of the primary beam. Events 1 and 2 occur when the PDP was closest to the flux tube of the electron beam, and are the largest in magnitude.

The average potential measurements for events 1 through 5 are shown in Figure 4. The largest changes in the average potential measurements associated with the electron beam are seen during events 1 and 2, where the average potential of the probes goes from positive values of +2 to +4 volts to negative values of -2 to -4 volts. The spin period variation of the signal discussed above can be seen in the graphs for events 1 and 2 during the times before and after the large negative excursions of the signal. During events 3, 4, and 5, the average potential does not change by a large amount, but the smooth spin period variation of the signal is disrupted.

IV. INTERPRETATION

Because the determination of the quasi-static electric field with the PDP is based on measurements of the differential voltage between two floating probes, the results can be affected by energetic beam electrons striking the probes. It is easily shown that a small flux of energetic electrons may alter the floating potential of the probes by a large amount [Fahleson, 1967]. Arnoldy and Winckler [1981] reported a population of energetic electrons in the region around an electron beam, causing the floating potential of the Echo 3 rocket to become several volts negative. A similar observation was made on Echo 6 [Winckler et al. 1984]. Thus we might expect to find that the PDP potential is affected by energetic electrons around the beam. In fact, during each of events 1 through 5 discussed here, the Lepedea on the PDP detected energetic electrons at energies nearly up to the beam energy [W. R. Paterson, personal communication, 1987]. Further, data from the PDP Langmuir probe seems to indicate that the PDP charged to at least -4.3 volts during event 2, and to at least -7.6 volts during event 1 [A. C. Tribble, personal communication, 1987]. Therefore there is reason to suspect that the probes also charged. If the charging is different for the two probes, then V_{diff}/L cannot be safely interpreted as a good measure of the electric field.

To determine the possible effect of energetic electrons on our

measurements, we perform a simple calculation of the floating potential. This is done by considering the balance of currents to the object of concern (see, for example, Kasha, 1969). The possible current sources are: 1) thermal (background) electrons, 2) thermal (background) ions swept up by the motion of the spacecraft, 3) energetic electrons (energies $\gg kT_e$), 4) energetic ions (energies $\gg 5.0$ eV, the ramming energy), 5) secondary electron emission, and 6) photoelectron emission. Measurements made with the Lepedea indicate that the current from energetic ions is much less than that from the ramming ions [W. R. Paterson, personal communication, 1987], so this current can be neglected. The maximum secondary electron yields for aluminum (PDP surface material) and graphite (probe surface material), are 1.0 secondaries/primary for 300 eV primaries [Whetten, 1985]. Thus, secondary production would reduce the negative charging effect of the energetic electrons by some fraction. Photoemission would also reduce the negative charging. But since we wish to obtain a worst case estimate of the spacecraft potential, we neglect both secondary production and photoemission. We consider then the following current balance equation for an object at potential $V < 0$:

$$A_x n_e u_{sc} (1 - eV/E_i) - A_s n_e (kT_e/2\pi m_e)^{1/2} \exp(eV/kT_e) - A_s J_b = 0 \quad , \quad (1)$$

The first term in the above equation includes the ion current due to the sweeping up of the ionospheric ions by the spacecraft motion plus some effect of the attraction of ions to the negatively charged

object. The second term is the electron current from the thermal electrons. The third term is the current to the object due to energetic electrons. The variables in Equation 1 are identified in Table 3.

Using the representative parameters given in Table 3, Equation 1 was solved numerically for various values of J_b and n_e . The floating potential was determined from Equation 1 for both the spherical probes and for the PDP chassis. The current collecting area of the PDP was taken to be its surface area. Unfortunately, the current collecting properties of the spacecraft body are complicated, and this estimate is to be taken only as a rough approximation. The solution for the floating potential as a function of the energetic electron current density is plotted in Figure 5. Measurements from the Lepede during beam event 1 indicate that J_b was as high as 4×10^{-4} amp/m² [W. R. Paterson, personal communication, 1987]. The Langmuir probe measurements indicate that during event 1, n_e was of the order of 1×10^{11} m⁻³ [A. C. Tribble, personal communication, 1987]. From Figure 5 one can see that under the conditions of event 1 the PDP floating potential could easily be lower than -10 volts. This is consistent with the Langmuir probe observation mentioned previously that the PDP charged to at least -7.6 volts during event 1. More importantly for the V_{diff} measurements, under the conditions of event 1 differences in J_b on the order of 10^{-5} amp/m² lead to floating potential differences on the probes of several volts. During events 2, 3, 4, and 5 the Langmuir probe measurements indicate that n_e was on the order of

$1 \times 10^{10} \text{ m}^{-3}$ [A. C. Tribble personal communication, 1987]. For this lower ambient density, Figure 5 shows that differences in J_b on the order of 10^{-6} amp/m^2 lead to floating potential differences on the probes of several volts. Figure 5 also shows that for a fixed value of J_b , small differences in the ambient plasma density lead to floating potential differences of several volts.

Using the differential voltage between the probes to infer electric field values can produce erroneous results if the two antenna probes receive different amounts of current from any of the various current sources. Current differences can occur if one of the probes is shielded by the PDP chassis from a current source, or if the plasma environment is nonuniform over the length of the antenna. During events 2, 3, 4 and 5 the peaks in V_{diff} are associated with specific orientations of the antenna with respect to the velocity and the magnetic field, and therefore can be primarily attributed to shadowing effects. Shadowing effects of this type were observed by Winckler et al. [1984] during the Echo 6 experiment. In that experiment, large signals at the payload spin frequency were attributed to shadowing of one probe from a magnetic field aligned plasma flow. At the time, the electric probes were stowed in the payload body. During events 3, 4, and 5 the "double peak" character of the signals indicates that two different shadowing effects are occurring. These two effects are discussed separately below.

For events 3, 4, and 5 one finds a voltage peak, and therefore a probable shadowing of one probe, when the antenna is aligned with the

magnetic field projected onto the spin plane. Because the local ion larmor radius is much larger than the PDP, a shadowing along field lines suggests a shadowing of electrons. We explain the signal peak in the following manner. For events 3, 4, and 5 the beam was injected in the direction of \vec{B} . At the time when the antenna was aligned with \vec{B} in the spin plane, the probe on the boom pointing in the direction of \vec{B} was at a lower potential than the probe on the boom pointing in the direction of $-\vec{B}$. Thus, we conclude that some energetic electrons are moving in the direction of $-\vec{B}$, and one probe is shielded from them. So, for the three events when the PDP is 80 or more meters from the beam, the energetic electrons have a preferred direction, which is opposite to the injection direction. This explanation is consistent with the report by the Lepedea group of a secondary electron beam in the shuttle wake [Frank et al., 1987]. The shadowing of one probe from electrons moving down the field lines is pictured in Figure 6a. Consideration of Figure 6b. shows that if the angle θ of the magnetic field to the spacecraft spin plane is too large, then shadowing along the field lines will not occur. The range of angles where shadowing is possible is $\theta < 20.4^\circ$. Referring to the values of θ listed in Table 2, one finds that shadowing along field lines is possible for events 2, 3, 4, and 5.

The energetic electrons moving down the field lines and charging the probes in events 3, 4, and 5, may be attributed to reflection of beam electrons by collisions with atmospheric neutrals, or to a beam plasma interaction. First, consider reflection of electrons by

collisions. Given the distance of the PDP downstream from the beam for these events, and the spacecraft velocity, one can determine the time of flight for the energetic electrons to be around 10 to 20 msec. For 1 keV electrons, the corresponding total distance traveled is about 200 to 400 km. For comparison, the mean free path of electrons for collisions with oxygen atoms can be roughly estimated by $\lambda = 1/(n_n \sigma)$, where n_n is the atomic oxygen density and σ is the collision cross section. We use a value for σ of $7 \times 10^{-16} \text{ cm}^2$, the total scattering cross section for 100 eV electrons measured by Sunshine et al. [1967]. At an altitude of 300 km, n_n is approximately 10^8 cm^{-3} [Johnson, 1965], which yields a mean free path $\lambda \approx 140 \text{ km}$. Because the atomic oxygen density is larger at lower altitudes, λ will become shorter at lower altitudes. Thus, for events 1 and 3 where the beam was injected downward, it is quite reasonable that electrons reflected by collisions with neutrals could reach the PDP. Since the atomic oxygen density is smaller at higher altitudes, λ becomes longer at higher altitudes. At an altitude of 400 km, n_n is approximately 10^7 cm^{-3} , which yields $\lambda \approx 1400 \text{ km}$. So for electrons injected upward, the effective mean free path will be $\gg 1400 \text{ km}$. For events 2, 4, and 5 where the beam was injected upward, it may seem unlikely that the PDP could be affected by reflected electrons. However, it is not necessary that most of the beam particles be reflected. The solution of Equation 1 showed that the measured signals are explained by differential energetic electron currents of the order of 10^{-6} amp/m^2 , and this current can result from only a small percentage of beam

particles being reflected. An alternative explanation for the presence of energetic electrons is considered by Wilhelm et al. [1985]. In the SCEX experiment, Wilhelm et al. measured energetic electrons in the region downstream of an electron beam. They discuss the possibility that the energetic electrons are the product of a beam plasma interaction. Both explanations are possible, and without a further more detailed analysis we cannot say which is correct.

A different shadowing effect occurs for events 2, 3, 4 and 5 when the antenna is aligned with the velocity vector. Because the local ion thermal speed is less than the spacecraft velocity, ions are swept up by the spacecraft motion. The electron thermal velocity is much greater than spacecraft velocity, so the electrons are not swept up. However, because quasineutrality must be maintained, both the ion and the electron densities are reduced behind the spacecraft, forming a plasma wake. The sweeping of the antenna through the wake as the PDP spins is indicated in Figure 6a. Because the velocity vector lies in the PDP spin plane as shown, the antenna always passes through the wake region. In order to estimate the plasma density in the wake at the location of the antenna probe, we use the self-similar solution for the expansion of a plasma into a vacuum as shown by Samir et al. [1983] and Singh and Schunk [1982]. In the standard treatment one assumes initially a plasma of density N_0 for the region $x < 0$, and a vacuum for the region $x > 0$. At time $t = 0$ the plasma is allowed to expand into the vacuum region. The solution for the density at later times is given by

$$N = N_0 \exp \left[- \left(\frac{x}{S_0 t} + 1 \right) \right] \quad (2)$$

where S_0 is the ion sound speed. To obtain an estimate of the density at the probe when the probe is in the wake, we use Equation 2 and take for x the radius of the PDP, $x = 0.53$ m, and for t the time for the ionospheric plasma to flow a distance of half of the antenna length relative to the PDP, $t = 2.5 \times 10^{-4}$ sec. Assuming an electron temperature of 0.2 eV, and assuming ions are atomic oxygen, the ion sound speed is estimated to be about 1.4×10^3 m/s, yielding a wake density

$$N = 0.08 N_0 \quad (3)$$

This solution corresponds to the expansion of the plasma in one direction only. The wake fills in from all directions, so we expect the density in the wake at the location of the antenna probe to be greater than $0.08 N_0$, but still significantly less than N_0 . Examination of Figure 5 shows that if both probes receive the same amount of energetic electron current, but one probe is in the wake where the density is lower, then the probe in the wake will be several volts lower in potential than the probe upstream. This explanation is consistent with the observed signals.

Event 1 does not lend itself to explanation in terms of probe

shadowing, as the other events do. The angle θ between the magnetic field and the spin plane (see Table 2) is greater than 20.4° , so that probes are not shadowed along field lines. Figure 2 shows that the peaks in voltage are not consistently centered about the times the antenna is aligned with the velocity vector or the magnetic field. The peaks are also broader than expected if due only to a shielding effect. Thus, the signal is due either to a gradient in the fluxes of energetic electrons reaching the probes, or both a gradient in fluxes of energetic electrons and an electric field. We cannot rule out the possibility that we have measured the electric field. However, because the entire region where the large electric field signals and the energetic electrons are observed is only 20 meters wide (refer to Figure 3), gradients over the antenna length are expected. As will be discussed below, we consider it likely that the large V_{diff} signal in event 1 is caused mainly by a gradient in energetic electron fluxes.

In order to investigate the possible interpretation of the large signals associated with event 1, the V_{diff} signals were analyzed as follows. Due to the spacecraft rotation, the V_{diff} signal varies sinusoidally with the PDP spin period of 13.1 seconds, and we assume that V_{diff} attains peak value when the antenna is aligned with the direction of strongest gradient in the energetic electrons. The direction and relative magnitude of the gradient is then obtained by using a least squares method to fit a 13.1 second segment of the V_{diff} signal to the function

$$F(t) = F_1 + F_2 \cos(2\pi t/T - \Phi) \quad (4)$$

where $T = 13.1$ seconds, and F_1 , F_2 , and Φ are parameters determined by the fit procedure. If the signal is interpreted as a measure of the gradient of the energetic electron flux, then the constant F_2 gives the magnitude of the gradient and Φ gives the direction of the gradient in the spin plane. We do not expect the energetic electron flux to vary much along the direction of \vec{B} , so we assume that the gradient lies in the plane perpendicular to \vec{B} and that we have measured the component of the gradient projected onto the PDP spin plane. Using this assumption, the magnitude of the gradient vector in the plane perpendicular to \vec{B} was determined. In order to establish a "goodness of fit" of the curve fit performed for each measurement, the following test variable was calculated:

$$X = [\Sigma(F(t_i) - x_i)^2 / (N - 3)]^{1/2} / F_2 \quad (5)$$

where x_i is the V_{diff} signal at time t_i , and N is the number of sample points used in one curve fit. Measurements were retained if $X < 0.25$, corresponding roughly to 25% error.

The vectors obtained by the above analysis are shown in Figure 7. The vectors are plotted along the trajectory of the PDP relative to the electron beam where the coordinate directions are the same as in Figure 3. The V_{diff} signals first becomes larger than $|(\nabla \times \vec{B}) \cdot \vec{L}|$, and the gradient in the energetic electron flux first becomes significant,

when the PDP is about 10 meters away from a line extending directly downstream from the center of the beam. The V_{diff} signal, and thus the gradient in the electron flux, become larger as the PDP gets closer to this line. The gradient vectors tend to point toward the line. The indicated picture is that of a region of energetic electrons downstream from the primary electron beam. The region is not homogeneous but rather the electron flux is peaked along the line extending directly downstream from the primary beam.

The presence of a gradient in energetic electron flux can account for the large magnitude (larger than 8 volts) of the V_{diff} signals during event 1. If the magnitude of the gradient in J_b is estimated from the Lepedea measurements, then the V_{diff} signal that would result from such a gradient can be estimated. As stated previously, the Lepedea measured a peak value of J_b of about 4×10^{-4} amp/m². We assume that the flux of energetic electrons is peaked on a line extending directly downstream from the center of the beam, and is symmetric about that line. Since the region where large signals are detected is about 20 meters wide, the spatial gradient $\Delta J_b / \Delta x$ is approximately $(4 \times 10^{-4} \text{ amp/m}^2) / (10\text{m}) = 4 \times 10^{-5}$ amp/m. The resulting V_{diff} can be estimated by:

$$V_{diff} = (\Delta J_b / \Delta x) (\Delta V / \Delta J_b) (L \sin \theta) \quad (6)$$

where the quantity $\Delta V / \Delta J_b$ must be determined from Figure 5, L is the antenna length, and θ is the angle of \vec{B} to the spin plane. For $n_e =$

$1 \times 10^{11} \text{ m}^{-3}$ and $J_b > 4 \times 10^{-5} \text{ amp/m}^2$, $\Delta V / \Delta J_b$ is $-1.6 \times 10^5 \text{ volts/amp/m}^2$. The antenna length is 3.89m (see Table 1) and θ is about 23° (see Table 2). Using equation 4 with the given values, we obtain $V_{\text{diff}} \approx 9.7 \text{ volts}$. Thus, a gradient in the energetic electron flux of the magnitude indicated by the Lepedea measurements could easily produce the V_{diff} signals recorded during event 1.

Analysis of all 5 events suggests that energetic electrons are found in a region about 20 meters wide extending up to 170 meters downstream from the injected electron beam. Consideration of event 1 indicates that very close to the beam, there is a large spatial gradient in the energetic electron flux: the flux increases as one approaches the line extending directly downstream from the center of the beam. We expect that the energetic electron flux is symmetric about this line. For events 3, 4, and 5, in which the PDP was 80 or more meters away from the beam, the signals are explained by the presence of energetic electrons having a preferential direction of motion along the magnetic field line, but in a direction opposite to the beam injection.

Although the main features of the V_{diff} signals during events 1 through 5 are understood in terms of the discussion given above, some features remain unexplained. For example, the voltage peaks during event 4 are bumps on a signal that is otherwise sinusoidal. The peaks in event 4 are explained by alignment of the antenna with the magnetic field or with the velocity vector in the presence of energetic electrons. However, the V_{diff} signal for event 4 shown in Figure 2

would also provide a reasonably good fit to the function in Equation 4. Yet, since the shadowing effects are apparent in the measurements, a fit of the signal to Equation 4 would be difficult to interpret. It is not clear why event 4 has a more sinusoidal character than events 3 or 5. Similarly, the large peaks in the signal during event 2 can be attributed to alignment of the antenna with the velocity vector in the presence of energetic electrons, but the signal remains $> |(\vec{V} \times \vec{B}) \cdot \vec{L}|$ when the probes are not in the spacecraft wake.

Finally, we consider the average potential measurements. The measurements show that during periods of no beam operation, the average probe floating potential was several volts higher than the PDP chassis floating potential. The solution of Equation 1 (see Figure 5) indicates that the probes should float to a potential which is much less than a volt higher than the PDP potential. During events 1 and 2 the average probe floating potential became lower than the PDP potential. The solution of Equation 1 indicates that the average probe floating potential should always be higher than the PDP chassis potential. The reasons for these discrepancies are not clear. However, we speculate that explanation involves the properties of the PDP surface materials. In solving Equation 1 for the PDP potential, we assumed the PDP to have a uniformly conducting surface. However the potential of the aluminum mesh on the PDP surface may be influenced by the fiberglass cloth which underlies it. The fiberglass cloth may be charging to a different potential than the aluminum mesh. Katz and Davis [1987] analyze some of the effects of the fiberglass

cloth-aluminum mesh arrangement for the situation of the PDP attached to the shuttle. The ultimate effect on the mesh potential for the PDP in free flight is uncertain.

V. CONCLUSIONS

Our conclusion from this analysis is that the large signals measured by the PDP quasi-static electric field instrument during electron beam operation can primarily be attributed to three causes. First, at times when the electric antenna is aligned with the projection of the magnetic field into the spin plane, the spacecraft body shields one probe from energetic electrons moving along the magnetic field lines. The two probes receive different amounts of electron current, thereby causing large signals. Second, at times when energetic electrons are reaching both probes, but one probe is in the PDP wake, the wake produces asymmetries in the plasma density at the two probes, thereby causing large signals. Finally, spatial gradients in the energetic electron fluxes between the two antenna probes produce differences in the energetic electron current to the two probes, thereby causing large signals. When the electron beam generator is operating, energetic electrons are found in a region about 20 meters wide and up to 170 meters downstream from the injected electron beam. Because the region is so narrow, the spatial gradients are significant even over the length of the PDP antenna. For events 80 or more meters away from the beam, the electric field results are explained by the presence of energetic electrons having a preferential motion back down the magnetic field line on which the beam was

injected.

On the Spacelab-2 mission, it was demonstrated that with the shuttle it is possible to carry out detailed studies of electron beam effects under carefully controlled conditions. Thus, it should be possible to obtain a good map of the electric field near an electron beam. However, our experience indicates that double probe floating potential measurements are not reliable in the region near the beam. The floating potential of an object in a region with substantial fluxes of energetic electrons can be many times kT_e/e more negative than the plasma potential. A small difference in energetic electron current collected by each probe of a double probe system can then lead to differential voltages much higher than those due to any electric field in the plasma. Reliable potential measurements probably will require biased probes, such as described by Fahleson [1965], or emissive probes such as described by Bettinger [1965]. These active potential measurements are not as sensitive to energetic electrons. An example of a biased probe system is found on the ISEE-1 spacecraft [Mozer et al., 1978]. In general though, active potential measurements have not been widely used because of the appealing simplicity of floating potential measurements. However, for future spacecraft electron beam experiments, active instead of passive potential measurements will probably have to be considered.

ACKNOWLEDGMENTS

The authors thank Dr. Louis A. Frank and William R. Paterson for the use of the Lepedea measurements, and for their help. We thank Dr. Nicola D'Angelo for use of the Langmuir probe measurements. We also acknowledge the useful discussions with Rock Bush, William M. Farrell, Dr. Karl Lonngren, Gerald B. Murphy, Jolene S. Pickett and Alan C. Tribble. This research was supported by NASA through contract NAS8-32807 with Marshall Space Flight Center, contract NAG3-449 with the Lewis Research Center, and grant NGL 16-001-043 with NASA Headquarters.

REFERENCES

- Arnoldy, Roger L., and John R. Winckler, The hot plasma environment and floating potentials of an electron beam-emitting rocket in the ionosphere, J. Geophysical Research, 86, 575-584, 1981.
- Banks, P. M., W. J. Raitt, A. B. White, R. I. Bush, and P. R. Williamson, Results from the Vehicle Charging and Potential Experiment on STS-3, J. Spacecraft and Rockets, 28, 138-149, 1987.
- Bettinger, Richard T., An in situ probe system for measurement of ionospheric parameters, in Interactions of Space Vehicles With an Ionized Atmosphere, ed. S. F. Singer, 163-270, Pergamon Press, New York, 1965.
- Denig, W. F., Wave and particle observations associated with the beam plasma discharge in a space simulation chamber, Ph.D. Thesis, Utah State University, 1982.
- Fahleson, U., Theory of electric field measurements conducted in the magnetosphere with electric probes, Space Science Reviews, 7, 238-262, 1967.
- Frank, L. A., D. A. Gurnett, M. Ashour-Abdalla, W. R. Paterson, W. S. Kurth, N. Omid, P. M. Banks, and W. J. Raitt, The secondary electron beams and plasma waves associated with electron beam injection in space (abstract), Bulletin American Physical

Society, 32, 1823, 1987.

Jacobsen, T. A., and N. C. Maynard, Polar 5 - An electron acceleration experiment within an aurora. 3. Evidence for significant spacecraft charging by an electron accelerator at ionospheric altitude, Planet. Space Sci., 28, 291-307, 1978.

Johnson, Francis S., Structure of the Upper Atmosphere, in Satellite Environment Handbook, ed. by Francis S. Johnson, 3-20, Stanford University Press, Stanford, California, 1965.

Kasha, Michael A., The Ionosphere and Its Interaction With Satellites, Gordon and Breach, Science Publishers, New York, 1969.

Katz, I., and V. A. Davis, Ram ion scattering caused by space shuttle $\nabla \times \mathbf{B}$ induced differential charging, J. Geophys. Res., 92, 8787-8791, 1987.

Kellogg, P. J., H. R. Anderson, W. Bernstein, T. J. Hallinan, R. H. Holzworth, R. J. Jost, H. Leinbach, and E. P. Szuszczewicz, Laboratory simulation of injection particle beams in the ionosphere, in Artificial Particle Beams in Space Plasma Studies, ed. by B. Grandel, pg. 289, Plenum Press, New York, 1982.

Mozer, F. S., R. B. Torbert, U. V. Fablesen, C. G. Falthammer, A. Gonfalone, and A. Pedersen, Measurements of quasistatic and low-frequency electric fields with spherical double probes on the ISEE-1 spacecraft, IEEE Trans. Geosci. Elect., GE-16, 258-261, 1978.

Samir, U., K. H. Wright, Jr., and N. H. Stone, The expansion of a plasma into a vacuum: Basic phenomena and processes and

applications to space plasma physics, Rev. Geophys. and Space Phys., 21, 1631, 1983.

Shawhan, S. D., Description of the plasma diagnostics package (PDP) for the OSS-1 shuttle mission and JSC chamber test in conjunction with the fast pulse electron gun (FPEG), in Artificial Particle Beams In Space Studies, ed. by B. Grandel, 419-430, Plenum, N. York, 1982.

Shawhan, S. D., G. B. Murphy, P. M. Banks, P. R. Williamson and W. J. Raitt, Wave emissions from dc and modulated electron beams on STS-3, Radio Science, 19, 471-486, 1984.

Singh, N., and R. W. Schunk, Numerical calculations relevant to the initial expansion of the polar wind, J. Geophys. Res., 87, 9154, 1982.

Sunshine, Gabriel, Bertrand B. Aubrey, and Benjamin Bederson, Absolute measurements of total cross sections for the scattering of low-energy electrons by atomic and molecular oxygen, Phys. Rev., 154, 1-8, 1967.

Tribble, A. C., N. D'Angelo, G. Murphy, J. Pickett, and J. T. Steinberg, Exposed high-voltage source effect on the potential of an ionospheric satellite, accepted for publication by J. Spacecraft and Rockets, 1987.

Whetten, N. R., Secondary electron emission, in CRC Handbook of Chemistry and Physics, 65th Edition CRC Press, Inc., Boca Raton, Florida, 1985.

Wilhelm, Klaus, Willian Bernstein, Paul J. Kellog, and Brian A.

Whalen, Fast magnetospheric echoes of energetic electron beams,
J. Geophys. Res., 90, 491-504, 1985.

Winckler, J. R., J. E. Steffen; P. R. Malcolm, K. N. Erickson, Y.

Abe, and R. L. Swanson, Ion resonances and ELF wave production by
an electron beam injected into the ionosphere: Echo 6, J.
Geophys. Res., 89, 7565-7571, 1984.

Winckler, J. R., and K. N. Erickson, Plasma heating, plasma flow and
wave production around an electron beam injected into the
ionosphere, JPL Symposium on Space Technology Plasma Issues in
2001, ed. by Henry Garrett, Joan Feynman, Stephen Gabriel, pg.
295-306, JPL Publication 86-49, Oct. 1, 1986.

FIGURE CAPTIONS

- Figure 1. The Plasma Diagnostics Package. Dimensions are given in meters.
- Figure 2. Large differential voltage signals associated with times of the electron beam generator operation. Arrows at the top indicate times the antenna was aligned with the spacecraft velocity vector. Arrows at the bottom indicate times the antenna was aligned with the magnetic field.
- Figure 3. Dashed lines indicate the trajectory of PDP in the plane perpendicular to \vec{B} during times of electron beam generator operation. The trajectories for events 1 through 5 are shown as solid segments. The origin represents the position of the magnetic field line on which the beam lies. V_{\perp} is the component of velocity perpendicular to \vec{B} .
- Figure 4. Average potential measurements during times when large differential voltage signals were detected.
- Figure 5. Solution of Equation 1 using values from Table 3. Model of floating potential as a function of energetic electron current. Antenna probe and PDP chassis have

different floating potentials because of their different current collecting surface areas.

- Figure 6a. The PDP with the spin plane corresponding to the plane of the page. Energetic electrons move along the field lines. As the PDP spins, the antenna periodically becomes aligned with the magnetic field, and one probe is shielded from the electron flux. The probe also passes through the PDP wake.
- Figure 6b. The PDP viewed with the spin axis in the plane of the page. The angle θ of the magnetic field to the spin plane is shown. If θ is small, then particles moving along field lines can be shadowed from one probe.
- Figure 7. Vectors showing the gradient in energetic electron flux along the trajectory of the PDP during event 1. Note that the beam will have a finite width, and the location of the beam center shown is accurate only to within a few meters.

TABLE 1. INSTRUMENT PARAMETERS AND DYNAMIC RANGES

Electric field high gain range	± 0.064 volts/m
Electric field high gain precision	± 0.51 millivolts/m
Electric field low gain range	± 2.0 volts/m
Electric field low gain precision	± 0.017 volts/m
Electric field sample rate	20.0 samples/second
Average potential range	± 8.0 volts
Average potential sample interval	1.6 seconds/sample
Spherical probe separation	3.89 meters
Spherical probe diameter	10.2 cm

TABLE 2. BEAM PARAMETERS, SUNLIGHT CONDITIONS, PDP ORIENTATION

Event	1	2	3	4	5
Distance from PDP to shuttle	206m	218m	93m	90m	235m
Distance from PDP to Flux Tube of Beam	26-3m	9-40m	87m	84m	143m
θ - Angle of B to Spin Plane	22.9° -23.6°	15.4° -15.7°	15.1° -19.4°	10.8° -12.1°	15.4° -16.6°
Day/Night	day	night	night	night -sunrise	night -sunrise
Beam Current	50 ma	100 ma	100 ma	100 ma	100 ma
Beam Injection Direction	down	up	down	up	up
Beam Injection Pitch Angle	$<7.5^{\circ}$	2.4° - 10°	54° - 70°	68° - 69°	38° - 45°
Beam Mode	DC	1.2 kHz	54s DC 115s pulsed 600 Hz stepped down to 10 Hz	DC	DC

TABLE 3. PARAMETERS USED IN EVALUATION OF EQUATION 1

U_{sc} spacecraft velocity	7.8×10^3 m/s
A_x cross sectional area for ion collection: PDP	0.869 m ²
probe	8.11×10^{-3} m ²
A_s total surface area: PDP	4.52 m ²
probe	3.24×10^{-2} m ²
E_i ion energy in spacecraft reference frame	5.08 eV
T_e electron temperature	0.2 eV
n_e plasma density	5.0×10^{11} m ⁻³
J_b current density of energetic electrons	$0-5.5 \times 10^{-4}$ amp/m ²

PDP CONFIGURATION

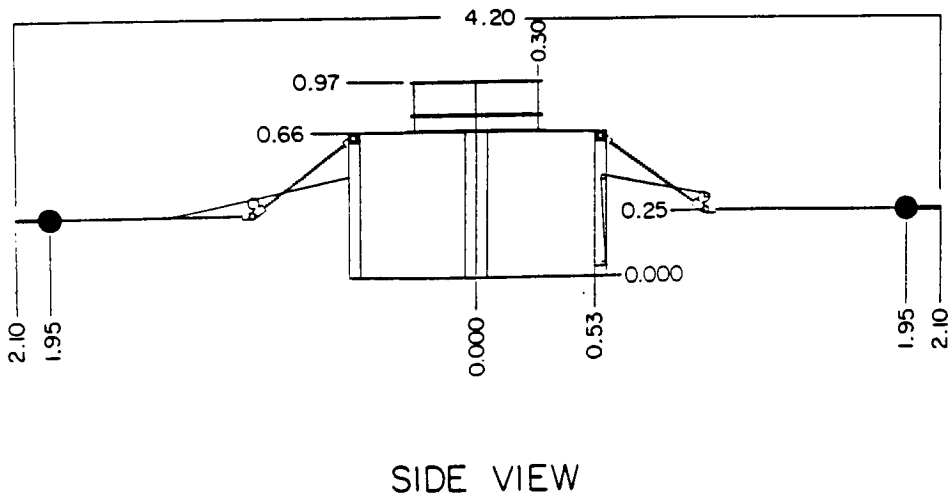
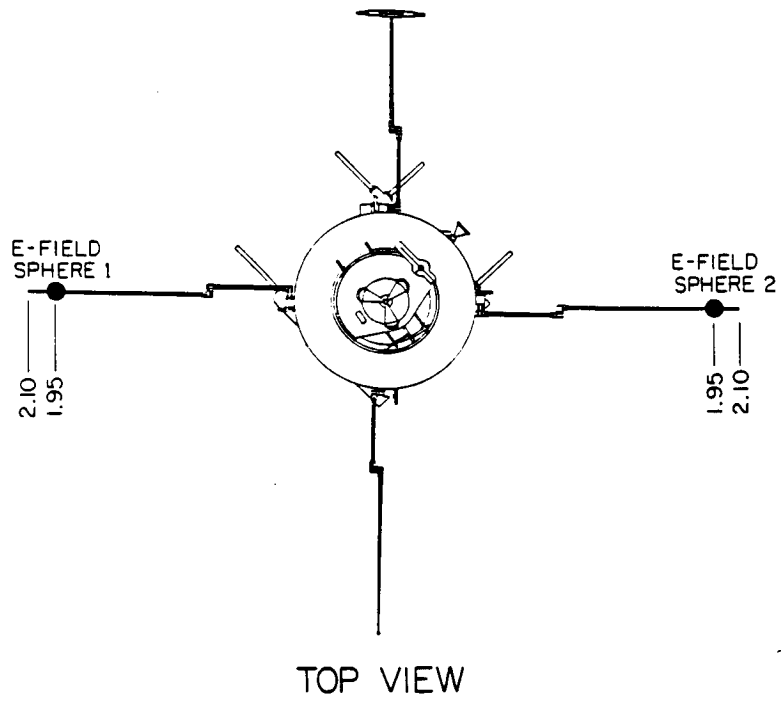


Figure 1

D-G88-72

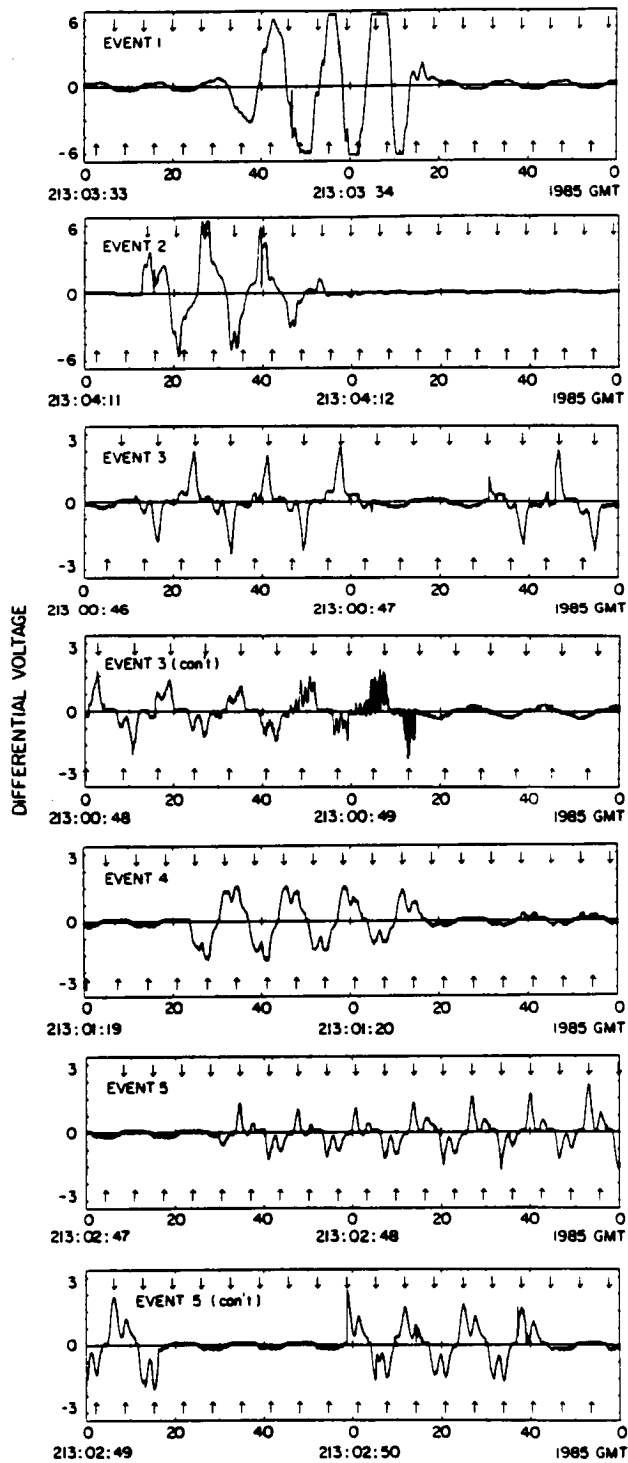


Figure 2

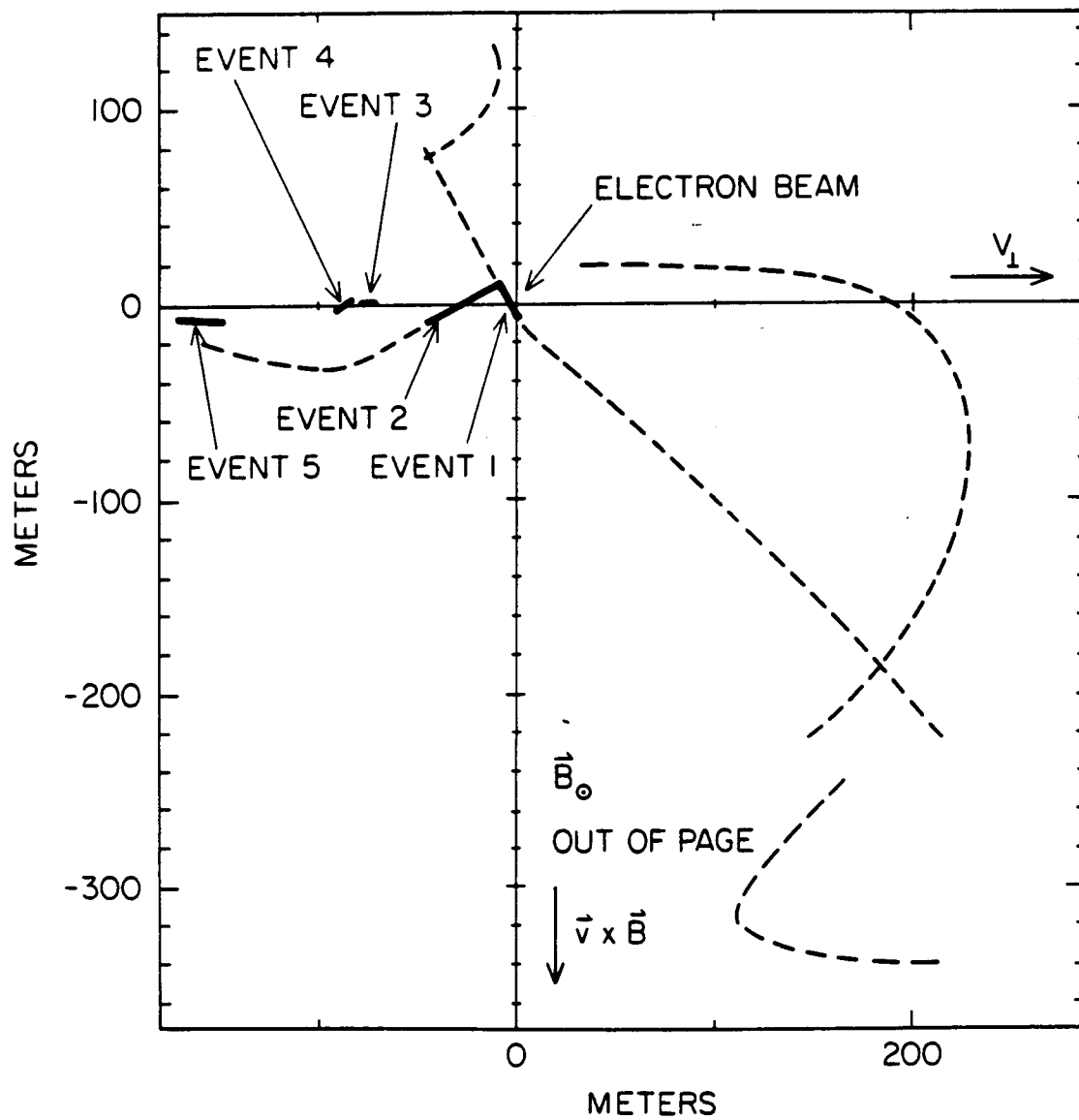


Figure 3

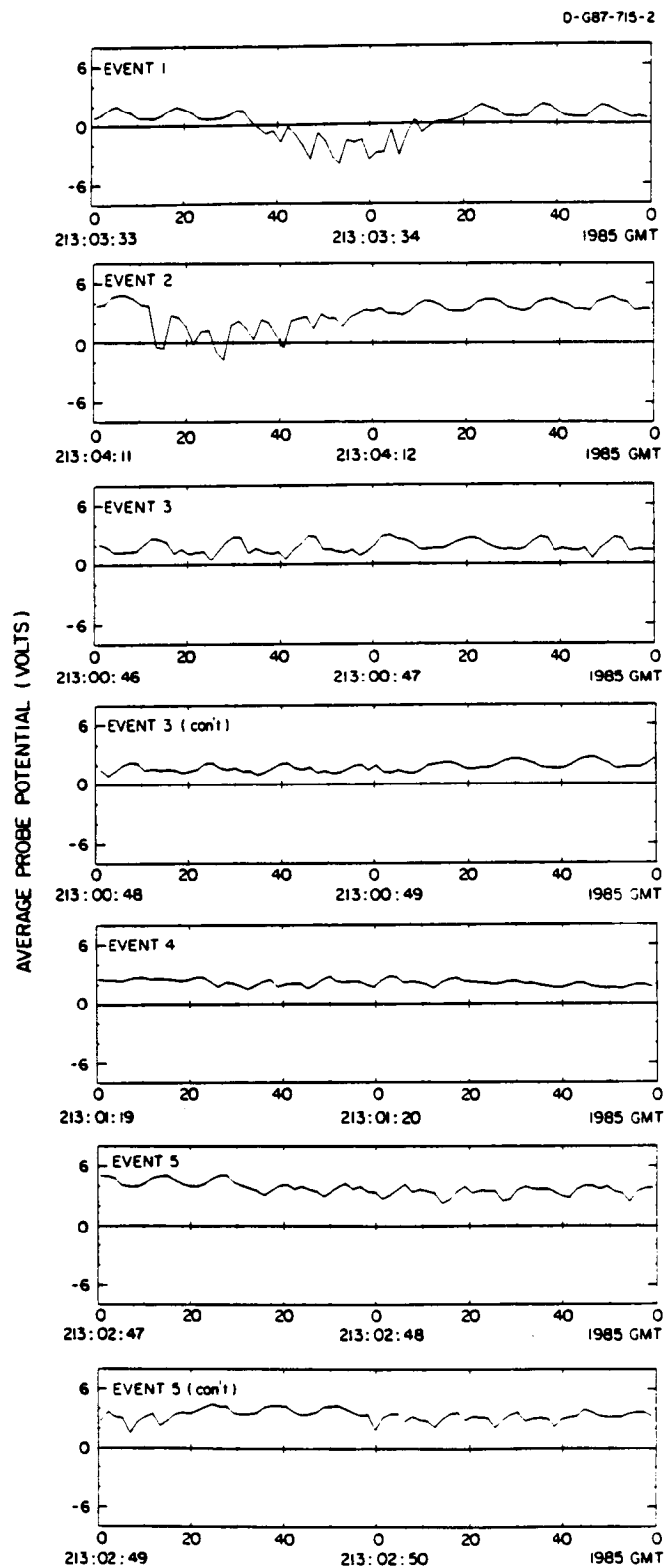


Figure 4

PROBE FLOATING POTENTIAL

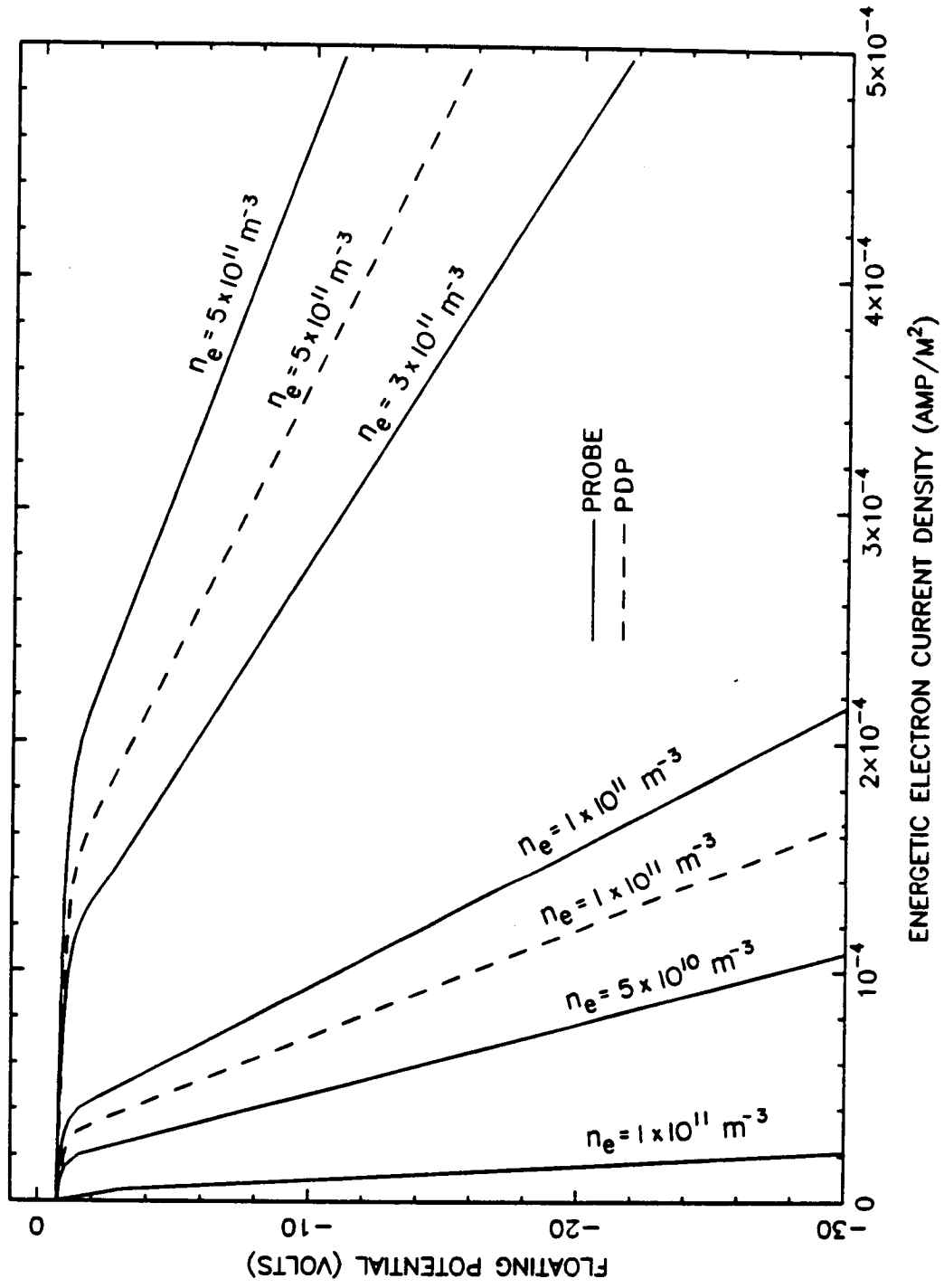


Figure 5

A-G87-681

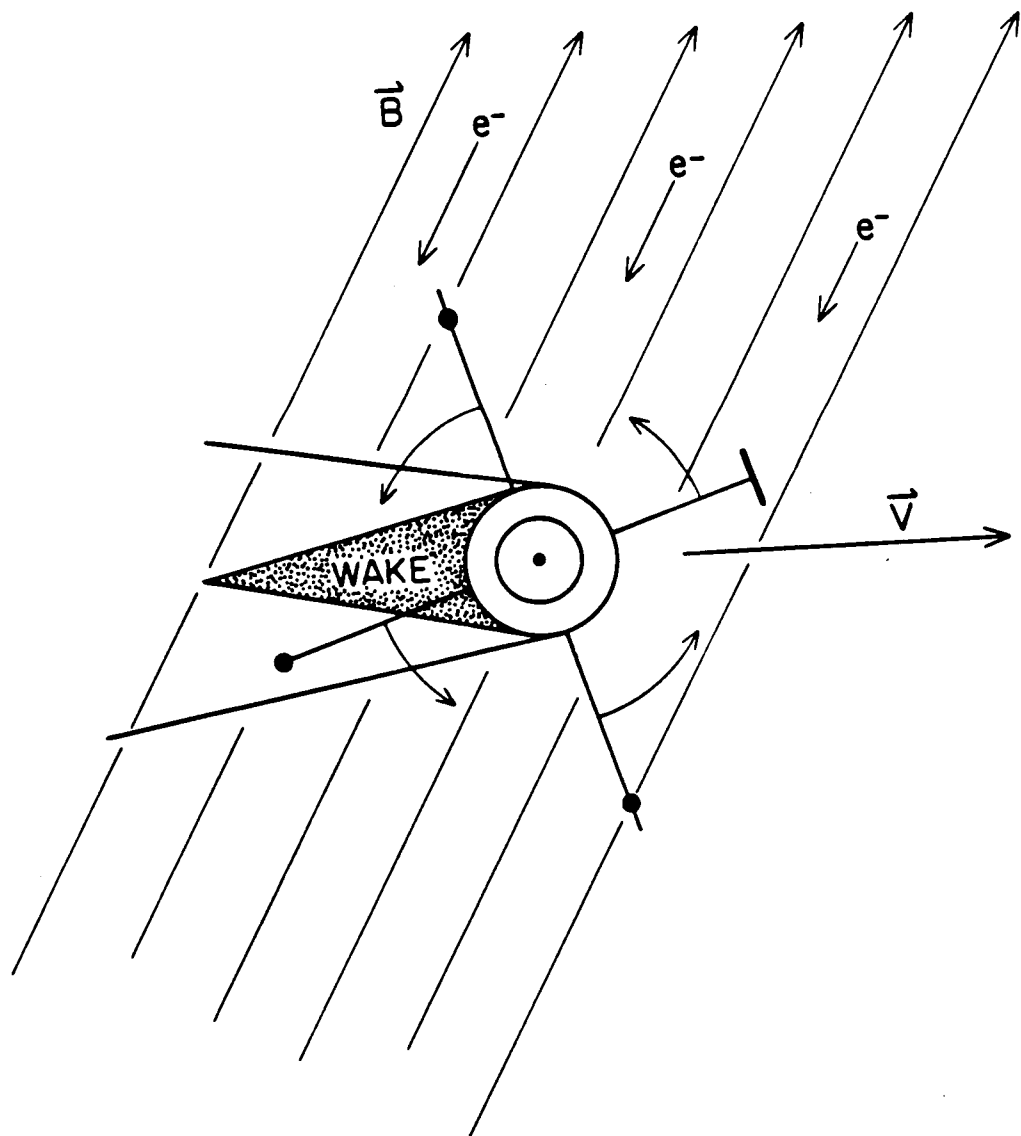


Figure 6a

A-G87-682

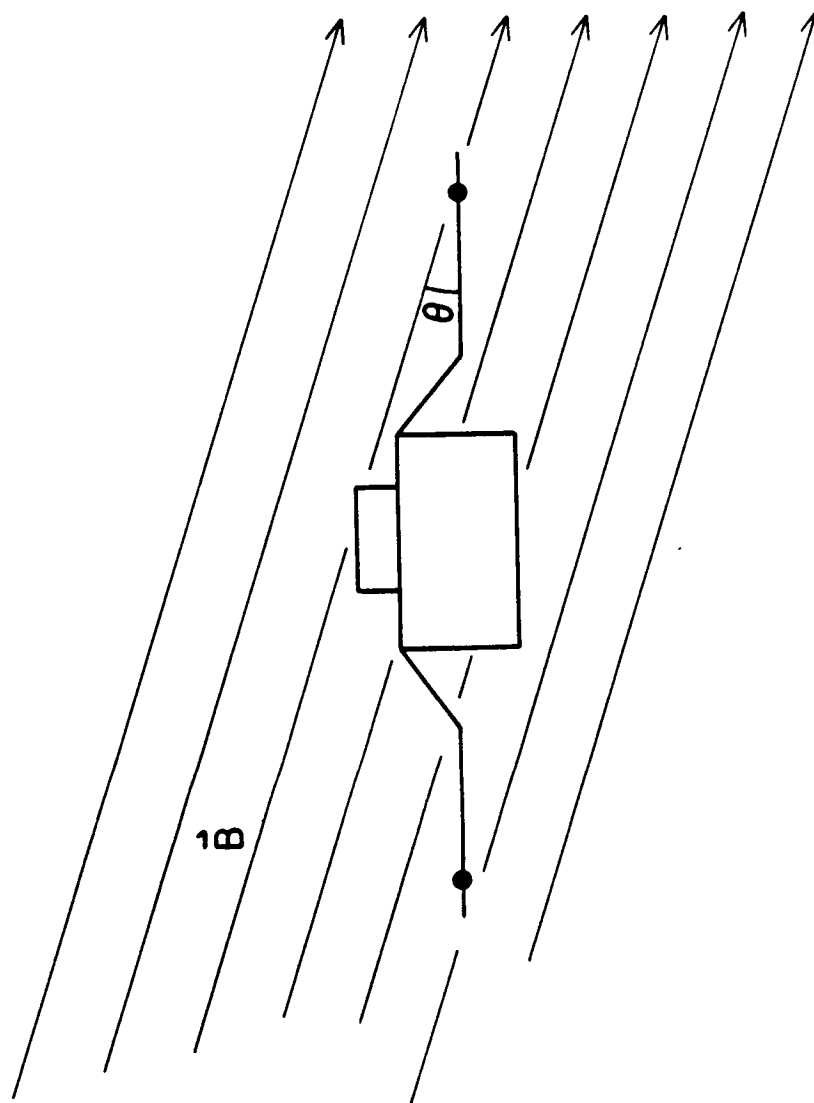


Figure 6b

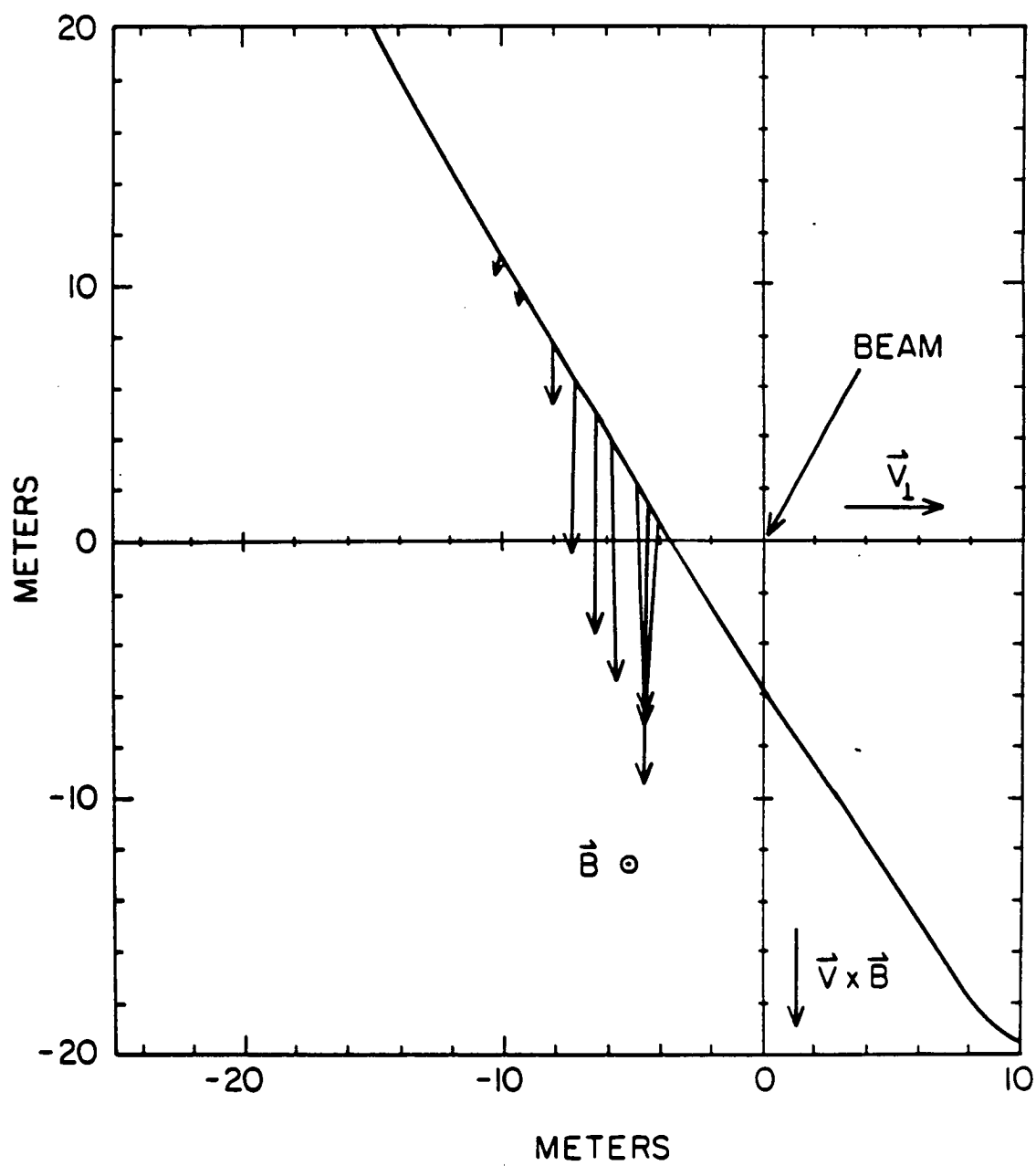


Figure 7

COHERENT CERENKOV RADIATION FROM
THE SPACELAB-2 ELECTRON BEAM

by

W. M. Farrell, D. A. Gurnett,
and C. K. Goertz

October 1987

May 1988

Submitted to Journal of Geophysical Research

Department of Physics and Astronomy
The University of Iowa
Iowa City, IA 52242

ABSTRACT

During the Spacelab-2 mission, a spacecraft called the Plasma Diagnostics Package (PDP) was released from the space shuttle to investigate the surrounding plasma environment. During an interval when the shuttle and PDP were magnetically connected, a continuous 1 keV-50 mA electron beam was ejected along a field line from an electron generator onboard the shuttle. As the PDP flew by the beam, the PDP plasma wave instrument detected intense whistler-mode radiation originating from the beam. It is believed that coherent Cerenkov radiation from bunches of beam electrons is responsible for the whistler-mode radiation, where an electrostatic beam-plasma instability forms the coherently radiating bunches. In this paper, a detailed model of the coherent Cerenkov emission process is presented. A one-dimensional computer simulation of the beam is used to model the expected phase-space structure of the electrons, and power emitted from Cerenkov radiation is computed using an analytical expression. The calculated power from the modeled 200-meter beam segment is $\sim 5 \times 10^{-8}$ W/Hz which can easily account for the measured whistler-mode wave power. The inclusion of coherent effects in the

beam increases the wave powers by nearly 90 dB above incoherent power levels. These calculations demonstrate that a spontaneous emission process, alone, can account for the observed whistler-mode wave powers.

I. INTRODUCTION

During the Spacelab-2 (SL-2) mission, intense whistler-mode radiation from an electron beam ejected from the space shuttle was detected by radio receivers onboard the Plasma Diagnostics Package (PDP) which was in free-flight around the shuttle (Gurnett et al., 1986). Simple calculations have indicated that coherent Cerenkov radiation emitted by bunches of beam electrons may produce such whistler-mode signals (Bell, 1968; Farrell et al., 1988), with the bunches being formed by a beam-plasma instability. This paper presents a detailed model of this wave generation process, including a determination of the expected radiated power.

In July of 1985, the space shuttle carried the SL-2 payload into the upper ionosphere. One of the experiments onboard was the University of Iowa's Plasma Diagnostics Package, which contained ten experiments designed to study the plasma environment around the shuttle orbiter. Another experiment, the Vehicle Charging and Potential experiment (VCAP), also flew on the mission to study the charging and potential of the shuttle. Part of this package included a

Fast Pulsed Electron Generator (FPEG) designed to eject a 1 keV-50 mA electron beam.

The PDP was released from the shuttle for a six-hour period on August 1, 1985, to investigate the plasma environment in an extended region around the shuttle. At specific times, the PDP intersected geomagnetic field lines that connected to the shuttle orbiter. These times are known as magnetic conjunction. During one magnetic conjunction event, the FPEG, located in the shuttle cargo bay, continuously ejected a 1 keV-50 mA electron beam with a pitch angle that varied from 0° to 20° . The PDP, located 200 meters from the shuttle, passed within 6 meters of the magnetic flux tube containing the beam. During this magnetic conjunction, the PDP plasma wave instrument detected intense whistler-mode radiation. Figure 1 displays a frequency-versus-time spectrogram from the PDP plasma wave instrument during the 1 keV-50 mA beam ejection (3:30 to 3:37 UT). The whistler-mode emission is the funnel-shaped structure extending in frequency from about 30 kHz to about 1 MHz.

The whistler-mode emission observed during the beam firing has been the subject of two studies (Gurnett et al., 1986, and Farrell et al., 1988). Evidence presented in both studies indicates that the emission is quasi-electrostatic and is propagating with wave normals near the

resonance cone. The emission is also believed to be generated by a Landau resonance interaction, since its index of refraction values are near those expected for such an interaction (Farrell et al., 1988) and $\bar{\mathbf{k}} \cdot \bar{\mathbf{v}}_b > 0$ (Gurnett et al., 1986). The radiated whistler-mode power from the first 200 meters of the beam was calculated by integrating the Poynting flux through a surface that contained the PDP trajectory (Farrell et al., 1988). The resulting power spectrum is displayed in Figure 2. Note that the power spectral density, dP/df , is about $\sim 10^{-9}$ W/Hz. The total power radiated in the whistler-mode from the 200-meter beam segment has been estimated to be 1.6 mW, which corresponds to a linear emissivity of about 8×10^{-6} W/m. Since the total power in the beam is 50 watts, the beam converted only 3.2×10^{-5} of its power to whistler-mode radiation in the first 200 meters of its trajectory.

Due to the low efficiency of converting beam power to wave power, incoherent Cerenkov radiation from the beam electrons was initially considered as the source of the emission. However, the estimated power from this radiation process is 10^7 times smaller than those detected (Farrell et al., 1988). In reality, the beam cannot be considered an incoherent radiator since a beam-plasma instability is operating in the beam forming quasi-periodically spaced density perturbations or "bunches" which can radiate

coherently. Therefore, an emission process involving coherent Cerenkov radiation from these bunches was considered (Farrell et al., 1988). Strong instability-related electrostatic turbulence near the local plasma frequency, f_{pe} , was detected in the beam by the PDP plasma wave instrument. These waves interact with the beam and form the "bunches" which can spontaneously emit powerful Cerenkov radiation due to the increased coherence of the beam electrons. The Cerenkov radiation emitted from these coherent structures is then detected by the PDP plasma wave receiver as the whistler-mode radiation. As demonstrated previously (Farrell et al., 1988), the frequency range of the emitted Cerenkov radiation closely corresponds to that of the detected whistler-mode radiation and the bunching may create enough coherence among the beam electrons to yield the measured wave powers.

In this paper, we will present a model of the coherent Cerenkov radiation from a bunched electron beam like that on the SL-2 experiment. We note that there are other possible mechanisms for generating the whistler-mode radiation, such as a whistler-mode instability in the beam (Lin and Wong, 1988) or some nonlinear mode conversion process. However, we will only consider the coherent Cerenkov radiation model and attempt to demonstrate that

this process alone can account for the measured wave powers. In Section II, an expression is derived that describes the coherent Cerenkov radiated power from a field-aligned electron beam. This expression will be applied to a model of the SL-2 electron beam obtained from a one-dimensional particle simulation, the results of which are outlined in Section III. In Section IV, the power from the modeled beam is calculated and compared to the measured power in the whistler-mode from the actual SL-2 electron beam.

II. EXPRESSION FOR THE RADIATED POWER

In this section an expression is derived for the power emitted from an electron beam by a coherent Cerenkov radiation process. The derivation presented here is similar to that of Mansfield's (1967), who calculated the radiated power from a single test particle in a plasma medium using the Fourier transforms of the source current and radiated electric field. Using a similar analytical technique, Harker and Banks (1983) derived an expression for the power radiated from a pulsed electron beam in a plasma medium which included coherent effects between the radiating electrons in the pulses. In their derivation, it was assumed that all beam electrons travelled with the same velocity, \bar{v} , in pulses of length, ℓ , with a distance, d , separating each pulse and that the pulsing is imposed by the generator that produces the beam. Compared to the incoherently-radiated power from a beam, the inclusion of coherent effects between radiating beam electrons in a pulse leads to much higher powers. The calculations performed in our analysis are similar to theirs, except that we are now considering the radiation from an initially continuous beam that becomes modulated or "bunched" due to the beam-plasma instability.

In the derivation of the radiated power presented here, it is assumed that the beam is a line source radiator of electromagnetic waves. This assumption is valid since the whistler-mode wavelength, λ_{em} , is on the order of 20 meters and is several times greater than the beam diameter, d , which is at most 2 cyclotron radii or about 6 meters (Farrell et al., 1988). It is also assumed that the beam electrons only act as test particles and do not significantly alter the plasma medium. In this case, the medium is represented by a homogeneous, cold, collisionless plasma in a static magnetic field, and terms in the dielectric tensor, \vec{K} , describing the beam are not included. In reality, the 1 keV-50 mA electron beam ejected from the shuttle was initially overdense ($n_b > n_a$); but, as indicated in pictures of beams (Sasaki et al., 1986; Banks et al., 1987) and in beam simulations (Winglee and Pritchett, 1987), the beam tends to expand quickly and become underdense ($n_b < .1 n_A$), and it is in the underdense region where the test particle assumption can be considered valid. According to the simulations of Winglee and Pritchett (1987), the beam becomes underdense within the first $100 \lambda_D$ of the injection point.

We write the equation for a wave in a cold plasma including the external current source, $\vec{J}_q(\vec{k}, \omega)$ as

$$\vec{T} \cdot \vec{E}(\vec{k}, \omega) = \frac{i \vec{J}_q(\vec{k}, \omega)}{\omega \epsilon_0} \quad , \quad (1)$$

where $\vec{T} \cdot \vec{E}(\vec{k}, \omega) = \vec{n} \times \vec{n} \times \vec{E}(\vec{k}, \omega) + \vec{K} \cdot \vec{E}(\vec{k}, \omega)$ and \vec{K} is the cold plasma dielectric tensor. The form of the dielectric tensor used here can be found in Mansfield (1967). The electric field, $\vec{E}(\vec{r}, t)$, is obtained by taking the inverse Fourier transform of $\vec{E}(\vec{k}, \omega)$,

$$\vec{E}(\vec{r}, t) = \frac{1}{\epsilon_0} \iint \vec{T}^{-1} \cdot \vec{J}_q(\vec{k}, \omega) \vec{e}^{i(\omega t - \vec{k} \cdot \vec{r})} d\vec{k} \frac{d\omega}{\omega} \quad . \quad (2)$$

The current density can be expressed in a generalized form for a line source as

$$\begin{aligned} \vec{J}_q(\vec{r}, t) = & (\hat{x} J_x(x, t) + \hat{y} J_y(y, t) + \hat{z} J_z(z, t)) \\ & \delta(x - R_c \cos \omega_c t) \delta(y - R_c \sin \omega_c t) \end{aligned} \quad (3)$$

where the beam displacement is

$$\vec{r} = \hat{x} R_c \cos \omega_c t + \hat{y} R_c \sin \omega_c t + \hat{z} z \quad (4)$$

and R_c and ω_c are the cyclotron radius and frequency, respectively. The Fourier transform of this current is

$$\begin{aligned}
\overline{J}_q(\vec{k}, \omega) &= \frac{1}{(2\pi)^4} \int \overline{J}_q(\vec{r}, t) e^{i(\vec{k} \cdot \vec{r} - \omega t)} d\vec{r} dt \\
&= \frac{1}{(2\pi)^4} \int (\hat{x} J_x(x, t) + \hat{y} J_y(y, t) + \hat{z} J_z(z, t)) \\
&\quad e^{i(k_z z - \omega t)} [e^{i k_x R_c \cos \omega_c t}] [e^{i k_y R_c \sin \omega_c t}] dz dt .
\end{aligned} \tag{5}$$

The exponential factors in the brackets can be reexpressed as

$$e^{i k_x R_c \cos \omega_c t} = \sum_{s=-\infty}^{\infty} J_s(k_x R_c) e^{-i s \omega_c t}$$

and

$$e^{i k_y R_c \sin \omega_c t} = \sum_{s'=-\infty}^{\infty} J_{s'}(k_y R_c) e^{i s' \omega_c t} \tag{6}$$

where J_s is the s -order Bessel function. Inserting these into (5) yields the following expression for the transformed current:

$$\begin{aligned}
\overline{J}_q(\vec{k}, \omega) &= \frac{1}{(2\pi)^4} \int (\hat{x} J_x(x, t) + \hat{y} J_y(y, t) + \hat{z} J_z(z, t)) \\
&\quad e^{i(k_z z - \omega t)} \left[\sum_{s=-\infty}^{\infty} J_s(k_x R_c) e^{-i s \omega_c t} \right] \left[\sum_{s'=-\infty}^{\infty} J_{s'}(k_y R_c) e^{i s' \omega_c t} \right] \\
&\quad dz dt .
\end{aligned} \tag{7}$$

During the SL-2 beam firing, the beam pitch angle was at most 20° , and for a three-minute period, from 3:32:30 to 3:35:30 UT, was less than 10° . As a consequence, $V_{\parallel} \gg V_{\perp}$ which implies that $J_z(z,t) \gg J_x(x,t)$ and $J_y(y,t)$. Also, $R_c = V_{\perp}/\omega_c \ll \lambda_{em}$ and, therefore, the factors in the brackets in (7) are near unity. Equation (7) then becomes

$$\bar{J}_q(\bar{k}, \omega) = \frac{\hat{z}}{(2\pi)^4} \iint J_z(z,t) e^{i(k_z z - \omega t)} dz dt \quad . \quad (8)$$

Consider a group of particles ejected from a particle generator. Ideally, if all the particles are moving at the same velocity, V_s , a simple transformation can be made to a frame moving with the particles, $z' = z - V_s t$. In this frame, the current density does not depend explicitly on time,

$$J_z(z,t) = J_z(z') \quad , \quad (9)$$

and, consequently, the beam particles appear stationary. In order to solve the time integral in (8), a transformation to z' is made where the current density is considered time independent. In reality, it is not expected that all particles have identical velocities (i.e., they may have a spread ΔV about V_s) and the validity

of the power expression derived assuming (9) must be established for the particular case in question.

Assuming that a transformation can be made to a frame where (9) is valid, expression (8) becomes

$$\bar{J}_q(\bar{k}, \omega) = \frac{\hat{z}}{(2\pi)^4} \int_{-\infty}^{\infty} J_z(z') e^{ik_z z'} dz' \int_{-\infty}^{\infty} e^{i(k_z V_s - \omega)t} dt. \quad (10)$$

The quantity $\int_{-\infty}^{\infty} J_z(z') e^{ik_z z'} dz' = \sqrt{2\pi} J_z(k_z)$ where $J_z(k_z)$ is the Fourier transform of $J(z')$. Using the definition of the delta function, $\int_{-\infty}^{\infty} e^{i(k_z V_s - \omega)t} dt = 2\pi \delta(k_z V_s - \omega)$, and the fact that $k_z = n\omega \cos \theta/c$, (10) is now

$$\bar{J}_q(\bar{k}, \omega) = \frac{\hat{z}}{(2\pi)^3} (\sqrt{2\pi} J_z(k_z)) \delta(n\omega \cos \theta\beta - \omega) \quad (11)$$

where $\beta = V_s/c$.

In order to determine the radiated electric field, (11) is substituted into (2) to obtain:

$$\begin{aligned} \bar{E}(\bar{r}, t) = & \frac{1}{(2\pi)^3 \epsilon_0} \iint (T^{-1} \cdot \mathbf{z}) (\sqrt{2\pi} J_z(k_z)) \delta(n\omega \cos \theta\beta - \omega) \\ & e^{i(\omega t - \bar{k} \cdot \bar{r})} d\bar{k} \frac{d\omega}{\omega}. \end{aligned} \quad (12)$$

Knowing the electric field and source current, an expression for the radiated power can now be found:

$$P(t) = \int \bar{E}(\bar{r}) \cdot \bar{J}(\bar{r}) d\bar{r} \quad (13)$$

$$= \frac{1}{(2\pi)^2 \epsilon_0} \iint (\hat{z} \cdot \vec{T}^{-1} \cdot \hat{z}) [(2\pi) J_z(k_z(n, \theta)) J_z^*(k_z(n, \theta))] \delta(n\omega \cos \theta \beta - \omega) e^{i(\omega - n\omega \cos \theta \beta)t} n^2 \omega^2 dn \sin \theta d\theta d\omega$$

where $n^2 (\omega^3/c^3) dn \sin \theta d\theta d\phi$ has been substituted for the element $d\bar{k}$ and the trivial integration over ϕ has been performed. Integrating over θ , an integral of the form

$$I = \int f(x) \delta(Ax - B) dx = \frac{f(x_0)}{A}$$

must be solved, where $A = |n \omega \beta|$, $B = \omega$ and $x_0 = \cos \theta_0 = 1/n\beta$. It should be noted that to obtain a nonzero solution to the integral, the condition $\cos \theta_0 = 1/n\beta$ must be satisfied, which is the Landau resonance condition. Upon evaluating the integral the radiated power becomes

$$P(t) = \frac{-i}{(2\pi)^2 \epsilon_0 c^3 \beta} \iint (\hat{z} \cdot \vec{T}^{-1} \cdot \hat{z}) [(2\pi) J_z(k_z(n, \theta_0)) J_z^*(k_z(n, \theta_0))] |n| |\omega| dn d\omega \quad (14)$$

From Mansfield, the quantity $(\hat{z} \cdot \vec{T}^{-1} \cdot \hat{z})$ is

$$(\hat{z} \cdot \vec{T}^{-1} \cdot \hat{z}) = \frac{T_{33}(n)}{\epsilon_1(n^2 - n_2^2)(n_2 - n_1^2)} \quad (15)$$

where

$$T_{33} = \epsilon_1^2 - \epsilon_2^2 - \epsilon_1 n^2 + (n^4 - \epsilon_1 n^2) \cos^2 \theta_0, \quad (16)$$

$$n_{1,2}^2 = [-B \pm (B^2 - 4C\epsilon_1)^{1/2}] / 2\epsilon_1, \quad (17)$$

$$B = \left(\frac{c}{V_s}\right)^2 (\epsilon_3 - \epsilon_1) + \epsilon_2^2 - \epsilon_1^2 - \epsilon_1 \epsilon_3. \quad (18)$$

and

$$C = \left(\frac{c}{V_s}\right)^2 (\epsilon_1^2 - \epsilon_2^2 - \epsilon_1 \epsilon_3) + \epsilon_3 (\epsilon_1^2 - \epsilon_2^2). \quad (19)$$

Using the Plemelj formula, the complex integration over dn is performed to yield the final expression for the radiated power:

$$P(t) = \bar{P} = \int_{-\infty}^{\infty} \left(\frac{\omega d\omega}{8\pi\epsilon_0\epsilon_1 c^2 V_s} \right) \frac{1}{(n_2^2 - n_1^2)} \sum_{k=1}^2 T_{33}(n_k) \quad (20)$$

$$[2\pi J_z(k_z(n_k, \theta_0)) J_z^*(k_z(n_k, \theta_0))] \quad .$$

Note that the radiated power is proportional to the square of the Fourier transform of the current density. This result is similar to that obtained by Harker and Banks (1983), who found that the radiated power varies as the square of the transform of the current pulses. Once the current density and its transform are known, it can be used in Equation (20) to easily calculate the radiated power. We will use a modeled beam to obtain the beam current, $J_z(z, t)$, since the available plasma instruments flown on the PDP cannot directly measure the electron bunching which occurs on time scales of $1/\omega_{pe} \sim 10^{-7}$ seconds. The results of the beam simulation are presented in the next section.

III. A ONE-DIMENSIONAL ELECTROSTATIC SIMULATION OF THE SL-2 ELECTRON BEAM

To obtain the required beam current, a one-dimensional electrostatic model of an electron beam propagating through an ambient plasma is simulated on a computer. A one-dimensional beam model was chosen since the length scales being considered are very long, about 200 meters (many thousand Debye lengths), and cannot be reasonably modeled using a two- or three-dimensional system due to the practical limits on computer CPU time. In the one-dimensional model, it is assumed that the velocity of the particles is directed along a static magnetic field line, which allows the particle trajectories to be unaffected by this field. Since the SL-2 electron beam was nearly field-aligned during injection, this assumption is acceptable. In this analysis, we also assume that the magnitude of the electric field of the generated Cerenkov radiation is much smaller than that of the electrostatic wave generated within the beam, $E_{ES} \gg E_{RAD}$. This assumption implies that the radiated electric field did not significantly alter the SL-2 beam electron trajectories, and is consistent with the modeling of the beam where radiation field effects are

neglected. This assumption is also consistent with observations made during the SL-2 experiment, where $E_{ES} \geq .3$ V/m in the beam while $E_{RAD} \sim 10^{-3}$ V/m for the whistler-mode waves.

The simulation is designed so that initially the system is charge neutral. The particles representing the ambient electrons can move freely; however, they are confined to the system by re-injection boundaries. Ambient electrons leaving the system at these boundaries are re-injected with a Gaussian-weighted velocity between zero and the electron thermal speed. The electron beam is represented by particles of negative charge that are injected into the system at the $z = 0$ boundary with velocities greater than the ambient electron thermal speed. In order to keep the net charge in the system equal to zero, a positive charge equal in magnitude to the amount of negative beam charge in the system is placed at the $z = 0$ boundary. This boundary charge draws a return flow of ambient electrons which, for low beam flux ($n_b V_b A < n_A V_{AA} A$), is sufficient to keep the boundary almost completely neutralized.

In a one-dimensional simulation, the particles are charged sheets of infinite extent in the transverse direction, and of finite thickness ($\sim \lambda_D$) along the direction being modeled. Consequently, the modeled beam has an infinite cross-section. This infinite cross-section

model, however, is contrary to the true SL-2 electron beam, which had a cross-sectional radius of no more than six meters (Farrell et al., 1988). Assuming such a model ignores finite radius electrostatic effects associated with the SL-2 electron beam and is only justified if the wavelength of the longitudinal electrostatic mode, λ_{ES} , is less than the SL-2 electron beam diameter, d , which is not the case. Therefore, we must demonstrate that the electrostatic nature of a finite radius beam, like the SL-2 electron beam, is not significantly different from an infinite radius beam. To show this, a comparison will be made between our one-dimensional beam model and a two-dimensional radially finite beam model (Winglee and Pritchett, 1987) to verify that finite radius effects are insignificant.

Figure 3 displays a beam phase space configuration from Winglee and Pritchett's (1987) two-dimensional simulation of a radially finite beam. In their model, an initially overdense beam is injected into a model ionosphere, with the ratio of the beam density to ambient density, n_b/n_A , equal to 4 and beam velocity to ambient thermal velocity, V_b/V_{TH} , equal to 20. Both ratios used in the simulation are representative of the conditions during SL-2 electron beam injections. From this figure we see that the beam can freely propagate from the injection

boundary (located at $x/\Delta = 125$). In this case, the spacecraft charging potential at the injection boundary is much less than the initial beam energy, $\phi < \frac{1}{2}m_e V_b^2$, and will allow the beam to escape from the near injection region. This low spacecraft potential is consistent with potential measurements made during the SL-2 mission where the shuttle obtained only a 40 volt potential during ejections of a 1-keV electron beam (Williamson et al., 1985; Hawkins et al., 1987). According to Winglee and Pritchett, the simulated beam expands radially from the initial injection radius of $2 \lambda_D$ out to $7 - 13 \lambda_D$ in its first $100 \lambda_D$ of propagation due to the Coulomb repulsion of the electrons in the beam. After the beam has expanded, it is underdense, with $n_b < n_A$, and the interaction of the beam with the ambient ionosphere is typical of underdense beams modeled in one-dimensional simulations (Okuda et al., 1987; Okuda and Kan, 1987; Winglee et al., 1987). As seen in the figure, the classic particle trapping structures created in this beam are very similar to those obtained in the one-dimensional simulations referenced above, thereby indicating that finite radius effects are not altering the beam structure significantly.

Due to the limitations of a one-dimensional simulation, we will not self-consistently model the spacecraft charging

and expansion region of the beam as was done by Winglee and Pritchett; but instead, will model the beam after it has already propagated $100 \lambda_D$ through the expansion region. The modeling of the beam will start at point A labeled in Figure 3, where the beam is considered underdense and still relatively cold.

Figure 4(a), (b), and (c) displays the beam phase space configuration from our one-dimensional simulation after 50, 100 and $840 \omega_{pe}^{-1}$, respectively. In this model, $n_b/n_A = 1/16$, $V_b/V_{TH} = 20$ and the beam is initially cold at $z = 0$. Each unit of distance represents $2\lambda_D$ or about 10 cm; thus, Figure 4(c) displays the beam phase space configuration for a 200 meter beam segment. The simulation was run for 840 plasma periods to allow the transient front edge of the beam to leave the system. Consequently, the model displayed in Figure 4(c) represents the steady state beam. Note from the figures that the wave-particle trapping structures are similar to those of the two-dimensional beam displayed in Figure 3, implying that both are undergoing similar electrostatic interactions. Also note that the beam phase space configuration appears very similar to those modeled by Okuda et al. (1987), who performed a one-dimensional simulation similar to the one presented here. Figure 5(a), (b), and (c) displays the number of beam

particles as a function of z at times corresponding to those in Figure 4. Note from both Figures 4 and 5 that the beam is undergoing strong interactions with the background ionospheric medium. In the first 100 meters ($z = 0$ to 1000), the beam-plasma instability is creating the classic trapping structures associated with such instabilities, which gives rise to significant perturbations in the density. Beyond 100 meters ($z > 1000$), the beam is strongly thermalized, with the beam particles becoming randomized in phase space due to the wave-particle interactions. Such randomization of the particles signifies the transfer of free energy from the beam to the electrostatic turbulence. Even though the beam becomes randomized, some significant density fluctuations are still present out past 100 meters ($z > 1000$), as indicated in Figure 5(c).

According to expression (20), the current density of the beam is needed to obtain the radiated power. Figure 6(a) displays the beam current density, $J_z(z, t = 840 \omega_{pe}^{-1})$ in the 200-meter beam segment. Note from the figure that current density perturbations are clearly evident in the beam. It is the radiative coherence within and between these perturbations that yield significant wave powers, since the randomized background beam component only

contributes to the incoherent power level. Figure 6(b) displays the Fourier transform of the current, $J_z(k_z)$, as a function of k_z . The resulting transform appears as a white-noise type k-spectra for $k_z > 20$; however, for $k_z < 20$, $J_z(k_z)$ appears to increase as k_z decreases. The white-noise type k-spectra found in $k_z > 20$ results from the randomized component of the electrons in the computer model. Although not feasible, if electrons with real mass and charge had been modeled, this noise would be significantly reduced. The average noise level was obtained by calculating the arithmetic average of the $J_z(k_z)$ values between 23.6 and 31.4. This level is represented by the dotted line in Figure 6(b). The increase in $J_z(k_z)$ found at $k_z < 20$ results from wave-particle interactions within the beam that create current density perturbations or "bunches." If bunching had not occurred, the simulated beam electrons would be completely randomized in phase space and the resulting values of $J_z(k_z)$ would appear as white-noise at all k_z values.

IV. THE RADIATED POWER FROM A MODEL OF THE SL-2 ELECTRON BEAM

Equation (20) will now be applied to the simulated SL-2 electron beam discussed in the last section. In applying this expression to waves propagating in the SL-2 electron beam environment, some further approximations can be made. Specifically, in the frequency range of consideration, $n_1 \gg n_2$, $n_1 \approx n$ where n is the whistler-mode index of refraction obtained from cold plasma theory and $T_{33}(n_1) \approx 10^3 T_{33}(n_2)$. Also, based on arguments of the typical density structure size in the beam, $J_z(k_z(n_2, \theta_0)) > J_z(k_z(n_1, \theta_0))$. Consequently, the $k=2$ term in the summation of Equation (20) is very small and can be neglected. The radiated power can then be expressed as

$$P(t) = \bar{P} \approx \int_{-\infty}^{\infty} \left[\frac{-|\omega| d\omega}{8\pi\epsilon_0\epsilon_1 c^2 V_s} \frac{1}{(n_2^2 - n_1^2)} \right] 2\pi J_z(k'_z) J_z^*(k'_z) T_{33}(n_1) \quad (21)$$

where $k_z' = n \cos \theta_0 \omega / c$. Note that $n_1 > n_2$ which makes the term in brackets positive for the frequency range considered. To derive (21), it was assumed that a frame of reference exists where the current density is time independent and, thus, all current density perturbations propagate

at the same speed, V_s . In this case, the transform of the current density is properly represented by Equation (11), where the delta function specifies the propagation speed, V_s , of the perturbations. In reality, however, all the perturbations may not be propagating at the same speed; and the validity of using Equation (21) to estimate the coherent radiated power must be established. Consider a more realistic case where the density perturbations propagate with a speed $V \pm \Delta V$, where ΔV represents a velocity spread of the perturbations. In this case, the delta function in Equation (11) should be replaced by a function that approximates this spread in velocity, such as a Gaussian function. As demonstrated in the Appendix, as long as this spread is not too great, the values of the radiated power are not significantly different from those obtained from perturbations all moving at identical velocities.

The velocity of the perturbations, V_s , must be determined in order to obtain a solution to (21). This velocity can be found by examining the spatial and temporal evolution of the current density perturbations in the simulation. By plotting the current density values above the average, $J_z(z,t) > .05$ A, as a function of z and t , the evolution of the individual perturbations can be followed. Such a plot is displayed in Figure 7. From this figure we see that the current density perturbations drift from the

injection point at nearly the initial beam speed of 1.89×10^7 m/sec. However, not all the perturbations move at the same identical speed since, at certain times, merging of a number of perturbations occurs. Examples of such current density enhancements are at $x = 100$ meters, $t = 2.1 \times 10^{-5}$ seconds and at $x = 85$ meters, $t = 3 \times 10^{-5}$ seconds, and are circled in the figure. It is the creation of these structures coupled with the perturbations near the injection boundary that yield the large values of $J_z(k_z)$ at small wave numbers ($k_z < .2$) shown in Figure 6(b). The Fourier transform of the current density, $J_z(k_z, \omega)$, is displayed in Figure 8. Note from this figure that the most intense values of the current corresponding to the perturbations lie near $V_g = 1.89 \times 10^7$ m/sec, which is represented by the solid line in the figure. We also see that there is a spread in these values about V_g ; but this spread is not very large and Equation (21) can be readily applied. It is interesting to note that even though the beam, itself, develops a significant velocity spread, as indicated in Figure 4, the perturbations which generate significant radiation continue to propagate at the injection speed with little spread.

To obtain the radiated power from (21), $J_z(k_z)$ evaluated at $k_z'(\omega) = n \cos \theta_0 \omega / c$ is required, where the wave number, $k_z'(\omega)$, represents those of the whistler-mode

that satisfy the Landau resonance condition. This wavenumber varies from .01 at 31.1 kHz to .332 at 1 MHz. The current density values that correspond to these wavenumbers are indicated in Figure 6(b). Using Equation (21) and the calculated values of $J_z(k_z)$ with the noise level subtracted, the radiated power spectral density, dP/df , from the modeled 200-meter beam segment is evaluated. These power spectral density values are plotted as a function of wave frequency in Figure 9 (represented by x's), along with the log average of these values (represented by the straight line). The calculated incoherent Cerenkov power spectra (represented by o's) and measured whistler-mode power spectra (represented by .'s) from the 200-meter SL-2 electron beam segment is also displayed in the figure. Note from the figure that the inclusion of coherent effects amongst the beam electrons increases the wave powers by nearly a factor of 10^9 (90 dB's) above incoherent power levels and yields values that are relatively close to the measured whistler-mode powers. It is clear from the figure that coherent Cerenkov radiation from the beam can indeed account for the measured whistler-mode wave power.

It can also be seen from Figure 9 that the calculated power from the modeled beam actually overestimates the measured power by a factor of 40. This over estimate may

result from the fact that the SL-2 electron beam is not an ideal line source radiator as assumed in our analysis, and a more accurate estimate of the power may be obtained by including the beam's radial dimension. The overestimate of the power may also be due to the assumption that the beam electrons are completely field aligned. Even if the electron generator is perfectly aligned with the geomagnetic field, electrical and fluid edge effects between the beam and the generator orifice may impart enough perpendicular momentum to the beam electrons to reduce the size of the density perturbations as we have modeled them. Consequently, the radiated power will be reduced. Interactions between the beam electrons and neutrals may also impart significant perpendicular momentum to the beam electrons, which will again reduce the size of the density perturbations and the radiated power. It might be expected that Landau damping of the Cerenkov radiation as it propagates in the ionospheric plasma will also significantly reduce wave powers; but it is suspected that this effect is not significant since the Cerenkov wave phase speed from the current density perturbations is still well above the thermal velocity of the ionosphere. Based on the limiting assumptions used in our model, the calculated power should be considered as an upper limit of the possible whistler-mode wave power. The effects

mentioned above should all tend to reduce the beam's radiative coherence as compared to our one-dimensional model; and, consequently, lower the radiated powers. Therefore, it is not surprising that the powers obtained via the one-dimensional analysis are higher than those measured.

VI. CONCLUSION

Previously, the measured power of the whistler-mode waves emitted by a continuous electron beam ejected from the shuttle was found to be almost 10^7 greater than the expected power from an incoherent Cerenkov radiation process. Due to this discrepancy, it was suggested that these waves might result from coherent Cerenkov radiation effects in a beam naturally modulated by a beam-plasma instability. In this case, the enhanced radiated power would result from the coherence between electrons in the instability-related density perturbations or "bunches."

In order to verify that this process is indeed viable, a one-dimensional electrostatic simulation of the beam was performed that verified the existence of the bunches. The coherent Cerenkov-radiated power from the modeled beam was then calculated using an analytical expression similar to that presented by Harker and Banks (1983), and was found to be within a factor of forty of the measured wave power.

It should be noted that two very critical assumptions were made to simplify the above analysis. The first assumption was that the beam could be treated as a line source radiator of the whistler-mode waves, and was invoked to obtain a manageable expression for the radiated power.

Although the beam was not an ideal line source, the electromagnetic wavelengths were still significantly greater than the beam diameter, making the assumption valid. The second assumption is that finite radius electrostatic effects in the beam were not significant, which allowed us to model the beam using only a one-dimensional simulation. As mentioned previously, a one-dimensional simulation was advantageous since a long beam length was required. We demonstrated, via simulation, that the phase space structure of a two-dimensional, radially-finite beam was indeed comparable to that of a one-dimensional beam. Without these two simplifying assumptions, the expression for the radiated power and the modeled beam could not have been used in the analysis.

Since we have demonstrated that a spontaneous emission process alone can account for the whistler-mode wave powers, other more sophisticated emission processes operating in the beam, such as a whistler-mode instability, are not required. Both a Cerenkov radiation process and a whistler-mode instability could be present in the beam; but, in this case, the powers from the Cerenkov process are at least comparable to those from the instability. Consequently, effects from spontaneous Cerenkov radiation

processes cannot be ignored in the generation of the whistler-mode waves from the SL-2 electron beam.

ACKNOWLEDGEMENTS

We would like to thank Terry Whelan and Shinobu Machida for their timely ideas concerning the simulation and radiated power calculations, John Steinberg for his useful discussions, Terry Averkamp for his valuable input on PDP data analysis, and John Birkbeck for a fine drafting job.

Part of this research was funded by NASA Graduate Student Researchers Training Grant NGT-50034. The research at the University of Iowa was also supported by NASA through contract 32807, and grants NAG3-449, NSG-7632, NGL 16-001-002 and NGL 16-001-043. The research at Stanford University was supported by NASA through grant NAGW-235.

REFERENCES

- Banks, P. M., Active electron beam experiments with rockets and space shuttles, EOS Trans. AGU, 68, 1400, 1987.
- Bell, T. F., Artificial production of VLF hiss, J. Geophys. Res., 73, 4409-4415, 1968.
- Farrell, W. M., D. A. Gurnett, P.M. Banks, R. I. Bush, and W. J. Raitt, An analysis of whistler-mode radiation from the Spacelab-2 electron beam, J. Geophys. Res., 93, 153-161, 1988.
- Gurnett, D. A., W. S. Kurth, J. T. Steinberg, P. M. Banks, R. I. Bush, and W. J. Raitt, Whistler-mode radiation from the Spacelab-2 electron beam, Geophys. Res. Lett., 13, 225-228, 1986.
- Harker, K. J., and P. M. Banks, Radiation from pulsed electron beams in space plasmas, Radio Sci., 19, 454-470, 1983.
- Hawkins, J. G., P. M. Banks, P. R. Williamson, R. I. Bush, and W. J. Raitt, Rise times in the vehicle charging and return current measurements during electron beam emission experiments from the shuttle orbiter, EOS Trans. AGU, 68, 1400, 1987.

- Lin, C. S., and H. K. Wong, Plasma instabilities of a finite size electron beam-plasma system, Proceedings, 1988 URSI Meeting in Boulder, CO, p. 195, 1988.
- Mansfield, V. N., Radiation from a charged particle spiraling in a cold magnetoplasma, Astrophys. J., 147, 672, 1967.
- Okuda, H., R. Horton, M. Ono, and M. Ashour-Abdalla, Propagation of a nonrelativistic electron beam in a plasma in a magnetic field, Phys. Fluids, 30, 200-208, 1987.
- Okuda, H., and J. D. Kan, Injection of an electron beam into a plasma and spacecraft charging, Phys. Fluids, 30, 209-220, 1987.
- Sasaki, S., K.-I. Oyama, N. Kawashima, W. J. Raitt, and N. B. Myers, VLF and HF wave characteristics observed from an active experiment tethered mother/daughter rocket payload (Charge-2), EOS Trans. AGU, 67, 1170, 1986.
- Williamson, P. R., J. G. Hawkins, R. I. Bush, P. M. Banks, W. J. Raitt, Vehicle charging measured during electron beam emission on Spacelab-2 (abstract), EOS Trans. AGU, 66, 1051, 1985.
- Winglee, R. M., and P. L. Pritchett, Comparative study of cross-field and field-aligned electron beams in active experiments, J. Geophys. Res., submitted, 1987.

Winglee, R. M., P. L. Pritchett, and G. A. Dulk, Energy transport by energetic electrons released during solar flares: 1. Thermal versus nonthermal processes, Astrophys. J., submitted, 1987.

APPENDIX

As mentioned in the text, all the current density perturbations or bunches in the modeled SL-2 electron beam are not propagating at exactly V_s , but instead propagate in a range of velocities, $V_s \pm \Delta V$, where ΔV is the typical velocity spread. Consequently, in the frame moving with these bunches, they are not all stationary as assumed in the derivation of (21), but have second-order temporal variations that can alter the radiative coherence of the beam. The effect of these temporal variations on the radiated power can be accounted for by changing the delta function in Equation (11) to a Gaussian function that represents the spread in bunch velocity. The corresponding transform of the current density in space and time is then written as

$$J_q(\bar{k}, \omega) = \frac{\hat{z}}{(2\pi)^3} \sqrt{2\pi} J_z(k_z) \left[\frac{t_0}{2\sqrt{\pi}} e^{-a^2 t_0^2/4} \right] \quad (A1)$$

where $J_z(k_z)$ is the spatial transform of the current density, $a = k_z V_s - \omega$, and t_0 is the typical coherence time scale of the temporal variations in the current density. If the transform of the current density is peaked at $\omega/k_z = V_s$

with little or no spread in ω or k_z , then the current density is properly represented by (11). However, as Figure 8 indicates, the transform of the current density, $J_z(k_z, \omega)$, has some spread about $V_s = \omega/k_z = 1.89 \times 10^7$ m/sec. Consequently, this transform is best represented by (A1), where the Gaussian function is used to represent the spread in ω - k_z space. Note as $t_0 \rightarrow \infty$, (A1) and (11) become identical.

Following a similar analysis as was done previously, the power spectral density from a current density, $J_z(k_z, \omega)$, with a spread is found to be

$$\frac{d\bar{P}}{d\omega} \Big|_{\omega=\omega_0} = \int F(k_z, \omega_0) \frac{t_0}{2\sqrt{\pi}} e^{-\frac{a^2 t_0^2}{4}} dk_z \quad (A2)$$

where

$$F(k_z, \omega_0) = \frac{1}{(2\pi)^2 \epsilon_0 c^2} \int (\hat{z} \cdot \vec{T}^{-1} \cdot \hat{z}) [2n J_z(k_z) J_z^*(k_z)] n \omega_0 dn \quad (A3)$$

Thus, to obtain the power spectra density, a Gaussian weighted integration of $F(k_z, \omega_0)$ over dk_z must be performed. Using (13) a similar expression can be written when $J_z(k_z, \omega)$ has no spread about $\omega/k_z = V_s$:

$$\begin{aligned}
\left. \frac{d\bar{P}}{d\omega} \right|_{\omega=\omega_0} &= \int F(k_z, \omega_0) \delta(k_z V_s - \omega_0) e^{i(k_z V_s - \omega_0)t} dk_z \\
&= \frac{F(k_{z0}, \omega_0)}{V_s} \Big|_{k_{z0} = \frac{\omega_0}{V_s}}
\end{aligned}
\tag{A4}$$

Expression (A2) and (A4) should yield similar results as long as $F(k_z, \omega_0)$ approximates $F(k_{z0}, \omega_0)$ in dk_z . A numerical integrating of (A2) was performed and this result was indeed found to be true. The radiated power varied by only about 10% when considering a spread in $J_z(k_z, \omega)$ equal to k_{z0} . From these results it is evident that the radiated power does not vary significantly when considering a spread in $J_z(k_z, \omega)$ about $\omega/k_z = V_s$. Consequently, the radiated power calculated using the much simpler expression (21) should be a sufficiently accurate estimate of the radiated power from the modeled beam.

FIGURE CAPTIONS

- Figure 1 A frequency vs. time spectrogram from the PDP plasma wave instrument showing intense emissions during a continuous electron beam event (3:30 - 3:37 UT). The funnel-shaped structure that extends from the electron cyclotron frequency, f_c , to about 30 kHz is whistler-mode radiation from the beam.
- Figure 2 The calculated power spectral density from the first 200 meters of the beam in the whistler mode is shown as a function of frequency.
- Figure 3 This figure displays the phase space configuration of beam electrons from Winglee and Pritchett's (1987) two-dimensional simulation. The beam is initially injected overdense ($n_b/n_A = 4$); however, the beam expands in the first $100 \lambda_D$ to where it is underdense. In this model, $V_b/V_A = 20$ and the figure displays the beam phase space after about $38 \omega_{pe}^{-1}$. Note that the wave trapping structures created in the beam are very similar to those typically created in one-dimensional simulations of underdense beams.

Figure 4(a), (b), and (c) The beam phase space configuration from our one-dimensional simulation is displayed after $50 \omega_{pe}^{-1}$, $100 \omega_{pe}^{-1}$ and $840 \omega_{pe}^{-1}$, respectively. In this simulation, the beam model represents the underdense part of the beam displayed in Figure 3 starting from point A. The simulation was run with $n_b/n_A = 1/16$ and $V_b/V_A = 20$.

Figure 5(a), (b), and (c) Displayed are the number of beam electrons as a function of z at times corresponding to those of Figure 4. Note from all three figures that significant density perturbations are created in the beam.

Figure 6(a) and (b) Figure (a) displays the beam current density as a function of z at $840 \omega_{pe}^{-1}$, while (b) displays the corresponding transform of this current. Note from (a) that significant perturbations in the current density are present in the beam, which increases the values of $J_z(k_z)$ displayed in (b) at wavenumbers less than 20.

Figure 7 Displayed are the current density values, $J_z(z,t)$, above the average of .05 A as a

function of z and t . The evolution of the current density perturbations is clearly displayed. Note that these perturbations drift at $V \sim 1.89 \times 10^7$ m/sec, which is the beam injection speed. Also, note that merging of the current density perturbations occurs in the beam, as indicated by the structures circled in the figure.

Figure 8 To determine the velocity of the perturbations, the Fourier transform of the current density in time and space, $J_z(k_z, \omega)$, was calculated and plotted as a function of k_z and ω . Note that the values lie near $\omega/k_z = 1.89 \times 10^7$ m/sec.

Figure 9 This figure shows the power spectra of the measured whistler-mode radiation from the first 200 meter of the SL-2 electron beam along with the calculated power spectra of the incoherent and coherent Cerenkov radiation from a 200-meter beam segment. Note that the inclusion of coherent radiation effects increases the calculated powers near to those measured from the SL-2 electron beam. Based on these results, it is concluded that

coherent Cerenkov radiation from a bunched electron beam can generate the detected whistler-mode radiation.

A-G85-807-1

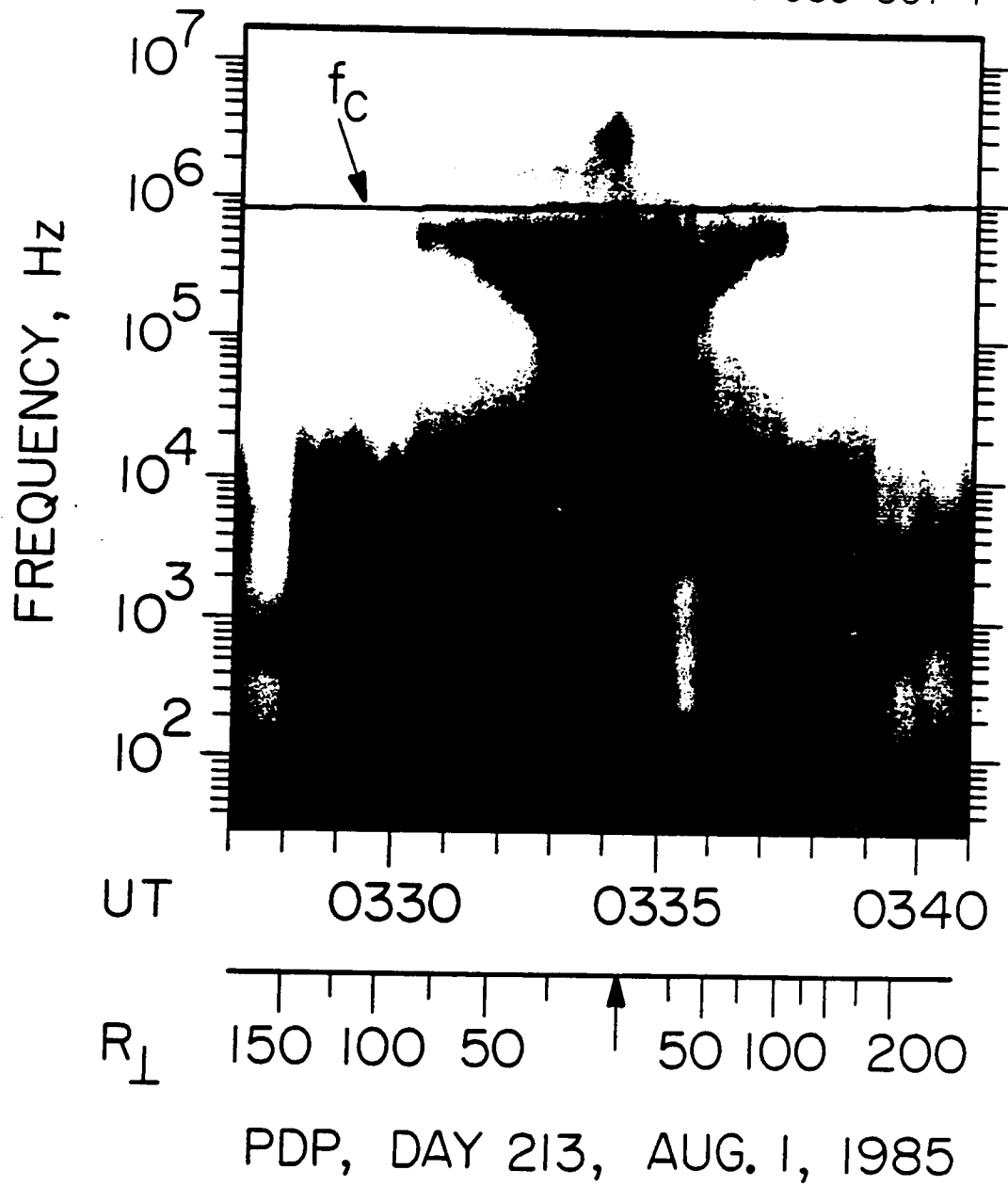


Figure 1

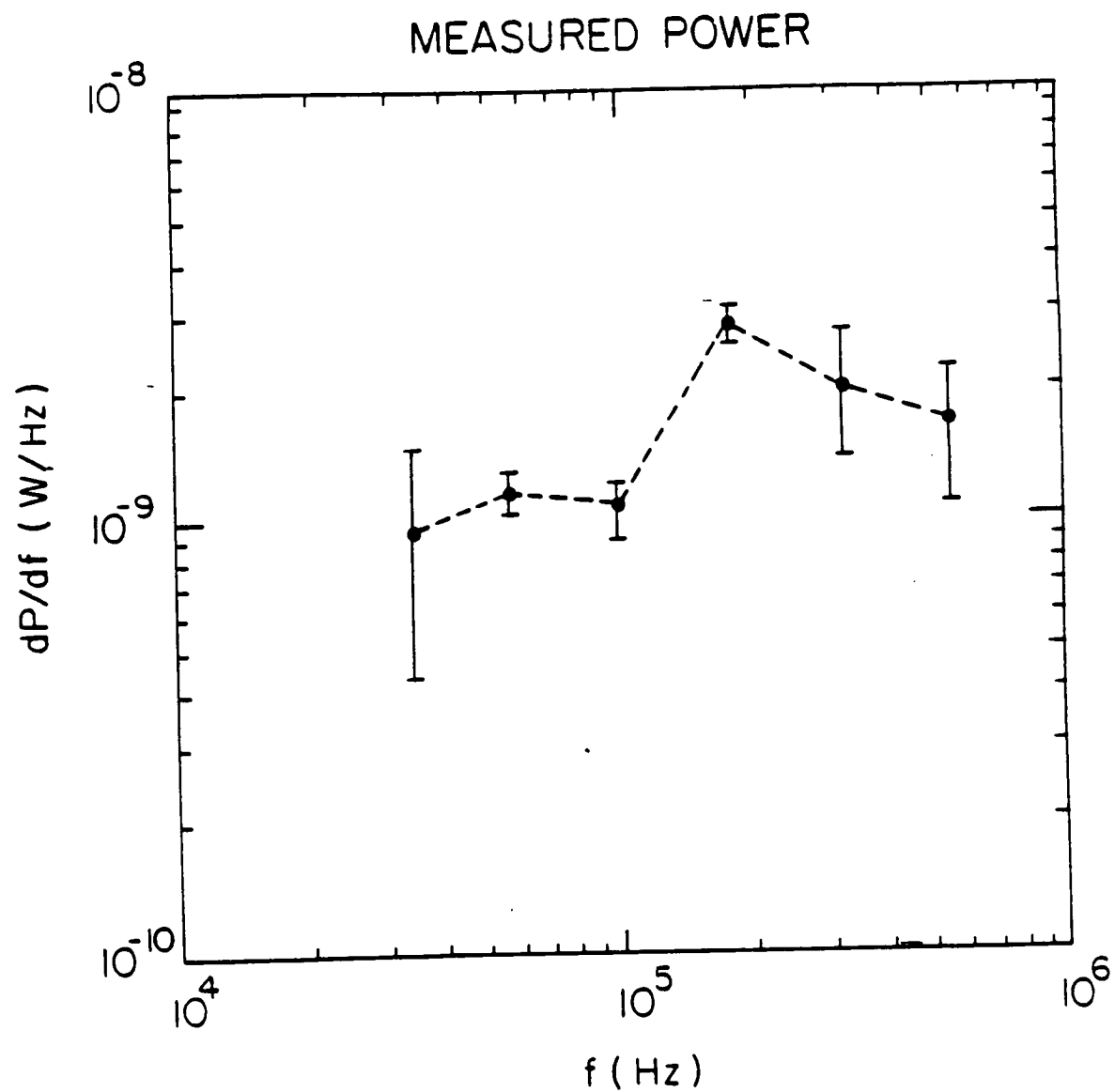


Figure 2

A - G88 - 359

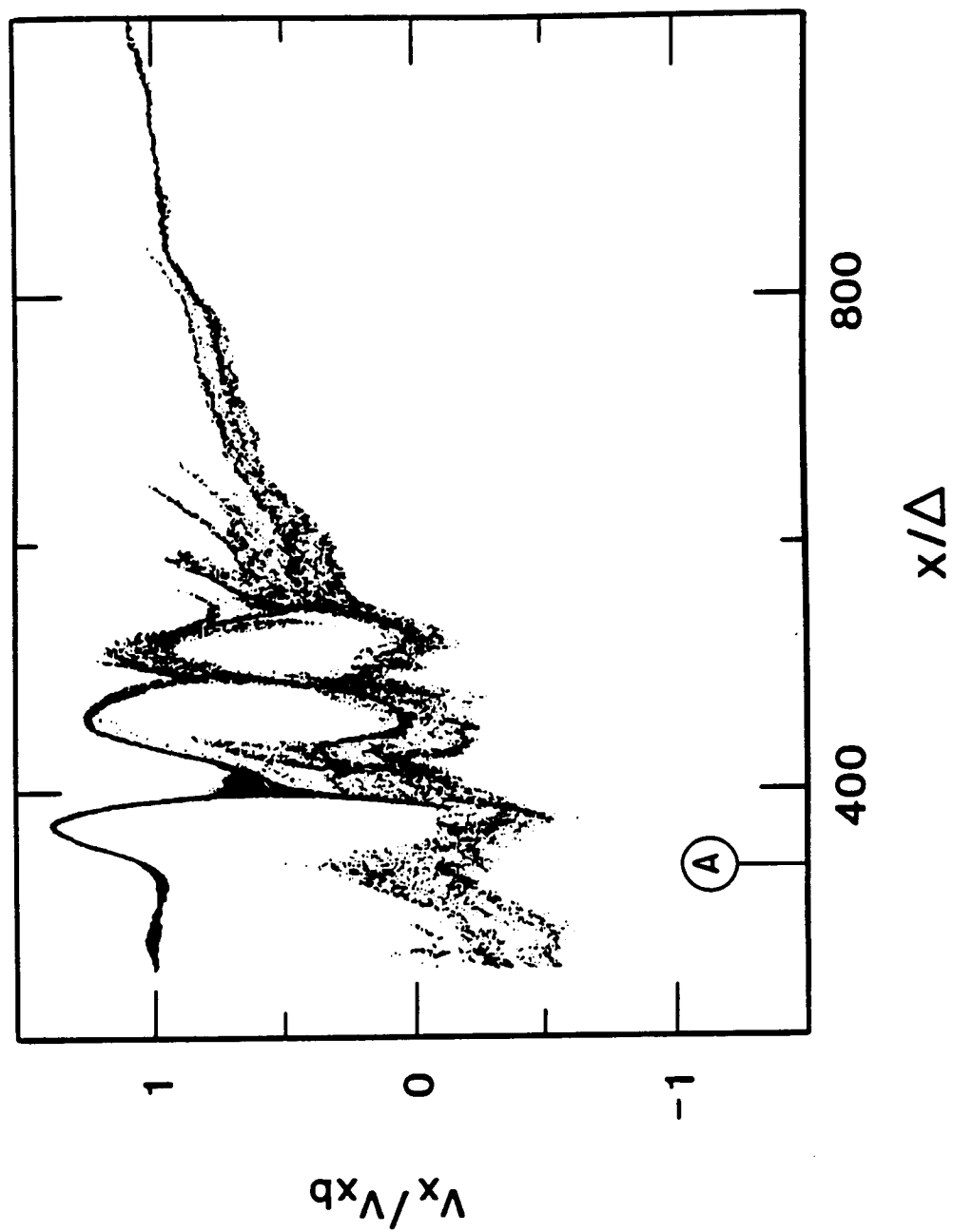
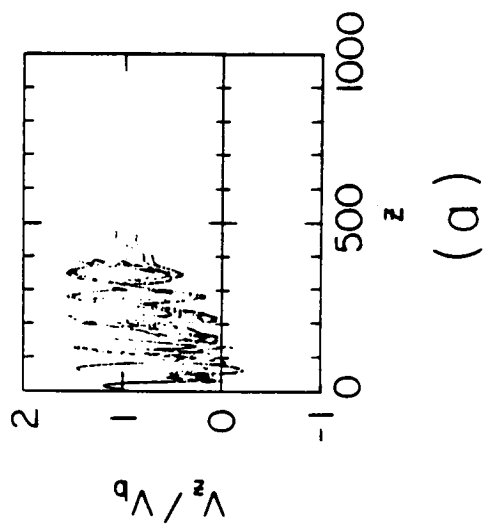
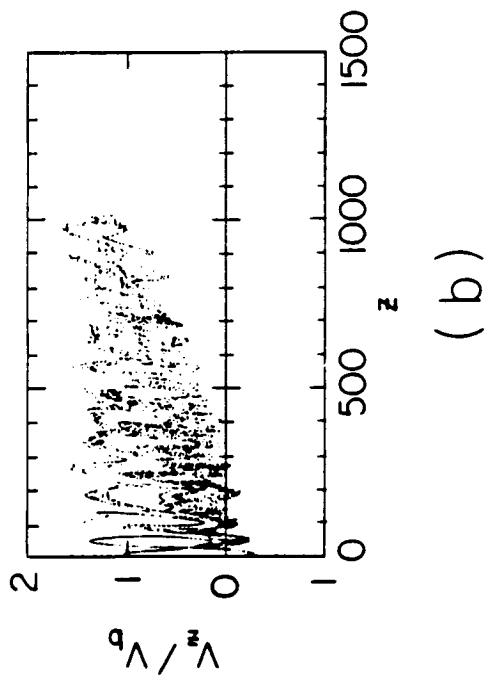


Figure 3

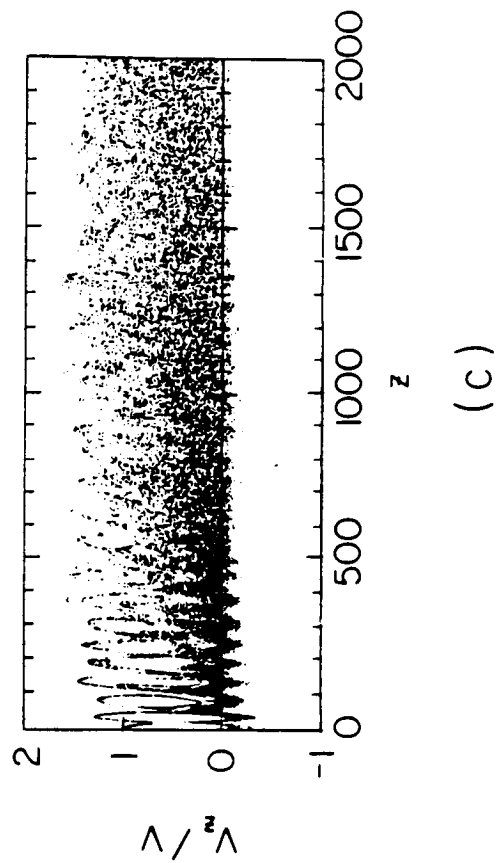
A-G88-75-1



(a)



(b)



(c)

B-G88-74-1

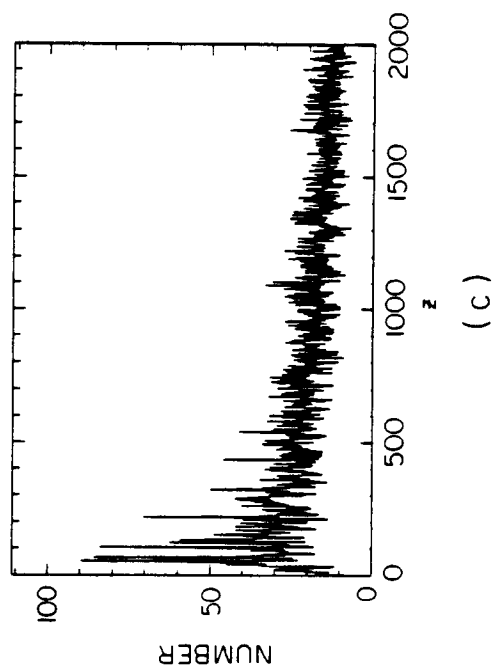
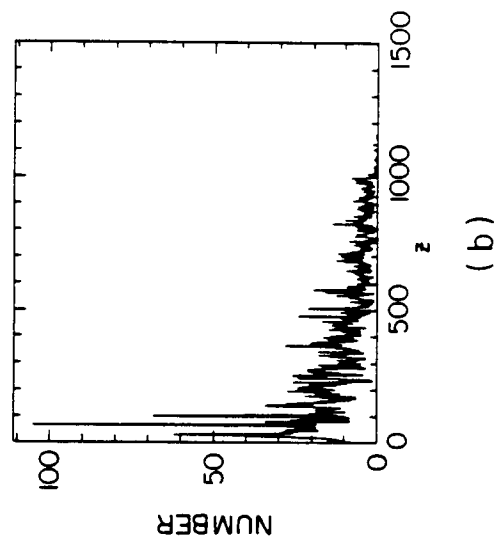
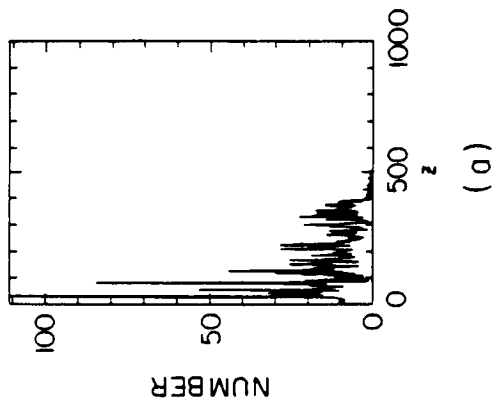
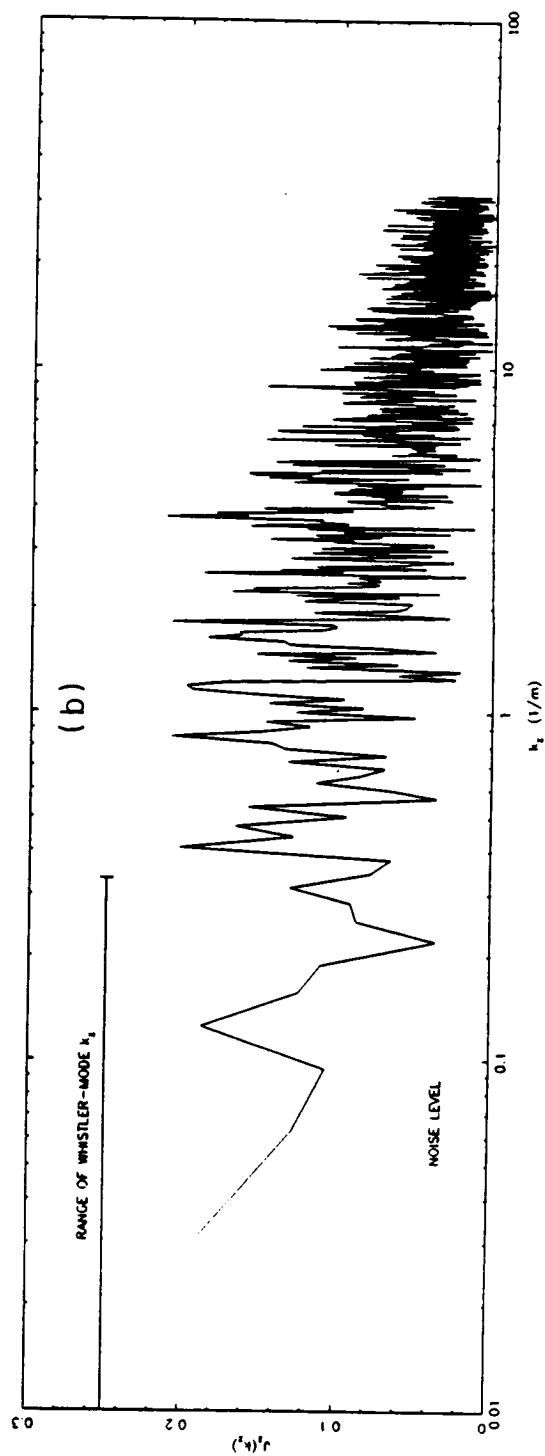
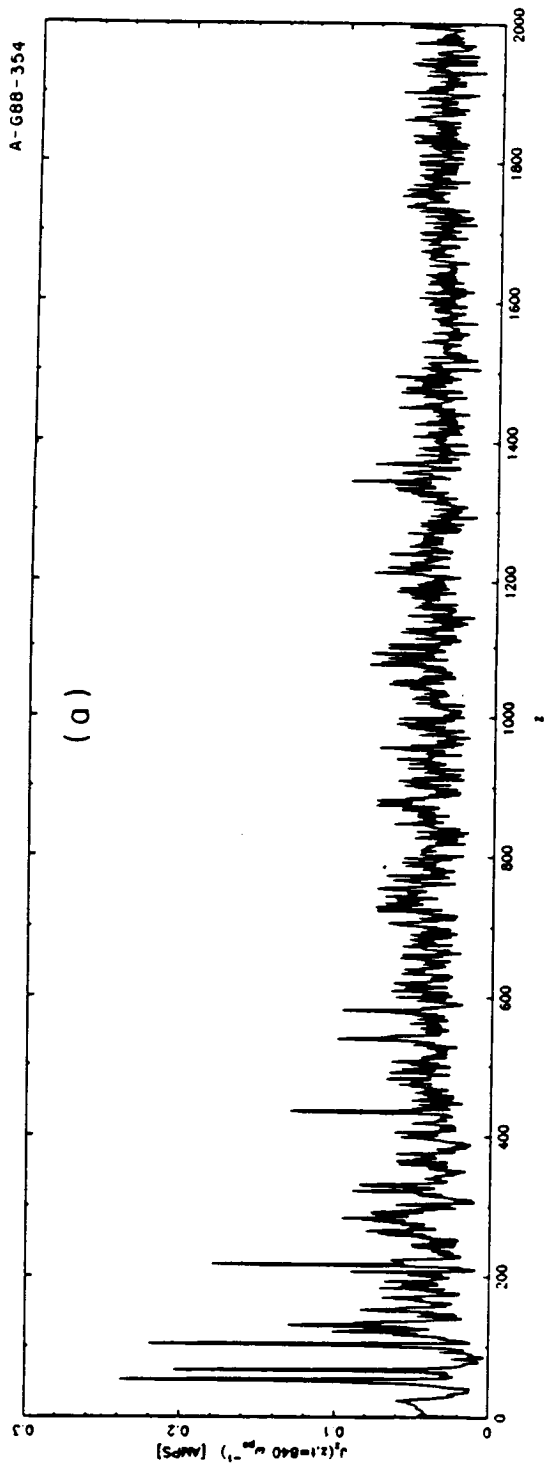


Figure 5



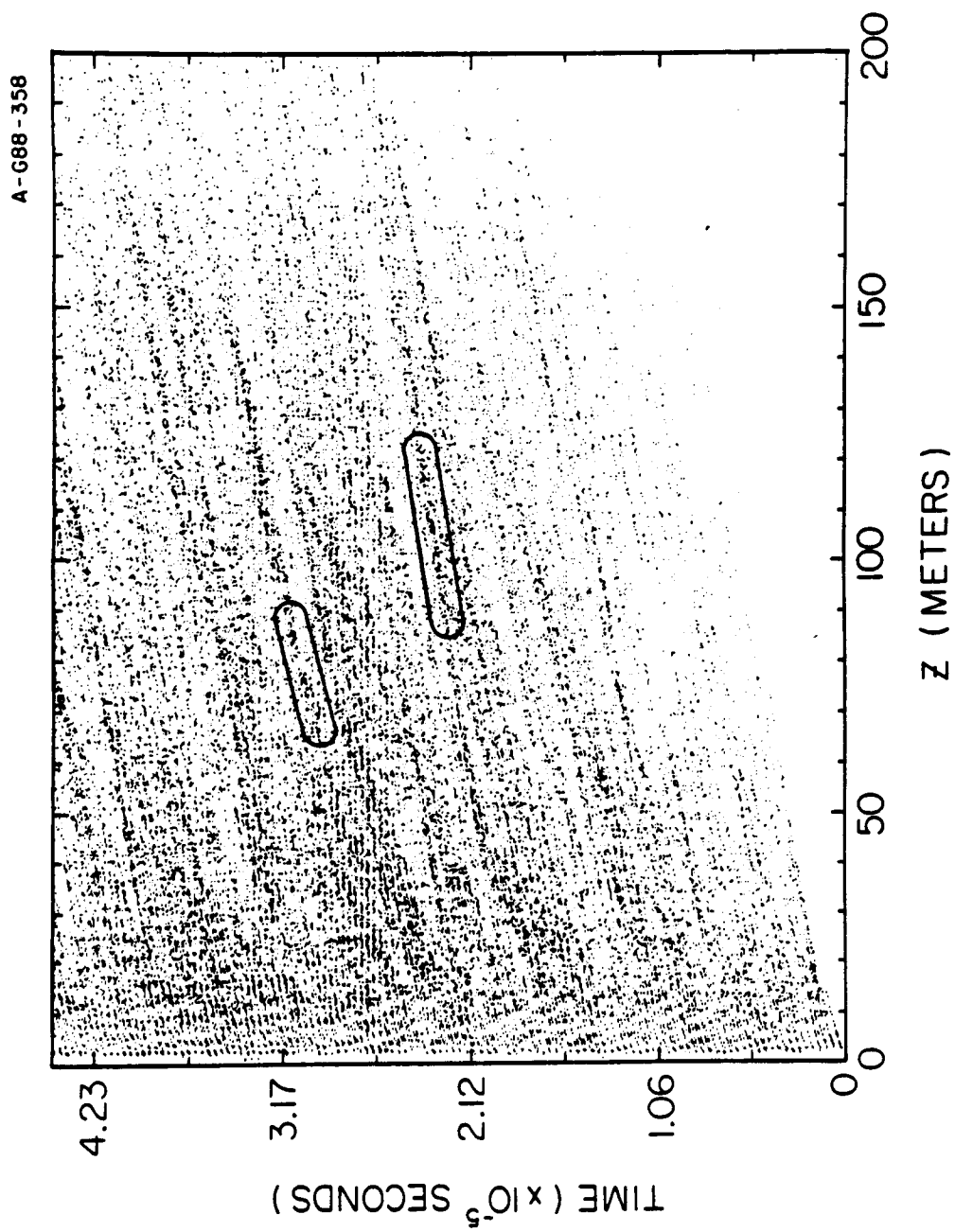


Figure 7

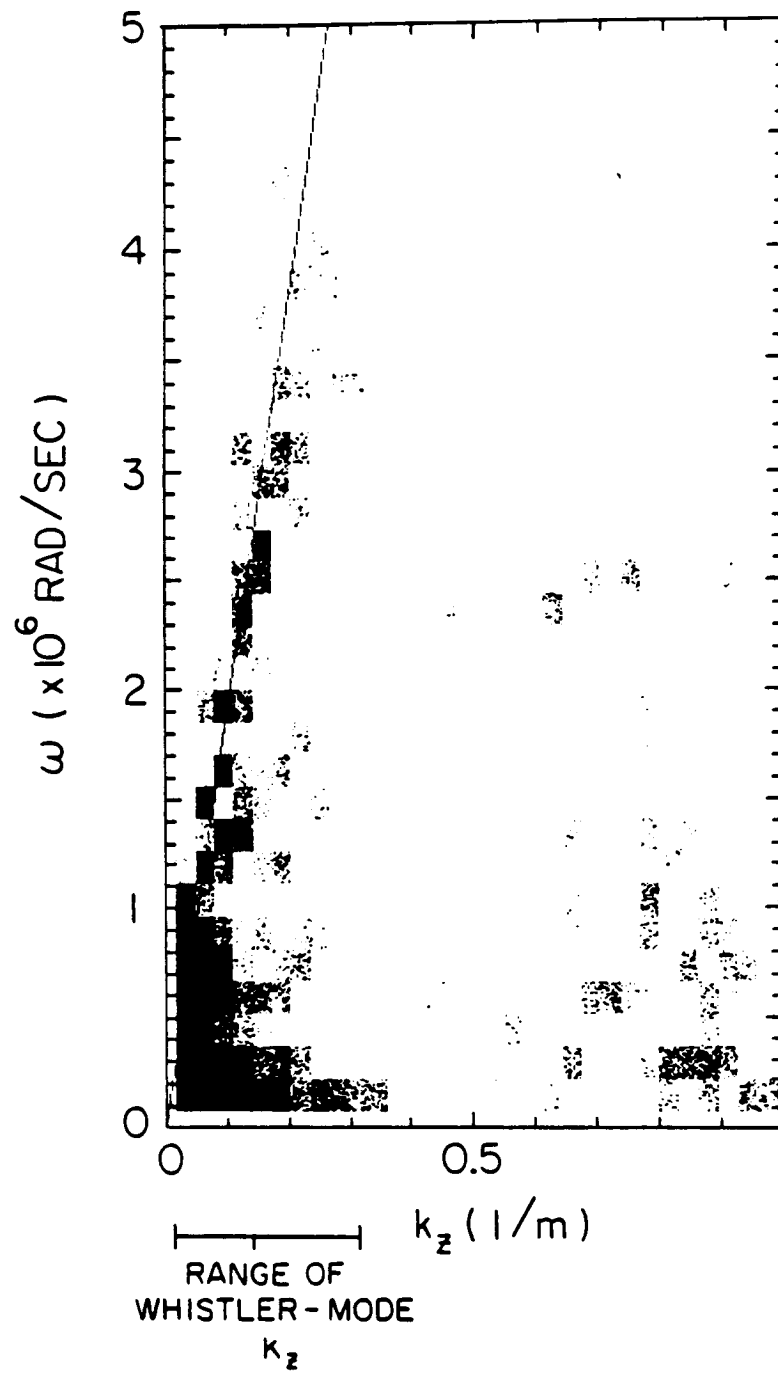


Figure 8

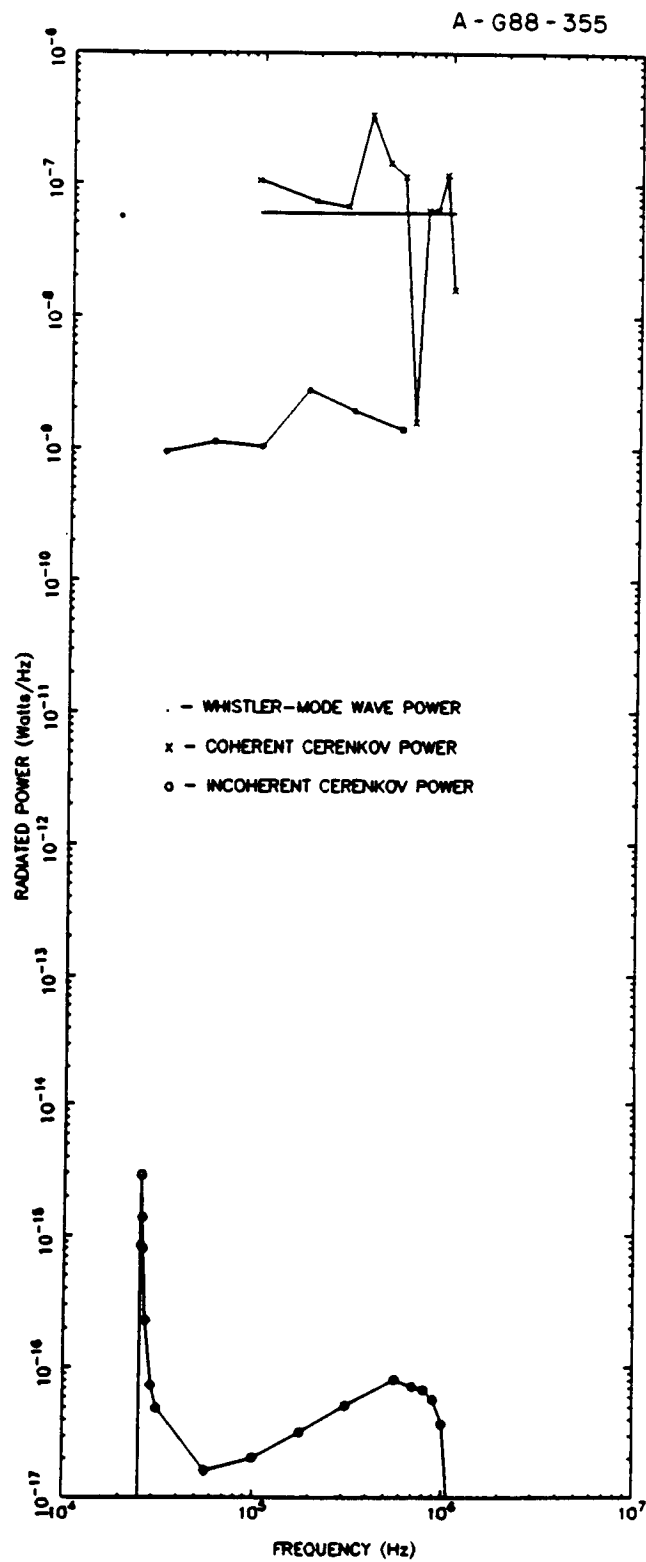


Figure 9

THE PLASMA WAKE
OF THE SHUTTLE ORBITER

by

G. B. Murphy,¹ D. L. Reasoner,² A. Tribble¹

N. D'Angelo,¹ J. S. Pickett,¹ W. S. Kurth¹

Submitted to Journal of Geophysical Research

December 1987

Revised May 1988

¹Department of Physics and Astronomy, The University of Iowa, Iowa City,
Iowa 52242

²Code ES53, NASA/MSFC, Huntsville, AL 35812

ABSTRACT

One of the principal objectives of Experiment 3 on Spacelab 2 was to use the Plasma Diagnostics Package (PDP) instrumentation to obtain more information about the plasma wake of a large body such as the shuttle orbiter. We present plasma density and temperature data taken both while the PDP was attached to the RMS and while it was a free flying satellite. Cross-sections of the wake taken from 10 meters to 240 meters behind the orbiter give a first look at the structure of the electron and ion wake. We conclude that the wake is "smooth" with no wave-like density disturbances (as expected for a plasma with $T_i \approx T_e$), and that the near wake may be influenced by the magnetic field and a significant contaminant plasma population. Enhanced plasma temperatures are observed at the wake boundary, but no definitive heating mechanism is established. An increase in the sophistication of the instrumentation as well as the experiment itself will be required to further examine the physics of the fill process for objects of this scale size.

INTRODUCTION

For more than 20 years experimentalists and theorists alike have struggled with the characterization of plasma wakes. The many variables such as relative ion and electron temperature, ion composition, body size, and body potential have divided the generic problem into a series of problems each with its own appropriate approximations and solution. The regime of very large body size $\gtrsim 10^3 \lambda_D$ has been one that is difficult to explore in the laboratory. Several ionospheric experiments have been performed but none exceeded the $\sim 10^2$ -- $10^3 \lambda_D$ scale size until the advent of the shuttle orbiter. More significantly, there has been relatively little done in the laboratory where the object size is large compared to both the ion and electron gyroradius [e.g., Schmitt et al., 1973; D'Angelo et al., 1986]. The orbiter satisfies all of these conditions but unlike laboratory experiments can have magnetic field/flow vector orientations which are at arbitrary angles. It is important to note that the wake characteristics may vary because of this magnetic field orientation. In the regime where a body is larger than an ion gyro radius the orbiter offers unique investigative capabilities.

This paper will discuss measurements in this large-body regime made by the Plasma Diagnostics Package (PDP) during Spacelab 2. The first section describes the nature of the wake experiment, the second details the ionospheric conditions and establishes the scale sizes of interest. In the next we present the electron and ion density data and discuss the enhanced electron temperature in the wake. Finally, a comparison between this data set and those from other spacecraft and missions is presented.

EXPERIMENT

The PDP, a small recoverable scientific satellite, designed and built at The University of Iowa, was one of 13 experiments aboard Spacelab 2 on Shuttle 51F in July-August 1985. One of its principal objectives was to determine the characteristics of the wake associated with a large scale structure such as the orbiter. A complete description of the PDP and its instrumentation can be found in Shawhan et al. [1984]. This paper will focus on electron density and temperature data collected by the Langmuir Probe (LP) instrument described in Murphy et al. [1986] and on ion density measurements taken by the Retarding Potential Analyzer (RPA) described in Reasoner et al. [1986]. It will build the database of previously reported shuttle wake investigations e.g. Murphy et al. [1986], Stone et al. [1986], Raitt et al. [1987].

Two key sets of experiments were performed during this mission which enabled the PDP to characterize the orbiter wake at distances downstream which ranged from ~ 10 m to 240 m. The first configuration was designed to measure cross sections of the near wake.

The PDP was positioned by the RMS at approximately 10 m directly above the orbiter cargo bay (Figure 1). The orbiter then underwent a slow roll, at the rate of 1 degree per second, so that the PDP would pass alternately from the ram of the plasma flow into the orbiter wake. This effectively measured the wake across its narrowest dimension (the orbiter's y-axis) and occurred nine times during a one-hour period. During this maneuver the orbiter's

x-axis, as defined in Figure 1, remained perpendicular to the plasma flow vector. For our purposes we consider the orbiter as the stationary frame with the plasma moving past it.

A second type of experiment was performed during a 6-hour period of the SL-2 mission devoted to the PDP "free-flight" experiment, an interval when the PDP was released from the orbiter and operated as a spin-stabilized satellite. The orbiter performed a series of maneuvers designed (among other things) to cause the PDP to pass through its wake at varying distances. This measured the orbiter wake along its widest dimension (the orbiter x-axis). At the end of this 6-hour free-flight period the orbiter approached the PDP and the Remote Manipulator System (RMS) arm was used to recapture it.

We may subdivide the free-flight into two experiments of particular importance in the context of wake studies. The first is the orbiter back-away where, after releasing the PDP from the RMS at a distance of ~ 5 m above the payload bay, the orbiter separates along the velocity vector. This maneuver is illustrated in Figure 2. The approach phase proved to be less useful since it occurred in a region where the ionosphere was quite variable and so normalization was not practical. During the second period of interest wake transits associated with an "elliptical fly-around" were performed. These wake transits, as well as some performed in a zig-zag fashion at the end of the free-flight period, constitute a series of wake crossings made in the orbit plane. These maneuvers are illustrated in Figure 3a. The wake transits resulting from the "fly-around" and "zig-zag" maneuvers are highlighted and numbered in Figure 3b.

A word about the coordinate system is in order. The system used throughout is the Local Vertical Local Horizontal (LVLH) or "airplane-mode" coordi-

nates which are non-inertial and move along with the objects in orbit. We have chosen to place the PDP at the origin of this system since it is the passive object. X is positive in the direction of the orbital velocity vector, Z is positive downward, or toward nadir, and Y is positive perpendicular to the orbit plane and in a southerly direction (see Figure 2). All wake transits take place within the X-Z plane (± 5 meters). Knowing the spacial relationship between the orbiter and PDP is critical in the analysis of wake data. The trajectory reconstruction for Figure 3 was done by an elaborate Kalman filter and backward-smoothing program called RELBET which uses the orbiter's rendezvous radar data as its input. Details of this process are discussed in Huysman [1985], and in Pieniazek [1985]. The reconstructed trajectory is accurate to a typical 1-sigma sphere of diameter 10 meters. Construction of the trajectory during back-away out to approximately 40 meters was performed by integration of the separation velocity obtained from on-board navigation software.

IONOSPHERIC CONDITIONS

The altitude of the orbiter during the PDP RMS and free-flight experiments was 325 km and the orbit inclination was 49.5 degrees. Typical ionospheric densities on the dayside are 1×10^5 to $5 \times 10^5 \text{ cm}^{-3}$. Ion and electron temperatures are typically 1500 to 3000 Kelvin with $T_i/T_e \sim 1$. The dominant ionic component is O^+ . The orbiter velocity of 7.7 km/sec results in the interaction with the ionosphere being supersonic with respect to ions (Mach 4-8) but subsonic with respect to electrons (Mach $\lesssim 0.05$). The size of the orbiter is $\sim 10^3 - 10^4$ times the Debye length, $\sim 10^3$ times the electron gyroradius, and is even large (\sim a factor of 5) compared to the ion gyroradius. This places the orbiter wake investigation in a unique position in the parameter space heretofore unexamined by laboratory and small satellite experiments.

OBSERVATIONS

Since wake observations are generally presented in the literature as densities normalized to ambient we attempt to consistently do so as well. Cautions about how this normalization is done, however, are warranted under certain circumstances and these will be discussed as the data are presented.

We first examine the roll maneuver data taken while the PDP was on the RMS as illustrated in Figure 1. These data are normalized to the value of density obtained when the PDP is in front of the orbiter. An important point to note is that after the first 360° orbiter roll, the PDP is rotated by the RMS as the orbiter revolves so as to maintain a constant geometric relationship between the probe, the body of the PDP and the velocity vector.

Figures 4a and 4b plot the normalized density for two typical roll scans of the orbiter's near wake. The X-axis has been converted to equivalent distance in meters from the center of the wake. These data presented were taken on the relatively stable dayside mid-latitude ionosphere in order to prevent naturally occurring variations from obscuring the data. Data near the center of the wake are missing because of limits in instrument sensitivity. The slight offset of the center of the wake is due to the physical offset of the probe from the center of the spacecraft.

Figure 5 illustrates a slightly longer segment of raw un-normalized data which center about the wake crossing of Figure 4b. This particular segment of data had the PDP fixed with respect to the orbiter instead of fixed with

respect to the velocity vector and as a result shows two smaller wakes which result from the RMS "wrist" grappled to the top of the PDP. Also illustrated are the effects of thruster firings which occurred during this time interval to initiate and stabilize the roll maneuver. (The thruster data had been cleaned from Figure 4b in order to more clearly present the orbiter wake data). The significance of these smaller "RMS wakes" and the thruster firings will be discussed in the last section.

Also illustrated in Figure 5 are electron temperature measurements made at regular intervals during this time period. The rise in temperature as the probe enters the wake of either the RMS (small wakes) or the orbiter is evident. Temperatures are not calculated near wake center where the density is too low to permit reliable calculations. In all, a total of nine wake crossings were observed but due to lower background densities near dusk and on the night side, the above two cases are the most meaningful to discuss. Figures 6 and 7 present the wake observations from the free-flight segment. To obtain normalized densities for this experiment, we tried initially to compare wake data to those data which were taken either one orbit earlier or one orbit later (similar local time and latitude). In principal, this should help to remove the effects of the slowly varying background.

This, however, is not possible with either the back-away data or wake transits 1 and 2 since they occur on consecutive orbits at the same local time. Various attempts at normalizing the data led us to the conclusion that the simplest and least misleading method would be to normalize to a constant density for the back-away data and to a linear extrapolation of the density on either side of the wake for transits 1 and 2. It was unfortunate that another

instrument capable of continually monitoring the background density for comparison was mounted on a pallet in the orbiter bay and in deep wake during all of these experiments.

Figure 6a plots the observed electron and ion density depression during the back-away maneuver with a constant $10^6/\text{cm}^3$ chosen as the reference density. In this case, the ion density is plotted only for times during spin-up of the PDP when the ion instrument is pointed in the ram direction ("+" symbols). Ion densities are calculated assuming a mass of O^+ . The dots are the electron density (small periodic depressions result when the boom-mounted probe passes through the wake of the spinning PDP). During the back-away the PDP and orbiter pass from a latitude of approximately -20 to $+30$ degrees in early afternoon local time. It should be noted that over the range of the data shown the RPA and LP data agree on density within $\sim \pm 10\%$. Figure 6b shows the measured ionospheric electron density one orbit later and will be discussed further in the next section.

Figure 7a shows the observed density for Wake Transits (WT) 1, 2, 3 and 4 in order of increasing distance. In the case of WT's 1 and 2 the density value used to compute the wake/ambient ratio is indicated by the dashed line in the figure which is a linear fit to density on either side of the wake. In the case of WT's 3 and 4 the dotted line used for normalization value is that of the ionosphere one orbit later and earlier respectively.

Figure 7b illustrates the same measurements for ion density with normalization values chosen identically to those in Figure 7a.

DISCUSSION

Beginning with data taken while on the RMS during the roll maneuver, we find three relevant observations.

1. At this distance downstream, which is $\lesssim 1R_0$, there is no evidence of any sharp transition in density or any rarefaction cone propagating away from the wake zone. The wake structure is smooth and if the data were extrapolated they indicate an approximate three order of magnitude depletion at wake center.
2. By comparing Figures 4a and 4b one can observe an asymmetry of the wake in 4b. The only variable that changes appreciably between these two cases is the direction of the magnetic field.
3. Temperature measurements made at the edges of the wake zone where density is still high enough to permit such analysis indicate a definite increase in this parameter.
4. The changes in density associated with thruster activity indicate depletion in background density but show that there is evidently a contaminant electron and ion population generated by the thruster. This thruster-generated plasma can raise density by $\gtrsim 1$ order of magnitude over what is expected by extrapolating the curve to wake center (see Figure 5a).

Laboratory investigations of the very near wake are non-existent for cases that scale both the Debye length, electron and ion gyroradii.

Most differences between distinct cases, (i.e. varying ratios of body size to Debye length, varying Mach number [Stone, 1981], or different ratios of T_i/T_e [Fournier and Pigache, 1975]) show fundamental differences only in the mid or far-wake zone. The only space experiment involving objects of this approximate scale size, within a factor of 2 to 5, were those conducted during the Gemini/Agena docking [Medved et al., 1969]. However, no clear cross sections of the near wake are available.

Thus, there exists no other data sets for direct comparison. One can argue, however, that for $R_0 \gg \lambda_D$ (let's say $R_0 \gtrsim 20 \lambda_D$ at a minimum) little difference in wake physics should exist between varying body sizes. A specific experiment which addressed the issue of the effects of body potential was conducted by Merlino and D'Angelo [1987]. They found in a laboratory experiment with an ion beam (energy ~ 17 eV) that appreciable changes in ion density could be observed at object biases of $\lesssim -4V$ at distances of $1.5 R_0$ downstream. For our observations at $z \lesssim 1R_0$, the orbiter dielectric surface at a potential of ~ -0.7 volts, and the ram O^+ energy of 5 eV, we believe the effect of the body potential can only be a secondary one. This depends, of course, on the "thickness" of the body and the specific potential at all the given transit paths of ions but, on the average, the sheath electric field would not seem to dominate the effect of the space charge field present in the void behind the vehicle. For very large objects we assume, therefore, that reasonable estimates of density at a given value of z/R_0 and ratio of T_i/T_e can, to first order, be scaled by the Mach number. Only when we get to a regime where the body size becomes large compared to an ion gyroradius or the

body potential becomes "large" should other fundamental differences become apparent.

In this case we may have an example of the effect of the magnetic field on the plasma dynamics of the near wake. Schmitt [1972] has investigated the effect of the magnetic field in a Q-machine. His experiment supports the following conclusions: (1) If the magnetic field is perpendicular to V , ions will be free to move along the field and the wake fill process will be unaffected along an axis parallel to B . (2) If, however, the magnetic field is aligned with V it can inhibit the void-filling process once the object becomes large enough to alter the distribution function of ions flowing past it. This implies that the object must be $\gtrsim 2 \rho_i$ in size. (3) Ion "bunching" occurs with a spacial periodicity related to the ion gyro period. Bogashchenko et al. [1971] have also observed periodicity in the far wake associated with a magnetic field where the object was on the order of an ion gyroradius in diameter.

Our experiment has met the condition that $R_0 \gtrsim 2 \rho_i$. Instead of being purely parallel or perpendicular to the field lines we have a case where the magnetic field has components both along and perpendicular to the velocity vector. This is a condition which would be extremely difficult to simulate in the laboratory. Table 1 indicates the different magnetic field geometries for the two cases depicted in Figure 4.

Clearly the principal difference is related to the fact that the magnetic field in Case A is closer to being parallel to the velocity vector than in Case B. Also there is a much larger component of the magnetic field along the Y-axis in Case B. Although the RMS roll observations occur at a distance

which is too close to the orbiter to observe the ion bunching, the asymmetry observed in 4b may be a result of this magnetic field.

Turning briefly to the electron temperature of Figure 5, we see that electrons appear "hotter" in the wake than in the "ambient" conditions sampled while the PDP was in front of the orbiter. The absolute error in determining temperature is approximately 50% so the enhancement is real (see Murphy et al., [1986] for a discussion of errors). This agrees with results reported by Murphy et al. [1986] for PDP observations of the orbiter wake during the OSS-1 mission. In those initial results, data taken while the PDP was in the payload bay and the orbiter was executing a roll maneuver (an inertial roll in that case) showed enhancements in temperature by a factor of about four at the edges of the wake. RMS data taken on that flight were less conclusive, but indicated an increase of what appeared to be about a factor of two in T_e .

Here, in a more cleanly defined experiment, we have clear evidence of this temperature increase at a distance of $Z \approx R_0$ downstream. This data combined with results of others (Medved, 1969; Samir and Wrenn, 1972; and Samir and Fontheim, 1981) would seem to lead to the inevitable conclusion that in front of a spacecraft (in this case about 10 m in front) the typical ionospheric values of .1 -.2 eV are encountered while the wake contains an electron population which appears hotter in the sense of equivalent temperature of a Maxwellian electron distribution. Studies of the RPA data in this time frame show no evidence of an increased ion temperature.

The ion motion into the wake is controlled by (a) the potential of the body (for small body sizes); (b) the thermal motion of the ions; (c) the space charge electric field created by the electrons in the wake; (d) the magnetic field. An enhanced electron temperature may imply that a larger space charge

field may exist in the wake. This could mean that models which assume $T_e \gg T_i$ (process 'c' above dominates process 'b') may be a better approximation for ionospheric wake models than heretofore expected. It has yet to be explained, however, what process causes this electron heating. Several mechanisms have been discussed including: (1) the hot electrons result from a selection effect by the negative potential found in the wake; (2) energization by wave-particle interactions; (3) adiabatic compression of electrons as they enter the low potential region [Murphy et al., 1986]. None of these processes can be ruled out from these data.

Last of all we note that electron density depletions associated with thruster firings are consistent with previous observations and with the postulate that H_2O acts to create a "plasma hole" which in this case is short lived because the orbiter moves rapidly out of the spatially small depletion area.

Let us now discuss data from the free-flight segment presented in Figures 6 and 7. The back-away data of Figure 6 pick up about where the RMS data leave off. As discussed in the previous section these data have been normalized to $1 \times 10^6/\text{cm}^3$. In studying the data of Figure 6 several observations are relevant.

- (1) Both ion and electron data agree to within $\sim 10\%$.
- (2) Although most data have a narrow scatter about a line, a large number of points appear below the line. These points correspond to the time when the Langmuir Probe is in the wake of the spinning PDP. Note that the period between these PDP wakes decreases as the spacecraft slowly comes up to speed while braking its momentum wheel.
- (3) There is a clear increase in density as the PDP moves away from the orbiter.

(4) Comparison between the two panels seem to indicate that there is considerable (spacial) variation in background ionospheric density.

One of the most significant conclusions results when one compares the density right before release (slightly less than $10^4/\text{cm}^3$) to that observed under similar plasma conditions during the roll maneuvers illustrated in Figure 4.

Let us examine the different geometric configurations for these two cases. Examining Table 1, we see that the data taken during the first roll maneuver and depicted in Figure 4a, have a similar magnetic field vector in the LVLH frame as the free-flight case. The PDP was held in a different attitude by the RMS for the data in Figure 4a than it was after release. The result was that the position of the Langmuir Probe was slightly forward (+X in orbiter coordinates) and slightly closer to the cargo bay (smaller value of -Z). This difference was small, however, and resulted in a relative position shift of only a few feet. More significantly, the attitude for the two cases differed by 90° . During the RMS roll maneuver the orbiter +Z-axis was aligned with the velocity vector (at wake center) and its X-axis was perpendicular to the orbit plane (Figure 1). When the PDP was released for free-flight the +Z-axis was aligned with the velocity vector but the orbiter X-axis was in the orbit plane (Figure 2). The importance of this difference will be revealed below.

How can we reconcile the deep wake observed during the roll maneuver (no current detection at wake center implies a density of $< 10^2/\text{cm}^3$) with the $\sim 10^4$ density observed while slightly closer to the orbiter right before

release? The answer requires going beyond the study of the ambient plasma wake to consider the effects of contaminant ions.

A number of authors have investigated the contaminant ion population in the vicinity of the orbiter. Hunton & Calo [1985] observe that at a particular time early in the STS-4 mission, ion species in the orbiter bay consisted of 36% ambient O^+ , 13% H_2O^+ and 48% H_3O^+ . Since two serial reactions are required to produce the H_3O^+ , the second being H_2O^+ with the H_2O cloud, this water cloud must indeed be quite extensive. Shawhan et al. [1984] indicate payload bay pressures in the 10^{-5} Torr range near ram which would also be consistent with high outgassing rates. A detailed investigation by Pickett et al. [1985] of the effects of chemical releases in the ionosphere by the orbiter FES, thrusters, and outgassing attributes high energy ions, observation of plasma turbulence, electrostatic waves, and DC E-field modification to a halo of H_2O^+ pick-up ions that exist around the orbiter.

To understand the wake measurements near the payload bay we must then look not only at the ion density but at its composition. Grebowsky et al. [1987] discuss the ion composition measurements made with a Bennett Ion Mass Spectrometer which was also a part of the PDP experiment. In a plot of ion composition, obtained once per spin cycle, they find the first ion peak detected after PDP release (at a distance of $\sim 12-15$ meters) to be H_2O^+ , not O^+ . In fact O^+ does not become the dominant ion species until the PDP gets to a distance of $\gtrsim 25$ m. Several explanations have been explored for the origin of these H_2O^+ and even H_3O^+ ions so near the orbiter, particularly in the wake. One possibility is that the water contaminant cloud is dense enough that the mean free path allows the creation of water ions within the first few meters

of the surface. This may be plausible but is unlikely even for non-wake ion measurements. For H_2O^+ to exist in an O^+ wake, they must originate elsewhere because the O^+ is needed to create H_2O^+ . Grebowsky et al. [1987] observe these water ions to distances of several hundred meters even in front of the orbiter. Paterson [1987] observes hot ions during the entire PDP free-flight period and verifies the ring distribution characteristic of such pick-up ions created in the $\text{O}^+/\text{H}_2\text{O}$ charge exchange reaction. Paterson calculates an average outgassing rate of water to be $\sim 10^{22}$ molecules/sec, assuming known cross sections for the reaction and a spherically expanding cloud at 300K. This model is valid to distances of a few km where loss processes begin to affect the density and it predicts densities close to those observed by Grebowsky et al. [1987] at distances of a few hundred meters. Caledonia et al. [1987] have modeled the chemistry of this cloud and find that water densities of $\sim 10^{10}/\text{cm}^3$ are consistent with observed pressures in the 10^{-6} Torr regime. They also indicate that using 5ev rate constants for the charge exchange interaction is a valid assumption for pressures $< 10^{-5}$ Torr. The gas cloud will have charge exchange ions with a guiding center motion in the direction of $\vec{E} \times \vec{B}$ where \vec{E} is the motional electric field, $\vec{v} \times \vec{B}$, measured in the shuttle frame. These ions will thus appear in the orbiter's reference frame, to be swept by in a direction perpendicular to that of the local magnetic field at velocity $V_{\perp} = V_0 \sin \alpha$ where α is the angle between V_0 , the orbiter velocity, and the earth's magnetic field. The motion of this contaminant cloud has recently been investigated and modeled by Eccles et al., [1988]. This results in a source of H_2O^+ ions which, when observed from the orbiter wake, will appear to approach at an angle $90-\alpha$ with respect to V_0 . The ambient O^+ ions approach along V_0 . This is consistent with

the Grebowsky et al. [1987] observations which indicated peaks in H_2O^+ occurring at angles as great as 77° to that of 0° . It is important to note that these observations reported by Grebowsky et al. were made at the same time as the data shown in Figure 6a.

Several conclusions are possible with the aid of Table 1, Grebowsky's observations, and the fact that the attitude of the orbiter with respect to the velocity vector (and magnetic field) was different for the two cases. The ions observed during the release of the PDP: (a) are contaminant ions; (b) are two orders of magnitude greater in density than the ambient O^+ in the near wake; (c) come from a direction, in the shuttle stationary frame, that is perpendicular to a field line. By studying the detailed B-field and orbiter attitude geometry we find that during the roll experiment the body, bay-doors and especially the wings of the orbiter shadowed the contaminant population in the deep wake. The magnetic field geometry after release did not allow the body to block the contaminant ions.

This points again to the necessity of careful evaluation of all these data and caution when comparisons are made with laboratory and other satellite data. It is possible that some of the asymmetry associated with data from Figure 4b may be due to the influence of this contaminant ion population. Note that this could also be called a magnetic field effect since the direction of motion of the contaminants is controlled by the magnetic field.

Last of all we examine the free-flight portion of data where WT's 1 through 4 occur. Table 2 summarizes the peak electron and ion density depressions normalized to the appropriately chosen background as shown in Figures 6 and 7. The Table is ordered with increasing wake distance. Note the relationship between the distance downstream and normalized density. The depth of the

wake and its width decrease as one moves to larger values of normalized Mach distance $X' = X/SR_0$. There is one inconsistent observation. For some reason WT 4 is not as pronounced as WT 2, which is actually further away. Looking for sources of error in this observation we find 1) error in determination of normalization value ($\sim \pm 10\%$); 2) an error in relative position (± 5 m); 3) an error in determining absolute values of T_e for normalization of Mach distance (± 500 K). These errors result in a total RMS error in observed normalized density as a function of mach distance of $\sim 20\%$ which is just enough to account for the observed inconsistency. It is useful, however, to examine real physical effects which could produce a wake which does not result in a monotonic increase in density behind an object. No ion species data is available at this time, so contaminant ions may not be totally ruled out. As discussed before, these contaminants are time variable and can be significant contributions. Grebowsky et al. [1987] show these contaminant species are, however, generally $\leq 10\%$ of ambient making it probable that they would only be a direct factor in the near wake density where depletions are greater than an order of magnitude (e.g. WT 3). Although the contaminants may not contribute significantly to the ion densities observed in the far wake they could affect this wake indirectly since they can alter the electric field of the near wake which affects the "rate of fill".

We postulate that the magnetic field may play a roll in the wake fill process and have tabulated the values of B_x , B_y and B_z in the LVLH frame in Table 2. One possible effect as presented during the discussion of asymmetries in the RMS roll data may be that for objects whose characteristic size projected into a plane perpendicular to the magnetic field is greater than ~ 2 ion gyroradii, the field will inhibit the wake fill process to some degree.

This may in effect skew the wake "off center" making simple cross sectional cuts presented in these WT data somewhat misleading. Schmitt [1972] and Bogashchenko et al. [1971] data would also suggest that some ion bunching may be observed. We note in Table 2 however, that both WT's 3 and 4 satisfy this condition that $r \geq 2 \rho_i$. We therefore conclude that although magnetic field effects are possible at these "mid-wake" distances, no strong evidence is available from this relatively limited data set.

A third possibility is that ion deflection due to body potential, as investigated by Merlino et al. [1987], may play a role at distances of ~ 100 meters behind the orbiter. Although this deflection has been observed in the laboratory the orbiter potential should be virtually the same for these two cases.

A more thorough investigation of all of these effects and a more complete characterization of the orbiter wake will simply require a larger data base that is not restricted to two-dimensional crossings. Accurate, concurrent measurements of ambient density, ion species, and neutral density would also improve the accuracy in determining the normalized density. It is hoped that on future missions such experiments may improve our observational data base so that further advances in our theoretical understanding will be possible.

Acknowledgements

This work was supported by NASA MSFC contract # NAS8-32807, NASA LeRC grant # NAG 3-449, and NASA Headquarters grant #NGT-50402.

REFERENCES

- Bogashchenko, I. A., A. V. Gurevich, R. A. Salimov, Yu. I. E'idel'man, Flow of Rarefied Plasma Around a Body, Soviet Phys. JETP, 32, 841, 1971.
- Caledonia, G. E., J. Person, D. Hastings, The Interpretation of Space Shuttle Measurements of Ionic Species, J. Geophys. Res., 92, 273, 1987.
- D'Angelo, N. and R. L. Merlino, The Effect of a Magnetic Field on Wake Potential Structures, IEEE Trans. Plasma Sci., PS-14, 609, 1986.
- Eccles, J. V., W. J. Raitt, P. M. Banks, A Numerical Model of the Electrodynamics of Plasma Within the Contaminant Gas Cloud of the Space Shuttle Orbiter at LEO, submitted to JGR 1988.
- Fournier, G. and D. Pigache, Wakes in Collisionless Plasma, Phys. Fluids, 18, 1443, 1975.
- Grebowsky, J. M., H. A. Taylor, Jr., M. W. Pharo III, N. Reese, Thermal Ion Perturbations Observed in the Vicinity of the Space Shuttle, Planet. Space Sci., in press, 1987.
- Hunton, D. E., and J. M. Calo, Low Energy Ions in the Shuttle Environment: Evidence for Strong Ambient-Contaminant Interactions, Planet. Space Sci., 33, 945-951, 1985.
- Huysman, B. P., L. A. Pieniazek, STS Post-flight On-orbit Relative Trajectory and Ancillary Data Products, TRW Report #85:W482-1-57, 1985.

Medved, D. B., Measurement of Ion Wakes and Body Effects with the Gemini/Agena Satellite, Rare. Gas Dyn., 2, 1525, 1969.

Merlino, R. L. and N. D'Angelo, The Interaction of a Conducting Object with a Supersonic Plasma Flow: Ion Deflection Near a Negatively Charged Obstacle, J. Plasma Phys., 37, 185, 1987.

Murphy, G., J. Pickett, N. D'Angelo, and W. S. Kurth, Measurement of Plasma Parameters in the Vicinity of the Space Shuttle, Planet. Space Sci., 34, 993, 1986.

Paterson, W. R., Ion Plasmas in the Vicinity of the Orbiter: Observations and Modeling, M. S. Thesis, University of Iowa, July, 1987.

Pickett, J. S., G. B. Murphy, W. S. Kurth, C. K. Goertz, S. D. Shawhan, Effects of Chemical Releases by the STS-3 Orbiter on the Ionosphere, J. Geophys. Res., 90, 3487, 1985.

Pieniazek, L. A., Relbet User's Manual V.2 Update, TRW Report #85:W482.8-24, 1985.

Raitt, W. J., J. V. Eccles, D. C. Thompson, P. M. Banks, P. R. Williamson, R. I. Busch, Plasma Parameters in the Near Wake of the Space Shuttle Geophys. Res. Lett., 14, 359, 1987.

Reasoner, D. L., S. D. Shawhan, G. B. Murphy, Plasma Diagnostics Package Measurements of Ionospheric Ions and Shuttle-Induced Perturbations, J. Geophys. Res., 91, 463, 1986.

Samir, U., and E. G. Fonthelm, Comparison of Theory and In-Situ Observations for Electron and Ion Distributions in the Near Wake of the Exp 31 and AE-C Satellites, Planet. Space Sci., 29, 975, 1981.

Samir, U., and G. L. Wrenn, Experimental Evidence of an Electron Temperature Enhancement in the Wake of an Ionospheric Satellite, Planet. Space Sci., 20, 899, 1972.

Schmitt, J. P. M., Wake Past an Object in a Magnetized Plasma Flow, Plasma Phys., 15, 667, 1973.

Shawhan, S. D., G. B. Murphy, J. S. Pickett, Plasma Diagnostics Package Initial Assessment of the Shuttle Orbiter Plasma Environment, J. of Spacecraft and Rockets, 21, 387, 1984.

Stone, N. H., K. H. Wright, Jr., K. S. Huang, U. Samir, G. B. Murphy, S. D. Shawhan, Further Observations of Space Shuttle Plasma --Electrodynamic Effects from OSS-1/STS-3, Geophys. Res. Lett., 13, 217, 1986.

Stone, N. H. NASA TP 133, 1981.

FIGURE CAPTIONS

Figure 1. The RMS roll maneuver is illustrated here. The position of the PDP with respect to the orbiter is fixed, but is rotated about an axis parallel to the orbiter's X-axis to maintain constant orientation to the velocity vector. The orbiter's X-axis is perpendicular to the orbit plane. The width of the near wake along this axis is ~ 10 m corresponding to a body size of approximately $10^3 \lambda_D$.

Figure 2. The RMS arm releases the PDP approximately 5 m above the payload bay. The orbiter then separates from the PDP along the velocity vector at approximately .1 m/sec. The reference system used places x along the velocity vector, y perpendicular to the orbit plane (southward) and z positive toward earth's center.

Figure 3a. The entire 6 hours of PDP free-flight is reconstructed in this figure. The PDP is at the center of this coordinate system and the times of interest for this study occur when the orbiter passes through the shaded region. While in this region, characteristics of the orbiter's wake can be measured by the PDP. Note that unlike laboratory experiments, the probe (PDP) is held stationary and the object (orbiter) is moved.

Figure 3b. The "wake transits" are enlarged and labeled 1 through 4 for future reference. Note the range varies from ~ 50 m to ~ 250 m.

Figure 4. Electron density, for the first two wakes encountered during the RMS roll maneuver, are normalized to the ambient density obtained in front of the vehicle.

Figure 5. Unnormalized roll data show the effect of thruster operations and the smaller wakes associated with the RMS in 5a. In Figure 5b the temperature enhancement typical of the wake boundary region is indicated.

Figure 6. Ion and electron data during the back-away are plotted normalized to $n_e = 1 \times 10^6 \text{ cm}^{-3}$. Beyond $t \approx 25$ background density varies considerably as is illustrated in Figure 4b which are data for one orbit later at approximately the same station-keeping position.

Figure 7a. The smoothed values of ion and/or electron data for each wake transit are shown in the four panels. The decimal value indicated by the arrow is the fractional density at wake center. WT #3 has the ion data from Figure 7b superimposed to show the similarity in results.

Figure 7b. Only ion data is shown for the same time intervals of Figure 7a. Agreement with electron data is typically better than 10%. Accurate density is obtained once per spin cycle of the PDP. The spin modulation is evident in the data.

TABLE 1

Magnetic field geometry for Figure 4 (LVLH Coordinates)

	B_x^*	B_y	B_z	ϕ^{**}	θ	α^{***}
Figure 4a	.234	-.140	.091	-30.8	71.5	35.5°
Figure 4b	.188	-.131	.242	-35.0	43.5	55.7°
Free Flight (back-away)	.259	-.146	-.068	-30	77	32°

* B is in Gauss.

** Theta and Phi are defined in the conventional spherical coordinate sense from the right-handed XYZ system.

*** α is the angle between B and the velocity vector.

TABLE 2

Distance (meters)	Wake Transit#	Latitude (degrees)	Mach Distance*	$B_x B_y B_z$ (gauss)	Observed Normalized Ion/Electron Density $\pm 10\%$	α (angle between B and V)	Projected Ion Gyrodiameter
45($\pm 11\%$)	3	+10	0.2($\pm 23\%$)	(0.24, -0.21, 0)	0.17/0.18	41	5.3
105($\pm 9.5\%$)	4	+35	0.4($\pm 22\%$)	(0.15, 0.25, -0.2)	0.80/0.90	65	3.0
125($\pm 4\%$)	2	-45	0.5($\pm 20\%$)	(-0.06, -0.4, -0.35)	0.60/0.61	84	0.7
242($\pm 2\%$)	1	-35	0.9($\pm 20\%$)	(0.04, -0.15, -0.5)	0.75/0.80	86	0.5

* Assumes $R_0 \sim 20$ meters and $S = 4.8$ ($T_e = 2500^\circ$).

(T_e is accurate in an absolute sense to about ± 500 K.)

These are absolute errors in determining Mach distance. Relative errors from one

WT to the next are less and believed to be $\lesssim 10\%$.

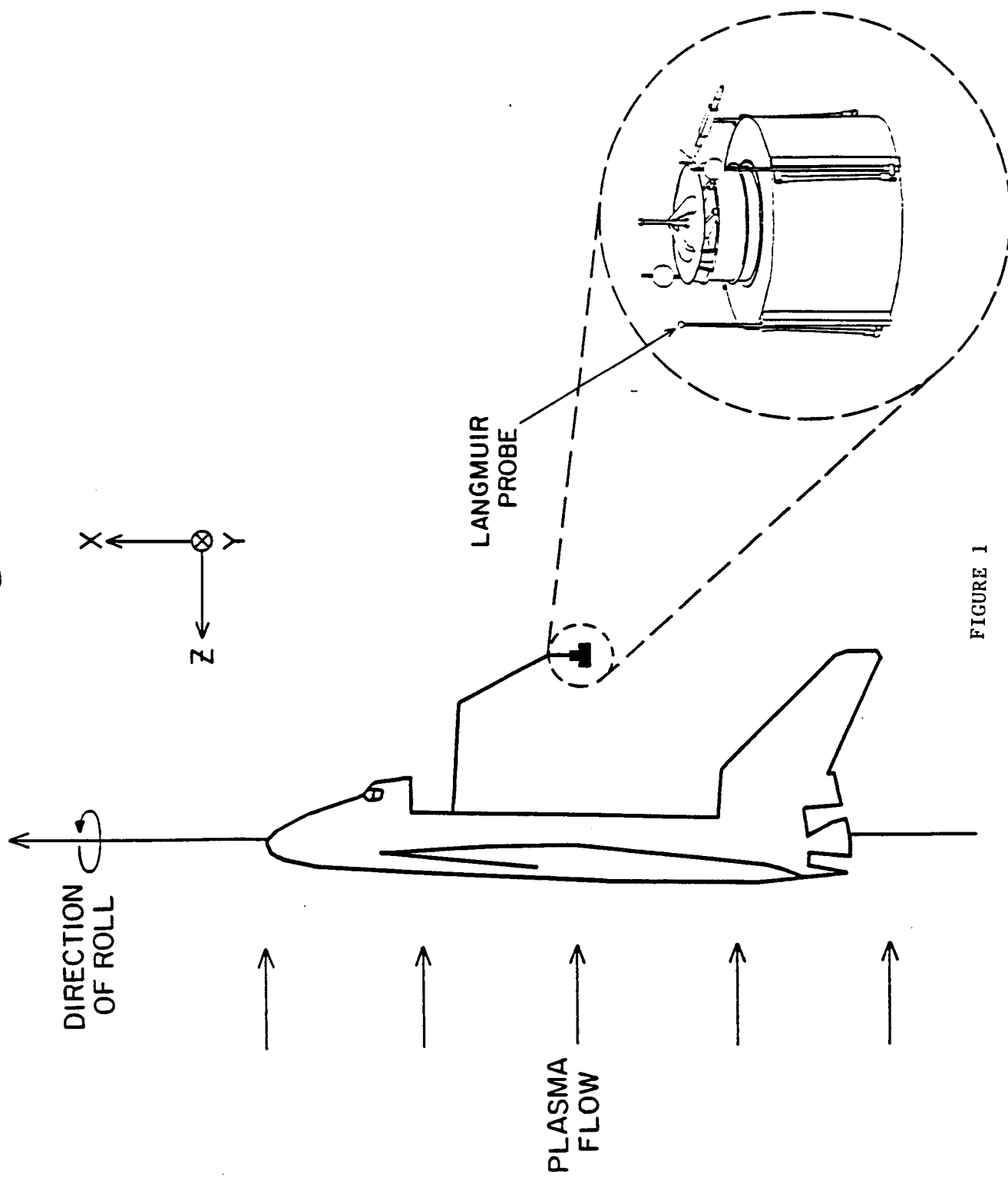


FIGURE 1

ORBITER SEPARATION MANEUVER

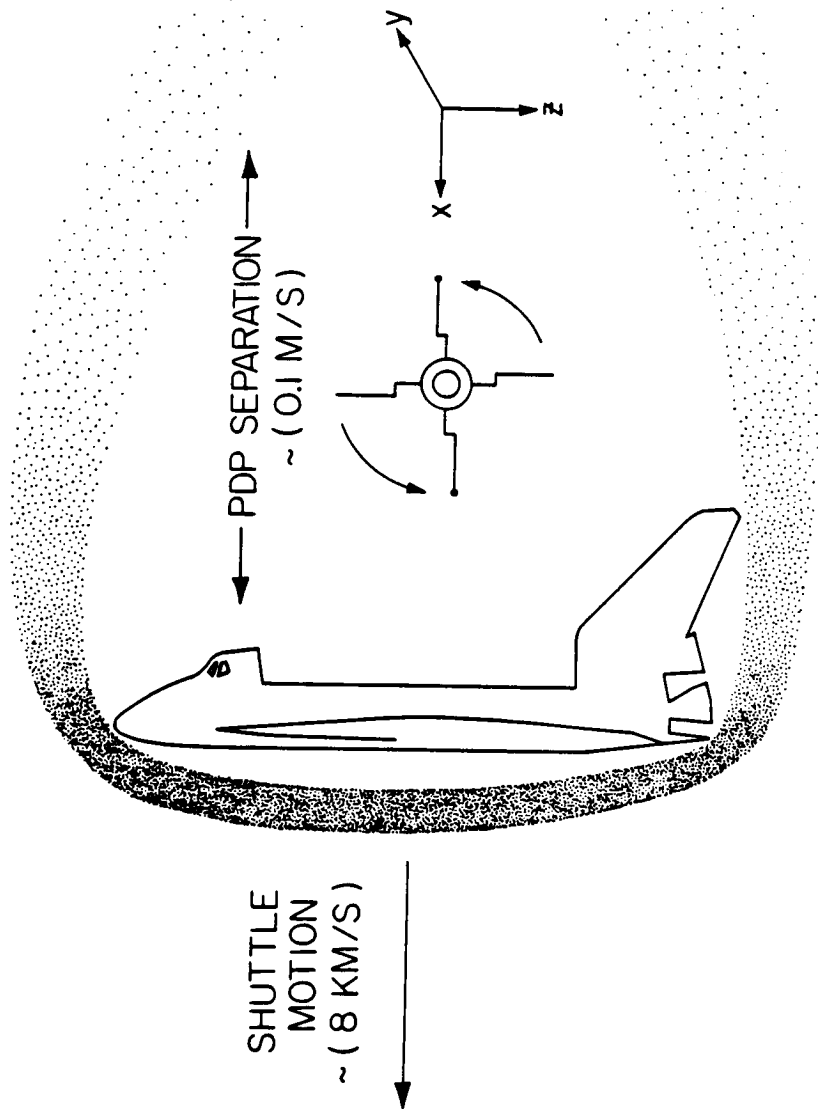


FIGURE 2

FIGURE 3a

X-G87-291

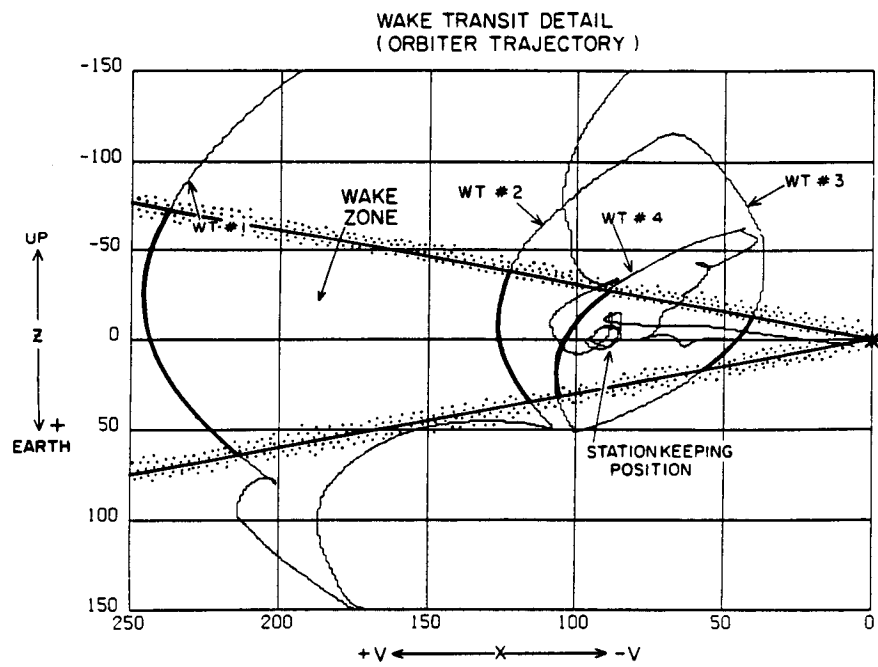
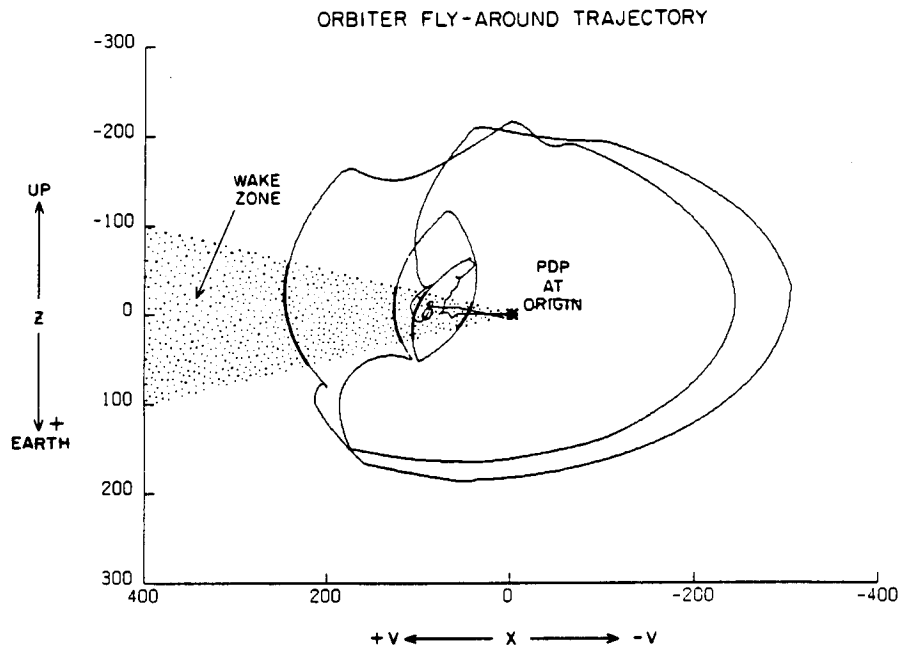


FIGURE 3b

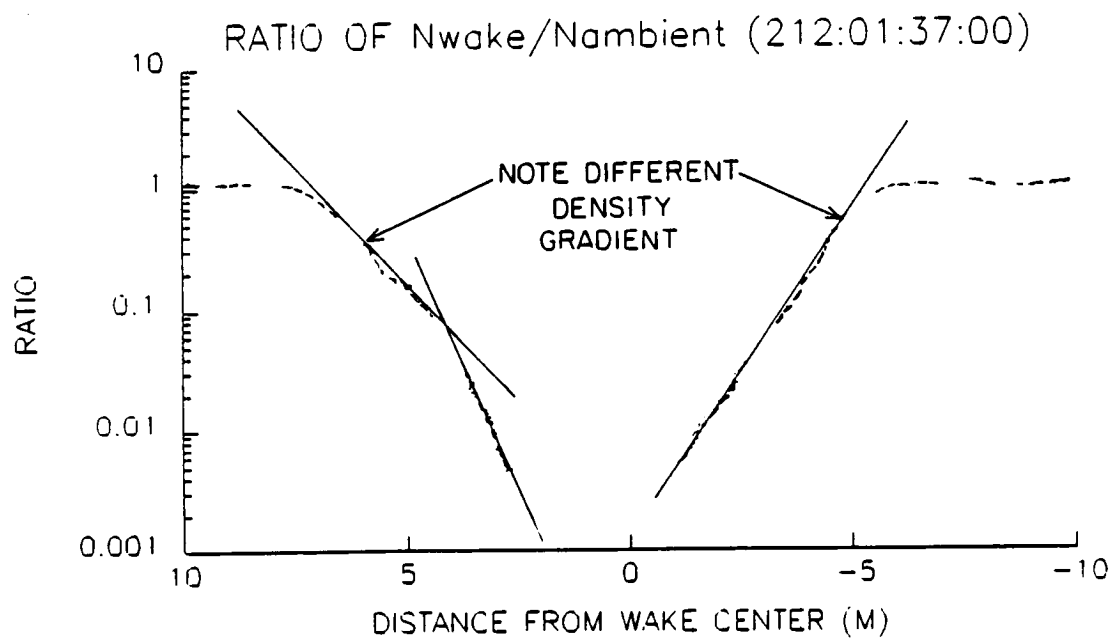
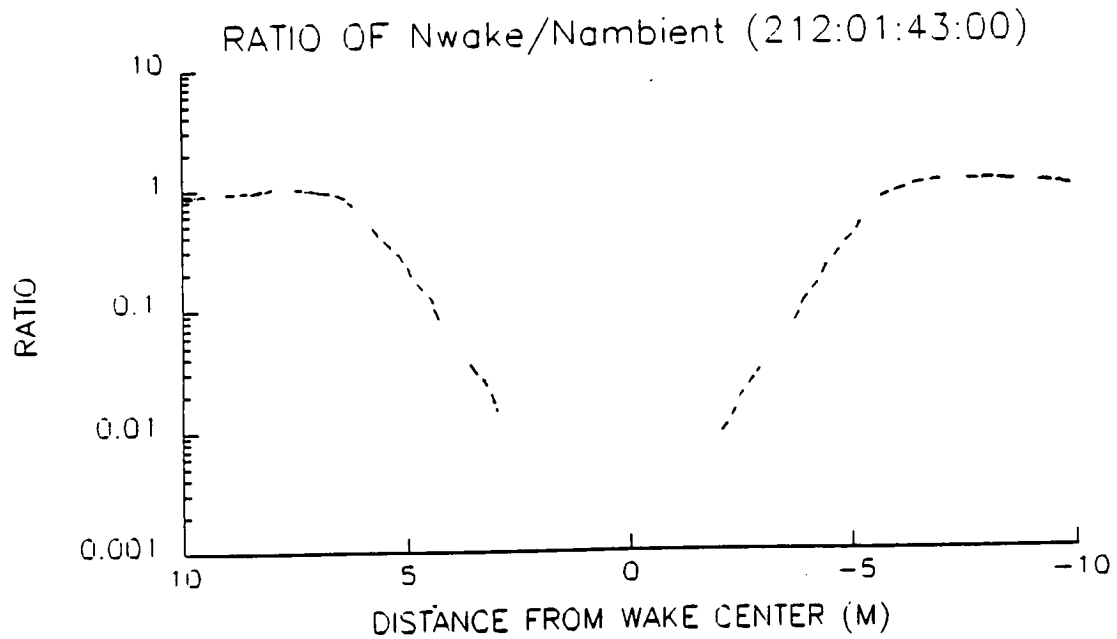


FIGURE 4

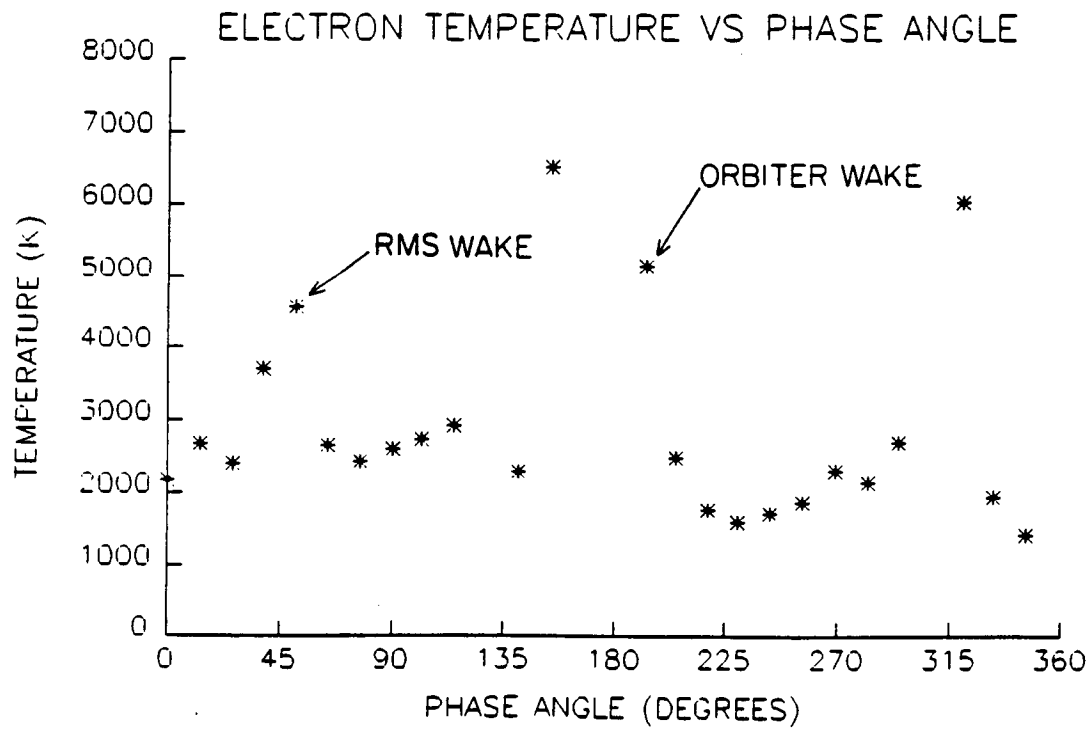
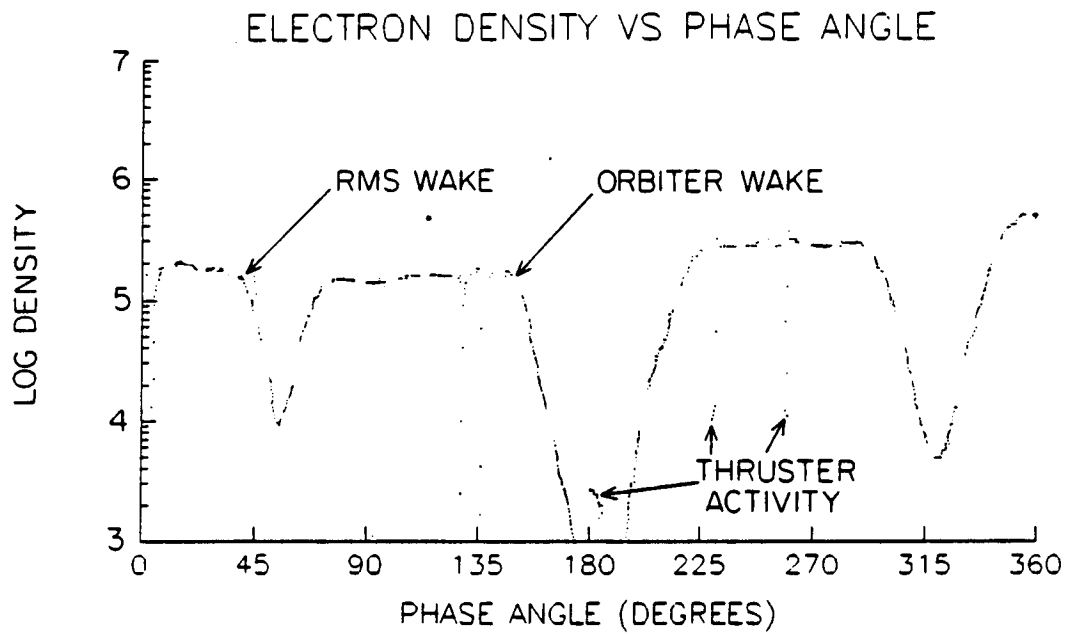
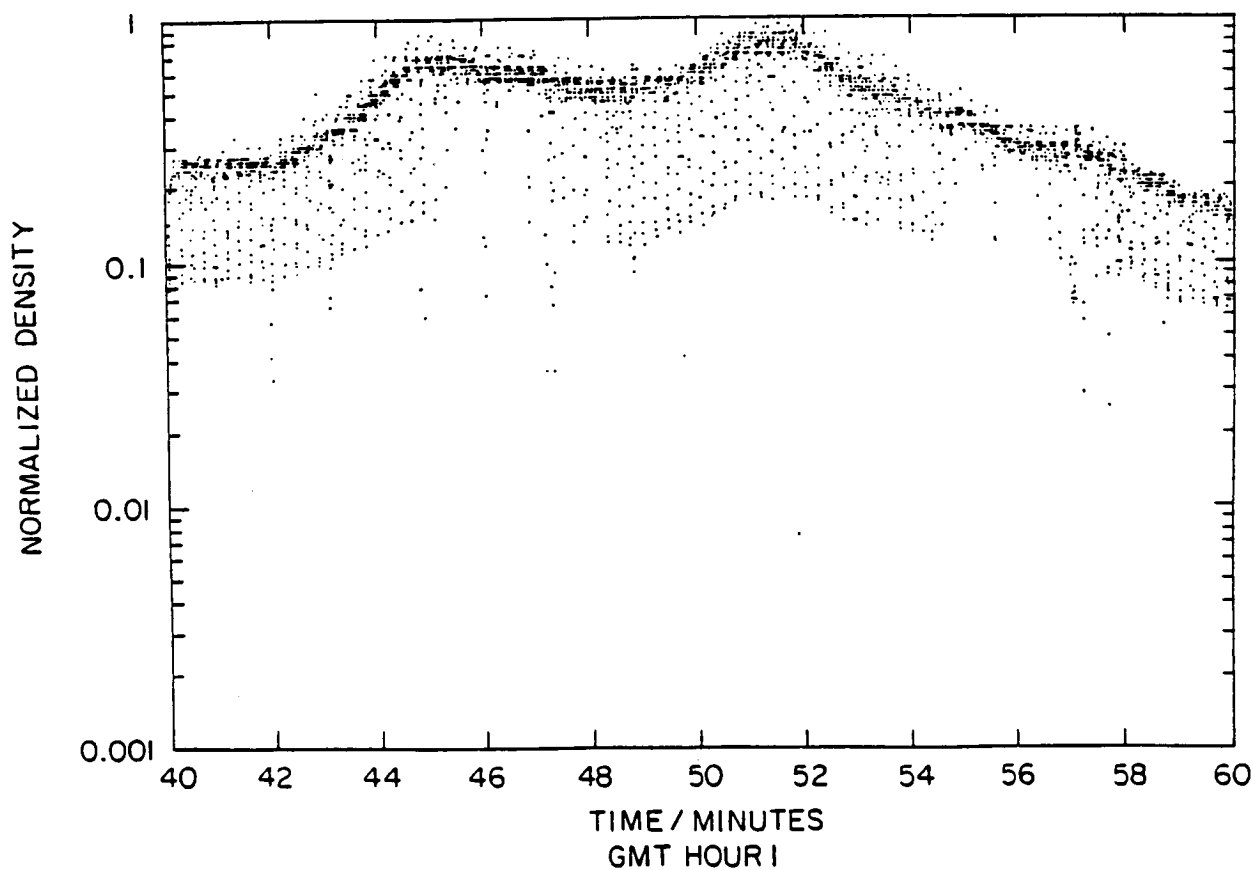
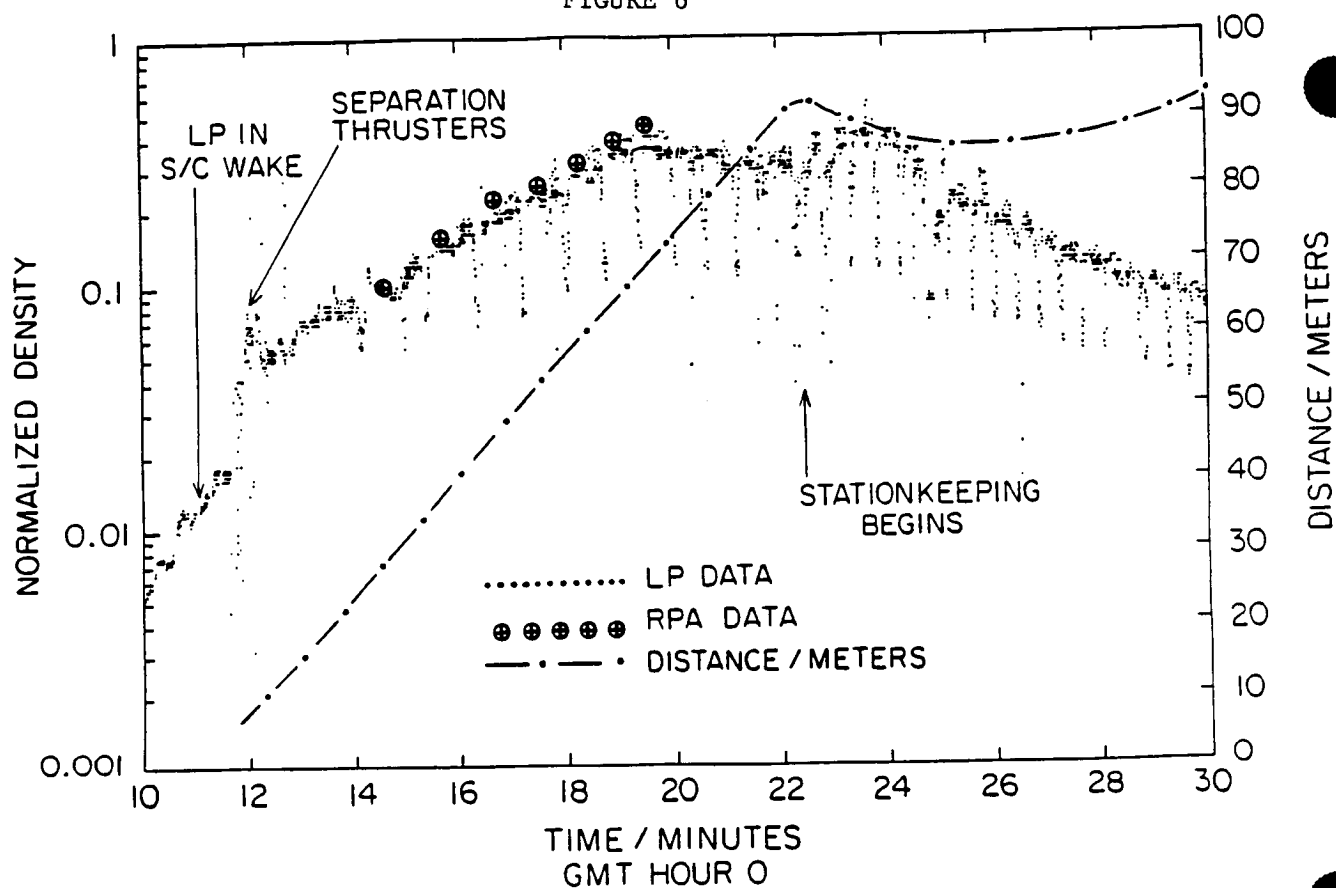


FIGURE 5

FIGURE 6

B-G87-864



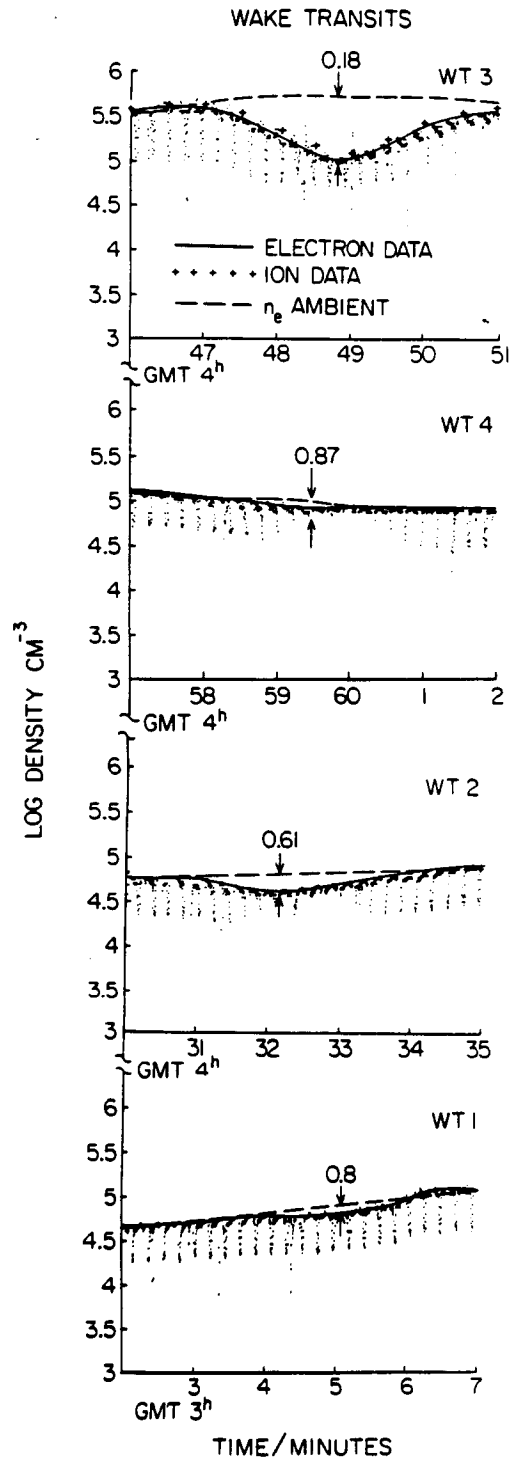


FIGURE 7a

C-88-376

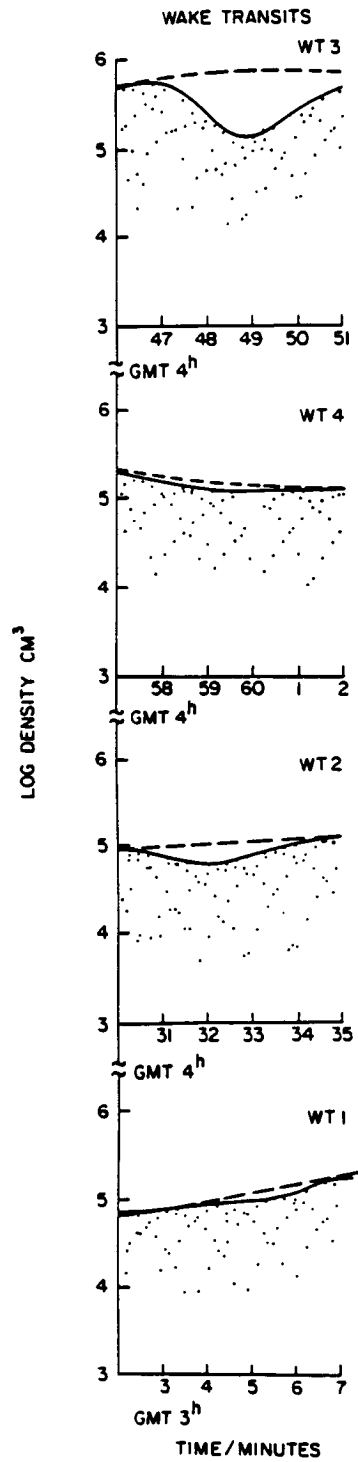


FIGURE 7b

THE POLAR CODE WAKE MODEL:
COMPARISON WITH IN-SITU OBSERVATIONS

G. Murphy,* I. Katz,‡

*Department of Physics and Astronomy

The University of Iowa

Iowa City, Iowa 52242

‡S-Cubed

P.O. Box 1620

La Jolla, California 92038

Submitted to Journal of Geophysical Research

December, 1987

Revised May, 1988

ABSTRACT

Measurements of the ion and electron densities associated with the wake of the shuttle orbiter were made by the Plasma Diagnostics Package (PDP) during the 1985 Spacelab 2 mission. Cross sections of the wake at distances of 50-200 meters downstream and measurements along the wake axis from 5 m to 100 m were obtained. The POLAR wake model, developed for The Air Force Geophysics Laboratory to study charging of spacecraft in low altitude high inclination orbits, was used to perform a 3-dimensional simulation of the plasma wake evaluated at points along the PDP's relative trajectory. The POLAR code uses several simplifying assumptions to predict wake densities. These include neglecting the magnetic field, assuming the plasma is quasi-neutral, and modeling the plasma density behind the expansion front by using the self-similar solution of the expansion of a plasma into a vacuum. This approach is computationally very efficient. The results presented here are the first known comparison between such a model and actual in-situ data obtained for objects of scale size $\sim 10^4 \lambda_d$. Excellent qualitative and quantitative agreement are found at distances greater than ~ 30 m indicating that, at least to first order, the model's approximations are justified. An intriguing disparity between the model and data suggest that the orbiter's near wake may be filled predominantly by a pick-up ion population created from neutral contaminants and that these would have to be included if accurate wake models of large gas-emitting objects are required.

INTRODUCTION

In this paper we discuss measurements made by the Plasma Diagnostics Package (PDP) during Spacelab 2, which are presented in the accompanying paper, and compare those results with predictions from AFGL's POLAR wake code which uses a complex geometric model of the orbiter and the self-similar solution of the expansion of a plasma into a vacuum as its model basis. Previous reports [Katz et al. 1985] have compared the predictions of POLAR to observations of $T_i \approx T_e$ plasmas in the laboratory. In this paper we apply the same model to the wake in a space plasma environment.

Caution should be exercised in extending conclusions about the accuracy of the POLAR model to conclusions regarding verification of the underlining physical processes it contains. Several other investigations have studied the applicability of the self-similar mathematics [Samir et al. 1983, Santwana et al. 1986, Gurevich et al. 1969] to wakes. It is our purpose only to determine if POLAR provides a reasonable model for the wakes of 'large' objects in the ionosphere as it has for $T_i \approx T_e$ plasmas in the laboratory.

We describe briefly the POLAR model and review the physics it contains, compare the data with the model, and then discuss the range of validity of the code.

THE POLAR CODE

To develop a code that can adequately describe the plasma wake behind a large object, particularly one of complex geometry, careful consideration of assumptions and approximations are required as are simplifications allowing for computational efficiency. The POLAR code has evolved with such considerations in mind. A detailed description of the POLAR wake model is given by Katz et al. [1985] and it is the purpose here only to review the basic physics and processes in POLAR so the reader may have some insight into the validity of the code.

The model of the wake structure used by POLAR depends on the position relative to the so-called ion front. This ion front marks the boundary where electron density begins to change on a scale commensurate with the Debye length and the ion density takes a sudden and dramatic drop. Several authors discussed the relationship between the wake fill process and the theoretical problem of the expansion of a plasma into a vacuum. In particular, problems applicable to ionospheric conditions have been treated by Gurevich et al. [1966], Gurevich and Pitaevsky [1975] and Singh and Shunk [1982] to name a few.

The solution to the Vlasov-Poisson equation system is in general quite difficult to obtain but for the expansion of a plasma into the void it can be solved explicitly [Gurevich et al., 1969]. Ahead of the ion front the plasma is treated as rarefied; its motion is controlled by the thermal spread in ion

velocities. Behind the front the motion is controlled by the electron temperature and ion mass. Figure 1 illustrates these regimes and defines the coordinate system used.

The governing equations in this region ahead of the front, considering that electrons are more mobile than ions and that they maintain equilibrium with a local potential, are:

$$\text{The Boltzman relation; } n_e = n_o \exp (e \phi / k T_e) \quad (1)$$

$$\text{continuity; } \frac{\partial n_i}{\partial t} + \frac{\partial}{\partial z} (n_i v) = 0 \quad (2)$$

$$\text{equation of motion; } \frac{\partial v}{\partial t} + \frac{v \partial v}{\partial z} = \frac{-e}{M} \frac{\partial \phi}{\partial z} \quad (3)$$

$$\text{Poissons equation; } \frac{\partial^2 \phi}{\partial z^2} = 4\pi e (n_e - n_i) \quad (4)$$

where n_o = ambient density

n_i = ion density

n_e = electron density

T_e = electron temperature

e = electron charge

ϕ = local potential

k = Boltzman's constant

Z is a variable representing distance parallel to the front velocity or in this case perpendicular to the orbital velocity.

Crow et al. [1975] have numerically solved the above equations to predict the position of the ion front. Katz et al. [1985] developed an analytical fit to the Crow results:

$$Z_F(t) = 2\lambda_d \left\{ \left(\omega t + \frac{1}{\alpha} \right) \ln (1 + \alpha \omega t) - \omega t \right. \quad (5) \\ \left. - \left(1 - \frac{.429}{\alpha} \right) \left(\omega t - \frac{1}{\alpha} \ln (1 + \alpha \omega t) \right) \right\}$$

where $\omega = \frac{(4\pi n_0 e^2)^{1/2}}{M}$, $\lambda_d = \frac{(kT_e)^{1/2}}{4\pi n_0 e^2}$

are the ion plasma frequency and Debye length. α is a free parameter determined to be ~ 1.6 .

Katz et al. [1985] showed that this formula agrees well with laboratory data from Wright et al. [1985] and incorporated it in POLAR. Ahead of this front Z_F , the plasma is assumed to expand due to thermal motion, the so-called "neutral approximation". Behind Z_F the plasma evolves into a state which is self-similar [Chan et al., 1984]. The self-similar solution of equations 1-4 for $z > -S_0 t$ is

$$n = n_0 \exp \left\{ - \left(\frac{z + S_0 t}{S_0 t} \right) \right\} \quad (6)$$

where $S_0 = (kT_e/M)^{1/2}$ is the ion acoustic speed.

We take the time variable to be specially defined as:

$$t = \frac{x}{V_0} \quad (7)$$

where x is the distance behind the object (perpendicular to z) and V_0 is the orbital velocity. We define the self-similar variable ζ as $\zeta = \frac{z}{S_0 t}$.

Thus the self-similar solution essentially states that between the region bounded in positive z by the front, Z_F , and in negative z by the line $z = -S_0 t$ the density rises exponentially to be equal to the ambient value along $z = -S_0 t$ which is an intuitively reasonable result.

In summary, the wake routines in POLAR employ two limiting cases.

1) Ahead of the ion front the electric field is negligible and the motion of ions is identical to neutrals. 2) Behind the ion front, whose position is determined by equation 5, the quasi-neutral self-similar solution of equation 6 is implemented.

POLAR has routines which model accurately the geometry of the object and the "neutral ion" trajectories are calculated from:

$$f_1(\vec{x}, \vec{v}) = g(\vec{x}, \Omega) f_{10}(\vec{v}) \quad (9)$$

where $f_{10}(\vec{v})$ is the unperturbed distribution function for a drifting Maxwellian;

$g(\vec{x}, \Omega)$ has value "0" if a ray starting from \vec{x} and going in the direction Ω would strike the vehicle and "1" if it would not.

The local density is given by:

$$n_1(\vec{x}) = \int f_1(\vec{x}, \vec{v}) d\vec{v} = \int g(\vec{x}, \Omega) \{ \int f_{10}(\vec{v}, \Omega) v^2 dv \} d\Omega \quad (10)$$

This initial density calculated in three dimensions for neutral particles is compared with density calculated assuming the complex geometric object is replaced by a flat plate at a position where the dominant source appears at the object edge. This ratio provides a "geometric correction factor" which is applied to the quasi-neutral one dimensional solution discussed above for

positions behind Z_F . In this way POLAR can calculate quite rapidly an approximate value for the ion and electron densities in the wakes of complex objects.

Note that the assumptions behind the front are 1) the electron temperature and ion mass govern the equation of motion, 2) the plasma is quasi-neutral, 3) the magnetic field does not affect the ion or electron motion, 4) equation 5 serves as a good approximation for determining the boundary of the ion front and 5) the geometric correction factor calculated in detail with the 3-D neutral model can be approximately applied to correct the plasma densities as well. Therefore, the algorithm can address complex geometries but takes advantage of the smooth wake structure characteristic of ionospheric plasmas where $T_i/T_e = 1$.

COMPARISON OF RESULTS

Figure 2 is a plot of the normalized density as a function of time predicted by POLAR for the PDP/orbiter relative trajectory. The density ratio $N_{\text{wake}}/N_{\text{ambient}}$ varies from approximately .9 for Wake Transit (WT) #1 which is at a distance of 245 meters to .2 for the closest WT#3 at 45 meters.

One must be careful when comparing the model to the data since the model assumes a fixed background density of $10^5/\text{cm}^3$ whereas the actual ionospheric density can and does vary considerably. The background density chosen for the model is typical of that observed in the dayside ionosphere. The assumed model temperature is also constant 2500 K. The observed temperature varies plus or minus $\sim 25\%$ from this assumed value during times of interest. The wake transits were all planned to occur in the relatively stable dayside ionosphere and over the time span of a given wake transit the background density is believed to be stable to $\pm 10\%$ [Murphy et al., 1988]. In the following discussion we will always compare the observed density ratio during a wake transit to the percentage change predicted by the model.

Figure 3a plots the observed electron and ion density depression during the back-away maneuver with a constant $10^6/\text{cm}^3$ as the reference density [Murphy et al., 1987]. The dots are the electron density (small periodic depressions result when the boom mounted probe passes through the wake of the spinning PDP). The '+' symbols are the ion density obtained once per spin cycle. During the back-away the PDP and orbiter pass from a latitude of approximately -20 to $+30$ degrees in early afternoon local time. Figure 3a

also shows the predicted normalized density calculated by the POLAR model described above. As can be seen, good agreement exists at distances from than ~ 30 meters to ~ 75 meters. It should also be noted that, over the range of the data shown, the RPA and LP data agree on density within $\sim \pm 10\%$.

As discussed in Murphy et al. [1987], we cannot easily normalize to either the previous or following orbit so we use a constant value of $10^6/\text{cm}^3$ for N_{ambient} . This value appears to be the peak density observed after the PDP has left the wake approximately $1^{\text{h}} 40^{\text{m}}$ later. Over the relatively long period of this maneuver the ionosphere has surely changed by more than 10% and this may explain the disparity after $t \approx 20$ minutes since the PDP to orbiter distance is changing relatively little. Figure 3b is a plot of the predicted density calculated by the IRI ionosphere model and the measured density one orbit later (same local time and latitude). Note that the gradual variations observed are consistent with the general trend predicted by the model.

Let us turn now to the wake transit observations. Table 1 lists the wake transits and compares the predicted and observed depletions as well as conditions at the time of the center of the wake. Note that in this entire range of 50 m to 250 m the calculations and observations agree to $\sim 10\%$.

Since the orbiter has a complex geometry, the details of the wake structure at a distance of 43 m (WT#3) downstream may be affected. Figure 4 plots a detail of that wake transit and the POLAR model as a function of time. The data are normalized to a constant value since it is clear some variation in background density occurs but it is not clear exactly what that variation is. To normalize to any unknown value other than a constant would introduce artificial variation and skew the results. The companion paper discusses this issue in detail and in that case, WT#3 is normalized by the data from the

prior orbit. However, the companion paper is attempting no comparison to a model. During this wake transit the background is believed to vary by as much as 10% [Murphy et al. 1988] so the model cannot be tested to accuracy greater than that.

DISCUSSION

In examining the back-away density profile we find three relevant observations from Figure 3.

1. Close to the orbiter (≤ 30 m) the model underestimates the observed density by one to two orders of magnitude.
2. In the range 30-75 m the model predicts quite accurately the gradual increase in density until the time $t \approx 20$ in Figure 3.
3. After $t \approx 20$ minutes, the observed density seems to have a variation which is not believed to be wake related. These density changes result from ionospheric variability as the spacecraft approaches the dawn-dusk meridian plane and are predicted by empirical models such as IRI.

Considering the first observation: recall that the assumptions incorporated within the POLAR wake model require a quasi-neutral plasma, assume a self-similar solution, and neglect magnetic fields. Considering that the electron and ion densities observed even at the beginning of the release and back-away period agree within 10%, it would seem that quasi-neutrality would be valid. It has been shown by Chan et al. [1984] that after a few ion plasma periods ($\sim .1$ msec in this case) the plasma expansion becomes self-similar. For the case of the shuttle orbiter this takes place within the first ~ 1 meter of the wake. The magnetic field, if it is to be considered for this case, would always act to limit plasma flow rather than enhance it. Therefore, it too can be eliminated from serving as an explanation for the

poor fit at less than 30 meters. The answer to the disparity between model and observation would seem to lie in the role played by contaminant ions. The companion paper Murphy et al. [1987] discusses these ions and offers their presence as an explanation for the disparity between these data and that taken at similar distances while on the RMS.

Let us turn now to the 30 m to 75 m distance regime. The most dominant characteristic of both the data and model are the relatively smooth increase in density as the PDP moves axially along the orbiter wake.

This midwake region has been studied extensively in the laboratory and the wake-fill process depends strongly on the body size, body potential, and ratio of ambient ion to electron temperature. Wright et al. [1985], Fournier and Pigache [1975], Hester and Sonin [1970] and many others have performed laboratory experiments and observed fine structure in wakes including ion density peaks along the wake axis and wave-like condensation disturbances. It is important, however, to note that for the case of large bodies in Low Earth Orbit (LEO): 1) the body potential is not too different from the plasma potential (a few kT_e at most); 2) the plasma is cold and collisionless; and 3) the ambient ion and electron temperatures are close to being equal.

An excellent review of laboratory work before 1975 is given by Fournier and Pigache [1975]. Another excellent review of the subject of ion acceleration into the wake is given by Samir et al. [1984]. In these cases the authors agree with the basic finding of Gurevich and Pitaevskii [1969] that the fine structure and ion peaks observed in certain laboratory investigations vanishes as T_i approaches T_e . We see in this case that in spite of (or perhaps because of) the effect of contaminant ions we have a large-scale wake which is basically devoid of any fine structure at least in the sense of total electron or ion density. It should be emphatically noted, however, that this does not

imply we know all there is to know about the wake structure. The overall plasma density is only the zeroth order parameter. Ion and electron composition [Grebowsky et al., 1987], vector measurements of ion velocities [Stone et al., 1983] electron temperature [Murphy et al., 1986; Raitt et al., 1984], wave disturbances [Shawhan et al., 1984], plasma turbulence [Raitt et al., 1984] all play roles in understanding the total physics of the wake structure for such a complex, gas-emitting, large object.

As discussed above, the structural differences between predictions and observations after $t = 20$ minutes in Figure 3a are attributed to natural ionospheric variation (not modeled by POLAR). Figure 3b illustrates the density profile one orbit after the back-away maneuver and shows this similar structure.

Finally, let us compare the model predictions to observations for WT#1 through 4. The agreement is quite remarkable and affirms that the "well-behaved" wake structures associated with $T_i/T_e \sim 1$ plasmas can be adequately modeled by the physics contained in the POLAR model. There is only one significant difference between model and data. WT#2 which occurs at ~ 125 m seems to be considerably deeper than WT#4 which occurs at a little more than 100 meters. Murphy et al. [1988] discuss this extensively in the companion paper and we do not believe that, considering approximations made by the model, and errors made in normalization, we could expect any better agreement. If the magnetic field and contaminant ions do play some role it is clear from both the model and the data that it must be a secondary one.

Studying the detail of the wake transit #3 observations and POLAR'S predicted profile we also find good agreement. This is significant because at 43 m ($> 1 R_0$) downstream the details of the orbiter geometry and its effect on the wake can not yet be "washed out". The good agreement seems to imply

that the geometric model assumptions are valid and it is permissible to use the geometric correction factor calculated from the neutral flow model, at least to first order.

Note that the center of the predicted wake seems to be offset slightly from that observed and that the predicted density gradient seems slightly greater than observed. Murphy et al., [1988] in the companion paper discusses the accuracy with which the trajectory reconstruction takes place. This offset error is consistent with that level of precision.

The difference in density gradients may be due to a slightly different plasma temperature than that modeled or may be consistent with the role played by contaminant ions in the neutralization of the space charge electric field.

Electric Field data is difficult to discern from the PDP because of interference from another instrument, but Steinberg [1988] has examined data from the time period of WT#3 and finds an electric field which changes sign at the wake center. This field is within a factor of two of that expected from a self similar expansion. No attempt has been made to compare the predicted field computed by POLAR to the actual data since error bars on the data are rather large. The authors may examine this as well as the RMS data in more detail in a future paper. The RMS roll data may be more useful for comparison since those data are taken at $< 1 R_0$ where the density depletion and electric fields are greater.

CONCLUSIONS

Comparisons of the PDP ion and electron densities to those predicted by the POLAR code verify that for ionospheric plasma conditions ($T_i \approx T_e$) the orbiter wake is relatively smooth in its structure to distances ~ 10 body radii downstream and that POLAR predicts this wake with an accuracy of about ~ 10 -20%. For large and complex systems such as the orbiter, outgassed products may play a significant role in the structure of its wake at distances less than the characteristic body dimension. Adequate modeling in this regime requires input that details the outgassed species and rates, chemistry describing their interaction with the ionosphere, and inclusion of magnetic field to account for the pick-up ion population in the wake.

At mid wake distances the magnetic field effects if any, would appear to be secondary to the dominate role of the electric field and thermal motion already modeled by POLAR in the wake fill process. However, for slightly larger objects or high inclination orbits the magnetic field may have to be considered if accurate results are required. In addition, the fundamental scientific questions associated with large body wakes will eventually require its inclusion.

For comparisons between in-situ observations and models such as POLAR to be meaningful at levels better than a few 10's of percent, more than simple axial or planar profiles of density are needed. The future experiments will also require good background measurements and inclusion of vector ion velocity, electric field, and particle distribution functions.

ACKNOWLEDGEMENTS

The Authors wish to express their thanks to the reviewers for their constructive comments and suggestions. This work was supported by NASA MSFC contract # NAS8-32807, NASA LeRC grant # NAG 3-449, and by Air Force Geophysics lab under contract # F19628-86-C-0056.

REFERENCES

- Chan, C., N. Hershkowitz, A. Ferreira, T. Intrator, B. Nelson and K. Lonngren, Experimental Observations of Self-Similar Plasma Expansion, Phys. Fluid, 27, 266, 1984.
- Crow, J. E., P. J. Aver, and J. E. Allen, The Expansion of a Plasma into a Vacuum, J. Plasma Phys., 14, 65, 1975.
- Fournier, G. and D. Pigache, Wakes in Collisionless Plasma, Phys. Fluids, 18, 1443, 1975.
- Grebowsky, J. M., H. A. Taylor, Jr., M. W. Pharo III, N. Reese, Thermal Ion Perturbations Observed in the Vicinity of the Space Shuttle, Planet. Space Sci. in press, 1987.
- Gurevich, A. V., L. V. Paryiskaya, and L. P. Pitaevsky, Self-Similar Motion of a Rarefied Plasma, Sov. Phys. J.E.T.P., 22, 449, 1966.
- Gurevich, A. V. and L. P. Pitaevskii, Non-Linear Dynamics of a Rarefied Ionized Gas, Prog. Aerospace Sci., 16, 227, 1975.
- Gurevich, A. V., L. P. Pitaevskii and V. V. Smirnova, Ionospheric Aerodynamics, Space Sci. Rev., 9, 805, 1969.
- Katz, I., D. E. Parks, and K. H. Wright, Jr., A Model of the Plasma Wake Generated by a Large Object, IEEE TNS, Vol. NS-32, #6, 1985.
- Hester, S. D., and A. A. Sonin, A Laboratory Study of Wakes of Ionospheric Satellites, AIAA J., 8, 1090, 1970.

- Murphy, G., J. Pickett, N. D'Angelo, and W. S. Kurth, Measurement of Plasma Parameters in the Vicinity of the Space Shuttle, Planet. Space Sci., 34, #10, 993, 1986.
- Raith, W. J., D. E. Siskind, P. M. Banks, and P. R. Williamson, Measurements of the Thermal Plasma Environment of the Space Shuttle, Planet. Space Sci., 32, 457, 1984.
- Samir U., K. H. Wright, Jr., and N. H. Stone, The Expansion of a Plasma into a Vacuum-basic Phenomena and Processes and Application to Space Plasma Physics, Rev. Geophys. Space Sci., 21, 1631, 1983.
- Shawhan, S. D., G. B. Murphy, J. S. Pickett, Plasma Diagnostics Package Initial Assessment of the Shuttle Orbiter Plasma Environment, J. of Spacecraft and Rockets, 21, #4, 387, 1984.
- Singh, N. and R. W. Schunk, Numerical Calculations Relevant to the Initial Expansion of the Polar Wind, J. Geophys. Res., 87, 9154, 1982.
- Stone, N. H., U. Samir, K. H. Wright, Jr., D. L. Reasoner, and S. D. Shawhan, Multiple Ion Streams in the Near Vicinity of the Space Shuttle, Geophys. Res. Lett., 10, 1215, 1983.
- Santuana, R., J. Hill, H. Chang, E. Tsikio, K. Lonngren, An Experiment on the Plasma Expansion into a Wake, Phys. Fluids, 29, 289, 1986.
- Steinberg J., private communication, March , 1988.
- Wright, K. H., Jr., N. H. Stone, and U. Samir, A Study of Plasma Expansion Phenomena in Laboratory Generated Plasma Wakes: Preliminary Results, J. Plasma Phys., 33, 71, 1985.

TABLE 1

<u>Wake #</u>	<u>Latitude (degrees)</u>	<u>T_e Kelvin</u>	<u>Distance (meters)</u>	<u>POLAR Normalized Density</u>	<u>Observed Normalized Density</u>
1	-35	2500	242	.9	.80
2	-45	3000	125	.75	.61
3	+10	1500	45	.20	.18
4	+35	2000	105	.65	.90

Figure 1. The POLAR wake code distinguishes three regions of interest. The ambient plasma, region of self similar model, and neutral approximation spaces are bounded by the Mach cone $Z = -S_0 t$ and ion front respectively. The coordinate system used is consistent with equations 1 through 7.

Figure 2. Using relative positions illustrated in Figure 2, POLAR calculates the density as a function of time for the entire free-flight time period. Areas of interest are labeled in the figure. The assumed normalization values for the plasma are $n_e = 1 \times 10^5 \text{ cm}^{-3}$ and $T_e = 2500 \text{ K}$.

Figure 3. Ion and electron data during the back-away are plotted in 4a normalized to $n_e = 1 \times 10^6 \text{ cm}^{-3}$. Note the relatively good agreement between model and data beyond 30 meters. Beyond $t \approx 20$ background density varies considerably as is illustrated in Figure 4b which are data for one orbit later at approximately the same stationkeeping position and a predicted density for this orbit from the IRI ionosphere model.

Figure 4. Detail of data from WT#3 is compared to POLAR predictions. Data are normalized to a constant. Since there may be variation in background of $\sim 10\%$, differences of that order between data and model are not significant.

"POLAR" WAKE MODEL

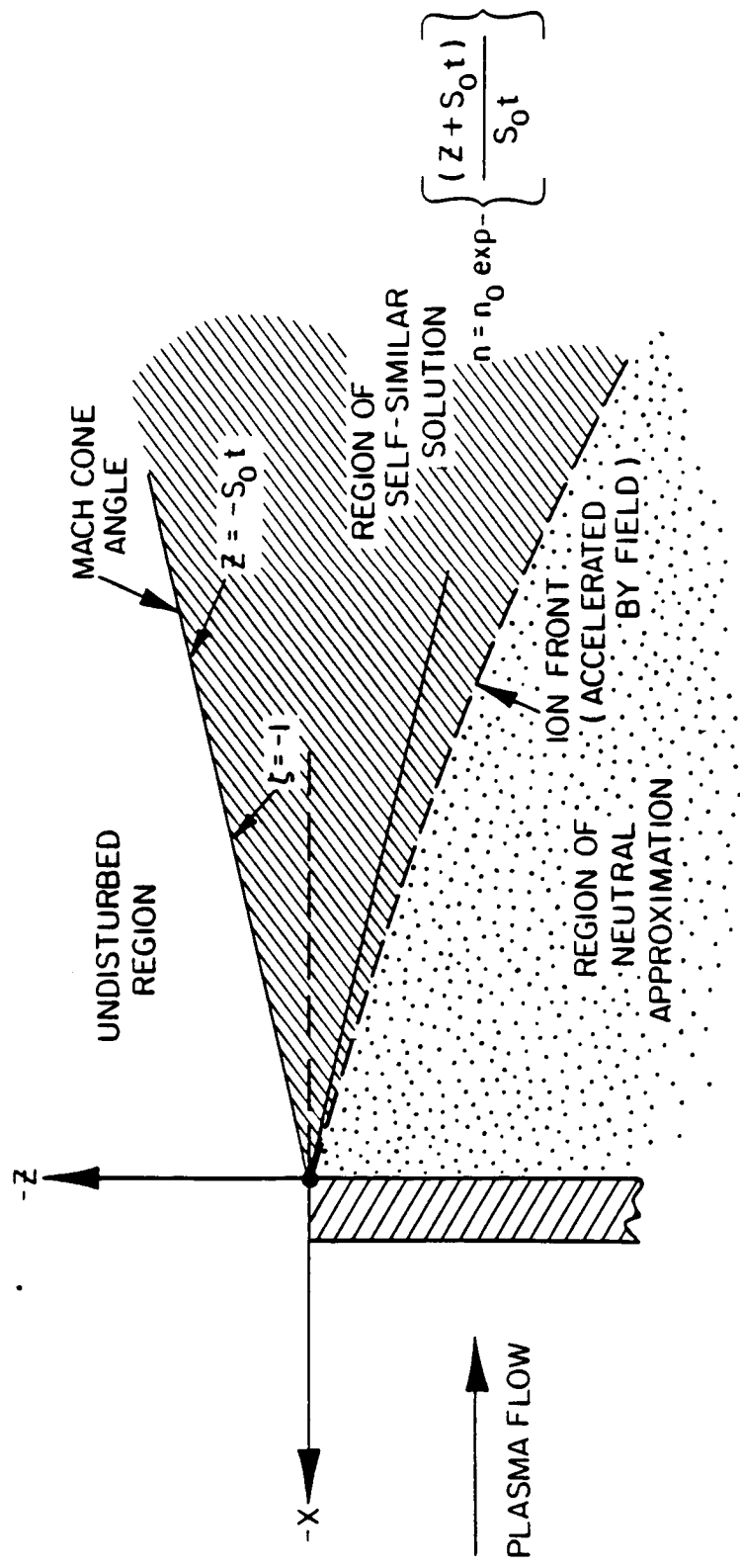


FIGURE 1

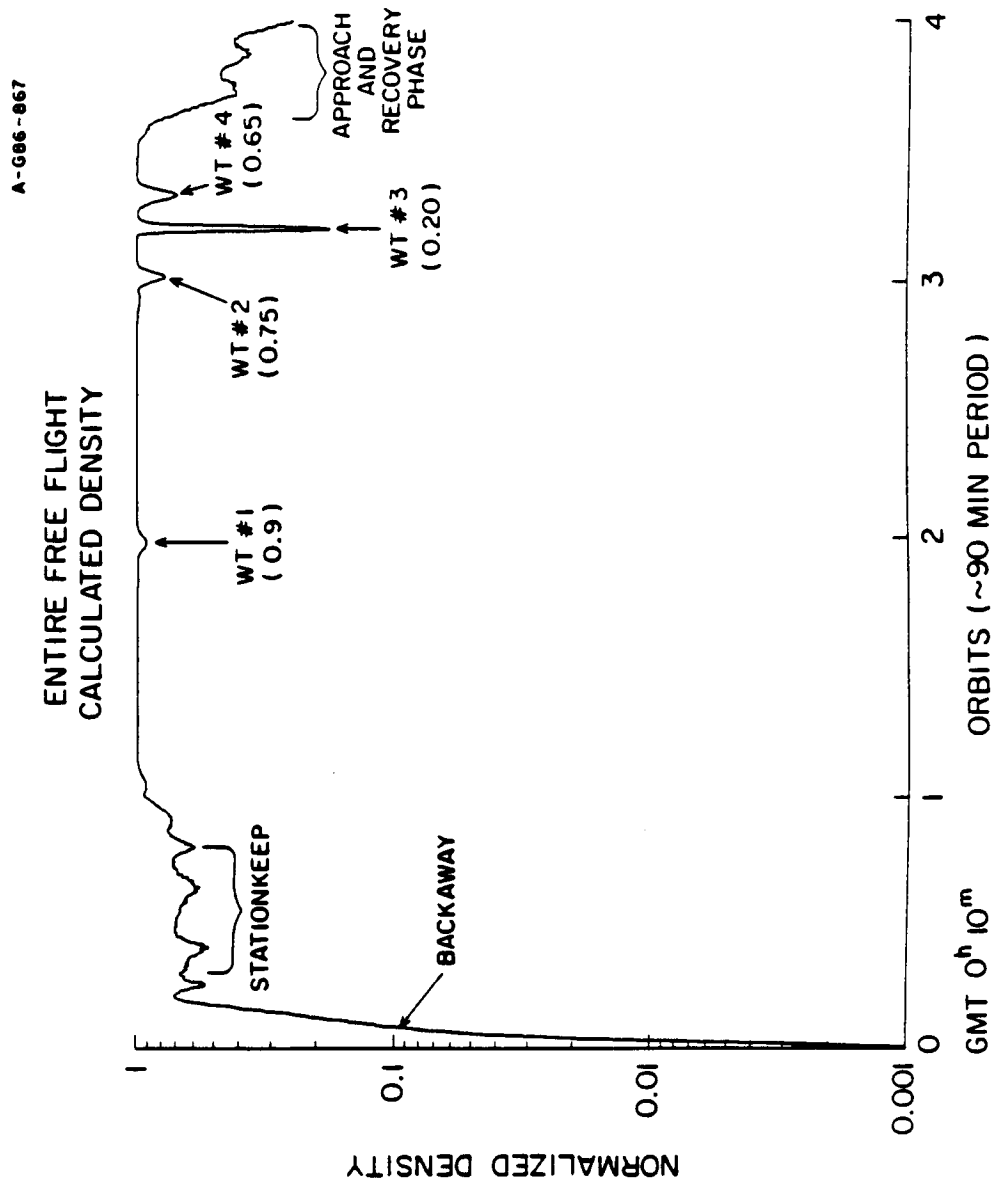


FIGURE 2

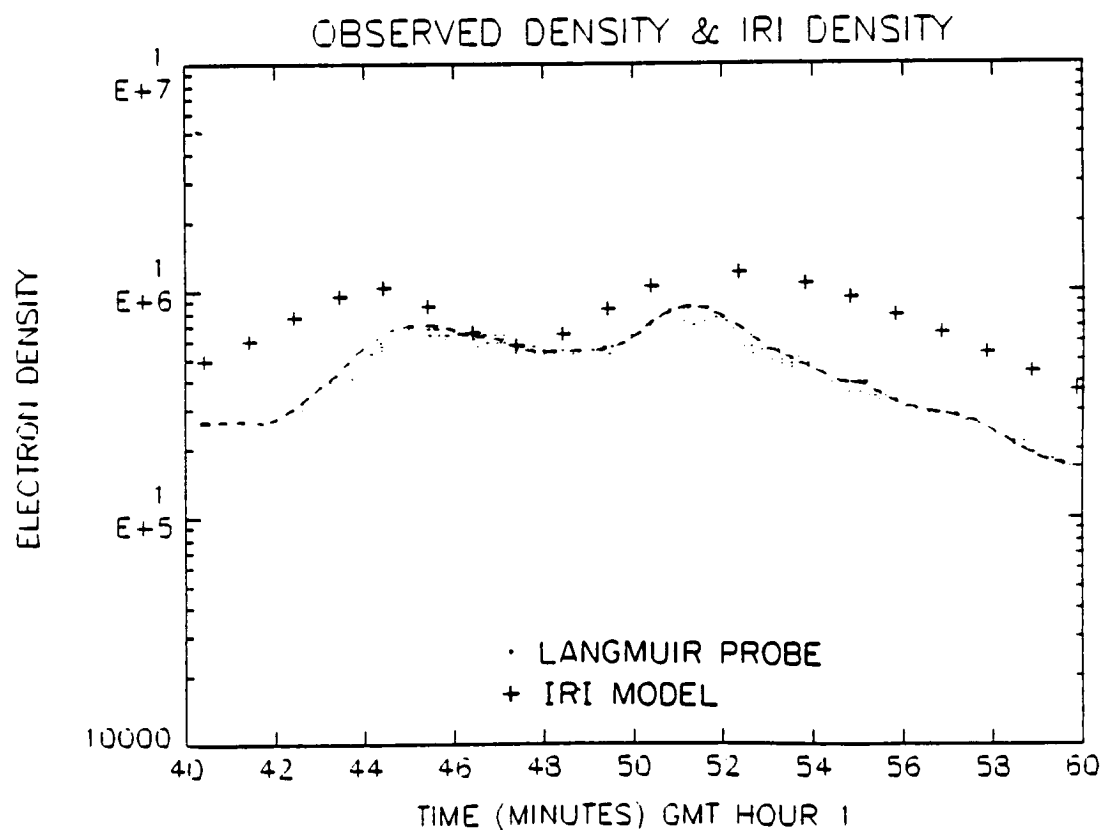
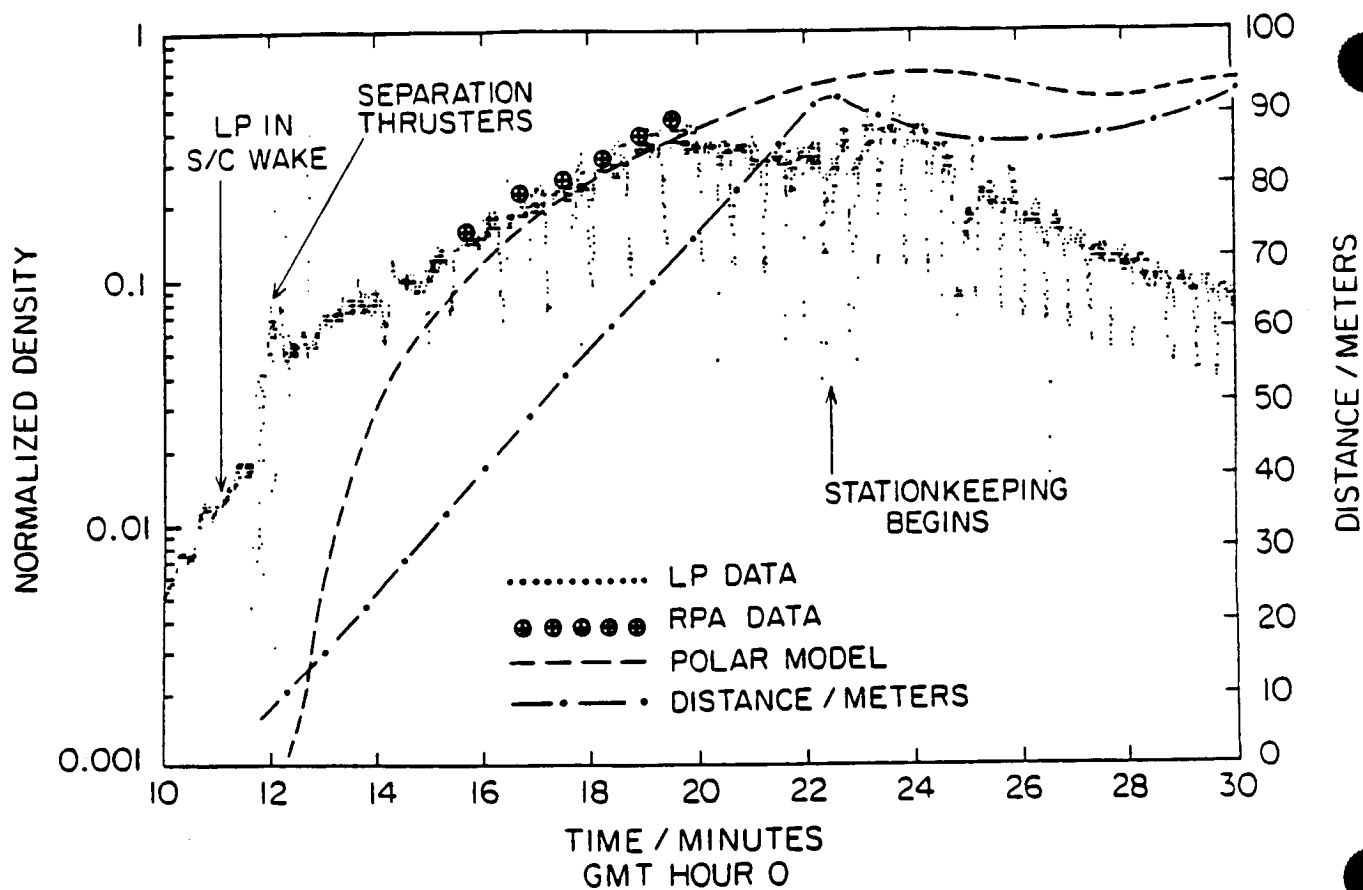


FIGURE 3

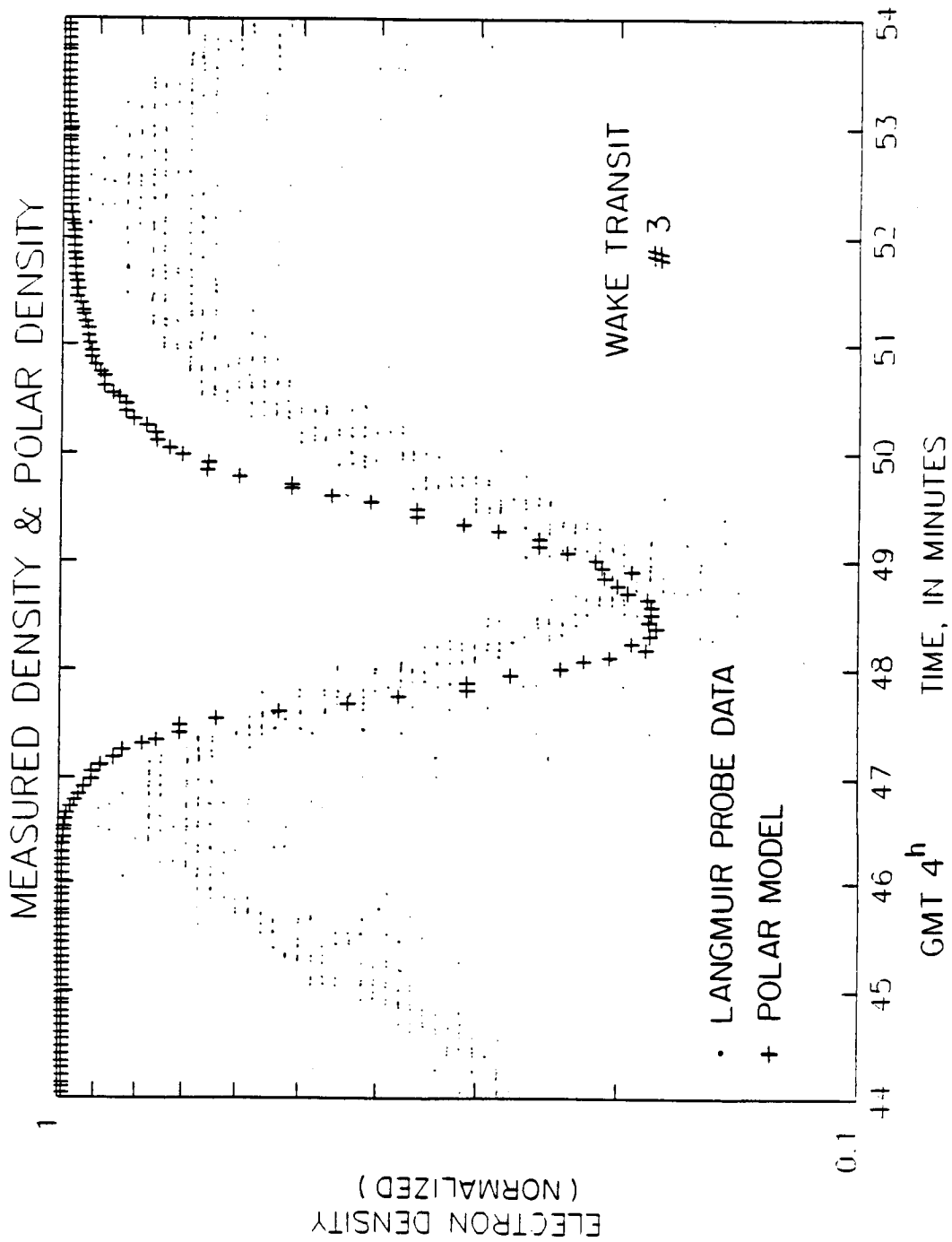


FIGURE 4

Exposed High-Voltage Source Effect on the Potential of an Ionospheric Satellite

A. C. Tribble,* N. D'Angelo,† G. B. Murphy,‡ J. S. Pickett,§ and J. T. Steinberg¶
University of Iowa, Iowa City, Iowa

A pulsed, high-voltage source, which is able to draw a current from the surrounding plasma, is seen to induce large changes in the potential of an ionospheric satellite (the Iowa Plasma Diagnostics Package flown on Space Shuttle flight STS-51F). This, in turn, may affect the operation of other instruments that use the chassis of the satellite as a ground for electrical circuits. The magnitude of the change in satellite potential is dependent upon both the orientation of the high-voltage source, relative to the plasma flow, and the characteristics of the high-voltage source. When the satellite is grounded to the Shuttle Orbiter, this effect is sufficient to change the potential of the Orbiter by a small, but noticeable, amount.

Nomenclature

A_e	= surface area of the PDP that will collect electrons
A_i	= surface area of the PDP that will collect ions
e	= charge of the electron
h	= height of the main body of the PDP
h'	= height of the "top cap" of the PDP
$I_{e, ins}$	= electron current collected by all of the PDP's instruments
$I_{e, pr}$	= electron current collected by the Langmuir probe
$I_{e, LEP}$	= electron current collected by the LEPEDA
$I_{e, sc}$	= electron current collected by the PDP chassis
$I_{i, ins}$	= ion current collected by all of the PDP's instruments
$I_{i, sc}$	= ion current collected by the PDP chassis
k	= Boltzmann's constant
m_e	= mass of the electron
n_e	= electron density
n_i	= ion density
r	= radius of the main body of the PDP
r'	= radius of the "top cap" of the PDP
T_e	= electron temperature
v_o	= orbital velocity of the PDP

Introduction

A SPACECRAFT traveling in the Earth's ionosphere has no external electrical ground available for it to use as a reference for potential measurements. As a consequence, such spacecraft are susceptible to different types of charging phenomena that may alter the potential of the spacecraft chassis.^{1,2} From July 29 to August 6, 1985, a satellite designed and built by the University of Iowa's Department of Physics and Astronomy, the Plasma Diagnostics Package (PDP), was flown as part of the Spacelab 2 payload on Space Shuttle flight STS-51F at an altitude of 325 km. The PDP is a cylindrical spacecraft 106.68 cm (42 in.) in diameter and 66.04 cm (26 in.) in height composed of 14 different instruments designed to study the plasma and electromagnetic environment near the Shuttle Orbiter. A diagram is shown in Fig. 1.

Received March 9, 1987; revision received June 23, 1987. Copyright © American Institute of Aeronautics and Astronautics, Inc., 1987. All rights reserved.

*Graduate Research Assistant, Member AIAA.

†Professor of Physics, Department of Physics and Astronomy.

‡Research Engineer, Department of Physics and Astronomy. Member AIAA.

§Staff Research Assistant, Department of Physics and Astronomy. Member AIAA.

¶Graduate Research Assistant, Department of Physics and Astronomy.

The PDP skins are constructed of aluminum and are covered by multilayered insulation (MLI) blankets followed by an outer dielectric layer of beta cloth (teflon-coated fiberglass) overlaid with a conducting aluminum wire mesh electrically grounded to the chassis of the PDP via bolts and staples through the MLI. The MLI consists of a singly aluminized kapton layer on the outside (aluminum sides facing inward) and 10 layers of doubly aluminized mylar separated by dacron net on the inside with grounding straps used to electrically bond the MLI to the structure.

During the Spacelab 2 mission, the PDP made measurements from the payload bay, from the Remote Manipulator

PDP BOOMS DEPLOYED CONFIGURATION

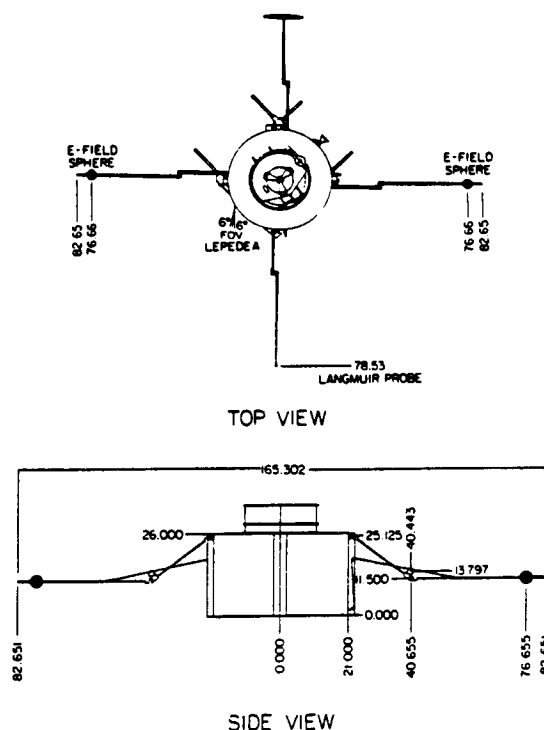


Fig. 1 Diagram of the PDP with booms deployed. Relevant distances are indicated in inches.

System (RMS), and for a period of 6 h as a free-flying subsatellite. This paper will show how some of the measurements made with a Langmuir probe and a dc Electric Fields instrument (utilizing the E-field spheres) on the PDP were affected by a pulsed, high-voltage source (LEPEDEA).

Instrumentation

A Langmuir probe on the PDP was used to make measurements of electron temperature, electron density, fluctuations in the electron density, and plasma potential. The Langmuir probe consisted of a 3-cm-diam spherical, gold-plated sensor and supporting circuitry. This circuitry was designed to alternate between two modes, which we refer to as the sweep mode and the lock mode.

During the sweep mode the bias voltage of the Langmuir probe was swept from 10 to -5 V, relative to the chassis of the PDP, in discrete steps of 0.125 V at a rate of 120 steps/s. A graph of the log of the current collected by the Langmuir probe during this time as a function of the bias voltage is typically referred to as a Langmuir curve. As shown, for example, by Huddleston and Leonard,³ a Langmuir curve allows us to calculate the electron density, electron temperature, and plasma potential. An example of a typical Langmuir curve is shown in Fig. 2a. In Fig. 2a and in all subsequent figures, the times given are in Universal Time (UT).

Following the sweep mode, the bias voltage on the Langmuir probe returned to 10 V where it remained for 11.8 s. During this time, the data collected by the probe, which were again sampled at a rate of 120 steps/s, allow us to measure electron density fluctuations. An example of the lock mode data, sampled through a 6-40-Hz filter, is shown in Fig. 2b. A Langmuir probe similar to the one used on the Spacelab 2 mission is discussed in more detail by Murphy et al.⁴

The dc Electric Fields instrument on the PDP consisted of two spherical unbiased high-impedance probes and associated electronics. The two sensors are visible in Fig. 1 and are labeled E-field spheres. In this paper, we are concerned with only one type of dc measurement that was made. The average of the dc potentials of the two spheres, V_a and V_b , relative to the chassis of the PDP, $(V_a + V_b)/2$, was measured once every 1.6 s. It is important to note that the measurements made by the Langmuir probe and the dc Electric Fields instrument complement each other in that the Langmuir probe was a low-impedance sensor that measured current at a controlled bias level and the dc Electric Fields instrument utilized high-impedance floating probes that measured the potential at near-zero current.

The last instrument that will be discussed in this paper is the Low Energy Proton Electron Differential Energy Analyzer (LEPEDEA). As can be seen in Fig. 1, the LEPEDEA was mounted on the circumference of the PDP. It has two particle collectors open to the ionosphere, one designed to detect electrons and the other, ions. The two openings are separated by a curved plate to which a pulsed high-voltage is applied. The combined cross-sectional area of the openings to the electron and ion detectors is 6.69 cm² (1.04 in.²). The high-voltage plate is 5.26 cm (2.07 in.) wide and extends into the LEPEDEA for a distance of 9.83 cm (3.87 in.). At time $t = 0$, the bias voltage on the LEPEDEA plate switched from 0 to 2.2 kV, relative to the chassis of the PDP, where it remained for 0.2 s. During the following 1.4 s, the bias voltage then decayed exponentially with a $1/e$ time of 0.16 s, the entire cycle requiring 1.6 s. The operation of the LEPEDEA is discussed in more detail by Frank et al.⁵

Anomalous Results

During the 6 h of free flight, an anomaly was detected in both the sweep and lock mode data collected by the Langmuir probe. An example is shown in Fig. 3. Figure 3a indicates that the normal Langmuir curve is interrupted by a "bite out" in the current collection. This bite out always maximizes approximately 0.2 s after the start of the voltage sweep.

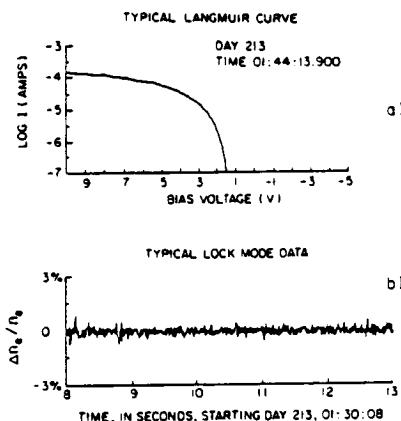


Fig. 2 Examples of: a) a typical Langmuir curve and; b) typical lock mode data.

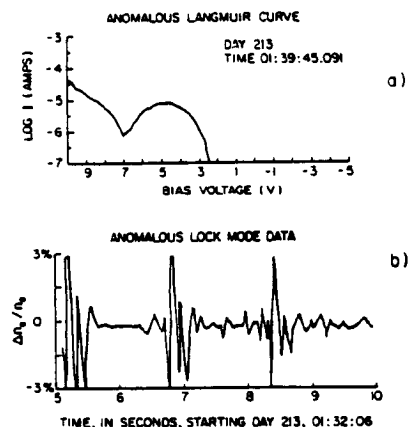


Fig. 3 Examples of: a) an anomalous Langmuir curve and; b) anomalous lock mode data.

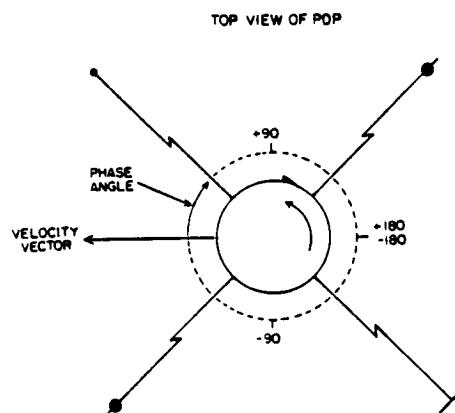


Fig. 4 Definition of the Langmuir probe phase angle. The PDP is rotating counterclockwise in the plane of the paper.

Further examination of a series of Langmuir curves indicates that the magnitude of the anomaly is dependent upon the orientation of the PDP, which was spinning about its cylindrical axis with an inertial period of 13.06 s. This orientation is defined by a phase angle, which is the angle between the velocity vector of the PDP and the vector that points from the center of the PDP to the Langmuir probe,

Fig. 4. In this figure, the PDP is rotating counterclockwise in the plane of the paper. The Langmuir probe entered the sweep mode every 12.8 s. Consequently, if the PDP started a voltage sweep when the phase angle was -180 deg, the next sweep would have begun when the phase angle was -172.9 deg. The difference in phase angles occurs because the PDP rotates through 352.9 deg in 12.80 s. Therefore, even though the PDP is rotating in a counterclockwise direction, a graph of phase angle at the start of a sweep mode vs time would show the Langmuir probe apparently precessing in a clockwise direction. A series of Langmuir curves that shows the dependence of the anomaly on the phase angle is shown in Fig. 5. These data indicate that the anomaly maximized at a phase angle of about -55 deg.

As seen in Fig. 3b, the lock mode data indicate that some type of interference, which we hereafter refer to as noise, was affecting the Langmuir probe once every 1.6 s. The anomaly in the lock mode data was present even during times when the PDP was grounded to the RMS of the Shuttle Orbiter. However, the magnitude of the resulting anomaly was reduced in comparison to that seen during free flight.

Like the Langmuir probe measurements, the dc potential measurements taken during free flight also had an unexpected character. As is shown in Fig. 6, the average potential of the spheres relative to the PDP varied with the spin phase of the spacecraft. In Fig. 6, the potential between the spheres and the PDP varies by about 2.1 V over the spin cycle. At other times during free flight, this variation in potential was as much as 3.0 V, depending on the local plasma conditions. The variation in potential always reached its maximum positive value when the phase angle of the Langmuir probe was about -55 deg.

Source of the Interference

Several reasons led us to believe that the noise detected by the Langmuir probe during PDP free flight was not due to an instrument malfunction. First, at all other times throughout the mission, the probe appeared to function as expected, and no anomaly was detected until data reduction had begun. Second, noise seen by the dc Electric Fields Instrument was coincident in time with the noise seen by the Langmuir probe. Also significant was the fact that the Langmuir probe noise recurred with a period of 1.6 s. This is important in that several instruments on the PDP were designed so that one complete "cycle" would require 1.6 s. As was mentioned previously, the LEPDEA is just such an instrument. The temporal relation between the bias voltage on the LEPDEA and the bias voltage on the Langmuir probe is illustrated in Fig. 7. The "ringing" detected in the lock mode data occurred at precisely the times that the bias voltage on the LEPDEA switched from 0 to 2.2 kV. This, and the fact that, throughout the mission, whenever the LEPDEA was turned off, the anomalies seen by the Langmuir probe and the dc Electric Fields Instrument disappeared, led us to believe that, in some way, the LEPDEA was responsible for the anomalous data.

This suspicion was strengthened by the fact that the phase-angle dependence, Fig. 5, shows strong indications of being a dependence upon the orientation of the LEPDEA. In Fig. 5, we see that the Langmuir curves, which have an anomalous character, occur between a phase angle of about -110 and 30 deg. This corresponds to time when the LEPDEA phase angle was between -53 and 87 deg. Sweeps taken when the Langmuir probe phase angle was -55 deg corresponded to times when the LEPDEA was approximately in ram. Thus, the anomalies were largest when the LEPDEA was in the ram of the plasma flow and smallest when it was in wake. The reason for this dependence will be discussed in the next section.

Discussion

When working with laboratory plasmas, it is possible to use an externally grounded electrode, whose potential will not change, as a reference point for potential measurements.

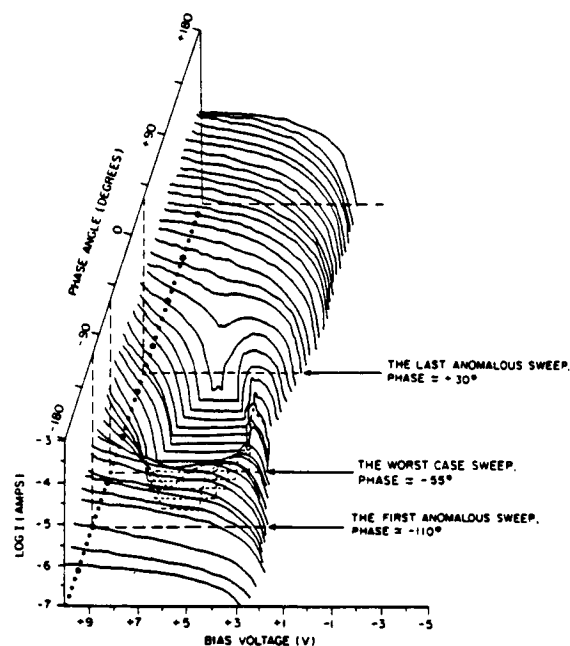


Fig. 5 Series of Langmuir curves taken at various phase angles. Time increases with increasing phase angle.

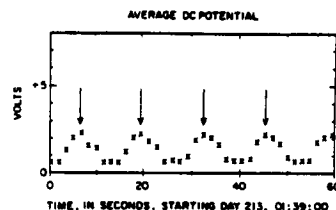


Fig. 6 Average dc potential of the PDP as measured by the dc Electric Fields instrument. The arrows indicate the times when the LEPDEA is approximately in ram.

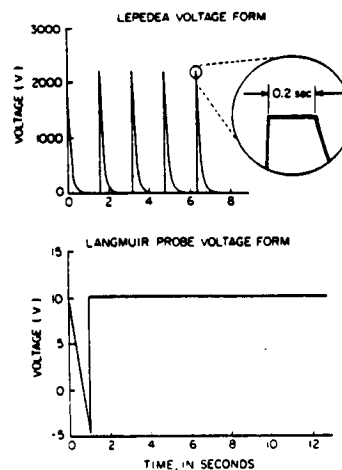


Fig. 7 Temporal relation between the Langmuir probe and the LEPDEA bias voltages.

However, no such electrical ground is available when dealing with a spacecraft in the ionosphere. In such a situation, we must treat the system of the spacecraft and the instruments

mounted on it as a "double probe," following the method originally proposed by Johnson and Malter.⁶ When two probes are biased with respect to one another but insulated from ground, the entire system will "float." An important consequence of this is that the total current collected by the system must be zero. That is, any electron current collected by the system must be balanced by an equal ion current. In our case, the condition that the system be floating is

$$I_{i, sc} + I_{i, ins} - I_{e, sc} - I_{e, ins} = 0 \quad (1)$$

where $I_{i, sc}$, $I_{e, sc}$, $I_{i, ins}$, and $I_{e, ins}$ are defined as the ion and electron currents to the PDP spacecraft structure and the instruments, respectively. We are able to obtain expressions for $I_{i, sc}$ and $I_{e, sc}$ in the following manner.

After release from the Shuttle, the PDP had an orbital velocity of about 7.7 km/s. Analysis of the uncontaminated Langmuir probe data indicated that the electrons had a typical temperature of about 2500 K and a typical density of $1.5 \times 10^3 \text{ cm}^{-3}$, in general agreement with previous measurements. If we assume that the ions and electrons are in thermal equilibrium, we find that the thermal velocity of an electron was about 180 km/s and the thermal velocity of atomic oxygen, the predominant ion in the F2 region, about 1.1 km/s. Since the orbital velocity of the PDP was approximately a factor of 7 greater than the thermal velocity of the ions, most of the ions would have impacted the PDP on the side facing the ram of the plasma flow, the ion current thus consisting of the ions swept out by the front surface of the PDP. The equation describing ion current collection by the spacecraft is

$$I_{i, sc} = A_i n_i v_o \quad (2)$$

where A_i is the front surface area of the PDP, e the charge of the ion, n_i the ambient ion density (we assume $n_i = n_e$), and v_o the orbital velocity of the PDP. Since the ion current consists of those ions that are rammed out by the motion of the PDP, we will approximate A_i by $(2rh + 2r'h')$, where r , h are the radius and height of the main body of the PDP, and r' , h' are the radius and height of the "top cap," Fig. 1.

The thermal velocity of the electrons is greater than the orbital velocity of the PDP by almost a factor of 25. Consequently, all surfaces of the PDP will collect electron current, not just the ram side. We assume that the electrons had a Maxwellian distribution given by

$$f_e(v) = n_e \left[\frac{m_e}{2\pi k T_e} \right]^{3/2} \exp \left[-\frac{m_e v^2}{2k T_e} \right] \quad (3)$$

The electron current to the PDP at a potential V less than the plasma potential V_p , and measured relative to V_p , consists of those electrons with energies greater than $|eV|$ that strike the PDP, and is given by

$$I_{e, sc} = A_e n_e \left[\frac{k T_e}{2\pi m_e} \right]^{1/2} \exp \left[\frac{eV}{k T_e} \right] \quad (4)$$

where A_e is the surface area of the PDP that will collect electrons, e the charge on the electron, n_e the electron density, k Boltzmann's constant, T_e the electron temperature, and m_e the electron mass. Since the electrons may strike all surfaces of the PDP, we approximate A_e by $(2\pi r^2 + 2\pi rh + 2\pi r'h')$.

We now need expressions for $I_{i, ins}$ and $I_{e, ins}$. The cross-sectional collecting areas of all of the instruments on the PDP are several orders of magnitude smaller than A_i ; consequently, we should be justified in neglecting $I_{i, ins}$ altogether. The only instruments on the PDP expected to draw significant amounts of electron current from the plasma, due to their positive bias voltages, are the Langmuir probe and the LEPDEA. We can rewrite Eq. (1) as

$$I_{i, sc} - I_{e, sc} - I_{e, pr} - I_{e, LEP} = 0 \quad (5)$$

where the subscripts pr and LEP refer to current collected by the Langmuir probe and LEPDEA, respectively. We can solve the preceding equation to determine the potential of the chassis of the PDP. Since the LEPDEA has a very small collecting area and its bias voltage is large only for about 0.3 s, during most of its 1.6-s operational cycle it should draw negligible current from the ionosphere. Therefore, we will first solve for the floating potential by setting $I_{e, LEP}$ to zero. Substituting Eqs. (2) and (4) into Eq. (5), with $I_{e, LEP}$ set to zero, we find that the "floating potential" of the PDP is given by

$$V = \frac{+k T_e}{e} \ln \left[\frac{A_i n_i v_o - I_{e, pr}}{A_e n_e (k T_e / 2\pi m_e)^{1/2}} \right] \quad (6)$$

Using the values for n_e , T_e , and the additional constants given in Table 1, we may determine the nominal floating potential of the PDP once we know $I_{e, pr}$. Analysis of Langmuir curves collected under the plasma conditions listed in Table 1 reveals that the corresponding value of $I_{e, pr}$ is approximately $14 \mu\text{A}$, which would give a value of -0.90 V for the floating potential of the PDP. The resulting magnitudes of $I_{e, sc}$ and $I_{i, sc}$ would be about 93 and $107 \mu\text{A}$, respectively. (Ignoring the presence of $I_{e, pr}$, i.e., setting $I_{e, pr}$ to zero, would have given a value for V_f of -0.86 V . As we shall see momentarily, a change of 0.04 V is about 2 orders of magnitude smaller than the effect that is responsible for the appearance of the anomalous data. Consequently, we would be justified in ignoring $I_{e, pr}$ altogether.)

We turn next to the intervals when the LEPDEA voltage was large and positive. As was mentioned previously, we believe that the cause of the anomalous data discussed in the preceding sections was somehow related to the operation of the LEPDEA. The most likely explanation for the appearance of the anomalous Langmuir curves is that the bias voltage of the Langmuir probe, relative to the plasma, was changing unexpectedly during the course of a sweep. One other possible explanation, that the conditions in the plasma itself were changing, was not supported by data from other instruments on the PDP. An examination of all anomalous Langmuir curves showed that, by the time the Langmuir probe bias voltage had stepped to 4 V , the cause of the anomaly seemed to have subsided, as the remainder of the anomalous Langmuir curve appeared nominal. Under the assumption that whatever was responsible for the anomaly had completely subsided by the time the probe's bias voltage was 4 V and that the conditions in the plasma remained unchanged during the course of a sweep, we were able to analyze the anomalous sweeps as follows. The Langmuir curve shown in Fig. 8 was taken when the plasma conditions were similar to those given in Table 1. In this figure, when the bias voltage of the Langmuir probe was 9 V , the probe collected about $6 \mu\text{A}$ of current from the plasma. Under normal conditions we would not collect this current until the bias voltage of the probe was 7.3 V . Therefore, we conclude that, at the time the probe bias voltage was supposed to be 9 V , relative to the original floating potential of the PDP, it was actually 7.3 V . As is shown in Fig. 9, this procedure allowed us to determine the potential of the PDP, relative to the original floating

Table 1 Constants used in the calculation of the floating potential

Geometry of satellite:	
Electron collecting area A_e , m^2	4.395
Ion collecting area A_i , m^2	0.830
Height of main body h , cm (in.)	66.04 (26)
Height of "top cap" h' , cm (in.)	21.97 (8.65)
Radius of main body r , cm (in.)	53.34 (21)
Radius of "top cap" r' , cm (in.)	28.58 (11.25)
Orbital parameters:	
Electron density n_e , $\times 10^3 \text{ cm}^{-3}$	1
Ion density n_i , $\times 10^3 \text{ cm}^{-3}$	1
Electron temperature T_e , K	2500
Orbital velocity of PDP v_o , km/s	7.7

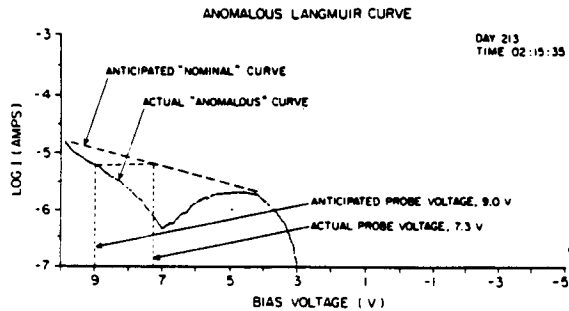


Fig. 8 Illustration of the method used to determine the actual Langmuir probe bias voltage, relative to the original floating potential of the spacecraft.

potential, as a function of time. (This cannot be done with the average dc potential measurements by the E-field spheres, since the dc potential is sampled only once every 1.6 s.) The potential of the PDP dropped for about 0.2 s after the beginning of a sweep and then spent the next 0.2 s recovering to its original value. The implications of this are as follows.

Recall that the current balance equation, Eq. (5), must be satisfied at all times. We have four currents contributing to current balance. $I_{i,sc}$ is a constant, independent of the floating potential of the PDP, $I_{e,sc}$ depends on the floating potential, which we can determine as in Fig. 9, and $I_{e,pr}$ was measured directly. This allows us to solve for our one remaining unknown, $I_{e,lep}$. A graph of $I_{e,lep}$ as a function of time, assuming the plasma conditions given in Table 1, is given in Fig. 10. Time $t = 0$ is the time when the bias voltage on the LEPEDA switches from 0 to 2.2 kV. Due to the sampling rate of the Langmuir probe data, 120 Hz, we were unable to determine the form of $I_{e,lep}$ between 0 and 0.050 s. Consequently, this portion of the graph has been left blank. Also, we were unable to obtain $I_{e,lep}$ after about 0.4 s, since it was difficult to establish with any accuracy when the predominant source of electron current changed from $I_{e,lep}$ to $I_{e,sc}$.

In spite of these difficulties, the significance of Fig. 10 is that it shows conclusively that the LEPEDA must be drawing significant amounts of electron current from the ionosphere. At time $t = 0.2$ s, the LEPEDA is drawing about 100 μ A of electron current, compared with 107 μ A for the magnitude of $I_{i,sc}$. Thus, the LEPEDA current is large enough that the potential of the PDP must drop by several volts in order to maintain current balance. In the example presented here, $n_e = 1 \times 10^5 \text{ cm}^{-3}$, $T_e = 2500 \text{ K}$, the potential of the PDP dropped by about 4 V. However, in some cases, when the Langmuir probe phase angle was about -55° , the resulting Langmuir curves indicated an even larger drop in spacecraft potential, Fig. 5. Also, by comparing the magnitude of the noise seen in the lock mode data during these worst-case events with the noise seen when the plasma conditions were similar to those in Fig. 8, we believe that, in some cases, the potential of the PDP may have dropped by as much as 10 V.

The previous discussion indicates that it is current collection by the LEPEDA that is responsible for the anomalous data reported by both the Langmuir probe and the dc Electric Fields instrument. We must now show that this can explain the actual appearance of the anomalous data and also the dependence of the anomaly on the phase angle. We begin with a discussion of the Langmuir probe sweep mode data. As was shown in Fig. 7, the bias voltage on the LEPEDA switches from 0 to 2.2 kV at the same time that the Langmuir probe enters the sweep mode. However, as was shown in Fig. 9, the maximum change in spacecraft potential does not occur until 0.2 s after the start of the sweep. This 0.2-s delay occurs because at time $t = 0$ the bias voltage on the LEPEDA switches from 0 to 2.2 kV and remains at this level for 0.2 s. The situation is similar to what happens when one charges/

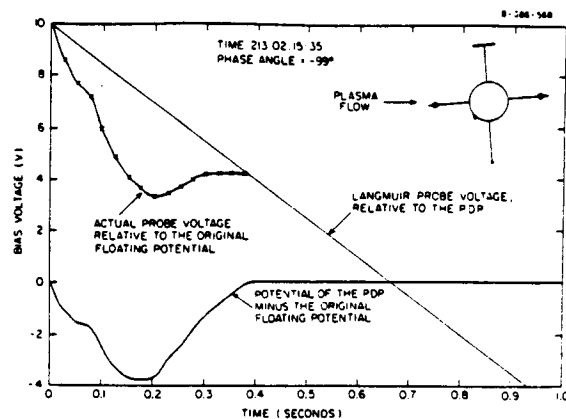


Fig. 9 Potential of the Langmuir probe and the PDP relative to the original floating potential.

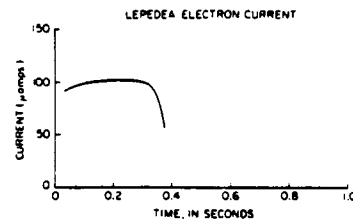


Fig. 10 Predicted value of the LEPEDA electron current, $I_{e,lep}$, vs time. Time $t = 0$ corresponds to the time when the LEPEDA bias voltage switched from 0 to 2.2 kV.

discharges a capacitor. At $t = 0$, the LEPEDA bias voltage is large and positive, thus the LEPEDA can draw a large electron current from the ionosphere and the PDP begins to charge to a negative potential. At $t = 0.2$ s, the bias voltage on the LEPEDA begins to decrease. Consequently, the electron current collected by the LEPEDA also decreases and the PDP begins to "discharge" to its original potential.

As can be seen in Fig. 9, the PDP potential wave form appears "rounded off" at early times. We have examined the possibility that this rounding could be related to a spacecraft-plasma circuit. Based on an electron density of $1 \times 10^5 \text{ cm}^{-3}$, we calculate a plasma sheath resistance of about 10 k Ω , ignoring magnetic field effects. If the rounding off of the spacecraft potential waveform occurred because the current to the spacecraft could only vary with a time constant given by $\tau = L/R = 0.2 \text{ s}$ or $\tau = RC = 0.2 \text{ s}$, for a simple circuit this would require values for the inductance L or the capacitance C , which are unrealistically large. Similarly, an examination of the Langmuir probe circuit gives no indication that any of its components could be responsible for producing the effect either. We have been informed that the LEPEDA voltage form was nominal in the high-voltage range during the time of observation,⁷ consequently, a satisfactory explanation of the PDP potential waveform is lacking.

The appearance of the lock mode (6–40 Hz) data is understood as follows. As was shown in Fig. 9, we were able to deduce the potential of the chassis of the PDP, as a function of time, after the voltage pulse to the LEPEDA. Consequently, we also know that the actual bias voltage of the Langmuir probe would be, relative to the plasma, during the lock mode. This is shown in Fig. 11a, where time $t = 0$ again corresponds to the start of the voltage pulse on the LEPEDA and the plasma conditions are those given in Table 1. Using a nominal Langmuir curve, Fig. 2a, we then determine the current collected by the Langmuir probe during the lock mode by reversing the process illustrated in Fig. 8. The current curve in the lock mode is shown in Fig. 11b for the initial 1.0 s of the 1.6-s cycle of the LEPEDA voltage. By taking the fast

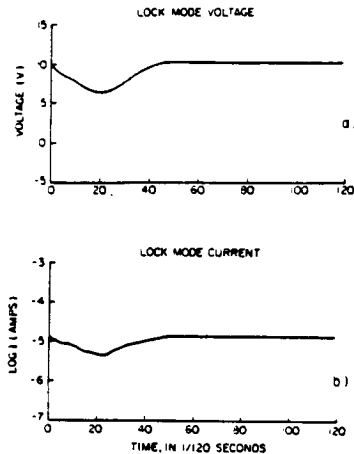


Fig. 11 Actual Langmuir probe bias voltage during the lock mode, relative to the original floating potential (a) and computation of the current collected by the Langmuir probe during lock mode (b). Time $t = 0$ corresponds to the time when the LEPEDA bias voltage switched from 0 to 2.2 kV.

Fourier transform of these data, Fig. 11b, we then isolate the contribution of the 6–40-Hz components, see Fig. 12. In comparing Fig. 12 with Fig. 3b, we notice that the general oscillatory form seen in Fig. 12 is very similar to that seen in the actual data, although the finer details appear somewhat different. We should note that, in an attempt to recreate the ringing seen in Fig. 3b, we have ignored the presence of any rapid density fluctuations, and, thus, cannot expect our prediction, Fig. 12, to agree entirely with the actual data, Fig. 3b.

Next, we need to explain the dependence that the anomaly has on the orientation of the PDP. As was previously mentioned, the magnitude of the anomaly recorded by both the Langmuir probe and the dc Electric Fields instrument maximizes whenever the LEPEDA is in ram. We would expect the LEPEDA to draw less current when the local electron density, i.e., the electron density near its opening, is small, and more current when the local electron density is large. If we ignore $I_{e,pr}$, we may rewrite Eq. (5) as

$$I_{e,LEP} = e n_e^*(\theta) f(V) \\ = e n_e (A_{v0} - A_p [kT_e / 2\pi m_e]^{1/2} \exp[eV/kT_e]) \quad (7)$$

where $n_e^*(\theta)$ is the local electron density "seen" by the LEPEDA, θ the LEPEDA phase angle, and $f(V)$ some function of its bias voltage. It is well established that the wake of an ionospheric satellite is a region of depleted electron densities. Therefore, when the LEPEDA is facing the wake of the PDP, the local electron density, $n_e^*(\theta)$, will be significantly less than the local electron density seen in ram. Thus, the magnitude of $I_{e,LEP}$ when the LEPEDA is in the wake will be correspondingly reduced and current balance will be achieved with virtually no change in spacecraft potential. Consequently, no anomaly is detected when the LEPEDA is in the wake.

Finally, the measurements of the average potential on the E-field spheres, relative to the chassis of the PDP, can also be easily understood. With the LEPEDA voltage pulsed to 2.2 kV, the potential between the PDP (which becomes more negative) and the spheres (still close to the original floating potential) must increase. We note that this potential measurement was taken once every 1.6 s and always 0.166 s after the LEPEDA voltage pulse. We can compare the potential change measured by the dc Electric Fields instrument with that determined from the Langmuir probe as in Fig. 9. In so doing, we find that the former is generally somewhat smaller

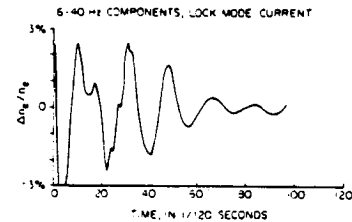


Fig. 12 Computed lock mode output from the 6–40-Hz channel. Time $t = 0$ corresponds to the time when the LEPEDA bias voltage switched from 0 to 2.2 kV.

than the latter, an effect due to low-pass filtering in the dc Electric Fields instrument. The Langmuir probe measurements and the dc potential measurements are, however, in general agreement.

Conclusions

Our experience suggests that an exposed, positive high-voltage source on an ionospheric satellite can act as a source of electron current to the spacecraft chassis. This may, in turn, affect the operation of other instruments that use the chassis of the satellite as an electrical ground by altering the spacecraft potential. This change in spacecraft potential is dependent upon the orientation of the high-voltage source, relative to the plasma flow. It is believed that this problem can be minimized in the future by placing a grounded grid on the opening of the high-voltage source so as to limit the collection of thermal electrons.

The fact that the effect was also detectable in the lock mode data when the PDP was grounded to the Orbiter indicates that the pulse of electron current collected by the LEPEDA was sufficient to change the potential of the Shuttle by a small, but noticeable, amount. Most of the body of the Shuttle is covered with an insulating material. The area of the Shuttle believed to be most responsible for current collection is the main engines. Because the surface area of the main engines is approximately one order of magnitude greater than that of the PDP, the current pulse to the LEPEDA may have shifted the potential of the Orbiter by as much as -1 V when the main engines were in the Orbiter's wake. If the potential of the Orbiter had shifted by more than -1 V the appearance of the Langmuir probe sweep mode data would have been affected. Since this did not occur, -1 V is an upper bound on the change in potential of the Shuttle.

Acknowledgments

This work was supported by Grant NAG3-449 from the NASA Lewis Research Center and Contract NAS8-32807 from the NASA Marshall Space Flight Center. We gratefully acknowledge the assistance of Prof. Donald A. Gurnett for providing the dc Electric Fields data and of the LEPEDA science/engineering team, in particular Bill Paterson, for their help in describing the operation of the LEPEDA.

References

- ¹DeForest, S. E., "Spacecraft Charging at Synchronous Orbit," *Journal of Geophysical Research*, Vol. 77, No. 4, Feb. 1972, p. 651.
- ²Olsen, R. C. and Purvis, C. K., "Observations of Charging Dynamics," *Journal of Geophysical Research*, Vol. 88, No. A7, July 1983, p. 5657.
- ³Huddleston, R. H., and Leonard, S. L., eds., *Plasma Diagnostic Techniques*, Academic Press, New York, 1965.
- ⁴Murphy, G., Pickett, J., D'Angelo, N., and Kurth, W. S., "Measurements of Plasma Parameters in the Vicinity of the Space Shuttle," *Planetary and Space Science*, Vol. 34, Oct. 1986, p. 993.
- ⁵Frank, L. A., Yeager, D. M., Owens, H. D., Ackerson, K. L., and English, M. R., "Quadrilateral LEPEDAs for ISEE's-1 and -2 Plasma Measurements," *IEEE Transactions on Geoscience Electronics*, Vol. GE-16, July 1978, p. 221.
- ⁶Johnson, E. O. and Malter, L., "A Floating Double Probe Method for Measurements in Gas Discharges," *Physical Review*, Vol. 80, Oct. 1950, p. 58.
- ⁷Cravens, J., private communication, 1987.

Orbiter Environment at S- and K_u-Band Frequencies

G. B. Murphy*

The University of Iowa, Iowa City, Iowa
and

W. D. Cutler†

The Aerospace Corporation, El Segundo, California

Detailed measurements of the electric field strength associated with the K_u-band radar and S-band communication link were made by the Plasma Diagnostics Package (PDP) on STS 51F. These measurements were made while the PDP was attached to the Remote Manipulation System arm and again while the PDP was released as a subsatellite. The results indicate that cargo elements that remain inside of the scan limits of the radar should experience fields less than 2 V/m and that elements that may encounter the main beam can use 300 V/m as a design guideline with adequate safety margin. S-band fields tended to be several dB lower than worst case predictions. Safe design practice indicates that an electric field $E = 100/r$ (r in meters) should be used as a guideline for deployable systems. S-band electric fields within the cargo bay envelope should be < 2 V/m even with edge diffraction effects and reflections from other payloads taken into account. The absolute accuracy of these measurements is ~ 2 dB.

I. Background

THE Space Shuttle Orbiters were designed to haul cargo into orbit as well as retrieve it from orbit. Because the cargo can be extremely varied in its application, a great effort has been made to define as much of the environment as possible in and near the Orbiter in launch, orbit, and landing phases. By knowing precisely what environment to expect, engineers can appropriately design the payloads to operate safely and reliably within that environment.

The Plasma Diagnostics Package (PDP) is a cluster of fourteen instruments designed primarily to define the way in which the Orbiter perturbs the natural plasma environment. A complete description of this instrumentation may be found in Shawhan.¹ Since plasma-wave instruments were part of the cluster in the PDP, measuring electric and magnetic fields to approximately 200 kHz, it was logical to use the PDP to measure Orbiter-induced electromagnetic interference (EMI) as well. The wave measurements were therefore extended in frequency range to measure fields generated by the Orbiter's intentional transmitters. An S-band receiver was added specifically to measure field magnitudes due to the PM and FM communication link. Shawhan² summarizes the EMI results obtained from the PDP wave instruments on the third test flight of the Orbiter Columbia (STS-3).

Detailed measurements at S-band communication frequencies on STS-3 indicated that field strengths were on the high side of predictions but with an uncertainty factor that made a refined set of measurements desirable.³ The S-band detector system was upgraded, and a receiver was added that had the ability to measure the fields of the K_u-band integrated radar and communications link. A detailed description of this hardware, referred to as the KUSR, may be found in Murphy⁴ and a brief overview is given in Sec. II.

Upon completion of the hardware calibration and integration, the PDP was reflown on Challenger 51F (Spacelab 2), and a number of specific experiments were implemented to characterize the S-band and K_u-band links. These experiments are described in Sec. III.

Before engaging in a detailed discussion of the experiment and results, it will be appropriate to review briefly the Orbiter's S-band and K_u-band communications system.

Challenger S-Band Communication Link

There are several communication systems in the S-band frequency range, but only the one with highest power output is of concern for our measurements. This system, the CW phase modulated link, operates at a frequency of 2287.5 MHz through the four S-band "Quad" antennas located above and below the cabin area. It should be noted that the configuration of the antenna beams has changed from that which was measured on the STS-3 mission. The configuration on the Columbia allowed the selection of one of four antenna beams mounted in equal quadrants at four points around the crew cabin. For the Spacelab 2 mission, the Orbiter Challenger had been modified to provide eight possible antenna beams.

The eight beams are created by the use of four sets of waveguide slot antennas that are centered about four points around the circumference of the cabin area. See Table 1 for the location of these antennas in Orbiter body axis coordinates. By properly phasing each set of antennas, a broad beam can be made to point slightly forward or slightly aft of the Z axis. Since the antennas are located at angles of approximately 45 deg to the X-Y and X-Z plane, they are referred to as upper left (UL), upper right (UR), lower left (LL), and lower right (LR) antennas. (See Fig. 1 for a definition of the coordinate system used.) In addition, the designation "F" or "A" (e.g., ULA) is added to indicate, for a given antenna, whether the forward or aft pointing beam is selected for a specified antenna.

Table 1 Quad antenna locations^a

	X	Y	Z
UL	-551	-71	-472
UR	-551	+71	-472
LL	-556	-96	-295
LR	-556	+96	-295

^aGiven in Orbiter body axis coordinates.

Received Feb. 9, 1987; revision received June 16, 1987. Copyright © American Institute of Aeronautics and Astronautics, Inc., 1987. All rights reserved.

*Antenna Engineer, Department of Physics and Astronomy, Member AIAA.

†EMC Engineer. Member AIAA.

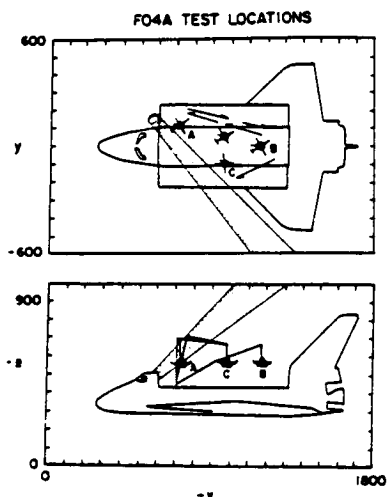


Fig. 1 Schematic representation of the FO4A sequence.

The high-frequency mode (2287.5 MHz) has the highest output power of all the possible S-band links and was selected when the KUSR made its measurements. The maximum measured output power of the high-frequency PM link transmitter is 163 watts (52 dbm). With 3.5 dB minimum cable loss, the maximum power available to the antenna is approximately 73 watts. (Measured cable loss varied from -3.5dB to -3.9dB.) Considering the maximum predicted gain of antennas at boresight is 7.1 dB (power ratio 5.12), the maximum expected field in a limited solid angle would be

$$E(V/m) = (1/r)[(1/4\pi)P \cdot G \cdot Z]^{1/2}$$

where P = transmitting power (watts), G = antenna gain, Z = free-space impedance, 377 Ω and r = distance (meters).

It is this worst-case electromagnetic field estimate that the experiment attempts to verify.

Shuttle K_u -Band Radar and Communications System

Since the Orbiter uses the same amplifier and parabolic antenna for operation of its TDRS data link (15.0034 GHz CW) and its radar link (five frequencies between 13.779 GHz and 13.987 GHz pulsed) and their peak output is essentially the same, it is sufficient to measure one or the other to determine worst-case fields. The radar field is linearly polarized in its passive mode, whereas in the communication mode the polarization is circular. Because of the flexibility of the radar system and the fact that it will be tracking the PDP while it is a free flyer, it was decided to make all measurements in radar mode. All details of the radar system may be obtained from Ref. 5 but are given below in a summary form.

The K_u -band radar and communications system is folded inside the payload bay for ascent and entry and deployed over the starboard sill next to the forward bulkhead when in use. Details of the antenna pattern and its predicted fields will be discussed in Sec. IV. The antenna has a 2-axis positioner and is pointed by rotation around a pivot point 21 inches from the antenna centroid when tracking satellites but employs an adjustable "obscuration mask" to prevent its pointing at certain elements of the Orbiter and into the payload bay.

The radar system is designed to track a standard Swerling target from approximately 30 m (100 ft) to 35 km (20 n.mi.). Since this is a range-gated radar, both the pulse width (pw) and pulse-repetition frequency (prf) are variable depending on the target distance. Table 2 lists the various pulse widths and prf's available depending on target distance and whether the radar is in its search or track mode.

In order to minimize scintillation effects, the radar frequency is automatically varied over the band indicated above

Table 2 Signal parameters for RR radar and radar power output

Mode	RR Radar		
	Range (n.mi.)	prf	pw (μ s)
Track	> 9.5	2987	33.2
	3.8 — 9.5	6970	16.6
	1.9 — 3.8	6970	8.3
	0.95 — 1.9	6970	4.15
	0.42 — 0.95	6970	2.07
Search	< 0.42	6970	0.122
	> 0.42	2987	66.4
	< 0.42	6970	0.122

Radar Power Output

Mode (Radar)	Output Power Level	Maximum Near Field (V/m) ^a	
		Far Field ^b	
Hi power	70 watts	280 ^c	2320/R
12 dB pad	4.4 watts	70	583/R
24 dB pad	0.3 watts	17	146/R
TWT bypass	~ 4 mwatts	3	26/R

^aMaximum in Communication Mode is 300 V/m. ^bBegins at ~ 77 m from dish. ^cIn Fresnel Zone extending to ~ 10 m.

in steps that are 52 MHz apart giving the following operational frequencies: 13.779, 13.831, 13.883, 13.935, and 13.987 GHz. This frequency switching happens rapidly compared to our KUSR measurement cycle and will not be important in data analysis.

Because there is a wide range in the possible return power (depending on target size and distance), it would be difficult to design the front end of the radar receiver section to handle such a dynamic range. Thus several output power levels are available. The power levels of these modes and the predicted field strength in the main beam at a distance of 100 m are contained in Table 2. The output power depends not only on the distance to the target but also on the radar mode selected. By choosing the proper mode, the PDP was able to make measurements of the radar beam even when it was too close to the orbiter to be tracked by the radar.

II. KUSR Instrumentation

The K_u -band/S-band receiver (KUSR) built and integrated into the PDP for the Spacelab 2 mission was designed and calibrated with the goal of measuring the S-band and K_u -band fields to a precision of 1 dB. This goal, since it was quite ambitious, could not be achieved, but accuracies on the order of 2 dB were attained. Although a complete and detailed description of the system is not within the scope of this paper (see Ref. 4), it is appropriate for the reader to have some basic understanding of the instrument.

The K_u -band subsystem consists of an optimal gain conical horn coupled to two orthogonal linear probes in a circular waveguide. The RF probe output is converted to DC through a zero-bias Schottky detector. This detector output is then routed to dual amplifier/peak detector systems, one high gain and one low gain. The outputs of both channels are multiplexed with S-band data and sampled by the PDP telemetry encoder at the rate of 10 Hz. Table 3 contains data on the sensitivity of this system.

The S-band subsystem differs somewhat from that which was flown on the STS-3 mission. A broadband, low-gain, ridge-guide horn was used for an antenna. Output was mixed to IF with a 2.20 GHz L.O. and the signal detected by both a linear detector (diode type), where output voltage was proportional to measured E-field, and a log detector. In front of the log detector was a bank of four filters; 25-65 MHz, 65-165 MHz, 165-400 MHz and 400-800 MHz, whose outputs were multiplexed to the log detector. Since we are only interested in the 2287.5 MHz PM link, only the output from the second filter (65-165 MHz) will be used in this report.

The test program for calibration of the KUSR was designed such that all absolute calibration ultimately depended on the accuracy of three things: 1) the repeatability of a measurement setup, 2) the absolute calibration of a power meter, and 3) the absolute accuracy of a standard gain horn. Table 4 delineates the instrument calibration error budget.

Calibration of the K_u-band subsystem was done for orthogonal linear polarizations, for five radar frequencies, and at all nominal pulse widths expected. These calibrations were performed in an anechoic chamber and compared to data from a standard gain horn. The system is slightly less sensitive at the lowest pulse width (0.122 μ s) but becomes flat above that 1.5 μ s. There is no frequency sensitivity because the radar changes frequencies rapidly compared to the peak detector sample rate. Only the frequency to which the system is most sensitive determines the output response on orbit.

By combining output from both polarizations, the total E-field may be determined independently of rotation about the line-of-sight axis to the source.

The S-band system was also calibrated in an anechoic chamber against a standard gain horn and its sensitivity is summarized in Table 3.

Both the K_u-band and S-band antenna patterns were plotted in azimuth and elevation so that measurements made at angles other than boresight could be reliably used in the analysis. In all cases these chamber measurements were made with the KUSR integrated into the PDP and with the PDP in its flight configuration.

III. Experiment Objectives

As with all experiments on Spacelab missions, detailed procedures, requirements, and configurations are determined far in advance of a mission and then timed as resources will allow. The following Functional Objectives (FO's) defined the goals of the KUSR experiment on PDP. These are met either by maneuvering the PDP on the RMS or by making measurements of the generated fields while the PDP is some distance away as a free-flying satellite.

F04A—K_u-band EMI

The RMS sequence pictured in Fig. 1 is used to move the PDP along the payload bay at a level near the top of the cargo doors. (The coordinate system used in Figs. 1-3 is the Orbiter Body Axis System (x/foreward, y/starboard, z/down).) The origin of this system is the nose of the external tank.) The radar dish is pointed over the payload bay (elevation +60, azimuth +50) at the edge of its allowable scan limit. The shaded portion of Fig. 1 depicts the beam at this scan angle. Low-power mode is chosen for the first part of the scan while the PDP continuously points its receiving antenna at the dish. During the last half of the scan, the PDP is rotated and points its receiving antenna at the vertical stabilizer allowing possible measurement of reflected fields. High-power mode was selected for this segment of the scan. This FO allows the instrument to characterize the worst-case electric fields expected near the cargo-bay envelope.

K04B—K_u-band Antenna Pattern—Near Field

The RMS sequence depicted in Fig. 2 is used to make direct measurements of the near-field radar beam. The radar is pointed up the -Z axis of the Orbiter, and the PDP scans along the beam axially from approximately 2.5 m (8 ft) to 10 m (35 ft).

Table 3 K_u-band and S-band sensitivity

K _u -Band, Single Channel	
Hi gain 13.887 GHz	2.07 μ s pw
0.8 V/m.....	4 V/m ^a
Lo gain	
3.5 V/m.....	63 V/m ^a
S-Band	
Log detector	2287 MHz
-42 dB V/m.....	+29 dB V/m
(0.008) V/m.....	(28 V/m)
Linear detector	2287 MHz
-18 dB V/m.....	+13 dB V/m
(0.126 V/m).....	(4.45 V/m)

^aVariation exists between the 2 polarizations. These data are typical.

Table 4 Instrument error budget

Source of Error	Magnitude of Error (dB)	
	K _u -Band	S-Band
Setup repeatability	± 0.5	± 0.5
Gain of standard horn	± 1	± 1
Calibration of detector	± 1	± 1
Mismatch detector/antenna	± 0.5	± 0.5
Sensitivity	± 0.25 (typ)	± 0.6 (typ)
Temperature correction	± 0.2	$\pm 0.5^a$
Total RMS error		
± 1 dB desired	± 1.6 dB	± 1.76 dB

^aLog Detector was not calibrated over temperature.

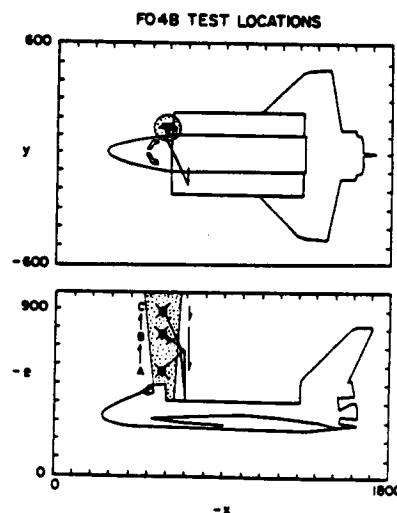


Fig. 2 The 4B scan sequence used to determine near-field strength of the radar beam.

At distances of 8 m (25 ft) and 10 m (35 ft) (points B and C in Fig. 2), the PDP is moved in X and Y to scan the beam radially. This scan was performed with the radar in both low and high power.

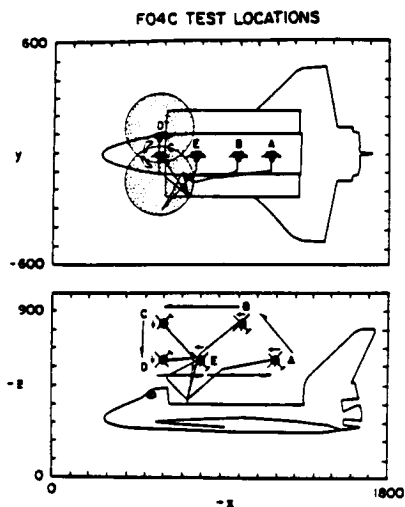


Fig. 3 The 4C scan sequence used to survey fields associated with Quad aft beams (2287.5 MHz.).

F04C—S-band Fields Near the Payload Bay

Figure 3 illustrates the RMS sequence used for this field survey. This is essentially a repeat of the experiment performed on STS-3. The scan is executed twice, once with the ULA beam selected (2287.5 MHz) and once with the URA beam selected. The small arrows in the figure indicate the pointing direction of the S-band horn.

F08—S-band Antenna Patterns

Figure 4 illustrates the objective that came to be called the "F08 roll." Since there are eight possible antenna beams on the Orbiter, it is desirable to get as much pattern information as possible on all of them. The PDP was a free-flying, spinning satellite, and the Orbiter was stationkeeping at ~ 90 meters along the velocity vector in front of PDP. Once stationkeeping was established, the Orbiter started a slow roll about its X-axis (0.75 deg/s). By selecting the proper antenna, a 90-deg scan of each of the eight beams was performed over a period of two complete rolls.

Another KUSR measurement goal, although not flight-test data are within approximately 3 dB of the theoretical prediction and in all cases are lower than the predicted value. Error bars on the PDP measurements would be ± 1.6 dB, easily obtained because the orbiter tracks the PDP during its free-flight at distances up to approximately 0.5 km.

IV. Results of K_u -Band Measurements

F04A was executed only one time, but the results are significant in that they provide guidelines for the EMI design specifications of hardware to be carried in the payload bay. During the first half of the scan depicted in Fig. 1 (A-B-C), the antenna, positioned against software limits at az-50 el-60, was operated in low power. No fields above the level of instrument sensitivity were detected (< 2 V/m) even though the PDP receiving antenna was directed toward the K_u -band radar dish. It should be noted that the original goal of pointing the radar directly at the vertical stabilizer was not achievable. Some higher reflected fields may have been expected in that case. During the second half of the scan (C-B-A), the radar antenna was operated in high-power mode. The only time any field above noise level was detected was at position C, where the PDP measured fringe fields associated with the beam per se. It should be noted that during this second half of the scan,

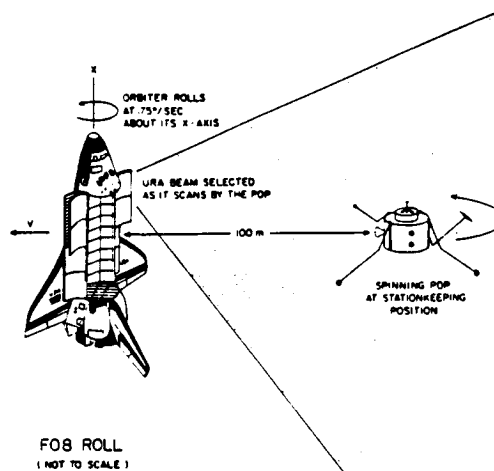


Fig. 4 Configuration for the F08 roll.

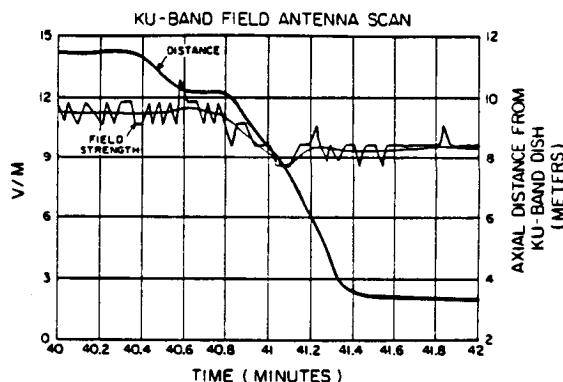


Fig. 5 Field strength measured during F04B scan.

the PDP receiving antenna was pointed in the general direction of the aft cargo bay and vertical stabilizer to look for reflected fields. The fact that no signals were detected implies that fields associated with power reflected from developing sidelobes many degrees from the main beam are negligible. F04B results discuss off-axis intensity in more detail.

Results of the above experiment would seem to confirm that instruments operating entirely within the obscuration mask or scan limits should not experience fields in excess of 2 V/m. Within the primary beam no reflections from other payload bay elements would seem to contribute enough to the field intensity to be of concern if instruments are not sensitive to 2 V/m fields. However, any instrument that is operated outside of this protective envelope should design to fields associated with the main beam.

The purpose of F04B was to measure the fields associated with the near-field beam. Figure 5 is a plot of the intensity of the K_u -band electric field in low-power radar mode and the axial distance from the center of the radar dish as a function of time for the first execution of F04B. As can be seen in the figure, the field is not strongly dependent on distance along the beam center. The intensity has a minimum at a distance of ~ 7.5 m and a broad maximum of ~ 11-12 V/m from 10-12 m. Although two scans were done with this RMS value, only the first scan, done in low-power mode, is plotted in Fig. 5 since the second scan, which was in high power, saturated the instrument when it was on axis of the antenna. Assuming the specified 24 dB difference between low and high power shown in Table 2, the maximum expected electric field in the near-field beam interpolated from the data would be ~ 190 V/m.

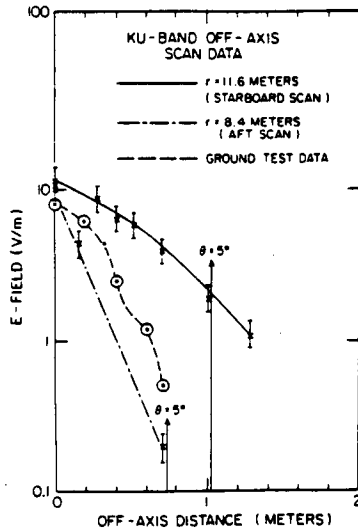


Fig. 6 Near-field off-axis scan data.

Figure 6 illustrates the radial dependence of the electric field intensity as the RMS scanned the PDP perpendicular to the beam axis. The figure is a compilation of data from 2 scans. For reference, data taken during ground testing⁶ at a distance of 8.4 m is also shown in Fig. 6.

A look at the raw data taken during the second F04B scan, which had the radar in high-power mode, reveals some interesting characteristics. Figure 7 plots the total measured field as a function of time. The two large dips in the field are the manual X and Y off-axis scans. The actual fields plotted are incorrect except during these X and Y scans because the instrument is in saturation (the actual field should be ~ 190 V/m based on low-power scan data). Several conclusions can be drawn from these data. The apparent increase in the total field at the beginning and end of the Y-scan indicates a shift in the polarization. This is noticeable because of a difference in sensitivity of the orthogonal detectors. At an angle of 6.5 deg away from the main beam, the field is still 18 V/m, yet a closer distance and 5 deg from the beam, the field is below the level of sensitivity of the low-gain detector. It is also interesting to note the apparent variation in intensity from time = 28 to time = 32. This change (a result of increasing the distance from the dish) is not only a real amplitude change but also indicates a polarization shift. The X-scan is notable because small "sidelobes" are beginning to form at this location. It is not clear if these are real or an artifact of multiple reflections between the probe (PDP) and the dish.

Additional measurements of the Orbiter's radar were obtained during the free-flight portion of the PDP's experiments. At distances greater than ~ 200 m (640 ft), the radar is in high-power mode during passive track and additional data points on the beam intensity were obtained at several distances. Figure 8 is a plot showing the superposition of a theoretical 25 dB Taylor distribution, Rockwell ground test data, and the points obtained both during F04B and free flight. [Figure 8 ground-test data ran 7.26 dB below a "hot" (hypothetical) system that would have 1) the highest output power of any production TWT, 2) the least observed waveguide loss, and 3) the highest antenna gain ever measured. There are natural variations in these parameters between systems.] The flight-test data are within approximately 3 dB of the theoretical prediction and in all cases are lower than the predicted value. Error bars on the PDP measurements would be ± 1.6 dB.

Discussion of the comparison between the measured values for K_u-band electric fields and design specifications will be continued in the summary section.

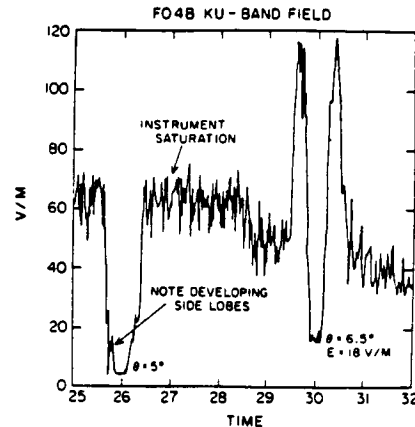


Fig. 7 Magnitude of the electric field as a function of time during the high-power F04B scan.

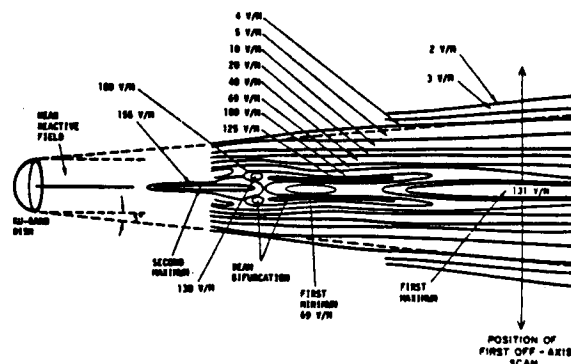
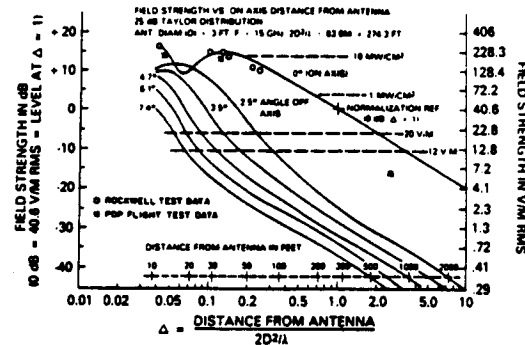


Fig. 8 Comparison of flight data to ground test results.

V. Results of S-Band Measurements

RMS test objective 4C, which was discussed in Sec. III, resulted in tabulated values of electric field intensity at several locations in and over the cargo bay. The RMS sequence was executed twice with either the URA or ULA quads selected since they produce the worst-case fields in and around the cargo bay. Table 5 summarizes the results of the measurements at each of the test locations shown in Fig. 3. These data have been corrected for the receiving antenna directivity, but it should be noted that the receiving antennas are linearly polarized and the transmitting antennas (quads) are circularly polarized. This implies that the total E-field at boresight is 3 dB greater than we measure.

Table 5 FO4C Summary

RMS Point (Fig. 3)	Distance from XMTR (m)	Angle from boresight (deg)	Measured field dB (V/m)	Antenna directivity correction (PDP) dB	Equiv. E-field V/m	Antenna Directivity correction (XMTR) dB	Far-field constant ^a $k = Er$
<i>Upper Left Aft</i>							
A	16	70	-4	1.35 ± 0.1	0.74	6 ± 1	23.5
B	14.3	58	4	2.7 ± 0.5	2.2	6 ± 1	61.7
C	9.2	54	11	1.05 ± 0.1	4.0	5 ± 1	65.1
D	6.0	86	5	5.8 ± 1	3.5	8.5 ± 1	55.4
E	6.9	64	4	3.5 ± 1	2.4	6 ± 1	32.6
<i>Upper Right Aft</i>							
A	16	69	-6	1.3 ± 0.1	0.58	5 ± 1	16.6
B	14.3	56	2	2.5 ± 0.3	1.7	4 ± 1	38
C	9.3	51	8	1.2 ± 0.1	2.9	2 ± 0.5	33.8
D	4.1	31	17	1.15 ± 0.1	8.1	1 ± 0.5	37.4
E	7.0	60	8	2.4 ± 0.5	3.3	4 ± 1	36.7

^aNot corrected for polarization loss.

Column 8 in Table 5 shows the value of $k = E \cdot r$ calculated for each measurement point, where r is the distance between transmitter and receiver. Note that for measurement angles far from boresight (points A and E for URA and points A, D, and E for ULA), there tends to be some divergence from the trend. This is consistent with the purity of the polarization from the transmitting antenna degrading at angles from boresight. Measurements taken at small angles from boresight give the best indication of the output of the transmitting antennas; however, measurements at larger angles from boresight do provide a realistic assessment of the fields encountered by a single linear polarized aperture at these locations. It would be wise for the designer to assume all of the power from the transmitting antenna, P_t , not $P_t - 3$ dB, is available to excite an aperture of any given orientation at these points in the cargo bay.

Measurements made during Orbiter back-away after PDP release provide the best measure of the $E \cdot r$ constant. Figure 9 is an illustration of the data taken during this maneuver. (These data have not been corrected for polarization loss.) The PDP was released from the RMS at 213:00:10:00; at 213:00:12:05 the Orbiter began a series of thruster firings that caused it to separate from the PDP at a rate of ~ 0.5 ft/s. Within 30 seconds after release from the RMS, the PDP began to slowly spin up. This generated the spin modulation evident in the data of Fig. 9. Figure 9 has been fitted to a k/r curve, where the best-fit value of k is 31.1 ± 0.5 . Correcting for the 3 dB polarization loss, the expected value of electric field from an upper quad antenna (it is not known if it was ULA or URA) is $E = 62/R$. These data are in close agreement with FO8 roll data for the ULA antenna discussed below.

In order to obtain measurements on all eight antennas, the FO8 roll maneuver (see Sec. III) was performed at a distance of approximately 90 meters from the Orbiter. Figure 10 illustrates the data taken during this objective. (The peaks are a result of the 13 s spin period of the PDP modulating the receiving antenna gain.) The PDP was located at a distance of about 90 m behind and slightly to the aft of the Orbiter. The roll maneuver about the Orbiter X axis thus produced a good principal plane scan of the aft beams but did not pass through the center of the forward pointing beams. The minimum angle

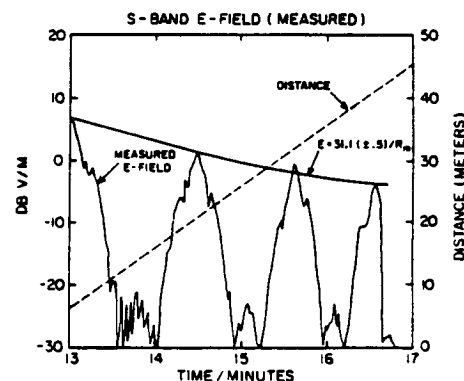


Fig. 9 S-band data from Orbiter back-away maneuver.

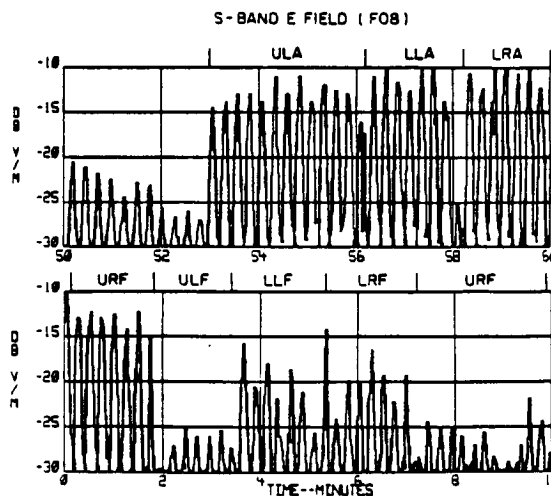


Fig. 10 FO8 roll data uncorrected for 3 dB polarization loss.

Table 6 FO8 S-band fields

Antenna Selected	Peak field measured dB (V/m)	Distance (m) (± 5)	Angle from boresight ^a (deg)	$k = E/r$	+ 3 dB polarization loss (XMTR)
ULA	-10	93	0 ± 2	29.4	58.8
LLA	-9	92	0 ± 2	32.6	65.2
LRA	-9	91	2 ± 2	32.3	64.6
URA	-12	86	3 ± 2	21.6	43.2

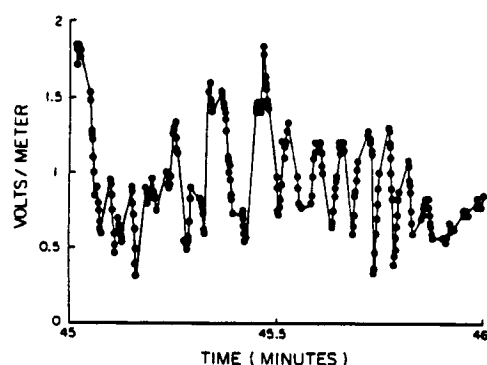
^aClosest approach of pattern cross section to transmitter boresight.

Fig. 11 Standing wave pattern observed as the PDP was moved from location D to E of FO4C scan.

to boresight for measurement of the forward beams was ~ 40 deg. This is evident in Fig. 10 from the lower intensity for all of the forward antennas. Using the ground-test data⁷ for antenna patterns illustrated in Fig. 10, a correction for directivity of the transmitting antenna can be made and an estimate of boresight intensity obtained. Table 6 summarizes the results, corrects for the 3 dB polarization loss, and provides an estimate of the worst-case fields for the aft beam of each antenna at this measurement distance.

An additional topic of interest for S-band fields in or near the cargo bay is how much electric field enhancement can be expected due to reflections from payload elements in the cargo bay and possible diffraction effects associated with the edge of the forward bulkhead. The RMS scan for FO4C yielded interesting results in this regard. Figure 11 is a sample of S-band data taken during FO4C scan from point D to E. The quasi sinusoidal variations observed can be explained by the PDP being moved through a standing wave pattern resulting from interference of multiple sources. (This standing wave pattern is not observed external to the cargo bay.) It is not possible with the complex geometry of the payload bay elements of 51F (Spacelab 2) to discriminate possible multiple source reflections, which would produce a standing wave pattern, from the diffracted fields that could also be present.

If we assume that this pattern is due to one primary and one secondary source, the worst-case VSWR observed indicates that the secondary source has a power approximately 20% that of the primary source. Since these observations are highly dependent on position within the cargo bay envelope and would, of course, be dependent upon payload geometry, it

would not be unreasonable to expect reflection enhancements to be as high as 50% over that of the primary source. Several dB margin of error over the measured E/R constant should be allowed to account for field enhancement from these reflections.

VI. Summary

For the EMC design of Shuttle payloads, several general conclusions can be gathered from the above data.

Under normal conditions, K_u-band electromagnetic fields experienced by cargo elements remaining inside the radar-scan limits set by either hardware limits or observation mask will be less than 2 V/m. Payloads that will be deployed or operated in any way outside of the mask, or those that need to operate concurrently with the radar and depend only on operational guidelines to prevent the radar antenna from pointing at them, should design to the guidelines given in the JSC, 07700, Volume XIV, Attachment 1 (ICD 2-19001). This specification lists the maximum field in the high-power beam to be 300 V/m. Experience dictates that this is probably an overestimate by $\sim 50\%$ of what fields may actually exist. Since there can be intrinsic variation in TWT output power and waveguide losses among orbiters, the 300 V/m value should be used to provide an adequate safety margin. Our measurements on Challenger can serve only to provide additional credibility to these guidelines.

S-band electric fields also tended to be somewhat lower than worst-case predictions. Figure 10.7.2.2.6-1 in ICD 2-19001 gives worst-case fields at boresight of slightly more than $100/r$. Our measurements that have an absolute accuracy of ± 2 dB predict $\sim 60/r$, which is about 4.4 dB low. This is not unreasonable since the ICD gives worst-case numbers. Safe design practice would indicate that for any point near the Orbiter payload bay, $100/r$ field prediction provides an adequate margin of safety. E-fields within the cargo bay should always be < 2 V/m even with reflections and/or diffractions taken into account.

Acknowledgements

The authors wish to thank Mr. Arthur Reubens and Mr. Bob Castle, NASA JSC, for their assistance in the preparation and analysis of this experiment. This work was supported by the Air Force Space Division through NASA MSFC Contract NAS8-32807.

References

- ¹Shawhan, S. D., Murphy, G. B., and Pickett, J. S., "Plasma Diagnostics Package Initial Assessment of the Shuttle Orbiter Plasma Environment," *Journal of Spacecraft and Rockets*, Vol. 21, July-Aug. 1984, pp. 387-391.
- ²Shawhan, S. D., Murphy, G. B., and Fortna, D. L., "Measurements of Electromagnetic Interference on OV102 Columbia Using the Plasma Diagnostics Package," *Journal of Spacecraft and Rockets*, Vol. 21, July-Aug. 1984, pp. 392-397.
- ³Murphy, G. B. and Shawhan, S. D., "Radio Frequency Fields Generated by the S-Band Communications Link on OV102," *Journal of Spacecraft and Rockets*, Vol. 21, July-Aug. 1984, pp. 398-399.
- ⁴Murphy, G. B., "KUSR Final Engineering Report," Department of Physics and Astronomy, University of Iowa, Iowa City, Iowa, April 1985.
- ⁵"Integrated Communications and Radar Equipment, K_u Band," Space Division, Rockwell International, Document Number MC409-0025, Rev. D.
- ⁶Griffen, B. L. and Blount, R. L., "The Electromagnetic Environment for the Space Shuttle Orbiter," AIAA Paper 83-0332, Jan. 1983.
- ⁷Shuttle Orbiter OV-099 S-Band Quad Switch Beam Antenna Pattern Data," Lockheed Engineering and Management Services Co., NASA Report EE3-84-14202, Sept. 1984.

Log No.: A8097

U. of Iowa 87-2

THE GASEOUS ENVIRONMENT OF THE SHUTTLE
EARLY IN THE SPACELAB 2 MISSION

Jolene S. Pickett,* Gerald B. Murphy,*
and William S. Kurth†

Department of Physics and Astronomy
The University of Iowa
Iowa City, Iowa 52242

Submitted to Journal of Spacecraft and Rockets
February, 1987
Revised June, 1987
Accepted July, 1987
Volume 25, No. 2

Presented as Paper 85-6054-CP at the AIAA Shuttle Environment
and Operations II Conference, Houston, TX, Nov. 13-15, 1985.

*Staff Research Assistant, Member AIAA.

†Research Scientist.

ABSTRACT

A cold cathode ionization gauge was flown on space shuttle flight STS-51F as a part of the Spacelab 2 payload. Neutral pressure data which were taken in the payload bay during the first few hours on orbit are presented. These data show that when the payload bay is oriented such that the atmospheric gases are ramming into it, the pressure rises to a peak of 4×10^{-6} Torr. Pressure is also slightly higher during the sunlit portion of each orbit. Outgassing of the payload bay causes the pressure to be elevated to a few times 10^{-6} Torr early in the mission. In addition, several effects on pressure have been identified which are due to chemical releases. Substantial increases (50-150%) are seen during another experiment's gas purge. Orbiter chemical release effects include the following: pressure increases of 200% up to 7×10^{-6} Torr due to OMS burns, minor perturbations in pressure due to vernier thruster firings and little or no increase in pressure due to water dumps. In the case of vernier thruster firings, effects are seen only from down-firing thrusters in the back of the Orbiter which are probably due to the reflection of thruster gases off of Orbiter surfaces.

INTRODUCTION

The Plasma Diagnostics Package (PDP), is a cylindrical subsatellite that has flown on two space shuttle flights to date. The PDP carried a complement of fourteen instruments, including a cold cathode ionization gauge, that measured various plasma parameters. Data were taken in the payload bay and on the Remote Manipulator System (RMS) arm on both flights and as a free-flying satellite on its most recent shuttle flight.

The PDP first flew on STS-3 (Space Shuttle Columbia) as part of the Office of Space Science's first payload (OSS-1) from March 22-30, 1982.¹ The pressure gauge on that flight obtained approximately 100 hours of neutral pressure measurements from two locations--in the payload bay and on the RMS arm up to 15 meters (~ 50 feet) from the Orbiter. Neutral pressure results from that flight can be found in Shawhan et al.² and Shawhan and Murphy.³

The PDP's second flight was on STS-51F (Space Shuttle Challenger) as part of the Spacelab 2 (SL-2) payload from July 29-Aug. 6, 1985.⁴ On this flight the pressure gauge obtained only 3 hours of data on the first day of the mission due to a mechanical failure in the gauge electronics box which occurred 7.5 hours after launch. However, these data were obtained during a time in which other instruments were being activated, the payload bay was still outgassing and two OMS burns occurred. For these reasons, these data are vital in understanding the neutral pressure environment of the space shuttle early in a mission.

INSTRUMENTATION

The vacuum measurement system on the PDP utilizes a cold cathode magnetron gauge similar in configuration to the Redhead magnetron gauge developed in the late 1950's.⁵ The gauge aperture contains a baffle to prevent ram effects of neutrals and ions. A six-inch extension tube is added to the aperture to allow access to the orbiter payload bay pressure environment outside of the PDP skin. The gauge works on the principle that a discharge current in a transverse magnetic field is dependent on the pressure of the gas. The gauge transforms the vacuum input signal into a 0-5 volt output signal which is proportional to the logarithm of the input pressure. The range of the instrument on SL-2 was from 10^{-7} to 10^{-3} Torr, of equivalent nitrogen pressure. The sampling frequency of the pressure gauge on SL-2 was 20 Hz.

Since all of the data that are presented in this paper were obtained while the PDP was located in the payload bay, it is important to know the orientation of the pressure gauge. Figure 1 shows the PDP in its stowed (i.e., pallet) configuration. As can be seen, the pressure gauge tube is located near the bottom of the spacecraft and points in a direction midway between starboard and aft of the Orbiter. The extension tube exits the PDP skin 45° to the radial direction. The tube aperture is only 1/2 inch from the PDP skin at its closest point. Figure 2 shows the location of the PDP within the SL-2 payload. It is obvious from this figure that other experiments closely surround the pressure gauge. In fact, the pressure gauge looks

directly at the Infrared Telescope (IRT) instrumentation, which is located only a few inches from the PDP structure. This is in contrast to the pressure gauge on OSS-1 which had an open field of view in the middle of the pallet where no other instrument was mounted close to it.

NEUTRAL PRESSURE RESULTS

Orbit-Related Effects

A plot of the 3 hours of neutral pressure data obtained by the PDP cold cathode ionization gauge on Spacelab 2 is shown in Fig. 3. This plot shows neutral pressure in Torr (equivalent N_2) vs. time. The time of this plot, which begins about 4.5 hours after launch, is from 0130 to 0430 GMT on day 211 of 1985. The pressure gauge actually received power at the time the spacecraft was powered up at 0039 GMT. However, it did not begin to ionize until 50 minutes later. The possible reasons for this will be discussed below.

One feature to note in Fig. 3 is the rise in pressure from a low of about 1.5×10^{-6} Torr that begins shortly before 0300 GMT. At this time the payload bay is rapidly rotating into the ram of the gas flow, reaching maximum ram at 0302 GMT, and then gradually rotating out of it as indicated by the angle of attack in Fig. 3. The angle of attack is defined as the angle between the -Z axis of the orbiter (up from the payload bay) and the velocity vector. Thus, maximum ram is obtained at an angle of attack equal to 0 degrees and deep wake at 180 degrees. During the ram event centered at 0302 GMT, the pressure is seen to rise rapidly and then gradually decrease to its previous level during this time, indicating a dependence on the direction of gas flow with respect to the payload bay. The rise actually begins to occur during a one-minute interval of lower pressure which will be explained in the next section. The PDP is in wake at 0203-0206 GMT but this wake appears to have no significant effect on pressure.

The entire payload bay is briefly in a deep wake condition (i.e., angle of attack equal to 180 degrees) around 0250 GMT, but once again no significant effect is noted.

It is also evident that there is some outgassing in the payload bay since ambient pressure for an altitude around 300 km would be $< 10^{-7}$ Torr and contributions from ram flow would only increase the pressure to about 1×10^{-6} Torr. Also evident are the brief, random one order of magnitude increases in pressure to about 2×10^{-5} Torr throughout the plot. These increases are believed to be due to outgassing in the gauge itself. This effect was also seen on the OSS-1 flight³ and during thermal-vacuum testing prior to the SL-2 launch.

There is also an indication in Fig. 3 that the neutral pressure in the payload bay is slightly less on the night side than on the day. For example, the slight rise in pressure (approximately 50%) seen at 0350 GMT is probably attributable to the shuttle entering daylight.

Payload-Related Effects

One of the more striking features of the plot shown in Fig. 3 is a periodic variation in pressure which begins at 0216:44 GMT. At this time the pressure is seen to rise, thus beginning a cycle of 20 minutes at a higher pressure and 1 minute at the lower pressure which was being recorded before the cycle began. Subsequent to the flight it was discovered that at about 0216:00 GMT the Cosmic Ray Nuclei Experiment (CRNE) of the University of Chicago, which is shown in Fig. 2, began a gas purge which consisted of releasing a mixture of 80% N₂ and 20% CO₂ for 20 minutes, pausing for 1 minute, and then releasing the gas for another 20 minutes, and so on. The amount of gas being released was about 500 liters per hour. Its composition

changed from the N_2 , CO_2 mixture to a mixture of 15% CH_4 , 25% Xe, and 50% He with a time constant of about one hour.⁶ Before the CRNE release we assume that the gaseous environment of the payload bay is predominantly water based on measurements taken by an ion mass spectrometer mounted on the PDP on SL-2⁷. Summers⁸ states that the relative sensitivity of H_2O normalized to N_2 is 0.97 over the pressure range 10^{-7} to 10^{-5} Torr for a cold cathode ionization gauge. Therefore, when the CRNE release, consisting primarily of N_2 , begins, we expect to see a maximum increase in pressure of 3% due to the gauge's greater sensitivity to N_2 than H_2O . Since the increase (about 150%) is, in fact, quite large, we know that the CRNE release has a marked effect on the payload environment.

If the payload bay environment is not dominated by water as reported in Reference 7, but instead consists primarily of atomic oxygen as expected at shuttle altitudes, then a lower limit on the pressure increase due to the CRNE release can be derived. Since the sensitivity of the gauge to atomic oxygen is not given in Reference 8, we can arrive at an approximate value based on the data given by Summers⁸ and the ionization cross sections published in the literature. Redhead et al.⁹ state that provided the ions, which are produced within the gauge, are formed with zero kinetic energy, the relative gauge sensitivities should be nearly proportional to the magnitude of the ionization cross-sections near their maximum (approx. 100 eV electron energy). Assuming this to be the case, the sensitivity of the gauge to atomic oxygen would be > 0.5 . This implies that the increase in pressure due to the CRNE release is only around 50% rather than 150% for the case of a water-dominated environment.

At least two other experiments on SL-2 - the Infrared Telescope (IRT) from the Smithsonian Astrophysical Observatory and the Super Fluid Helium Experiment (SFHE) from the Jet Propulsion Laboratory - were steadily venting helium at the sill of the Orbiter payload bay at the rate of 20-30 mg/s (approximately 0.4-0.6 liters/h at STP). The relative sensitivity of He normalized to N₂ for this gauge is 0.15.⁸ The effects, if any, from helium ventings cannot be determined.

Another effect on the pressure which we believe may be due to one of the other experiments located in the payload bay is shown in Fig. 4. This plot covers 30 minutes from 0200 to 0230 GMT on day 211. At about 0205 GMT we see a square wave pattern in the data with a period of about 3.5 minutes. At about 0216:00 GMT the square wave begins to look more like a rectified sine wave with a period of about 0.5 minutes. (Note that the jump at 0216:44 GMT is the result of the CRNE gas purge.) We considered the possibility that the scanning IRT, which is located very close to the pressure sensor, is the cause of this effect, however, available data appear to rule this out. The drop to zero output seen at 0204 GMT is probably an indication of the impending mechanical failure.

Orbiter-Related Effects

Figure 5 shows the effects of two types of chemical releases associated with thruster activity on the Orbiter--a continuous firing of two vernier thrusters, which take place over about 1.1 seconds, and an Orbital Maneuvering System (OMS) burn. The effect of the OMS-3 burn, which was used on SL-2 to circularize the orbit at approximately 325 km altitude, begins at 0230:27 GMT during daylight, lasts for about 35 seconds, and is directed antiparallel to the velocity vector. This burn raises the neutral pressure by about a factor

of 2 up to 7×10^{-6} Torr. Once the OMS engines are shut off, the pressure returns to its previous level after only 3 to 4 seconds. Acceleration data from the SFHE experiment¹⁰ show a sharp drop at 0231:01.0 GMT until about 0231:01.7 GMT and then an exponential decay which approaches zero at about 0231:05 GMT, which is consistent with the pressure data. The reason for the pressure spike (lasting about half a second) at the beginning of the burn is not known. However, the post-mission flightcrew report¹¹ states that exceptional ignition transients were associated with all OMS burns on STS-51F with the exception of the final deorbit burn. The ignition transient was termed a "hard light" by the crew and was manifested by larger than normal acceleration at the beginning of the burn. The report states further that Johnson Space Center has been unable to confirm this effect or show a cause for it. It is possible that the momentary sharp pressure increase to 10^{-5} Torr seen at the beginning of the OMS-3 burn is related to the effect reported by the crew.

Another OMS burn which occurs at 0322:17 GMT during nighttime (not shown in Fig. 5) and which is directed antiparallel to the velocity vector over Millstone Hill Observatory in Westford, Massachusetts also raises the pressure by about a factor of 2 over its pre-burn level. The pressure spike is also present at the beginning of this burn. We are not able to determine the recovery time associated with this burn since there is a data dropout which begins in the middle of the burn and lasts well past engine shut off. During the two OMS burns just discussed, both OMS engines were fired, each of which has a thrust of 26,688 N (6,000 lb) and burn at a rate of about 85.27 N/s (19.17 lb/s) using a propellant of monomethylhydrazine (MMH) as fuel and nitrogen tetroxide (N_2O_4) as an oxidizer.

The Reaction Control System (RCS) thruster firings pointed out at 0229:38 GMT in Fig. 5 are vernier thrusters which have a thrust of 111 N (25 lb.) and use a propellant of MMH/N₂O₄. The effect of this series of continuous firings is to raise the neutral pressure in the vicinity of the payload bay by only a small amount. A more detailed analysis of all thruster firings which occur during the time in which pressure data were taken was done in order to determine whether specific thrusters affect the pressure more than others. We ascertained that no primary RCS thrusters, which have a thrust of 3870 N (870 lb.), were fired during the 3 hours of interest. That leaves only six vernier thrusters. Two of them are located in the nose section of the Orbiter and have thrust vectors that point down and slightly starboard or port (F5R, F5L). The remaining four are in the RCS pods in the tail section of the Orbiter. Two of these four are located on the starboard side and point in the starboard (or +Y) direction (R5R) and down along +Z (R5D). The other two in the tail section are on the port side of the Orbiter and point in the port (or -Y) direction (R5L) and down along +Z (L5D).

Figure 6 is 2-minute plot which shows two sets of vernier thruster firings. Notice that at 0202:22 GMT the continuous firing of two vernier thrusters in the back of the Orbiter for a period of 2.8 seconds has a noticeable effect on the pressure, whereas the continuous firing of one forward and one aft verniers for a period of 2.1 seconds has no effect. Our analysis of all thruster firings from 0130 to 0430 GMT on day 211 shows that all vernier thruster firings from the back of the Orbiter which involve thrust vectors that are directed down along the Orbiter +Z axis (R5D, L5D) produce similar effects on neutral pressure as those shown in Fig. 6 at

0202:22 GMT. Vernier thruster firings from the front directed down and slightly out (F5R, F5L) and from the back directed along the $\pm Y$ axes (R5R, L5L) have little or no effect on the neutral pressure as shown in Fig. 6.

Other factors which may be important in the study of thruster-firing effects are discussed in the next section. More details on the thrusters and their effects on the ionosphere during the OSS-1 flight are provided in Refs. 12 and 13.

Finally, an Orbiter water dump which begins at 0414 GMT (see Fig. 3) and continues for about 40 minutes may be the cause of the slight increase in pressure seen at about that time. However, due to the fact that the angle of attack has significantly started to decrease and the pressure increase is so slight, no definite conclusions can be drawn.

DISCUSSION AND CONCLUSIONS

The unusually long time taken for the pressure gauge to begin to ionize (about 50 minutes) may be related to several factors, such as the length of time it was stored at sea level, the temperature at which it is powered up and the degree to which it has been contaminated during preflight testing. The PDP was at sea level for a considerable length of time due to its integration into the SL-2 payload at Kennedy Space Center over a year prior to launch. The temperature of the deck on which the pressure gauge is mounted was about 20° C at the time it was powered up on orbit so temperature was probably not a factor. One of the biggest factors could have been the fact that the pressure gauge was not cleaned after the completion of all preflight testing and prior to launch. Thus, it is possible that contamination may have contributed to the delay in onset of ionization.

Neutral pressure in the payload bay depends to a great extent on the orientation of the gas flow to it and to a lesser extent on the day/night conditions prevailing at the time. SL-2 results show slightly higher pressures during daytime than nighttime, which is in accord with the MSIS-83 atmosphere model,¹⁵ and enhancements in the pressure under ram conditions. The wake conditions which were encountered produce no significant effects on the pressure probably due to payload bay outgassing. OSS-1 results show a definite modulation in the pressure from ram to wake conditions.^{2,3} This effect has also been reported by Yanagisawa et al.¹⁶ from measurements obtained by a BN-type ionization pressure gauge which was part of the SEPAC investigation flown on Spacelab 1.

A relation is given by Hedin et al.¹⁷ for determining ram pressure for a gauge consisting of an enclosure within a rocket with a small entrance hole or orifice. Hedin et al.¹⁷ state that if the diameter of the entrance hole is large compared to the length of the hole, but small with respect to the mean free path of the gas, and the gas in the gauge comes to thermal equilibrium with the walls of the gauge, the result is:

$$n_g = n_a (T_a/T_g)^{1/2} F(S) \quad (1)$$

where

n_g = number density of particles in the gauge

n_a = ambient particle number density

T_g = temperature of the gauge walls

T_a = ambient temperature

$$F(S) = \exp(-S^2) + S\pi^{1/2} (1 + \operatorname{erf} S) \quad (2)$$

where

$$S = V/C_{pa}$$

V = component of rocket velocity normal to gauge opening

C_{pa} = most probable speed of ambient particles

The significance of equation (1) is that the number of particles entering the gauge per unit time is equal to those leaving. Substituting gauge pressure, P_g , and ambient pressure, P_a , for n_g and n_a respectively, in equation (1) we obtain

$$P_g = P_a \left(\frac{T_a}{T_g} \right)^{1/2} F(S) \quad (3)$$

For the one maximum ram condition on SL-2 (0302 GMT) we ran the MSIS-83 atmospheric model¹⁵ and found that $P_a = 7.7 \times 10^{-8}$ Torr, $T_a = 894$ K and $C_{pa} = 1.07$ km/sec. At 0302 GMT, $T_g \sim 293$ K and $V =$ orbiter velocity normal to the payload bay $= 7.8$ km/sec. Substituting these values in equation (3) gives $P_g = 3.5 \times 10^{-6}$ Torr, which is in good agreement with the SL-2 data. In applying equation (3) to the orbiter, it is assumed that the oriface is the payload bay.

The enhancement under ram conditions is most likely primarily related to the fact that under ram conditions there is a great increase in the number of atmospheric molecules in the vicinity of the payload bay which are reflected from various Orbiter and instrument surfaces at thermal velocities corresponding to the temperature of the bay.^{16,18} A much smaller contribution may come from the erosion of materials due to atomic oxygen bombardment.

Outgassing in the payload bay and ram flow to the bay as discussed above cause the neutral pressure in the bay to be elevated to a few times 10^{-6} Torr early in the mission. Shawhan et al.² state that it took nearly 24 hours for the payload bay to outgas to the ambient level on OSS-1. Koch¹⁴ reports that pressure measurements obtained by an identical pressure gauge to the PDP's as a part of the IRT investigation on SL-2 are around an order of magnitude higher than the PDP's. However, the IRT pressure gauge, including sensor, were located inside a box that had only a two-inch diameter opening at the top. Due to the greatly decreased volume of this box compared to the relatively openness of the payload bay and the outgassing within the box itself, it is expected that the IRT gauge would obtain consistently higher pressure measurements than the PDP gauge. Scialdone¹⁹ derived an equation for open bay pressure as a function of time based on previous measurements from

the payload bay. The pressure for open bay is:

$$P_s(t) = 1.3 \times 10^{-5} t^{-1} \quad (\text{Torr}) \quad , \quad (4)$$

where t is in hours and greater than 0240 MET (Mission Elapsed Time). The data shown in this paper appear to follow this relationship until the CRNE gas purge begins. Scialdone¹⁹ states that the outgassing pressure will vary depending on temperatures of outgassing materials, which are related to the angle of the payload bay to the sun and length of time at that angle.

Experiments which release gas in the operation of their instruments can and do affect the neutral pressure environment in the payload bay. These gas releases, together with outgassing of the payload bay and ram flow pressure enhancements early in a shuttle mission, can lead to a substantial increase in the neutral pressure over ambient.

Orbiter OMS burns on SL-2 are shown to increase the neutral pressure in the payload bay by a factor of 2. A review of PDP pressure gauge data from OSS-1 shows no increase in pressure during the two OMS burns which occur late in the mission. However, these two burns are performed under ram conditions which produce higher pressures than those shown to be associated with OMS burns. Further, the pressure spikes seen at the beginning of the SL-2 OMS burns are not present at the beginning of the OSS-1 burns. However, the sampling frequency was only 1 Hz on the earlier flight. Thus, if these sharp pressure increases, which last about 0.5 seconds, are present, they would probably not be evident in the data. Narcisi et al.²⁰ report results similar to those shown in this paper for OMS burns. Their instrument, a quadrupole mass spectrometer flown on an early shuttle flight, shows the spike at the beginning of the burn, a pressure pulse of about 10^{-6} Torr and a return to background in 1-2 seconds.

Although no primary thrusters are fired during the time of interest on SL-2, it is important to mention them in light of the fact that they can affect neutral pressure more than an OMS burn. The L2U primary thruster firing sequence which occurs during the OSS-1 flight raises the pressure to 3×10^{-4} Torr^{2,3,12}. This sequence consists of the pulsed firing of 2 primary thrusters in the back and the continuous firing of one in the front, all of which have thrust vectors which point up (parallel to the Orbiter -Z axis).

Even though the emission rate for the OMS firing is twice as great as for the combination of the three up-firing primary thrusters, the OMS burn on SL-2 causes the pressure in the payload bay to rise to a value which is at least 1 1/2 orders of magnitude less than that for the L2U primary thruster sequence test. There are several factors which probably contribute to this. The L2U sequence takes place when the payload bay is in the wake of the orbiter. There is probably some reflection of the thruster plumes of the 2 primaries in the back off of the vertical stabilizer. Further, the PDP is closer to the primary thruster plumes than to the OMS plumes, thus being in a better position to see any backscatter from the plumes and their interactions with each other. Finally, the PDP is in a more open environment during the L2U event on OSS-1.

A summary of the questions which must be given consideration in order to adequately analyze the effects from any thruster firings are the following:

1. Is the payload bay in wake or ram? If it is in wake, any measurements which are made during thruster firings will probably show a much greater pressure increase in a relative sense than at non-wake times due to the lower background pressure in the wake. If it is in ram, effects may not be seen at all if the ram pressure is extremely high.

2. What is the location of the pressure gauge with respect to each thruster? The closer the gauge is to the thruster and its exhaust plumes, the greater the possibility of recording an effect due to backscatter from the plume. This means that the emission pattern of the plume is also important. For instance, the exhaust plume of the primary thrusters is much broader than that of the verniers. Coupled with this is the fact that certain thruster plumes are reflected into the payload bay by various Orbiter surfaces, such as the wings, elevons and vertical stabilizer. Another important consideration is the presence of barriers and obstructions between the pressure gauge and the thruster which may tend to hinder the gauge's ability to detect an effect.

3. What is the direction of the velocity vector with respect to the thrust vector? Although no one has yet done a thorough study of this, the possibility exists that a thruster fired upstream of the Orbiter may have a different effect than one fired downstream. If such an effect was detected for a thruster fired upstream, it would most likely be a second order effect. Although the velocity of the Orbiter is much greater than the thruster exhaust, the thruster plume interacts with the environment on a much faster timescale.

4. How many thrusters are firing simultaneously? In the case of vernier thrusters it is most often the case that two or three will fire simultaneously throughout a given period of time. This being the case, it is very difficult to determine the effects due to any one thruster. Thus, it is often

necessary to study the effects of groups of thrusters, such as the down-pointing ones. In this connection it has been reported by Wulf and Von Zahn²¹ that there is some evidence that the simultaneous firing of several vernier thrusters produces higher signals than would be calculated for the sum of the individual contributions. Primary thrusters are more likely to be fired one at a time, however, they are not used as extensively on orbit as verniers and so the study of their effects may be limited.

In our analysis of vernier thruster firing effects on neutral pressure, the following conclusions are drawn based on the above:

1. In general, vernier thruster firings are only minor perturbations to the pressure. Although we have no examples of firings while the payload bay is in wake, the ones which were made while in ram show a very small enhancement in pressure.
2. The fact that we see effects from only downward-pointing verniers (along +Z) in the back is probably due to the thruster plume impinging on Orbiter surfaces, such as the body flap, elevons, main engines, etc., and thus being reflected into the payload bay. The two forward-mounted vernier thrusters have a relatively unobstructed path in the primary direction of the expanding thruster plume compared to the aft verniers, which could partially explain why we see little or no effect on neutral pressure during those firings. In addition, the location of the pressure gauge on SL-2, well down in the center of the payload bay near other structures, may have been another factor particularly in the case of the aft sideways-pointing verniers whose plumes can be

reflected off the wings. It is not possible to do a thruster direction dependence analysis on the OSS-1 data set since the sampling frequency was only 1 Hz. However, the SL-2 thruster direction dependence results with regard to forward and aft downward-firing verniers are certainly borne out by Wulf and von Zandt,²¹ from neutral mass spectrometer results from the SPAS-01 subsatellite on the STS-41B flight, and by Narcisi et al.²⁰ on an early shuttle flight. Their results for these thrusters differ from the SL-2 results only in that the effects they see are substantially greater. In addition, they see effects from port and starboard firing verniers which may be due, in part, to their instruments being located in a more advantageous position with respect to these thrusters than the SL-2 pressure gauge.

3. No conclusions can be drawn with regard to the relationship of the velocity vector to the direction of thrust since the data set is limited.

4. No conclusions can be drawn with regard to the effects of one thruster firing versus several firing simultaneously since single firing events were not available.

A definitive conclusion as to whether Orbiter water dumps affect the neutral pressure in the payload bay cannot be made since enough cases under varying conditions have not been tested. The data seem to indicate, however, that the effect, if any, is minimal. As reported by Pickett et al.,¹³ neutral pressure readings on OSS-1 are slightly greater with water being dumped than without it when the payload bay is in wake. Narcisi et al.²⁰ report there is no increase in neutral pressure during a water dump.

Finally, a comment is in order with regard to the magnitude of effects seen by the SL-2 pressure gauge versus those seen by other pressure monitors on this and other shuttle flights. Effects of thruster firings seen by the PDP pressure gauge are less in magnitude than those seen on previous shuttle flights. This could be related to a number of things such as location of the sensor in relation to other instruments, Orbiter altitude and attitude, and degree of outgassing in the payload bay. In fact, had the PDP pressure gauge on SL-2 been able to obtain measurements later in the flight when outgassing in the payload bay had decreased significantly, the relative effects of thruster firings, OMS burns, and payload bay into ram may have been much greater although the absolute magnitude may have remained about the same due to the gauge's location in the bay. Further measurements on future space shuttle flights need to be made in order to adequately quantify the various effects on neutral pressure seen as a result of Orbiter and payload operations.

ACKNOWLEDGMENTS

The authors wish to thank Dr. S. Swordy of the University of Chicago, Dr. D. Koch of the Smithsonian Astrophysical Observatory and Dr. P. Mason and Dr. D. Petrac of the Jet Propulsion Laboratory for supplying them with the times of their experiments' gas releases and with results from their experiments. JSP thanks Mr. P. Simeth of Sentran Company for providing useful information about the pressure gauge and Dr. L. Leger of JSC and Col. G. Fullerton of Dryden Flight Center for helpful comments on thruster firing and OMS engine effects.

We gratefully acknowledge the permission granted by Cambridge University Press to use and modify Fig. 2 of this paper, which originally appeared on page 158 of Spacelab Research in Earth Orbit by David Shapland and Michael R. Rycroft published in 1984.

This research was supported by NASA through Grant NAG3-449 from Lewis Research Center and through Contract NAS8-32807 with Marshall Space Flight Center.

REFERENCES

- ¹Neupert, W. M., "OSS-1: A Pathfinder Mission for Space Science on the Space Shuttle," Journal of Spacecraft and Rockets, Vol. 21, July-Aug. 1984, pp. 382-386.
- ²Shawhan, S. D., Murphy, G. B., and Pickett, J. S., "Plasma Diagnostics Package Initial Assessment of the Shuttle Orbiter Plasma Environment," Journal of Spacecraft and Rockets, Vol. 21, July-Aug. 1984, pp. 387-391.
- ³Shawhan, S. D. and Murphy, G. B., "Plasma Diagnostics Package Assessment of the STS-3 Orbiter Environment and Systems for Science, AIAA Paper 83-0253, Jan. 1983.
- ⁴"Spacelab 2 90 Day Post-Mission Science Report," edited by E. W. Urban, Marshall Space Flight Center, AL, Nov. 14-15, 1985.
- ⁵Redhead, P. A., "The Magnetron Gauge: A Cold-Cathode Vacuum Gauge," Canadian Journal of Physics, Vol. 37, 1959, pp. 1260-1271.
- ⁶Swordy, S., Private communication, University of Chicago, Chicago, IL, April 1986.
- ⁷Grebowsky, J. M., Taylor, H. A. Jr., Pharo, M. W. III, and Reese, N., "Thermal Ion Perturbations Observed in the Vicinity of the Space Shuttle," Planetary and Space Science, in press, 1986.
- ⁸Summers, R. L., "Gas Sensitivity Tables," NASA Technical Note TN D-5285, June 1969.
- ⁹Redhead, P. A., Hobson, J. P., Kornelsen, E. V., "The Physical Basis of Ultrahigh Vacuum," Chapman and Hall Ltd., 1968.
- ¹⁰Mason, P., Private Communication, Jet Propulsion Laboratory, Pasadena, CA, December 1986.
- ¹¹"51-F Flightcrew Report," Johnson Space Center, Houston, TX, 1985.

¹²Murphy, G. B., Shawhan, S. D., and Pickett, J. S., "Perturbations to the Plasma Environment Induced by the Orbiter's Maneuvering Thrusters," AIAA Paper 83-2599, Oct. 1983.

¹³Pickett, J. S. et al., "Effects of Chemical Releases by the STS 3 Orbiter on the Ionosphere," Journal of Geophysical Research, Vol. 90, 1985, pp. 3487-3497.

¹⁴Koch, D., Private communication, Smithsonian Astrophysical Observatory, Cambridge, MA, Oct. 1986.

¹⁵Hedin, A. E., "A Revised Thermospheric Model Based on Mass Spectrometer and Incoherent Scatter Data: MSIS-83," Journal of Geophysical Research, Vol. 88, 1983, pp. 10,170-10,188.

¹⁶Yanagisawa, M. et al., "Vacuum-Environment around Spacelab-1," The Institute of Space and Astronautical Science, Tokyo, Japan, ISAS Report No. 617, Aug. 1985.

¹⁷Hedin, A. E., Avery, C. P., and Tschetter, C. D., "An Analysis of Spin Modulation Effects on Data Obtained with a Rocket-Borne Mass Spectrometer," Journal of Geophysical Research, Vol. 69, 1964, pp. 4637-4648.

¹⁸Scialdone, J. J., "Self-Contamination and Environment of an Orbiting Satellite," NASA TM TN-D-6645, May 1972.

¹⁹Scialdone, J. J., "Shuttle Measured Contaminant Environment and Modeling for Payloads--Preliminary Assessment of the Space Telescope Environment in the Shuttle Bay," NASA TM-8511, Dec. 1983.

²⁰Narcisi, R. et al., "The Gaseous and Plasma Environment around Space Shuttle," AIAA Paper 83-2659, Oct. 1983.

²¹Wulf, E. and von Zahn, U., "The Shuttle Environment: Effects of Thruster Firings on Gas Density and Composition in the Payload Bay," Journal of Geophysical Research, Vol. 91, No. A3, Mar. 1986, pp. 3270-3278.

FIGURE CAPTIONS

- Fig. 1. The Plasma Diagnostics Package subsatellite with neutral pressure gauge aperture pointed out.
- Fig. 2. Layout of the Spacelab 2 pallets showing the location of the PDP in relation to the other instruments.
- Fig. 3. Three-hour neutral pressure plot from early in the Spacelab 2 mission.
- Fig. 4. Neutral pressure changes on a short time scale possibly related to another experiment.
- Fig. 5. Effects on neutral pressure of Orbiter gas releases.
- Fig. 6. Comparison of vernier thruster firing effects on neutral pressure.

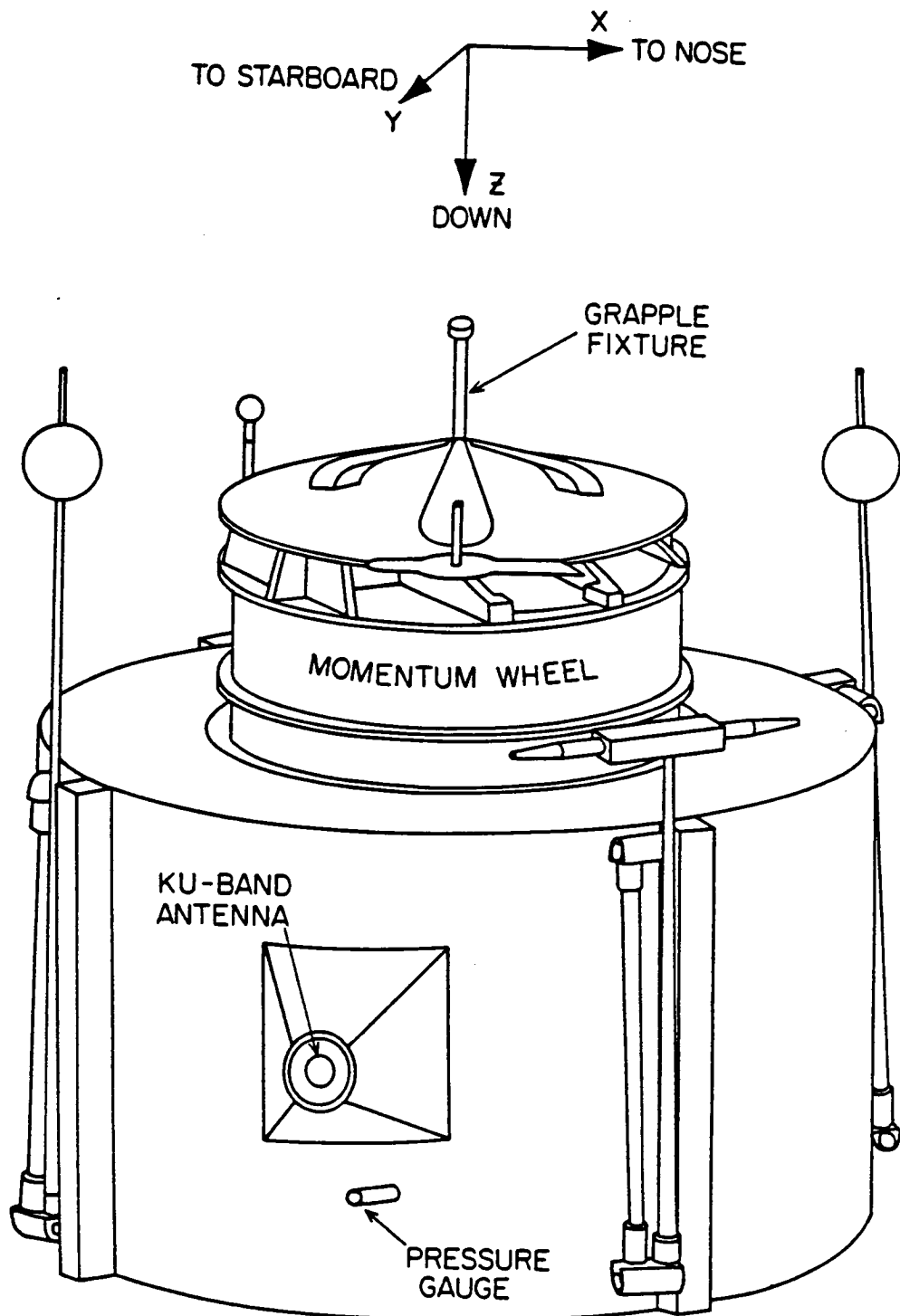


Fig. 1

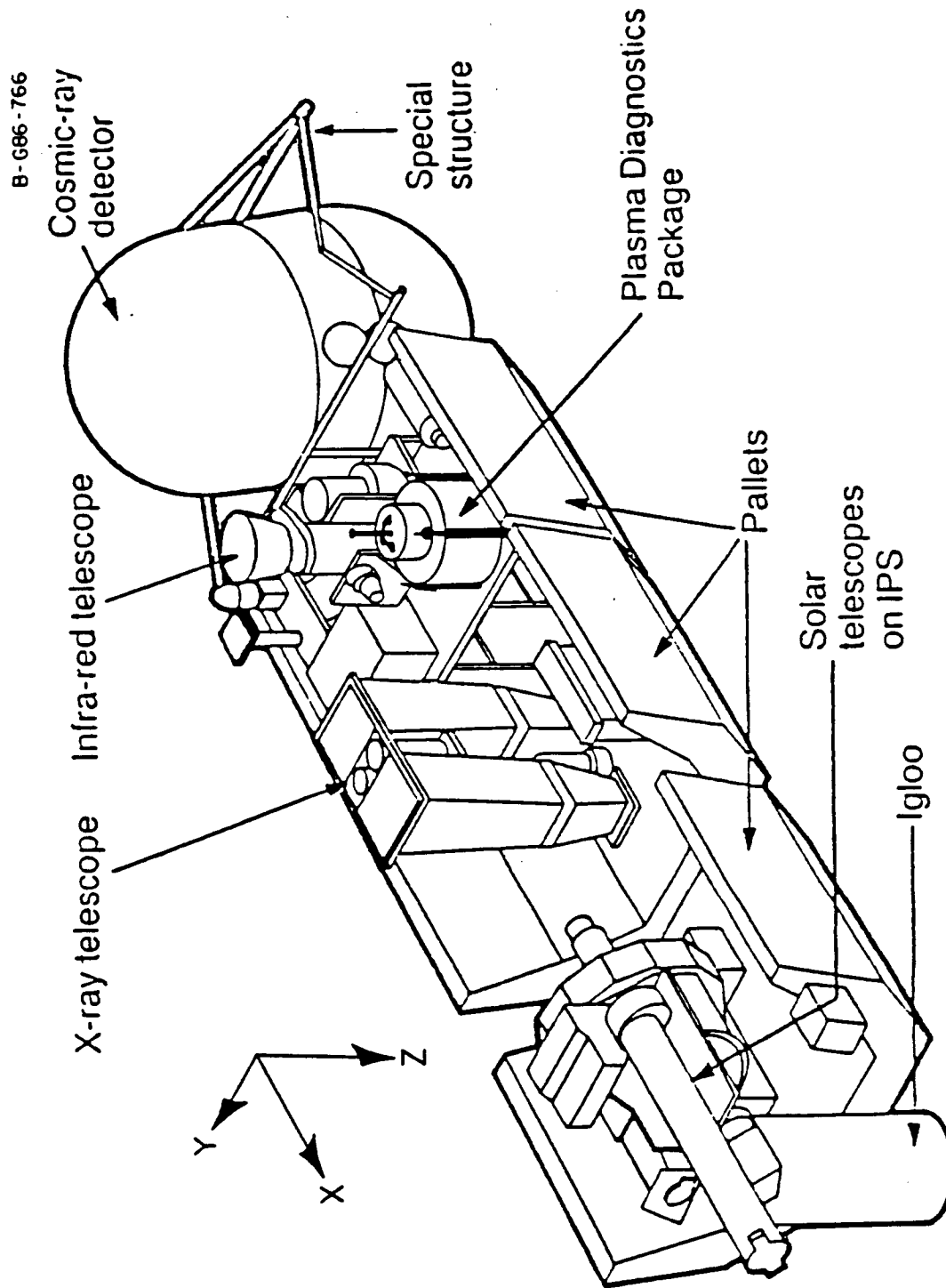


Fig. 2

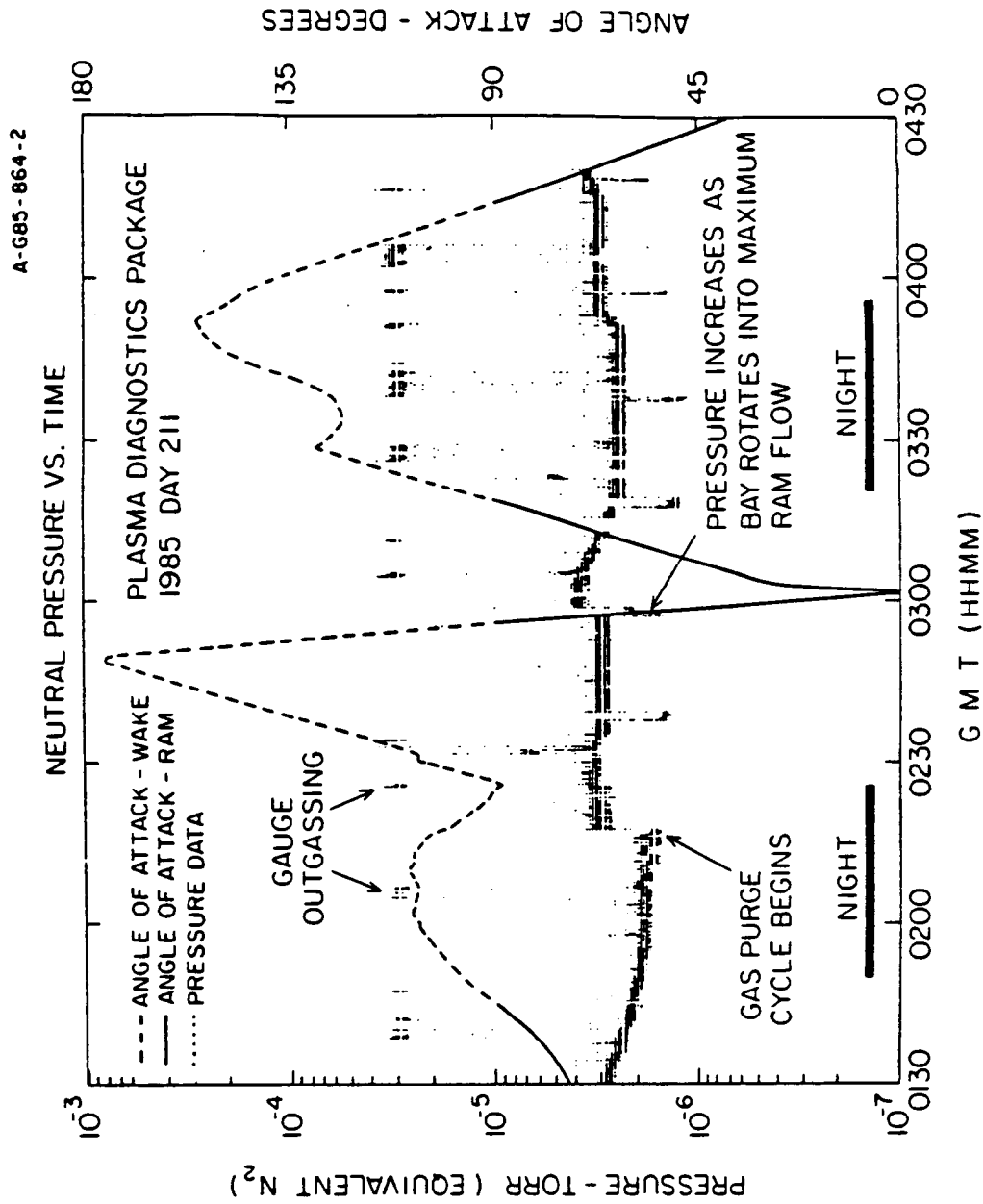


Fig. 3

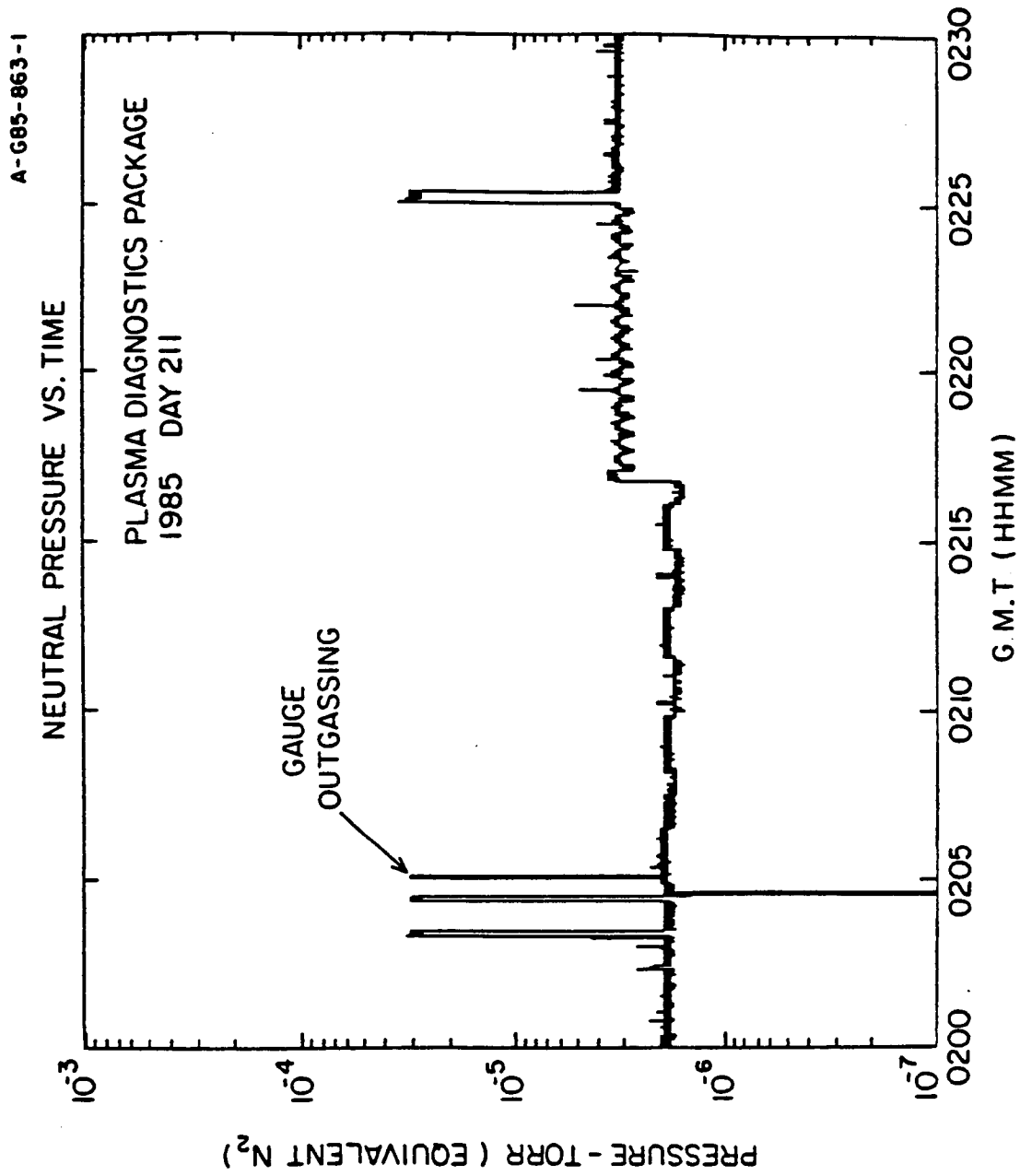


Fig. 4

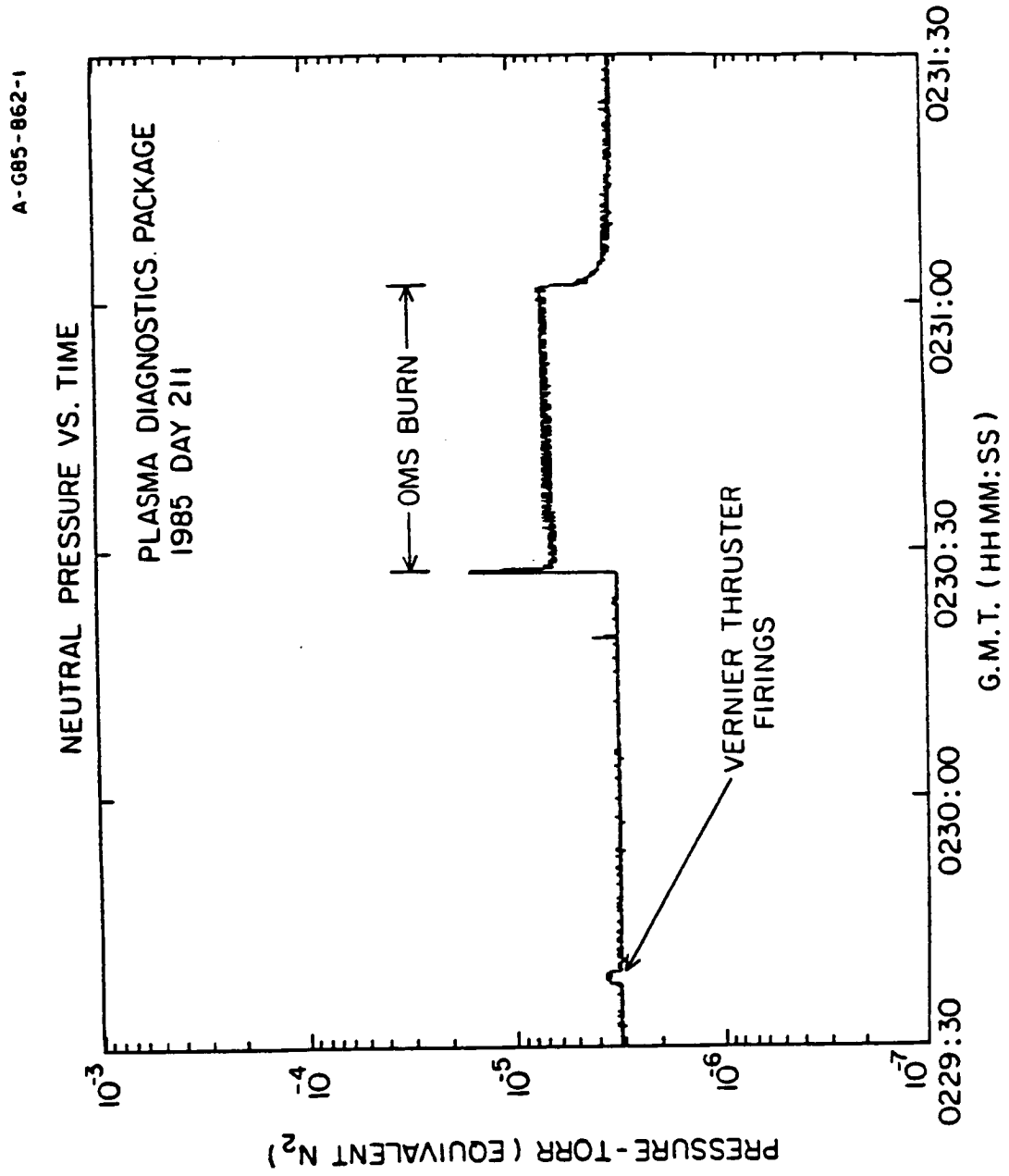


Fig. 5

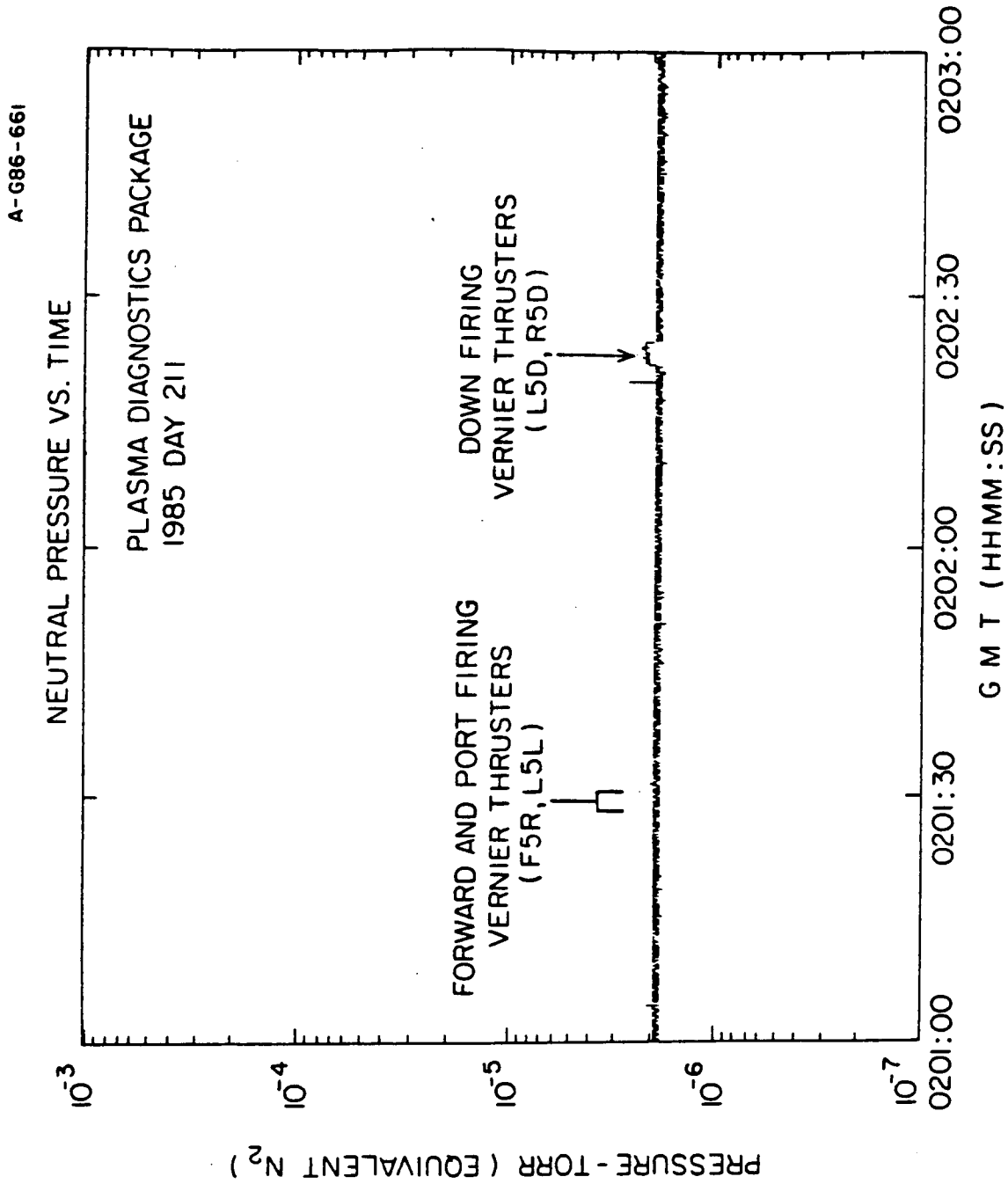


Fig. 6

PULSED ELECTRON BEAM EMISSION IN SPACE

Torsten Neubert, Joseph G. Hawkins, Geoffrey D. Reeves,
Peter M. Banks, Rock I. Bush, and P. Roger Williamson

STARLAB, Stanford University, Stanford, CA 94305, USA

Donald A. Gurnett

Department of Physics and Astronomy, University of Iowa,
Iowa City, Iowa 52242, USA

W. John Raitt

Center for Atmospheric and Space Sciences, Utah State University,
Logan, Utah 84322, USA

Abstract

During the Spacelab-2 mission of July, 1985, electron beams (1 keV, 50-150 mA) pulsed at ELF and VLF frequencies were emitted from the Space Shuttle Orbiter. The wave fields generated by the beam were monitored by a Plasma Diagnostics Package (PDP), which was released as a free-flying sub-satellite during a six hour period. Measurements of the Orbiter potential and the return current during beam emissions were obtained from a Charge and Current Probe (CCP) mounted in the payload bay. Results from the PDP and CCP are presented.

1. INTRODUCTION

Some effort in recent years has gone into the study of the radiation generated by pulsed electron beams emitted from space platforms [*Bush et al.*, 1987; *Reeves et al.*, 1988; *Winckler et al.*, 1985; *Holzworth and Koons*, 1981]. The background for this interest is partly the possibility that pulsed beams may replace conventional antennas in space for communication purposes. An issue which must

2

be addressed when considering this option is the charging of the space platform during beam emissions and the formation of a region of enhanced negative space charge close to the beam nozzle. These effects are important to understand because they may limit the amount of beam current escaping the platform and distort the beam coherence. In the Space Experiments with Particle Accelerators (SEPAC) flown on the Spacelab-1 Shuttle mission, for instance, it was found that when the main thruster engine bells were in the wake (they constitute the largest conducting area of the Orbiter), the Orbiter may have charged to the beam potential of 5 keV when the beam current exceeded 100 mA, thereby partly inhibiting the beam from escaping the Orbiter [Sasaki *et al.*, 1986].

Recent numerical simulations show that when the electron beam density exceeds the ambient plasma density, a negative space charge may build up in a region close to the beam nozzle. This will reflect a portion of the beam electrons and greatly distort the escaping portions of the beam [Pritchett and Winglee, 1987].

The questions of spacecraft charging and loss of beam coherence are addressed in the paper by means of observations made during the Spacelab-2 mission of the Space Shuttle Orbiter. The observations include Orbiter charging and return currents during electron beam emissions and wave fields generated by pulsed and continuous beams.

Spacelab-2 was launched into an almost circular orbit with a nominal altitude of 325 km and an inclination of 49.5°. A Fast Pulse Electron Generator (FPEG) was mounted on the port side of the Orbiter. The beam energy was 1 keV and the beam current could be set to 50, 100, or 150 mA by selecting a combination of two separate electron sources. The beam could be emitted in a continuous mode (DC) or in a pulsed mode (AC), where the beam current was almost perfectly square-wave modulated with a nominal pulse rise time of 10^{-7} s.

A Charge and Current Probe (CCP) was mounted on the starboard side of the payload bay. The Charge Probe has a conducting surface covered by a dielectric layer, and it measures changes in the potential induced across the dielectric layer. The Current Probe measures the current flowing through a gold plated surface and is mounted next to the Charge Probe. The FPEG and the CCP were part of the Vehicle Charging and Potential experiment (VCAP), which was also flown on STS-3/OSS-1. It is described in more detail in *Banks et al.* [1987].

A Plasma Diagnostics Package (PDP) was stored in the payload bay. During a six hour period the PDP was released as a free-flying satellite to co-orbit at distances up to 300 m from the Shuttle. The PDP carried an array of plasma diagnostics equipment, including an electric dipole antenna and a magnetic search coil. The antennas were connected alternately for 52.2 s to the wide-band wave receiver. The receiver scanned a 30 kHz frequency range by selecting 10 kHz bands in the following order: 0-10 kHz (25.6 s), 20-10 kHz (12.8 s), and 20-30 kHz (12.8 s). The receiver output was controlled by an Automatic Gain Control system (AGC), which ensured a 100 dB dynamic range and a roughly constant output level. The output was telemetered in analog form and was later digitized at 25 kHz. In addition, the antennas were connected to a number of filterbank receivers with a coverage in frequency from 31 Hz to 800 MHz. For a description of the PDP instruments, see *Shawhan et al.* [1984].

2. OBSERVATIONS

2.1 Orbiter Charging and Return Currents

We have attempted to correlate the measurements of the CCP during DC electron beam emissions with the ambient ionospheric densities. This imposes a problem since the interactions between the Shuttle Orbiter and the ionosphere frequently prevent accurate

measurements of ambient plasma parameters from the payload bay [Siskind *et al.*, 1983; Raitt *et al.*, 1984; Grebowsky *et al.*, 1987].

During the the Spacelab-2 mission, the only in situ measurements of the plasma density away from the plasma perturbations associated with the Orbiter were performed during a 6 hour period when the PDP became a free-flying satellite. For other times of the mission, we must rely on values of the ambient density predicted by the International Reference Ionosphere (IRI) model [Bilitza, 1986]. The accuracy of the IRI model has been assessed by comparing its predictions with the measurements from a Langmuir probe on the PDP during the 6 hour free-flight. It was found that the predicted values of the density were, in general, higher than the measured ones, at times up to an order of magnitude higher, but that the general trend of day/night variations etc. was captured well by the model. Much of this difference can be attributed to the fact that the PDP measurements were made during a period of general magnetospheric disturbance with $K_p = 5+$ at the time of the PDP release. Deep electron density troughs were seen at high magnetic latitudes, while the plasma density at the geomagnetic equator dropped below 10^3 cm^{-3} . These features tended to become less visible as time went on in the PDP free-flight period.

With this caution in mind, results from the Charge Probe are shown in Figure 1 as function of ambient plasma density as predicted by the IRI model. The figure shows a summary of the Charge Probe measurements during all DC beam emissions performed during the Spacelab-2 mission [Hawkins, 1988]. For high ambient plasma densities the charging level of the Orbiter is low, while for low densities the Orbiter charges to high levels. The charge probe does not give absolute measurements of the Orbiter potential, but rather a measurement of the potential drop across a dielectric surface covering the probe. For low charging levels and thin potential sheaths, the probe measurement is close to the vehicle potential, while for higher potential levels and extended sheath regions, the

probe generally measures a potential which is lower than the vehicle potential.

A threshold in the ambient plasma density for which the Orbiter charges to high levels can be estimated from Figure 1. This is about $3 \times 10^5 \text{ cm}^{-3}$ for 100 mA beam current and $1.5 \times 10^5 \text{ cm}^{-3}$ for 50 mA current. If we consider the threshold density to be the density at which the thermal electron current from the ionosphere balances the beam current, then we find the effective current collecting area of the Orbiter to be about 42 m^2 for an electron temperature of 1000 K [Hawkins, 1988]. This area is comparable to, but somewhat larger than, the area of the main engine bells which have a surface area of about 30 m^2 . They constitute the largest, but not all, the current collecting area of the Orbiter. We thus interpret the threshold seen in the charging level as the ambient plasma density level at which the electron thermal current equals the beam current. At lower densities the Orbiter has to charge to high potentials in order to draw a sufficient return current.

Figure 2 shows Current Probe measurements during DC beam emissions as function of ambient plasma density predicted by the IRI model. Also shown is the electron thermal current that can be drawn to the probe for temperatures of 1000 K and 3000 K. Data show that the current to the probe depends on the Orbiter attitude. This is an ion wake phenomena, since the Orbiter velocity, V_s , is about 7.8 km/s, which is much larger than the ion thermal velocity (about 1 km/s). Thus the current to the probe varies greatly from ram to wake conditions [Raitt *et al.*, 1984; Grebowsky *et al.*, 1987]. Furthermore, the probe potential is shifted by the $(V_s \times B) \cdot L$ induced potential, where L is a vector pointing from the engine bells to the probe and B the earth's magnetic field. The potential shift is generally less than 5 V, which is enough to influence the electron current to the probe. The ion current is less affected since the ion energies seen from the reference frame of the Orbiter have energies larger than 5 eV [Raitt *et al.*, 1984].

In order to remove the obvious attitude bias in the Current Probe results, an Orbiter attitude called the airplane mode was selected. In this mode, the Shuttle orbits in the same manner as an airplane flies, and the wake structure around the Orbiter is constant. Furthermore, in this mode the $(V_S \times B) \cdot L$ induced potential is always small. The result of selecting data from observations during the airplane mode is shown in Figure 3. The probe current increases with ambient plasma density in a roughly linear fashion and seems independent of the emitted beam current. This trend in the data is important since it indicates that the beam does not fully escape the Orbiter. Rather it appears that the fraction of the beam that escapes is proportional to the ambient plasma density.

2.2 Wave Fields

During the course of the 6 hour period when the PDP was free-flying, care was taken to permit the PDP and the Shuttle to have two magnetic conjunctions per orbit. The trajectory of the PDP relative to the Orbiter during the fourth conjunction is shown on the top panel of Figure 4, with tick marks for every one minute of flight. The vertical axis is the distance to the PDP measured along the earth's magnetic field, and the horizontal axis the distance perpendicular to the field. A pulsed electron beam sequence was started at approximately 04:11 UT and lasted for about 7 min. The beam current was 100 mA and the beam was square-wave modulated at 1.22 kHz with a 50% duty cycle (beam on time equals beam off time). The period of beam emission and the antenna switching pattern of the wide-band wave receiver is indicated by shaded areas.

The Orbiter attitude was adjusted during this sequence so that the initial velocity of the beam electrons was always directed towards the PDP. The variation of the beam pitch angle is shown on the bottom panel of Figure 4.

The conjunction occurred during nighttime. The ambient plasma density, estimated from the measurements of the Langmuir probe on

the PDP, was $3.2 \times 10^4 \text{ cm}^{-3}$ [D'Angelo, personal communication], corresponding to a plasma frequency of 1.6 MHz, and the electron gyrofrequency varied from 560 kHz to 600 kHz. Assuming the ambient ion population consisted mainly of O^+ , the lower hybrid frequency varied from about 3.1 kHz to 3.3 kHz.

An example of the magnetic field observed by the search coil on the PDP is shown in Figure 5. The relative signal intensity (the AGC is not incorporated here) is color coded showing the fundamental and odd harmonics of the 1.22 kHz modulation frequency as horizontal lines. The first half of the panel, 0-25 s, the bandwidth is 0-10 kHz, the following quarter of the panel, 25-38 s, the band is 20-10 kHz, with 20 kHz being at the bottom of the frequency scale and 10 kHz at the top. The final quarter of the panel presents 20-30 kHz. During the time interval shown on Figure 5 the perpendicular distance to the beam was about 75 m.

For comparison, Figure 6 shows the electric field intensity observed 51.2 s earlier when the PDP was at a distance of about 40 m from the beam. As before, emissions are seen at the odd harmonics of the modulation frequency in the whole band. However, in addition to these coherent emissions, strong broad-banded electrostatic noise is also seen. This noise is about 40 dB above the background noise level observed prior to the beam emission and partly inhibits the detection of higher harmonics in the 0-10 kHz band.

The amplitude of the harmonics of the beam pulsing frequency have been estimated using a pre-flight calibration of the wide-band receiver and the AGC. The result of this calibration for the 0-10 kHz range is shown in Figure 7 for the three time intervals during the pulsed beam emission that the receiver was connected to the magnetic search coil.

The Fourier transform of a square-wave function with a 50% duty cycle has vanishing even harmonics and possesses odd harmonics with amplitudes that vary with frequency as $1/f$. We note that the

observed magnetic wave field does have strong odd harmonic components while the even harmonics, although present, are almost an order of magnitude weaker. This leads us to believe that the beam source, at least within the first couple of hundred meters, is able to retain much of its square-wave modulated structure (coherence in v_{II}), in spite of the low ambient plasma density.

The electric field amplitudes are shown in Figure 8. At larger distances from the beam, the second and third harmonic become relatively strong, while the first harmonic is strongly damped. This effect may be caused by the change in topology of the wave refractive index, which changes at the lower hybrid frequency (3 kHz for the experiment).

During its free-flight, the PDP was spinning with a period of 13 s. Both the magnetic and the electric sensors measured a component of the wave field perpendicular to the spin axis. This induces a modulation of the measured field amplitudes with a period of 6.5 s. The modulation is very noticeable in the magnetic field at all harmonic numbers and in the electric field for the harmonics with frequencies larger than 10 kHz. We expect an analysis of the amplitude modulation to give us important clues as to the polarization of the fields, and a means to check existing theories for wave generation by pulsed electron beams.

3. DISCUSSION

Recent numerical simulations (*Winglee and Pritchett, 1988*) show that an electron beam will be strongly disrupted by the accumulation of negative space charge in a region close to the beam nozzle if the beam density at injection is much larger than the ambient ionospheric density. The formation of such a virtual cathode is found to develop if $t_{rp}/t_s > 0.4$, where t_{rp} is the plasma response time and t_s is the beam stagnation time. The plasma response time is about $\sqrt{3}/\omega_{pe}$, where ω_{pe} is the electron plasma frequency of the ambient ionosphere. The beam stagnation time depends on the spacecraft

size, the beam width and the beam energy and is for Spacelab-2 conditions in the range $5/\omega_{pb}$ to $15/\omega_{pb}$, where ω_{pb} is the beam plasma frequency at beam injection. The FPEG beam density at injection has been estimated to be about $3 \times 10^7 \text{ cm}^{-3}$ [Banks and Raitt, 1988] and the ambient plasma density during the pulsed flux tube connection was about $3.2 \times 10^4 \text{ cm}^{-3}$. Thus for the the experimental conditions we have $\omega_{pb}/\omega_{pe} = 30.6$, or $t_{rp}/t_s = 3.5$ to 10.6 . These values are much larger than the threshold value of 0.4 , and according to the computer simulations we should expect strong beam disruption and limitations in the amount of beam current escaping the Orbiter.

The Current Probe measurements shown in Figure 3 seem to be in accordance with the predictions of *Winglee and Pritchett* [1988]. At low ambient plasma densities, the fraction of the beam that escapes the Orbiter increases with the ambient density. The voltage measured by the Charge Probe during the pulsed flux-tube connection was about 40 V , a value in accordance with the results shown in Figure 1 for 50 mA beams (100 mA , 50% duty cycle). The Orbiter is charging to a relatively high potential, because the ambient plasma density of $3.2 \times 10^4 \text{ cm}^{-3}$ is lower than the threshold value of $1.5 \times 10^5 \text{ cm}^{-3}$ for 50 mA beams. As mentioned earlier, the Orbiter potential may have been higher than indicated by the Charge Probe.

However, we are reluctant to draw any firm conclusions on beam escape on the basis of the limited dataset presented in Figure 3. The return current distribution is probably strongly non-uniform and sensitive to small changes in the attitude and magnetic field variations. Furthermore, the wave data indicate that the beam retains its coherent structure during the pulsed flux-tube connection, with at least a substantial portion of the beam fully escaping the Orbiter.

First, we note that the magnetic component of the coherent signals has strong odd harmonic components as compared to the even harmonic components, with the amplitude of the odd harmonics roughly varying like $1/f$. This indicates that the source is basically

square-wave modulated and that little distortion in the parallel electron beam velocity is occurring.

Second, during the previous magnetic conjunction, a 50 mA, DC beam was emitted. It was found that the high frequency wave intensity observed by the filterbank had a funnel like appearance in frequency time spectrograms and that this feature was consistent with whistler waves generated through a Landau resonance with beam electrons in a semi infinite beam [Gurnett *et al.*, 1986]. The radiation level was found to be in agreement with the level predicted by quasi coherent Cherenkov resonance provided the beam electrons have a coherence length of about 7 m [Farrell *et al.*, 1988]. The radiation level of Cherenkov resonance depends strongly on the beam coherence length, which in Farrell *et al.* [1988] was assumed to be determined by the wavelength of Langmuir oscillations generated inside the beam column. Thus a funnel shaped emission, while consistent with the radiation properties of a semi infinite beam does not at present allow us to estimate the fraction of the beam escaping the near region around the Orbiter. However, the noise level indicates that during the DC fluxtube connection a substantial fraction of the beam did escape at least out to the 200 m distance of the PDP and the Orbiter. The DC fluxtube connection was performed at daytime. The ambient density measured from the Langmuir probe mounted on the PDP was about 10^5 cm^{-3} , which gives $t_p/t_s = 2$ to 6, which again is larger than the value of 0.4. The potential measured by the Charge Probe was about 3 V or less.

During the pulsed beam sequence, the high-frequency/time intensity plots of the filterbank data also had a funnel shaped feature with an intensity comparable to the intensity observed during the DC beam emission. This indicates that at least a portion of the beam during the pulsed flux tube connection escaped the Orbiter.

Finally we point out that the intensity of the broad-banded, mainly electrostatic, noise observed both at low frequencies by the wide-band receiver and at high frequencies by the filterbank, was almost

the same for the DC and the pulsed flux-tube connections. The effective current was the same for the two sequences, 100 mA pulsed with a 50% duty cycle and 50 mA DC. The fact that they were performed for different ambient plasma conditions, with the Orbiter charging to high levels during the pulsed sequence, and low levels during the DC sequence, indicate that either the two beams were both strongly disrupted, or both escaped the Orbiter largely unaffected by space charge effects. The spectral structure of the magnetic wave fields and the funnel shaped emissions points to the latter option.

The question of the fraction of the beam current that, in given circumstances, can escape a space platform is fascinating, but experimentally very hard to solve. Our experience from the SL-2 experiment indicates that wave measurements may prove to be a powerful tool to answer this question, once the power levels generated by a beam are more thoroughly understood. We also find that a space platform with current probes spread over the surface of the platform in a number sufficient to resolve the return current distribution may prove to be very helpful.

ACKNOWLEDGMENTS

One of the authors (T. Neubert) thanks Kyoto University for travel support to the Kyoto WACTEXS meeting. The work done at Stanford was sponsored by NASA under contracts NAGW-235 and NAG5-476. NASA's Space Physics Analysis Network (SPAN) was used in the preparation of this report.

REFERENCES

Banks, P. M., W. J. Raitt, A. B. White, R. I. Bush, and P. R. Williamson, Results from the vehicle charging and potential experiment on STS-3, *J. Spacecraft*, 24, 138-149, 1987.

Banks, P. M., and W. J. Raitt, Observations of electron beam structure in space experiments, accepted for *J. Geophys. Res.*, 1988.

Bilitza, D. International reference ionosphere: recent developments, *Radio Science*, 21, 343-346, 1986.

Bush, R. I., G. D. Reeves, P. M. Banks, T. Neubert, P. R. Williamson, W. J. Raitt, and D. A. Gurnett, Electromagnetic fields from pulsed electron beam experiments in space: Spacelab-2 results, *Geophys. Res. Lett.*, 14, 1015-1018, 1987.

Farrell, W. M., D. A. Gurnett, P. M. Banks, R. I. Bush, and W. J. Raitt, An analysis of whistler mode radiation from the Spacelab-2 experiment, *J. Geophys. Res.*, 93, 153-161, 1988.

Grebowsky, J. M., H. A. Taylor, and M. W. Pharo, Thermal ion perturbations observed in the vicinity of the space shuttle, *Planet. Space Sci.*, 35, 501-513, 1987.

Gurnett, D. A., W. S. Kurth, J. T. Steinberg, P. M. Banks, R. I. Bush, and W. J. Raitt, Whistler-mode radiation from the Spacelab-2 electron beam, *Geophys. Res. Lett.*, 13, 225-228, 1986.

Hawkins, J. G., Charging and return current measurements during electron beam experiments from the shuttle orbiter, *Thesis*, Stanford, 1988.

Holzworth, R. H., and H. C. Koons, VLF emissions from a modulated electron beam in the auroral ionosphere, *J. Geophys. Res.* 86, 853-856, 1981.

Pritchett, P. L., and R. M. Winglee, The plasma environment during particle beam injection into space plasmas, 1, Electron beams, *J. Geophys. Res.*, 92, 7637-7688, 1987.

Raitt, W. J., D. E. Siskind, P. M. Banks, and P. R. Williamson, Measurements of the thermal plasma environment of the space shuttle, *Planet. Space Sci.*, 32, 457-467, 1984.

Reeves, G. D., P. M. Banks, A. C. Fraser-Smith, T. Neubert, R. I. Bush, D. A. Gurnett, and W. J. Raitt, VLF wave stimulation by pulsed electron beam injected from the space shuttle, *J. Geophys. Res.*, 93, 162-174, 1988.

Sasaki, S., N. Kawashima, K. Kukuri, M. Yanagishawa, and T. Obayashi, Vehicle charging observed in SEPAC Spacelab-1 experiment, *J. Spacecraft*, 23, 194-199, 1986.

Shawhan, S. D., G. B. Murphy, P. M. Banks, P. R. Williamson, and W. J. Raitt, Wave emissions from dc and modulated electron beams on STS-3, *Radio Science*, 19, 471-486, 1984.

Siskind, D. E., W. J. Raitt, P. M. Banks, and P. R. Williamson, Interaction of the orbiting space shuttle and the ionosphere, *Planet. Space Sci.*, 32, 881-896, 1983.

Winckler, J. R., K. N. Ericson, Y. Abe, J. E. Steffen, and P. R. Malcolm, ELF wave production by an electron beam emitting rocket system and its suppression on auroral field lines: evidence for Alfvén and drift waves, *Geophys. Res. Lett.*, 12, 457-460, 1985.

Winglee, R. M., and P. L. Pritchett, Comparative study of cross-field and field-aligned electron beams in active experiments, accepted for *J. Geophys. Res.*, 1988.

FIGURE CAPTIONS

Figure 1. Vehicle charging during DC electron beam emissions measured by the CCP charge probe as function of ambient plasma density estimated from the IRI model.

Figure 2. Return current during DC electron beam emissions measured by the CCP current probe as function of ambient density estimated from the IRI model. As a reference is shown the ambient electron thermal current that can be drawn by the probe for two electron temperatures.

Figure 3. Return current during DC electron beam emissions for a selected Orbiter attitude, the airplane mode.

Figure 4. On the top panel is shown the trajectory of the PDP relative to the Shuttle during the pulsed flux-tube connection. The period of beam emission and the wide band antenna switching pattern are shown by shaded areas. The bottom panel shows the beam angle θ_B with respect to the earth's magnetic field.

Figure 5. The magnetic field in the frequency range 0-10 kHz, 20-10 kHz, and 20-30 kHz (see text) as a function of time. The perpendicular distance from the beam was about 75 m.

Figure 6. The electric field the frequency range 0-10 kHz, 20-10 kHz, and 20-30 kHz (see text) as function of time. The perpendicular distance to the beam was about 40 m.

Figure 7. Amplitude of the harmonics of the beam pulsing frequency (magnetic) at three radial distances from the beam. Also shown for reference is a $1/f$ -functional dependance, where f is frequency (or harmonic number).

Figure 8. Amplitude of the harmonics of the beam pulsing frequency (electric) at four radial distances from the beam.

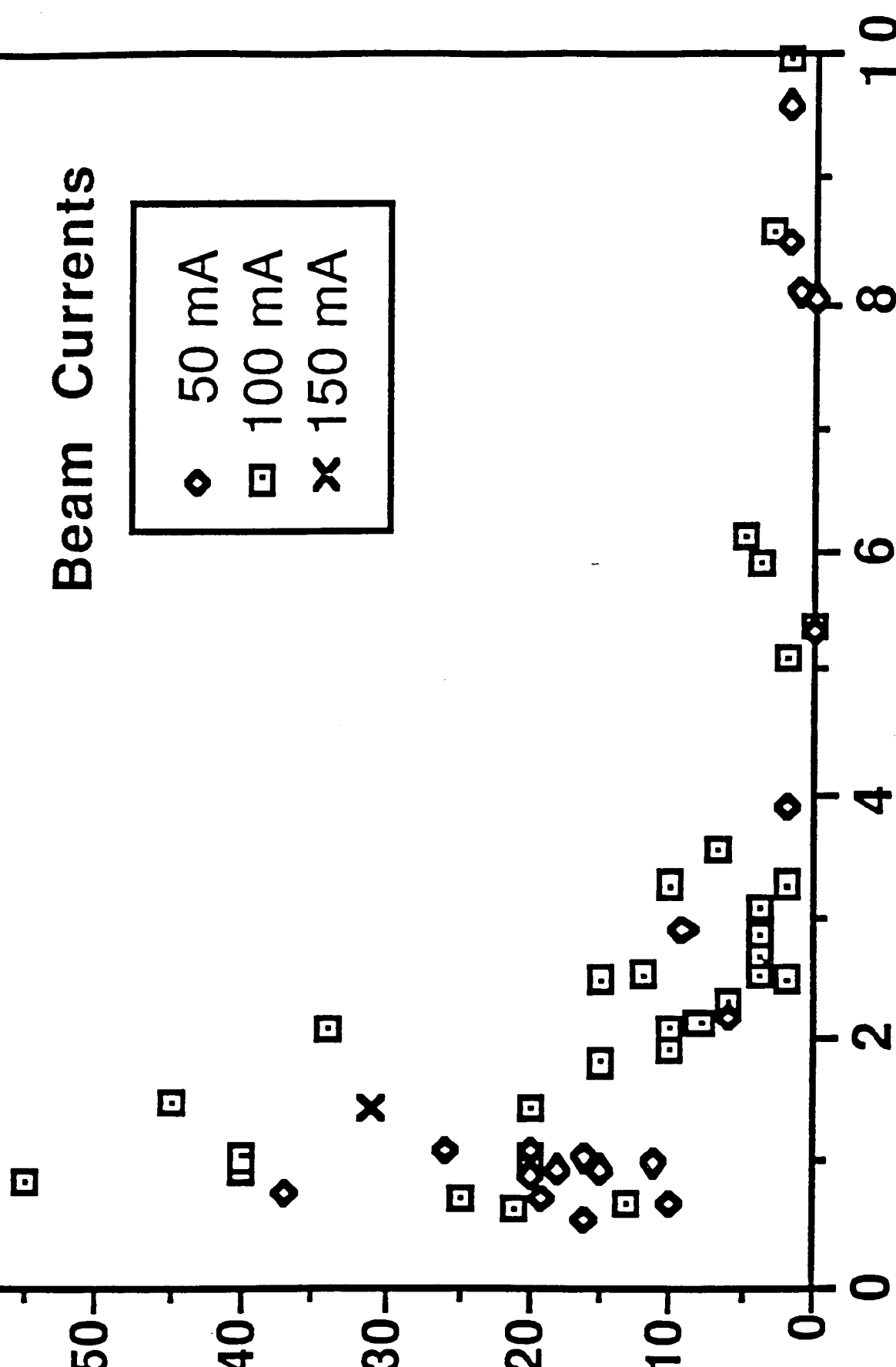
Beam Currents

- ◇ 50 mA
- 100 mA
- × 150 mA

Charging (volts)

Ambient Plasma Density (10^5 cm^{-3})

Fig 1



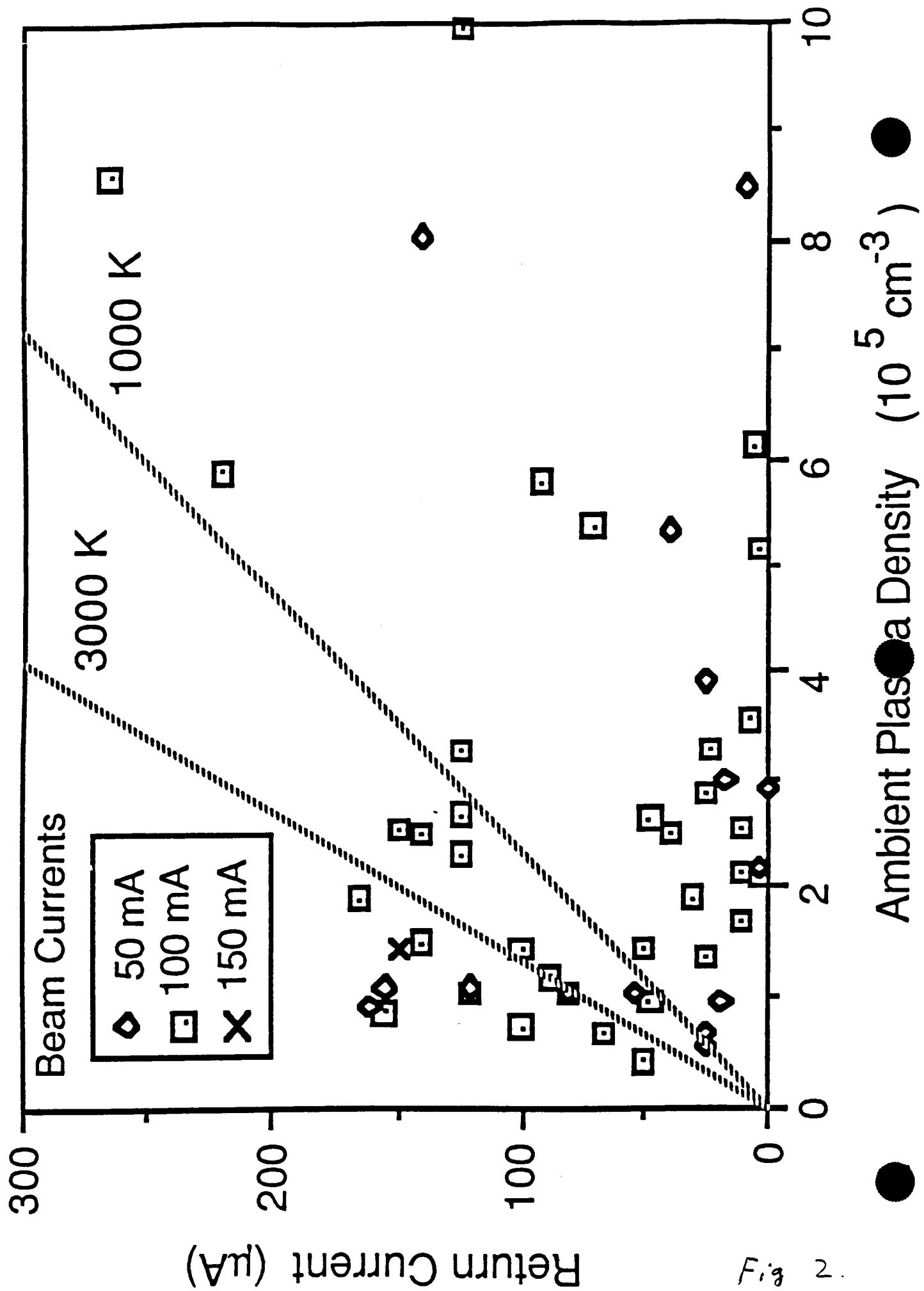
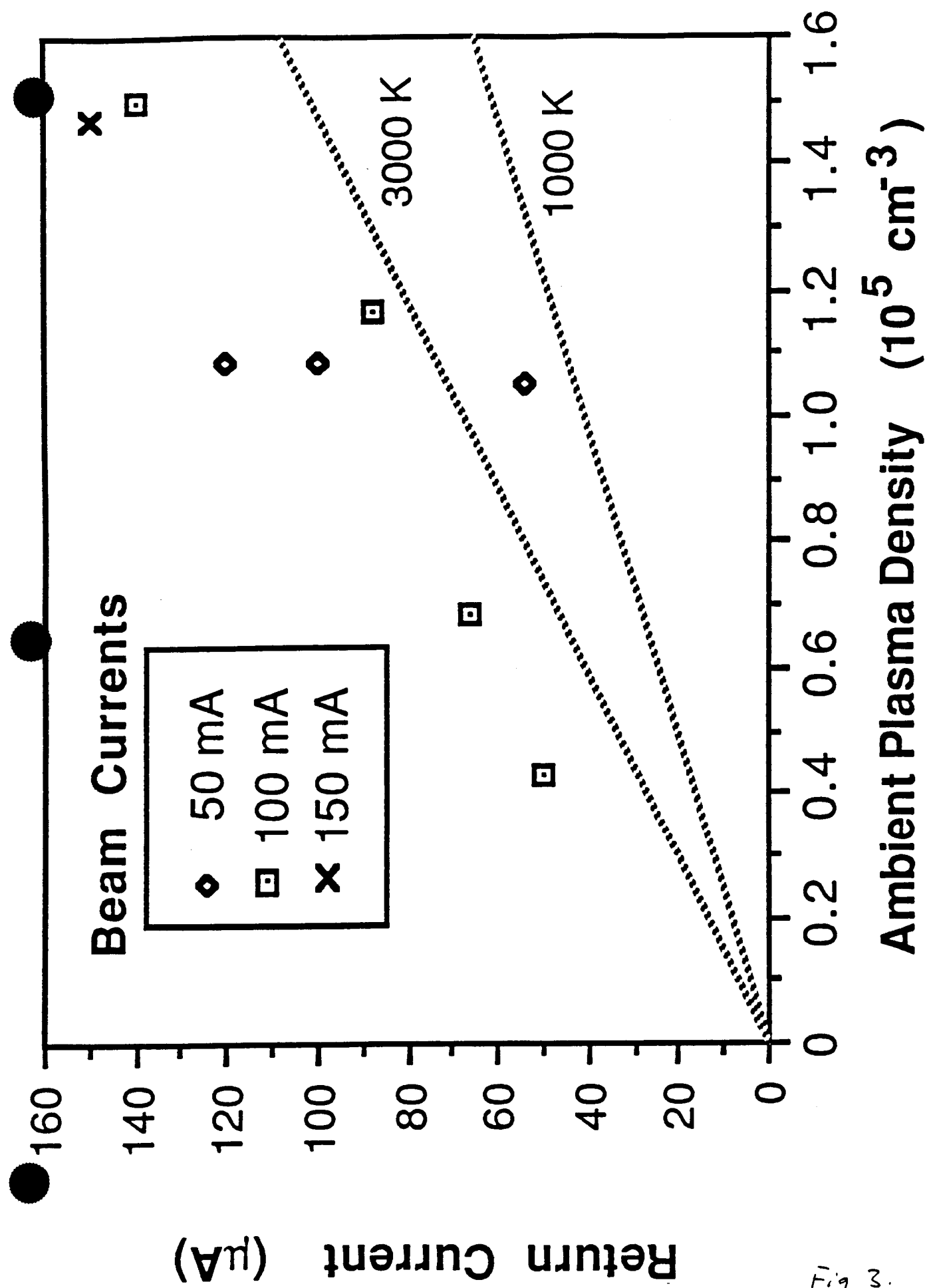


Fig 2.



SPACELAB-2

DAY 213, 1985

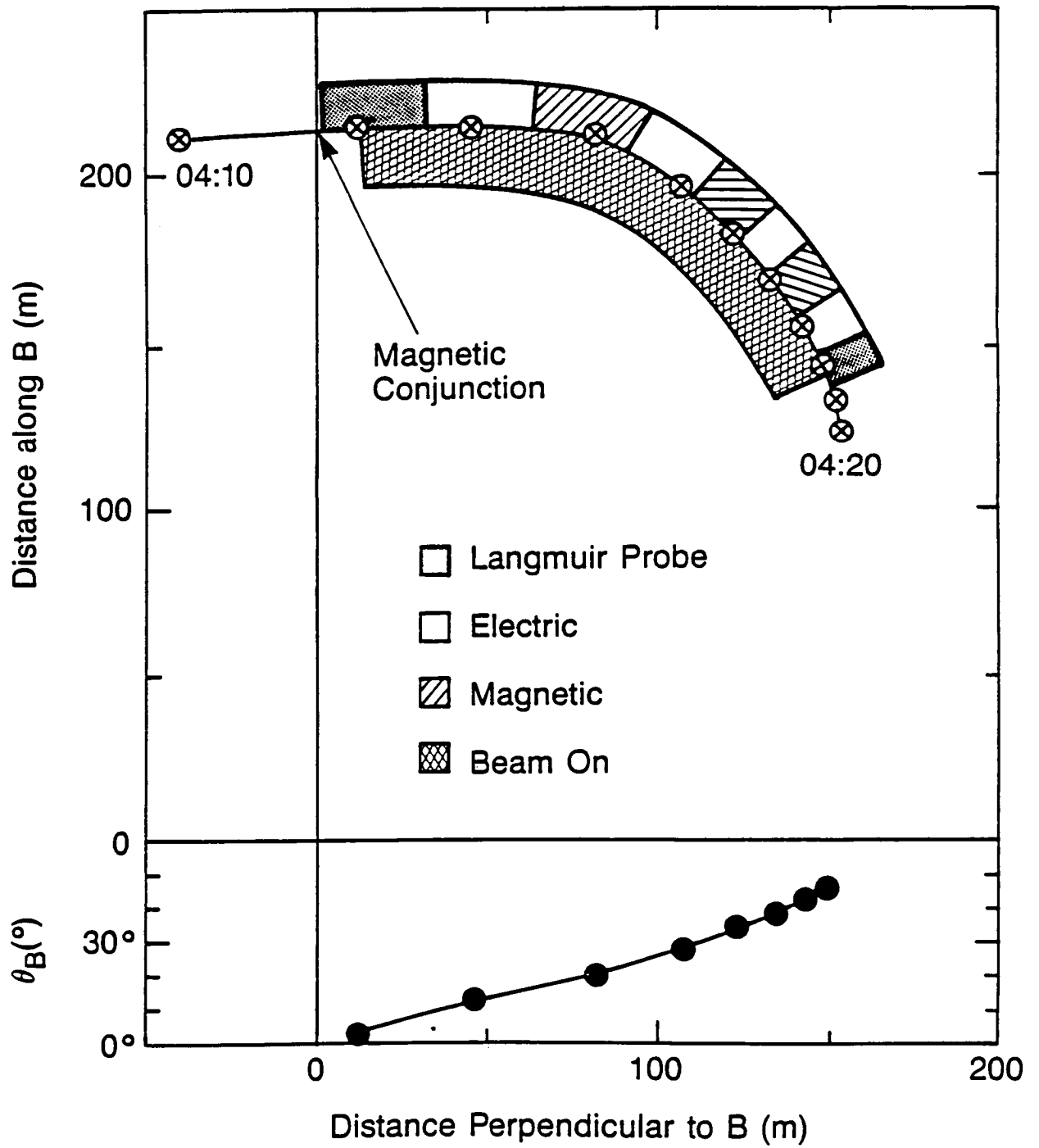


Fig 4.

ORIGINAL PAGE
BLACK AND WHITE PHOTOGRAPH

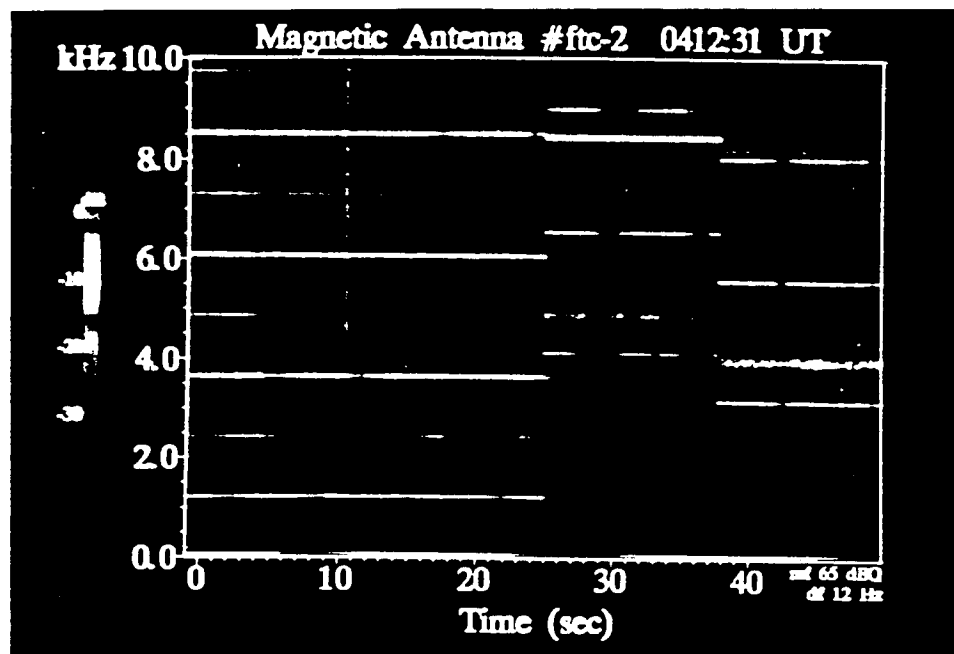


Fig. 5.

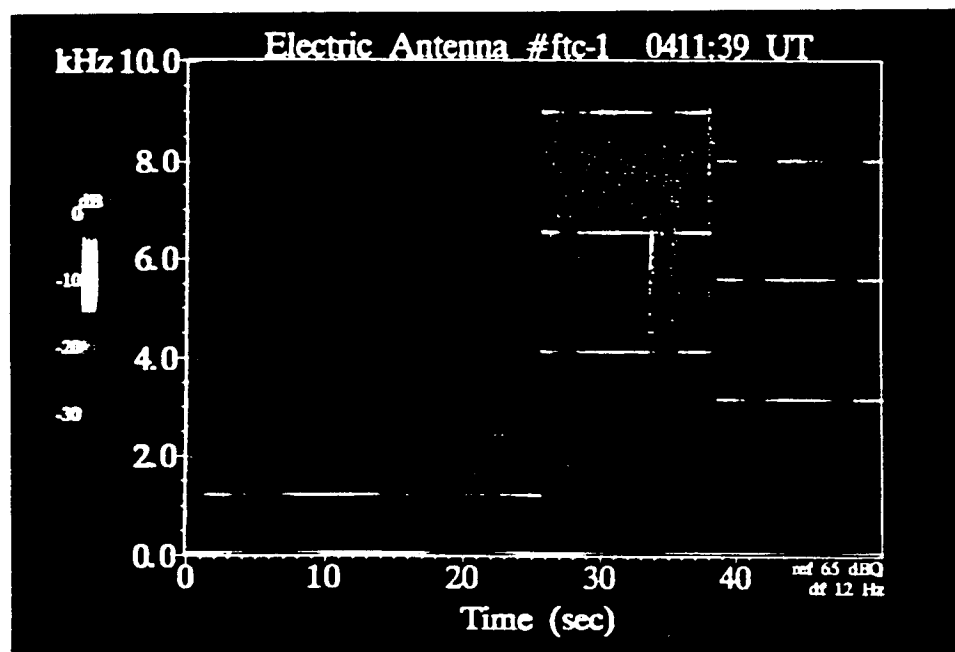


Fig. 6.

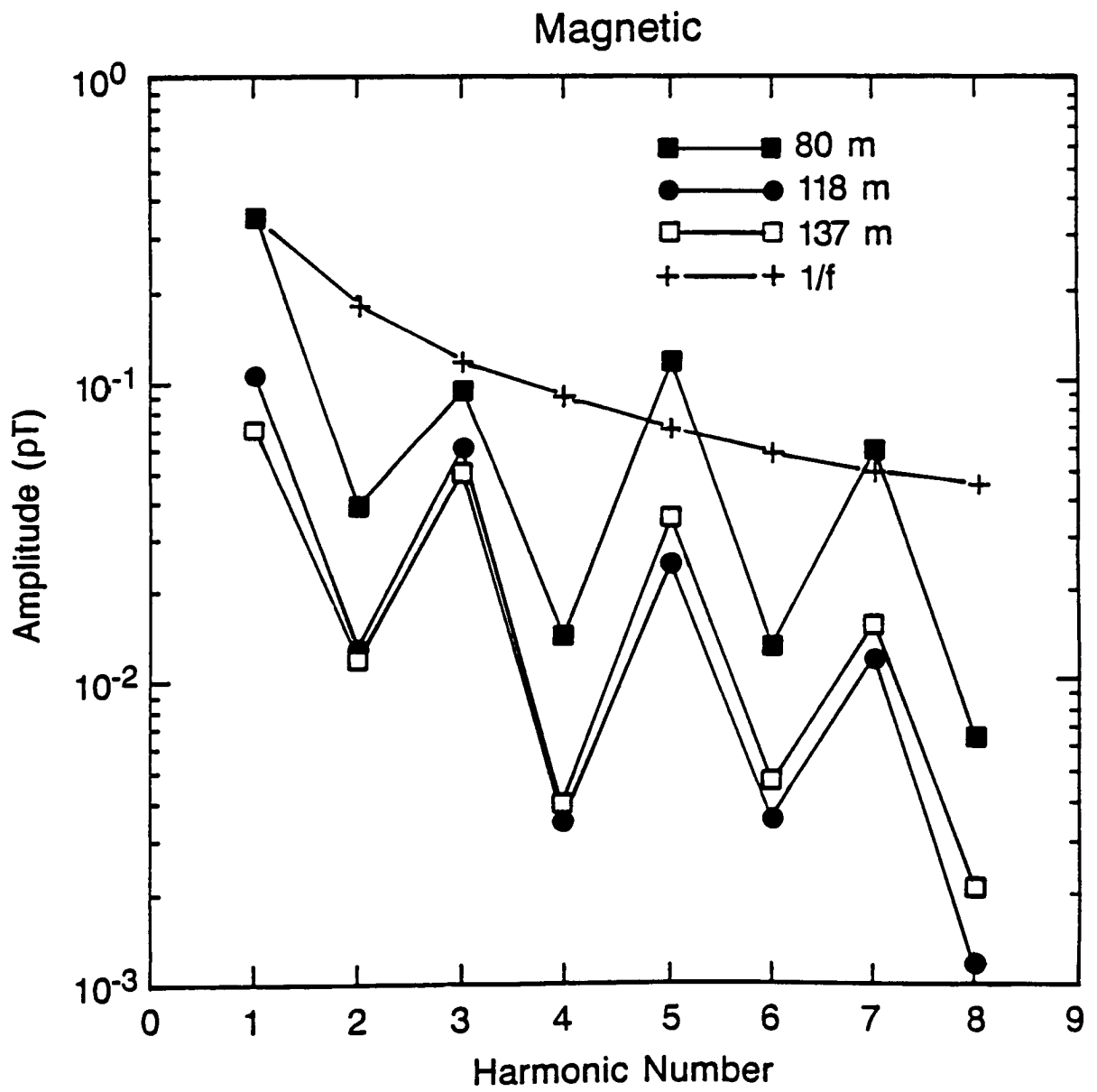


Fig 7.

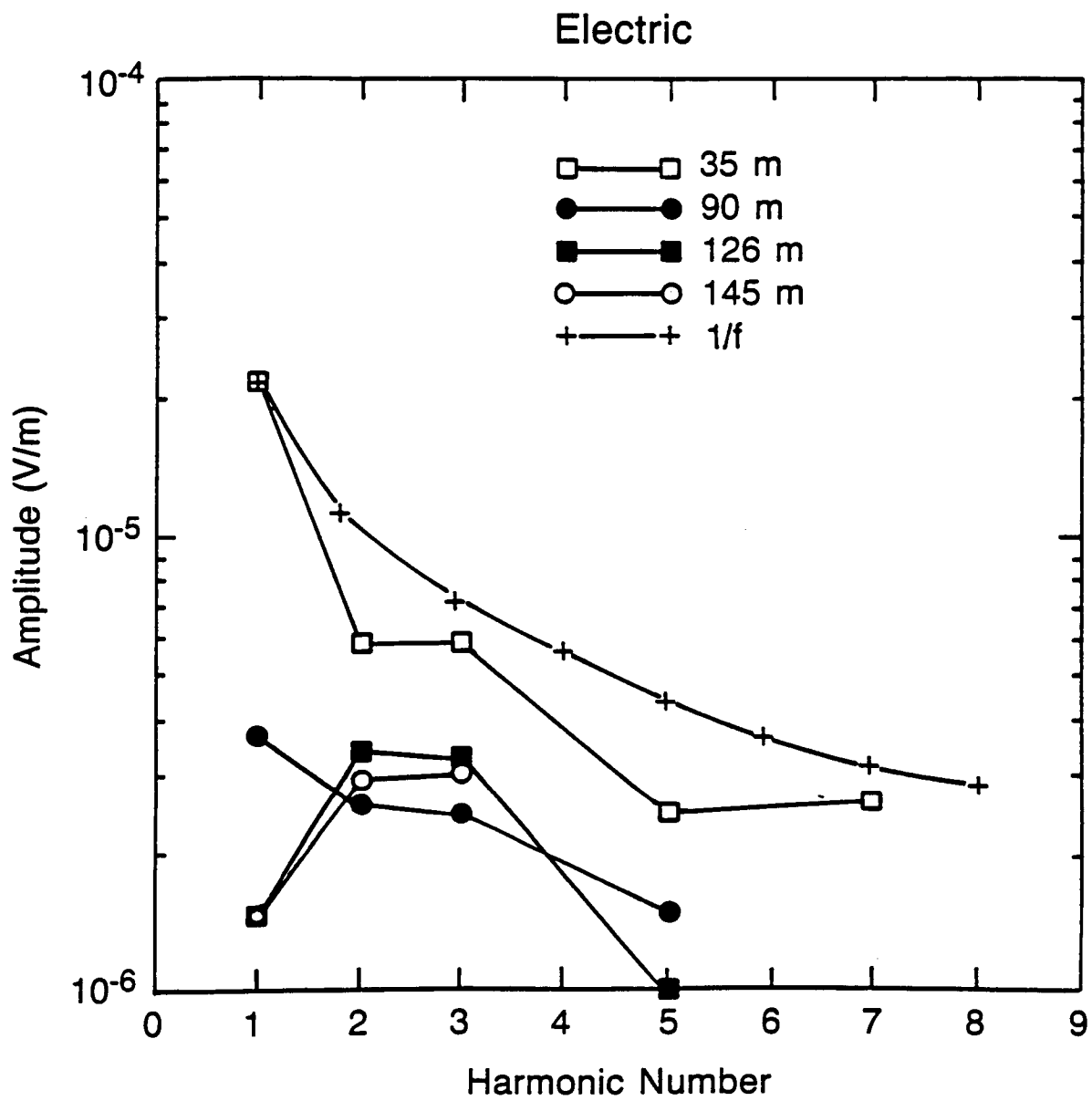


Fig 8

PLASMA WAVE TURBULENCE AROUND THE SHUTTLE:
RESULTS FROM THE SPACELAB-2 FLIGHT

D. A. Gurnett, W. S. Kurth, J. T. Steinberg

Department of Physics and Astronomy, The University of Iowa, Iowa City 52242

S. D. Shawhan

NASA Headquarters, 400 Maryland Ave., Washington, DC 20546

Submitted to Geophysical Research Letters

April, 1988

Abstract. During the Spacelab-2 flight, which occurred from July 29, to August 6, 1985, a spacecraft called the Plasma Diagnostics Package (PDP) was released from the shuttle to explore the plasma environment around the shuttle. The plasma wave instrument on the PDP detected a region of intense broadband turbulence around the shuttle at frequencies extending from a few Hz to about 10 kHz. The noise has broadband intensities ranging from 1 to 5 mV/m and was observed at distances of up to 400 m from the shuttle. The highest intensities occurred in the region downstream of the shuttle and along magnetic field lines passing near the shuttle. The intensities also tended to increase during periods of high thruster activity, which provides strong evidence that the noise is caused by an interaction of the ionosphere with gaseous emissions from the shuttle, similar in many respects to the interaction of a comet with the solar wind. Antenna interference patterns observed in the wideband data show that the wavelength of the turbulence is very short, a few meters or less.

Introduction

In this report we describe plasma wave turbulence observed around the shuttle by a spacecraft called the Plasma Diagnostics Package (PDP) which was released from the shuttle during the Spacelab-2 flight. The PDP was designed and constructed at the University of Iowa and is a reflight of the same spacecraft previously flown on the STS-3 flight [Shawhan et al., 1984a]. On STS-3 the PDP was carried on the remote manipulator arm, which restricted the measurements to about 15 meters from the shuttle. The principal new feature of the Spacelab-2 flight is that the PDP was released from the shuttle, thereby providing measurements at much greater distances. During the free-flight phase of the mission, the shuttle was maneuvered to provide two complete fly-arounds of the PDP at radial distances out to about 400 meters. The fly-arounds provided measurements both upstream and downstream of the shuttle, and along the magnetic field line through the shuttle. In addition to the fly-arounds, a series of maneuvers, called wake transits, was performed to survey the wake region directly downstream of the shuttle.

Included among the various experiments on the PDP was a plasma wave receiver designed to measure electric and magnetic disturbances produced by the motion of the shuttle through the ionosphere. The results presented here are mainly from this instrument. For a description of this and other instruments on the PDP, see Shawhan [1982]. The Spacelab-2 mission, which was launched on July 29, 1985, was flown in a nearly circular low-inclination orbit with a nominal altitude of 325 km and an inclination of 49.5°. The PDP was in free flight for a roughly 6-hour period, from 0010 to 0620 UT on August 1, 1985.

Observations

An electric field spectrogram showing the plasma wave intensities during the first of the two fly-arounds is shown in the bottom panel of Figure 1. The shuttle position relative to the PDP is given by the x, y, z coordinates at the bottom of each plot. The +z axis is directed downward toward the center of the Earth, the x axis is in the orbital plane with the positive axis in the direction of motion, and the y axis completes the right-handed coordinate system. The electric field spectral density, $E^2/\Delta f$, is indicated by the color code, with blue being least intense and red being most intense. The white line labeled f_{ce} is the electron cyclotron frequency, which is a basic characteristic frequency of the plasma. The points labeled 1 and 2 at the top of the spectrogram indicate magnetic conjunctions, which are times when the shuttle was maneuvered to intercept a magnetic field line through the PDP.

The spectrogram shows two types of noise. At selected times during the flight an electron gun on the shuttle was used to inject a beam of electrons into the ionosphere for purposes of studying beam-plasma interactions. This beam produced the series of whistler-mode emissions identified as "electron beam emissions" in Figure 1. These emissions have been described in a previous series of papers [Gurnett et al., 1986; Bush et al., 1987; Farrell et al., 1988] and will not be discussed further. In addition to the electron beam emissions, a broad band of noise can be seen at frequencies below about 10^4 Hz. The magnetic antenna indicates no comparable response, so the noise must be electrostatic. The same type of noise was detected on the STS-3 mission [Shawhan et al., 1984b; 1984c], and is usually referred to as "broadband electrostatic noise."

As can be seen, the broadband electrostatic noise consists of many impulsive short-term variations superimposed on a slowly varying, nearly continuous background. Most of the impulsive variations can be associated with thruster firings. For comparison, the rate of

gas ejection from the thrusters averaged over one-minute intervals is shown in the top panel of Figure 1. Major trajectory correction maneuvers, which typically involve gas injection rates of 10^2 to 10^3 gm/sec over periods of 30 sec or more, almost always produce an intense burst of broadband noise. Examples of such maneuvers occur near the first magnetic conjunction, at 0157 and 0204 UT. In addition to the trajectory correction maneuvers, an almost continuous level of thruster activity occurs in association with minor attitude corrections. These firings, which have durations of about 80 msec and occur at a rate of several per minute, are at least partly responsible for the nearly continuous low level of noise that is present most of the time.

Comparisons of the electric field spectrograms from the two fly-arounds and the wake transits indicate that the intensity varies systematically with the position of the PDP relative to the shuttle. This dependence is illustrated in Figure 2 which shows the x-z projection of the shuttle trajectory relative to the PDP. The solid black dots show the regions where the broadband electric field strength, integrated from 35 Hz to 31 kHz, exceeds 1 mV/m. As can be seen, the electrostatic noise tends to be strongest and most persistent along the +x axis, when the PDP is downstream of the shuttle, and weakest along the -x axis, when the PDP is upstream of the shuttle. The noise is also strong near the four magnetic conjunctions, which are labeled 1 through 4 in Figure 2.

The interpretation of the noise enhancements near the magnetic conjunctions is complicated by the fact that the thruster firing rate tends to be higher in these regions as the shuttle was maneuvered to intercept the magnetic field line through the PDP. Nevertheless, we believe that the intensification in this region is controlled to a significant degree by the magnetic field geometry. As evidence of this relationship note that thruster firings when the PDP is upstream of the shuttle, for example at 0216 and 0224 UT (see Figure 1), do not have nearly as large an effect as thruster firings near the magnetic

conjunction, for example at 0157 and 0204 UT. Also, even when the gas ejection rate is low, for example from 0159 to 0203 UT, the noise level in the magnetic conjunction region is higher than for comparable gas ejection rates when the PDP is upstream of the shuttle.

Representative electric field spectrums of the broadband electrostatic noise are shown in Figure 3. The top panel shows two spectrums selected from near the first and second magnetic conjunctions, and the bottom panel shows spectrums at two different distances ($x = 247$ m and $x = 87$ m) in the wake region directly downstream ($y = 0, z = 0$) of the shuttle. All four spectrums are remarkably similar. Typically, the spectrum is almost flat from 10 Hz to about 10^4 Hz, and then drops below the instrument noise level by 10^5 Hz. Sometimes a peak can be seen at a frequency of a few kHz, which is near the lower hybrid resonance frequency. This peak can be seen at various times in Figure 1, for example at 0150 and 0255 UT. The broadband electric field strength during the most intense thruster-related events ranges from about 2 to 5 mV/m. The nearly continuous background level in the wake region directly downstream of the shuttle is about 1 to 2 mV/m.

High-resolution wideband spectrograms of the electrostatic noise sometimes show a "fingerprint" pattern that repeats with a period of one-half of the spacecraft rotation period. An example of such a pattern is shown in Figure 4. This type of spin modulation pattern is well known in space plasma wave data and is an antenna pattern effect caused by wavelengths short compared to the antenna length [Temerin, 1979; Fuselier and Gurnett, 1984; Gallagher, 1985]. The nulls occur when the antenna separation projected in the direction of propagation is an integral number of wavelengths. Since the antenna length is only 3.9 meters, the existence of these nulls implies that the wavelengths of the electrostatic noise is substantially less than one meter. For such short wavelengths, the frequency spectrum is almost entirely determined by Doppler shifts. The fingerprint pattern tends to be most pronounced and easily recognized near the upper frequency cutoff (~ 10 to 20 kHz)

and in the region directly downstream of the shuttle.

Interpretation

The close correlation between thruster firings and enhancements in the broadband electrostatic noise provides a strong indication that the noise is associated with neutral gas emissions from the shuttle. Previous measurements [Shawhan et al., 1984b; 1984c; Pickett et al., 1985] have shown that the shuttle is surrounded by a neutral gas cloud with pressures as much as 10^2 to 10^3 above ambient. This gas cloud originates from a variety of transient and steady-state sources including thruster firings, water dumps, outgassing of water absorbed in the tiles, and leaks from pressurized compartments on the shuttle. The fact that the electrostatic noise displays both an impulsive component as well as a nearly steady component simply reflects the complex time variability of these various sources.

Since a neutral atom does not interact with an electric field, some mechanism is needed to generate the noise. This mechanism is believed to be charge exchange between the shuttle gas cloud and the surrounding ionosphere. Studies of the plasma distribution around the shuttle by Paterson and Frank [1987] and Frank et al. [1988] show that the shuttle is surrounded by an energized distribution of H_2O^+ ions and other heavy ions. These ions are believed to be produced by charge exchange between the shuttle gas cloud, which is primarily H_2O and ionospheric O^+ ions, which are streaming by at ~ 8 km/s. Once ionized, the newly born $\vec{\text{H}}_2\text{O}^+$ ions are immediately accelerated by the $\mathbf{V} \times \mathbf{B}$ electric field and carried downstream, more or less as illustrated in Figure 5.

The pick-up process causes two effects that could possibly account for the intense electrostatic noise observed around the shuttle. First, since the newly born ions are moving with respect to the ionosphere, these ions produce a beam or ring-like velocity distribution

that should be highly unstable [Krall and Trivelpiece, 1973; Papadopoulos, 1984]. Second, the pick-up process produces both a perpendicular and parallel current system, \vec{J}_\perp and \vec{J}_\parallel , which ultimately must close in the ionosphere via an Alfvén wave, more or less as shown in Figure 5. If the current density exceeds a critical value, then current-driven electrostatic waves could be excited, similar to the processes that are believed to occur in the auroral zone [Kindel and Kennel, 1971]. Just which mechanism provides the free-energy source for generating the intense electrostatic noise around the shuttle remains to be established. The unstable ion distributions associated with the pick-up ions appears to be the best possibility, since current-driven instabilities usually have a rather high threshold. However, the enhanced noise intensities near the magnetic conjunctions suggest that field-aligned currents may play some role. Although the main energization of the pick-up ions comes from the acceleration by the $\vec{V} \times \vec{B}$ electric field, the electrostatic turbulence may play an important role in thermalizing these ion distributions.

In comparing these results with other measurements, it is interesting to note the very close similarity between the noise observed near the shuttle and the electrostatic noise observed near the AMPTE artificial comet [Gurnett et al., 1985; 1986] and the comets Giacobini-Zinner [Scarf et al., 1986], and Halley [Grard, 1986]. Since charge exchange and ion pick-up are believed to be one of the dominant processes in the interaction of a comet with the solar wind, it appears that the interaction of the shuttle with the ionosphere may have a close similarity to the plasma processes occurring near a comet.

Acknowledgements. The research at the University of Iowa was supported by NASA through contract NAS8-32807, and grants NGL 16-001-043 and NAG3-449.

REFERENCES

- Bush, R. I., G. D. Reeves, P. M. Banks, T. Neubert, P. R. Williamson, W. J. Raitt, and D. A. Gurnett, Electromagnetic fields from pulsed electron beam experiments in space: Spacelab-2 results, Geophys. Res. Lett., **14**, 1015-1018, 1987.
- Farrell, W. M., D. A. Gurnett, P. M. Banks, R. I. Bush, and W. J. Raitt, An analysis of whistler mode radiation from the Spacelab 2 electron beam, J. Geophys. Res., **93**, 153-161, 1988.
- Frank, L. A., W. R. Paterson, P. M. Banks, R. I. Bush, and W. J. Raitt, Plasma observations in the vicinity of the shuttle, 1988 National Radio Science Meeting, Boulder, Colorado, Jan. 5-8, 1988.
- Fuselier, S. A., and D. A. Gurnett, Short wavelength ion waves upstream of the earth's bow shock, J. Geophys. Res., **89**, 91-103, 1984.
- Gallagher, D. L., Short-wavelength electrostatic waves in the earth's magnetosheath, J. Geophys. Res., **90**, 1435-1448, 1985.
- Grard, R., A. Pedersen, J.-G. Trotignon, C. Beghin, M. Mogilevsky, Y. Mikhailov, O. Molchanov, and V. F. Formisano, Observations of waves and plasmas in the environment of comet Halley, Nature, **321**, 290-291, 1986.
- Gurnett, D. A., R. R. Anderson, B. Häusler, G. Haerendel, O. H. Bauer, R. A. Treumann, H. C. Koons, R. H. Holzworth, and H. Lühr, Plasma waves associated with the AMPTE artificial comet, Geophys. Res. Lett., **12**, 851-854, 1985.
- Gurnett, D. A., W. S. Kurth, J. T. Steinberg, P. M. Banks, R. I. Bush, and W. J. Raitt, Whistler-mode radiation from the Spacelab-2 electron beam, Geophys. Res. Lett., **13**, 225-228, 1986.

- Gurnett, D. A., T. Z. Ma, R. R. Anderson, O. H. Bauer, G. Haerendel, B. Häusler, G. Paschmann, R. A. Treumann, H. C. Koons, R. Holzworth, and H. Lühr, Analysis and interpretation of shock-like electrostatic noise observed during the AMPTE solar wind, J. Geophys. Res., 91, 1301-1310, 1986.
- Kindel, J. M., and C. F. Kennel, Topside current instabilities, J. Geophys. Res., 76, 3055-3078, 1971.
- Krall, N., and A. W. Trivelpiece, Principles of Plasma Physics, McGraw-Hill, N. York, 473, 1973.
- Papadopoulos, K., On the shuttle glow (the plasma alternative), Radio Science, 19, 571-577, 1984.
- Paterson, W. R., and L. A. Frank, Observations and modeling of ion pickup in the vicinity of the orbiter, EOS, 68, 1399, 1987.
- Pickett, J. S., G. B. Murphy, W. S. Kurth, C. K. Goertz, and S. D. Shawhan, Effects of chemical releases by the STS-3 orbiter in the ionosphere, J. Geophys. Res., 90, 3487-3497, 1985.
- Scarf, F. L., F. V. Coroniti, C. F. Kennel, D. A. Gurnett, W.-H. Ip, and E. J. Smith, Plasma wave observations at comet Giacobini-Zinner, Science, 232, 377-381, 1986.
- Shawhan, S. D., Description of the plasma diagnostics package (PDP) for the OSS-1 shuttle mission and JSC chamber test in conjunction with the fast pulse electron gun (FPEG), Artificial Particle Beams in Space Plasma Studies, ed. B. Grandel, 419-430, Plenum, N. York, 1982.
- Shawhan, S. D., G. B. Murphy, P. M. Banks, P. R. Williamson, and W. J. Raitt, Wave emissions from dc and modulated electron beams on STS-3, Radio Science, 19, 471-486, 1984a.
- Shawhan, S. D., G. B. Murphy, and J. S. Pickett, Plasma Diagnostics Package initial

assessment of the shuttle orbiter plasma environment, J. Spacecraft and Rockets, 21, 387-391, 1984b.

Shawhan, S. D., G. B. Murphy, and D. L. Fortna, Measurements of electromagnetic interference on OV102 Columbia using the Plasma Diagnostics Package, J. Spacecraft and Rockets, 21, 392-397, 1984c.

Temerin, M., Doppler shift effects on double-probe-measured electric field power spectra, J. Geophys. Res., 84, 5929-5934, 1979.

Fig. 1. The bottom panel shows a spectrogram of the electric field intensities observed by the PDP during the first fly-around and the top panel shows the gas flux associated with thruster firings on the shuttle. The broad band of noise below about 10^4 Hz is closely associated with the thruster firings and is believed to be caused by an interaction between a cloud of neutral gas around the shuttle and the ionosphere, which is streaming by at ~ 8 km/sec .

Fig. 2. An orbital plane plot showing the regions (black dots) where the broadband shuttle-induced noise exceeds 1 mV/m. The noise is strongest and most persistent in the region downstream of the shuttle and weakest in the region upstream of the shuttle. Strong enhancements also occur near the magnetic conjunctions.

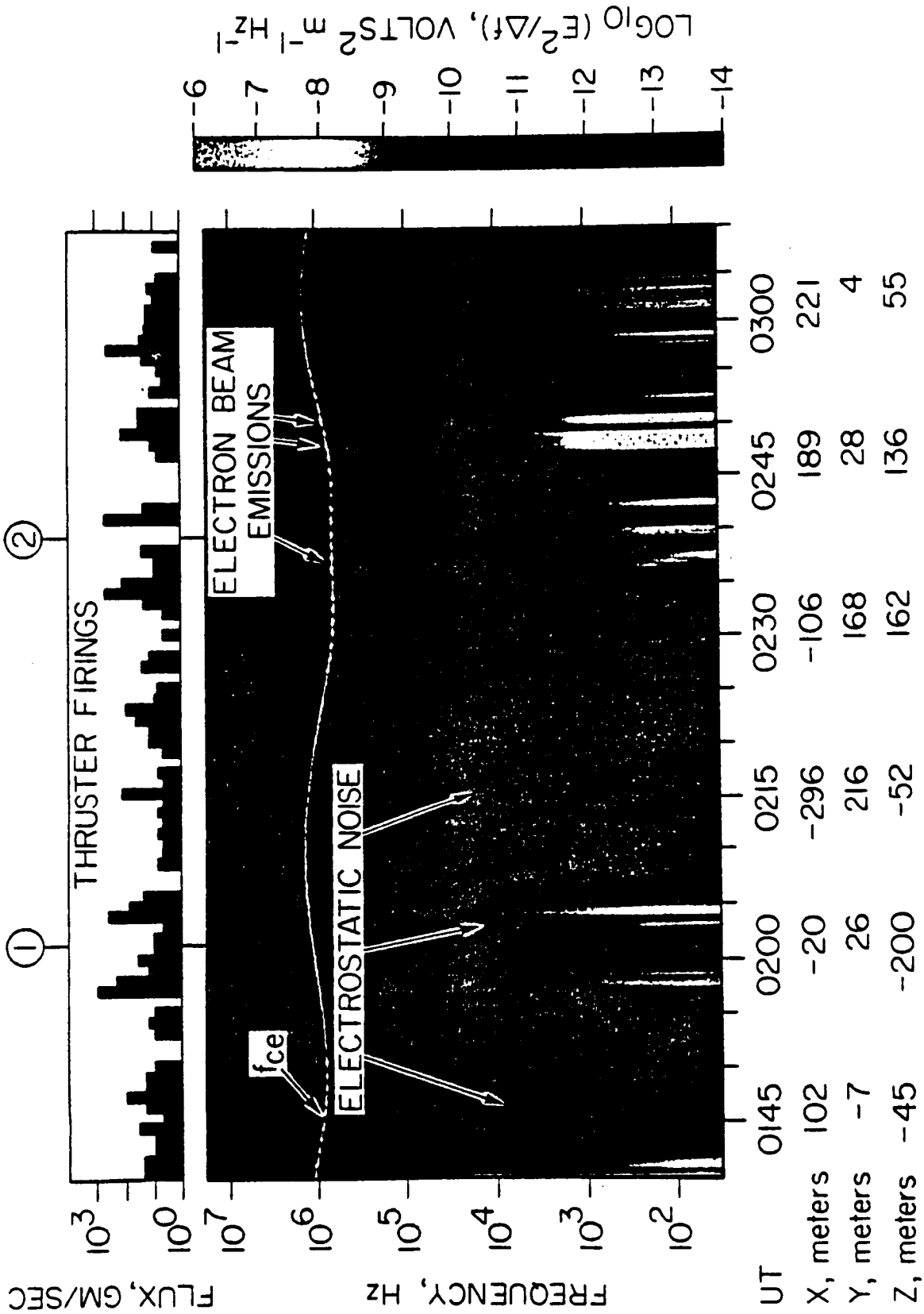
Fig. 3. Selected spectrums of the broadband noise near the first and second magnetic conjunctions, and at two positions in the wake region downstream of the shuttle.

Fig. 4. A high-resolution wideband spectrogram showing "fingerprints" in the broadband noise. This effect is caused by nulls in the antenna pattern as the spacecraft rotates and is indicative of wavelengths shorter than the 3.9 meter length of the electric antenna.

Fig. 5. Charge exchange interactions with ionospheric ions are believed to partially ionize the neutral gas cloud around the shuttle (6), thereby producing pick-up ions which are accelerated and carried downstream by the convection electric field. The pick-up ions produce a highly unstable ion distribution which is believed to be responsible for the intense electrostatic noise observed downstream of the shuttle.

ORIGINAL PAGE
BLACK AND WHITE PHOTOGRAPH

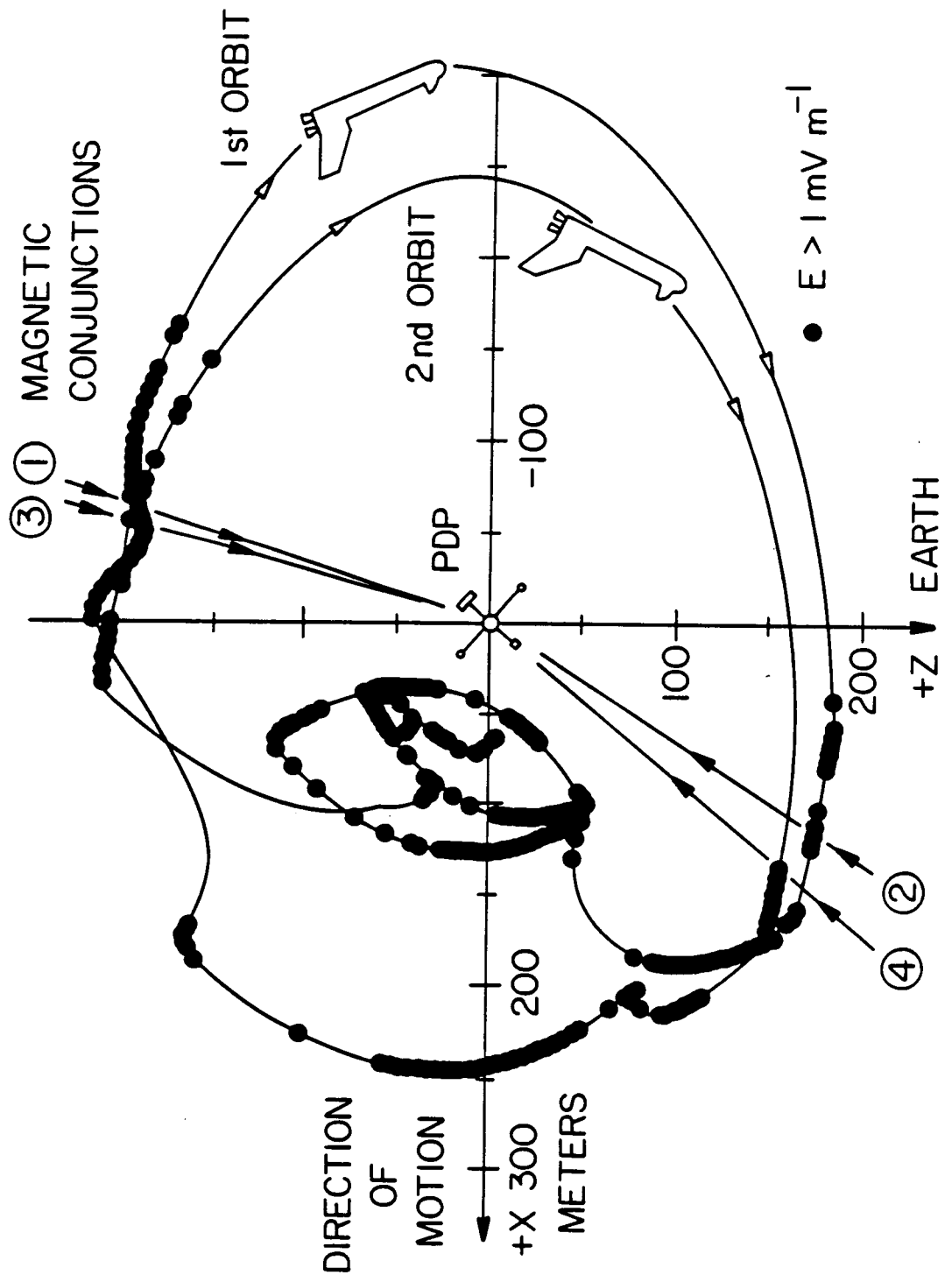
A-G86-861-1



PDP, AUG. 1, 1985

Figure 1

A-G86-860



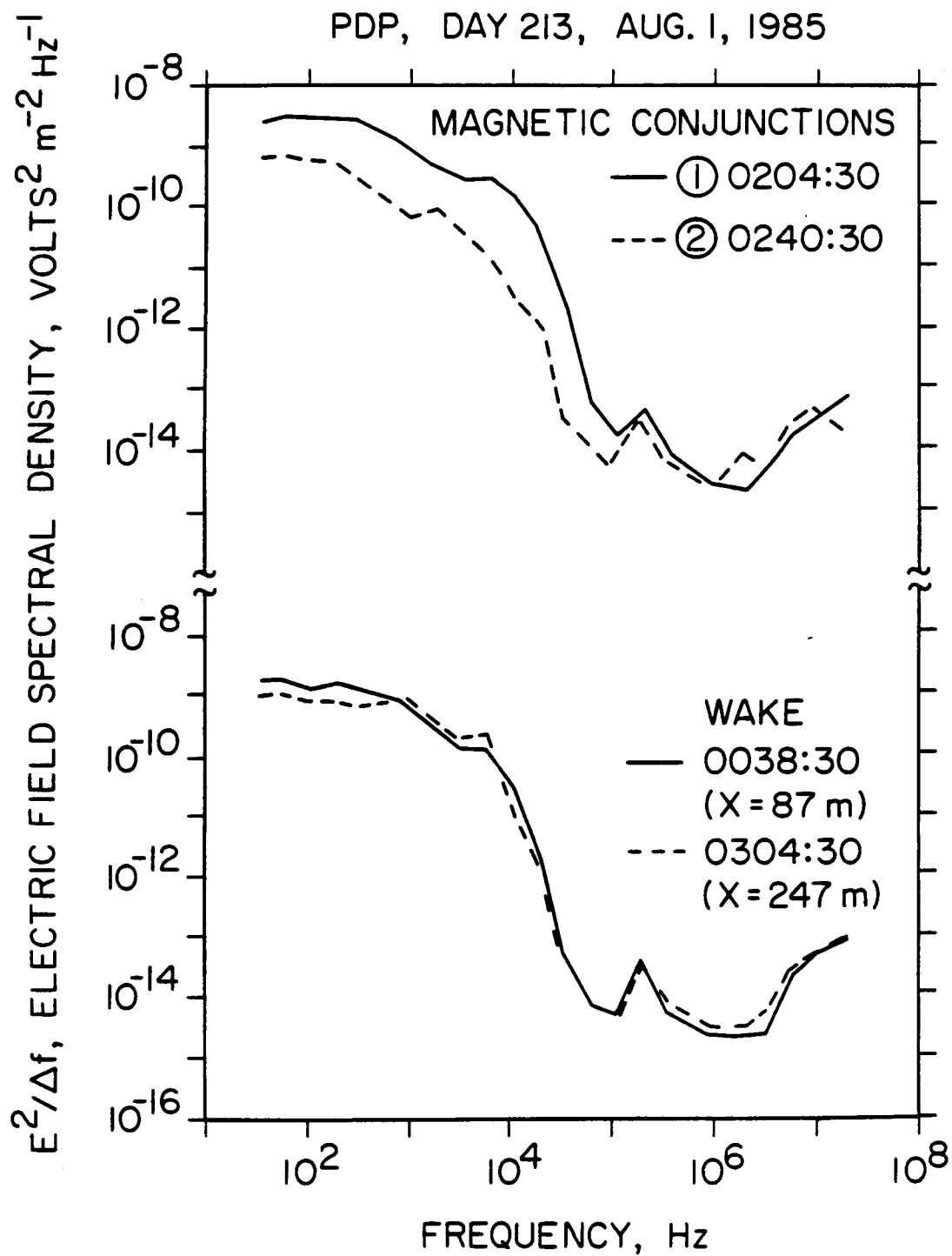
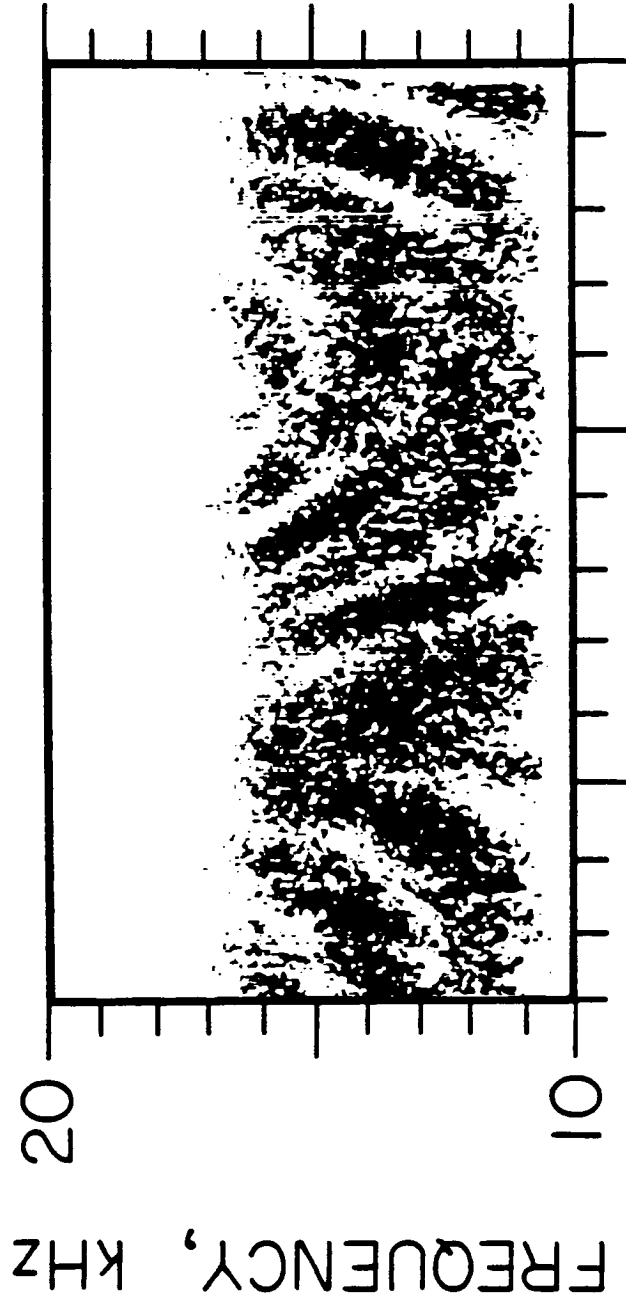


Figure 3

C-4

A-G85-1019



X = 87 m, Y = 1 m, Z = -5 m

PDP, DAY 213, AUG. 1, 1985

C-G87-320

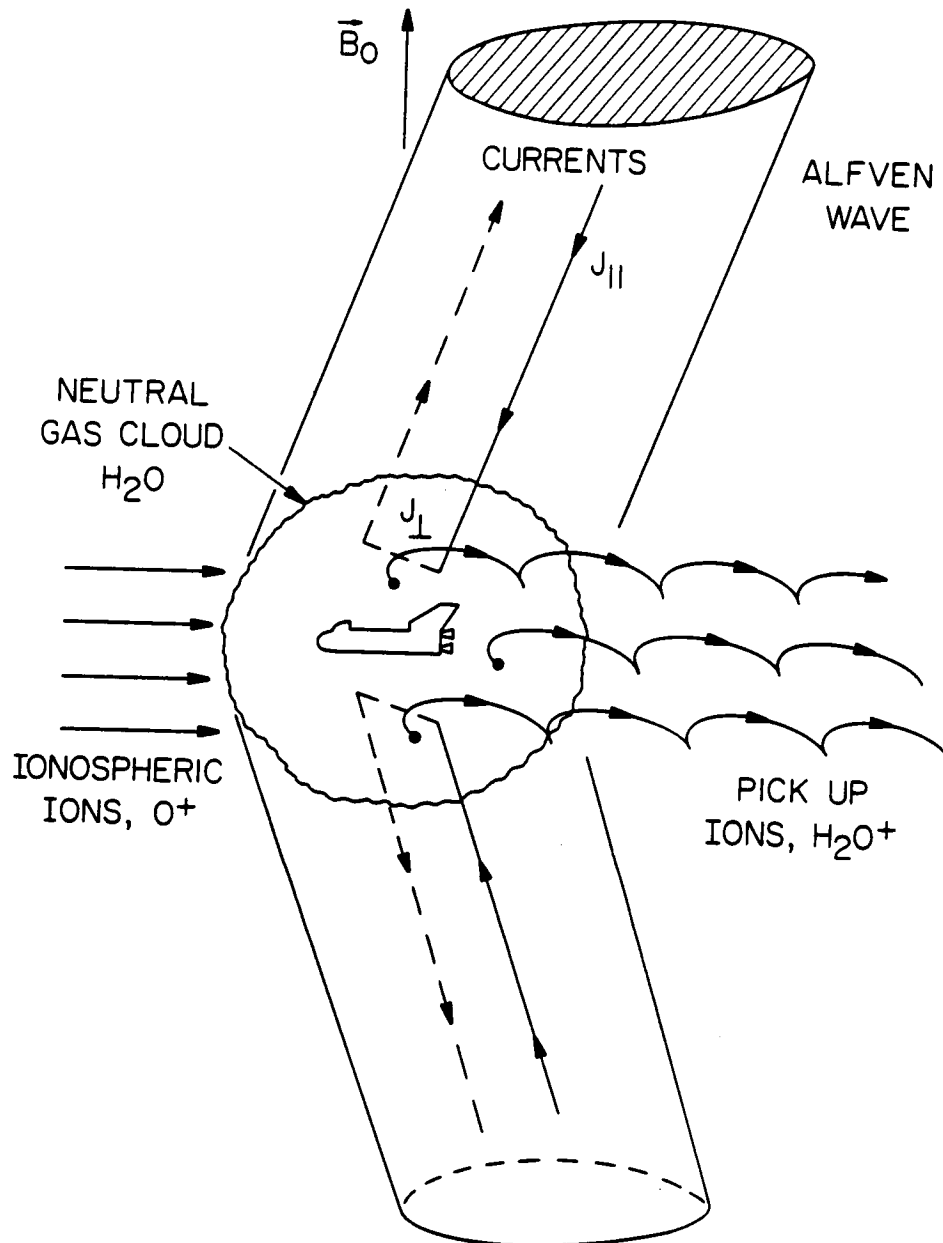


Figure 5

**ON THE EXPANSION OF IONOSPHERIC PLASMA
INTO THE NEAR-WAKE OF THE SPACE SHUTTLE ORBITER**

**N. H. Stone, K. H. Wright, Jr.,* U. Samir,^{1,2}
and K. S. Hwang³**

Submitted To:

Geophysical Research Letters

SPACE SCIENCE LABORATORY
PREPRINT SERIES
NO. 88-124

April 1988

* National Research Council Associate

¹ Department of Geophysics and Planetary Science
Tel-Aviv University
Ramat-Aviv, Israel

² Space Physics Research Laboratory
The University of Michigan
Ann Arbor, MI 48109

³ Department of Mechanical Engineering
The University of Alabama in Huntsville
Huntsville, AL 35899

Abstract

The Spacelab 2 mission provided the first opportunity to measure the extended plasma wake of the Space Shuttle Orbiter. While the Plasma Diagnostics Package was attached to the Remote Manipulator System, differential ion vector measurements were obtained in the near wake at a distance of 4-5 Shuttle radii. The Orbiter's wake was found to fill in at a much faster rate than can be explained by simple thermal motion. The measurements show that ion acceleration must have occurred along the wake boundary in a direction normal to the orbital motion. This behavior implies the existence of a spatially extended electric field and strongly suggests the process of "plasma expansion into a vacuum." The level of plasma depletion in the wake is in agreement with the results from laboratory experiments and small ionospheric satellites that were obtained at comparable normalized distances downstream, suggesting that the near wake plasma depletion is not sensitive to the body scale size for bodies up to an ion gyroradius in size.

INTRODUCTION

The Space Shuttle has greatly increased the range and fidelity of possible space experiments and, as a result, has reopened and generated renewed interest in the physics of spacecraft-space plasma interactions. The STS-3 mission, which took place on March 22-30, 1982, offered the first opportunity to measure the plasma and field environment of the Shuttle Orbiter. An ensemble of 14 plasma instruments was included in the Plasma Diagnostics Package (PDP), a self-contained, deployable satellite that could be deployed up to 15 m above the Orbiter payload bay by the Remote Manipulator System (RMS) (Shawhan et al., 1984).

No measurements were obtained in the Orbiter's wake during STS-3 and it is the wake aspect of spacecraft-space plasma interactions that is most intense and with which the preponderance of ground-based simulations and theoretical models has dealt. However, the PDP experiment was reflown on the Spacelab 2 mission, which took place on July 29-August 6, 1985. Measurements were obtained in the Orbiter's near wake during the PDP RMS maneuvers and in the far wake when the PDP was deployed as a free-flyer. In this paper, we present a brief assessment of measurements obtained in the Orbiter's near wake with one of the PDP instruments, the Differential Ion Flux Probe (DIFP), during the PDP attached, RMS maneuvers.

EXPERIMENTAL CONDITIONS

The DIFP was originally developed for the diagnosis of complex, nonparallel ion flows found to exist in the wakes of laboratory test bodies (Stone, 1977). Details of the flight model design are described in Stone et al. (1985). Its mounting arrangement and field of view on the PDP are given in Stone et al. (1983). It should be noted that the PDP is a clean (no solar

cells) and geometrically simple body. The PDP surface was made conducting by covering its thermal blanket with a grounded, fine mesh wire screen.

The data discussed in this paper were obtained on Julian day 214, 1985, with the Orbiter in a bi-inertial mode that resulted in the payload bay being pointed at the Sun when the Orbiter was in sunlight, and into deep space when in the Earth's shadow. The Orbiter was oriented with its X-axis (the axis of symmetry) approximately normal to the orbital plane; i.e., the axis of symmetry was always approximately perpendicular to the direction of motion. During this period, the PDP was parked on the Orbiter's port side, 13.7 m from the Orbiter's axis of symmetry, approximately in the plane of the payload bay forward bulkhead, and oriented so that the DIFP was pointed at the Orbiter as shown in Figure 1 (see the normal vector \hat{n}). In this configuration, the DIFP electronically swept a 5° acceptance window for ions $\pm 50^\circ$ across the Orbiter's axis of symmetry while the PDP was swept through the Orbiter's wake once per orbit near the sub-solar point. Ions streaming into the instrument from above and below the Orbiter were deconvolved by the differential angular scan and their characteristics (i.e., flow direction, drift energy, current density, and temperature) measured independently.

Figure 1 also shows the effect of the changing geometry of the Orbiter's cross section on the characteristics of the plasma wake and the position of the PDP within the wake. The angle shown beside each panel is the projection of the plasma ram velocity into the Y-Z plane of the Orbiter. (The variation of the out-of-plane ram velocity component during the indicated attitude change was about 11.5° .) Note that in the top panel the ionospheric plasma flows directly across the payload bay and the PDP is located well outside of the geometric wake (the cross-hatched region) approximately at the Mach line. In the middle panel, the Orbiter has rotated 17.5° placing the PDP in

the center of the geometric wake subtended by the starboard payload bay door radiator and bottom port side of the Orbiter. Finally, the bottom panel depicts the situation as the PDP exits the wake region. Note, also, that the effective body size varies greatly with rotation, e.g., approximately 3 m for the top panel and 6 m to 7 m for the bottom panel. Therefore, two things become apparent that must be accounted for in the analysis of the wake measurements: (1) the variation of the Orbiter's effective scale size and (2) the actual position of the PDP with respect to the leading edges of the Orbiter (initiation points for each side of the wake)--both of which vary with the Orbiter's angle-of-attack.

EXPERIMENTAL OBSERVATIONS

The ion flow direction and current density from one of the wake transits are shown in Figures 2a and 2b, respectively. Note that the DIFP was exposed to the "ambient" ionospheric ram current for the period 0 to 5 minutes (Figure 2a). These ions have not undergone any significant deflection as evidenced by their near zero angle-of-attack (i.e., the ion flow direction is approximately aligned with the orbital velocity vector). Once the PDP entered the wake region as denoted by the Mach line in the top panel of Figure 1, the ion current direction abruptly changed and strong perturbations of the ion current density, shown in Figure 2b, were observed as the PDP moved into the Orbiter's wake. Note that the angles-of-attack, shown in Figure 2a, have been corrected for PDP sheath effects and that the current values, shown in Figure 2b, have been adjusted for the variation in DIFP sensitivity with angle (Stone et al., 1985).

Shortly after passing the Mach line, beginning at 7 minutes and continuing through 13 minutes, two ion streams are observed simultaneously

(Figures 2a and 2b). The occurrence of the two ion streams coincides roughly with the geometric wake region. At the wake boundary, the ram current that was initially aligned with the orbital velocity vector is now deflected downward and into the void region of the Orbiter's wake. This stream increases monotonically in angle-of-attack while decreasing in intensity with the motion of the PDP across the wake (Figures 2a and 2b). The second stream, which is deflected upward from beneath the Orbiter, follows the opposite sequence. (The dropout in current for stream 2 at about 14 minutes into the wake transit is possibly due to a dense burst of neutral gas from the Orbiter.) Figure 2a shows that the direction of each stream varied linearly over a range of 30° in angle-of-attack (relative to the Orbiter velocity vector) as the PDP moved across the wake.

DISCUSSION OF RESULTS

First we note that the Orbiter's wake is filled at a much faster rate than would be possible as the result of simple thermal diffusion. This is shown by the fact that (1) although the ion acoustic Mach angle for the Orbiter in this case is $10^\circ \pm 1^\circ$, Figure 2a shows that the measured angles-of-attack for the observed ion streams at the wake axis (see middle panel of Figure 1) are in the range of 15° to 17° , indicating supersonic ion motion into the wake; and (2) the ion void filling actually began well upstream of the point of measurement (13.7 m downstream), evidenced by the continuous observation of ion currents well above the instrument sensitivity threshold across the entire wake, as shown in Figure 2b. Note that at the axial crossing point of the stream lines in the leading edge of the inflowing ion flux, the current density profile is expected to dip to very low levels. This point will occur approximately 18 m downstream for ion thermal motion. It is apparent, therefore, that the ions have been accelerated into the Orbiter's wake.

The required ion acceleration could be produced by an electric field in the Orbiter's plasma sheath, or by an electric field generated along the plasma wake void boundary by the basic process of collisionless plasma expansion (Samir et al., 1983). Because of its large scale size (~ 1000 Debye lengths), the Orbiter has a thin sheath. Since the effectiveness of the currents deflected by the plasma sheath in filling the wake void must be proportional to the ratio of the cross-sectional area of the sheath to that of the body, this is not expected to be an important wake filling mechanism for the Orbiter.

Regarding the possibility of collisionless plasma expansion, experimental and theoretical investigations have shown that this process can occur almost any time a sufficient density gradient exists in a plasma. In the case of the Orbiter, a strong density gradient is created in the very near wake at the boundary of the plasma void region. Moreover, collisionless plasma expansion has been shown to occur in streaming laboratory plasmas under similar, steady state conditions in which the density gradient was created in the near wake of a large plate oriented normal to the plasma flow (Wright et al., 1985, 1986; Wright, 1988). The linear increase in the transverse velocity of the ions to values exceeding the ion acoustic speed, shown by the linear variation in angle-of-attack for the converging streams shown in Figure 2a, is inconsistent with ion thermal diffusion, but consistent with both sheath and plasma expansion induced accelerations. However, the processes differ in that the expansion electric field accelerates ions over an extended region, resulting in curved trajectories and, therefore, greater angles-of-attack than can be produced by an "impulse-like" deflection within the Orbiter's plasma sheath (see Figure 3).

To test this point, a more exact analysis of the effects of the changing Orbiter geometry is needed. In Figure 4, the locations of the vector ion flow measurements are given in terms of distance from the initiation point of the wake at the corresponding side of the Orbiter, i.e., distance downstream from the initial point of contact of the Orbiter with the ionospheric flow and lateral distance from the edge of the geometric wake (see Figure 1). Note that the effective downstream location of the measurements for ion streams having positive and negative angles-of-attack is different because of the difference in the position of the leading edge on the respective sides of the Orbiter.

At each measurement position, the direction of the ion stream is given and the following observations are now permitted: (1) with the exception of the outer-most measurement obtained during transition out of the wake, all points outside of the Mach line are approximately aligned with the ambient rammed plasma; (2) the points inside the Mach line show measurable angles-of-attack, indicating acceleration into the wake; (3) the angle-of-attack (acceleration) of ion streams deflected from both above and below the Orbiter increases with penetration into the wake beyond the Mach line; and (4) a line extended back upstream at the angle-of-attack from each measurement point, that lies within the Mach line, intercepts the Mach line downstream from the Orbiter and intercepts the plane of the Orbiter well beyond the limits of any reasonable sheath thickness, i.e., approximately 2 m from the Orbiter's surface for the ion streams deflected into the wake from above the Orbiter. (Note that observation (4) does not hold strictly for the ion streams arriving from below the Orbiter. Since the point at the largest distance outside the wake does not return to ambient, some other effects may be present. (The reason for this is being investigated further.)

It is apparent from observation (4) that, at least for the ion streams originating from above the Orbiter, the angles-of-attack are too large for the deflection to have occurred within the Orbiter's sheath. However, as previously mentioned, "plasma expansion into a vacuum" will produce curved streamlines and larger angles-of-attack that are consistent with the above measurements. These observations, therefore, strongly suggest that the collisionless plasma expansion (or "plasma expansion into a vacuum") process is a significant factor in the near wake of the Orbiter.

Comparing the plasma depletion, $\alpha \equiv I(\text{wake})/I(\text{ambient}) \approx 0.14$, obtained from Figure 2b, with previous results, we find that at this point in the wake of the Orbiter (for which $R_d > 1000$), α is greater than the value ($\alpha \approx 0.5$) measured at a similar distance ($5 R_0$) downstream in the wake of the Ariel I satellite where $R_d \sim 10$ (Henderson and Samir, 1967), but comparable to the values ($\alpha \approx 0.17$) obtained in laboratory simulation experiments for $R_d \sim 1-10$ at $z/R_0 = 3$ (Stone, 1981). We can speculate that the Ariel I wake was less depleted because of the difference in Mach numbers (3.75 compared to 5-6 for the Orbiter) since Samir et al. (1986) have shown that the amount of depletion increased with ion acoustic Mach number for the Dynamics Explorer 1 satellite. The two results are, therefore, consistent.

The laboratory plasmas are non-magnetized and the gyroradius is not a significant factor for the near wakes of either the Orbiter or ionospheric satellites since orbiting spacecraft move ~ 95 m in one-half of a gyroperiod (the "effective gyroradius for orbital motion"). It, therefore, appears that R_d is not a significant factor for the plasma in the near wakes of bodies whose size is much less than the "effective gyroradius for orbital motion."

Finally, we note that the current profile for the ion stream coming from above the Orbiter with a positive angle-of-attack (stream 1 in Figure 2b)

consistently exhibited a region of ion rarefaction just outside of the ion acoustic Mach cone of the Orbiter. This structure is not understood at present, although similar structures have also been observed in space in the wake of the Ariel I satellite (Samir, 1973) and during the Gemini-Agena 10 wake experiment (Troy et al., 1970).

CONCLUSIONS

The data shown in Figure 2 are the first from an in situ experiment in which differential, vector measurements were obtained of ion streams in the disturbed, nonparallel plasma flow produced in the wakes of ionospheric satellites. The significant conclusions and speculations supported by these measurements are:

(1) The plasma wake of a large ionospheric spacecraft closes much faster than would be possible from simple thermal motion. Therefore, we conclude that the ions filling the wake have been accelerated at some point, or over an extended region, by an electric field.

(2) The source of the electric field could be either a plasma sheath surrounding the Orbiter or charge separation extending along the wake boundary created by collisionless plasma expansion into the void region behind the Orbiter. The fact that the intrushing ions converge on the wake axis at angles greater than would be allowed by an "impulse-like" sheath deflection at the Orbiter strongly suggests the operation of the collisionless plasma expansion process and its spatially extended electric field.

(3) The depth of the Orbiter's wake void is in agreement with laboratory experiments and previous in situ data where the measurements were obtained at a comparable normalized distance downstream. In view of the wide variation in

Debye ratios in these examples, we conclude that the plasma depletion in the near wake of bodies that are much smaller than the effective gyroradius for orbital motion is not sensitive to the body scale size in the plasma.

Acknowledgments. The authors thank D. A. Gurnett of the University of Iowa for providing the dc electric field measurements. We also wish to acknowledge the assistance of Kay Babine of Boeing Computer Support Services for her assistance in flight data reduction and display. U.S. acknowledges support from NASA grant NGR-23-005-320. K.S.H. acknowledges support under NASA contract NAS8-37107.

REFERENCES

Henderson, C. L., and U. Samir, Observations of the disturbed region around an ionospheric spacecraft, Planet. Space Sci., 15, 1499, 1967.

Samir, U., Charged particle distribution in the nearest vicinity of ionospheric satellites - Comparison of the main results from the Ariel I, Explorer 31, and Gemini-Agena 10 spacecraft, in Photon and Particle Interactions with Surfaces in Space, edited by R.J.L. Grard, p. 193, D. Reidel Publ. Co., Dordrecht, Holland, 1973.

Samir, U., K. H. Wright, Jr., and N. H. Stone, The expansion of a plasma into a vacuum: Basic phenomena and processes and application to space plasma physics, Rev. Geophys., 21, 1631, 1983.

Samir, U., R. H. Comfort, C. R. Chappell, and N. H. Stone, Observations of low-energy ions in the wake of a magnetospheric satellite, J. Geophys. Res., 91, 5725, 1986.

Shawhan, S. D., G. B. Murphy, and J. S. Pickett, Plasma Diagnostics Package initial assessment of the Orbiter plasma environment, J. Spacecr. Rockets, 21, 387, 1984.

Stone, N. H., Technique for measuring the differential ion flux vector, Rev. Sci. Inst., 48, 1458, 1977.

- Stone, N. H., The aerodynamics of bodies in a rarefied ionized gas with applications to spacecraft environmental dynamics, NASA Tech. Paper 1933, Washington, DC, November 1981.
- Stone, N. H., U. Samir, K. H. Wright, Jr., D. L. Reasoner, and S. D. Shawhan, Multiple ion streams in the near vicinity of the space shuttle, Geophys. Res. Lett., 10, 1215, 1983.
- Stone, N. H., B. J. Lewter, W. H. Chisholm, and K. H. Wright, Jr., Instrument for differential ion flux vector measurements on Spacelab 2, Rev. Sci. Instr., 56, 1897, 1985.
- Troy, B. E., Jr., D. B. Medved, and U. Samir, Some wake observations obtained on the Gemini/Agena two body system, J. Astron. Sci., 18, 173, 1970.
- Wright, K. H., Jr., N. H. Stone, and U. Samir, A study of plasma expansion phenomena in laboratory generated plasma wakes: Preliminary results, J. Plasma Phys., 33, 71, 1985.
- Wright, K. H., Jr., D. E. Parks, I. Katz, N. H. Stone, and U. Samir, More on the expansion of a collisionless plasma into the wake of a body, J. Plasma Phys., 35, 119, 1986.
- Wright, K. H., Jr., A study of single and binary ion plasma expansion into laboratory generated plasma wakes, NASA Contractor Report 4125, February 1988.

Figure Captions

Fig. 1. Experimental configuration. Schematic of the PDP traversal through the Orbiter's wake. The angle indicated is the projection of the plasma ram velocity into the Orbiter's Y-Z plane. The cross-hatched region indicates the geometric wake and the vector \hat{n} is the DIFP normal. The time notation beside each panel is the relative time used in Figure 2.

Fig. 2. Experimental data. (a) Ion flow direction, relative to the Orbiter velocity vector versus time (or position in wake); the tic marks indicate when the PDP crosses the Mach lines shown in Figure 1. (b) Ion current density for each individual stream versus time. Note that the geometric wake of the Orbiter extends approximately from 7.7 to 13.5 min. The dip in stream 2 at 14 min is thought to be due to a dense burst of neutral gas from the Orbiter.

Fig. 3. A comparison of ion trajectories produced by a localized acceleration of ions within a thin plasma sheath, and by an extended acceleration of ions by an "expansion electric field."

Fig. 4. Ion flow direction at various measurement locations given in terms of distance from the wake origin (leading edge of the Orbiter). ξ is the distance downstream measured along the geometric wake axis and χ is the lateral (perpendicular) distance from the edge of the geometric wake, where $-\chi$ lies inside the wake. O and \square indicate ion streams flowing over the Orbiter top and bottom surfaces, respectively.

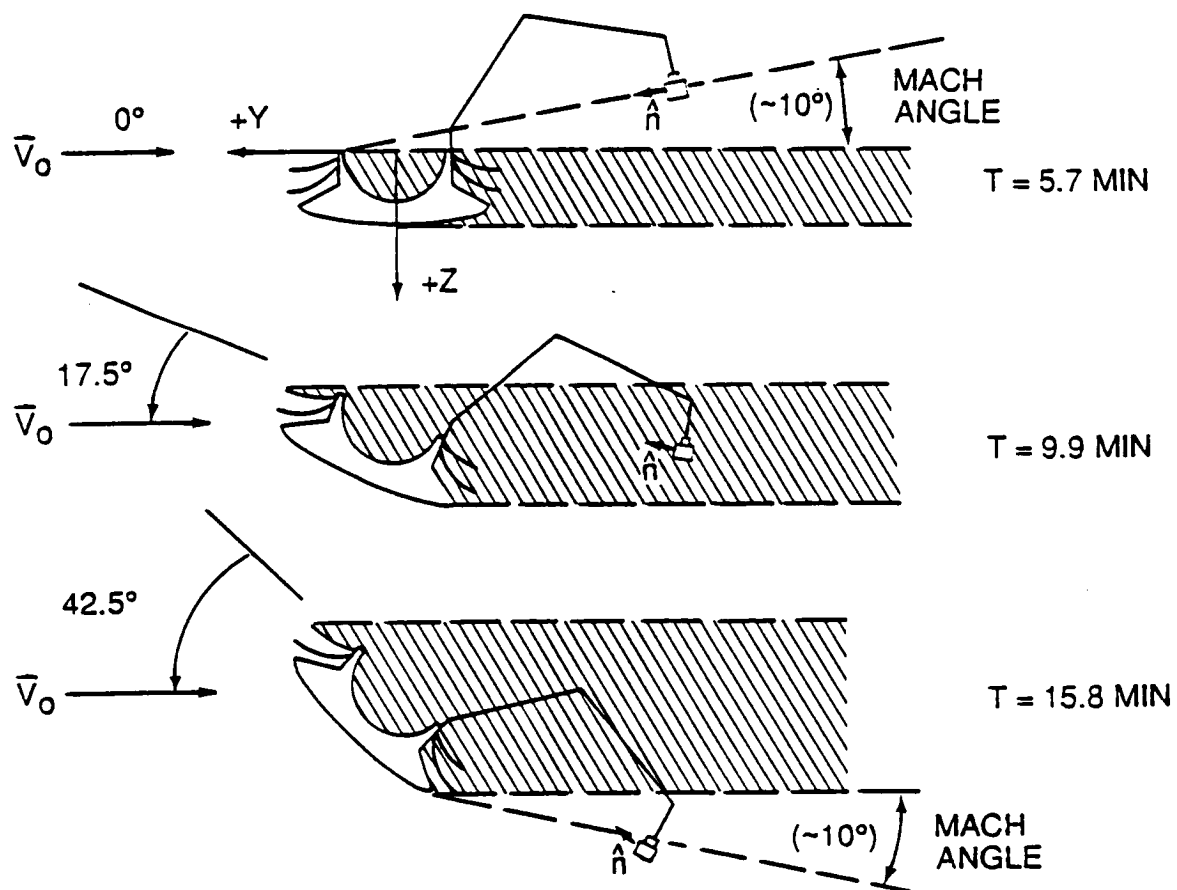


Fig. 1

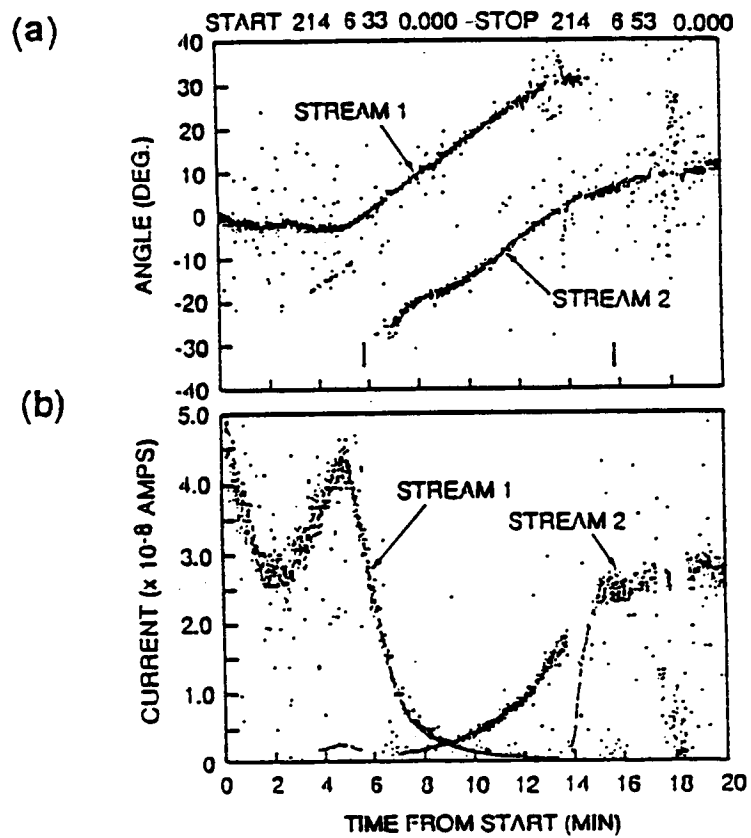


Fig. 2

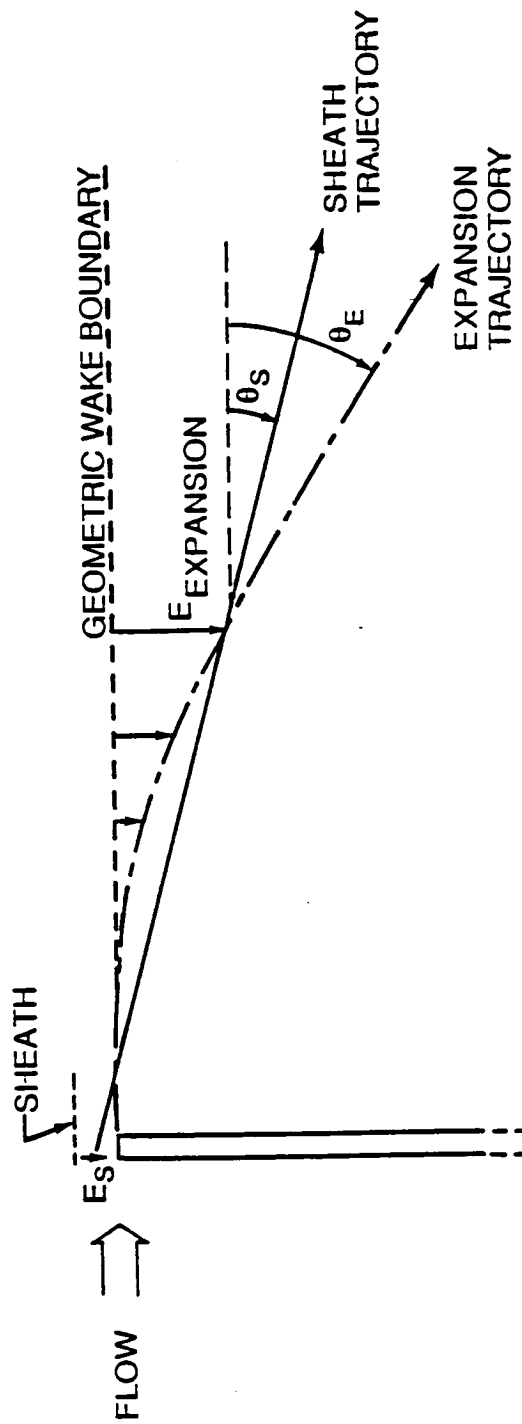


Fig. 3

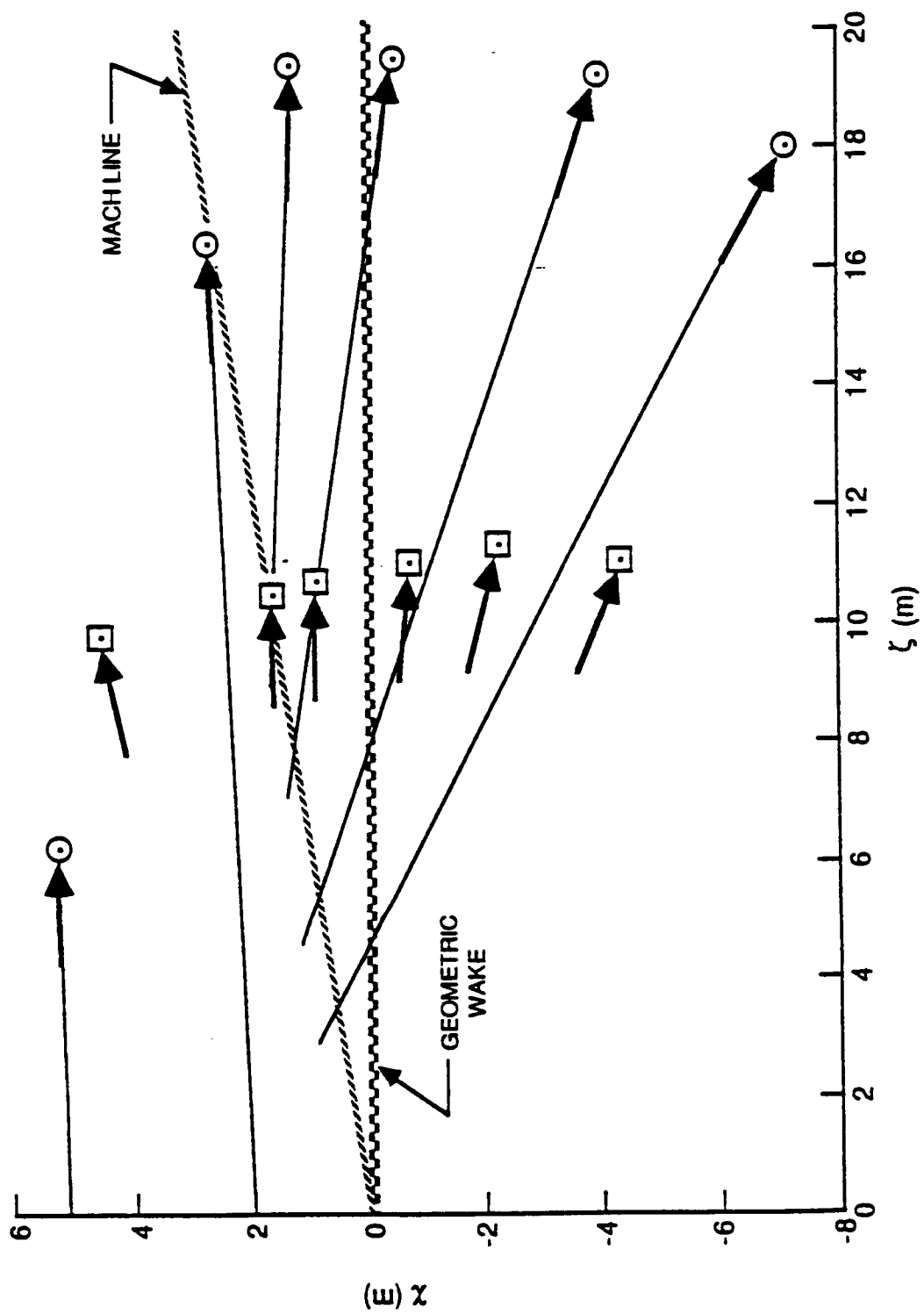


Fig. 4

VLF Wave Emissions by Pulsed and DC Electron Beams in Space 1: Spacelab-2 Observations.

G. D. REEVES, P. M. BANKS, T. NEUBERT, R.I.
BUSH, P.R. WILLIAMSON, AND A.C. FRASER-SMITH

Space Telecommunications and Radioscience Laboratory, Stanford University, Stanford California

D. A. GURNETT

Department of Physics and Astronomy, University of Iowa, Iowa City

W. J. RAITT

Center for Atmospheric and Space Science, Utah State University, Logan

During the Spacelab-2 Space Shuttle mission a 1 keV, 100 mA, square wave modulated, electron source (FPEG) and a plasma diagnostics sub-satellite (PDP) were used to investigate the properties of radio waves generated by electron beams in space. A variety of electron beam pulsing sequences were executed to investigate specific properties of the beam-plasma-wave interaction. In addition to operations conducted with the PDP in the payload bay, several investigations were conducted with the PDP operated as a free-flying satellite at distances of several hundred meters from the Orbiter. In this paper we present the results of three beam operation sequences which provide new information about the characteristics of wave generation by electron beams. Those sequences are: (1) the 'DC flux tube connection' sequence in which the FPEG was operated with continuous electron emission while the Orbiter maneuvered to connect the PDP and the Orbiter on the same magnetic field line; (2) A 'Pulsed flux tube connection' sequence for which the electron beam was square wave modulated at 1.22 kHz; and (3) A 'Prox Ops' sequence in which the FPEG was again pulsed at 1.22 kHz while the PDP was mounted in the Orbiter payload bay rather than operating as a free-flying satellite. Analysis of the amplitudes of VLF emissions from these FPEG sequences allows comparison of broadband emissions from the DC and pulsed electron beams, comparison of broadband and narrowband emissions during the pulsed electron beam emissions, and investigation of the production and propagation properties of radio waves generated by DC and pulsed electron beams in space plasmas. Spectrograms showing the general characteristics of the ambient wave environment and the wave environment

generated during these three sequences are presented. The results of electron beam generated wave observations from the STS-3/OSS-1 mission were verified. Both DC and modulated electron beams produce copious broadband emissions. Square-wave modulated electron beams produce narrowband radiation at the pulsing frequency and its harmonics along with the broadband emissions. The time evolution and spectral structure of broadband and narrowband emissions are analyzed. Our observations indicated that DC, 50 mA electron beams and pulsed, 50% duty cycle, 100 mA beams produce broadband radiation which is comparable in intensity and spectral shape at all points for which the wave field was sampled. Observation of the waves produced by the electron beam during the flux tube connections indicate that there are three zones of wave emissions characterized by the amplitude of waves in those spatial regions. Zone 1 is a highly disturbed region near the beam with very intense wave activity. Zone 2 is the region of propagating waves and zone 3 contains lower amplitude emissions which are near-field contributions. The amplitude of narrowband emissions appear to be in good agreement with the predictions of theory for waves generated through the Cherenkov resonance with wave normal angles less than the resonance cone angle and the harmonic structure of the narrowband radiation is found to be dependent on the beam propagation characteristics.

1. INTRODUCTION

Since the first experiment with electron beams in space plasmas [Hess, et al., 1969] there has been continued and growing interest in beam-plasma experiments conducted in the ionosphere and magnetosphere. Rocket-borne electron beam experiments have been used to investigate a large range of phenomena including propagation of an electron bunch in the magnetosphere [Winckler, 1980], electrical charging of rockets [e.g., Maehlum et al., 1980; Myers et al., 1988], electric fields at geosynchronous altitudes [Meltzner, 1978], radio wave emission from modulated electron beams [Gendrin, 1974; Holzworth and Koons, 1981; Winckler et al., 1984 and 1985], and the charging and wave generation mechanisms involved in a tethered rocket system [Sasaki et al., 1986a].

The first electron beam experiment to be carried on the space shuttle was flown on the March 1982 flight, STS-3, as part of the Vehicle Charging and Potential (VCAP) experiment on the Office of Space Science-1 (OSS-1) mission [Banks et al., 1987]. Cooperative use of a square-wave modulated (1 keV, 50/100 mA) Fast Pulsed Electron Generator (FPEG) and the instruments on the University of Iowa Plasma Diagnostics Package (PDP) permitted numerous observations of the interaction of the electron beam with the ambient plasma environment in the vicinity of the Orbiter. These experiments, because of the relatively long duration of the orbit, could be used to investigate

the disturbed plasma environment around the Orbiter [Shawhan et al., 1984a; Banks et al., 1987], charging of the Orbiter during passive conditions and during electron beam injection in a variety of plasma environments [Hawkins 1988], and the production of waves produced by both DC and square wave modulated electron beams [Shawhan et al., 1984b; Reeves et al., 1988].

Three shuttle based electron beam experiments have followed. The Space Experiments with Particle Accelerators (SEPAC) beam-plasma experiments were flown on the Spacelab-1 mission in 1983. The SEPAC experiments utilized a higher power electron beam (up to 5 keV, 300 mA), a plasma plume injector, a neutral gas plume injector, a TV camera, and a diagnostics package to investigate the properties of spacecraft charging, neutralization, and return currents for relatively high power electron beams. The results of these experiments have been reported by Obayashi et al., [1982], Akai [1984], Sasaki [1986b], Cai et al. [1987], and Neubert et al. [1986a]. The separate PICPAB experiment investigated the radiation produced by operation of the electron beam [Beghin et al., 1984].

More recent electron beam experiments in space took place on the Spacelab-2 mission in July and August 1985. Spacelab-2 included a reflight of VCAP and the PDP. During this mission the PDP was released as a free-flying satellite for a period of six hours. During the free-flight the Orbiter and the PDP completed six earth orbits while the Orbiter maneuvered around the PDP allowing measurement of the plasma and wave environment out to separations of several hundred meters. Four periods of the free-flight included carefully planned magnetic flux tube connections in which the Orbiter maneuvered into a position such that it passed through the same geomagnetic field lines as the PDP. Two flux tube connections were used to study the effects of the passive interaction of the Orbiter with the ionosphere, one flux tube connection took place with the FPEG operating in DC mode with a 50 mA current, and during the final connection the FPEG was pulsed at 1.22 kHz, 100 mA with a duty cycle of 50% (beam on-time equals beam off-time). A total of 325 electron beam pulsing sequences were conducted with the PDP free-flying and mounted in the payload bay.

An overview of the Spacelab-2 mission is forthcoming in Banks et al. [1988]. Gurnett et al. [1986] and Farrell et al. [1988] reported on resonance cone, whistler-mode radiation observed during the DC flux tube connection using filter bank data in the range 31 Hz-17.8 MHz. Results from the PDP wideband VLF wave receiver during the Pulsed flux tube connection were reported by Bush et al. [1987] and Neubert et al. [1988].

2. EXPERIMENT DESCRIPTION

This paper presents the results of the electron beam wave generation results from three separate pulsing sequences. These are the 'DC flux tube connection', the 'Pulsed flux tube connection', and the 'Prox Ops' sequences. Details of the orbital and instrumental parameters for these sequences

are given in Table 1. During the DC and Pulsed flux tube connections, the PDP was released as a free-flying satellite and the Orbiter maneuvered around it so that the separation of the Orbiter and the PDP would allow the sampling wave fields in a range of positions with respect to the beam.

Figure 1 shows the trajectory of the PDP relative to the Orbiter. The start and stop times for each sequence are noted and one point is plotted every 30 s. The coordinate system is picked with the Orbiter at the origin. The vertical axis is the distance parallel to the magnetic field line which passes through the Orbiter, hereafter referred to as the 'conjunction field line', and the horizontal axis is the distance perpendicular to that field line. (Note that the conjunction field line refers to the instantaneous field line connected to the Orbiter, not a geomagnetic field line which is fixed in space.) Negative distances on the horizontal axis correspond to times when the PDP was approaching the conjunction field line and positive distances correspond to times when the PDP was receding. For $r_{\perp} = 0$, the PDP and the Orbiter lie on the same geomagnetic field line and this is referred to as the flux tube connection. The attitude of the Orbiter was such that at all times the Orbiter z-axis (rising out of the payload bay, perpendicular to the plane containing the wings) pointed toward the PDP. Beam electrons follow a helical trajectory along the field line so the angle between the conjunction field line and a line connecting the Orbiter to the PDP defines the pitch angle of the electron beam as well as the ray angles of wave emissions detected by the PDP. During the Prox Ops sequence the PDP was mounted in the payload bay 6.62 m from the FPEG aperture (figure 2) and the FPEG was operated in the same mode as during the Pulsed flux tube connection.

The data presented in this paper were acquired using the wideband receiver on the University of Iowa Plasma Diagnostics Package. A description of the use of the wideband receiver for making VLF wave observations can be found in Reeves et al. [1988] and is summarized here. The wideband receiver measured two frequency bands, ELF and VLF, with frequency limits 40–1000 Hz and 0.4–10 kHz respectively. Data in the two bands were obtained simultaneously. The wideband receiver was connected alternately to a 3.89 m electric dipole antenna and a 16 inch long, 10,000 turn magnetic field search coil. Every fourth magnetic antenna period was replaced by an antenna period when the wave receiver was connected to a Langmuir probe and during those times the broadband wave data cannot be used. In addition to this antenna switching pattern, the VLF band could measure signals heterodyned from higher frequency ranges into the 0–10 kHz frequency range. The VLF band monitored the approximate frequency ranges 0–10 kHz for 26 s, 20–10 kHz (with inverted frequency response) for 13 s, and 20–30 kHz for 13 s. The antenna switching pattern is illustrated in figure 3. The antenna switching pattern is the origin of many of the apparent gaps or discontinuities in the wave data as well as the lack of simultaneous electric and magnetic field data.

In addition to the wideband wave receiver, the PDP contained a Langmuir probe which was used to measure the plasma electron density, a Low Energy Proton and Electron Differential Energy

Analyzer (LEPEDEA) which measured electron and proton energy spectra, a tri-axial fluxgate magnetometer which measured the magnitude and direction of the ambient magnetic field, the IMP/HELIOS filter bank, and a variety of other instruments which were not used in this experiment [Shawhan *et al.*, 1984a]. The IMP/HELIOS instrument consisted of 16, 10% band-width filters in the range 31 Hz to 17.8 MHz which were connected to the electric dipole and magnetic search coil antennas to provide additional wave field information. The Vehicle Charging and Potential (VCAP) experiment package contained the FPEG, a Langmuir probe, a spherical retarding and potential analyzer and charge and current probes. These instruments provided information on vehicle charging and return current collection during ambient conditions and during electron beam injection [Banks *et al.*, 1988].

3. OBSERVATIONS

The wideband wave receiver data is in the form of an analog broadband audio waveform. The amplitude of the signal is kept within strict limits with an automatic gain control (AGC) with a 100 dB dynamic range. In order to analyze the amplitude of the spectral components of the received wave signal select periods of VLF band wave data were digitized at a rate of 25000 samples/sec which, in conjunction with the bandpass of the receiver, leaves the frequency ranges of interest without aliased signals. This data was then Fourier transformed into time-frequency spectrograms with a resolution of 12.207 Hz and 40.96 ms. At this point the spectrograms can be displayed to observe the general wave characteristics but the AGC modulation of the signal is still superimposed on the data (See, for example, figure 4 of this paper and figures 2 and 3 of Bush *et al.* [1987]). In the following section we present spectrograms from the three sequences under consideration and discuss the general observations.

General Results

Figure 4 shows four spectrograms produced from the VLF wideband electric antenna data. In each spectrogram one antenna period is shown. The antenna switching pattern is most obvious in figures 4c-d. We note again that the first 26 s are 0-10 kHz, the next 13 s are 10-20 kHz and is inverted (with 10 kHz at the top of the scale), and the final 13 s are 20- 30 kHz. The AGC modulation of the signal keeps the total wave amplitude in the band roughly constant therefore amplitudes are relative.

The Ambient Wave Environment.

Figure 4a is the electric response during the Pulsed flux tube connection before the FPEG is turned on. At this time the PDP is located at a position with respect to the Orbiter which is 100 m along the conjunction field line and 250 m perpendicular to it (-250 m in figure 1). The electric field is seen to be very highly time varying with the strongest wave response occurring

due to natural atmospheric, including whistlers, and to wave emissions due to Orbiter thruster operation. (Orbiter thruster firings are frequent during the flux tube connections.) During this antenna period the wave spectrum is dominated by small dispersion atmospheric. The whistlers can be identified in the spectrograms by a slight 'hook' in the frequency response at frequencies low frequencies. They were found to have amplitudes of up to 5×10^{-5} V/m as measured with the electric dipole antenna and 10^{-5} nT as measured with the magnetic search coil antenna during daytime conditions. During nighttime conditions, the maximum amplitudes were 10^{-7} V/m and 10^{-6} nT. The amplitudes of the whistler signals observed in figure 4a peak between 3-4 kHz which is in the range of the lower hybrid frequency which was approximately 3.6 kHz at this time. The maximum amplitude of whistlers reported by Hayakawa et al. [1986] during daytime conditions were 6×10^{-4} V/m at 25° latitude and 2.5×10^{-4} V/m at 35° latitude. It has also been reported in the literature [Helliwell, 1965] that whistlers are often observed to have enhanced amplitudes near the lower hybrid frequency so we find that our measurements are in general agreement with previous observations.

The effect of the Orbiter reaction control system (RCS) and attitude control system (ACS) on the plasma wave response was usually to enhance plasma wave amplitudes by up to an order of magnitude above existing levels. The effects of thrusters upon the VLF wave signals and return current distribution during electron beam operation are active areas of investigation and will be reported elsewhere.

Another feature observed in the ambient wave spectrum during the flux tube connections, is the presence of variable frequency, narrowband emissions between 7 and 16 kHz with amplitudes which can exceed 10^{-6} V/m. The frequency of the narrowband emissions varies with time and appears to repeat with a period of ~ 13 s. During the free-flight, the PDP was spin stabilized and rotated with a period of ~ 13 s. It is curious that the variation of these narrowband signals appears with the spin period of the PDP rather than with half the spin period as would be expected for a symmetric single axis antenna. Although the whistlers are observed with both the electric and the magnetic antennas, these narrowband emissions are observed only through their electric field signature. Waves with similar features have been observed from rockets and satellites. They are thought to be generated by the interaction of the spacecraft with the ambient plasma as discussed in Neubert et al. [1986b] and references therein.

The DC Flux Tube Connection.

Figure 4b shows the electric field response during the DC flux tube connection when the FPEG is firing and the PDP is near the conjunction field line. During this antenna period the PDP is located 225 m along and 45 m perpendicular to the conjunction field line. It is apparent that operation of the FPEG produces broadband emissions at all frequencies within the limits of the receiver. The broadband emissions dominate the ambient wave fields at all times that the FPEG is

firing. In this spectrogram, the strongest emissions are seen between 4 and 8 kHz, near the lower hybrid frequency ($f_{LHR} \approx 6.6$ kHz) and these emissions show spin modulation due to the rotation of the PDP. The effects of thrusters are also observed and are most apparent at 1 and 21 s in the figure. Although it appears that wave activity is diminished, this is only an effect of the AGC. In fact, wave amplitudes are enhanced at all measured frequencies during thruster operations but the dominance of lower frequency wave amplitudes suppresses the apparent amplitude at higher frequencies.

The Pulsed Flux Tube Connection.

The electric field response during the Pulsed flux tube connection is shown in figure 4c. The PDP was at a distance of approximately 210 m parallel and 35 m perpendicular to the conjunction field line and the FPEG was being modulated at 1.22 kHz. Broadband emissions are observed in all frequency ranges as was the case for DC beam operation. It will be seen below (figure 6) that the amplitude of broadband emissions from the pulsed beam are comparable to those from the DC beam but appear less prominent in the spectrograms shown here due to the action of the AGC. Figure 4c also shows that the pulsed electron beam produces narrowband emissions superimposed on the broadband signals. These occur at the beam pulsing frequency of 1.22 kHz and at higher harmonics. The even harmonics are visible but with significantly reduced amplitude as is predicted by Fourier transform theory for a 50% duty cycle, square wave modulated beam.

The PDP was spinning with a period of ~ 13.6 s during its free-flight and many wave emissions show significant amplitude variations as a result. The spin modulation of the broadband and narrowband emissions is particularly apparent in figure 4c. Since the antennas are symmetric, the PDP spin period gives a wave modulation period of one half the spin period or 6.8 s. In figure 5 the magnetic field amplitude of the fundamental (1.22 kHz) is plotted as a function of time along with the function $\sin^2(\omega t)$. From the phase of the modulation and the known position and orientation of the PDP, the polarization of the observed signals can be deduced. The analysis is, however, complicated by secondary instrumental effects. It has been found, for example, that the LEPDEEA instrument aboard the PDP can make anomalous periodic changes to the potential of the PDP and that these shifts can affect the wave results [Tribble et al., 1988]. It appears that the spin modulation and instrumental effects can be separated and the polarization of the signals analyzed. Results will be presented in a later paper. Figure 5 also shows perturbations to the wave signals due to thruster operation on the Orbiter. In this case the duration of the thruster operation (0.24 s) is much less than the AGC sample rate (1.6 s) so the amplitudes are unreliable.

The Prox Ops Sequence.

The final spectrogram, figure 4d shows an antenna period from the Prox Ops sequence. At ~ 20 s in the figure, the FPEG is turned on and modulated at 1.22 kHz. Throughout this time the PDP is mounted in the payload bay and the presence of Orbiter interference lines below 500 Hz reduces the

apparent amplitude of the other emissions. Prior to FPEG turn-on the spectrum is broadband and low amplitude. When the FPEG begins pulsing narrowband emissions up to 30 kHz are observed with odd harmonics dominating. Notably absent is the effect of spin modulation which, of course, does not occur when the PDP is mounted in the payload bay.

Discussion.

The spectrograms shown in figures 4a-d provide an overview of the wave response to electron beam operation but are lacking in some respects. They do not, however, provide absolute amplitude information so the wave intensities from one sequence to another or even from one time within a sequence to another. This must come from the more detailed analysis in the next section. Also, the Pulsed flux tube connection and the Prox Ops sequences span seven antenna periods and the DC flux tube connection spans ten. Figure 4 provides only one antenna period from each of the three sequences and cannot show the time evolution for the duration of the sequences.

To quantify the analysis of radiation from the electron beam, the data was numerically processed to compensate for the effects of the AGC. This was done by using the telemetered values of the gain applied to the signal and the pre-flight calibration of the receiver system. To determine the accuracy of the AGC compensation procedure, the results were compared with the wave amplitudes from the IMP/HELIOS instrument, which measured wave field amplitudes with a filter bank which was not connected to the AGC. Agreement within a factor of two was found at times when the total wave amplitude changed slowly on the scale of the 1.6 s AGC data sample rate. (See Reeves, [1988] for a full explanation of the AGC compensation procedure.) It is important to note that, as result of the Fourier transforming of digitized data, 'amplitude', as used in this paper, means the amplitude of a 12 Hz Fourier spectral component. Although one could transform amplitude (in say, V/m) into spectral amplitude (in $V/m \cdot Hz^{1/2}$) this would be appropriate only for the broadband signals but would not apply to narrowband signals. Because some spectra contain both broadband and narrowband signals, all amplitudes in the VLF band are the amplitudes of the 12 Hz Fourier components.

The result of the AGC compensation procedure is that absolute wave amplitudes can be obtained. By averaging over time, the average wave spectra (amplitude as a function of frequency) for the sequences can be compared. This has been done for electric and magnetic wave fields for the three sequences and our results are presented in the following section. The long term variation from one antenna period to another can also be investigated by considering the amplitude in a selected frequency range as a function of time. Results from this analysis are presented for each of the three sequences in the final observation section.

Wave spectra from the three sequences

Using the technique, described above, composite spectra have been be created showing the cal-

ibrated wave response of the plasma to electron beam injection. Figure 6 shows the time averaged amplitude vs. frequency for the DC and Pulsed flux tube connections and for the Prox Ops sequence. In this paper we have used the convention that, where figures are to be compared with the spectrograms such as in figure 4, time is plotted on the horizontal axis and frequency is plotted on the vertical axis.

The spectra are complicated by some instrumental and processing effects which deserve consideration. The magnetic spectrum for the DC flux tube connection (figure 6a lower panel) shows these effects most clearly. The spectra are composites produced by adjoining the spectra from the 0-10, 10-20, and 20-30 kHz frequency ranges of the VLF band. They are not measured simultaneously and, for the flux tube connections, the PDP is moving with respect to the conjunction field line. Therefore there can be discontinuities at 10 and 20 kHz. There is also an effect due to the receiver filter sensitivity. In the 0-10 kHz range the filter function is fairly flat from .9 to nearly 10 kHz. From .9 down to .4 kHz there is some roll-off (as is verified by comparison with the ELF band data) and below .4 kHz the signal is dominated by spurious noise. The 10-20 and 20-30 kHz ranges were heterodyned down into the 0-10 kHz range and then re-scaled for display. As noted, the 10-20 kHz range was also inverted in frequency. Thus the 'lower end' of the filter response is seen near 20 kHz for both frequency ranges and is the explanation for the noise at those frequencies. In addition it is seen that the frequency response of the heterodyned signals is not as flat as it is for the 0-10 kHz frequency range although this effect is considerably reduced for the Prox Ops sequence, which measured more intense signals and was not spinning or moving in time.

There are also narrowband signals which are attributable to instrumental effects. Virtually all the narrowband emissions observed in the spectra for the DC flux tube connection are instrumental in origin. The most prominent of these is seen in the magnetic spectrum at 11.5 kHz which is likely to be from a source on the PDP. The slightly broader signal at 24.8 kHz is spin modulated and has an amplitude which varies with distance from the conjunction field line and hence is likely originate on the Orbiter. In addition there are small amplitude, narrowband signals which can be found at 1.1 or 2.2 kHz from the 'lower end' of the 10 kHz wide frequency bands. They are clearly instrumental and have not been investigated in detail. We can note that, when the PDP is mounted in the payload bay, there is a considerable magnetic, narrow band noise which complicates the appearance of the magnetic spectra. This is in contrast to the OSS-1 mission in which there was significant electric, narrowband noise but little magnetic interference [Shawhan *et al.*, 1984a; Reeves *et al.*, 1988]. The instrumental effects are also present, but not labeled, in the other spectra in figure 6.

The DC Flux Tube Connection.

The relevant orbital and instrumental parameters for this and the other two sequences are given in Table 1. The DC flux tube connection sequence took place at relatively high latitudes

during daytime with an ambient electron density of $\sim 10^5 \text{ cm}^{-3}$. Figure 6a shows the electric field measured at $\sim 50 \text{ m}$ from the conjunction field line and the magnetic field measured at $\sim 25 \text{ m}$ while the electron beam is operated in DC mode with a current of 50 mA. In the VLF range at these locations, broadband electric and magnetic emissions are generated by the beam. The electric field wave amplitudes fall in the range $10^{-8} - 10^{-6} \text{ V/m}$ and the magnetic amplitudes are between 2×10^{-7} and $2 \times 10^{-5} \text{ nT}$. The amplitude of the signals, at this distance, decreases with frequency, at a steady rate, up to the 30 kHz limit of the receiver. The ratio of $c\langle B \rangle / \langle E \rangle$ (where $\langle \rangle$ denotes time average) is of order 1 and is fairly constant with frequency.

The Pulsed Flux Tube Connection.

The spectra for two antenna periods during the Pulsed flux tube connection are shown in figure 6b. The electric and magnetic field measurements were made at perpendicular distances of approximately 35 and 70 m respectively. It is notable that the broadband signals from the 100 mA, 50% on-time, pulsed electron beam are comparable in amplitude to the 50 mA, 100% on-time, DC electron beam for both the electric and the magnetic fields and at all frequencies measured. The narrowband emissions are considerably stronger than the broadband emissions. Narrowband wave amplitudes lie between 5×10^{-8} and $5 \times 10^{-4} \text{ V/m}$ for the electric antenna and between 10^{-6} and 10^{-3} nT for the magnetic antenna. The amplitudes of the narrowband emissions generally decrease with frequency but show a greater variation than the broadband emissions. The narrowband emissions are more electromagnetic than the broadband emissions with $c\langle B \rangle / \langle E \rangle$ of order 10.

The Prox Ops Sequence.

During the Prox Ops sequence the electron beam was modulated at 1.22 kHz, 100 mA, 50% duty cycle and the PDP was mounted in the payload bay. The spectra are shown in figure 6c. We see that the broadband emissions again have $c\langle B \rangle / \langle E \rangle$ of order 1 and have a similar spectral shape to the broadband emissions from the DC and Pulsed flux tube connection sequences. However, the emissions are an order of magnitude stronger due to the proximity of the PDP to the FPEG (6.62 m). The narrowband emissions again show strong response at the pulsing frequency and its harmonics but $c\langle B \rangle / \langle E \rangle$ is only of order 1. Some of the variation of harmonic structure is seen by comparing the amplitudes of the even harmonics with those measured during the Pulsed flux tube connection. The magnetic field amplitudes are quite similar but the electric field amplitudes during the Prox Ops sequence are considerably enhanced. This is not simply a result of the PDP being in the payload bay since a variety of harmonic structures are observed with the PDP both mounted and free-flying.

The time-variation of wave amplitudes

Investigation of the long-term evolution of the wave amplitudes as a function of time were made. To do this, the data was processed to extract the average amplitude in the frequency band

1.7–1.8 kHz. The frequency range 1.7–1.8 kHz was chosen because it lies between harmonics of 1.22 kHz and contains only broadband emissions but is near enough in frequency to the 1.22 kHz fundamental frequency so a comparison of broadband and narrowband amplitudes can be made.

Data was extracted for all the antenna periods which measured the 0–10 kHz range during the DC and Pulsed flux tube connections. The average wave amplitude in the frequency range 1.7–1.8 kHz is shown as a function of time for the DC flux tube connection (figure 7) and for the Pulsed flux tube connection (figure 8).

The DC Flux Tube Connection.

The DC flux tube connection data starts at day 213, 03:28 GMT. At this time the Orbiter is on the Earth's day side. The PDP passes closest to the conjunction field line at approximately 03:34:01 and this is referred to as the 'flux tube connection'. The sequence ends at 03:39 still in daytime conditions. During both flux tube connection sequences, the electron beam is freely escaping and has a pitch angle given by the angle between the magnetic field line and a line connecting the Orbiter and the PDP. (See figure 1.) The electron beam emission began at 03:30:12. Before this time the PDP measured highly time varying ambient fields. As was the case for the Pulsed flux tube connection, the strongest emissions are due to natural whistlers and to the effects of the Orbiter thrusters. (See figure 4a.)

When the FPEG is turned on the measured fields become more structured with the second magnetic and third electric antenna periods showing the most clear spin modulation of the signals. The electric field amplitudes show less structure but the average field amplitudes are only slightly enhanced above the pre-gun-turn-on levels of about 10^{-6} V/m. The magnetic field amplitudes are also enhanced above background levels but still lie close to the range of 5×10^{-6} nT seen before FPEG turn-on to 5×10^{-5} nT after FPEG turn-off. While the FPEG is on, field amplitudes remain fairly constant with the exception of the fourth electric antenna period when intense electric fields are measured which saturate the Automatic Gain Control for nearly 10 s and then drop rapidly back down to the 10^{-6} V/m level. The strongest signal was measured when the PDP was at its closest approach to the conjunction field line. This distance has been calculated to be less than 5 m.

The Pulsed Flux Tube Connection.

The Pulsed flux tube connection data starts on day 213 at 04:04 GMT, lasts for 13 min, and takes place on the night side of the earth. For this sequence, the FPEG is off throughout the period of approach to the conjunction field line and is turned on when the PDP is near its closest approach, unfortunately while the wideband receiver is connected to the Langmuir probe, preventing the acquisition of wave data. The FPEG is then on for the remainder of the sequence while the PDP completes a trajectory very similar to that for the DC flux tube connection (figure 1). We see that

the ambient fields, measured with the FPEG off, are nearly 100 times weaker for the electric and 10 times weaker for the magnetic field measurements. As seen from the spectrograms in figure 4, the ambient fields, although slightly spin modulated, are dominated by natural whistlers and thruster wave effects as they were in the DC case. With the FPEG on we see enhanced electric and magnetic field amplitudes that drop off as the PDP moves away from the conjunction field line. The electric field amplitudes at about 100 m perpendicular distance from the beam are on the order of 10^{-6} V/m and the magnetic field amplitudes range from 10^{-6} to 10^{-5} nT. These values are very nearly the same as the amplitudes of broadband emissions in the DC case and, as we have seen, the amplitude of broadband emissions during the two flux tube connections tend to be the same for all frequencies in the 0-30 kHz range.

For the Pulsed flux tube connection we can also compare the dependence of field amplitude as a function of distance from the conjunction field line for narrowband as well as broadband emissions. This dependence is shown in figure 9a for the electric antenna and figure 9b for the magnetic antenna. The amplitude plotted is the amplitude averaged over the 26 s duration of the 0-10 kHz frequency range and the distance is the average distance during that period. The electric field amplitude of the narrowband emission at 1.22 kHz is five times stronger than the average broadband amplitude in the 1.7-1.9 kHz frequency range and the magnetic field amplitude at 1.22 kHz is fifteen times stronger than the broadband amplitudes. This ratio stays fairly constant and thus relatively independent of where the wave field is measured.

It should be noted that a comparison of broadband and narrowband emissions at higher harmonic frequencies shows different behavior because the harmonic structure of the narrowband emissions varies in time and/or distance. Figure 10 shows the harmonic structure at four distances for the electric antenna (a) and at three distances for the magnetic antenna (b). One interesting feature is that for greater distances from the conjunction field line, the electric field amplitudes of the second and third harmonics are larger than the amplitude of the fundamental. The magnetic field data does not display this behavior but instead shows the even harmonics (the 'forbidden' frequencies) at greatly reduced amplitudes for all distances. The unexpected strength of the second and third harmonic electric field amplitudes at large distances may be due to their proximity to the lower hybrid resonance frequency which is approximately 3.6 kHz for the conditions during the Pulsed flux tube connection.

The Prox Ops Sequence.

The Prox Ops sequence begins on day 212 in sunlight. The Orbiter velocity vector was directed toward the nose and slightly down (below the plane of the wings) so the payload bay was in light wake conditions. (See table 1.) At 18:31:42 the electron beam was turned on and the electric field broadband and narrowband amplitudes increased over previous background levels by roughly a factor of 10 and 100 respectively (figure 11). The amplitude of broadband and narrowband

emissions stays fairly constant up to 18:35:15 when the electron beam was determined to have hit the Orbiter starboard payload bay door. We observe that the amplitude of both the narrowband and the broadband electric emissions abruptly increase at this time while the magnetic field amplitudes do not. When the FPEG turns off at 18:36:52, the broadband signals are at their pre-sequence levels while the 1.22 kHz signals are an order of magnitude higher indicating that the Orbiter environment is still 'ringing' at the pulsing frequency. The spectra shown in figure 6c are from the earlier portion of the sequence when the electron beam was escaping. Spectra from the later portion of the sequence are considerably different with the 0-10 kHz, even and odd harmonics of comparable amplitude (figure 12).

4. DISCUSSION

Comparison with STS-3/OSS-1

The wave spectra from pulsed electron beam operations on Spacelab-2 were found to confirm and extend the results from the STS-3/OSS-1 mission [Reeves *et al.*, 1988]. Broadband electromagnetic emissions are produced by beam operations and narrowband emissions at the pulsing frequency and its harmonics are observed both during the free-flight and when the PDP was mounted in the payload bay (as it was for STS-3). The harmonic structure of narrowband emissions varies from one sequence to another. As in figure 4c, it is often observed that narrowband frequencies for which $\sin(\gamma\pi b/d) = 0$ (where γ is the harmonic number and b/d is the duty cycle) are not observed or are observed with significantly reduced amplitudes. For this reason, these frequencies are referred to as 'forbidden frequencies'. The presence of emissions at the forbidden frequencies is thought to reflect a loss of coherence of the square-wave structure of the current source, as will be discussed further below.

An important observation from STS-3/OSS-1 was the detection of 'satellite lines' and 'sub-harmonics'. Satellite lines were identified as narrowband emissions associated with the harmonics of the beam pulsing frequency. During the STS-3 mission, they were often observed in conjunction with harmonics particularly in the higher frequency ranges (20-30 kHz). The difference between the frequency of the harmonic and the satellite line (Δf) was found to be the same for each harmonic which had an associated satellite line, but Δf itself varied with time. Sub-harmonics are narrowband emissions observed well below the pulsing frequency, usually in the ELF band. It was found that the frequency of the sub-harmonics (f_{sub}) was equal to the difference in frequencies between the satellite lines and the harmonics ($f_{sub} = \Delta f$). (See figure 9 of Reeves *et al.* [1988].) Satellite lines and sub-harmonics have been observed on the Spacelab-2 mission during the Pulsed flux tube connection sequence. As with STS-3, it was observed that the satellite lines are more commonly associated with higher harmonics, that $f_{sub} = \Delta f$, and that f_{sub} and Δf vary in time. These observations are mentioned here for completeness. An analysis of the production of satellite lines and sub-harmonics will appear in a later publication.

The results from the STS-3/OSS-1 mission presented by Reeves et al. [1988] and preliminary observations from Spacelab-2 presented by Bush et al. [1987] were primarily qualitative observations of the characteristics of electron beam wave generation. The development of a technique for extracting wave amplitude from the broadband data has allowed for a more quantitative discussion for the results of Spacelab-2.

Broadband emissions from pulsed and DC electron beams

Figures 6, 7, and 8 reveal some basic information about the amplitude of broadband emissions generated by electron beams in space plasmas. It appears that DC and pulsed electron beams that deliver the same power into the plasma medium produce broadband emissions of comparable amplitude and comparable spectral shape when measured at similar locations with respect to the magnetic field line along which the electron beam propagates. The background fields during the DC flux tube connection were considerably stronger than the background fields during the Pulsed flux tube connection. When the FPEG is on, the measured field amplitudes range from saturated values at locations very near the conjunction field line to 10^{-6} V/m and 10^{-8} – 10^{-5} nT at larger distances from the conjunction field line. In the case of the DC flux tube connection, the amplitudes of beam generated electromagnetic fields at larger distances are of the same order as the background fields while for the Pulsed flux tube connection, the beam generated fields are above the background levels at all points of measurement. Although, as we would expect, the amplitude is a function of the frequency and the position at which the wave field is measured, we can make some general comments about broadband wave production by electron beams propagating along magnetic field lines in the ionosphere.

From figures 7 and 8 we identify three zones of wave amplitude. Zone 1 occurs very near the conjunction field line and is a narrow region of very intense wave activity. Zone 2 spans a somewhat wider region of space than zone 1 and is characterized by a very rapid decrease in amplitude with increasing distance from the conjunction field line. Zone 3 contains wave fields that are of significantly lower amplitude than those in zones 1 and 2 but often above the amplitude of ambient, background wave activity.

Zone 1 is a region of very disturbed plasma which exists in a region near the electron beam and in the wake of the beam. For the DC flux tube connection zone 1 extends approximately 20 m in diameter which is somewhat larger than the region in which the beam is expected to be propagating. It is characterized by a very turbulent plasma environment which makes measurement of temperature and density unreliable. As observed, it is also a region of intense wave activity which saturated the wideband receiver. These waves include the Cherenkov, resonance cone radiation which at higher frequencies produces the funnel-shaped emissions observed by Gurnett et al. [1986]. At frequencies below 30 kHz those waves propagate at less than 5° to the magnetic field and thus occupy a region of very small spatial extent.

The waves in zone 2 have been identified as produced by the Cherenkov resonance with wave normal angles less than the resonance cone angle [Reeves *et al.*, *this issue*]. Zone 2 can be defined by the region of propagation of this radiation. Although the free-flight of the PDP allowed sampling of the wave environment to distances of several hundred meters perpendicular to the conjunction field line it still lay within a distance which is less than or of the order of a perpendicular wavelength of radiation in this mode.

The emissions observed in zone 3 lie outside the region of propagation for Cherenkov radiation with wave normal angles less than the resonance cone angle. However, the enhanced amplitude of emissions observed in this region compared to ambient wave fields can be attributed to near-field radiation which is observable within a few perpendicular wavelengths of the conjunction field line. The reader is referred to the accompanying paper [Reeves *et al.*, *this issue*] for a more detailed theoretical analysis of the waves found in these zones.

Narrowband emissions

We have seen that the amplitudes of narrowband emissions produced by pulsed electron beams share some of the same characteristics as broadband emissions. The theory of Harker and Banks [1987] was developed to predict the electric field amplitudes of narrowband, near-field radiation from pulsed electron beams in space. Neubert and Harker [1988] extended this theory narrowband magnetic field amplitudes. A detailed comparison of the observed and predicted amplitudes of the narrowband radiation can be found in the accompanying paper [Reeves *et al.*, *this issue*]. There it is shown that the best agreement between observation and theory occurs for the predictions for Cherenkov radiation with wave normal angles less than the resonance cone angle. The predicted wave amplitudes for the conditions during the Pulsed flux tube connection sequence are presented in figure 13. The electric and magnetic field amplitudes are plotted vs. harmonic number for the distances at which measurements were made. Comparison of figures 13 and 10 show that the observed wave amplitudes for the odd harmonics are somewhat lower than those predicted by theory but are comparable in amplitude and spectral shape. The theory does not predict amplitudes for the even harmonics because of the assumption of perfect square-wave coherence.

The harmonic structure of narrowband emissions

The prediction that the even harmonics are 'forbidden' is specific to the case of an electron beam which is pulsed with a 50% duty cycle. In general, any harmonic for which the harmonic number times the duty cycle of the beam pulse is integral will be predicted to be forbidden. This is a result of the Fourier decomposition of the square wave shape of the electron beam current and is independent of the details of the calculation. We observe that the even harmonics have a substantially reduced magnetic component but that the electric component may have an amplitude which exceeds the amplitude of the odd harmonics (figures 6 and 10). The presence of narrowband harmonics at the forbidden frequencies is most likely due to a degradation in the coherence of the

beam making the assumption of a perfect square wave current source invalid. This possibility is supported by an analysis of the harmonic structure during the Prox Ops sequence.

During the Prox Ops sequence the PDP measures fields in the Orbiter payload bay 6.62 m from the FPEG aperture. Both the broadband and narrowband amplitudes are therefore higher than those measured during the free-flight at times other than the period of AGC saturation in zone 1. During the Prox Ops sequence the PDP is fixed in position. However, the relative orientations of the Orbiter with respect to the ambient magnetic field vector changes so that the Prox Ops sequence begins with the electron beam freely escaping the Orbiter bay but ends with the beam hitting the Orbiter. Using the measured values of the ambient magnetic field strength and direction and the nominal electron beam energy of 1 keV, the trajectory of the electrons can be calculated. This information was used with a three-dimensional computer model of the Orbiter and the instruments in the payload bay to determine that, as the magnetic field direction changed from 120° to 114° from the Orbiter z-axis, the electron beam hit the Orbiter on the starboard payload bay door approximately 4 m from the FPEG aperture. The calculations were done assuming each electron in the beam acts independently and follows the classical helical trajectory around the magnetic field. Observations of the electron beam hitting the tail of the Orbiter using the Low Light Level TV camera on the OSS-1 mission have shown that this is not the case. Rather, the electrons spread both along and across the magnetic field direction to form a hollow cylinder defined by the gyro-radius of the electrons and the magnetic field which will be referred to as the 'beam column' [Banks and Raitt, 1988]. This spreading takes place within a distance of several meters so the intersection of the beam column and the Orbiter surface is more likely an arc defined by the intersection of the beam column and the payload bay doors. The result of the change in the propagation of the electron beam away from the Orbiter is a change in the characteristics of radiation from the electron beam. The fact that electric field amplitudes increase when the electron beam hits the Orbiter while the magnetic field amplitudes do not (figure 11) suggests that the fields measured very close to the beam are near-field, incoherent emissions but that the current distribution still defines the spectral structure. The spectral structure of the narrowband emissions give some clues as to the radiating portion of the electron beam pulse. When the beam is freely escaping, the spatial distance between two 1.22 kHz pulses is 15 km in free space. When the beam hits the Orbiter its length is only several meters and the harmonic structure of the beam changes as is shown in figure 12. The even harmonics in the 0-10 kHz frequency range become comparable in amplitude to the odd harmonics because the square wave current structure is lost.

5. CONCLUSIONS

The VLF wave observations from the wideband wave receiver on Spacelab-2 confirm and extend the results of electron beam wave stimulation experiments on the STS-3/OSS-1 mission [Reeves et al., 1988]. It was found on both missions that a 1 keV electron beam injected from the

Space Shuttle Orbiter produced copious broadband electromagnetic emissions. When the electron beam was square-wave modulated, narrowband emissions at the pulsing frequency and harmonics of that frequency are observed to be produced along with the broadband emissions. The harmonic structure of the narrowband emissions was often consistent with the assumption of a square-wave current source but, at times, forbidden frequencies were observed indicating some loss of coherence in the square-wave structure. Satellite lines and sub-harmonics with $f_{sub} = \Delta f$ were observed during the Pulsed flux tube connection but the production of satellite lines does not appear to have been as common during the Spacelab-2 beam firings as during beam firings on the STS-3/OSS-1 mission.

The Spacelab-2 mission included a 6 hour free-flight of the PDP which allowed sampling of the wave environment out to several hundred meters from the Orbiter. In addition, a technique was developed wherein the broadband analog signal was digitized and the effects of the automatic gain control could be removed. This allowed the determination of absolute wave amplitudes. These two improvements allow more quantitative observations and more detailed analysis of the electron beam wave generation results than was possible for the STS-3 experiments.

It was found that the wave environment at distances of several hundred meters from the Orbiter when the FPEG was not firing was dominated by broadband natural atmospheric and Orbiter thruster-generated wave disturbances. Ambient wave fields can have amplitudes up to 10^{-6} V/m; 10^{-5} nT but the higher amplitude wave fields tend to be observed mainly in regions of higher ambient plasma density. The broadband ambient wave amplitudes may be spin modulated but are often more highly time varying. Narrowband, electrostatic, variable frequency emissions are also observed in the ambient wave environment.

During both DC and Pulsed electron beam operations, broadband electromagnetic radiation is produced throughout the 0-30 kHz range of the wideband receiver. The observations of wave amplitudes from the wideband receiver and the IMP/HELIOS filter bank indicate that this is radiation produced by the Cherenkov resonance. During the flux tube connections it is possible to observe the wave fields at various locations with respect to the conjunction field line. Three zones of wave activity were identified. Zone 1 occurs closest to the conjunction field line. It is characterized by a region of very turbulent plasma and by large amplitude waves with wave normal angles on the resonance cone ($\theta = \theta_{res}$). These waves saturate the wideband VLF wave receiver and are responsible for the funnel shaped emission identified by Gurnett et al. [1986]. Broadband VLF emissions in the range $100 < f < 30,000$ Hz are identified in Reeves et al. [this issue] as Cherenkov resonance waves with $\theta < \theta_{res}$. Zone 2 is defined by the region of propagation of those waves. Zone 3 contains near-field contributions to the wave environment which exist within a few perpendicular wavelengths from the conjunction field line. The amplitude of these emissions, in some cases, still exceeds the amplitude of waves in the ambient environment.

The amplitude of broadband emissions during the Pulsed flux tube connection sequence was

found to be approximately equal to those for the DC flux tube connection sequence when measured at similar positions with respect to the conjunction field line. This was true throughout the measured frequency range. These results indicate that 100 mA, 50% duty cycle, pulsed beams produce broadband emissions through the same mechanism as for 100 mA, DC beams.

In addition to broadband radiation, pulsed electron beams produce narrowband radiation at the pulsing frequency and its harmonics. Comparison of measured amplitudes with predictions using the theory of Harker and Banks [1987] for near-field, narrowband radiation from pulsed electron beams show good agreement for the $s = 0$, Cherenkov resonance solutions with wave normal angles less than the resonance cone angle ($\theta < \theta_{res}$). The observed waves generally have amplitudes less than those predicted by Harker and Banks but are less than a factor of 30 lower in amplitude than predicted. The observed harmonic structure is consistent with the predictions with the exception of the electric field measurements at distances greater than 100 m from the conjunction field line. For those measurements, the second and third harmonics, which have frequencies near the lower hybrid frequency, appear with slightly enhanced amplitudes. The observation that the broadband and narrowband amplitudes near the beam pulsing frequency have the same variation in amplitude with perpendicular distance to the conjunction field line is also consistent with the conclusion that both are produced through $s = 0$, Cherenkov resonance with $\theta < \theta_{res}$.

The presence of emissions at the forbidden frequencies is not predicted by theory but appears to be the result of loss, or partial loss, of the coherence of the square-wave structure of the current source. In the case of a 50% duty cycle beam pulsing, the even harmonics are forbidden. Observations during the Prox Ops sequence show that, when the beam is freely escaping, the amplitude of the forbidden, even harmonics is as much as two orders of magnitude lower than the odd harmonics. As the inclination of the earth's magnetic field with respect to the Orbiter changed during the Prox Ops sequence, the electron beam hit the Orbiter payload bay doors instead of escaping. At this time the wave amplitudes measured in the payload bay increased and the harmonic structure changed such that forbidden, even harmonics appeared with amplitudes equal to the amplitude of the odd harmonics. It is believed that this is the result of the inability of the beam to maintain square-wave structure. In general it is found that observations of the magnetic field components at the forbidden frequencies are in better agreement with theory and that the harmonics at forbidden frequencies are more electrostatic than the other harmonics.

REFERENCES

- Akai, K., Electron beam-plasma interaction experiment in space, ISAS Res. Note 285, Inst. of Space and Astronaut. Sci., Tokyo, 1984.
- Banks, P.M., W.J. Raitt, A.B. White, R.I. Bush, and P.R. Williamson, Preliminary results from the Vehicle Charging and Potential experiment on STS 3, *J. Spacecr. Rockets*, 24, 1987. Banks, P.M. and W.J. Raitt, Observations of electron beam structure in space experiments, *J. Geophys. Res.*, submitted 1988.
- Banks, P.M., W.J. Raitt, P.R. Williamson, T. Neubert, R.I. Bush, J.G. Hawkins, G.R. Reeves, and B. White, Results of vehicle charging, plasma densities, and wave generation experiments on Spacelab-2., *J. Spacecr. Rockets*, to be submitted, 1988.
- Beghin, C., J.P. Lebreton, B.N. Maehlum, J. Troim, P. Ingsoy, and J.L. Michau, Phenomena induced by charged particle beams., *Science*, 225, 1984.
- Blitza, D., International reference ionosphere: recent developments., *Radio Science*, 21, 1986.
- Bush, R.I., G.D. Reeves, P.M. Banks, T. Neubert, P.R. Williamson, W.J. Raitt, and D.A. Gurnett, Electromagnetic fields from pulsed electron beam experiments in space: Spacelab-2 results., *Geophys. Res. Lett.*, 14, 10, 1015, 1987.
- Cai, D., T. Neubert, L.R.O. Storey, P.M. Banks, S. Sasaki, K. Abe, and J.L. Burch, ELF oscillations associated with electron beam injections from the space shuttle., *J. Geophys. Res.*, 92, 1987.
- Farrell, W.M., D.A. Gurnett, P.M. Banks, R.I. Bush, and W.J. Raitt, An analysis of the whistler-mode radiation from the Spacelab-2 electron beam., *J. Geophys. Res.*, 93, 153, 1988.
- Gendrin, R., The French-Soviet ARAKS experiment, *Space Sci. Rev.*, 15, 905, 1974.
- Gurnett, D.A., W.S. Kurth, J.T. Steinberg, P.M. Banks, R.I. Bush, and W.J. Raitt, Whistler-mode radiation from the Spacelab-2 electron beam, *Geophys. Res. Lett.*, 13, 225, 1986.
- Harker, K.J., and P.M. Banks, Near fields in the vicinity of pulsed electron beams in space, *Planet. Space Sci.*, 35, 1, 1987.
- Hawkins, J.G., Vehicle charging and return current measurements during electron beam emission experiments from the Shuttle Orbiter., PhD dissertation, Stanford University, 1988.
- Hayakawa, M., Y. Tanaka, K. Ohta, and J. Okuda, Absolute intensity of daytime whistlers at low and middle latitudes and its latitudinal variation., *J. Geophysics*, 59, 1986.
- Helliwell, R.A., *Whistlers and Related Atmospheric Phenomena*, Stanford University Press, Stanford CA, 1965.
- Hess, W.N., Generation of artificial aurora, *Science*, 164, 1512, 1969.
- Holzworth, R.H., and H.C. Koons, VLF Emissions from a modulated electron beam in the auroral ionosphere., *J. Geophys. Res.*, 86, 853, 1981.
- Maehlum, B.N., K. Maseide, K. Aarsnes, A. Egeland, B. Grandal, J. Holtet, T.A. Jacobsen, N.C. Maynards, F. Soraas, J. Stadsnes, E.V. Thrane, and J. Troim, Polar 5-An electron accelerator experiment within an aurora, 1-4, *Planet. Space Sci.*, 28, 259, 1980.
- Melzner, F., G. Metzner, and D. Antrack, The GEOS electron beam experiment S 329, *Space Sci. Instrum.*, 4, 45, 1978.
- Myers, N.B., W.J. Raitt, A.B. White, P.R. Williamson, P.M. Banks, R.I. Bush, S. Sasaki, K-I. Oyama, N.

- Kawshima, CHARGE-2: A sounding rocket payload to investigate vehicle charging effects due to electron beam emissions., *J. Spacecr. Rockets.*, submitted 1988.
- Neubert, T., W.W.L. Taylor, L.R.O. Storey, N. Kawashima, W.T. Roberts, D.L. Reasoner, P.M. Banks, D.A. Gurnett, R.L. Williams, and J. Burch, Waves generated during electron beam emissions from the space shuttle., *J. Geophys. Res.*, 91, 11,321 1986a.
- Neubert, T., G. Holmgren, E. Ungstrup, and K. Melgard, Waves with harmonic structure below and above the lower hybrid resonance observed on the CENTAUR 35.001 and 35.002 rockets., *Can. J. Phys.*, 64, 1986b.
- Neubert, T. and K.J. Harker, Magnetic fields in the vicinity of pulsed electron beams in space., *Planet. Space Sci.*, in press, 1988.
- Neubert, T., J. G. Hawkins, G.D. Reeves, P.M. Banks, R.I. Bush, P.R. Williamson, D.A. Gurnett, and W.J. Raitt, Pulsed electron beam emissions in space, *J. Geomag. Geoelectr.*, in press, 1988.
- Obayashi, T., N. Kawashima, K. Kuriki, N. Nagatomo, K. Ninomiya, S. Sasaki, A. Ushirokawa, I. Kudo, M. Ejiri, W.T. Roberts, R. Chappell, J. Burch, and P.M. Banks, Space experiments with particle accelerators (SEPAC), in *Artificial Particle Beams in Space Plasma Studies*, edited by B. Grandal, p. 659, Plenum, New York, 1982.
- Reeves, G.D., P.M. Banks, A.C. Fraser-Smith, T. Neubert, R.I. Bush, D.A. Gurnett, and W.J. Raitt, VLF Wave stimulation by pulsed electron beams injected from the space shuttle., *J. Geophys. Res.*, 93, 162, 1988.
- Reeves, G.D., Very low frequency radio waves produced by electron beam injection in space plasmas., PhD dissertation in preparation, Stanford University, 1988.
- Reeves, G.D., P.M. Banks, T. Neubert, and K.J. Harker, VLF Wave emissions by pulsed and DC electron beams in space 2: Analysis of Spacelab-2 results., *J. Geophys. Res.*, *this issue*.
- Sasaki, S., K-I. Oyama, N. Kawashima, W.J. Raitt, and N.B. Myers, VLF and HF Wave characteristics observed from an active experiment tethered mother/daughter rocket payload (CHARGE-2), *EOS*, 67, 1170, 1986a.
- Sasaki, S., N. Kawashima, K. Kuriki, M. Yanagisawa, and T. Obayashi, Vehicle charging observed in SEPAC Spacelab-1 experiment., *J. Spacecr. Rockets*, 23, 194, 1986b.
- Shawhan, S.D., G.B. Murphy, and J.S. Pickett, Plasma Diagnostics Package initial assessment of the STS 3 orbiter plasma environment, *J. Spacecr. Rockets*, 21, 387, 1984a.
- Shawhan, S.D., G.B. Murphy, P.M. Banks, P.R. Williamson, and W.J. Raitt, Wave emissions from DC and modulated electron beams on STS-3., *Radio Sci.*, 19, 2, 471, 1984b.
- Tribble, A.C., N. D'Angelo, G.B. Murphy, J.S. Pickett, and J.T. Steinberg, Exposed high-voltage source effect on the potential of an ionospheric satellite., *J. Spacecr. Rockets*, submitted, 1988.
- Winckler, J.R., The application of artificial electron beams to magnetospheric research, *Rev. Geophys.*, 19, 3, 659, 1980.
- Winckler, J.R., J.E. Steffen, P.R. Malcolm, K.N. Erickson, Y. Abe, and R.L. Swanson, Ion resonances and ELF wave production by an electron beam injected into the ionosphere: Echo 6, *J. Geophys. Res.*, 89, 7565, 1984.
- Winckler, J.R., K.E. Erickson, Y. Abe, J.E. Steffen, and P.R. Malcolm, ELF Wave production by an electron

beam emitting rocket system and its suppression on auroral field lines, Geophys. Res. Lett., 12, 457, 1985.

6. FIGURE CAPTIONS

Table 1. Instrumental and orbital parameters for the Spacelab-2 mission which are relevant to the DC and Pulsed flux tube connections and the Prox Ops sequences. Orbital parameters are from the best estimated trajectory tables for Spacelab-2. Characteristic frequencies are calculated for the measured or estimated magnetic field strengths and electron densities. For the Prox Ops sequence, the electron density was taken to be one third of that predicted by the International Reference Ionosphere model [Blitza, 1986] based on comparison of measured and predicted densities for the other two sequences.

Figure 1. The trajectory of the PDP for two flux tube connections. The Orbiter is at the origin and parallel and perpendicular refer to the conjunction field line connected to the Orbiter. The trajectories for the DC and the Pulsed flux tube connections are shown. Sequence start and stop times are noted and one point is plotted for every 30 s.

Figure 2. The position of the FPEG, the PDP, the CCP, and other instruments mounted in the payload bay on Spacelab-2. The orbiter coordinate system is also indicated in the figure.

Figure 3. The antenna switching pattern. One antenna switching cycle consists of 8 'antenna periods' which alternate between electric and magnetic antennas with the final magnetic antenna period being replaced by a Langmuir probe period. Both the ELF and VLF bands are subject to the same, synchronized, switching pattern. In addition, the VLF band is subjected to a frequency switching pattern. In both the electric and magnetic antenna periods, 0- 10 kHz is measured for half a period and 20-10 kHz (inverted) and 20-30 kHz are measured for a quarter period.

Figure 4. Spectrograms of four antenna periods during the Spacelab-2 mission. The antenna switching pattern is superimposed on the data so the first 26 s are 0-10 kHz, the next 13 s are 10-20 kHz (with 10 kHz at the top) and the final 13 s are 20-30 kHz. The AGC modulation of the amplitudes has not been removed so amplitudes are relative. (a) An antenna period from the Pulsed flux tube connection sequence before FPEG turn-on. The ambient wave field includes natural atmospheric, including whistlers; Orbiter thruster-generated waves; and narrowband, variable frequency emissions. (b) An antenna period from the DC flux tube connection sequence. The FPEG is operating in DC mode with a 50 mA beam current. Broadband beam-generated emissions are observed and the amplitude if these emissions are modulated by the spin of the PDP. (c) An antenna period from the Pulsed flux tube connection when the FPEG is pulsing with a 100 mA beam current and a 50% duty cycle at 1.22 kHz. Narrowband harmonics and broadband emissions are observed and are spin modulated. (d) An antenna period from the Prox Ops sequence when the PDP is in the payload bay and the FPEG is pulsing at 1.22 kHz, 100 mA, 50% duty cycle. Strong narrowband harmonics are seen beginning 19 s into the antenna period when the FPEG is turned on.

Figure 5. The amplitude of the 1.22 kHz narrowband emission observed with the magnetic field

search coil plotted as a function of time. Spin modulation of the amplitude due to the rotation of the PDP is observed and may be compared with the function $\sin^2(\omega t)$. A transient disturbance due to the operation of the orbiter thrusters is also observed.

Figure 6. The 0-30 kHz wave spectra for (a) the DC flux tube connection, (b) the Pulsed flux tube connection, and (c) the Prox Ops sequence. The upper plots in each figure show the electric field amplitude (in V/m) vs. frequency. The lower plots show magnetic field amplitude (in nT) vs. frequency. To facilitate comparison with the spectrograms of figure 4, frequency is plotted on the vertical axis.

Figure 7. The amplitude of electric (top) and magnetic (bottom) field components in the frequency range 1.7-1.9 kHz as a function of time for the DC flux tube connection sequence. The trajectory of the PDP is shown in figure 1. Three zones of beam-generated wave emissions and the region of ambient wave fields may be identified with various amplitudes. Gaps in the wave data are times when the wave receiver is observing waves in the 10-30 kHz frequency range.

Figure 8. The amplitude of electric (top) and magnetic (bottom) field components in the frequency range 1.7-1.9 kHz as a function of time for the Pulsed flux tube connection sequence. The trajectory of the PDP is shown in figure 1. At the time of closest approach to the conjunction field line the FPEG is turned on. The wave receiver was connected to the Langmuir probe at this time and there is an additional gap in the wave data.

Figure 9. A comparison of narrowband and broadband field strengths as a function of perpendicular distance to the conjunction field line during the Pulsed flux tube connection as measured by the (a) electric dipole antenna and (b) the magnetic search coil antenna. The ratio of amplitudes is observed to be a fairly constant function of distance from the conjunction field line.

Figure 10. The measured (a) electric (b) and magnetic field harmonic structure during the Pulsed flux tube connection at various distances from the conjunction field line. For distances greater than 100 m the electric field amplitudes of the second and third harmonics are observed to be slightly enhanced. For the magnetic field measurements the even, forbidden harmonics are plotted with dashed lines and are observed to be of significantly lower amplitude than the odd harmonics.

Figure 11. The time-variation of the electric and magnetic field amplitudes during the Prox Ops sequence showing the increase in electric field strength when the beam is turned on and the further increase when the electron beam hits the Orbiter instead of propagating away from the Orbiter. The amplitude of the 1.22 kHz emission observed with the magnetic antenna does not increase when the beam hits the orbiter.

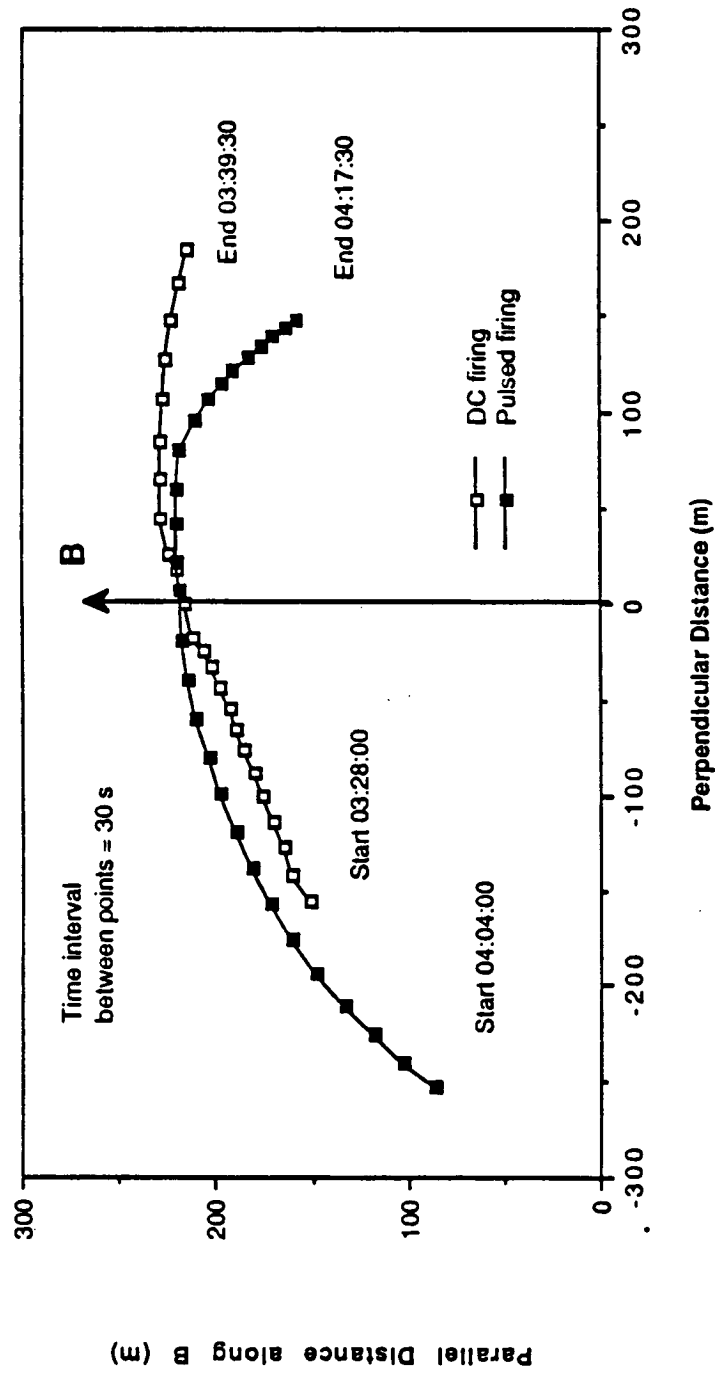
Figure 12. A comparison of the amplitudes of narrowband harmonics of the 1.22 kHz pulsing frequency during the Prox Ops sequence. When the beam is freely escaping from the Orbiter, the even 'forbidden' harmonics appear with significantly reduced amplitude compared to the odd

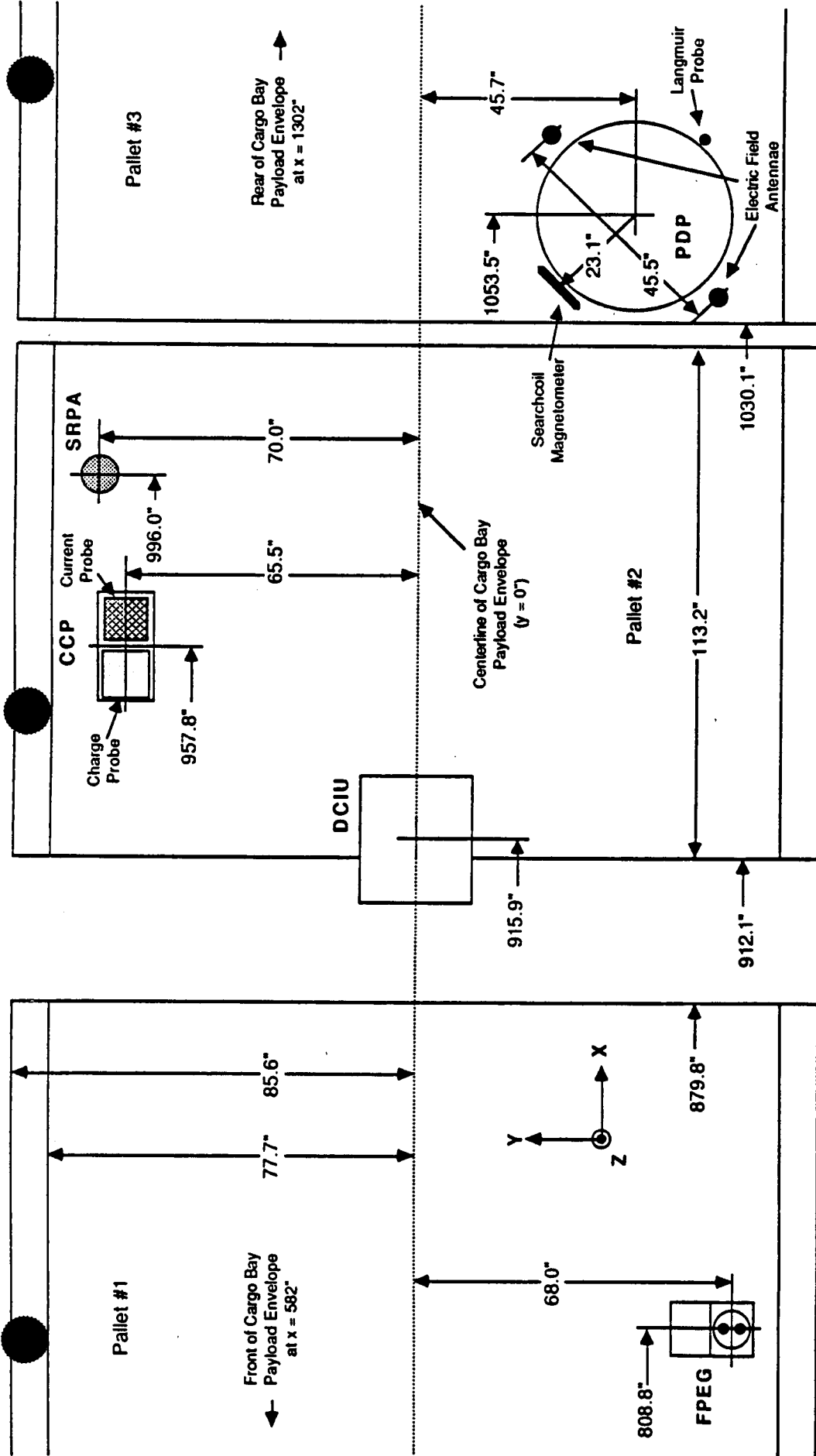
harmonics. When the beam hits the Orbiter, its square-wave current structure is lost and the even harmonics appear with amplitudes which are comparable to the amplitudes of the odd harmonics.

Figure 13. The (a) electric and (b) magnetic field amplitudes predicted using the theory of Harker and Banks [1987]. Plots show the predicted amplitude for the $s = 0$, Cherenkov resonance with $\theta < \theta_{res}$ as a function of harmonic number. The measured magnetic field strength, electron density, and pitch angle appropriate for the Pulsed flux tube connection were used for the calculation. Comparison with the measured amplitudes (figure 10) show fairly good agreement.

Table 1			
Instrumental or Orbital Parameters	DC Flux Tube Connection	Pulsed Flux Tube Connection	Prox Ops Sequence
beam energy	1 keV	1 keV	1 keV
beam current	50 mA	100 mA	100 mA
duty cycle	100%	50%	50%
location of PDP	free-flight	free-flight	payload bay 6.62 m from FPEG
sequence start time	213/03:28	213/04:04	212/18:31
sequence stop time	213/03:39	213/04:17	212/18:39
FPEG turn-on	213/03:30:12	213/04:11:13	212/18:31:42
FPEG turn-off	213/03:37:22	213/04:18:23	212/18:38:52
altitude of the Orbiter	325 km	321 km	327 km
start latitude	28°	3°	48°
stop latitude	54°	-38°	48°
start longitude	15°	1°	14°
stop longitude	18°	4°	27°
day/night	day	night	day
measured electron density	$1 \times 10^5 \text{ cm}^{-3}$	$3 \times 10^4 \text{ cm}^{-3}$	unavailable
IRI predicted electron density	$3.5 \times 10^5 \text{ cm}^{-3}$	$8.1 \times 10^4 \text{ cm}^{-3}$	$6.5 \times 10^5 \text{ cm}^{-3}$
magnetic field strength †	.407 G	.225 G	.476 G
magnetic field azimuth †	356°	14°	99°
magnetic field elevation †	≈ 0°	≈ 0°	115°
shuttle velocity	7.7 km/s	7.7 km/s	7.7 km/s
velocity azimuth †	354°	166°	354°
velocity elevation †	75°	126°	118°
f_{pe} †	2.8 MHz	1.6 MHz	4.0 MHz
f_{ce}	1.1 MHz	.63 MHz	1.3 MHz
$f_{ci}(O^+)$	38.8 Hz	21.5 Hz	45.4 Hz
$f_{ci}(H^+)$	611 Hz	344 Hz	727 Hz
f_{LHR} †	6.6 kHz	3.6 kHz	8.4 kHz
† values are for the time of closest approach to the conjunction field line † calculated using 2% H^+ and measured electron densities for the DC and Pulsed flux tube connections and $n_e = \frac{1}{3} 6.5 \times 10^5 \text{ cm}^{-3}$ for the Prox Ops sequence.			

Trajectory of the PDP during the Flux Tube Connections

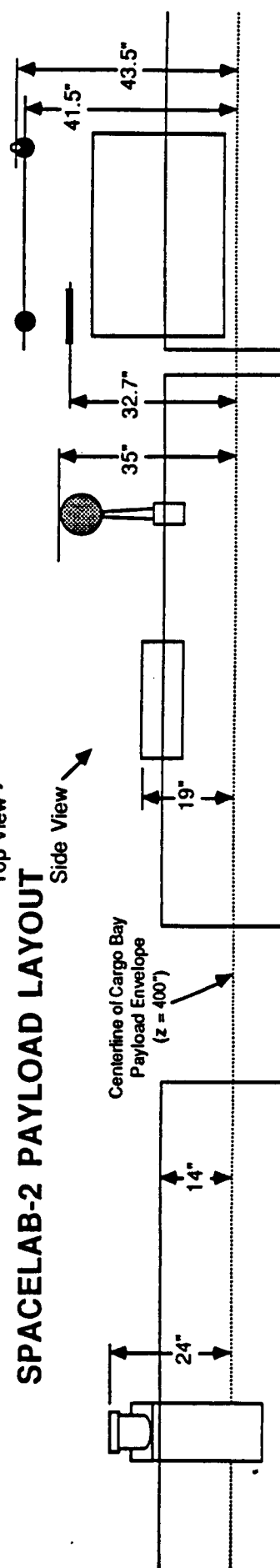


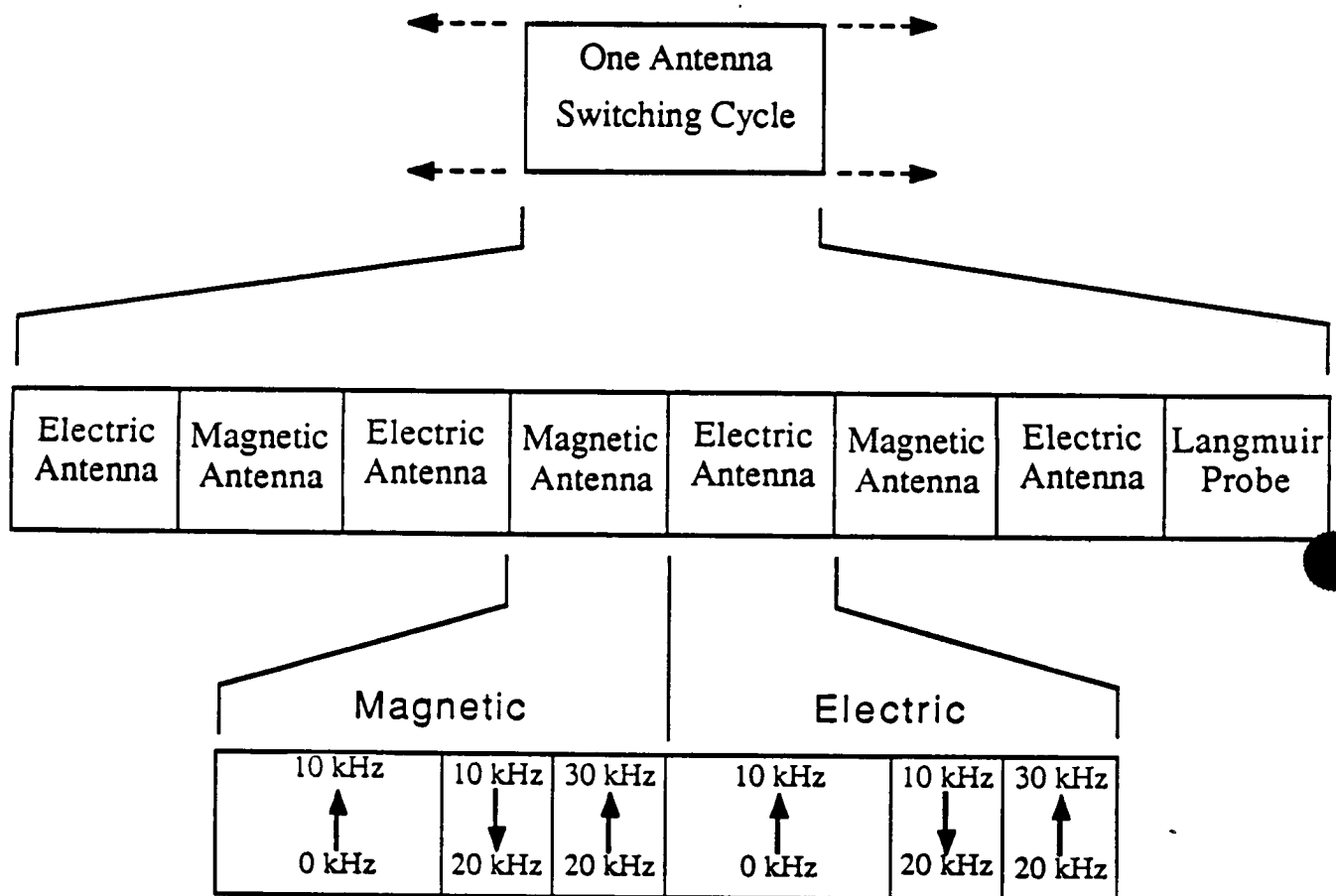


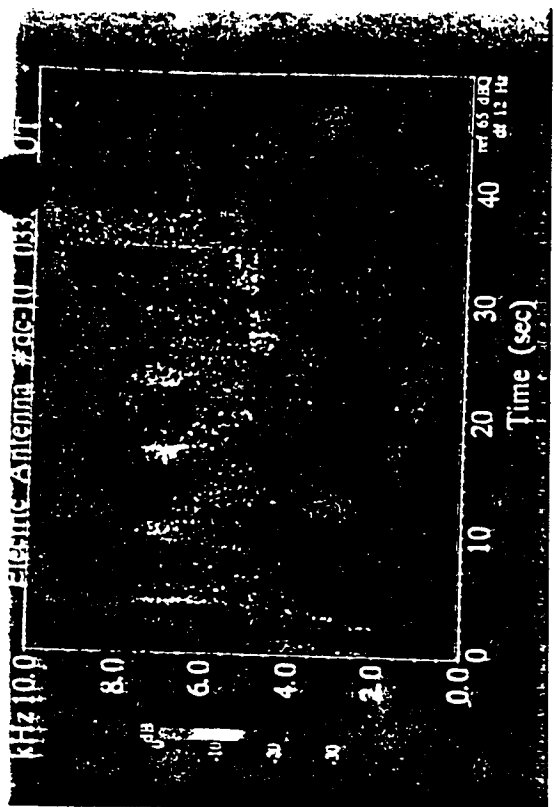
SPACELAB-2 PAYLOAD LAYOUT

Top View

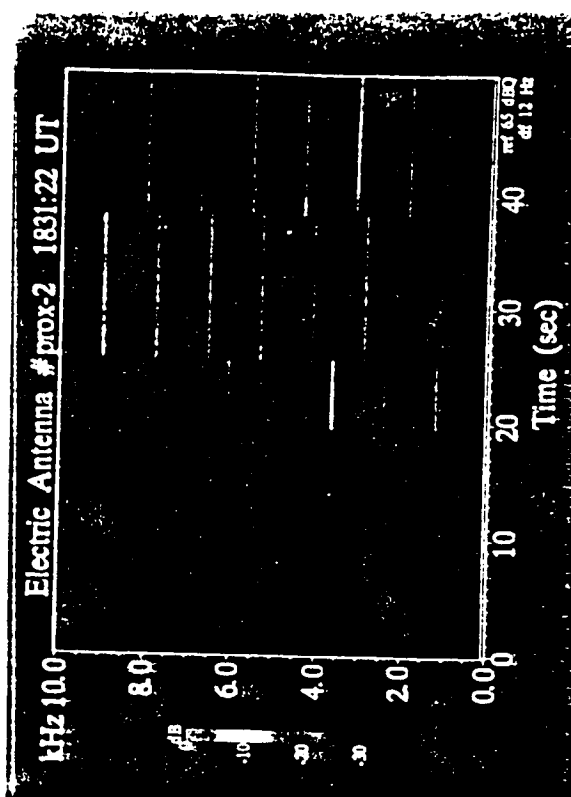
Side View



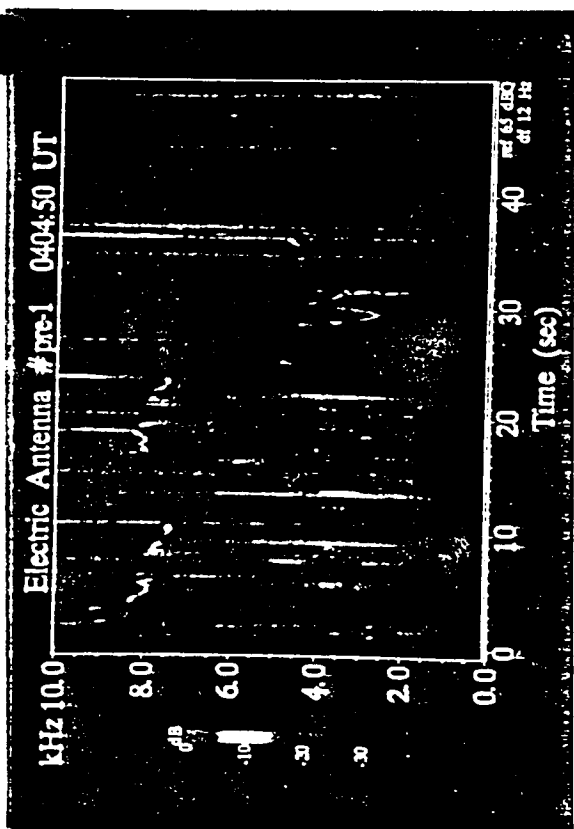




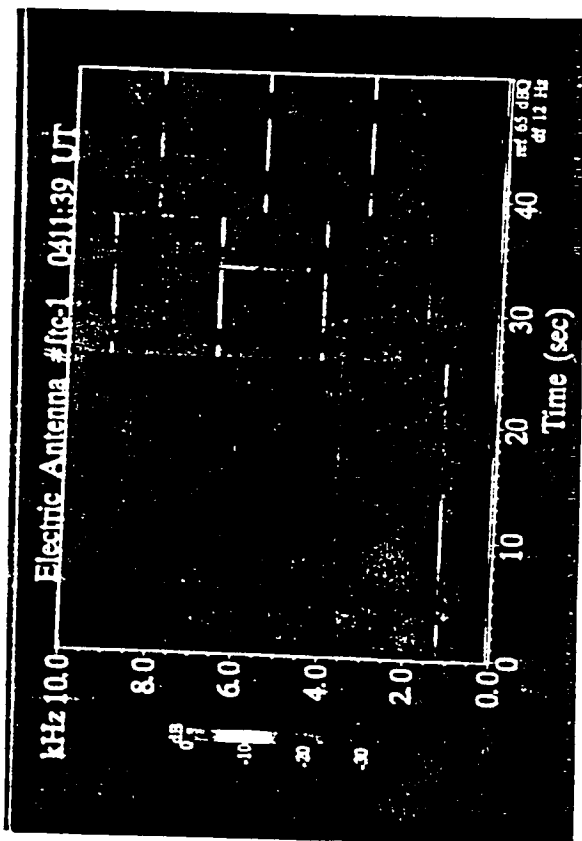
b



d

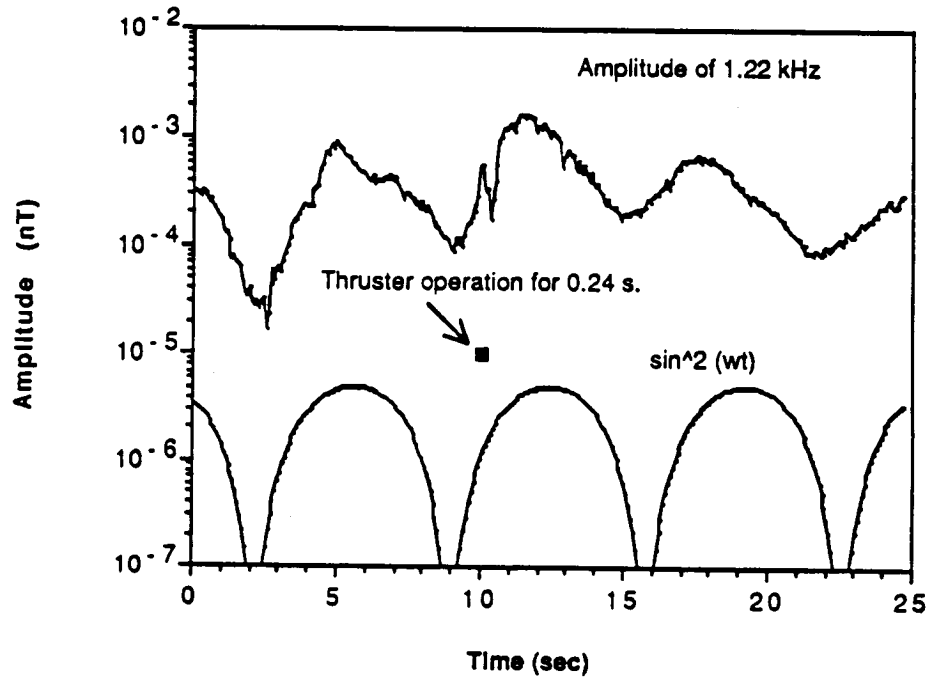


c



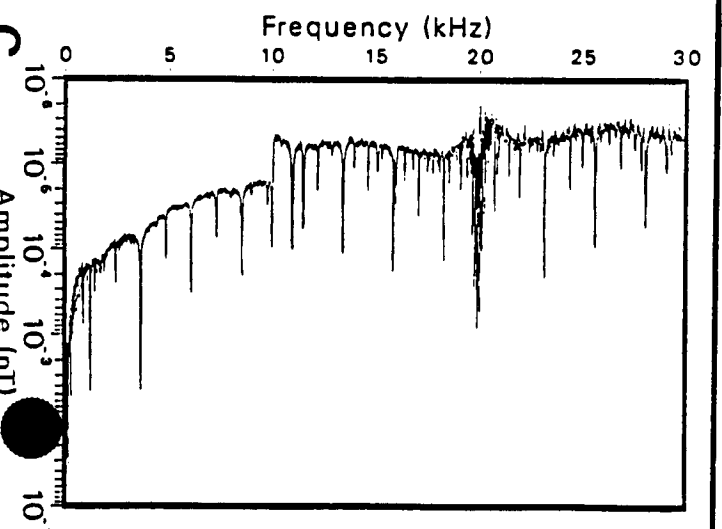
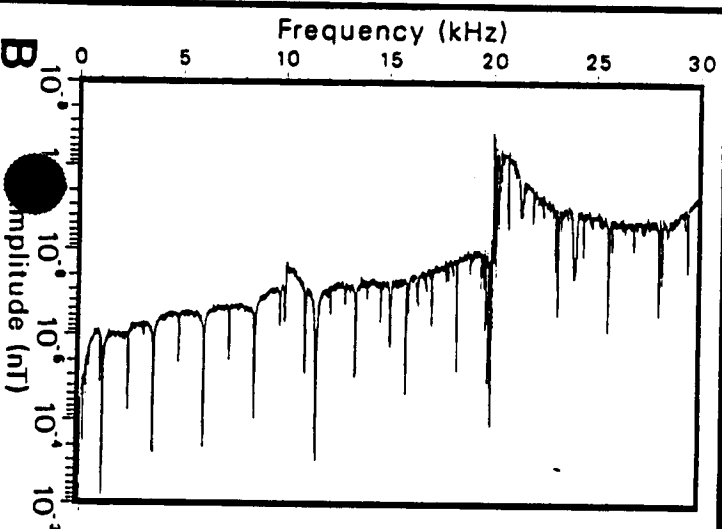
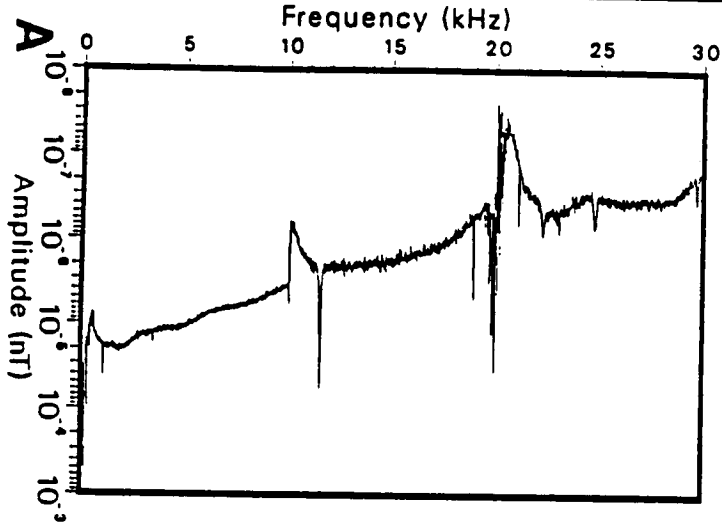
e

Spin Modulation of the Magnetic Amplitude of the 1.22 kHz Narrowband Emissions

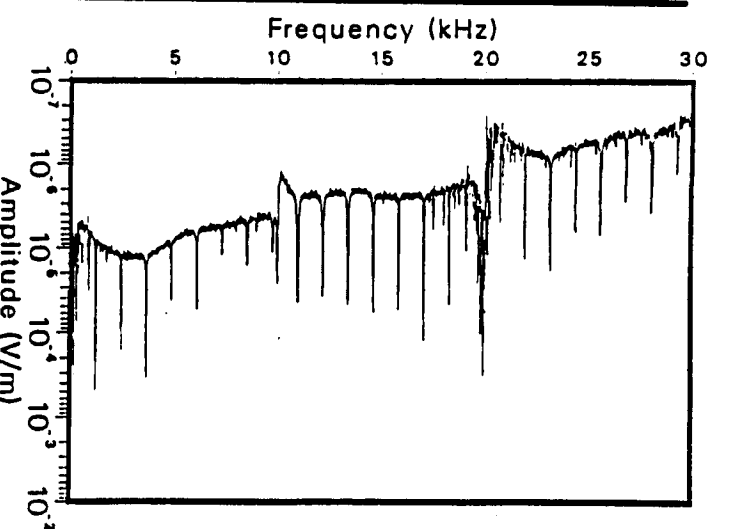
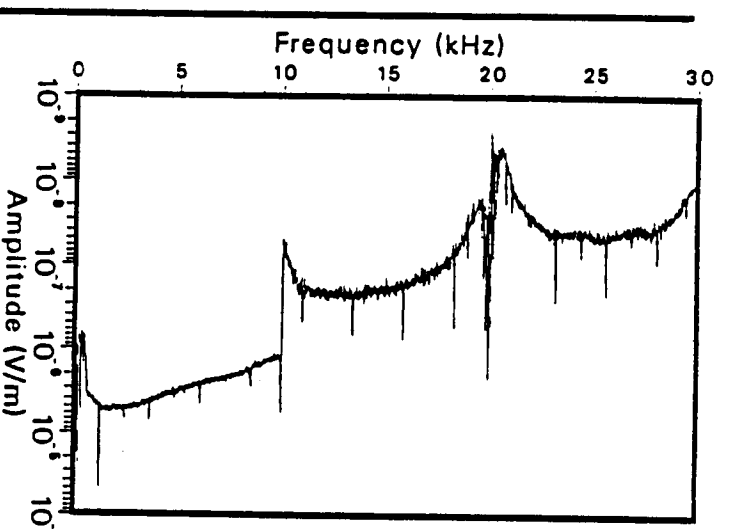
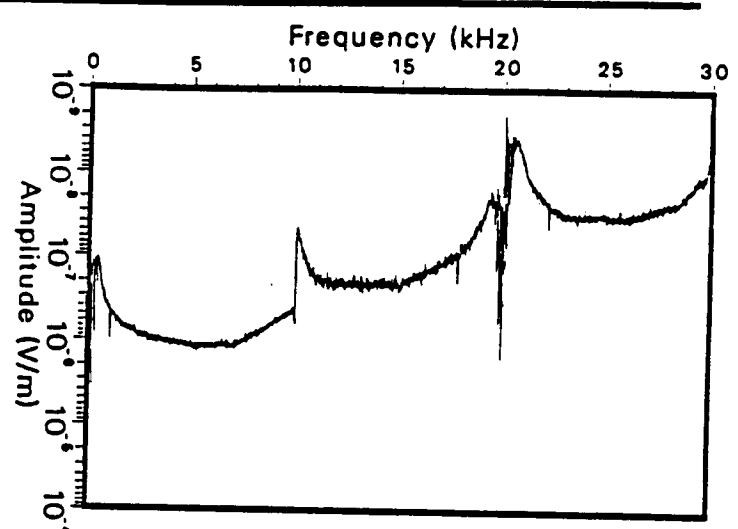




Magnetic Spectra

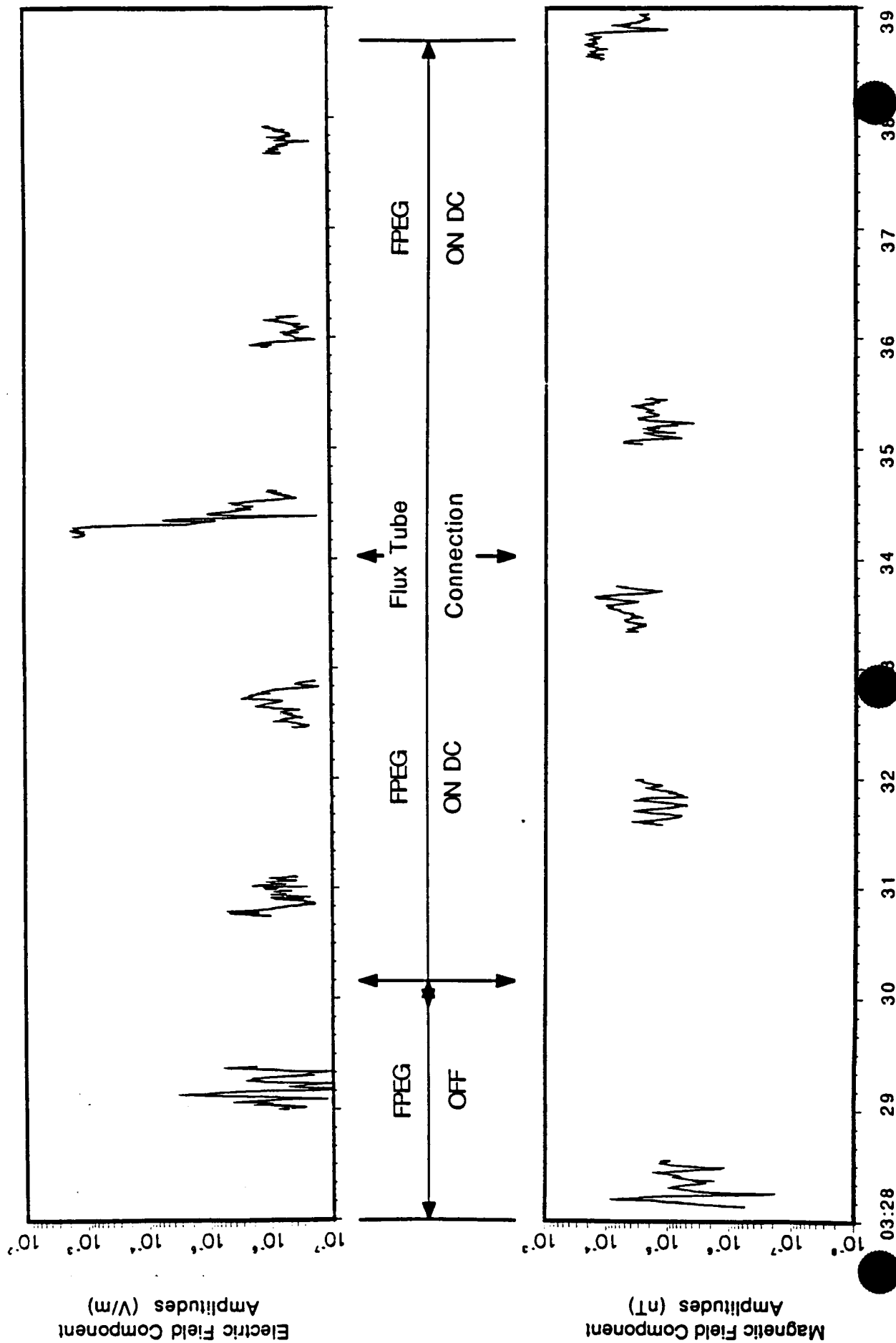


Electric Spectra



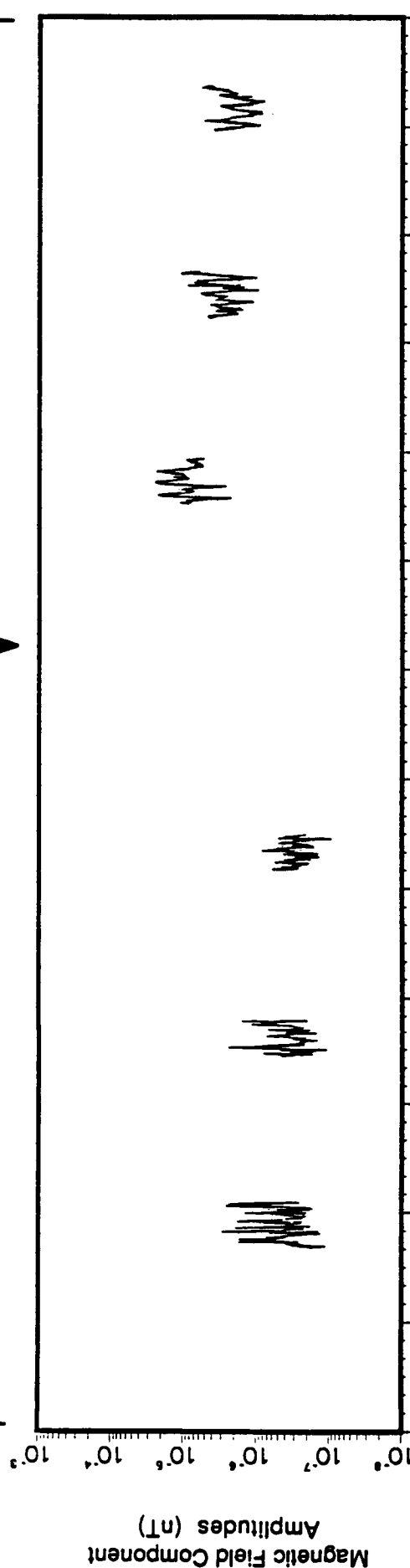
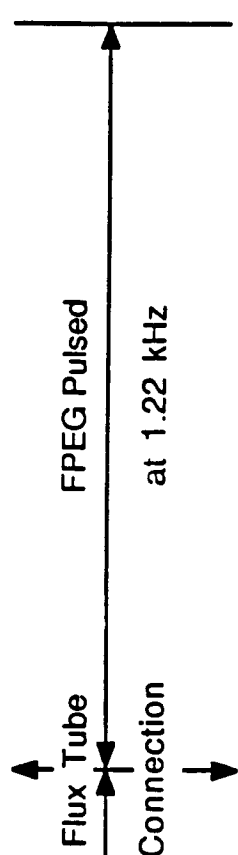
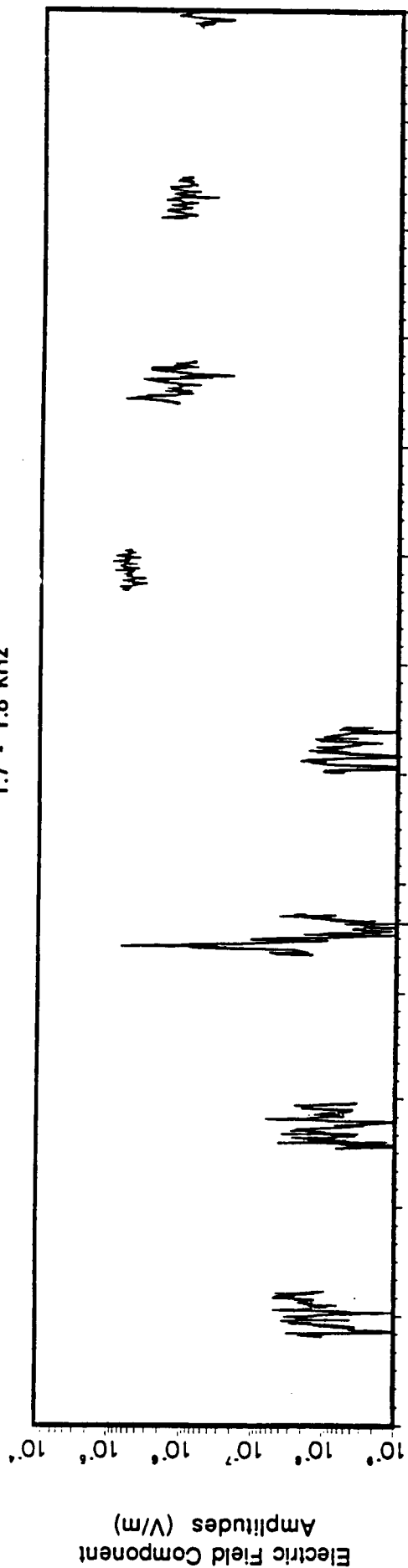
Field Amplitudes during the DC Flux Tube Connection

1.7 - 1.8 kHz

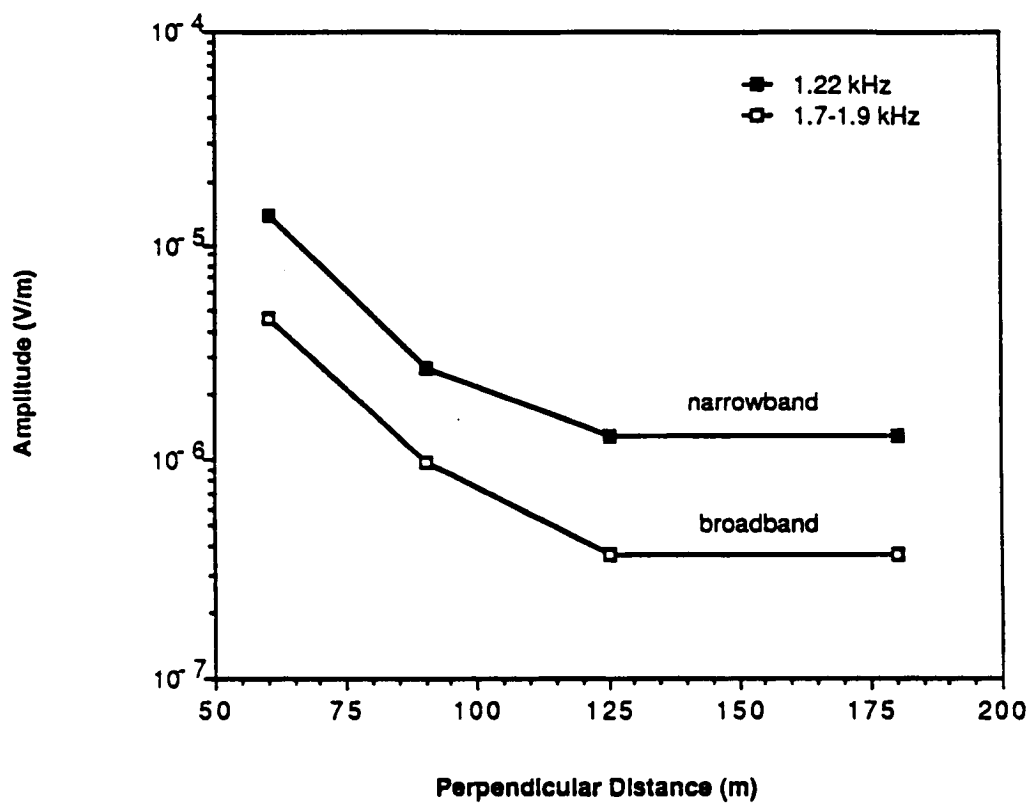


Field Amplitudes during the Pulsed Beam Flux Tube Connection

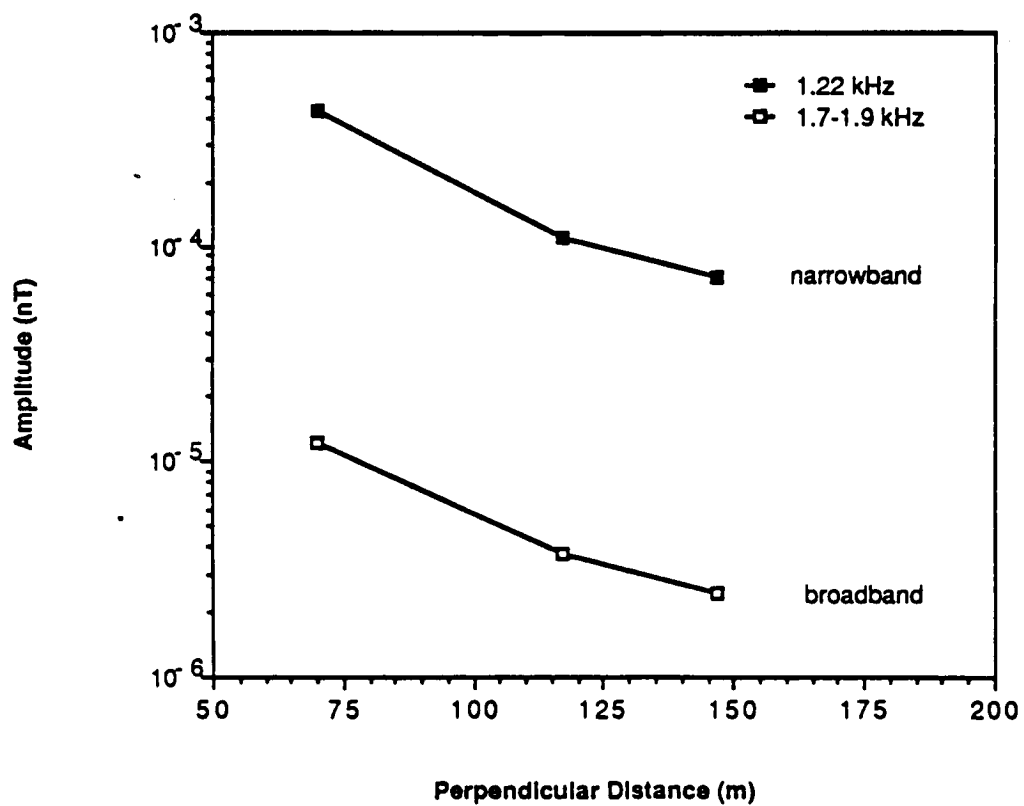
1.7 - 1.8 kHz



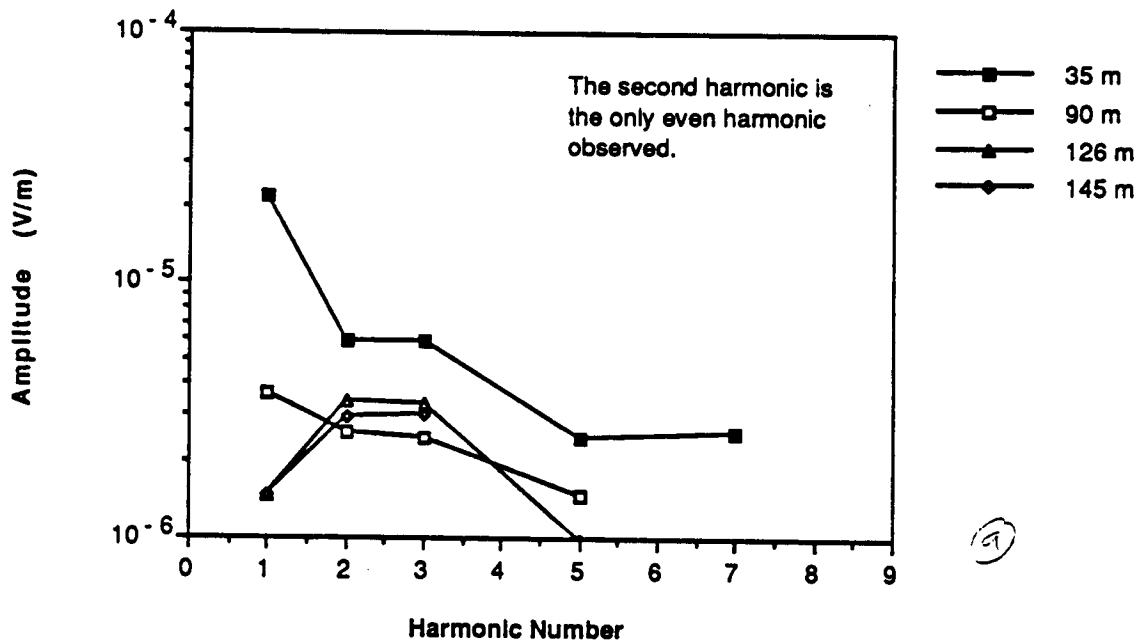
Electric Field Amplitudes



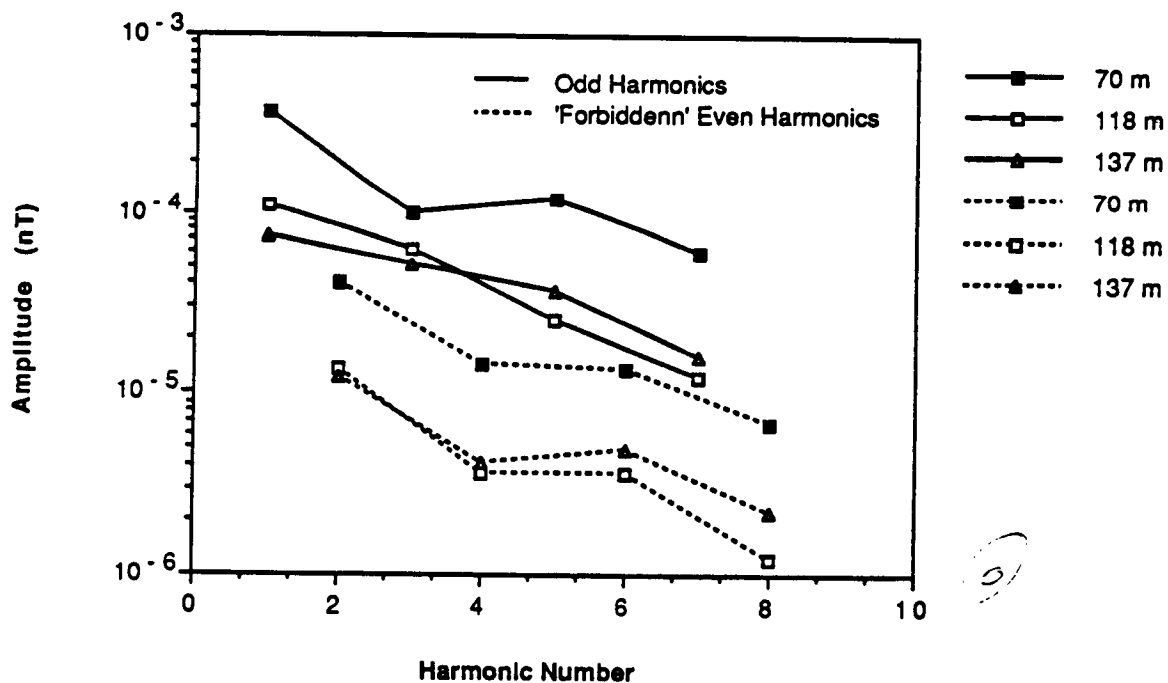
Magnetic Field Amplitudes



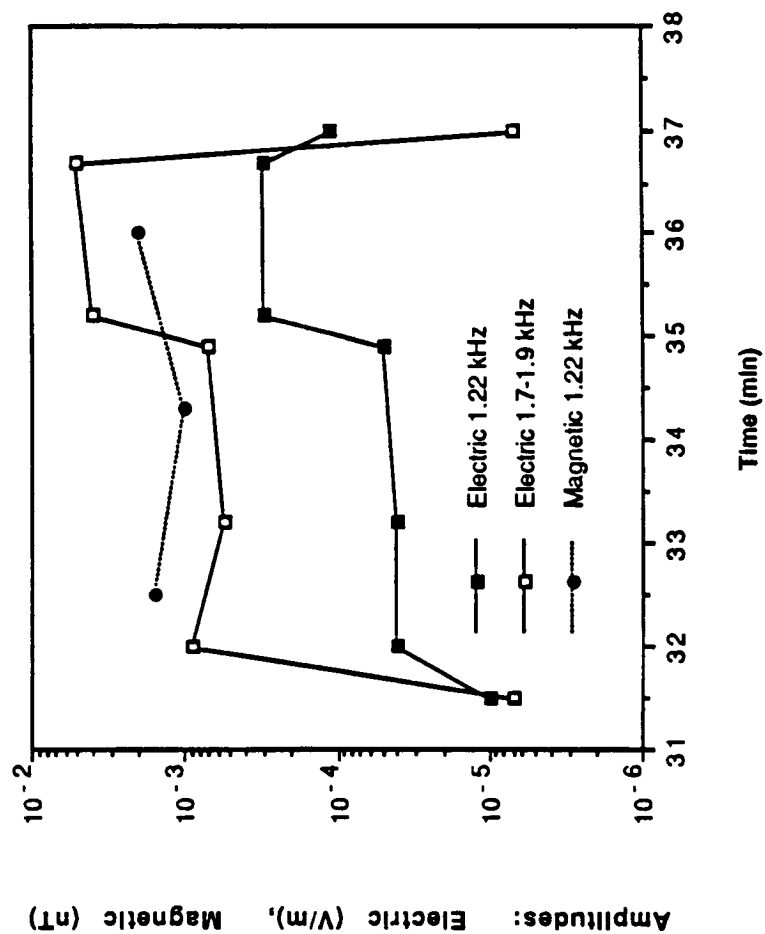
Measured Electric Field Amplitudes



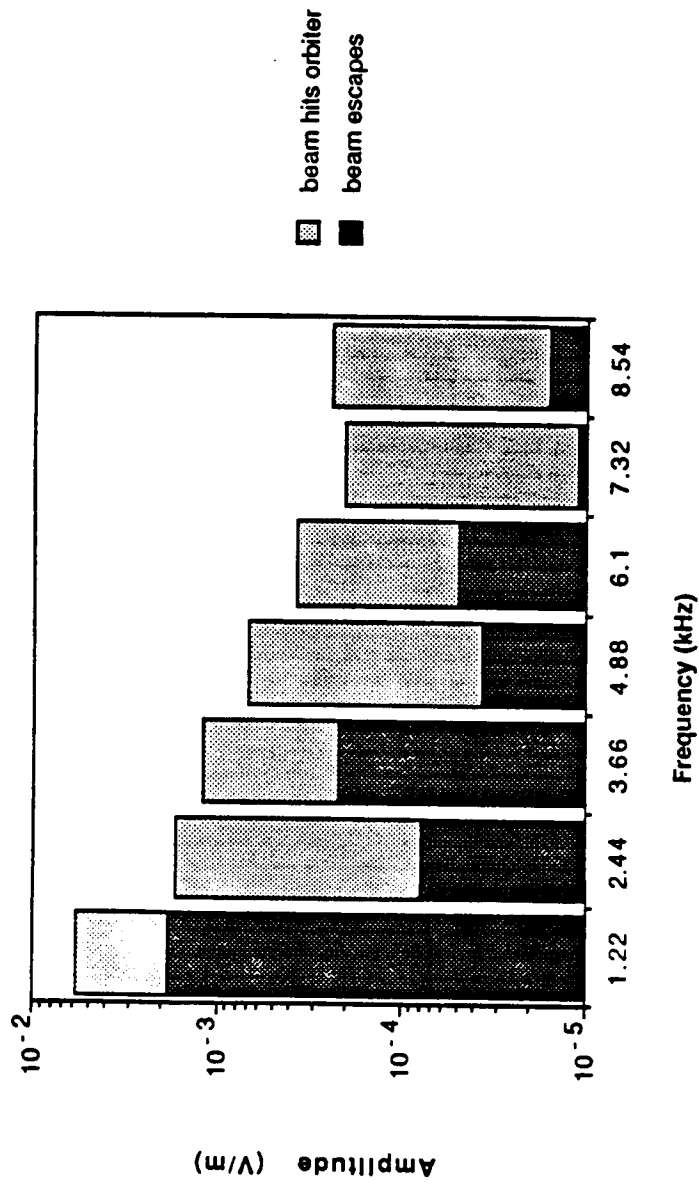
Measured Magnetic Field Amplitudes



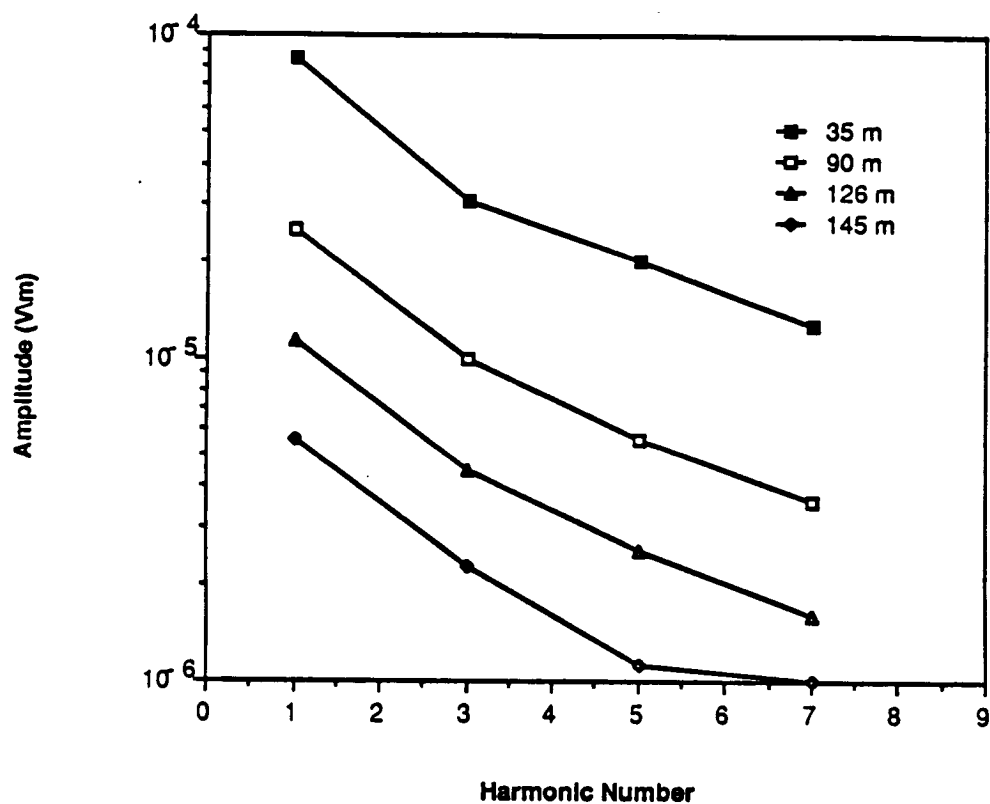
Field Amplitudes during the Prox Ops Sequence



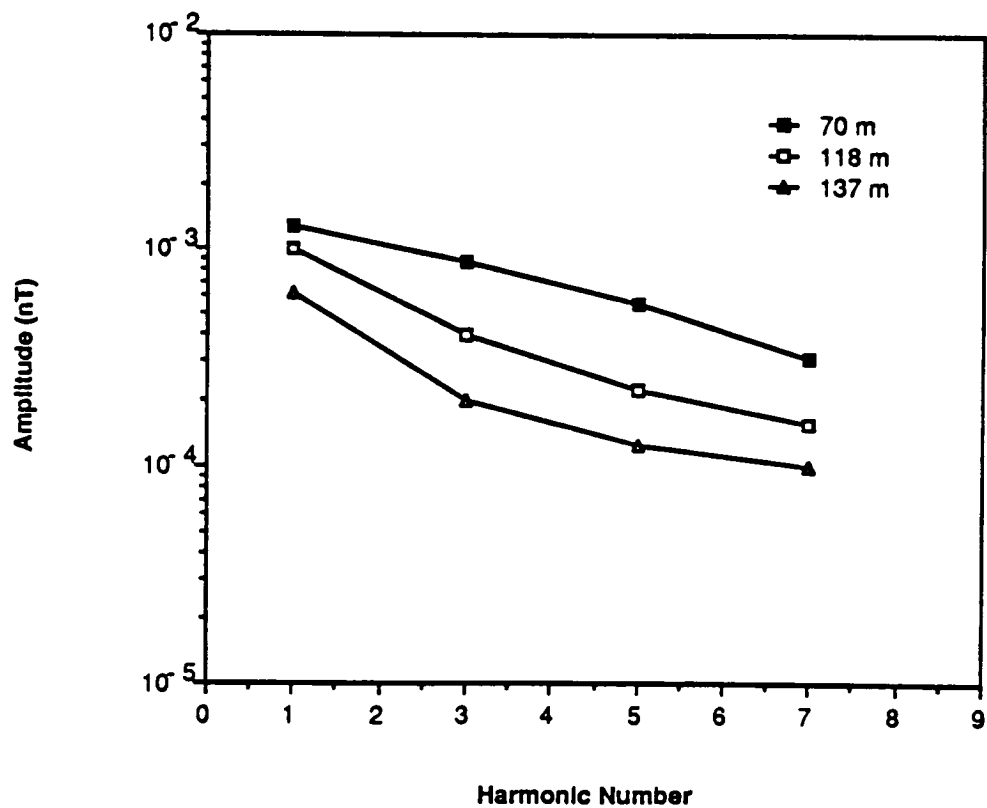
Relative Amplitudes of Odd and Even Harmonics



Predicted Electric Field Amplitudes



Predicted Magnetic Field Amplitudes



VLF Wave Emissions by Pulsed and DC Electron Beams in Space 2: Analysis of Spacelab-2 Results

G. D. REEVES, P. M. BANKS, T. NEUBERT, AND K.J. HARKER

Space Telecommunications and Radioscience Laboratory, Stanford University, Stanford California

D. A. GURNETT

Department of Physics and Astronomy, University of Iowa, Iowa City

Experiments investigating the generation of electromagnetic radio-frequency waves by the injection of electron beams into ionospheric plasmas were conducted in July and August of 1985 on the Spacelab-2 Space Shuttle mission. Among the results were the production of broadband electromagnetic emissions from continuous and square-wave modulated, low-power (1 keV, 50/100 mA) electron beams and the observation of narrowband radiation from pulsed beam operations [Reeves *et al.*, *this issue*]. This paper presents an analysis of the observations from Spacelab-2. Broadband emissions from DC and pulsed electron beams are found to be consistent with production of waves through the $s = 0$, or Cherenkov resonance. Broadband emissions at frequencies below 30 kHz have features which can be explained in terms of propagation characteristics of waves, produced through the Cherenkov resonance, which have wave normal angles less than the resonance cone angle. A single ion cold plasma theory is used to explain some of the general features observed in the data. The effects of the presence of a second ion species on the wave spectra at low frequencies and the effects of making wave measurements in the near-field of the beam are also considered. Comparison of observations of narrowband radiation with a theory of wave generation by pulsed electron beams [Harker and Banks, 1987] is also found to show the best agreement with measurements for predictions of Cherenkov resonance with wave normal angles less than the resonance cone angle.

1. INTRODUCTION

The Spacelab-2 electron beam wave generation experiments were part of a continuing effort to investigate the properties of beam-plasma-wave interactions using active experiments in space. Summaries of some of the research which has been conducted using electron beams in space can be

found in Reeves et al. [*this issue*]; Winckler [1980]; and Myers et al. [1988]. The results analyzed here were obtained by co-operative use of the instruments in the Stanford University/Utah State University, Vehicle Charging and Potential (VCAP) experiment [Banks et al., 1987; Hawkins 1988] and the University of Iowa Plasma Diagnostics Package (PDP) [Shawhan et al., 1984a]. The VCAP experiment included a Fast Pulsed Electron Generator (FPEG) which produced a 1 keV electron beam with currents of 50 or 100 mA. The beam was operated both continuously, in DC mode, and in pulsed mode with frequencies and duty cycles which were command controlled. The VCAP experiment package also included a spherical retarding and potential analyzer, a Langmuir probe, and charge and current probes which were used to investigate vehicle charging and the collection of return current during electron beam operations. More information on the VCAP instruments and their use on the Spacelab-2 and STS-3/OSS-1 missions can be found in Banks et al. [1988]; Hawkins [1988]; and Reeves et al. [1988].

The waves produced by the injection of electrons into the ambient plasma were measured using instruments on the PDP. The PDP is a sub-satellite which contained a variety of instruments for the investigation of the ambient plasma and wave environment around the Orbiter and the modifications to that environment due to electron beam injection. The PDP was operated both when it was mounted in the Orbiter payload bay and when it was released as a free-flying satellite out to distances of several hundred meters from the Orbiter. The PDP instruments included a wideband wave receiver and an array of band-pass filters known as the IMP/HELIOS instrument. These instruments were used to investigate the wave fields produced by the interaction of the electron beam with the ionospheric plasma. The wideband receiver recorded signals in the range 0–30 kHz using a 1 kHz wide channel (the ELF channel) which monitored the 0–1 kHz frequency range and a 10 kHz wide channel (the VLF channel) which was switched between the frequency ranges 0–10, 10–20, and 20–30 kHz. Both channels of the wideband receiver were connected, alternately, to an electric dipole antenna or a magnetic search coil antenna. The IMP/HELIOS instrument consisted of an array of 16, 10% bandwidth filters in the frequency range 31 Hz to 17.8 MHz. Filter bank data could be used to observe the general structure of electric fields produced by beam operations producing a continuous time record (1.6 s time steps) without the complications of antenna and frequency switching found in the wideband receiver data. Observations of wave fields produced by electron beam operations on Spacelab-2 using the wideband receiver have been reported by Bush et al. [1987] and Neubert et al. [1988]. Observations using the IMP/HELIOS instrument of funnel shaped wave emissions resulting from Cherenkov, resonance-cone propagation of radiation from electron beams have been discussed by Gurnett et al. [1986] and Farrell et al., [1988]. (These two papers will hereafter be referred to as ‘GF’.) More detailed descriptions of the instruments on the PDP and the use of those instruments for the investigation of the plasma and wave environment in the vicinity of the Orbiter can be found in Shawhan et al. [1984b]; Gurnett et al. [1986]; Tribble et al. [1988]; and Farrell et al. [1988].

2. A SUMMARY OF SPACELAB-2 WAVE OBSERVATIONS

The analysis presented here is based on the observations and discussion presented in Reeves et al. [*this issue*] which will be referred to as 'GR'. In GR, the amplitudes, spectral characteristics, and time evolution of waves generated by continuous and modulated electron beams were considered. GR presented results from three electron beam wave generation sequences on Spacelab-2. These sequences are referred to as the 'DC flux tube connection', the 'Pulsed flux tube connection' and the 'Prox Ops' sequences. In the flux tube connection sequences the PDP was operated as a free-flying sub-satellite and the Orbiter maneuvered such that the Orbiter and the PDP lay on the same geomagnetic field line: the so-called 'conjunction field line'. During the DC flux tube connection sequence the FPEG was operated continuously with a current of 50 mA. During the Pulsed flux tube connection sequence the FPEG was square wave modulated at 1.22 kHz with a 50% duty cycle and a 100 mA current. Both the DC and pulsed modes inject the same amount of power and it was found that both produce waves with the same amplitude when measured at similar distances with respect to the conjunction field line. (See figures 1 and 2 of this paper and figures 7 and 8 of GR.)

The spatial areas in which broadband waves of different amplitudes were observed were defined in terms of three zones. In zone 1, the plasma environment is disturbed by the interaction of the beam with the ambient plasma. Very intense wave activity which saturates the wideband receiver is within ≈ 10 m from the beam. These intense emissions occur in zone 1 which is a very disturbed region which exists in the vicinity and in the wake of the electron beam. Zone 2 contains waves of lower amplitude and the amplitude drops off rapidly with distance from the conjunction field line. The spatial extent of zone 2 is dependent on the frequency of the waves. Zone 3 contains waves of significantly reduced amplitude compared to zones 1 and 2 but amplitudes may still be greater than the amplitude of the ambient wave fields. Zone 3 extends out to distances greater than the maximum distance between the conjunction field line and the PDP.

During the Pulsed flux tube conjunction and the Prox Ops sequences, the FPEG was pulsed at 1.22 kHz with a 50% duty cycle. During the Pulsed flux tube connection, the PDP was operated as a free-flying satellite. For the Prox Ops sequence, it was stowed at a fixed point in the payload bay 6.62 m from the FPEG. Pulsed electron beams were found to produce narrowband emissions at the pulsing frequency and harmonics of that frequency. During the Pulsed flux tube connection it was found that there was a constant ratio of the amplitude of narrowband emissions at the pulsing frequency (1.22 kHz) to the amplitude of broadband emissions near that frequency (1.7-1.8 kHz). For the electric field measurements the narrowband emissions were approximately five times stronger than the broadband emissions. For the magnetic field measurements the narrowband emissions were about fifteen times stronger. These results were independent of where the fields were measured [GR, figure 9].

The electric field wave data from the IMP/HELIOS filter bank provides a good over-view of the wave environment during the DC and Pulsed flux tube connection sequences. Figure 1 is similar to those presented in GR. Spectral intensities (in $V^2/m^2\cdot Hz$) are presented in continuous frequency format by interpolating between values at the filter frequencies. Unlike the VLF wideband receiver, the IMP/HELIOS instrument had no AGC and the electric field measurements had no antenna switching pattern so a continuous time record could be obtained. Figure 1 can be compared with figure 7 of GR. The FPEG is operated continuously from 03:30:12 to 03:37:22. At earlier and later times in the figure, the FPEG is not on and the ambient wave fields are observed. At approximately 03:34:01 the PDP passes closest to the conjunction field line and the strongest emissions are seen at this time. Intense emissions are observed to be associated with a region which is disturbed by the injection of the electron beam. We see that waves are observed at larger distances from the conjunction field line (earlier and later times) at frequencies below 1 kHz. The wave amplitude drops off more rapidly with distance for frequencies above 1 kHz. At 10 kHz stronger emissions are again observed at earlier and later times ($\sim 03:33$ to $\sim 03:36$). A cut-off in the broadband, beam-generated, VLF emissions is observed between 2-5 kHz. These characteristics are interpretable in terms of the propagation properties of the electron beam produced waves as will be discussed below.

The filter bank data for the Pulsed flux tube connection sequence is shown in figure 2 and is in the same format as figure 1. Since there were only four filters per. decade of frequency, the narrowband emissions are not well represented. However, the enhanced amplitude of waves near 1 kHz compared to the DC flux tube connection is attributable to the contribution of narrowband signals. The narrowband wave signals are more clearly represented in the wideband receiver data presented in GR.

The IMP/HELIOS data for the Pulsed flux tube connection shows that the broadband wave production and propagation characteristics are similar for DC and pulsed electron beams. For the Pulsed flux tube connection, the FPEG was turned on at 04:11:13 when the PDP was near the conjunction field line. The FPEG was turned off at 04:18:23. At times when the FPEG was not firing, the ambient fields were observed. The ambient electric field amplitudes are two orders of magnitude lower during the Pulsed flux tube connection sequence than during the DC flux tube connection sequence [GR]. Zone 1 emissions are not observed because the FPEG was not operated when the PDP was within 10 m of the beam. Zone 2 and zone 3 emissions are observed as well as resonance cone emissions which form the 'funnel' above 10 kHz.

3. ANALYSIS OF ELECTRON BEAM-PLASMA-WAVE INTERACTIONS

Broadband emissions from pulsed and DC electron beams

We begin the analysis of the wave modes produced by pulsed and continuous electron beams

injected into space plasmas by considering the broadband radiation observed in the three zones identified in the Spacelab-2 wave data during the flux tube connection sequences. For simplicity we will begin by discussing a two component (O^+ and e^-), cold plasma in the frequency range $0 < \omega < \omega_{ce}$ where ω_{ce} is the electron cyclotron frequency ($f_{ce} \approx 1$ MHz). We will also assume oscillatory behavior of the fields which is equivalent to an assumption that we are in the far-field of the waves. In order to apply the theory of radiation in a cold plasma to the present situation, several cautions must be kept in mind. Electromagnetic radiation in the frequency range $0 < \omega < \omega_{ce}$ can have wavelengths which range from less than one Debye length to kilometers. Therefore, the PDP measured wave fields that were, in some circumstances, within one wavelength of the source. In such a situation, far-field radiation assumptions do not strictly apply. Further, the ambient plasma contains ion species other than O^+ (notably H^+), it has finite temperature, and is disturbed by thruster emissions, vehicle outgassing, and the 7.7 km/s velocity of the Orbiter and the PDP through the medium. Never the less, a first order treatment of radiation in a cold plasma can explain some of the observed phenomena and it is simpler to conceptualize. Therefore, we will begin with a first order treatment of the propagation of broadband radiation from pulsed and continuous electron beams and discuss some important refinements of that theory in the following section.

First Order Theory.

Following the treatment of Al'pert [1983] we first consider the cold plasma dispersion curves $n^2(\omega)$, where n is the complex index of refraction (figure 3). Since the dispersion relation is quadratic in n^2 there are two roots at any given frequency, n_1, n_2 , as given by the sign before the discriminant. In the frequency range $\omega_{ci} < \omega < \omega_{ce}$, where ω_{ci} is the ion-cyclotron frequency, only the n_2 root is real. This branch is called the whistler mode. At lower frequencies, this branch is sometimes referred to as the fast magnetoacoustic mode. In the range $0 < \omega < \omega_{ci}$, both roots are real and the n_1 branch is labeled the-ion whistler or Alfvén mode. The index of refraction, n , is a function of the angle, θ , between the wave normal direction and the direction of the magnetic field. For $0 < \omega < \omega_{LHR}$ (the lower hybrid frequency), the index of refraction surface, $n(\theta)$, is closed and n is finite for all θ . For higher frequencies the surface is open and $n(\theta)$ becomes infinite at the resonance cone angle, θ_{res} .

In the VLF spectra from Spacelab-2 we find that, in general, there is no distinct change in wave amplitude or spectral shape at the lower hybrid frequency [GR, figure 6]. The continuity of amplitude across the lower hybrid frequency suggests that the broadband emissions observed outside the disturbed region near the beam (zone 1) are whistler mode emissions that have wave normal angles less than the resonance cone angle.

To explore this idea in the context of Spacelab-2 observations, we consider the beam-generated wave amplitudes as a function of ray angle to the source. We define the ray angle, α , as the angle

between the ray direction and the magnetic field direction. (The geometry is sketched in figure 4.) The minimum observable ray angle at a particular location of the PDP will be given by the angle between the magnetic field line, \mathbf{B} , and the line connecting the Orbiter and the PDP. If we call this angle β then only waves with ray angles $\alpha \geq \beta$ will be observed by the PDP at that time. Waves with ray angles $\alpha = \beta$ will originate at the source of the electron beam. At the same location, waves with larger ray angles will originate at different segments along the length of the beam. During the free-flight, the PDP is moving with respect to the conjunction field line. When the PDP is far from the conjunction field line, β is large and only propagating radiation with large ray angles should be observed. As the PDP approaches the conjunction field line, β decreases and the range of observable ray angles increases.

Various wave-particle interaction processes can produce radiation in the whistler mode. The propagation characteristics of radiation from the electron beam can provide information which helps identify the type of interaction observed in the Spacelab-2 experiments. To determine the expected wave normal and ray angles we consider the resonance condition $k_{\parallel} = (\omega - s\omega_{ce})/v_{\parallel}$ where $s = 0$ is the Cherenkov or Langmuir resonance, $s = 1$ is cyclotron resonance, and $s = -1$ is anomalous cyclotron resonance. The index of refraction is given by $n = kc/\omega$. For $\omega < \omega_{LHR}$ only the $s = 0$ resonance is possible because the magnitude of the index of refraction is less than that required for $s = \pm 1$ resonance for all wave normal angles. Thus the continuity of amplitude across the lower hybrid resonance frequency suggests that the dominant mode of wave generation was the Cherenkov resonance. This was also determined to be the resonance condition for frequencies in the range ω_{LHR} to ω_{ce} by Gurnett et al. [1986] using wave propagation arguments to explain the funnel shaped emission observed during the DC flux tube connection at those frequencies.

To be specific, we will consider the conditions which existed during the DC flux tube connection sequence. (The instrumental and plasma parameters for various electron beam wave generation sequences on Spacelab-2 are given in Table 1 of GR.) Using $v_{\parallel} = 1.9 \times 10^7$ m/s for a 1 keV beam directed along the field line and $\omega_{ce} = 6.3 \times 10^6$ s⁻¹, the Cherenkov resonance condition, $s = 0$, gives $n_{\parallel} = 16$ and the Cherenkov resonance condition is independent of frequency. Using the value $n_{\parallel} = 16$ one can calculate the wave normal angle (or phase velocity angle), θ , and the ray angle (or group velocity angle), α . According to cold plasma theory, the ray angle then determines the maximum perpendicular distance at which one would expect to detect far-field radiation at a particular frequency because at larger perpendicular distances the angle β is larger than the ray angle, α .

The ambient magnetic field strength and background electron density during the DC flux tube connection were $B_0 = .40$ Gauss, $n_e = 10^5$ cm⁻³, respectively. Using these values we find that the composition of the VLF (0-30 kHz) wave spectra are consistent with an $s = 0$ resonance with $\theta < \theta_{res}$. At low frequencies ($f = 100$ Hz for example) the condition $n_{\parallel} = 16$ picks out very large wave normal angles, $\theta \approx 90^\circ$, which on a closed index of refraction surface implies large ray angles,

$\alpha \approx 90^\circ$. This situation is represented schematically in figure 5a. For $f = 1$ kHz, the index of refraction surface is flatter, $\theta < 90^\circ$, and α becomes small, $\alpha \approx 5^\circ$ (figure 5b). At higher frequencies a resonance cone develops but the wave normal angles with $\theta < \theta_{res}$ which satisfy $n_{\parallel} = 16$ lie in the central hump. At 15 kHz, $\theta \approx 60^\circ$ and again, larger ray angles, $\alpha \approx 20^\circ$, are found (figure 5c). As we continue to increase in frequency the index of refraction surface gets lower at small angles and the wave normal angle picked out by the resonance condition approaches zero. At 30 kHz, $\theta \approx 0^\circ$ and $\alpha \approx 0^\circ$ (figure 5d). For even higher frequencies, the value of the parallel index of refraction for $\theta < \theta_{res}$ becomes less than 16 and only resonance cone propagation will satisfy the $s = 0$ resonance condition (figure 5e).

The predicted propagation region for waves generated through the Cherenkov resonance propagating with wave normal angles less than the resonance cone angle is shown schematically in figure 6. The propagation region for broadband radiation is determined using cold plasma theory to determine the far-field ray angles of beam generated radiation for the conditions of the DC flux tube connection. The ray angles and perpendicular wavelengths for various frequencies are calculated assuming Cherenkov resonance and $\theta < \theta_{res}$. Frequency has been plotted vs. distance so that figure 6 may be more easily compared with figures 1 and 2. Angle is converted into distance by multiplying the sine of the ray angle by 200 m which is a nominal value for the distance from the Orbiter to the PDP. As indicated in figure 5, the ray angle, and hence the propagation region, is a function of frequency. Low frequency waves in Cherenkov resonance have large wave normal angles and the wave normal decreases with increasing frequency until the resonance condition can no longer be satisfied in the central hump of the index of refraction surface.

For frequencies above 30 kHz, only resonance cone emissions are observed and these form the funnel structure as explained by Gurnett et al. [1986]. Resonance cone propagating waves exist at all frequencies between f_{LHR} and f_{ce} , but below $f = 30$ kHz the resonance cone angle is nearly 90° and the ray angles are less than 5° . The VLF emissions that saturate the wideband wave receiver in zone 1 are most likely resonance cone propagating waves. The duration of observation of waves in zone 1 is not represented well in figures 1 and 2 because wave emissions are at the extreme end of the amplitude scale (red) at VLF frequencies both in zone 1 and in zone 2. The strong wave emissions observed at $\sim 03:34$ in figure 1 and at $\sim 04:11$ in figure 2 are, however, associated with the region of disturbed plasma near the beam and in its wake. Although the horizontal scale in figures 1 and 2 are time scales, the distance from the PDP to the conjunction field line for the DC and Pulsed flux tube connection sequences can be determined from figures 7a and 7b.

The above propagation properties can be observed in the IMP/HELIOS filter bank data (figures 1 and 2). Figures 1 and 6, for the DC flux tube connection, can be compared. The three wave zones can be identified, the cut-off of non-resonance cone emissions near 30 kHz is apparent, and the resonance cone emissions which form the funnel above 30 kHz can be observed. The Pulsed flux tube connection sequence occurred during slightly different ambient conditions and the FPEG was

not operated during the approach to the conjunction field line.

Refinements of the First Order Theory.

As noted, the analysis above assumes a two component (e^- and O^+) cold plasma and assumes far field propagation characteristics. Having determined the general characteristics of broadband wave production and propagation, we now consider the observed wave effects which are a result of performing measurements within the near-field of the beam and the spectral characteristics which are attributable to the presence of a second ion species.

Near-field Wave Observations.

During the Spacelab-2 experiments observations were made at locations that were outside the propagation region as determined from a far-field, cold plasma model. The waves observed at these locations are the zone 3 emissions. The reason that the amplitude of the waves measured at these locations does not drop down to ambient background levels is that the perpendicular wavelength of propagating waves can be quite large. The perpendicular wavelength is plotted vs. frequency in figure 6 which provides a measure of the validity and limits of the far-field approximation. Here the index of refraction for $s = 0$, $\theta < \theta_{res}$ is calculated using the conditions for the DC flux tube connection and is used to calculate the component of the wavelength which is perpendicular to the conjunction field line. For frequencies in the ELF range the wavelengths are several hundred to several thousand meters except near the ion-cyclotron frequencies. At VLF frequencies below 20 kHz the wavelengths are in the range 100-200 m. Thus, although most of the wave data is taken within one perpendicular wavelength of the conjunction field line, it is reasonable to assume that the results of far-field calculations can be applied to the general characteristics of the function of amplitude vs. ray angle. It is also reasonable to attribute the enhancement of wave amplitudes above ambient levels in locations outside the region calculated using the far-field assumption to the effect of near-field or 'evanescent' waves. The wavelength of resonance cone emissions is less than or on the order of 10 m and has therefore not been plotted.

The Effects of H^+ on Observed Wave Spectra.

The first order model of the propagation of far-field radiation derived using cold plasma theory for a plasma with a single ion species becomes more complex when one considers the presence of a second ion species. At the orbital altitude of 325 km, O^+ is the dominant ion species. There is, however, an appreciable amount of singly ionized hydrogen, H^+ . The effects of the presence of a second ion species on the spectral characteristics of beam-generated waves are more dramatic at lower frequencies than at higher frequencies. With H^+ present, there is an additional ion-cyclotron resonance which lies at 611 Hz for $B = .40$ Gauss. The ray angles predicted from cold plasma theory (figures 5 and 6) show the same general characteristics as for the single-ion species case for frequencies above the H^+ ion-cyclotron frequency, $f_{ci}(H^+)$. For frequencies just

below $f_{ci}(H^+)$, the model ray angle drops to zero but then rapidly increases to large angles with decreasing frequency until the O^+ ion-cyclotron frequency at 38 Hz.

The waves observations presented in GR were drawn primarily from the VLF channel of the wideband receiver. In considering the effects of H^+ , the spectra from the ELF (0–1 kHz) channel are more useful. The spectrum from a magnetic antenna period during the DC flux tube connection is shown in figure 8. Spectrograms are produced by digitizing the analog waveform from the wideband receiver and performing a discrete Fourier transform over a progressive series of time records. The ELF spectrograms are prepared in the same way as the VLF spectrograms with the exception of the data sampling rate (2600 s^{-1}) and the size of the Fourier transform (1024 pt) which result in a resolution of 2.54 Hz by .197 s. The wideband receiver data, and hence, the spectrograms contain amplitudes which are kept within a strict range of values by means of an Automatic Gain Control (AGC). Absolute amplitudes can be obtained by numerically compensating for the effects of the AGC. Gains applied by the AGC are removed in the same manner as for the VLF data and the calibrated spectrum averaged over the 51 s antenna period is shown in figure 9. (GR and Reeves [1988] contain further explanation of the digitization and calibration procedures.)

The ELF data shows clear spin modulation of the signals below 500 Hz and a cut-off which varies between 550–600 Hz. The cut-off is apparent in the ELF data both when the FPEG is firing and during ambient conditions. However, the amplitude of the waves is generally greater during beam operations. The amplitude of ambient wave fields at 150 Hz, for example, is between $10^{-6} - 10^{-5} \text{ V/m}$; $5 \times 10^{-5} - 5 \times 10^{-4} \text{ nT}$ for the DC flux tube connection and is approximately 10^{-7} V/m ; $5 \times 10^{-5} \text{ nT}$ for the Pulsed flux tube connection. When the FPEG is firing the amplitude at 150 Hz, for both sequences, is over 10^{-4} V/m ; 10^{-3} nT near the conjunction field line and decreases to 10^{-5} V/m at large distances. The cutoff in the ELF band (figures 8 and 9) has been identified as the two-ion cut-off which occurs at the so-called 'crossover frequency' ($\omega_{1,2}$ in the notation of Al'pert). This is the $L = 0$ cut-off in the notation of Stix [1962]. During ambient conditions, a band of noise above the crossover frequency is observed and has a similar appearance to the emissions during electron beam operations. This noise is referred to as Band-limited ELF Hiss (BLH). It was first described by Gurnett and Burns [1968] and was later studied by Muzzio [1971]. BLH is thought to originate just inside the plasmopause in the equatorial region. Frequencies below the crossover frequency are reflected as the wave propagates to low altitudes. The BLH is observed to disappear at equatorial latitudes with higher frequencies dropping off at higher latitudes as a result of propagation effects.

The two-ion cut-off provides a sensitive measurement of the ratio of densities of the ion species. The ratio of ion densities can be calculated by setting $1 - \sum_i \omega_{pi}^2 / (\omega^2 - \epsilon_i \omega \omega_{ci}) = 0$ where ω_{pi} , ω_{ci} , and ϵ_i are the plasma frequency, the cyclotron frequency and the sign of the charge for plasma species i (which are e^- , O^+ , and H^+). If the cut-off frequency is taken to be 550 Hz the density of hydrogen and oxygen ions is calculated to be $N_{H^+} = 10\% N_{e^-}$ and $N_{O^+} = 90\% N_{e^-}$. However, if we

calculate the density using a cut-off frequency of 600 Hz, $N_{H^+} = 2\% N_{e^-}$. This is simply indicative of the sensitive dependence of the equations on N_{H^+} . Calculations using the International Reference Ionosphere (IRI) model [Bilitza, 1986] for the conditions during the DC flux tube connection give $N_{H^+} = 1\% N_{e^-}$ and $N_{O^+} = 99\% N_{e^-}$. We conclude then that H^+ exists in quantities less than 10% of the electron density in the vicinity of the Orbiter. The presence of H^+ is responsible for the low frequency cut-off in the ELF band. The H^+ concentration is not large enough for it to have significant impact on the index of refraction surfaces at VLF frequencies. At 500 Hz a two-ion calculation of the index of refraction at wave normal angles of 30° with $N_{H^+} = 10\% N_{e^-}$ is 36% different than for the calculation using only O^+ and e^- . At 1 kHz the difference has dropped to 7% and at 5 kHz it is 0.7%.

Narrowband emissions

Pulsed electron beams injected into space plasmas produce narrowband radiation in addition to broadband emissions. It has been shown by GR that the narrowband emissions share some of the features with the broadband emissions. For example, the ratio of the amplitude of the fundamental frequency (1.22 kHz) to the amplitude of broadband emissions at frequencies near the fundamental (1.7–1.8 kHz) is roughly independent of where the wave fields are measured. Narrowband emissions are also present at harmonics of the pulsing frequency. The amplitudes of the fundamental and its harmonics are dependent on the resonance condition, the wave mode, the duty cycle of the modulated beam, and propagation properties of the waves. A theory of narrowband, near-field radiation from pulsed electron beams was developed by Harker and Banks [1987]. (This paper will be referred to as 'HB'.) It contains expressions for the electric field amplitudes produced by square wave modulated electron beams with arbitrary energies, currents, and pitch angles measured at any distance larger than one gyro-radius from the beam. These expressions can be applied to experimental conditions by using the parameters which are appropriate for the conditions at the time of the experiment. Neubert and Harker [1988] have extended this theory to predict the narrowband magnetic field amplitudes. Because the theory treats only coherent emissions, no broadband wave amplitudes are predicted.

The exact results for the amplitude of narrowband radiation from a pulsed electron beam are complicated but we can summarize some of the general features. Since the theory treats the near-field wave amplitudes we are justified in applying it to our observations. The mathematical treatment assumes a perfectly coherent infinitely long, thin beam. A value of the parallel index of refraction is found from the resonance conditions $s = 0, 1, -1$. The electric field amplitudes are related to the electron beam current density through a radiation condition which can be expressed in frequency-wave number space as a function of k_\perp , the perpendicular wave number. A contour integration over k_\perp selects the self consistent wave normal angles and the fields are transformed back into time-distance space. Results are presented for both (complex) values of k_\perp (labeled roots 1, and 2 in HB) for each of the three resonance conditions. The three components of the electric field

can then be read off the figures of HB or the expression for the electric field components can be evaluated numerically for a variety of experimental conditions.

For the conditions for the DC flux tube connection, $\log(f/f_{ce}) \approx -3$ for the fundamental frequency, $f = 1.22$ kHz. From Table 1 of HB, we find that only the $s = 0$, root 2 predictions have real solutions for this frequency. The fields for $s = \pm 1$ and for $s = 0$, root 1 are evanescent fields. This reflects the fact that the $s = \pm 1$ resonance conditions cannot be satisfied for a 1 keV beam at frequencies below the lower hybrid frequency and the fact that a resonance cone does not exist for those frequencies. Measurable near-field waves are still predicted to exist however. For the $s = \pm 1$ resonances, the root 1 solutions become highly oscillatory functions of frequency for frequencies below 30 kHz and no exact predictions can be made. Waves in these modes must be treated using hot plasma theory. However, the wave amplitudes can be estimated by extrapolation and the $s = \pm 1$, root 1 solutions could have amplitudes greater than 1 V/m. Although it is possible that the observed narrowband beam emissions are due to $s = \pm 1$ resonance but are observed with amplitudes well below those predicted by theory, we will see below that much better agreement between measurement and theory is found for the $s = 0$, or Cherenkov, mode.

The total electric field strength predicted by HB for the $s = 0, 1, -1$; root 2 and the $s = 0$, root 1 solutions are presented in figure 10 for a perpendicular distance of 50 m from the beam. The observed wave fields measured at 35 m and 90 m from the beam are plotted with dotted lines. The predicted amplitude of these four wave modes and the measured amplitude for the fundamental are plotted as a function of distance from the conjunction field line in figure 11. These two figures allow comparison of the variation with frequency and the variation with perpendicular distance for predictions and measurements for the different wave modes. Root 1 represents resonance cone propagation and solutions are imaginary below the lower hybrid resonance and real above it. Root 2 has real solutions throughout the frequency range of interest and describes waves which lie in the central hump of the index of refraction surface. The $s = \pm 1$, root 2 solutions are found to have amplitudes well below observed values.

Figures 10 and 11 and figures 10 and 13 of GR show that reasonable agreement between observations and the predictions of HB are found for the $s = 0$, root 2 solutions. For those solutions, HB predict electric and magnetic field amplitudes which are greater, but less than 30 times greater, than the measured field amplitudes at all distances and for all harmonics. The general features observed in the measured data are reproduced in the calculations. The electric field amplitudes range from 10^{-6} to 10^{-4} V/m and the magnetic field amplitudes range from 10^{-4} to 2×10^{-3} nT. For both the electric and the magnetic antennas, the amplitude of the narrowband harmonics decreases with increasing distance from the conjunction field line and, at all distances, the amplitude decreases for increasing harmonic numbers. The fact that the ratio of broadband to narrowband amplitudes stays fairly constant with distance to the conjunction field line [GR] appears to be consistent with the conclusion that both broadband and narrowband emissions are generated through the Cherenkov

resonance with wave normal angles less than the resonance cone angle ($s = 0, \theta < \theta_{res}$).

The difference in measured and predicted amplitudes could be accounted for by a reduction in coherent beam current from the nominal 100 mA level. This reduction could occur through such mechanisms as scattering or diffusion of beam electrons or the production of a virtual cathode as suggested by numerical simulations done by Winglee and Pritchett [1987, and 1988]. It may also simply be a result of the fact that measurements were made with single axis antennas and therefore measurements of the full field amplitudes could not be made.

The results of HB are used here with the following caveat. It has been determined that the contour integration over k_{\perp} in HB contains branch cuts in addition to simple poles. HB evaluates only the contributions to the integral from the simple poles, which correspond to surface waves, and therefore the solution is incomplete. In addition to the field components calculated, there will be field contributions due to terms which arise from the inclusion of these branch cuts which correspond to ray propagation. Those contributions can be evaluated and will be presented in an upcoming paper. It has been determined that the contributions from the branch cuts will be most significant at large distances from the beam but the effect at smaller distances has not been determined. In this paper we conclude only that the theory of HB, as it stands, provides the best agreement with experimental observations for the $s = 0$, root 2 mode which describes Cherenkov resonance with wave normal angles less than the resonance cone angle.

The ratio of the electric and magnetic field amplitudes

In considering the amplitude of radiation from electron beams in space, we implicitly assume that the waves are electromagnetic. For a 1 kHz wave with $n_{\parallel} = 16$ and $B_0 = .40 \text{ G}$, $n_e = 10^5 \text{ cm}^{-3}$, $|n| = n = 316$. From the calibrated amplitude of field components one can calculate the ratio $c\langle B \rangle / \langle E \rangle$ where $\langle B \rangle$ and $\langle E \rangle$ are the time averaged amplitudes of the magnetic and electric fields. For broadband emissions measured during the Prox Ops and the DC and Pulsed flux tube connection sequences, $c\langle B \rangle / \langle E \rangle$ was of order 1. Narrowband emissions during the Pulsed flux tube connection sequence were determined to have a ratio $c\langle B \rangle / \langle E \rangle$ of order 10 [GR]. Since $n \times E = cB$, there is an apparent discrepancy between the measured and the predicted values of n . We now consider the possible causes of this discrepancy.

Knowing the wave normal angle of radiation at a particular frequency, one can use Maxwell's equations to solve for the vector components of the electric and magnetic wave fields. Choosing a coordinate system in which the geomagnetic field defines the z-axis and k lies in the x-z-plane, and using conditions for the DC flux tube connection sequence and frequencies near 1.22 kHz we find that the wave normal angle is nearly 90° . The wave electric field has its largest component along the x-axis and virtually no component along the magnetic field. The wave magnetic field has its largest component along the direction of the geomagnetic field but also has a component along the y-axis. Since the PDP rotates with its antennas in a plane containing the geomagnetic field, it is

appropriate to consider the time average over all three components of the wave fields. Doing this we find that the average reduces the ratio $c\langle B\rangle/\langle E\rangle$ by a factor of ~ 10 ...

We would then expect ratios of $c\langle B\rangle/\langle E\rangle$ of order 10 for the coherent emissions observed. Although simultaneous electric and magnetic field measurements could not be made with the broadband wave receiver, comparison of the average magnetic and electric field amplitudes of natural whistlers observed during ambient conditions also gives values of $c\langle B\rangle/\langle E\rangle$ which are of order 10. It is not understood why the broadband emissions observed during the PDP free-flight or broadband and narrowband emissions observed in the payload bay have a ratio $c\langle B\rangle/\langle E\rangle$ of order 1. One would expect $n \times E = cB$ to be satisfied under all conditions. Although it is possible that the details of the measurements or analysis of the field amplitudes is responsible for the apparent reduction, it is not possible to resolve the issue given the limits of the observations.

We have considered the possible contribution to the observed electric field from ion-acoustic waves. In order that such waves be observed at distances of several hundred meters from the conjunction field line they must be propagating at oblique angles to the geomagnetic field. Such waves can exist in a warm plasma and have been observed in the laboratory to be produced by drifting electrons in a magnetoplasma [Gekelman and Stenzel, 1978]. Ion-acoustic waves produced by drifting return current electrons during electron beam injection from spacecraft have been predicted by Okuda and Ashour-Abdalla [1988] using a one dimensional numerical simulation. Although such waves may be present we have been unable to determine their contribution, if any, to the observed wave fields. We also note that purely ion-acoustic contributions do not account for the enhancement of the wave magnetic field above ambient levels or the propagation characteristics observed in the IMP/HELIOS data.

We find then that the measured values of $c\langle B\rangle/\langle E\rangle$ for coherent, narrowband emissions observed during the free-flight of the PDP are not inconsistent with the assumption that the electron beam generated waves which are electromagnetic. More accurate verification of this assumption could be accomplished by simultaneous three-axis measurements of the wave field. The wideband receiver measurements from Spacelab-2 were neither simultaneous nor three-axis. The IMP/HELIOS instrument provided periods of simultaneous electric and magnetic field measurements but without detailed knowledge of the orientation of the receivers at a particular time, the electromagnetic character of the observed radiation can not be investigated more rigorously than has been done here.

The lack of simultaneous three-axis field measurements also complicates rigorous determination of the Poynting flux, $S = \frac{1}{\mu_0} E \times B$. However, B has its maximum along the magnetic field line (B_0) and E has its maximum components perpendicular to B_0 . Thus if E_{max} and B_{max} are the maximum amplitudes measured during the spin period of the PDP, then $\frac{1}{\mu_0} E_{max} \cdot B_{max}$ gives an estimate of $|S|$. For the coherent emissions at the 1.22 kHz fundamental frequency during two antenna periods from the Pulsed flux tube connection, $\frac{1}{\mu_0} E_{max} \cdot B_{max}$ is of order $10^{-12} \text{ W/m}^2\text{-Hz}$

for a 12 Hz wide amplitude component. E_{max} is measured at 04:11:48 and B_{max} is measured at 04:12:36. At those times the PDP was 22 m and 61 m from the conjunction field line respectively. $E_{max} \cdot B_{max}$ is a very rough estimate of $|S|$ but it is comparable with the predictions of Bell [1968] who predicted powers up to 10^{-10} W/m²-Hz for coherent emissions with a coherence length of 10 m and 10^{-18} W/m²-Hz for incoherent emissions.

4. CONCLUSIONS

During both DC and Pulsed electron beam operations on Spacelab-2, broadband electromagnetic radiation is produced throughout the 0-30 kHz range of the wideband receiver. The observations of wave amplitudes from the wideband receiver and the IMP/HELIOS filter bank indicate that this is radiation produced by the $s = 0$, or Cherenkov, resonance. During the flux tube connections it is possible to observe the wave fields at various locations with respect to the conjunction field line. Three zones of wave activity were identified. Zone 1 occurs closest to the conjunction field line. It is dominated by waves with wave normal angles on the resonance cone ($\theta \approx \theta_{res}$). These waves saturate the wideband VLF wave receiver and are responsible for the funnel shaped emissions identified by Gurnett et al. [1986]. Broadband VLF emissions in the range $100 < f < 30,000$ Hz are identified as waves with wave normal angles in the central hump of the index of refraction surface ($\theta < \theta_{res}$). Zone 2 contains propagating radiation and is defined by the ray angle of the waves. The ray angle, and hence the region of propagation, is a function of frequency. In general, lower frequency ($f < 1$ kHz) waves propagate at larger angles to the magnetic field than higher frequency ($1 < f < 30$ kHz) waves. The cut-off near 30 kHz appears to be due to the inability to satisfy the $s = 0$ resonance for $\theta < \theta_{res}$ for a 1 keV beam at frequencies higher than this.

A simple single-ion, cold plasma, far-field radiation theory is not sufficient to explain all the features observed in the data. The waves in zone 3 have lower amplitudes than the waves in zones 1 or 2 but may still appear with amplitudes above ambient levels. These emissions are most likely evanescent waves which are observed within a few perpendicular wavelengths of the conjunction field line. The cut-off observed in the broadband ELF wave data at frequencies between 550-600 Hz requires consideration of a second ion species, H^+ , in addition to O^+ and e^- . The frequency of this cut-off allows a calculation of the density of hydrogen ions which indicates that the density is less than 10% of the electron density near the Orbiter, the remainder being predominantly oxygen ions.

The ratio of $c\langle B \rangle / \langle E \rangle$ is useful for checking the electromagnetic nature of electron beam generated waves but was found to be limited by the effects of the spin of the PDP and the lack of simultaneous electric and magnetic field observations. The ratio $c\langle B \rangle / \langle E \rangle$ was found to be of order 10 for the narrowband radiation observed during the Pulsed flux tube connection. This ratio is in rough agreement with the predicted values of the time averaged ratio of electric and magnetic field amplitudes for coherent emissions. The ratio of $c\langle B \rangle / \langle E \rangle$ for broadband emissions during the

free-flight and for broadband and narrowband emissions when the PDP is in the payload bay is of order 1.

Although the propagation characteristics of broadband and narrowband radiation from pulsed and DC electron beams observed on Spacelab-2 have some features which can be understood in terms of cold plasma far-field radiation theory, there are features and effects which require more detailed investigation. Among them are: (1) the question of the effects of thruster operation on the wave environment around the Orbiter, (2) the propagation characteristics of the beam electrons themselves, (3) the return current interaction and the generation of ion-acoustic waves by return currents, (4) the question of vehicle charging and beam escape and the effects of those on the generation of VLF radiation by the beam, (5) the power levels carried away from the electron beam by propagating radiation, and (6) the question of the ratio of the electric and magnetic field amplitudes for broadband and narrowband emissions. Although we may begin to address some of these questions using the results of observations from electron beam experiments which have been completed, some cannot be addressed given the limitations of those experiments and must await future research.

REFERENCES

- Al'pert, Ya.L., *The Near Earth and Interplanetary Plasma*, Cambridge University Press, NY, 1983.
- Akai, K., Electron beam-plasma interaction experiment in space, ISAS Res. Note 285, Inst. of Space and Astronaut. Sci., Tokyo, 1984.
- Banks, P.M., W.J. Raitt, A.B. White, R.I. Bush, and P.R. Williamson, Results from the Vehicle Charging and Potential experiment on STS 3, *J. Spacecr. Rockets*, 24, 1987.
- Banks, P.M. and W.J. Raitt, Observations of electron beam structure in space experiments, *J. Geophys. Res.*, submitted 1988.
- Banks, P.M., W.J. Raitt, P.R. Williamson, T. Neubert, R.I. Bush, J.G. Hawkins, G.R. Reeves, and B. White, Results of vehicle charging, plasma density, and wave generation experiments on Spacelab-2., *J. Spacecr. Rockets*, to be submitted, 1988.
- Bell, T.F., Artificial production of VLF hiss., *J. Geophys. Res.*, 73, 13, 1968.
- Blitza, D., International reference ionosphere: recent developments., *Radio Science*, 21, 1986.
- Bush, R.I., G.D. Reeves, P.M. Banks, T. Neubert, P.R. Williamson, W.J. Raitt, and D.A. Gurnett, Electromagnetic fields from pulsed electron beam experiments in space: Spacelab-2 results., *Geophys. Res. Lett.*, 14, 10, 1015, 1987.
- Farrell, W.M., D.A. Gurnett, P.M. Banks, R.I. Bush, and W.J. Raitt, An analysis of the whistler-mode radiation from the Spacelab-2 electron beam., *J. Geophys. Res.*, 93, 153, 1988.
- Gekelman, W., and R.L. Stenzel, Ion sound turbulence in a magnetoplasma., *Phys. Fluids*, 21, 1978.
- Gurnett, D.A. and T.B. Burns, The low frequency cut-off of ELF emissions., *J. Geophys. Res.*, 73, 1968.
- Gurnett, D.A., W.S. Kurth, J.T. Steinberg, P.M. Banks, R.I. Bush, and W.J. Raitt, Whistler-mode radiation from the Spacelab-2 electron beam, *Geophys. Res. Lett.*, 13, 225, 1986.
- Harker, K.J., and P.M. Banks, Near fields in the vicinity of pulsed electron beams in space, *Planet. Space Sci.*, 35, 1, 1987.
- Hawkins, J.G., Vehicle charging and return current measurements during electron beam emission experiments from the Shuttle Orbiter., PhD dissertation, Stanford University, 1988.
- Muzzio, J.L.R., ELF Propagation in the plasma sphere based on satellite observations of discrete and continuous forms., Stanford Electronics Lab., Tech. Rept. # 3439-2, 1971.
- Myers, N.B., W.J. Raitt, A.B. White, P.R. Williamson, P.M. Banks, R.I. Bush, S. Sasaki, K-I. Oyama, N. Kawshima, CHARGE-2: A sounding rocket payload to investigate vehicle charging effects due to electron beam emissions., *J. Spacecr. Rockets.*, submitted 1988.
- Neubert, T. and K.J. Harker, Magnetic fields in the vicinity of pulsed electron beams in space., *Planet. Space Sci.*, in press, 1988.
- Neubert, T., J. G. Hawkins, G.D. Reeves, P.M. Banks, R.I. Bush, P.R. Williamson, D.A. Gurnett, and W.J. Raitt, Pulsed electron beam emissions in space, *J. Geomag. Geoelect.*, in press, 1988.
- Okuda, H., and M. Ashour-Abdalla, Ion-acoustic instabilities excited by injection of an electron beam in space., *J. Geophys. Res.*, 93, 1988.
- Reeves, G.D., P.M. Banks, A.C. Fraser-Smith, T. Neubert, R.I. Bush, D.A. Gurnett, and W.J. Raitt, VLF Wave stimulation by pulsed electron beams injected from the space shuttle., *J. Geophys. Res.*, 93, 162,

1988.

- Reeves, G.D., Very low frequency radio waves produced by electron beam injection in space plasmas., PhD dissertation in preparation, Stanford University, 1988.
- Reeves, G. D., P. M. Banks, T. Neubert, R.I. Bush, P.R. Williamson, A.C. Fraser-Smith, D. A. Gurnett, and W. J. Raitt, VLF Wave emissions by pulsed and DC electron beams in space 1: Spacelab-2 observations., J. Geophys. Res., this issue.
- Shawhan, S.D., G.B. Murphy, and J.S. Pickett, Plasma Diagnostics Package initial assessment of the STS 3 orbiter plasma environment., J. Spacecr. Rockets, 21, 387, 1984a.
- Shawhan, S.D., G.B. Murphy, P.M. Banks, P.R. Williamson, and W.J. Raitt, Wave emissions from DC and modulated electron beams on STS-3., Radio Sci., 19, 2, 471, 1984b.
- Stix, T.H., The Theory of Plasma Waves, McGraw-Hill Book Co. Inc., SF, 1962.
- Tribble, A.C., N. D'Angelo, G.B. Murphy, J.S. Pickett, and J.T. Steinberg, Exposed high-voltage source effect on the potential of an ionospheric satellite., J. Spacecr. Rockets, submitted, 1988.
- Winckler, J.R., The application of artificial electron beams to magnetospheric research, Rev. Geophys., 19, 3, 659, 1980.
- Winglee, R.M. and P.L. Pritchett, Space-charge effects during the injection of dense electron beams into space plasmas., J. Geophys. Res., 92, 6114, 1987.
- Winglee, R.M. and W.L. Pritchett, Comparative study of cross-field and field- aligned electron beams in active experiments., J. Geophys. Res., submitted 1988.

5. FIGURE CAPTIONS

Figure 1. The spectral intensity of waves observed during the DC flux tube connection sequence plotted as a function of frequency and time. The data was obtained using the IMP/HELIOS filter bank which had four 10% band-width filters per. frequency decade. Among the features observed are the funnel shaped emissions due to resonance cone propagation, the cut-off of VLF emissions above 30 kHz, and the dependence on frequency of VLF emissions observed at various locations with respect to the conjunction field line. Lower frequency ($f < 1$ kHz) waves are observed at greater distances from the conjunction field line and therefore appear at earlier and later times than higher frequency ($1 < f < 30$ kHz) waves. See figure 7 for the location of the PDP for various times.

Figure 2. The spectral intensity of waves observed during the Pulsed flux tube connection sequence. The format is the same as for figure 1.

Figure 3. A schematic diagram of the square of the index of refraction as a function of frequency with the various wave branches labeled.

Figure 4. A representation of the effects of different propagation angles on the waves observed at the location of the PDP during the flux tube connection sequences. The angle between the conjunction field line and a line connecting the Orbiter and the PDP is labeled β . Frequencies for which waves have a ray angle $\alpha = \beta$ originate at the beam source. Frequencies for which $\alpha > \beta$ originate at points along the beam. Frequencies for which $\alpha < \beta$ will not be observed at the PDP except as evanescent waves.

Figure 5. A schematic of the index of refraction surfaces for various frequencies showing the wave normal and ray angles picked out by the Cherenkov resonance condition. (a) For low frequencies $n(\theta)$ is a closed surface and for $n_{\parallel} = 16$, $\theta \approx 90^\circ$, $\alpha \approx 90^\circ$. (b) For frequencies $f \geq f_{LHR}$, $n(\theta)$ is an open surface. For $\theta < \theta_{res}$, $n_{\parallel} = 16$ picks out wave normals in the central hump. For $f \sim f_{LHR}$ θ is large and $\alpha \approx 0^\circ$. (c) As f increases, θ decreases, and α increases up to a maximum of $\sim 20^\circ$. (d) For $f \rightarrow 30$ kHz, $\theta \rightarrow 0^\circ$, and $\alpha \rightarrow 0^\circ$. (e) Above a critical frequency the resonance condition. $n_{\parallel} = 16$ can no longer be satisfied for wave normal angles $\theta < \theta_{res}$ and only resonance cone propagation is possible

Figure 6. A schematic representation of the propagation effects which determine the three zones of wave amplitude. Zone 1 is identified as being associated a region of the plasma which is highly disturbed by the injection of the electron beam. The limits of zone 2 which contains propagating waves with wave normal angles less than the resonance cone angle is indicated with a bold line and is labeled 'VLF Propagation Region'. A cut-off is observed near the hydrogen ion-cyclotron frequency. The limits of the zone 1 and 2 propagation regions are indicated by plotting the sine of the ray angle times 200 m. The dotted line indicates the limits of zone 3 represented by a distance equal to one perpendicular wavelength from the conjunction field line. Although this figure implies

distinct borders, observations show that the transitions from one zone to another are smooth. Figure 7 can be used to compare this figure with figures 1 and 2.

Figure 7. The perpendicular distance from the conjunction field line as a function of time for (a) the DC flux tube connection sequence and (b) the Pulsed flux tube connection sequence. This figure can be used to compare the propagation region predicted by cold plasma theory (figure 6 - distance scale) to that observed in the IMP/HELIOS data (figures 1 and 2 - time scales).

Figure 8. A spectrogram from the ELF band of the broadband wave receiver showing the two-ion cut-off between 500-600 Hz. This cut-off was determined to be a result of the presence of hydrogen ions with a density of less than 10% of the ambient electron density.

Figure 9. The time-averaged amplitude as a function of frequency for the antenna period shown in figure 8. The change in amplitude at the two-ion cut-off frequency can be observed and the frequency of the cut-off identified.

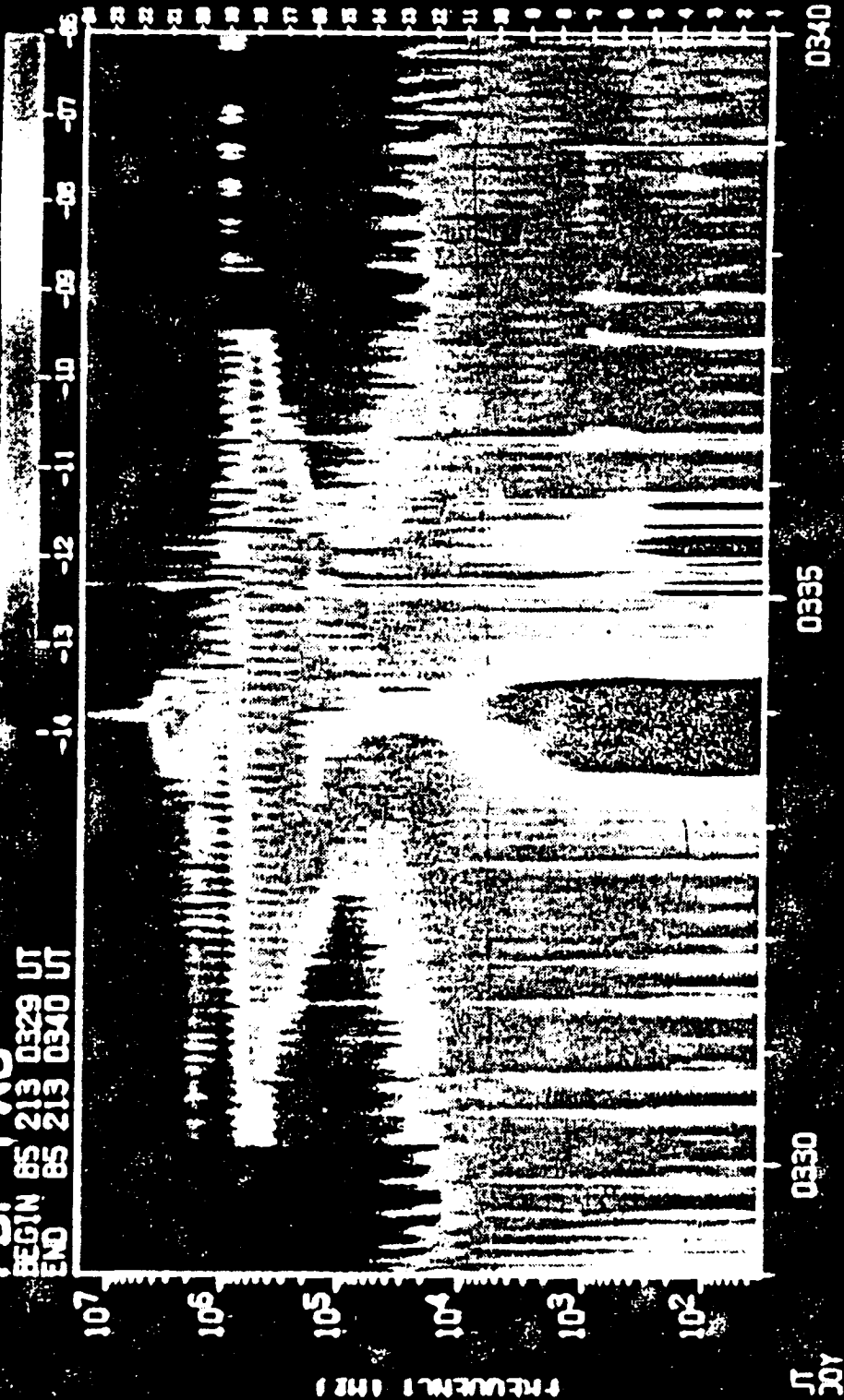
Figure 10. The amplitude of narrowband harmonics of the 1.22 kHz pulsing frequency. The log of the electric field wave amplitude is plotted vs. harmonic number for the predictions using the theory of HB for the $s = 0$, roots 1 and 2; for the $s = \pm 1$, root 2 solutions. Predicted amplitudes were calculated for a perpendicular distance of 50 m from the conjunction field line. Measured amplitudes (dotted lines) are plotted vs. harmonic number for the observations at perpendicular distances of 35 and 90 m.

Figure 11. The variation of amplitude with perpendicular distance to the conjunction field line for the 1.22 kHz fundamental frequency. The log of the electric field wave amplitude is plotted vs. harmonic number for the predictions using the theory of HB for the $s = 0$, roots 1 and 2; for the $s = \pm 1$, root 2 solutions. The $s = 0$, root 1 and the $s = \pm 1$, root 2 solutions represent evanescent waves and the amplitude drops off very rapidly with perpendicular distance. The measured amplitude of the 1.22 kHz signal is also plotted vs. distance (dotted line) and shows better agreement with the $s = 0$, root 2 solutions.

PDP PWS

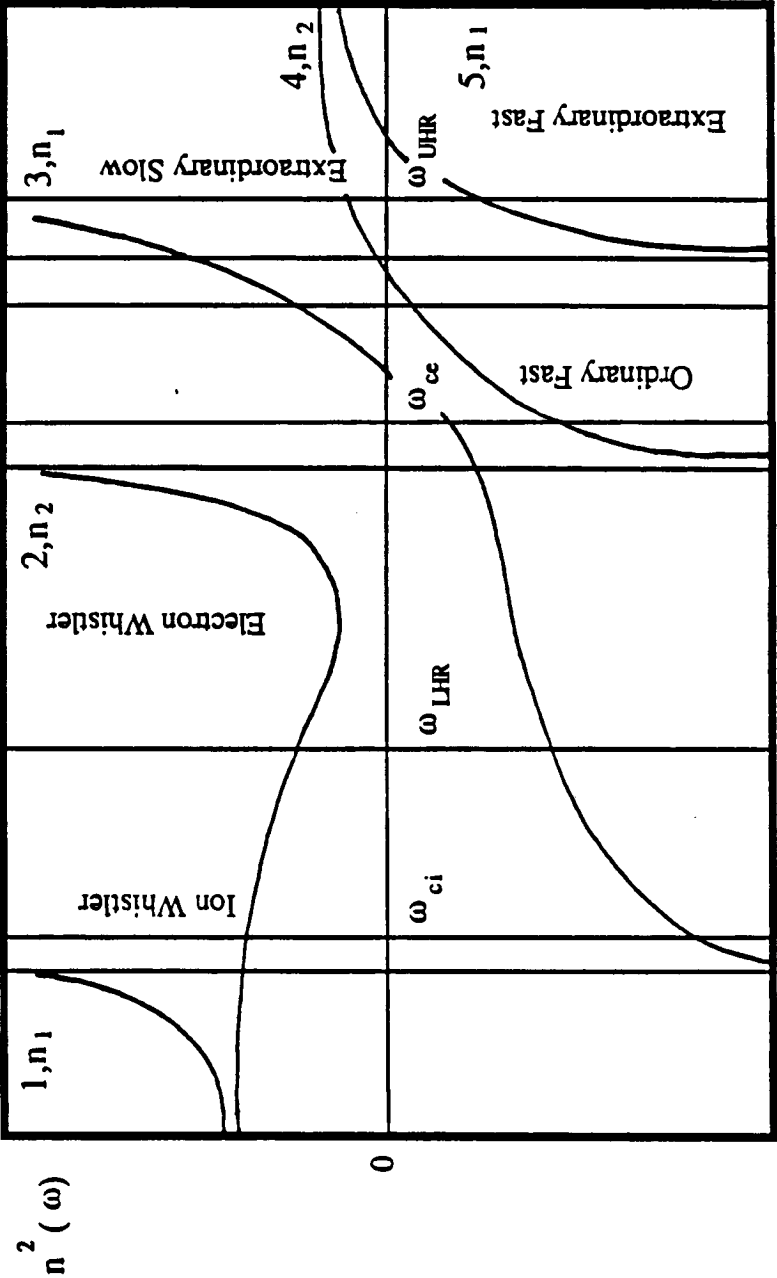
BEGIN 85 213 0329 UT
END 85 213 0340 UT

LOG SPECTRAL DENSITY (V_{rms}^2/Hz)

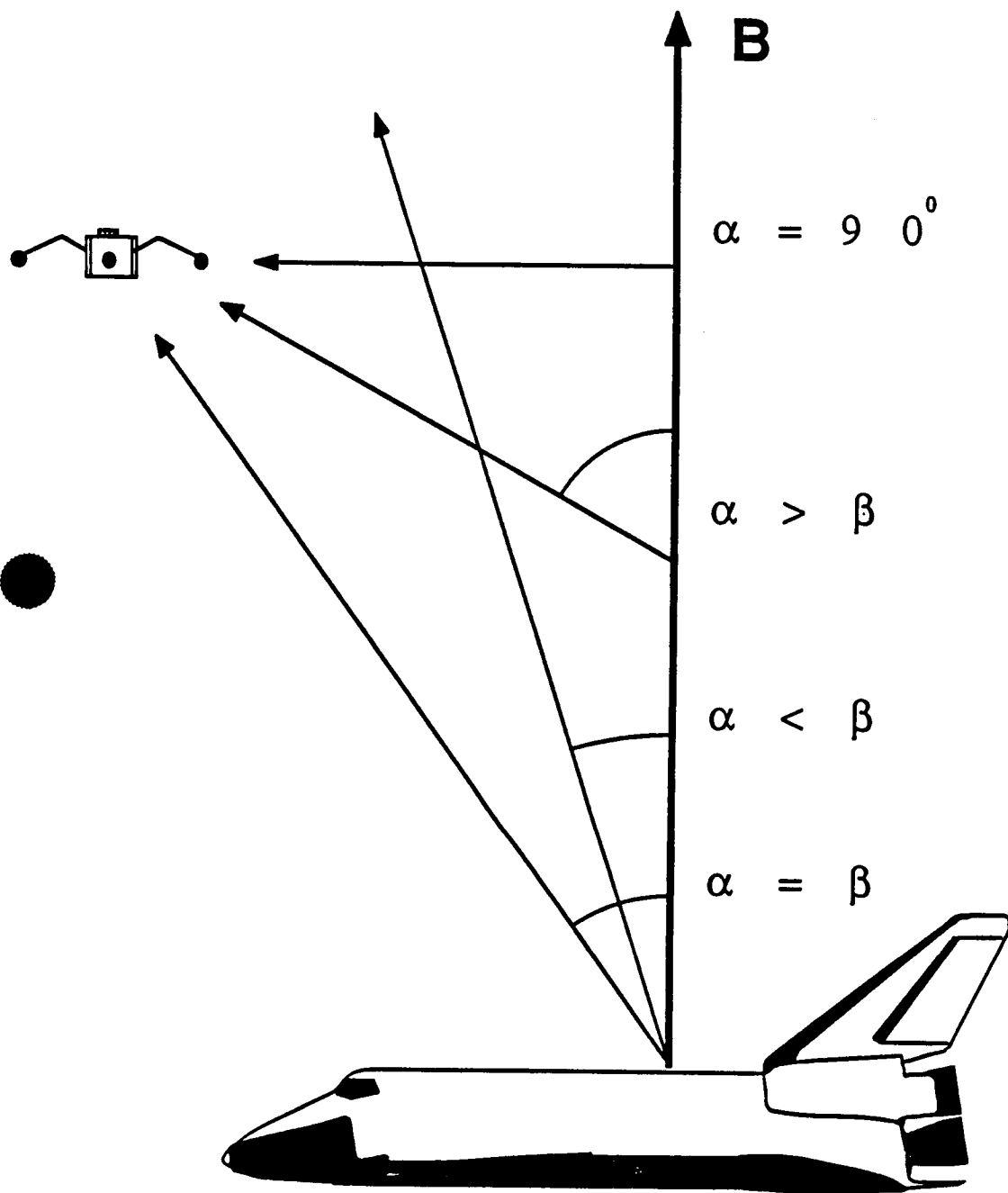




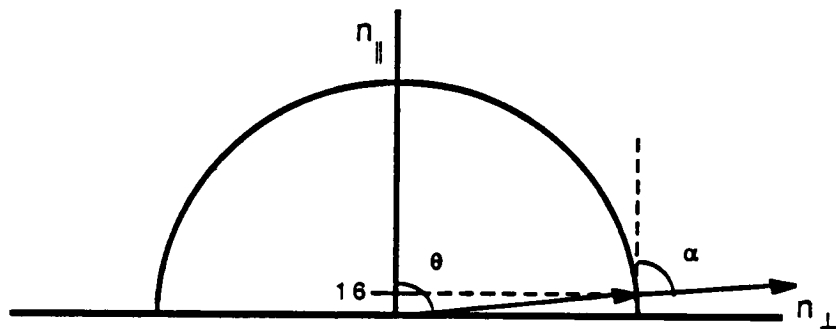
Schematic of the Index of Refraction Branches



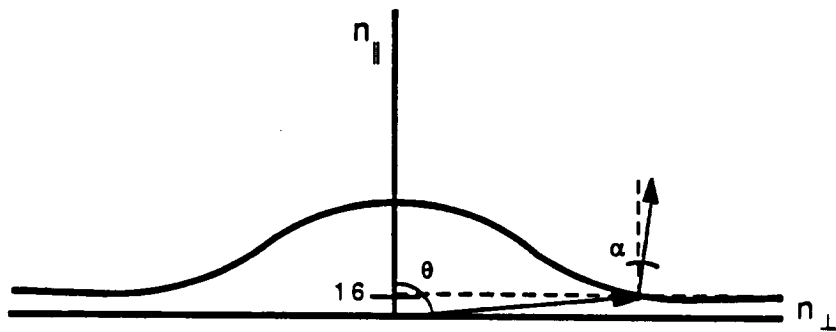
frequency



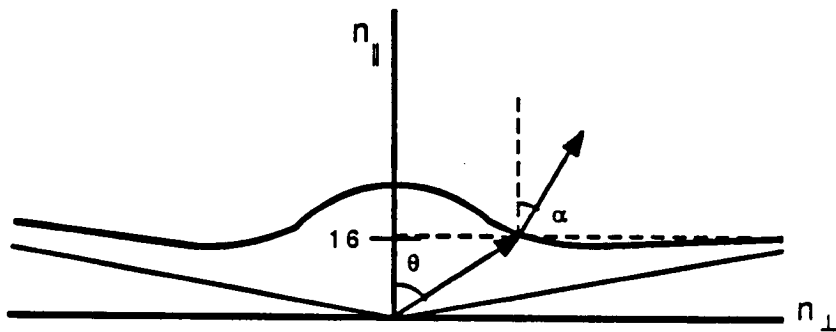
a



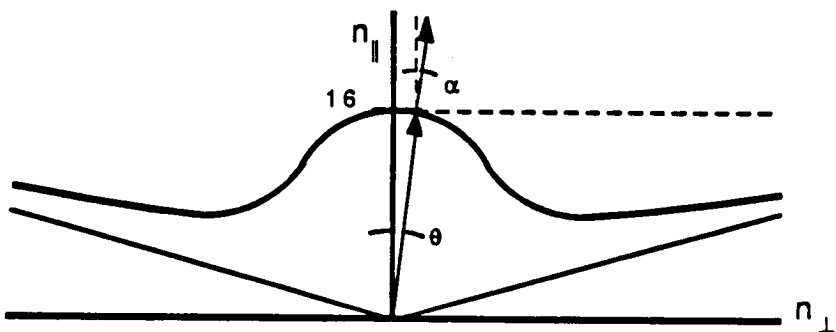
b



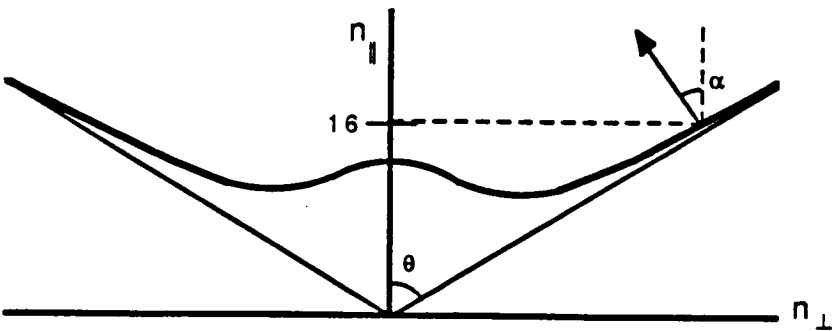
c



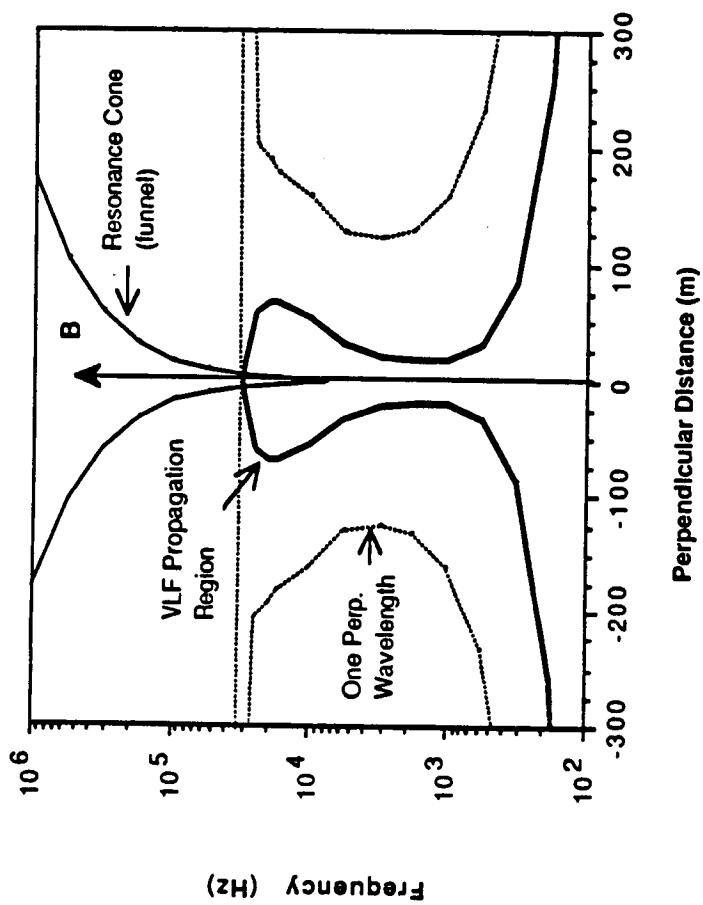
d

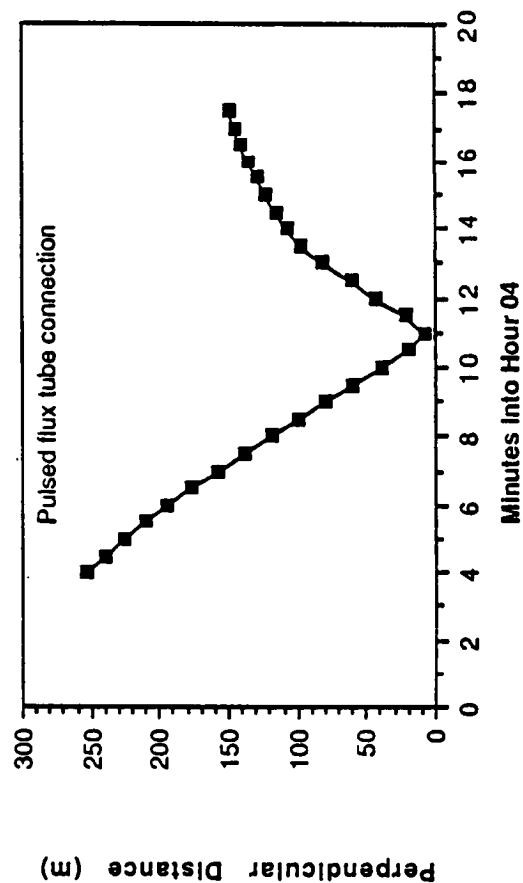
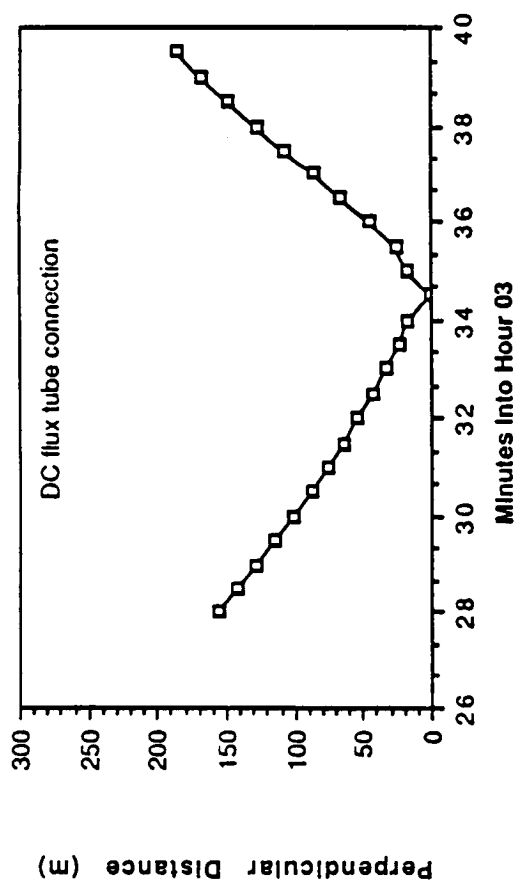


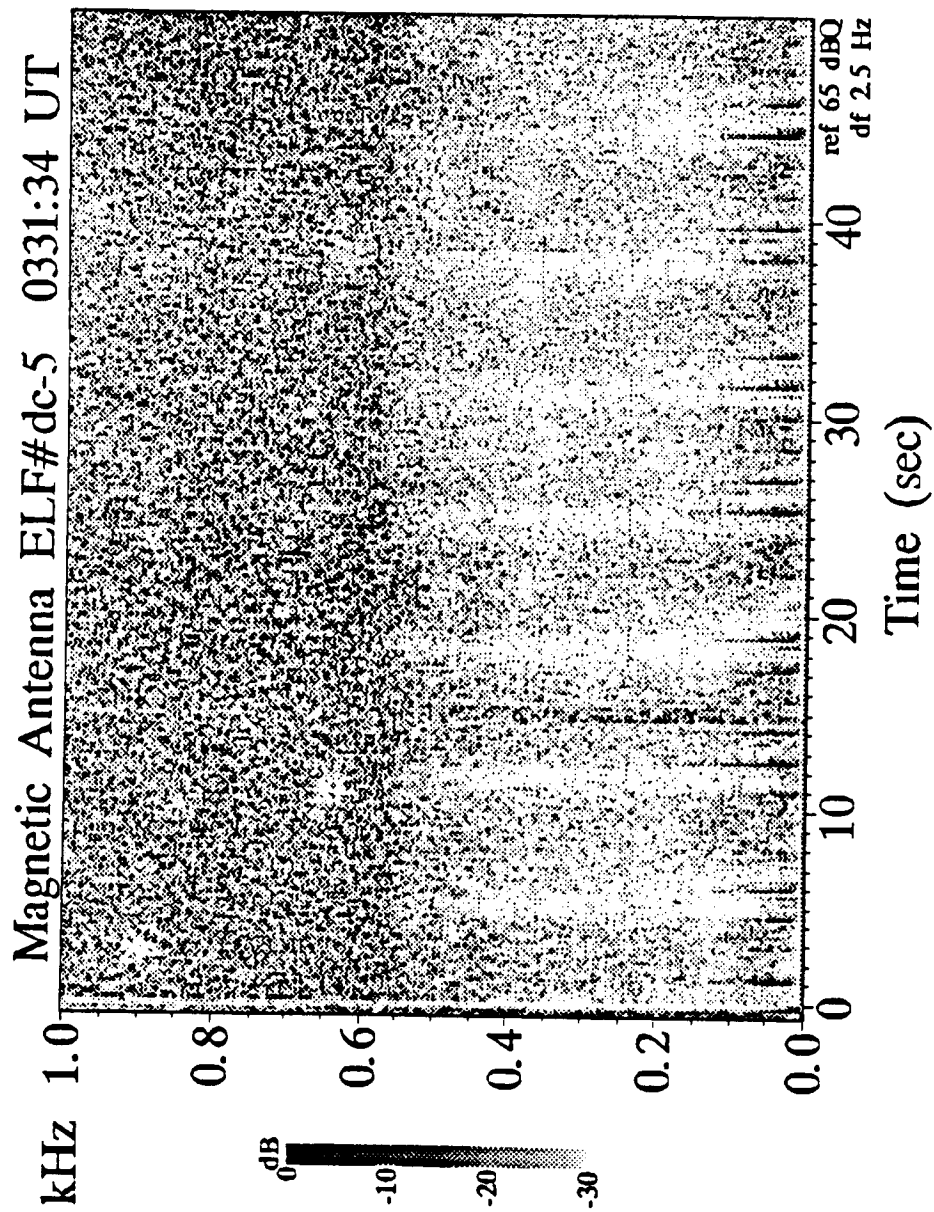
e



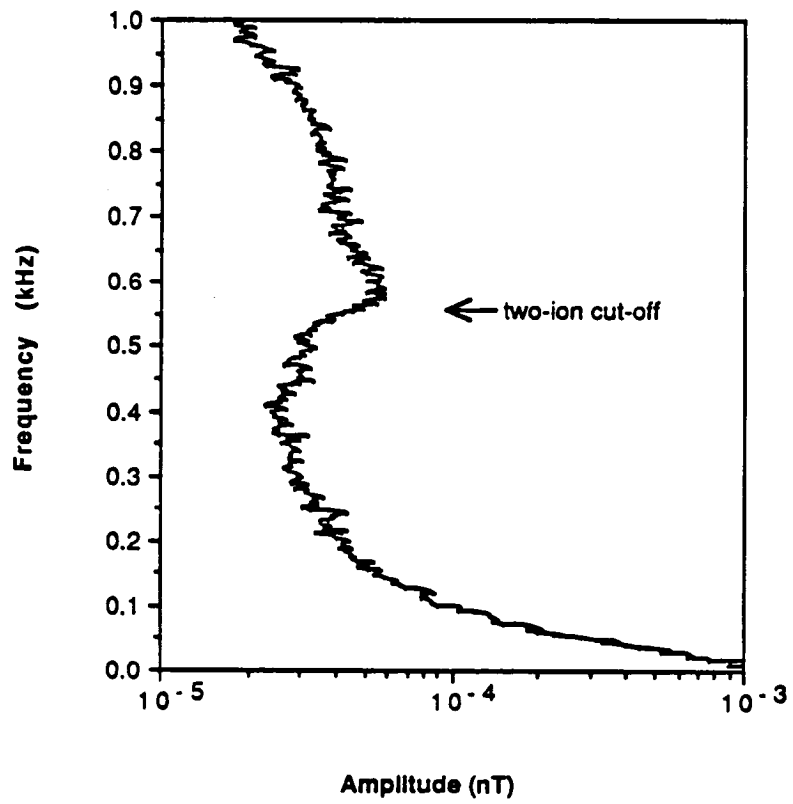
Propagation Regions near the Conjunction Field Line



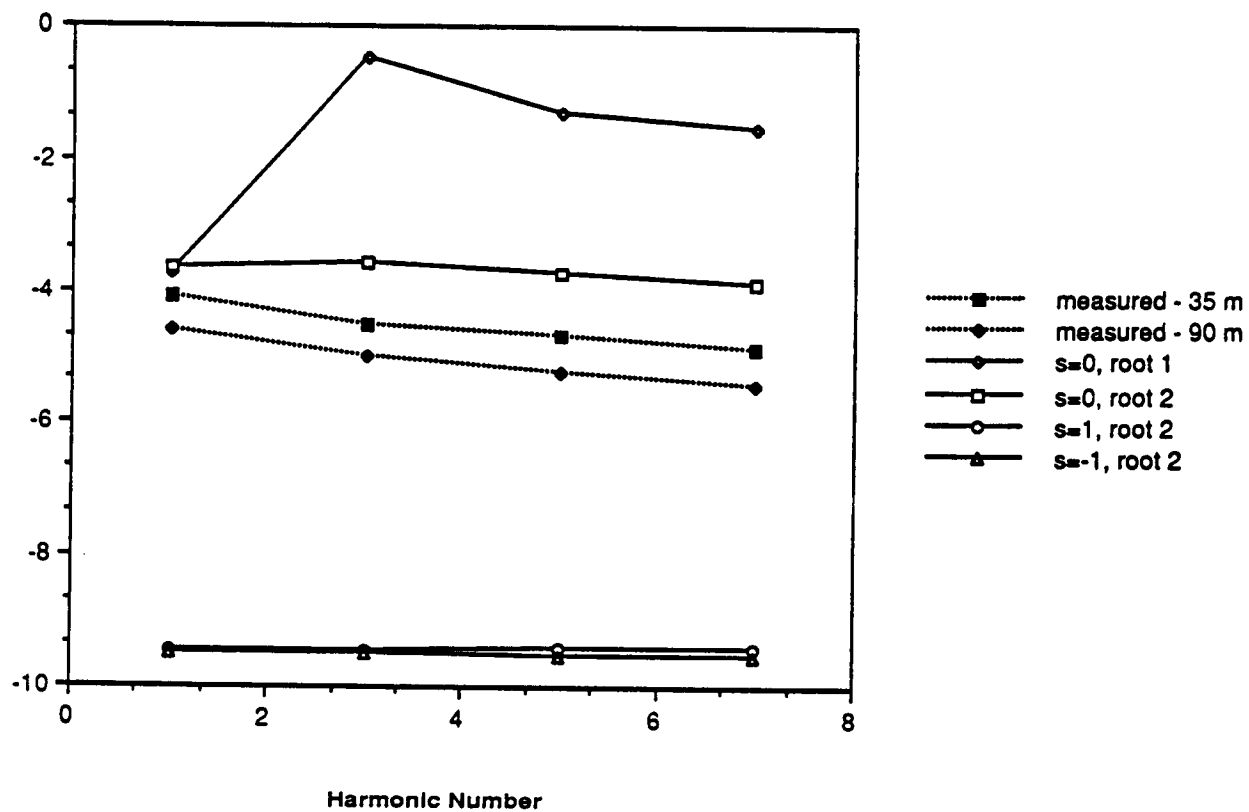




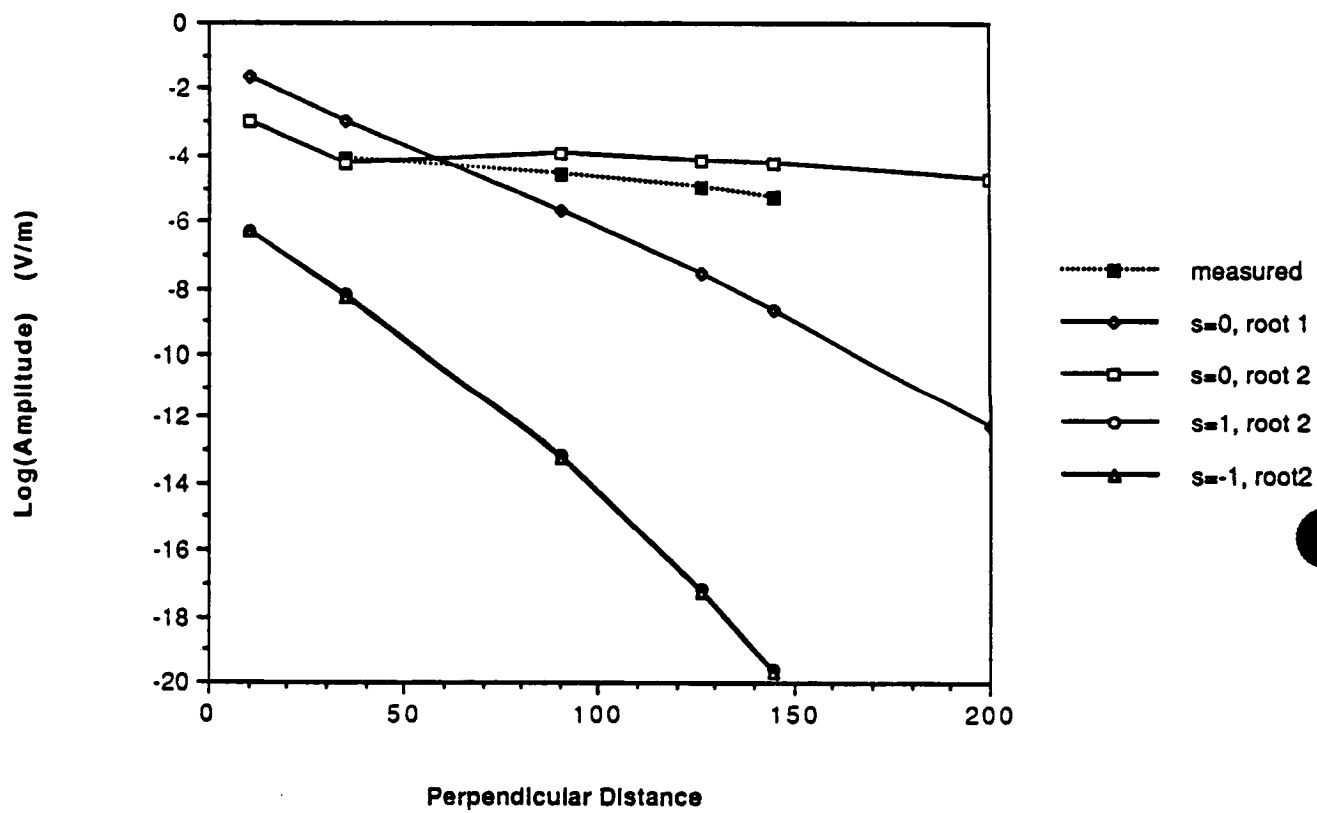
Average Magnetic field Spectrum



Amplitudes at 50 m for Various Modes



Amplitudes of 1.22 kHz for Various Modes



HOT ION PLASMAS FROM THE CLOUD OF NEUTRAL GASES
SURROUNDING THE ORBITER

W. R. Paterson and L. A. Frank

February 1988

To be submitted to Journal of Geophysical Research

Department of Physics and Astronomy
The University of Iowa
Iowa City, Iowa 52242

Abstract

Large intensities of hot positive ions are observed at distances of several hundred meters from the Orbiter with a plasma analyzer on board a small free-flying satellite, the Plasma Diagnostics Package. This ion plasma is inferred to be generated by the charge exchange of ionospheric O^+ ions with the water molecules in a large cloud of gases from the Orbiter. The hot ion plasma forms an ion trail in the Orbiter's wake. A model for the water vapor cloud provides the basis for density estimates as high as $10^9 \text{ H}_2\text{O molecules cm}^{-3}$ at a distance of 50 m from the Orbiter. Thus the Orbiter possesses a substantial co-orbiting atmosphere.

1. Introduction

We report on a series of measurements of hot ion plasmas in the vicinity of the space shuttle Challenger on August 1, 1985. These observations are made with a plasma instrument capable of determining the energy spectra of electrons and positive ions, separately and simultaneously, in the energy range-per-unit charge extending from 2 V to 36 kV. This plasma analyzer is included with other fields and plasma instrumentation in the free-flying, recoverable small satellite PDP, i.e., the Plasma Diagnostic Package.

The PDP spacecraft was one of the components of the Spacelab-2 mission flown on the space shuttle Challenger. Spacelab 2 was carried into orbit on July 29, 1985 and was landed on August 6, 1985. The orbital altitude and inclination were ~ 320 km and 49.5° . Instrumentation for the PDP includes the plasma analyzer, a Langmuir probe, an ion mass spectrometer, a retarding potential analyzer, a differential ion flux probe, a plasma wave receiver and electric field detector, an electrometer, a neutral pressure gauge, and radio receivers. The plasma analyzer is also known in the literature as a Lepedea (Low Energy Proton and Electron Differential Energy Analyzer) [Frank et al., 1978]. The diameter (without booms) and height of the PDP are 1.1 and 1.3 m respectively and the total mass is 285 kg.

Prior to Spacelab 2 the PDP was flown as part of the OSS-1 payload aboard the space shuttle Columbia [Shawhan et al., 1984]. During that flight the PDP was operated while berthed in the payload bay and in the immediate vicinity of the shuttle by means of the Remote Manipulator System

(RMS). During the Spacelab-2 mission the PDP also made measurements from within the bay and while attached to the RMS. In addition, the PDP was released from the Orbiter and flown as an independent satellite. Release of the PDP occurred at 0010 UT on August 1 and retrieval was successfully accomplished at 0620 UT on the same day. Our present interest lies in the plasma observations during free flight of the PDP at distances ranging to ~ 400 m from the space shuttle Challenger, henceforth referred to as the Orbiter. Remarkably intense, hot ion plasmas are found in the vicinity of the Orbiter. We interpret these plasmas in terms of a dense cloud of neutral gasses from and co-orbiting with the Orbiter.

2. Observations

The electrostatic analyzers are constructed of concentric, spherical-segment plates across which a known, variable potential is supplied in order to separate ions and electrons according to their energy-per-unit charge. Because it is necessary to measure the charged particle intensities with respect to both the directions of the local magnetic field \vec{B} and of the instantaneous orbital velocity \vec{V} of the Orbiter and PDP, and because these directions vary as the spacecraft orbit Earth, the electrostatic analyzer is configured to utilize the rotation of the PDP spacecraft so as to measure the particle intensities from almost all directions. One analyzer each for positive ions and electrons employs seven detectors and one entrance aperture for measurements in seven directions in a wide, fan-shaped field-of-view. The plane of this field-of-view is aligned parallel to the spin axis of the PDP such that, with the spin motion of this satellite,

most of the 4π -sr solid angle for particle velocity vectors is observed with the plasma analyzer. Such surveys of the entire angular distributions of hot electron and ion plasmas are acquired once each spin period of the PDP spacecraft, 13.1 seconds.

After the release of the PDP from the RMS the Orbiter's primary and vernier thrusters were fired to increase the distance between the two spacecraft to 90 m. This separation was maintained until 0120 UT. At that time the crew began maneuvering the Orbiter around the PDP. The Orbiter was flown around the PDP twice with each circuit taking place during one 90-minute orbit of Earth. The trajectory of the Orbiter relative to the PDP between 0130 and 0430 UT is depicted in Figure 1. This motion is shown projected into the orbital plane. The relative out-of-plane separation during this time was as large as 350 m while the total distance between the spacecraft ranged from 100 m to 420 m. Following these orbits the Orbiter was flown several times across the path of the PDP so that the PDP passed directly through the Orbiter's wake. At 0527 UT spin-down of the PDP was begun and the PDP was subsequently picked up with the RMS.

An example of the hot ion spectra observed in the vicinity of the Orbiter is shown in Figure 2. The position of the free-flying PDP is at a distance of 280 meters from the Orbiter. The differential, directional intensities of positive ions as a function of energy-per-unit charge are shown in Figure 2. These measurements are taken in the direction parallel to the velocity vector of the spacecraft, i.e., as seen looking into the ram direction due to the spacecraft orbital motion. At these altitudes of

~ 300 km above Earth's surface, the primary ionospheric ion is O^+ [Banks and Kockarts, 1973]. Because the orbital velocity of the spacecraft is 7.8 km s^{-1} , the ram energy-per-unit charge of the ambient O^+ ions is about 5 V. The large intensities of these O^+ ions can be seen in Figure 2. The characteristic thermal energies of the ambient ionospheric O^+ ions are ~ 0.1 eV, an energy below that of the energy resolution of the hot plasma analyzer that is designed for measurements of plasmas with energies greater than several electron volts-per-unit charge. Thus the presence of the ambient O^+ ions in the ionosphere is detected, but their temperatures and densities are not determined.

Large intensities of positive ions are detected at energies significantly greater than those expected for ambient ions. These hot ions are seen at energies-per-unit charge $\gtrsim 10 \text{ V}$ in Figure 2. Of particular interest is the maximum of intensities at ~ 18 V and the significant intensities of hot ion plasmas extending to ~ 60 V. We interpret these ions in terms of ion production by charge exchange in a large cloud of neutral gases that are outflowing from and co-orbiting with the Orbiter.

Consider the neutral gas cloud of the Orbiter. There are a variety of sources of neutral gases from the Orbiter, including waste water, water as a by-product of power generation by fuel cells, combustion from the Orbiter thrusters for attitude control, and He from the cooling of the infrared telescope. The thrusters utilize the reaction between monomethyl hydrazine and N_2O_4 , and several of the combustion products are H_2O , N_2 , CO_2 and CO [Pickett et al., 1985].

Outgassing of volatiles, in particular H_2O , is expected from the surfaces of the Orbiter. These neutral gases should radially outflow from the Orbiter at thermal speeds, \sim hundreds of meters per second. This cloud of neutral gases is moving with a bulk velocity of 7.8 km s^{-1} , i.e., the Orbiter orbital velocity, through the plasmas of Earth's ionosphere. The densities of the ambient ionospheric ions are $\sim 10^4$ to 10^6 cm^{-3} at these altitudes and sufficiently large to ionize a measurable fraction of the neutral molecules in the cloud by charge exchange, i.e., $\text{O}^+ + \text{H}_2\text{O} \rightarrow \text{O} + \text{H}_2\text{O}^+$. Momentum transfer is negligible. These positive ions produced by charge exchange are observed with our plasma instrument. After charge exchange the H_2O^+ ions do not co-orbit with the Orbiter gas cloud but are trapped in the terrestrial magnetic field by the Lorentz force, i.e., these ions form an ion trail in the wake of the Orbiter. The motion of these so-called 'pickup' ions in the reference frame of the Orbiter and PDP are of interest for our observations. In this reference frame, these ions appear to be executing cycloidal motion with an average drift speed due to an electric field $\vec{E} = -\vec{V} \times \vec{B}$. In other words, if the Orbiter velocity \vec{V} is directed perpendicular to the local magnetic field \vec{B} , then the apparent motion of the pickup ions is such that during one period of circular motion of the ion in the plane perpendicular to \vec{B} , the ion speed increases to a maximum of twice V and then decreases to values nearly zero. The average drift velocity of the ion with respect to the Orbiter is $-\vec{V}$ in the direction of the wake. As the angle α between \vec{V} and \vec{B} decreases or increases from 90° the maximum ion energy decreases in proportion to $\sin^2 \alpha$. At angles near 0° and 180° , the energy spectra of the pickup ions become

similar to that for the ionospheric ions and the two ion populations can be difficult to separate with the plasma analyzer. The phenomenon of pickup ions in plasmas moving with respect to neutral gases is of general interest to space plasma physics, e.g., the production of He^+ in the solar wind by infalling interstellar gas [Möbius et al., 1985], the formation of a plasma torus from volcanic gases of the Jovian satellite, Io [Goertz, 1980], and the interaction of cometary coma with the solar wind [Ip and Axford, 1986; Ipavich et al., 1986; Mukai et al., 1986].

Two features of the distributions of pickup ions are noted here in the case of the Orbiter in motion nearly perpendicular to the magnetic field. Because the maximum ion speed is twice the Orbiter and PDP orbital speeds, the maximum energy of the ion is equal to four times that of an ambient ionospheric ion of the same mass as seen at the PDP. Secondly, in a coordinate system referenced to the velocity components of the observed ions in the rest frame of the Orbiter, the distributions are pancake-shaped in a plane perpendicular to \vec{B} and are offset from the origin by the spacecraft velocity vector. For example, these ion velocity distributions are shown in Figure 3 as taken at 0208 UT on August 1, 1985. The distribution function for ion densities, i.e., ions per unit volume $\Delta x \Delta y \Delta z$, and per unit volume of velocity space $\Delta v_x \Delta v_y \Delta v_z$, is given for a plane perpendicular to the local magnetic field. The direction of the Orbiter motion is approximately $+V_x$. Thus the ambient ionospheric plasma is in bulk motion with respect to the Orbiter and is expected to appear as a compact series of circles at $V_x \approx -0.8 \times 10^6 \text{ cm s}^{-1}$. Evidence for this ambient ion plasma can

be seen in Figure 2, although as mentioned earlier this plasma is too cool to fully resolve with the instrument. The pancake distribution of pickup ions with higher energies is the dominant feature to be seen in Figure 3. For this figure and the following Figure 4, the ion mass-per-unit charge is assumed to be 16 a.m.u. (O^+). The results are changed little for masses nearly equal to this value, e.g., H_2O^+ , but must be recomputed if the ion is CO^+ or CO_2^+ . In order to demonstrate that the ion velocity distribution is pancake in shape, i.e., that the motions of the ions are mainly directed perpendicular to the magnetic field \vec{B} , it is necessary to exhibit these ion distribution functions in a plane parallel to \vec{B} . These ion distributions are shown in Figure 4 with the V_z axis taken parallel to \vec{B} , and V_x is perpendicular to \vec{B} and almost along the direction of the Orbiter orbital motion. It is seen that the component of ion motion, V_z , along \vec{B} is smaller relative to that perpendicular to \vec{B} , V_x . Thus the observed ions are found to be in motion primarily in a direction perpendicular to the magnetic field (the pancake distribution) with an offset from the coordinate origin (the average drift speed of the ions with respect to the Orbiter and PDP). These are the expected signatures of pickup ions from the interaction of the ionosphere with the neutral gas cloud of the Orbiter.

The species of the pickup ions are not directly determined with the plasma instrumentation, but may be inferred from energy spectra such as that shown in Figure 2. The energy-per-unit charge for the secondary peak is ~ 18 V. The most likely ion with this energy at twice the Orbiter speed is H_2O^+ . At higher energies, $\gtrsim 20$ V, the ions are heavier, CO^+ , CO_2^+ , and others from the thrusters. The identification of H_2O^+ as the dominant

pickup ion in the lower mass range is in agreement with independent ion mass analyses at lower energies [Grebowsky et al., 1987]. This identification is also consistent with observations of neutral water [Carignan and Miller, 1983; Narcisi et al., 1983; Wulf and Von Zahn, 1986] and water ions [Grebowsky et al., 1983; Narcisi et al., 1983; Hunton and Calo, 1985] in the near vicinity of the Orbiter during other Shuttle flights.

3. Model of the Water Cloud

We can use the observations of the densities of pickup H_2O^+ ions to develop a model of the water vapor cloud that co-orbits with the Orbiter. We assume that the radial velocity of the water molecules from the Orbiter is similar to that for thermal velocities corresponding to a temperature ~ 300 K, or $V_t \approx 5 \times 10^4$ cm s $^{-1}$. This velocity is much less than the spacecraft orbital velocity of $V \approx 8 \times 10^5$ cm s $^{-1}$. The water vapor expands radially outwards from the Orbiter until the molecules collide with those of the ambient neutral atmosphere, primarily atomic oxygen OI. The densities of OI, [OI], are in the range of $\sim 1 \times 10^8$ to 3×10^8 cm $^{-3}$. The MSIS-83 model [Hedin, 1983] for the neutral ambient atmosphere is used for our calculations. To estimate the cross section for collisions of H_2O with OI we assume hard-sphere collisions and typical diameters of 4.6×10^{-8} cm for H_2O and 2.6×10^{-8} cm for OI [McDaniel, 1964], where the diameter for Ne is used for OI. The cross section estimated in this way is $\sim 4 \times 10^{-15}$ cm 2 , and the mean free paths Λ are about 10 km. Thus, relative to the Orbiter, a water molecule moves an average distance $d \approx (V_t/V) \Lambda$, or ~ 700 m before its first collision with an atmospheric oxygen atom. The

number density of water molecules, $[H_2O]$, is assumed to vary with radial distance R from the Orbiter as

$$[H_2O] = C (R_0/R)^2 \exp(-(R-R_0)/d), \quad (1)$$

where R_0 is taken as 10 meters, or the approximate linear dimension of the Orbiter.

The relationship between the densities of pickup H_2O^+ ions and of the neutral water molecules must be found in order to determine the constant C in equation (1). The primary source of the H_2O^+ ions is charge exchange of H_2O with the ambient ionospheric O^+ . Photoionization by solar ultraviolet radiation and impact ionization by atmospheric photoelectrons proceed at much slower rates. Because O^+ is the dominant ionospheric ion at the Orbiter altitudes, the O^+ densities, $[O^+]$, are taken to be equal to the electron densities that are simultaneously measured by the Langmuir probe on the PDP spacecraft (data from courtesy of N. D'Angelo). The cross section for the charge exchange $H_2O + O^+ \rightarrow H_2O^+ + O$ appears uncertain. For the 5 eV energy of O^+ relative to the water cloud values of $2.6 \times 10^{-15} \text{ cm}^2$ [Turner and Rutherford, 1968] and $0.6 \times 10^{-15} \text{ cm}^2$ [Murad and Lai, 1986] have been reported. We adopt the cross section reported by Turner and Rutherford [1968], $2.6 \times 10^{-15} \text{ cm}^2$. The relationship between the water molecule densities, $[H_2O]$, and the ion densities, $[H_2O^+]$ and $[H_3O^+]$, is given by the following equations:

$$\frac{\partial}{\partial t} [H_2O^+] = \gamma_1 [H_2O] [O^+] - \gamma_2 [H_2O^+] [H_2O] - \alpha_1 [H_2O^+] [e^-] \quad (2)$$

$$\frac{\partial}{\partial t} [H_3O^+] = \gamma_2 [H_2O^+] [H_2O] - \alpha_2 [H_3O^+] [e^-] \quad (3)$$

where the rate coefficients are given in Table 1. To calculate the rate coefficient γ_1 for charge exchange between H_2O and O^+ we multiply the cross section for this reaction with the relative speed of the reactants, $7.8 \times 10^5 \text{ cm s}^{-1}$. The rate constant γ_2 is for the reaction $H_2O^+ + H_2O \rightarrow H_3O^+ + OH$. The kinetic energy of the H_2O^+ ions relative to the water cloud ranges from approximately 0 eV to 23 eV due to the gyratory motion of the H_2O^+ ions. For γ_2 we have used the rate at 300 K [Albritton, 1978]. The coefficients α_1 and α_2 for the dissociative recombination of H_2O^+ and H_3O^+ with electrons are estimates by Sjolander and Szuszczewicz [1979]. Equations (2) and (3) are expected to be applicable for ions and neutral atoms within distances up to $\sim 10 \text{ km}$ from the Orbiter. Also the densities of ionospheric O^+ ions are found to be sufficiently unperturbed that they may be taken as a constant as the water cloud moves through the ionosphere for distances $\gtrsim 20 \text{ m}$ from the Orbiter. Equation (1) for the radial dependence of water molecule densities and equations (2) and (3) for the relationship of the neutral water molecule and water ion densities are solved numerically with a fifth-order Runge-Kutta algorithm in a reference frame at rest with respect to the instantaneous position of the center of curvature for pickup ion motion, i.e., the guiding center. The constant C in equation (1) is then found by determining the H_2O^+ density, $[H_2O^+]$, by numerical integration of ion velocity distributions such as that shown in Figures 3 and 4. The specific time for determination of $[H_2O^+]$, and then C , is 0350 UT on August 1. If $[H_2O]$ is in units of molecules cm^{-3} , then

$C = 4 \times 10^{10}$. For our following discussion we assume that the water release rate from the Orbiter is constant. No major waste water releases occur during the PDP free-flight.

In Figure 5 is given an example of the results from the model calculations for the water vapor cloud surrounding the Orbiter and for the ion densities in its wake. The abscissa is taken parallel to the Orbiter motion but offset such that this coordinate axis lies at a distance of 50 m from the Orbiter at closest approach (at 0 km on abscissa scale). For this example, the Orbiter velocity \vec{V} is perpendicular to the geomagnetic field \vec{B} . The water vapor densities at 50 m from the Orbiter are large, $\sim 6 \times 10^9$ H_2O molecules cm^{-3} , and greater than that of the ambient atmosphere. These densities decrease to $\sim 1 \text{ cm}^{-3}$ at a distance of 8 km from the Orbiter. The column density as seen from the Orbiter is also large, $\sim 4 \times 10^{13}$ H_2O molecules cm^{-2} . This column density exceeds that corresponding to the threshold of the infrared telescope in the bay of the Orbiter by about an order of magnitude [Fazio, 1982]. The rate of water release from the Orbiter that is necessary to sustain the water cloud is $\sim 2.5 \times 10^{22}$ molecules s^{-1} . This rate implies a total water loss from the Orbiter, excluding direct losses from water dumps and thruster firings, of ~ 500 kg during the eight-day mission. Although there are inaccuracies inherent in our simple model, such as due to atmospheric ram effects in the immediate vicinity of the Orbiter, the above assessment of the properties of the neutral water cloud is probably accurate to within factors of 3.

4. The Water Ion Trail

The computed water ion densities in the wake of the Orbiter are also shown in Figure 5. These H_2O^+ densities are in the range of 5% of the ionospheric O^+ densities. This ion trail is long, $\gtrsim 10$ km, and is expected to be dissipated primarily by recombination with electrons and the impact of the hot water ions with the ambient oxygen atoms. This latter loss term is not included in equation (2) that is used for the water ion and molecule densities at closer distances to the Orbiter. The pickup ion velocity distributions are in substantial nonequilibrium with that of the ionospheric ions, a situation likely to drive plasma instabilities responsible for the generation of the observed broadband electrostatic noise in the wake [Gurnett et al., 1986; Scarf et al., 1986]. In order to obtain measurements of the unperturbed ionospheric plasmas it is evident from Figure 4 that these observations must be made at distances beyond 1 to 2 km upstream from the Orbiter.

In the rest frame of the ionosphere the pickup ions move along the magnetic field with a component of velocity equal to $\vec{V} \cdot \vec{B}/B$. The results of calculations with \vec{B} and \vec{V} at an angle of 60° are shown in Figures 6 and 7. Figure 6 is similar to Figure 5 in that the abscissa is parallel to the direction of motion of the spacecraft and passes within 50 m of the center of the water cloud. Ahead of the Orbiter the ion densities are nearly equal to the densities calculated for \vec{B} and \vec{V} at an angle of 90° (Figure 5). Behind the Orbiter, however, the ion densities decrease along this axis due to the ion motion along the magnetic field. Figure 6

displays contours of constant $[H_2O^+]$ in the coordinate plane parallel to \vec{B} and \vec{V} . It is clear from this figure that the trail of ions behind the Orbiter does not extend directly opposite \vec{V} , but points in a direction that is perpendicular to \vec{B} . The ion trail extends directly behind the Orbiter only when \vec{B} and \vec{V} are at an angle of 90° .

5. Observed Water Ion Densities

Observations of the densities of pickup H_2O^+ ions during approximately two Earth orbits of the PDP while this spacecraft is in free-flight are shown in Figure 8. Also shown in this figure are the calculated pickup ion densities as expected from the model of the water vapor cloud that surrounds the Orbiter, as presented in our previous discussion. The water vapor cloud is assumed to be time-independent for this period. The position angle θ is the angle between the velocity vector \vec{V} of the spacecraft orbital motion and the direction from the Orbiter to the PDP. The distance between the PDP and the Orbiter is given as R in Figure 8. In order to compute the pickup ion densities from the model of the water vapor cloud, the ambient O^+ density is assumed to be equal to the ionospheric electron densities as measured with the Langmuir probe on the PDP. Reliable measurements of these electron densities are not available during the two periods of ~ 0230 to 0250 UT and ~ 0405 to 0420 UT. The densities are assumed to be 10^4 cm^{-3} for these two periods. Inspection of Figure 7 shows that there is general qualitative agreement between the observed and computed H_2O^+ densities and, for a substantial fraction of this series of observations, quantitative agreement as well. However, for certain time

periods, e.g., 0310 - 0330 UT and 0445 - 0500 UT, discrepancies between observed and computed densities are evident. Such disparity may arise from a temporal fluctuation of the water vapor cloud of the Orbiter or from our inability to accurately separate the pickup ion densities from those of the ambient ionosphere. The diurnal variations of pickup ion densities as seen in Figure 8 are primarily due to a similar variation of the ionospheric O^+ densities that charge exchange with the neutral water molecules along the path of the Orbiter. No hot ion densities that greatly exceed those due to charge exchange are found with our observations. The somewhat higher densities relative to those from the model during the period 0230 to 0250 UT do not exceed the observational uncertainties.

6. Discussion

The velocity distributions of hot, positive ions observed during the PDP free flight are characteristic of ions picked up from a cloud of gases co-orbiting with the Orbiter. Because the cloud has a speed V through the ionosphere the ions form flat velocity distributions in the plane perpendicular to Earth's magnetic field. Distributions of this type were observed throughout the free flight with densities ranging from a few tens per cubic centimeter to nearly 10^4 cm^{-3} . In the reference frame of the spacecraft these ions are expected to have a maximum energy four times greater than the energy of ionospheric ions of similar mass. The observed energy spectra indicate that the dominant ion species is most likely H_2O^+ although more massive species appear to be present as well. This identification is consistent with measurements from the Ion Mass Spectrometer also on board the PDP [Grebowsky et al., 1987]. From these

observations we conclude that the Orbiter is surrounded by a substantial cloud of gases and that neutral water is a major constituent of this cloud. We infer that the observed ions are produced primarily by reactions of gases within the cloud with ambient ionospheric ions, the dominant reaction being charge exchange between H_2O^+ and OI .

In contrast to the shell-like velocity distributions of pick-up ions observed at comet Halley [Mukai et al., 1986] and in the solar wind [Möbius, et al., 1985], the pick-up ions observed during the PDP free flight are seen to have retained their initial pancake distributions. These ions are swept from the cloud by the terrestrial magnetic field. Since the time constant for recombination of H_2O^+ with electrons is approximately 10 s, an ion tail with a length $\gtrsim 10$ km is expected to extend behind the Orbiter. The Lorentz force on the ions acts transverse to the direction of the magnetic field, and the ion motion along the field is unaffected. In this way the ion tail can be driven either downwards into the atmosphere or upwards away from the atmosphere depending on the relative orientation of \vec{B} and \vec{V} .

Our simple model of the water cloud and the ion chemistry within that cloud accounts for much of the variation seen in the time-history of observed pick-up densities. We find that our assumption of radial flow at a constant rate is adequate in providing qualitative agreement between measured and calculated H_2O^+ densities. In particular, no increase in flow seems to occur at sunrise when Orbiter surfaces are suddenly exposed to sunlight. Instead, the observed increase in H_2O^+ density at sunrise appears to be due to the coincident increase in the density of ionospheric

O^+ . Higher ion densities could also be the signature of another heating mechanism for ions in the water cloud of the Orbiter. Enhanced ionization in the neutral water vapor cloud is not expected from the critical ionization velocity effect proposed by Alfvén [1954] for gases in bulk motion with respect to a plasma and with bulk speeds exceeding that corresponding to the ionization potential of the neutral molecules. The ionization potential for H_2O^+ is 12.6 eV, and the kinetic energy of the H_2O molecules with respect to the ionospheric plasmas is only 5.7 eV.

Acknowledgements

We express our appreciation to N. D'Angelo for kindly allowing us the use of the electron densities from the Langmuir probe. Our gratitude is also conveyed to the flight crew C. G. Fullerton, R. D. Bridges, Jr., and S. Musgrave, the mission specialists A. England and K. Henize, and the payload specialists L. Acton and J.-D. Bartoe, whose skills and efforts made our measurements possible. Similar acknowledgements are given to the alternate payload specialists D. Prinz and G. Simon, to the mission scientist E. W. Urban and his assistant K. S. Clifton, and to the mission manager R. C. Lester. At the University of Iowa the efforts of the project manager for the PDP spacecraft, R. F. Randall, and his engineering staff were essential to the successful implementation of our scientific investigation. This research was supported in part by the National Aeronautics and Space Administration under contract NAS8-32807 and grant NGL-16-001-002.

Figure Captions

- Figure 1. Orbiter trajectory during the free flight. The Orbiter motion relative to the PDP is shown projected into the Orbital Plane. The out-of-plane separation ranged from 0 m to 340 m. Maximum out-of-plane excursions occurred near 0215 and 0350 UT.
- Figure 2. Energy spectrum of positive ions as observed in the orbital ram direction with an electrostatic analyzer on the free-flying spacecraft PDP.
- Figure 3. The velocity distribution for hot ions in the vicinity of the Orbiter. The velocity vector for the Orbiter orbital motion is approximately along the $+V_x$ axis. The geomagnetic field vector is directed perpendicular to the plane of the figure. The density value for the outer contour is shown. Each successive inner contour corresponds to a factor of 10 increase in densities.
- Figure 4. Continuation of Figure 3, but for a plane rotated by 90° to include the direction of the geomagnetic field vector ($+V_z$).
- Figure 5. Densities of H_2O , H_2O^+ , and H_3O^+ as computed from a model based upon observations of pickup ion densities. The abscissa is taken along a line parallel to the velocity vector of the Orbiter, but displaced by 50 m, i.e., 0 km corresponds to a

distance of 50 m from the Orbiter. The ambient densities of OI and O^+ are $2.3 \times 10^8 \text{ cm}^{-3}$ and $4 \times 10^5 \text{ cm}^{-3}$, respectively. For this calculation the direction of orbital motion and the magnetic field are taken to be at an angle of 90° .

Figure 6. Densities of H_2O , H_2O^+ , and H_3O^+ computed from the model. The ambient densities of OI and O^+ are the same as for Figure 5. The direction of orbital motion and the magnetic field for this case are at an angle of 60° .

Figure 7. Contours of constant $[H_2O^+]$ calculated from the model for the case where \vec{B} and \vec{V} are at an angle of 60° . The coordinate origin is at the center of the water cloud (the Orbiter).

Figure 8. Comparison of the observed densities of pickup water ions with computed values from the model of the water vapor cloud that co-orbits with the Orbiter. Observations are shown for most of the free-flight period of the PDP. Orbiter thruster firings do not occur during the periods selected for determining the water ion densities.

References

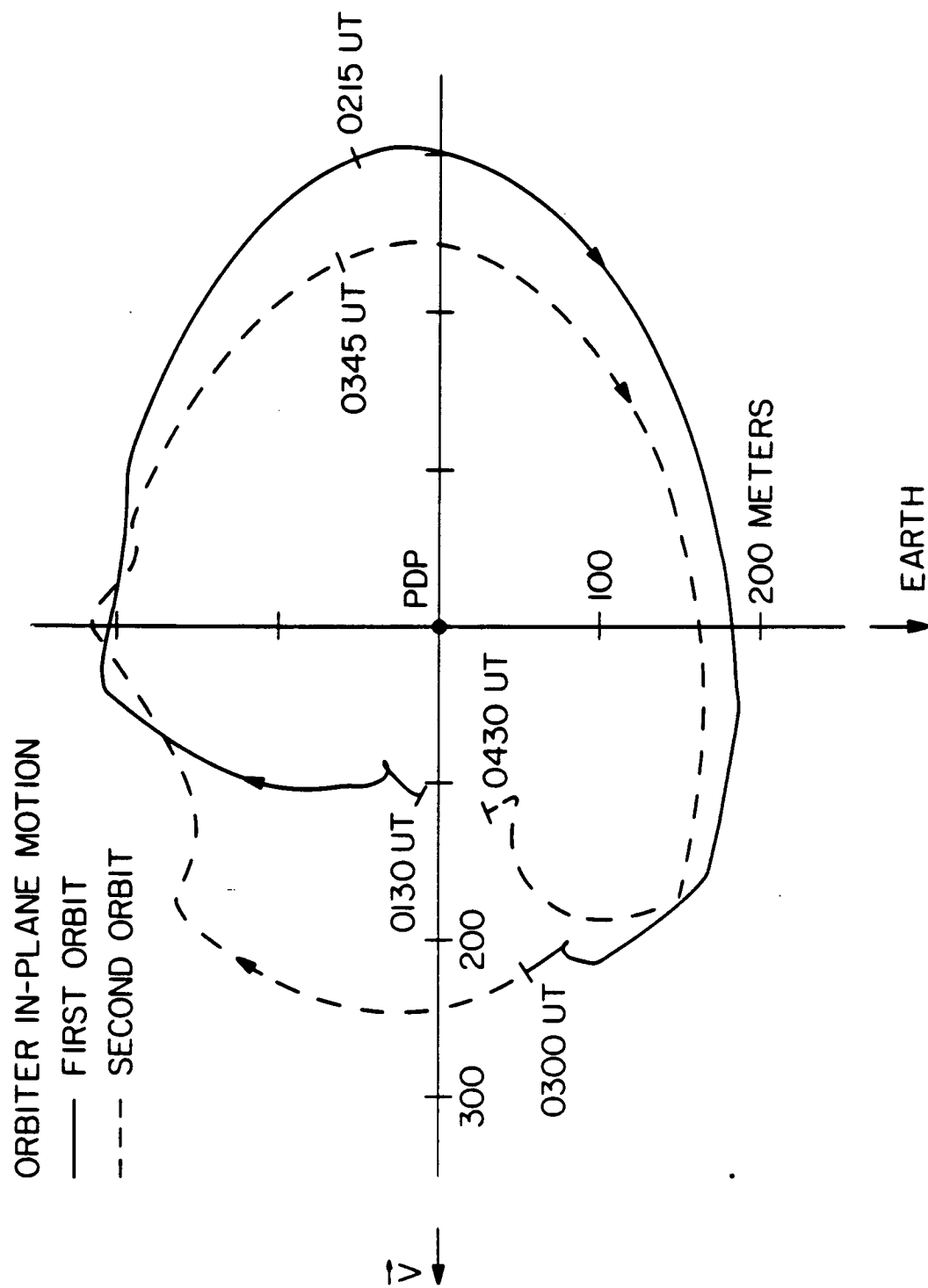
- Albritton, D. L., Ion-neutral reaction rate constants measured in flow reactors through 1977, At. Data Nucl. Tables, 22, 1-101, 1978.
- Alfvén, H., On the Origin of the Solar System, 194 pp., Clarendon, Oxford, 1954.
- Banks, P. M., and G. Kockarts, Aeronomy Part B, 355 pp., Academic, New York, 1973.
- Carignan, G. R., and E. R. Miller, in STS-2, -3, -4 Induced Environment Contamination Monitor (IECM) Summary Report, edited by E. R. Miller, pp. 87-101, NASA TM-82524, Marshall Space Flight Center, Alabama, 1983.
- Fazio, G. G., A small helium-cooled infrared telescope, in Spacelab Mission 2 Experiment Descriptions, edited by K. S. Clifton, pp. 13-16, NASA TM-82477, Marshall Space Flight Center, Alabama, 1982.
- Frank, L. A., D. M. Yeager, H. D. Owens, K. L. Ackerson, and M. R. English, Quadrispherical LEPEDAS for ISEE's-1 and -2 plasma measurements, IEEE Transactions on Geoscience Electronics, 16, pp. 221-225, 1978.
- Goertz, C. K., Io's interaction with the plasma torus, J. Geophys. Res., 85, pp. 2949-2956, 1980.
- Grebowsky, J. M., M. W. Pharo III, H. A. Taylor Jr., and I. J. Eberstein, Measured thermal ion environment of STS-3, AIAA Pap., 83-2597, 1983.
- Grebowsky, J. M., H. A. Taylor, Jr., and M. W. Pharo III, Thermal ion perturbations observed in the vicinity of the space shuttle, Planet. Space Sci., 35, pp. 501-513, 1987.

- Gurnett, D. A., T. Z. Ma, R. R. Anderson, O. H. Bauer, G. Haerendel, B. Häusler, G. Paschmann, R. A. Treumann, H. C. Koons, R. Holzworth, and H. Lühr, Analysis and interpretation of the shocklike electrostatic noise during the AMPTE solar wind lithium releases, J. Geophys. Res., 91, pp. 1301-1309, 1986.
- Hedin, A. E., A revised thermospheric model based on mass spectrometer and incoherent scatter data: MSIS-83, J. Geophys. Res., 88, pp. 10,170-10,188, 1983.
- Hunton, D. E., and J. M. Calo, Low energy ions in the shuttle environment: evidence for strong ambient-contaminant interactions, Planet Space Sci., 33, pp. 945-951, 1985.
- Ip, W.-H., and W. I. Axford, The acceleration of particles in the vicinity of comets, Planet. Space Sci., 34, pp. 1061-1065, 1986.
- Ipavich, F. M., A. B. Galvin, G. Gloeckler, D. Hovestadt, B. Klecker, and M. Scholer, Comet Giacobini-Zinner: In situ observations of energetic heavy ions, Science, 232, pp. 366-369, 1986.
- McDaniel, E. W., Collision Phenomena in Ionized Gases, 775 pp., John Wiley and Sons, New York, 1964.
- Möbius, E., D. Hovestadt, B. Klecker, M. Scholer, G. Gloeckler, and F. M. Ipavich, Direct observations of He^+ pick-up ions of interstellar origin in the solar wind, Nature, 318, pp. 426-429, 1985.
- Mukai, T., W. Miyake, T. Terasawa, M. Kitayama, and K. Hirao, Plasma observation by Suisei of solar-wind interaction with comet Halley, Nature, 321, pp. 299-303, 1986.

- Murad, E., and S. T. F. Lai, Some charge exchange reactions involving H_2O , Chem. Phys. Lett., 126, pp. 427-429, 1986.
- Narcisi, R., E. Trzcinski, G. Federico, L. Wlodyka, and D. Delorey, The gaseous and plasma environment around space shuttle, AIAA Pap., 83-2659, 1983.
- Pickett, J. S., G. B. Murphy, W. S. Kurth, C. K. Goertz, and S. D. Shawhan, Effects of chemical releases by the STS 3 orbiter on the ionosphere, J. Geophys. Res., 90, pp. 3487-3497, 1985.
- Scarf, F. L., F. V. Coroniti, C. F. Kennel, D. A. Gurnett, W.-H. Ip, and E. J. Smith, Plasma wave observations at comet Giacobini-Zinner, Science, 232, pp. 377-381, 1986.
- Shawhan, S. D., G. B. Murphy, and J. S. Pickett, Plasma diagnostics package initial assessment of the shuttle orbiter plasma environment, J. Spacecr. Rockets, 21, pp. 387-391, 1984.
- Sjolander, G. W., and E. P. Szuszczewicz, Chemically depleted F_2 ion composition: measurements and theory, J. Geophys. Res., 84, pp. 4393-4399, 1979.
- Turner, B. R. and J. A. Rutherford, Charge transfer and ion-atom interchange reactions of water vapor ions, J. Geophys. Res., 73, pp. 6751-6758, 1968.
- Wulf, E., and U. von Zahn. The shuttle environment: effects of thruster firings on gas density and composition in the payload bay. J. Geophys. Res., 91, pp. 3270-3278, 1986.

Table 1. Reactions and Reaction Rates

Reaction	Rate, $\text{cm}^3 \text{s}^{-1}$
$\text{H}_2\text{O} + \text{O}^+ \rightarrow \text{H}_2\text{O}^+ + \text{O}$	$\gamma_1 = 2 \times 10^{-9}$
$\text{H}_2\text{O}^+ + \text{H}_2\text{O} \rightarrow \text{H}_3\text{O}^+ + \text{OH}$	$\gamma_2 = 1.7 \times 10^{-9}$
$\text{H}_2\text{O}^+ + \text{e}^- \rightarrow \text{OH} + \text{H}$	$\alpha_1 = 1.7 \times 10^{-7}$
$\text{H}_3\text{O}^+ + \text{e}^- \rightarrow \text{products}$	$\alpha_2 = 1.9 \times 10^{-7}$



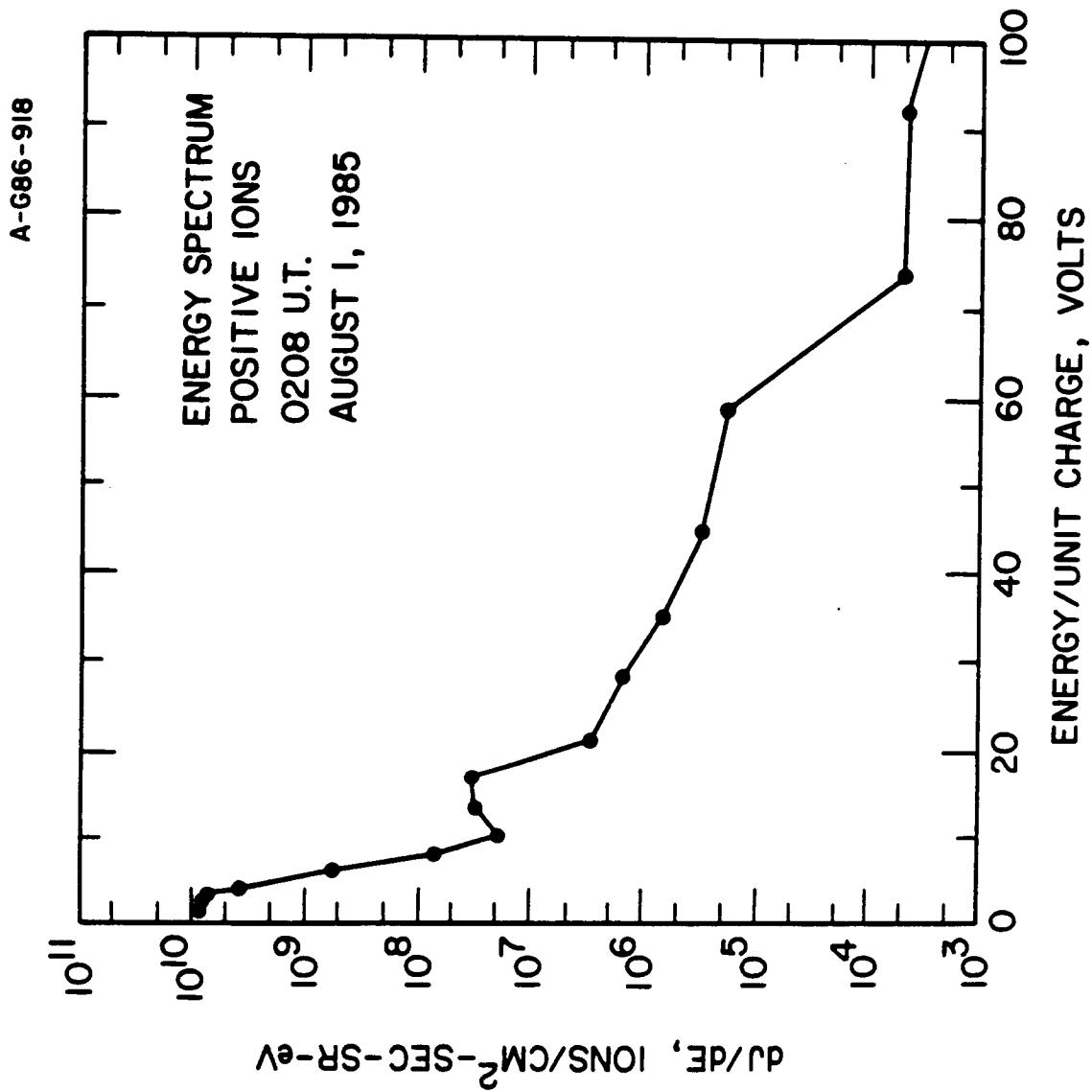
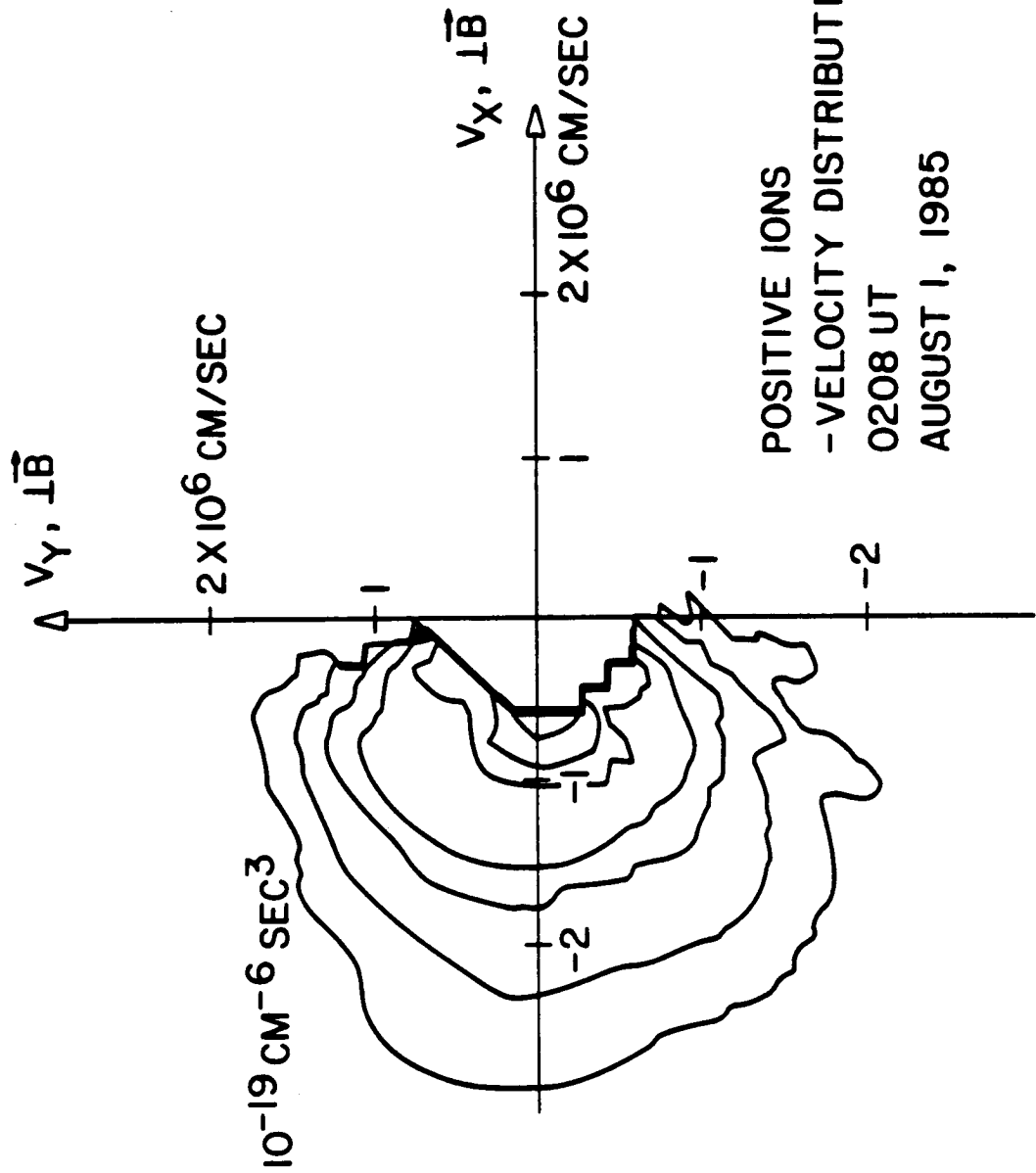


Figure 2

A-686-920



A-G86-921

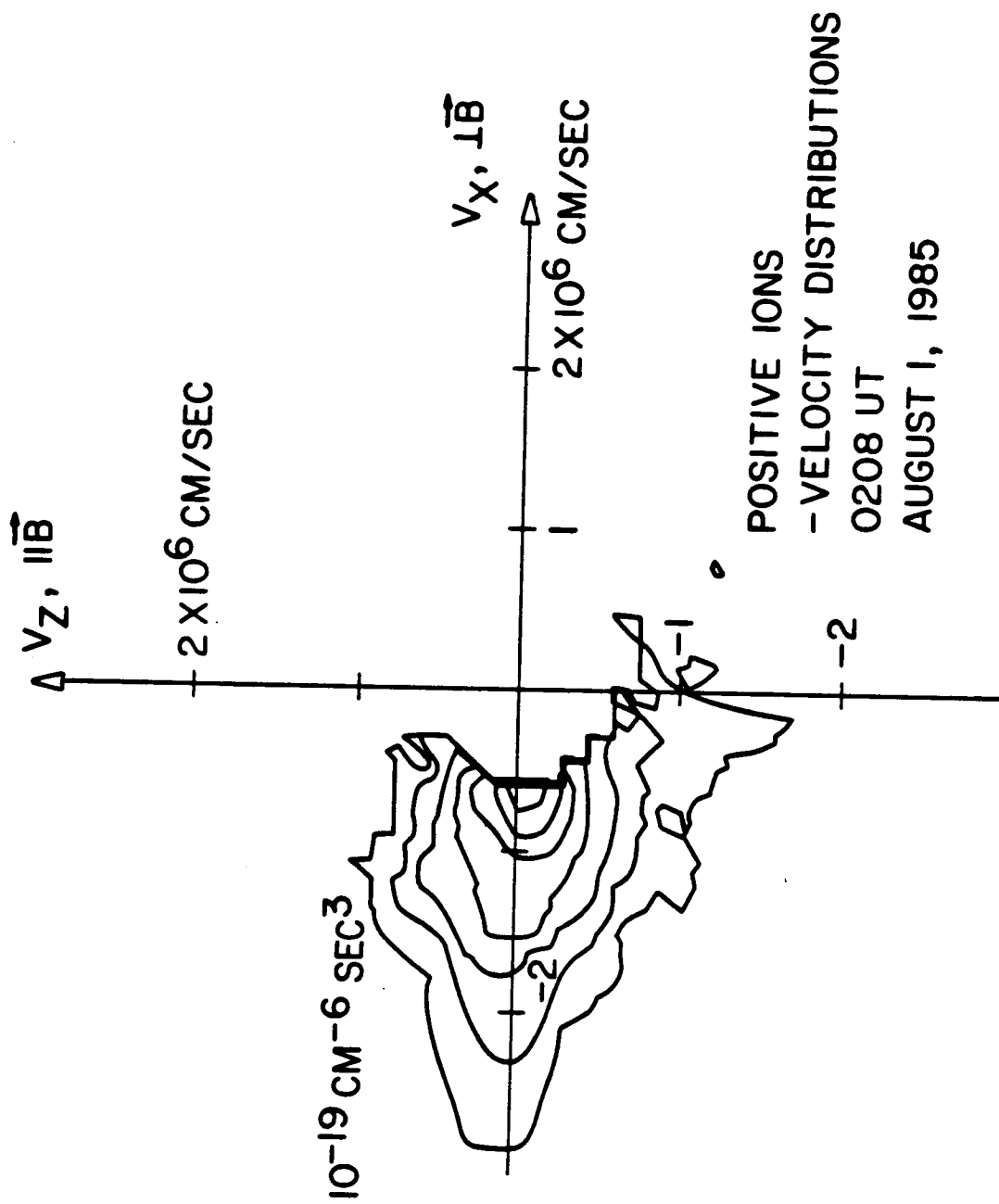
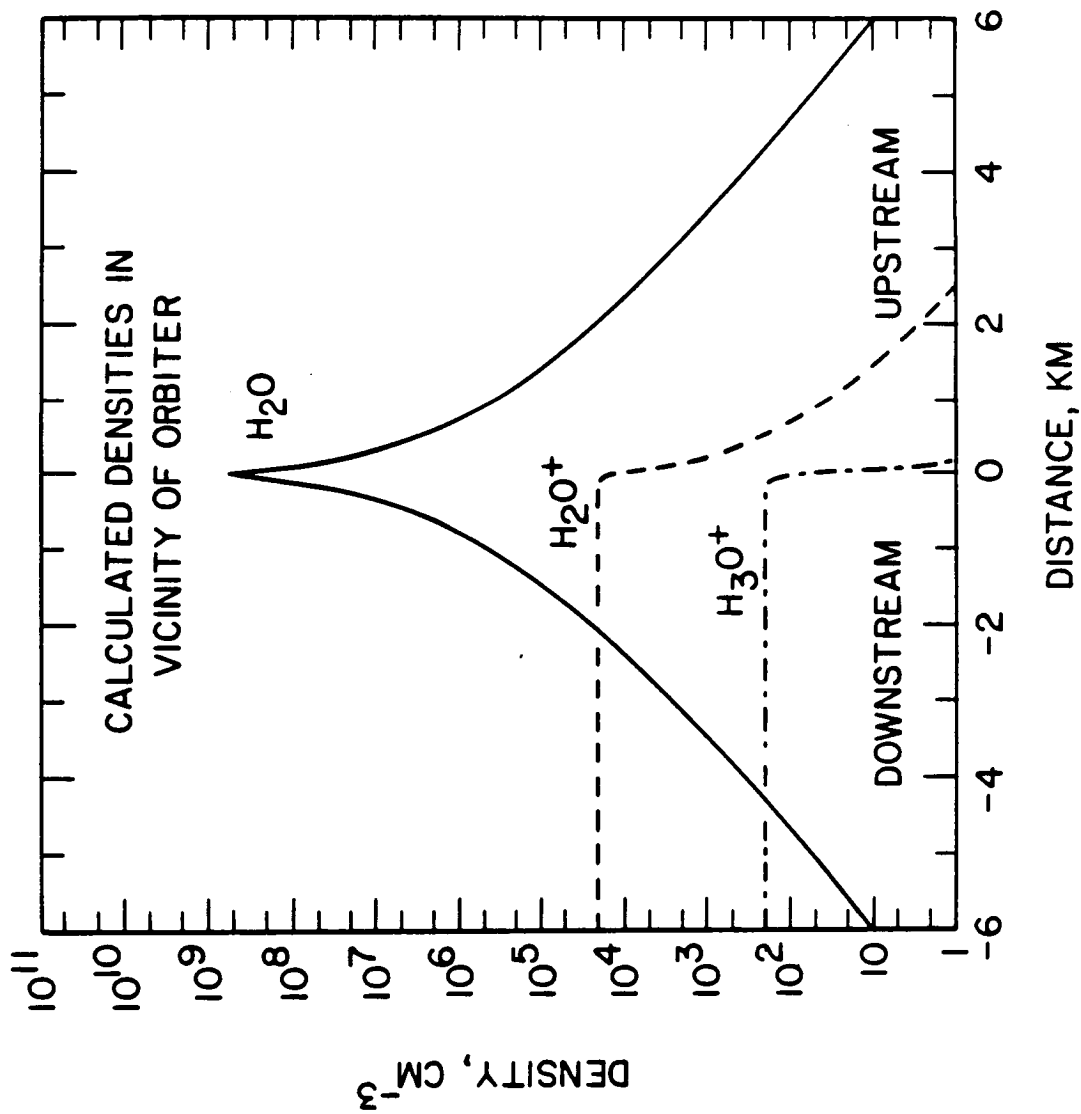


Figure 4



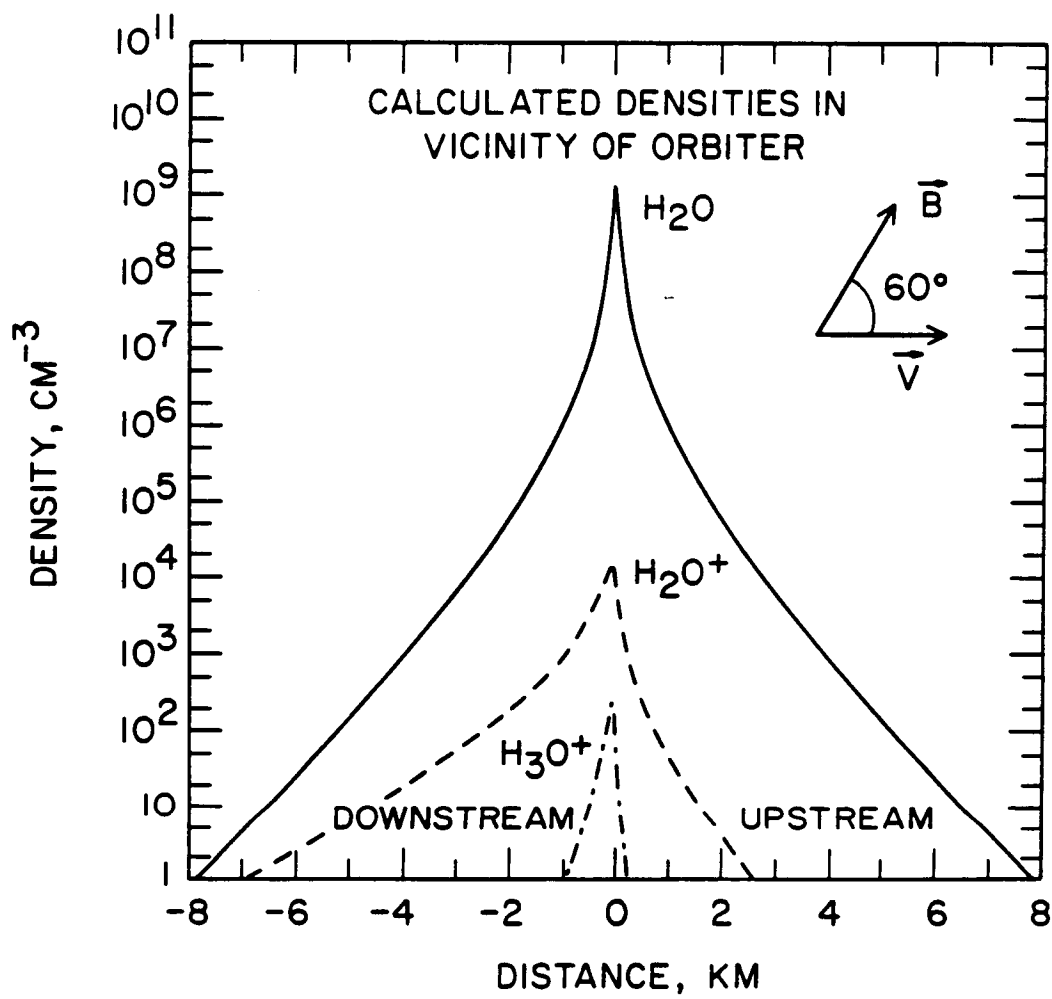


Figure 6

A-G87-508

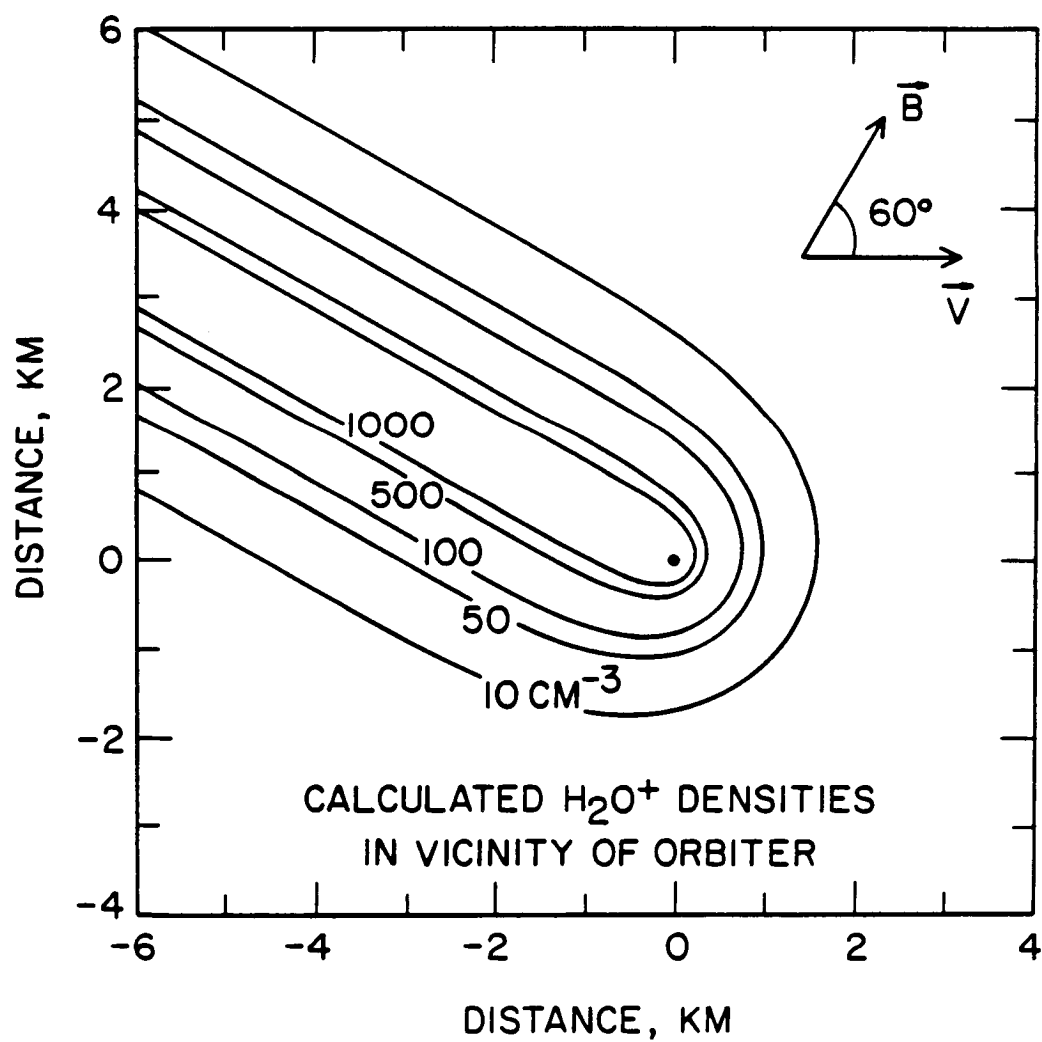


Figure 7

A-G86-922

H_2O^+ DENSITIES OBSERVED DURING
FREE-FLIGHT, AUGUST 1, 1985

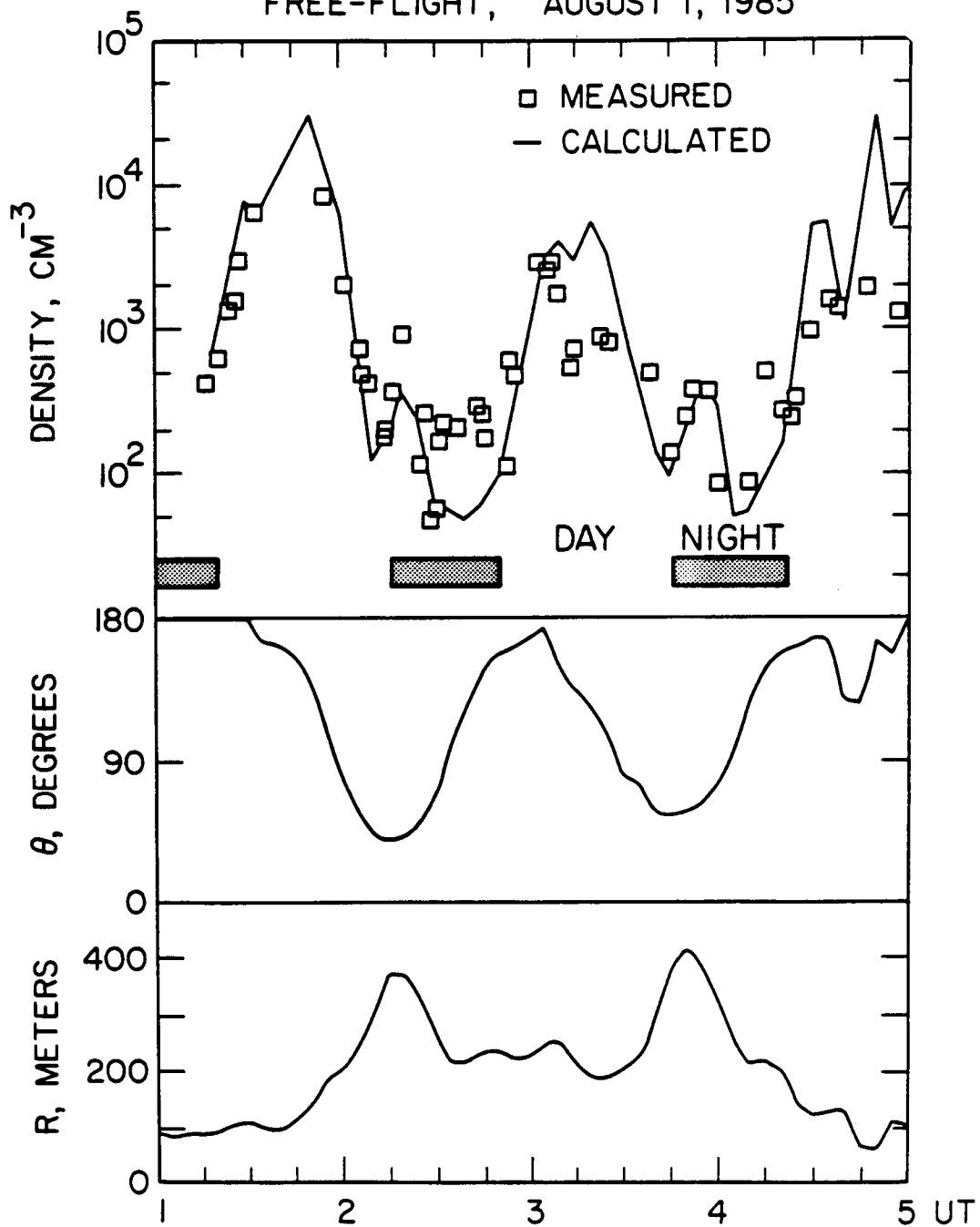


Figure 8

THE SPACELAB 2 PLASMA DIAGNOSTICS PACKAGE

by

W. S. Kurth and L. A. Frank

March 1988

The Department of Physics and Astronomy
The University of Iowa
Iowa City, Iowa 52242-1479

To be submitted to Journal of Geophysical Research

This research was supported by the National Aeronautics and Space Administration through Contract NAS8-32807 with the Marshall Space Flight Center.

ABSTRACT

The Plasma Diagnostics Package is a small deployable satellite designed to study the interaction of the shuttle with the ionospheric environment as well as to be used in joint experiments with the Plasma Depletion investigation and the Vehicle Charging and Potential investigation during the Spacelab 2 mission. This paper provides a brief description of the package, its instrumentation, its operation, and the scientific objectives of the investigation. A brief summary of the scientific results obtained thus far will also be presented.

1. INTRODUCTION

The University of Iowa's Plasma Diagnostics Package (PDP) was one of thirteen investigations which flew as part of the Spacelab 2 mission between July 29 and August 6, 1985. As its name implies the PDP is a coordinated set of sensors and instruments designed to measure a wide range of parameters characterizing the ionospheric environment surrounding the space shuttle in its orbit. The objectives of the investigation are to study the interaction of the shuttle with the ionosphere, the interaction of an electron beam with the ionospheric plasma, and various naturally occurring ionospheric phenomena.

During the Spacelab 2 mission, the PDP was operated in its launch configuration in the payload bay, at various vantage points around the shuttle while being maneuvered by the Remote Manipulator System (RMS), and at distances of up to about 400 m from the shuttle while operating as a free-flying subsatellite of the shuttle. In each of these operational configurations the PDP obtained measurements supporting the various scientific objectives. During much of the mission the PDP was operated jointly with the Plasma Depletion and Vehicle Charging and Potential experiments for correlative studies.

The Plasma Diagnostic Package flew previously on STS-3 as part of the first Office of Space Science payload (OSS-1) in March 1982.¹ The instrument complement was similar to the Spacelab 2 PDP, although not

identical and observations were obtained only from the payload bay and the RMS. There was no provision for the PDP to operate as a free-flyer on STS-3. The primary objectives for the PDP on STS-3 were to characterize the environment of the shuttle in terms of the plasma parameters and electromagnetic contamination and to study the interaction of an electron beam with the plasma.

In this paper we outline the general scientific objectives of the Plasma Diagnostic Package for the Spacelab 2 mission, describe the PDP and its complement of instruments, provide an overview of the operations of the PDP during the mission, and summarize the results gained to date from the PDP.

2. SCIENTIFIC OBJECTIVES

One of the major scientific objectives of the Plasma Diagnostics Package investigation on Spacelab 2 was to characterize and understand the interaction of the shuttle with the ionospheric environment through which it flies. The shuttle is a large object; in fact, it is large with respect to virtually all the important plasma scale lengths at its approximately 325 km altitude orbit, including the thermal ion gyroradius. Further, the shuttle moves with great velocity through the ionospheric plasma, typically about 8 km/s. This provides the opportunity to study the formation of wakes and turbulence by a large body moving through the plasma. Previous satellite measurements were all of bodies that were much smaller, and often in plasma regimes where the scale sizes were much larger.^{2,3} On Spacelab 2 the PDP carried out a coordinated set of wake observations at distances ranging from very close, i.e., a few meters, to nearly 400 m. In addition, the shuttle provides its own set of active experiment opportunities in the form of chemical contamination experiments. The most obvious examples of these are the joint experiments with the Spacelab 2 Plasma Depletion experiment for which the PDP provides supporting, in situ data for the ground-based observation of the effects of firing the Orbital Maneuvering System (OMS) engines in the plasma.^{4,5} The shuttle, however, is almost continuously depositing large quantities of contaminants into the ionosphere through

outgassing, leaks from pressurized vessels, the operation of the Reaction Control System (RCS) jets required to set and maintain various attitudes, and the deliberate discharging of both liquid and gaseous water as normal maintenance operations.^{6,7}

Another primary objective of the PDP on Spacelab 2 was to work jointly with the Fast Pulse Electron Generator (FPEG) portion of the Vehicle Charging and Potential (VCAP) experiment provided by Stanford University and Utah State University⁸ to investigate the interaction of an energetic (1 keV) beam of electrons with the ionospheric environment. This experiment has importance to the study of naturally occurring auroral phenomena observed elsewhere in the ionosphere but takes advantage of the active control of the electron beam to isolate various aspects of the beam-plasma interaction. The electron beam studies were also undertaken during STS-3, but Spacelab 2 offered experiments benefiting from the RMS STS-3 experience and the important opportunity to back off to distances a factor of 10 or more larger in the free-flight configuration.

Finally, it was planned to observe naturally occurring ionospheric phenomena with the PDP while in free-flight, but one of the most important discoveries of the Spacelab 2 PDP is that one must move much further away from the shuttle than the 400-m distances achieved during Spacelab 2 to fully escape the influence of the shuttle.^{6,7,9} Hence, the ambient ionospheric studies have been overshadowed by the more active shuttle and electron beam interaction studies. It should be noted that some natural phenomena were observed, such as VLF whistlers, so some such studies may still be possible.

3. INSTRUMENTATION

A. Spacecraft Description

The Plasma Diagnostics Package was designed and fabricated by the University of Iowa and is a unique Spacelab experiment in that it is designed to make observations while attached to the Spacelab pallet in the payload bay, while being maneuvered about the shuttle by the RMS, and also while operating as an independent satellite in orbit nearby the shuttle. To accomplish the latter, the PDP had to be designed primarily as a free-flying satellite, but with provisions to be carried aloft within the payload bay and be grappled and articulated by the RMS. Modifications late in the development of the PDP further allowed its recapture, preserving the possibility of re-using all or part of the spacecraft in future programs.

The PDP, shown in free-flight during the Spacelab 2 mission in Fig. 1 and in schematic form in Fig. 2, is cylindrically shaped with a diameter of about 42 inches and a weight of about 625 lbs. Various sensors are mounted on the four deployable booms and numerous instruments have view ports through the spacecraft skin situated around the circumference of the cylinder. The appendage at the top of the spacecraft is an electrical grapple fixture which allows the PDP to be grappled by the RMS as well as controlled electrically through cables in the RMS connected to a special switch panel on the aft flight deck of the shuttle.

The small cylinder just below the grapple fixture contains a momentum wheel loaned by the Smithsonian Institution from the ATS-G satellite. The wheel is used to store angular momentum in the PDP prior to release for free flight. The stored angular momentum was subsequently used to spin the PDP up to about 4.4 rpm during the free-flight phase by allowing the momentum wheel to spin down with respect to the PDP structure. Prior to recovery, the wheel was spun up again to transfer the angular momentum back out of the structure, thereby despinning the spacecraft to allow recapture by the RMS.

B. Instrument Summary

The Plasma Diagnostics Package contains an integrated set of instruments to provide a broad range of measurements of plasmas, DC and oscillatory electric and magnetic fields, and neutral pressure. Because of funding limitations, many of the scientific instruments are flight spare units from such projects as IMP, Helios, and ISEE. Table 1 provides an overview of the various scientific instruments flown on the Spacelab 2 Plasma Diagnostics Package, the investigators providing the instrumentation, and a brief summary of the measured parameters. The sensor locations are shown in Fig. 2.

4. PDP OPERATIONS

The PDP operations performed during the Spacelab 2 mission can best be organized by separating them into operations performed while on the Spacelab pallet, while being manipulated by the RMS, and while functioning as a free-flying satellite in orbit with the shuttle. In the subsections below we will briefly describe the operations in each of these phases.

A. Pallet Operations

The PDP was carried into orbit while latched onto the Spacelab pallet and was returned to Earth in the same configuration. The initial activation and check-out was performed just a few hours after launch, as soon as the payload bay doors were opened and the Spacelab support systems were activated. During the on-pallet operations early in the mission the PDP was able to monitor the activation of other instruments from an electromagnetic interference point of view as well as observe the initial outgassing of the shuttle and its payload.¹⁰ All PDP instruments were activated soon after the PDP was powered up with the exception of the Lepedea that utilizes a high-voltage power supply and is subject to coronal discharge prior to complete outgassing.

The PDP also spent the final four days of the mission positioned on the pallet while intensive solar and dark sky observations were being performed by other Spacelab investigations. During this time.

the PDP passively monitored the payload bay environment and supported the VCAP electron beam experiments. The solar observations required a bay-toward-sun attitude for many orbits in succession which led to overheating of a few of the PDP subsystems. In response to the overheating, the PDP was occasionally deactivated to allow temperatures to return to acceptable values. No thermal damage was experienced despite the elevated temperatures.

B. RMS Operations

The PDP was grappled by the RMS at 1 day, 2 hours, and 26 minutes into the mission (or mission elapsed time MET), corresponding to 2326 GMT on July 30, 1985. During the next 3 days the PDP was actively manipulated by the RMS in studies of the shuttle-ionosphere interaction and electron beam interactions for a total of about 11 hours. During the remaining portion of those 3 days, the PDP was either stowed in a non-interfering position over the port wing at a park point (Fig. 3d) or was in free flight.

During the active portion of the RMS operations, the PDP was moved about the orbiter in a number of pre-programmed maneuvers in support of the various scientific objectives. Several of these maneuvers are depicted in Figs. 3a-c. The primary maneuvers moved the PDP longitudinally parallel to the roll axis of the shuttle (X-scans), or parallel to the pitch axis of the orbiter (Y-scans), or vertically up and down over a fixed location in the bay (Z-scans). The maximum extension of the RMS is about 15 m. However, the PDP was never more than about 13 m from the orbiter while attached to the RMS. At various times during the scans the PDP could be rotated about its

spin axis by the wrist actuator of the RMS so that instruments with directed fields of view could be swept through different look angles or pointed in various special directions such as the velocity vector of the shuttle.

The RMS programs were specialized to the PDP scientific objectives. For example, the X- and Y-scans were used to execute beam searches, that is, to move the PDP through the electron beam in order to sample the region of direct beam plasma interaction as well as the surrounding environment. One particularly useful maneuver coupled the rotation of the PDP about the RMS wrist axis in one direction with the roll of the shuttle in the opposite direction at identical rates such that the PDP was swept alternately through ram and wake orientations while holding a specific instrument's look direction parallel to the velocity vector of the shuttle. This particular maneuver was designed to allow detailed studies of the near-wake of the shuttle.

C. Free Flight

The free-flight portion of the PDP operations was the most innovative part of the Spacelab 2 PDP investigation. Not only was this activity not undertaken during the previous STS-3 mission, but we believe the PDP free-flight experiments were the first of their kind in space plasma physics. Several rocket experiments have included detached payloads for the diagnosis of beam interactions, but none have included all the active control of relative position and attitude for the purposes of studying vehicle-plasma interactions as well as the beam-plasma interactions, especially in conjunction with a large body such as the shuttle.

The constraints on the free-flight activities were severe, especially from the point of view of time allotted against the requirements of other Spacelab 2 investigations and Reaction Control System propellant usage. The latter constraint was much more severe than planned due to the loss of about 4500 lbs of Orbital Maneuvering System (OMS) propellant during the abort-to-orbit procedure executed as a result of the premature shut-down of the center main engine on ascent.

The free-flight phase of the mission can be broken down into deployment and back-away, fly-around 'ellipses', wake transits, and approach and recovery. The total time for the free-flight was 6 hours. Fig. 4 shows the relative trajectory of the orbiter with respect to the PDP. The first panel shows the back-away and first fly-around ellipse. The second panel shows the the second fly-around ellipse, wake transits, and approach. Three hours were utilized during the two orbits of fly-arounds depicted in Fig. 4. During the fly-around 'ellipses' the shuttle was flown out of the orbit plane and to positions along the magnetic field line threading the PDP in order to look for Alfven waves generated by the shuttle and to do electron beam experiments. During the portion of the orbit when the shuttle preceded the PDP in orbit, the shuttle was brought back into the PDP orbit plane in order to study the shuttle's wake at distances between 50 and 250 m.

The back-away and approach maneuvers were completed with the shuttle upstream from the PDP, that is, with the PDP in or near the wake of the shuttle. This configuration allowed additional

observations to be made of the shuttle's wake at distances intermediate to those achieved while on the RMS or in the free-flight fly-around maneuvers. It was anticipated that the intervals in time when the PDP preceded the shuttle in orbit at distances of over 300 m that the PDP might be able to sample the unperturbed ionospheric medium. As it turned out, the PDP was never far enough upstream to avoid the neutral gas cloud and its associated effects so that a truly ambient ionospheric observation could be made.

5. SUMMARY OF RESULTS

A. Studies of the Shuttle Environment

Perhaps the most profound discovery of the PDP flight aboard Spacelab 2 is that the shuttle is accompanied in orbit by an extensive gas cloud of contaminants, consisting primarily of water.^{6,7,10,11} This conclusion is consistent with observations made by the ion mass spectrometer,^{6,11} pressure gauge,¹⁰ retarding potential analyzer, and Lepedea⁷ on the PDP. The shuttle releases contaminants through the operation of the RCS thrusters, normal operation of the orbiter fuel cells and cooling systems, leakage from pressurized vessels, and outgassing. The neutral water is subject to ionization by a number of processes in low earth orbit with charge exchange with the ambient O^+ ions being the primary reaction. As ions are created, they are immediately 'picked-up' by the magnetic field sweeping through the cloud at the orbital velocity of the shuttle, about 8 km/s and, hence, form a highly anisotropic distribution of ions known as a ring distribution. The Lepedea has measured these ring distributions from free-flight vantage points at several locations around the orbiter.⁷ The measurements indicate a neutral water production rate of about $2.5 \times 10^{22} \text{ s}^{-1}$ from the shuttle. The pick-up generally occurs within a sphere of about 100 m radius, but with the primary pick-up occurring in the region downstream from the shuttle. The contaminant water ions can actually be the dominant species in the region within a few meters of the shuttle.⁶ Models of the cloud suggest that it extends for a

few km in all directions with an extended tail in the downstream direction.

Since ring distributions are typically unstable to plasma waves, it is possible that these distributions are responsible for the generation of broadband electrostatic waves observed in the vicinity of the shuttle by the plasma wave receiver.^{9,12} This noise typically extends with a relatively flat spectrum from a few Hz to 20 or 30 kHz. The broadband electric field strength of the turbulence is about 10 mV/m. The waves are generally most intense in the region downstream of the shuttle, although high intensities are also observed near magnetic conjunctions. The wave intensity is correlated with RCS thruster activity, although some noise is still present when no thrusters are being fired.

The S- and K_u -band receivers assessed the electric fields associated with the operation of the orbiter communication links at various locations around the payload bay.¹³ For those systems which avoid the main beam of the radar, the maximum field strength is less than 2 V/m. For those payload elements which are subjected to the main beam, a design guideline of 300 V/m provides an adequate safety margin at K_u -band. The S-band fields measured were several dB below the worst-case predictions. S-band fields within the payload bay envelope should be < 2 V/m.

B. Wake Studies

The motion of the shuttle through the ionosphere leads to the formation of a well-developed wake in the downstream region.¹⁴ The PDP had operations both on the RMS and in free-flight specifically

designed to provide information on the characteristics of the wake both in the near vicinity of the shuttle (within a body radius of the obstacle) and in the distant wake, out to about 250 m. From RMS observations the density in the deep wake can be two or more orders of magnitude less than the ambient density while the electron temperature on the boundary of the wake region can be observed to increase by more than a factor of two. At larger distances, the magnitude of the density depletion is less, sometimes only about 10%. One striking result, however, is that even at distances of 250 m, the wake is still well defined and of simple structure. There is no evidence of large scale turbulence in the distant wake. It should be mentioned, however, that small-scale wave-like turbulence often characterizes the boundary of the wake region; it is possible this turbulence is similar in character to the broadband electrostatic noise discussed above.

Some work on comparisons of the Spacelab 2 PDP wake observations with wake models has been completed.¹⁵ The model used in these comparisons is the Polar code¹⁶ which neglects the magnetic field and uses a self-similar solution to the expansion of a plasma into a vacuum as its foundation. The observed electron and ion densities measured by the PDP during passages through the shuttle's wake at distances out to a few hundred meters are compared with predictions of the model. In the distance range less than 30 m, the model underestimates the density by as much as an order of magnitude and the conclusion is that outgassing from the shuttle can be a substantial contributor to the wake density within a few body scale sizes. Beyond

30 m, the agreement is very good (within about 10%) between the model and observations, provided one allows for variations in the ambient density with orbit position as predicted by the International Reference Ionosphere model. The observations show a lack of fine structure in the density of the wake and are, therefore, consistent with the behavior of wake in regimes where $T_e \approx T_i$. Further, some minor inconsistencies in the depth of the wake as a function of distance from the shuttle observed by the PDP suggest that magnetic field geometry is a second order albeit important effect.

C. Beam-Plasma Interactions

The PDP and VCAP jointly designed numerous experiments for the Spacelab 2 mission for the purpose of understanding various aspects of the interaction of an energetic (1 keV) electron beam with the ionospheric plasma. One of the primary characteristics of the interaction is the generation of waves. Early studies have concentrated on whistler mode waves called VLF hiss¹⁷ which are thought to be generated via a coherent Cerenkov process associated with bunching of electrons in the continuously firing beam.^{18,19} The VLF hiss was easily detected because of a funnel-shaped frequency-time signature observed in the plasma wave data set. The funnel-shaped spectrum is a result of well-understood propagation characteristics of the whistler mode waves and leads to an understanding of the emissivity of the beam as a function of distance along the beam. Further studies^{8,20,21} involve the study of the generation of waves by a pulsed beam where the pulsing frequency of the beam is in the VLF

frequency range. The resultant waves are found at harmonics of the pulsing frequency.

Other studies concerning the interaction of the electron beam with the ionosphere includes the DC electric fields set up in the vicinity of the beam in response to the current systems driven by the beam.²² A study using the PDP Lepedea measurements of the actual plasma distribution functions associated with the beam plasma interaction shows a sheet of energetic electrons on field lines downstream of the active field line.²³ These energetic electrons make up a net current returning the current carried by the beam. Simulations of the energetic electrons show the generation of low frequency, broadband electrostatic waves similar to those observed by the plasma wave receiver.

6. CONCLUSIONS

The PDP investigation on the Spacelab 2 mission was extremely successful. Virtually 95% of the objectives of the investigation were achieved and the results referred to in the previous section attest to the scope of the science results that were obtained during the flight. Those 5% of the objectives which were not met owing to the shortage of RCS propellant were primarily experiments that involved the firing of RCS thrusters in a predetermined way in order to measure their effects and those experiments that were to have been performed during a planned, third orbit of fly-around. The thruster-associated objectives were partially achieved via coincidental firings of RCS thrusters during the execution of various maneuvers. The loss of the third orbit of fly-arounds resulted primarily in the loss of repetitions of experiments achieved during the first two orbits.

ACKNOWLEDGMENTS

The PDP project would not have been possible without the support of a large number of people at the University of Iowa and within NASA. Unfortunately, we can not mention all of those persons here. However, we do wish to commend the flight crew, C. G. Fullerton, R. D. Bridges, Jr., T. England, S. Musgrave, K. G. Henize, J.-D. Bartoe, and L. W. Acton and the Alternate Payload Specialists, G. Simon and D. Prinz for their excellent job of carrying out the mission. We would also like to acknowledge the MSFC mission management team under R. C. Lester; the planning and operations teams under S. Perrine and A. Roth; and the data management team under M. Rives. B. Gwynes, D. Talley, R. Adams, W. Claunch, and B. Soutullo all served the PDP project as our MSFC liason and assured the success of the project. We thank E. Urban for his role as Mission Scientist. We are indebted to the mission planning and operations team at JSC, including K. Cannon, A. Austin, and M. Veres as well as the payload integration team at KSC, especially E. Lunceford. At the University of Iowa we express our appreciation for the professional job performed by the spacecraft engineering team under the direction of R. F. Randall, the operations team led by G. B. Murphy, and the data analysis team headed by R. L. Brechwald and J. S. Pickett. The research at the University of Iowa was supported by NASA through Contract NAS8-32807 with the Marshall Space Flight Center.

REFERENCES

¹Shawhan, S. D., Murphy, G. B., and Pickett, J. S., "Plasma Diagnostics Package Initial Assessment of the Shuttle Orbiter Plasma Environment," Journal of Spacecraft and Rockets, Vol. 21, July-Aug. 1984, pp. 387-391.

²Samir, U., and Wrenn, G. L., "Experimental Evidence of an Electron Temperature Enhancement in the Wake of an Ionospheric Satellite," Planetary and Space Science, Vol. 20, No. 6, 1972, pp. 899-904.

³Samir, U., and Fontheim, E. G. "Comparison of Theory and "In Situ" Observations for Electron and Ion Distributions in the Near Wake of the Explorer 31 and AE-C Satellites," Planetary and Space Science, Vol. 29, No. 9, 1981, pp. 975-987.

⁴Mendillo, M., Baumgardner, J., Allen, D. P., Foster, J., Holt, J., Ellis, G. R. A., Klekocivk, A., and Reber, G., "Spacelab 2 Plasma Depletion Experiments for Ionospheric and Radio Astronomical Studies," Science, Vol. 238, 1987, pp. 1260-1264.

⁵Bernhardt, P. A., Kashiwa, B. A., Swartz, W. E., Kelley, M. C., Tepley, C. A., Sulzer, M. P., and Noble, S. T., "xxxxxxxxxxxxxxxxx," Science, Vol. xx, No. xx 1987, pp. xxx-xxx.

⁶Grebowsky, J. M., Taylor, H. A. Jr., Pharo, M. W. III, and Reese, N., "Thermal Ion Perturbations Observed in the Vicinity of the Space Shuttle," Planetary and Space Science, Vol. 35, No. 4, 1987, pp. 501-513.

⁷Paterson, W. R., and Frank, L. A., "Hot Ion Plasmas from the Cloud of Neutral Gases Surrounding the Orbiter," Journal of Geophysical Research, submitted, 1988.

⁸Bush, R. I., Reeves, G. D., Banks, P. M., Neubert, T., Williamson, P. R., Raitt, W. J., Gurnett, D. A., "Electromagnetic Fields from Pulsed Electron Beam Experiments in Space: Spacelab 2 Results," Geophysical Research Letters, Vol. 14, No. 10 1987, pp. 1015-1018.

⁹Gurnett, D. A., Kurth, W. S., Steinberg, J. T., and Shawhan, S. D., "Plasma Wave Turbulence Produced by the Shuttle: Results from the PDP Free Flight," Geophysical Research Letters, in preparation, 1988.

¹⁰Pickett, J. S., Murphy, G. B., and Kurth, W. S., "Gaseous Environment of the Shuttle Early in the Spacelab 2 Mission," Journal of Spacecraft and Rockets, in press, 1988.

¹¹Grebowsky, J. M., Taylor, H. A. Jr., Pharo, M. W. III, and Reese, N., "Thermal Ion Complexities Observed Within the Spacelab 2 Bay," Planetary and Space Science, Vol. 35, No. 11, 1987, pp. 1463-1469.

¹²Hwang, K. S., Stone, N. H., Wright, K. H. Jr., and Samir, U., "The Emissions of Broadband Electrostatic Noise in the Near Vicinity of the Shuttle Orbiter," Planetary and Space Science, Vol. 35, No. 11, 1987, pp. 1373-1379.

¹³Murphy, G. B., and Cutler, W. D., "A Detailed Look at the Orbiter Environment at S- and K_u -Band Frequencies," Journal of Spacecraft and Rockets, in press, 1988.

¹⁴Murphy, G. B., Reasoner, D. L., Tribble, A., D'Angelo, N., Pickett, J. S., and Kurth, W. S., "The Plasma Wake of the Shuttle Orbiter," Journal of Geophysical Research, submitted, 1988.

¹⁵Murphy, G. B., and Katz, I., "The Polar Code Wake Model: Comparison with In-Situ Observations," Journal of Geophysical Research, submitted, 1988.

¹⁶Katz, I., Parks, D. E., and Wright, K. H. Jr., "A Model of the Plasma Wake Generated by a Large Object," IEEE TNS, Vol. NS-32, No. 6 1985, pp. 4092-4096.

¹⁷Gurnett, D. A., Kurth, W. S., Steinberg, J. T., Banks, P. M., Bush, R. I., and Raitt, W. J., "Whistler-Mode Radiation from the Spacelab 2 Electron Beam," Geophysical Research Letters, Vol. 13, No. 3, 1986, pp. 225-228.

¹⁸Farrell, W. M., Gurnett, D. A., Banks, P. M., Bush, R. I., and Raitt, W. J., "An Analysis of Whistler-Mode Radiation from the Spacelab 2 Electron Beam," Journal of Geophysical Research, Vol. 93, No. A1, 1988, pp. 153-161.

¹⁹Farrell, W. M., Gurnett, D. A., and Goertz, C. K., "Coherent Cerenkov Radiation from the Spacelab 2 Electron Beam," Journal of Geophysical Research, submitted, 1988.

²⁰Reeves, G. D., Banks, P. M., Fraser-Smith, A. C., Neubert, T., Bush, R. I., Gurnett, D. A., and Raitt, W. J., "VLF Wave Stimulation by Pulsed Electron Beams Injected from the Space Shuttle," Journal of Geophysical Research, Vol. 93, No. A1, 1988, pp. 162-174.

²¹Neubert, T., Hawkins, J. G., Reeves, G. D., Banks, P. M., Bush, R. I., Williamson, P. R., Gurnett, D. A., and Raitt, W. J., "Pulsed Electron Beam Emission in Space," Journal of Geophysical Research, submitted, 1988.

²²Steinberg, J. T., Gurnett, D. A., Banks, P. M., and Raitt, W. J.,
"Quasi-Static Electric Field Measurements Near the Electron Beam on
Spacelab-2," Journal of Geophysical Research, submitted, 1987.

²³Frank, L. A., et al., "xxxxxxxxxxxxxx," Geophysical Research
Letters, in preparation, 1988.

TABLE 1

Spacelab 2
Plasma Diagnostics Package
Scientific Instruments

<u>Instrument</u>	<u>Provider</u>	<u>Measurement</u>
Ion Mass Spectrometer (IMS)	J. M. Grebowsky GSFC	Thermal Ions 1-64 AMU; $20 - 2 \times 10^6 \text{ cm}^{-3}$
Retarding Potential Analyzer (RPA)	D. L. Reasoner MSFC	Ions; 0-15 eV; $20 - 10^7 \text{ cm}^{-3}$
Differential Ion Flux Probe (DIFP)	N. H. Stone MSFC	Ions; 0-15 eV; $6 \times 10^{-2} - 3 \times 10^5 \text{ cm}^{-3}$; 3° angular resolution in range of $\pm 45^\circ$ from PDP equator
Lepedea	L. A. Frank U. of Iowa	Ions and electrons; three-dimensional velocity distributions; 2 eV-36 keV; plus electrometer with range $10^9 - 10^{14} \text{ electrons cm}^{-2} \text{ s}^{-1}$
Langmuir Probe	N. D'Angelo U. of Iowa	Thermal electrons; $10^3 - 10^7 \text{ cm}^{-3}$; $500^\circ \text{ K} < T_e < 4000^\circ \text{ K}$; $\Delta N/N$ spectrum
Neutral Pressure Gauge	J. S. Pickett U. of Iowa	$10^{-7} < P < 10^{-3} \text{ Torr}$
Triaxial Fluxgate Magnetometer	S. D. Shawhan NASA Headquarters	± 1.5 gauss with 0.012 gauss resolution; 3 axes; 10-Hz sample rate each axis
DC Electric Fields	D. A. Gurnett U. of Iowa	$\pm 4.8 \text{ V/m}$ single axis; 4mV/m resolution Plasma potential $\pm 8 \text{ V}$; 20mV resolution; 20-Hz sample rate
Plasma Waves	D. A. Gurnett U. of Iowa	Electric: 30 Hz - 17.8 MHz in 24 channels Magnetic: 35 Hz - $\sim 10 \text{ kHz}$ in 11 channels Wideband analog 5 Hz - 30 kHz
S- and Ku-Band Monitor	G. B. Murphy U. of Iowa	S-band; 1.4 - 3.0 GHz Ku-band; 13.5 - 14.5 GHz

FIGURE CAPTIONS

- Fig. 1 A photograph of the PDP deployed in its free-flight configuration during the Spacelab 2 mission.
- Fig. 2 The top panel shows the locations of the various instrument viewports and sensors (see Table 1) in a schematic of the PDP shown with the sidewall of the spacecraft 'unrolled'. The bottom panel is a view of the PDP from the top showing the locations of the booms and boom-mounted sensors in the fully extended configuration.
- Fig. 3 Most of the RMS manipulations of the PDP during Spacelab 2 were composed of the combinations of the motions parallel to the principal axes of the orbiter shown above. A few other special sequences were also utilized that are not shown here.
- Fig. 4 The trajectory of the orbiter with respect to the PDP during the free-flight portion of the Spacelab 2 mission. The upper panel summarizes the release of the PDP through the completion of the first fly-around 'ellipse'. The lower panel shows the second 'ellipse', final wake transits, and the approach for recovery. When the orbiter was in the 'cone' on the left side of the panels, it was in the plane of orbit of the PDP so that the orbiter's wake would pass over the PDP at varying distances. In the remainder of the 'ellipses', the orbiter was flown out of the PDP's orbit

plan in order to intercept the magnetic field line threading the PDP.

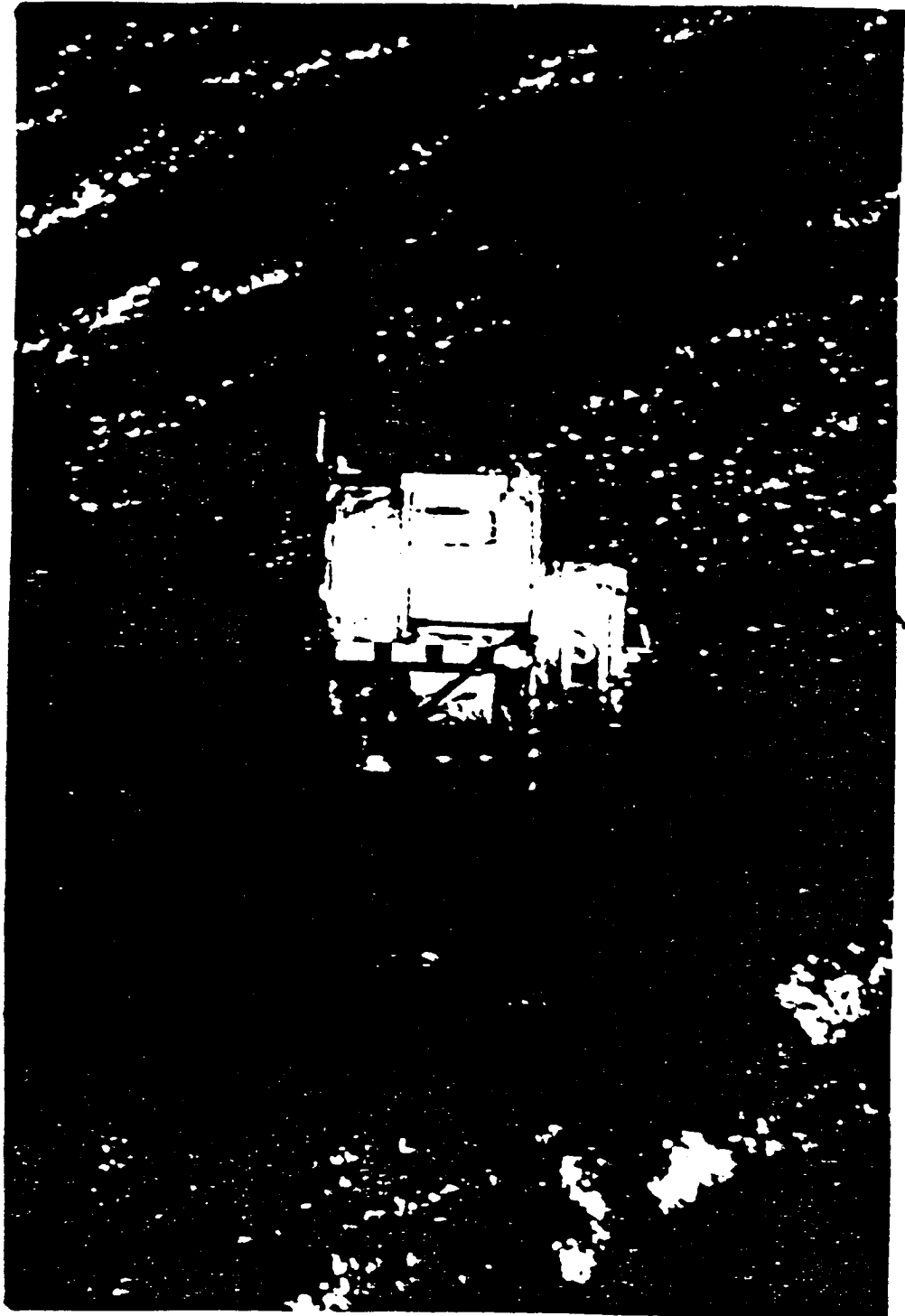


Figure 1

ORIGINAL PAGE
BLACK AND WHITE PHOTOGRAPH

PDP SENSOR LOCATIONS

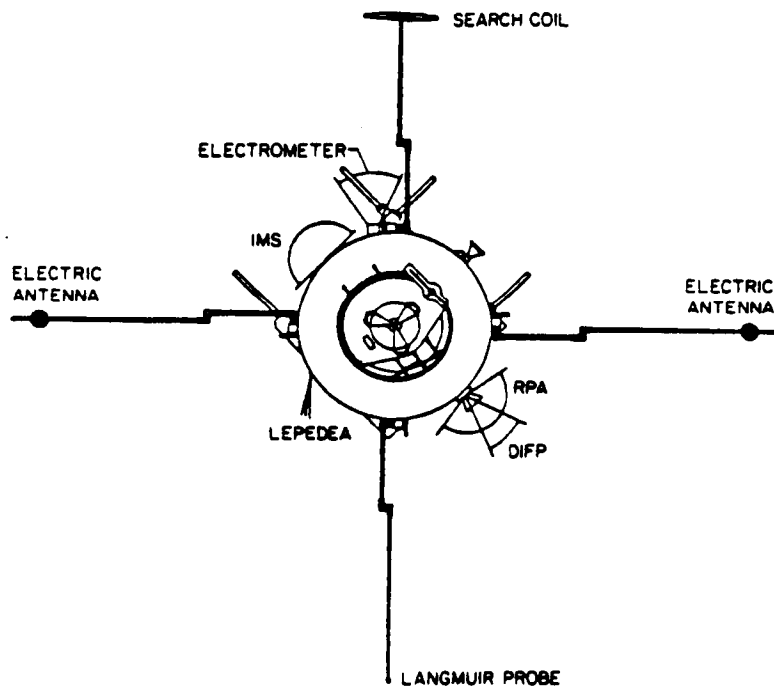
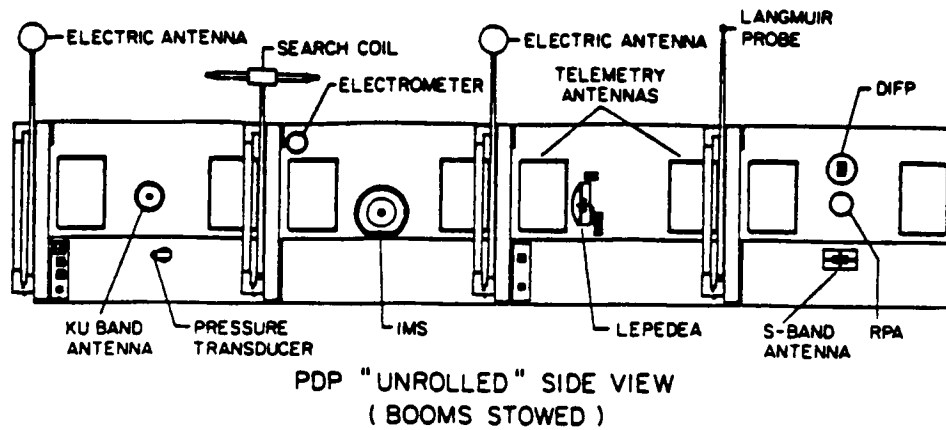
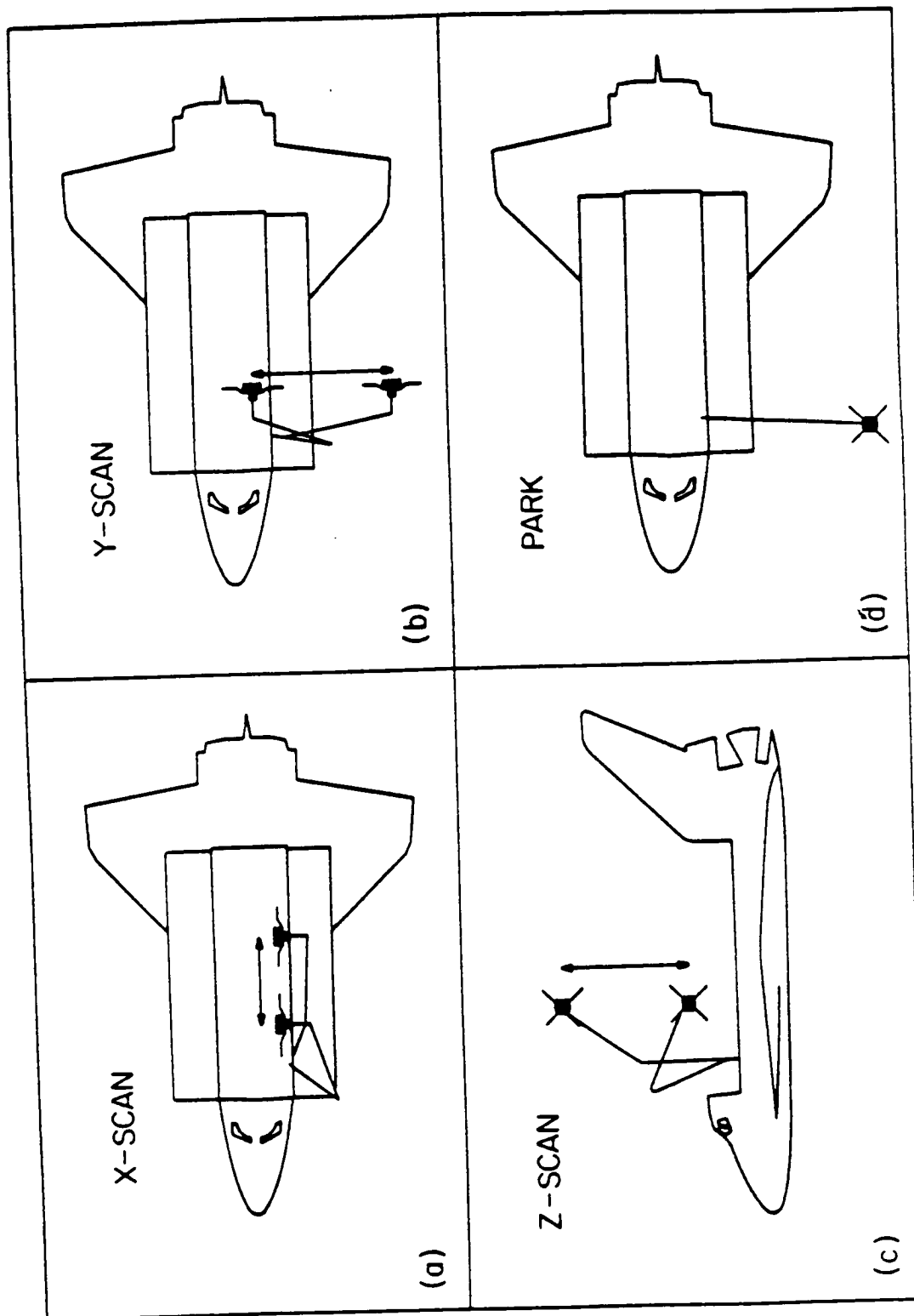


Figure 2



SPACELAB 2 PDP FREE-FLIGHT
AUGUST 1, DAY 213, 1985

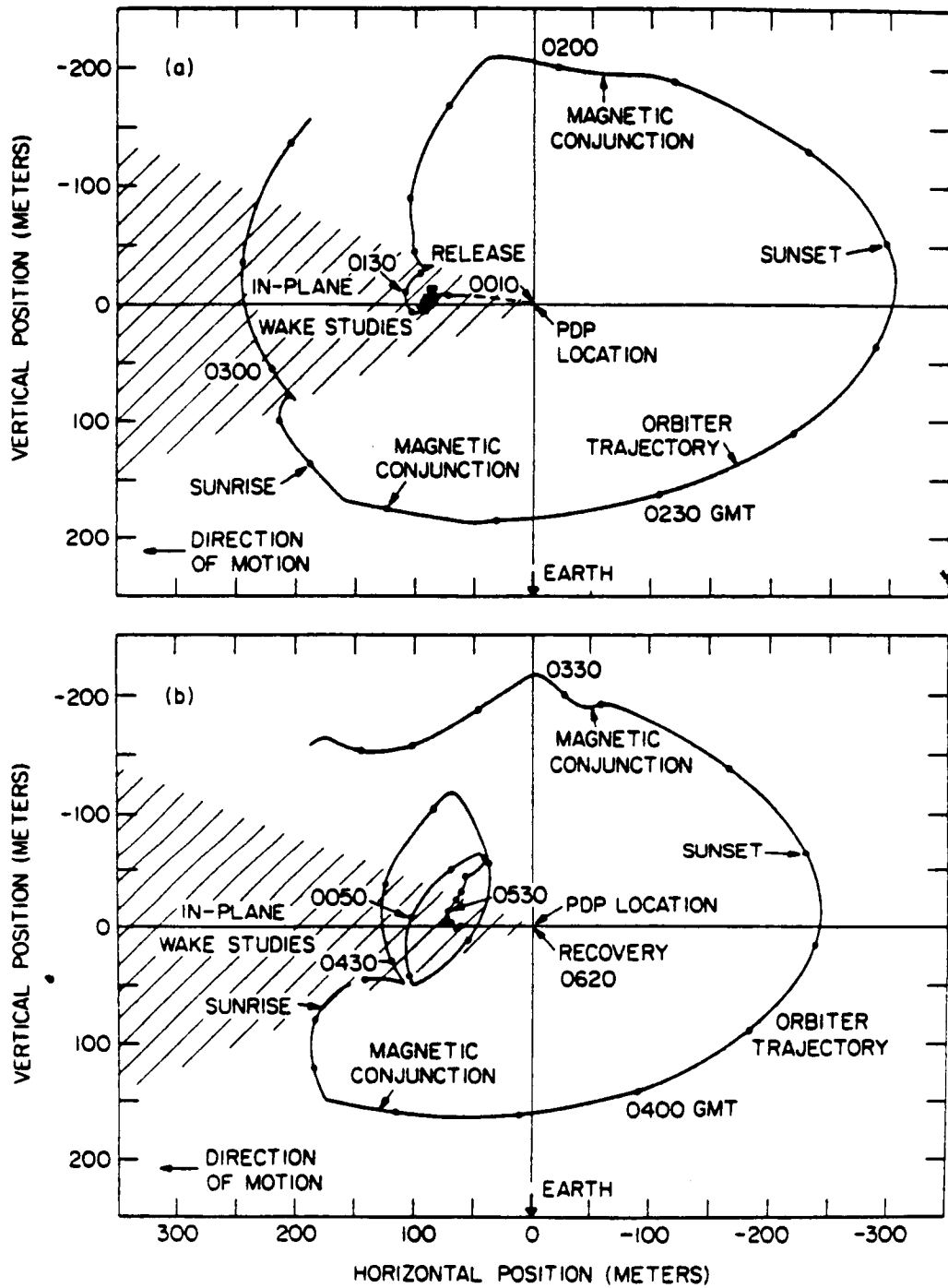


Figure 4

From: Proceedings of the Workshop on Space Technology Plasma Issues in
2001, Jet Propulsion Laboratory, Pasadena, CA, Sept. 24-16, 1986.

**A Review of the Findings of the Plasma Diagnostic Package and Associated
Laboratory Experiments: Implications of Large Body/Plasma
Interactions for Future Space Technology**

Gerald B. Murphy and Karl E. Lonngren

University of Iowa, Iowa City, Iowa 52242

1.0 Introduction

The purpose of this report is to review the discoveries and experiments of the Plasma Diagnostic Package (PDP) on the OSS 1 and Spacelab 2 missions, to compare these results with those of other space and laboratory experiments, and to discuss the implications for the understanding of large body interactions in a LEO plasma environment. The paper is logically divided into three sections. First a brief review of the PDP investigation, its instrumentation and experiments is presented. Next a summary of PDP results along with a comparison of those results with similar space or laboratory experiments is given. Last of all the implications of these results in terms of understanding fundamental physical processes that take place with large bodies in LEO is discussed and experiments to deal with these vital questions are suggested.

2.0 PDP instrumentation and experiments

The PDP is a small cylindrical satellite with a complement of instruments designed to measure plasma density and temperature, give ion composition, temperature and flow direction, provide complete electron and ion distribution functions, and measure electron flux from electron beams. In addition to these comprehensive particle measurements the PDP contains instrumentation to provide a complete set of single axis wave and field measurements. Waves (both electric and magnetic) are measured from approximately 10^1 to 10^5 hz and electric fields are measured both at DC and from 10^1 to 10^7 hz. A complete description of the PDP instrumentation is available in Shawhan 1984c.

The PDP was designed not only as a satellite, but because it was to be flown and deployed from the Orbiter; it was also capable of measuring the plasma environment in and around the orbiter bay by being maneuvered through various positions on the Shuttle Remote Manipulator System (RMS) arm. The initial experiments and measurements made by the PDP on the OSS-1 (STS-3) Mission were all made either in the payload bay on a pallet or within approximately 10 meters of the bay on the RMS. As will be seen in the next section these early shuttle experiments helped provide insight into the shuttle orbiter environment, conducted the first orbiter-based active plasma experiments, and provided some of the first insights in large body interactions at LEO. In addition, the OSS-1 experiments provided the baseline from which many of the future detailed interaction issues could be addressed. Spacelab 2, which repeated (with some modifications) some of the OSS-1 experiments and extended the range of interaction studies to nearly a kilometer from the orbiter, benefited greatly from the earlier OSS-1 experience. The PDP investigation was initiated by Prof. Stanley D. Shawhan (who is now at NASA Headquarters) and is currently under the leadership of Prof. Louis A. Frank at the University of Iowa. Other members of the PDP team

include Donald A. Gurnett and Nicola D'Angelo (U. of Iowa), Nobie H. Stone, David L. Reasoner (NASA/MSFC) and Joseph M. Grebowsky (NASA/GSFC). Numerous other scientists and engineers both at the U. of Iowa and NASA have played a major role in the program since its inception in 1978.

3.0 The early results

Early papers from the OSS-1/PDP program focused on defining the environment of the shuttle orbiter. This environment was a critical question mark in the eyes of many future users of the shuttle particularly in the areas of contamination, plasma, and electromagnetic environment.

3.1 The neutral environment

Early measurements of the neutral pressure environment of the orbiter revealed that the ambient pressure at orbital altitudes was only obtainable in the near wake of the vehicle and then only after a long period of outgassing. Even after seven days in orbit, pressure averaged at least an order of magnitude greater than ambient (Shawhan, 1984c). Not until Spacelab-2 analysis was available would the probable source of such a large vapor cloud be revealed.

More detailed investigation of the source of large pressure enhancements led to the study of thruster operations. It was reported that the thrusters (in particular Primary RCS and to a much less degree Vernier RCS) introduce major changes in plasma density, ion composition, neutral density, electric fields, and electrostatic plasma waves (Shawhan, 1984c; Murphy, 1983; Pickett, 1985). Other investigators have since reported similar results noting neutral density increase of up to $10^{18}/\text{m}^3$ inside the payload bay ($\sim 7 \times 10^{-5}$ Torr) with NO a major component of the enhancement (Wulf, 1986).

3.2 The plasma environment

The plasma density and apparent DC electric field shifts observed near the orbiter are not yet totally understood but may be related to interactions of the neutral constituent of the gas plume with the ambient plasma or to the plasma component per se.

Grebowsky et al. (1983) reported the surprising result that H_2O^+ is a major constituent of the plasma near the orbiter sometimes even dominating the ambient O^+ ionosphere. The source of these water ions is believed to be in charge exchange reactions between the ambient O^+ ions and a cloud of H_2O molecules generated by outgassing around the orbiter. This H_2O cloud may indeed be a major contributor to the enhanced neutral pressure environment.

The plasma environment near the orbiter not only has an altered ion composition but reveals the influence of a large body moving supersonically through its medium. Stone et al. (1986) observe the ions streaming by the orbiter and study in detail the structure of the wake behind the vehicle. They took particular note of multiple "beams" of ions with different apparent source directions and theorize that this is consistent with not only an additional source of ions close to the orbiter but may imply an E-field sheath associated with a boundary between the ion source region and the undisturbed plasma. It could in fact be that this additional source region is consistent

with observations of Grebowsky (1983) on the production of H_2O^+ near the orbiter.

Reasoner et al. (1986) have underscored the problem of making reliable ambient ionospheric density/temperature measurements near the orbiter. Combinations of contaminant ions, plasma turbulence generating heating, and ram/wake effects make it imperative to move well away from the orbiter before relying on an RPA to reliably characterize the ionosphere. This observation is of course consistent with all previously discussed results.

Electron densities and temperatures near the orbiter are reported by Murphy et al. (1986). To first order electron densities are dominated by the ram/wake effects associated with large bodies. The orbiter is not only large compared to the debye length (10^3 - $10^4 \lambda_D$) but also large compared to the electron and ion gyroradius. This size results in the investigation of a unique and unexplored region in parameter space and creates perhaps more questions than it answers. Murphy et al. (1986) report density depletions of as much as 5 orders of magnitude in the near wake of the orbiter (within the payload bay) and less dramatic though significant depletions of 1-2 orders of magnitudes at distances reachable by the RMS. Moreover, apparent temperature

enhancements of $>$ factors of 5 are observed in the wake transition region. This transition region is also characterized by plasma "turbulence" with $\Delta N/N$ values of typically several per cent. Secondary effects controlling the electron density spacial variation involve: 1.) the possible enhancement of electron density in ram (compared to ambient), Shawhan (1984c), Raitt (1984); 2.) the effect of the neutral cloud around the vehicle and the photoionization of that cloud, Pickett (1985); 3.) the role of the magnetic field both in the filling in of the wake and the production of $V \times B$ potentials in the orbiter reference frame.

3.3 Electromagnetic environment

The AC and DC electric and magnetic fields on and near the orbiter are driven by two sources: 1.) orbiter EMI associated with the hardware per se; 2.) fields associated with the interaction between the orbiter and its environment.

The orbiter EMI under JSC's leadership and Rockwell's cooperation proved to be much more benign than the original ICD specifications would indicate. Shawhan (1984b) and Murphy (1984b) reported in detail the measurement of that environment. By using the PDP's sensitive plasma wave receivers and various RMS maneuvering sequences a "map" of orbiter EMI revealed that the environment was dominated not by orbiter generated noise but by plasma interaction noise. This Broadband Orbiter Generated Electrostatic (BOGES) noise (Shawhan, 1984b) seemed to be associated with plasma turbulence around the orbiter and had field strengths as great as .1 v/m with a relatively flat spectrum up to ~ 10 khz. Although the exact mechanism was not understood, Murphy et al. (1984a), suspecting that it was similar to the turbulence observed by the Langmuir probe, indicated that it was noise of relatively short wavelength (< 1 m). This noise was observed to be enhanced by any sort of gas release (thruster, water dump, etc.) implicating the gas cloud as a production mechanism. Theoretical work by Papadopolous (1984) suggested that the gas

cloud may provide the "fuel" for enhanced plasma densities by the critical ionization velocity phenomenon and may be intimately involved in the production of this BOGES noise.

Thus we see that the understanding and characterization of the orbiter environment requires detailed investigation of the inter-reactions between the orbiter body, its contaminant cloud, and the ionospheric plasma.

For purposes of completeness it should also be emphasized that a large part of both the OSS-1 and Spacelab-2 missions were devoted to detailed study of the behavior and interactions of an electron beam propagating in the ionosphere. These studies were conducted jointly with the Vehicle Charging and Potential (VCAP) experiment (Banks, 1986). The OSS-1 results are reviewed by Banks (1986) and Shawhan (1984a). Since another paper in this proceedings describes the VCAP/PDP results in detail no further discussion will be given here.

4.0 Spacelab 2, laboratory results, and the emerging picture

Many of the results discussed above began to be published after the Spacelab-2 mission which was launched in July 1985 but early results had a significant influence on the science objectives and experiment planning of Spacelab-2. The landmark nature of the plasma experiments of Spacelab-2 will gradually emerge over the next several years and, in particular, the importance of the PDP free-flight activity, described briefly below, in understanding large vehicle interactions, will become quite obvious. This is especially true in light of the hiatus of Spacelab type missions in the coming years.

After performing about 12 hours worth of experiments on the RMS which consisted of wake studies, EMI surveys, and joint experiments with VCAP, the PDP was prepped for release as a sub-satellite of the orbiter. The PDP free-flight scenario consisted of approximately 6 hours of complex maneuvers by the shuttle orbiter which controlled, in a carefully planned sequence, the relative positions of the PDP and orbiter.

First, a release and back-away maneuver moved the PDP down the "throat" of the orbiter wake to a distance of ~ 100 meters. After several station-keeping experiments the orbiter began a "fly-around" of the PDP. Part of the fly-around was executed in plane so the PDP would transit the orbiter wake at distances from 40 to 200 meters. The other part of the fly-around was out of plane moving the orbiter above and behind the PDP and targeting two flux-tube-connections (FTC's) per orbit. These FTC's were planned so that they occurred out of the orbiter's wake with one in the daytime ionosphere and one at night. The FTC's were quite successful in placing the PDP and the orbiter on the same magnetic field line at a relative distance of ~ 200 meters. These FTC's were believed to be accurate to within several meters at best to a little more than 10 meters at worst. After two "fly-arounds" and several wake transits were completed the orbiter approached and captured the PDP along the velocity vector, again allowing the PDP to examine the near wake. Dealing with topics as a continuation and refinement of the OSS-1 results we first discuss the neutral environment.

4.1 Neutral environment and the contaminant gas cloud

Further measurements by the PDP neutral pressure gauge taken during pallet operations verified the high pressure environment due to early on-orbit outgassing. Analysis of vernier thruster operations verified that only the aft down pointing verniers affected pressure in the bay (Pickett, 1986). No further observations of primaries are possible because of an instrument malfunction. A strong point to be made from Pickett's observations are that large instruments which vent gases can also have dramatic effects of the payload bay environment, raising pressure to as high as 10^{-5} Torr. The orbiter's outgassing is now known to have a major effect on the local environment.

The contaminant ion gas cloud observations were extended to $\sim .5$ km from the orbiter. Grebowsky, 1986 observed contaminant H_2O^+ ions in all directions around the orbiter. The presence of contaminant NO and O_2^+ ions was also reported. It is important to note that the dominant ion in the wake of the shuttle appeared to be H_2O^+ instead of ambient O^+ .

If these ions are created by charge exchange with O^+ analysis of their distribution function would indicate a ring in velocity space. Reports by Paterson, 1986 provide evidence that this is indeed the case and an attempt to model the outgassing and chemical reactions associated with it is currently under way. Observations of the Infrared telescope on Spacelab-2 may provide additional data on outgassing rates and the structure of the water cloud which appears to surround the vehicle.

4.2 Further studies of the orbiter wake

Investigation of the structure and dynamics of the orbiter wake both on the RMS and as a free flyer are being continued. More detailed examination of the wake turbulence indicate that the magnetic field orientation may affect the structure of the turbulent zone (Tribble, 1986). Comparisons of the electron density observed in the wake are being made with predictions of the NASA POLAR code (Katz et al., 1984) and early results indicate the code may be quite accurate at predicting at least the first order effects on electron density. The details associated with magnetic field effects, the role of the plasma turbulence and pick up ions, and processes which produce the heated electrons (Murphy, 1986) still must be investigated. Although a detailed review of wake investigations conducted both in the laboratory and in space is presented elsewhere in the proceedings it is relevant to discuss briefly some laboratory results which complement the Spacelab studies.

4.3 Complementary laboratory investigations

In addition to observing the wake region behind large objects as they pass through the near earth plasma, it is found profitable to perform laboratory experiments in order to gain some insight into the plasma-wake environment. Although the parameters may not scale directly to the plasma that has been examined above, such experiments suggest new avenues for the spacelab investigations of the future. Herein, we shall review a few recent experiments performed in laboratory plasma environments whose volume is of the order one cubic meter, possessing plasma numbers of $n_e = n_i = 10^6 - 10^8$ electrons/cm³; $T_e \sim 1-3$ eV and $T_i < T_e/10$.

Alikhanov et al. (1971) studied the flow into the wake region created by a flowing plasma passing a rectangular plate that was at floating potential. In an extended study, Eiselevich and Fainshtein (1980) noted that the expansion of the plasma from the undisturbed region into the wake could be modeled with a self similar description. This can be understood from the governing fluid equations of continuity

$$v_b \delta n / \delta z + \delta(nv) / \delta x = 0$$

and motion

$$v_b \delta / \delta z + v \delta v / \delta x = -c_s^2 \delta(\ln n) / \delta x$$

where the quasineutral plasma has been assumed to be moving as a beam in the z direction with a velocity of v_b . The ion acoustic velocity is c_s . These equations are identical to the problem of a neutral gas or a quasineutral plasma expanding into a vacuum and solutions in terms of the self similar variable $\zeta = x/(z/v_b)$ can be obtained. The POLAR model discussed previously uses such a quasineutral approximation. Similar results concerning the self similar expansion into the wake region behind a grounded metal plate were reported by Wright et al. (1985). In the very near wake region where quasineutrality would be violated, it was found that the potential would be the important self similar dependent variable by Diebold et al. (1986). In this case, the dependent self similar variable becomes $\zeta = x/(z/v_b)^2$ as shown by Lonngren and Hershkowitz (1979).

As the wake region has a lower density than the ambient flowing plasma, one might conjecture that the electrons due to their higher mobility would rapidly enter the wake, creating an electric field which would accelerate the ions to velocities greater than the ion acoustic velocity. The accelerated ions have been noted in the experiments of Wright et al. (1985), (1986) and Raychaudhuri et al. (1986). The potential well that would result from such a space charge was observed in the orbiter wake by Murphy et al. (1986). That the electrons can speed ahead of the ions was recently detected by Chan et al. (1986). Ions could also enter the wake region by being deflected around the perturbing objects as was recently noted by D'Angelo and Merlino (1986a), (1986b) in an experiment performed in a plasma in a weak magnetic field oriented in the direction of the plasma flow. These experiments show results reminiscent of those by Stone 1986 where streams of converging ions were observed behind the orbiter. Finally, a series of experiments designed to examine the flow of plasma around magnetized objects has been described by Hill et al. (1986). These would be related to the TERRELLA type of experiments except that the present experiments were performed in a very low β plasma environment ($\beta \approx 10^{-4}$). A general characteristic of the observations in this experiment was that the magnetic object "appeared" to be larger for the electrons than the ions since the electron wake had dimensions that were larger than the ion wake.

Hence, we see that the laboratory experiment provides a controllable environment in which to suggest future paths for space experiments or to explain certain space observations. Future work needs to better define the role of the magnetic field and the charge on the object in question. It should be noted however that it is difficult to simulate in the laboratory conditions similar to the orbiter where the magnetic field can be perpendicular to the flow vector and where gas cloud interactions modify the

observations.

4.4 Electromagnetic environment and active experiments

Further definition of the electromagnetic environment has shown that the BOGES noise extends as far from the orbiter as the PDP observed, and was strongest along field lines connecting to the orbiter and in the turbulent wake zone (Gurnett, 1986a). Gurnett has also verified that the noise is electrostatic in nature and has very short wavelength. Considerable theoretical efforts are currently under way to determine the fundamental process creating such noise.

Of further interest may be a series of joint experiments with VCAP where, during two flux tube connection experiments, dramatic comparisons to the physics of whistler mode radiation in auroral arcs has been discovered (Gurnett, 1986b).

Further active experiments conducted by using the orbiter OMS engines to produce a cloud of water vapor and deplete the ionosphere (Mendillo, 1981; Mendillo et al., 1978) showed significant plasma depletion, as measured in the orbiter payload bay, recovering on the timescale of seconds after engine shutdown (Tribble et al. 1985). Tribble also reported a high level of plasma "turbulence" which lasted tens of seconds indicating the presence of instabilities. This phenomenon may be similar to that observed by RCS ignition and reported by Murphy et al., 1984a, and Shawhan et al., 1984b.

5.0 Summary

It is important, with such a wide range of data, to put together an emerging picture of the Shuttle orbiter interactions and then systematically address the experiments which need to be conducted in order to further the science/technology of large body interactions.

Although laboratory and small satellite observations can shed light on details of wake structures, and the electric fields associated with them, large bodies such as the orbiter pose some unique problems. Is the orbiter a comet? In many respects, there are similarities. It definitely carries its own gas cloud and understanding how large objects such as the orbiter, platforms, or space station interact with the plasma demands on more than a scaling of laboratory experiments.

Part of the interactions around large objects are due to the "scale size" effect while others are distinctly interrelated to outgassed products and the change in the balance of the ambient chemical equilibrium. As described by Grebowsky et al., 1986, the instrumentation required to completely disgrace the ionospheric chemistry and simultaneously determine all key plasma parameters requires careful consideration of the specific problems the spacecraft must study. The PDP is only a first generation experiment with instrumentation that was not optimized for studies such as "comet" problems.

Future experiments must be designed both for space and in complementary laboratory setting which can, if not solve the following problems, at least determine by appropriate empirical means their impact on future technologies. These problems include:

1. What is the effect of gas clouds associated with large objects on their interaction with the neutral atmosphere and plasma?
 - a. How does the cloud affect the wake fill process?
 - b. Is the orbiter cloud large enough to create a pick-up current of such magnitude that it partially screens the motional electric field? (Pickett, et al., 1985; Goertz, 1980; Katz et al., 1984).
 - c. For large objects such as space station, could the energy dissipation associated with such a cloud create significant anomalous drag?
 - d. How does the cloud affect the charge neutralization process and current loops associated with tethers, or particle beams?
 - e. What is the effect of such a cloud on the operation of a plasma contactor?
2. The interactions of large structures with the ionosphere through electromotive forces associated with differential charging, absolute charging, and closed current loops are not well understood.
3. The phenomena of vehicle glow, its relationship with the plasma, the neutral cloud and the interacting surface has given rise to conflicting theories with insufficient data to resolve the issue. (Green, 1985)
4. Understanding of the total picture associated with large body wakes involves more than models of electron and ion density. Wave particle interactions, atmospheric chemistry, vehicle charge, and magnetic fields must be included in the analysis.
5. Joint particle beam experiments such as those between PDP and VCAP have raised many questions about the propagation of beams from structures like the orbiter. This is an immature experiment because until SL-2 no experiments (other than short sounding rocket flights) have provided remote diagnostics on such beams. (See the paper by Banks et al. in this proceedings for more detail.)

6.0 Recommendations

The Challenger accident has dealt a severe setback to the space experiments associated with large body/plasma interactions. It is unfortunate that the space station is set to proceed on course with little opportunity in the next 6 years for detailed study of the technical issues that should be resolved before it proceeds.

Studying such problems requires a commitment by NASA to a program which must involve the development of instrumentation adequate to measure the appropriate parameters, flights of opportunity within the next five to six years for such instruments, support of working groups consisting of experimentalists who may have relevant data from past missions and theorists attempting to model the phenomena and, last of all, well designed and executed laboratory experiments.

Last of all it is of paramount importance that those scientists and engineers evolved with the state of the art of large body interactions, gas cloud dynamics, high voltage effects, etc. have effective knowledge transfer to those individuals and organizations making the design decisions of the future.

Acknowledgements

The authors wish to thank the PDP principal investigator, Professor Louis A. Frank and all co-investigators for their cooperation and input to this manuscript. We also acknowledge the efforts of Henry Garrott, Steve Gabriel and Joan Feynman for the organization of the conference. The PDP program has been supported by NASA/MSFC contract NAS832807 and NASA/Lewis Grant NAG 3-449. Laboratory investigations at the University of Iowa have been supported by NSF Grant # ECS 8519510.

References

- Alikhanov, S. G., V. G. Belen, G. N. Kichigin and P. Z. Chebotaev, Expansion of a Plasma in Vacuum and Flow of Collisionless Plasma Around a Plate, Sov. Phys. JETP, 32, 1061-1063, 1971.
- Banks, P.M., W. J. Raitt, P. R. Williamson, A. B. White and R. I. Bush, Results from the Vehicle Charging and Potential Experiment on STS-3, J. Spacecraft and Rockets, (in press), 1986.
- Chan, C., M. A. Morgan and R. C. Allen, Electron dynamics in the Near Wake of a Conducting Body, IEEE Transactions on Plasma Science, to be published, 1986.
- D'Angelo, N. and R. L. Merlino, The Effect of a Magnetic Field on Wake Potential Structures, IEEE Transactions on Plasma Science, PS-14, 609-610, 1986a.
- Diebold, D. N. Hershkowitz, T. Intrator and A. Bailey, Self-similar Potential in the Near Wake, Physics of Fluids, to be published, 1986.
- Eselevich, V. G. and V. G. Fainshtein, Expansion of Collisionless Plasma in a Vacuum, Sov. Phys. JETP, 52, 441-448, 1980.
- Goertz, C. K., Io's Interaction with the Plasma Torus, J. Geophys. Res., 85, 2949-2956, 1980.
- Grebowsky, J. M., M. W. Pharo III, H. A. Taylor, Jr., and I. J. Eberstein, Measured Thermal Ion Environment of STS-3, AIAA Pub., 83-2597, 1983.
- Grebowsky, J. M., H. A. Taylor, Jr., M. W. Pharo III, and N. Reese, Thermal Ion Perturbations Observed in the Vicinity of the Space Shuttle, submitted to Planetary and Space Science, May, 1986.
- Green, B. D., Review of Vehicle Glow, AIAA reprint #85-6095-CP, 1985.

- Gurnett, D. A., J. T. Steinberg, and W. S. Kurth, Short Wavelength Electrostatic Noise Observed in the Vicinity of the Shuttle During the SL-2 Mission, presented at URSI, Boulder, CO, Jan., 1986.
- Gurnett, D. A., W. S. Kurth, J. T. Steinberg, P. M. Banks, R. I. Bush, and W. J. Raitt, Whistler Mode Radiation from the SL-2 Electron Beam, Geophys. Res. Lett., 13, 225, 1986.
- Green, B. D., 'Review of Vehicle Glow, AIAA reprint #85-6095-CP, 1985.
- Hill, J. L., A. Seyhonzadeh, H. Y. Chang and K. E. Lonngren, Radio Science, to be published, 1986.
- Katz, I., D. E. Parks, D. L. Cooke, J. R. Lilley, Jr., Geophys. Res. Lett., 11, 1115-1116, 1984.
- Katz, I., D. L. Cooke, D. E. Parks, J. J. Mandrell, A. G. Rubin, Three Dimensional Wake Model for Low Earth Orbit, J. of Spacecraft and Rockets, 21, 125, 1984.
- Lonngren, K. E. and N. Hershkowitz, A Note on Plasma Expansion into a Vacuum, IEEE Transactions on Plasma Science, PS-7, 107-108, 1979.
- Mendillo, M., J. Forbes, Artificially Created Holes in the Ionosphere, J. of Geophys. Res., 83, 151, 1978.
- Mendillo, M., The effect of Rocket Launches on the Ionosphere, Advances in Space Research, 1, 275, 1981.
- Merlino, R. L., and N. D'Angelo, The Interaction of a Conducting Object With a Supersonic Plasma Flow: Ion Deflection Near a Negatively Charged Obstacle, J. Plasma Physics, to be published, 1986.
- Murphy, G. B., N. D'Angelo, J. S. Pickett and S. D. Shawhan, Characteristics of Strong Plasma Turbulence Created by the STS Orbiter, presented at URSI, Jan. 1984.
- Murphy, G. B., J. S. Pickett, N. D'Angelo, and W. S. Kurth, Measurements of Plasma Parameters in the Vicinity of the Space Shuttle, Planetary and Space Science, (in press), 1986.
- Murphy, G. B., S. D. Shawhan, Radio Frequency Fields Generated by the S-band Communication Link on OV102, J. of Spacecraft and Rockets, 21, #4, 398, 1984.
- Murphy, G. B., S. D. Shawhan, L. A. Frank, N. D'Angelo, D. A. Gurnett, J. M. Grebowsky, D. L. Reasoner, and N. H. Stone, Interaction of the Space Shuttle Orbiter With the Ionospheric Plasma, Proc. 17th ESLAB Symposium on Spacecraft/Plasma Interactions and Their Influence on Field and Particle Measurements, European Space Agency Publ., ESA SP-178, p. 73, Dec. 1983.
- Papadopolous, K., On the Shuttle Glow - the Plasma Alternative, Radio Sci., 19, 571, 1984.

- Paterson, W. R., L. A. Frank, and P. M. Banks, Charged Particle Distributions Measured in the Vicinity of the Space Shuttle, presented at Fall AGU, San Francisco, CA, 1985.
- Pickett, J. S., G. B. Murphy and W. S. Kurth, The Gaseous Environment of the Space Shuttle Early in the Spacelab-2 Mission, submitted to J. of Spacecraft and Rockets, 1986. (Presented as paper 85-6064-CP at AIAA Conference Shuttle Environment and Operations II, Nov. 1985)
- Pickett, J. S., G. B. Murphy, W. S. Kurth, C. K. Goertz, and S. D. Shawhan, Effects of Chemical Releases by the STS-3 Orbiter on the Ionosphere, J. Geophys. Res., 90, 3487, 1985.
- Raitt, W. J., D. E. Siskind, P. M. Banks, P. R. Williamson, Measurements of the Thermal Plasma Environment of the Space Shuttle, Planet. Space Sci., 32, 457, 1984.
- Raychaudhuri, J. Hill, H. Y. Chang, E. K. Tsikis and K. E. Lonngren, An Experiment on the Plasma Expansion into a Wake, Physics of Fluids, 29, 289-293, 1986.
- Reasoner, D. L., S. D. Shawhan, and G. B. Murphy, Plasma Diagnostics Package Measurements of Ionospheric Ions and Shuttle-Induced Perturbations, J. Geophys. Res., (in press), 1986.
- Shawhan, S. D., G. B. Murphy, P. M. Banks, P. R. Williamson and W. J. Raitt, Wave Emissions from DC and Modulated Electron Beams on STS-3, Radio Sci., 19, 471, 1984.
- Shawhan, S. D., G. B. Murphy, D. L. Fortna, Measurements of Electromagnetic Interference on OV102 Columbia Using the Plasma Diagnostics Package, J. Spacecraft and Rockets, 21, 392, 1984.
- Shawhan, S. D., G. B. Murphy, and J. S. Pickett, Plasma Diagnostics Package Initial Assessment of the Shuttle Orbiter Plasma Environment, J. Spacecraft and Rockets, 21, 387, 1984.
- Stone, N. H. and U. Samir, The Plasma Dynamics of Hypersonic Spacecraft: Applications of Laboratory Simulations and Active In Situ Experiments, this issue.
- Stone, N. H., K. H. Wright, Jr., K. S. Hwang, U. Samir, G. B. Murphy, and S. D. Shawhan, Further Observations of Space Shuttle Plasma - Electrodynamic Effects from OSS-1/STS-3, Geophys. Res. Lett., 13, 217, 1986.
- Tribble, A. C., J. S. Pickett, N. D'Angelo, and G. B. Murphy, Plasma Densities and Temperatures Near the Shuttle Orbiter, presented at Fall AGU, San Francisco, CA, 1985.
- Tribble, A. C., N. D'Angelo, G. B. Murphy, and J. S. Pickett, The Effect of the Earth's Magnetic Field on Plasma Turbulence Near the Shuttle Orbiter, presented at Fall AGU, San Francisco, CA, 1986.

Wulf, E., and U. von Zahn, The Shuttle Environment: Effects of Thrust Firings on Gas Density and Composition in the Payload Bay, J. of Geophys. Res., 19, 3270, 3278, 1986.

Wright, Jr., K. H., D. E. Parks, I. Katz, N. H. Stone and U. Samir, More on the expansion of a collisionless plasma into the wake of a body, J. Plasma Physics, 35, 119-123, 1986.

Wright, Jr., K. H., N. H. Stone and U. Samir, A study of plasma expansion phenomena in laboratory generated plasma wakes: Preliminary Results, J. Plasma Physics, 33, 71-82, 1985.

CONTAMINANT IONS AND WAVES IN THE SPACE STATION ENVIRONMENT

G. B. Murphy

Department of Physics and Astronomy
The University of Iowa
Iowa City, IA 52242

Introduction

It is a difficult task to estimate, with any degree of certainty, the probable environment of any large space structure or system given that the system has not been firmly defined. This environment is a product of the natural environment and its interactions with that structure and system. We shall distinguish between the so-called induced environment, the molecular, particulate, photon and wave environment which results from the disturbing effects of a large object flying at orbital speeds through the ionosphere, and the contaminant environment which is produced when solids, liquids or gases are released from the system and interact with the induced environment in an array of chemical and physical processes. Our task is made particularly difficult by two important unknowns: a firm definition of the system and its contaminants; incomplete knowledge of the chemical and physical processes which can take place. In this paper we will address the probable plasma environment of Space Station. That is, we will discuss the particles (ions and electrons) and waves which will likely exist in the vicinity of the Space Station and how these may affect the operation of proposed experiments. Differences between quiescent operational periods (as defined by JSC 30426) and non-operational periods as well as probable effects from Shuttle operations will also be discussed. Areas which need further work are identified and a course of action suggested.

Background

Much of our knowledge about the interactions between large bodies and the ionospheric plasma had, until the time before Shuttle flights, been obtained from observations aboard small scientific satellites and various scaled laboratory investigations. The recent era of Spacelab-type payloads aboard the Shuttle orbiter has provided a wealth of heretofore unobtainable information. The Shuttle is not only the largest body flown to date but, as was discovered over a period of time, carries with it a large gas cloud. The discovery of "Shuttle glow" (Banks et al., 1983), broadband electrostatic noise (Shawhan et al., 1984a), heated electron populations (McMahan et al., 1983), a modified ion environment (Hunton and Carlo, 1985), and contaminant ions in the wake (Grebowsky et al., 1987) have begun to fill in pieces in what appears to be a complex puzzle associated with the large body induced environment and contaminant interactions. Recent studies of the neutral and ion population during thruster operations (Wulf and Von Zahn, 1986; Narcisi et al., 1983; Shawhan et al., 1984b), modification of the plasma during FES

operations and H_2O dumps (Pickett et al., 1985), the discovery of pick-up ions consistent with chemistry of the H_2O , O^+ interaction (Paterson, 1987), as well as observations by neutral mass spectrometers (Wulf and Von Zahn, 1986; Miller, 1983), have helped to sort out the differences between interactions which are of the induced variety and those which result from release of contaminants by the orbiter. Observations by IR, optical, and UV instruments on board the orbiter (Torr, 1983; Torr and Torr, 1985; Koch et al., 1987), and by IR on the ground (Witteborn et al., 1987) have provided insight into the effects of both absorption and emission by this contaminant population. It is now clear as a result of these pathfinder experiments that in order to conduct experiments in plasma physics, provide long-term monitoring and a data base for the ionosphere, observe astronomical targets over a broad range of wavelengths, and provide sensitive remote sensing capability, the Space Station environment must be cleaner than that of the orbiter in many respects. Much work has already been done in assessing just how clean that environment must be in order to meet the minimum science requirements (Space Station Payload Contamination Compatibility Workshop, 1987). It will be the purpose of this paper to assess what the particle and wave environment might be and whether the current specifications are adequate in this regard. This assessment will be based on current contamination control requirements, knowledge of proposed space station configuration, and our best guess about the scaling laws for certain plasma interactions.

Particle Environment

A number of investigators have studied the composition of the Shuttle ion environment and compared it to that which was expected of the natural environment at the orbiter altitude (Grebowsky et al., 1987; Siskind et al., 1984; Reasoner et al., 1986). The studies observe large amounts of H_2O^+ which results from the rapid charge exchange reaction



as well as smaller amounts of H_3O^+ .



The amount of H_2O^+ (and H_3O^+) observed appears to be directly proportional to the surface temperature leading to the conclusion that most of this observed water is offgassed from Shuttle tiles or other porous surfaces (Narcisi et al., 1983). The amount of water can be estimated by neutral mass spectrometers but caution must be taken since frequently these instruments can only observe molecules which are scattered back toward the orbiter either by collisions with ambient molecules or the cloud itself. Several attempts have been made to estimate water density or by observing the ion population and then doing a kinetic analysis. This has been done with observations obtained within the orbiter bay (Narcisi, 1983) and with data which were obtained during the PDP free-flight on Spacelab 2 (Paterson, 1987). Other estimates have been obtained by observing the infrared signature and then estimating column densities (Koch et al., 1987). The remarkable thing about all of these methods is that although they have shown some decay in the amount of water during the lifetime of the mission and variation among missions, the neutral

observations, ion observations, and IR observations give a consistent picture which can be modeled within the accuracy of the known cross sections for the charge exchange reaction. The significance of this is that if we know one of the above parameters accurately, e.g., column density from IR observations, we can predict another, e.g., contaminant ion population, through a modeling of the chemistry and kinetics of the gas cloud. Several authors have developed models of this "gas-cloud" interaction; notably Patterson (1987) has modeled a steady state cloud and shown the production of H_2O^+ to scale with background O^+ density and Hastings et al. (1987a) have developed time-dependent models of clouds which would be associated with a brief gas release, such as the opening of a gas relief valve or a thruster operation.

This contaminant ion population can be a source of several problems.

(1) These ions create an additional wake which trails the object in a sense which is perpendicular to the magnetic field line instead of parallel to the velocity vector.

(2) Depending on the nature of the ions they may result in a deposition problem on some surfaces facing the ram direction.

(3) Depending on the excitation state of the ions, they may add to the IR, optical or UV spectrum which is sensed by a particular instrument.

(4) The current created by these pick-up ions is believed to be responsible for plasma instabilities which enhance the background wave environment.

(5) Molecules which have low ionization potential may be susceptible to the critical ionization velocity (CIV) process causing enhanced plasma density, production of wave turbulence, and possible photon emission.

Let us look at the above possibilities in light of Space Station operations. Although much of our shuttle experience has been gained by observing the H_2O/O^+ interaction, any process such as charge exchange, photoionization, ionization by CIV, etc., will produce the pick-up ion cloud and present a similar set of problems to experiments on the Space Station.

Figure 1 presents a cartoon of the composite nature of the Shuttle environment to illustrate the first point above. Superimposed on the induced environment (i.e., the neutral and plasma wake) is the wake produced by the pick-up ions. Generated in the orbiter rest frame they will appear to move past the vehicle perpendicular to field lines. Any experiment expecting to be in the neutral or plasma wake may in fact be in a location dominated by these contaminant ions. As mentioned in point 2, it is clear that these ions could interact with or stick to surfaces when they were presumed to be part of a freely expanding cloud. Possible surface degradation could result from the fact that they can strike the ram surfaces with near orbital velocity (their energy is dependent on the reaction that creates them as well as their mass). This implies chemistry which takes place in front of ram surfaces (e.g., glow) and that which takes place on surfaces must take these ions into account.

Regarding point 3, since these ions form an asymmetric distribution about the vehicle and since their column density is greatest in the wake direction, it is important to evaluate not only the atomic physics associated with the neutral molecule but its ionized and possibly excited state as well. If the

ionized species has a particular emission line which is undesirable optically, this may be particularly noticeable in the wake direction.

We will discuss in more detail the effects described by points 4 and 5 in the next section. Let us first, however, summarize the primary contributors to the ion environment.

Molecular contaminants resulting from outgassed or vented products can interact with the ambient population through several processes creating an ionized cloud which will trail behind the Space Station much like the tail of a comet. If the ionizable contaminants are held to levels well below that of the Shuttle (how much below will be discussed in the next section), the ion environment during operational periods should be acceptable to most experimenters. However, a very important gap exists in our knowledge. A study of the OSSA Space Station waste inventory (Rosley et al., 1986) reveals a large number of possible waste gas and liquid products. Although interactions of simple molecules like H_2O , N_2 , and CO_2 with the O^+ plasma are reasonably well understood, the chemistry of this large possible "soup" of waste products involves many unknowns. It would seem prudent to assess the possible interaction of some of these waste gases by realistic laboratory experiments before deciding that they are allowable vent gases.

Wave Environment

It will be difficult to assess whether the wave environment described in JSC 30420 and JSC 30237 can be met in its entirety. Analysis of the wave environment aboard the orbiter based on PDP data from OSS 1 and Spacelab 2 have led to the emerging picture, again depicted by the cartoon of Figure 1, that the broadband noise environment may be dominated not by the induced environment associated with the large body interaction as was originally believed, but by production of waves by the gas cloud itself. If this is the case it may be possible to correlate the general level of this background noise to the density of the water cloud. In Figure 2, we present data that have been compiled from the published literature (Pickett et al., 1985). The level of noise at 1 kHz (chosen as typical of the broadband noise spectra for these data) is plotted for three different cases of "small" gas cloud releases. The level of uncertainty in the measurement of H_2O density is represented by the vertical error bars. The three cases chosen represent almost 3 orders of magnitude in gas quantity. In all cases the dominant gas is H_2O . The first is the H_2O vapor cloud associated with the orbiter outgassing per se, the second an operation of the Flash Evaporator System (FES), and the third a typical operation of a VRCS thruster. In all cases the releases were on the dayside and in an ambient density of O^+ plasma of $\sim 10^5 \text{ cm}^{-3}$. Note that the data indicate that the noise is linearly proportional to the density of gas released. The best fit to the data is that the intensity (at 1 kHz) of electrostatic noise is proportional to the product of H_2O and O^+ density. The constant of proportionality is such that at a 1 g s^{-1} release rate the measured electric field anywhere within the general interaction region will be $\sim 1 \text{ mV m}^{-1}$ in a 150 Hz bandwidth. (150 Hz is the approximate bandwidth at which these measurements were made.) This law is certainly not absolute but leads the author to believe that most of the observed noise can be tied to this contaminant release. Further examination of turbulence measured by the Langmuir probe and electrostatic waves observed near the orbiter wake by the PDP on Spacelab 2 leads one to speculate that the wake

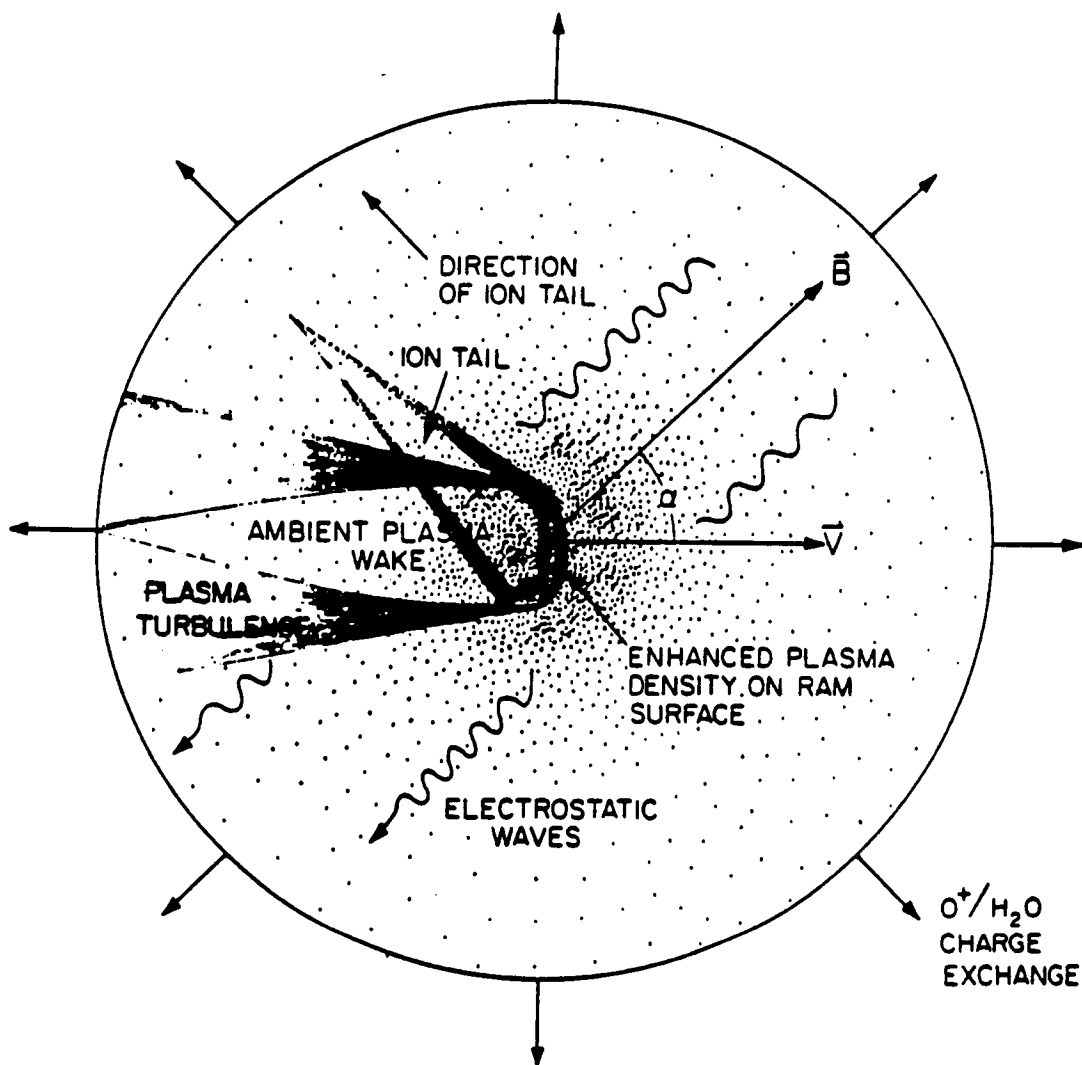


Fig. 1. The neutral cloud of gas which expands from the orbiter undergoes chemical interactions such as charge exchange which results in an ion tail and creates plasma waves presumed to be driven by the ion currents.

noise is dominant only in a region confined to the wake and wake boundaries and most wake noise observed elsewhere is dominated by the production of noise associated with instabilities resulting from ion pick-up current generated by the contaminant water cloud.

In order to properly scale this phenomena we must establish more firmly the instability that causes the wave growth and the process that saturates the

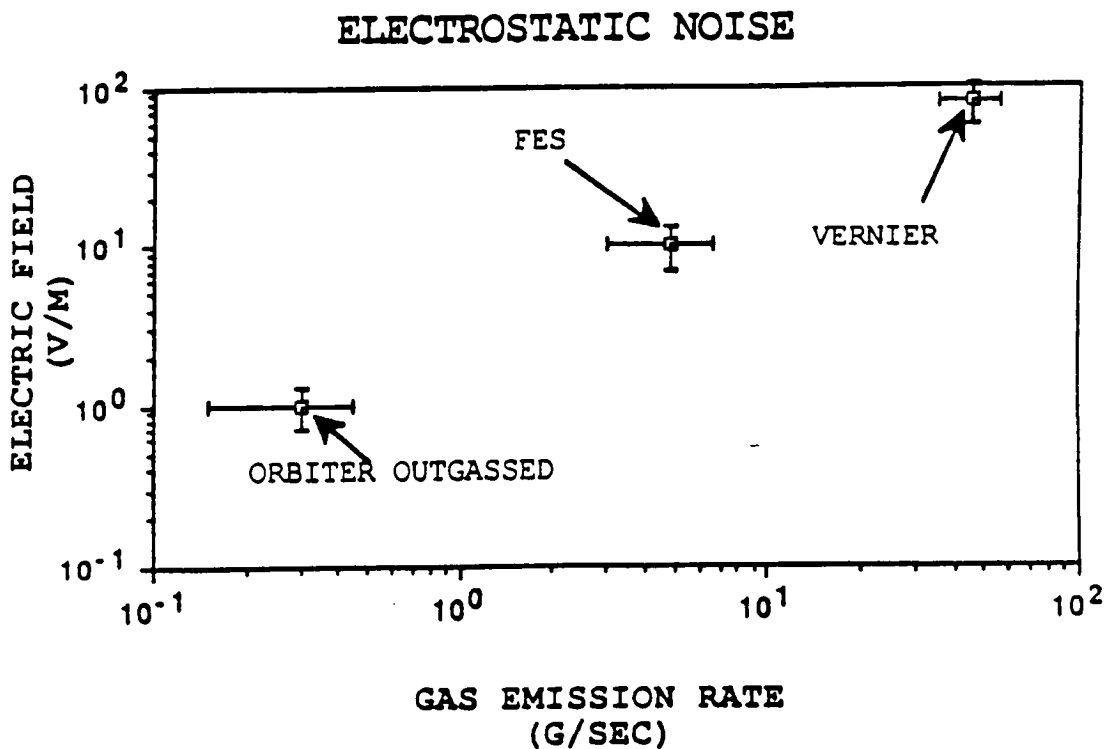


Fig. 2. Gas releases of three different magnitudes and the measured electrostatic noise show roughly a linear correlation. Estimates of outgassing rates for the first data point are a consensus of observations of inferred column density from IR and measurements of both ion and neutral densities. Emission rates of FES and VRCS are well defined.

instability. CIV may play a role in this process (Papadopoulos, 1984) but will again be very dependent on the gas composition. More experiments are required before we can definitely say that the above scaling law applies to molecules other than water, since the importance of a particular instability or CIV varies with molecular species.

Extrapolating this insight into the Space Station environment we are again led to conclude that the plasma environment will be acceptable and the JSC requirements met only during periods where ionizing components of the contaminant gases are minimized. Although the large modules and solar arrays may be a source of plasma noise generated by turbulence in their wake, at points midway along the transverse boom or on the upper or lower keel, this noise may be at an acceptable level at least for some geometric configurations of the velocity vector and magnetic field. Other sources of noise, currents carried by the structure to complete the $\vec{V} \times \vec{B}$ current loop (Hastings and Wang, 1987), radiation of noise by the cable trays or solar arrays or currents

(Hastings et al., 1987b), conduction of noise by sheath waves, etc. must be solved by appropriate design and are not within the scope of this discussion.

What numerical limits must be placed on the ionizing contaminants in order to meet the JSC 30237 specification and provide an environment free of this source of noise? Examining JSC 30237 for the spec on broadband emission for systems at standard locations, we find that at 1 kHz we must be less than $103 \text{ dB } \mu\text{V m}^{-1} \text{ MHz}^{-1}$. Scaling to the 150 Hz bandwidth of the measurements taken in compiling Figure 2, we find that these emissions must be less than $\sim 0.02 \text{ mV m}^{-1}$ which, using the linear scaling law of Figure 2, implies an emission rate of water of $< 20 \text{ mg s}^{-1}$. This should be manageable for a structure like the Space Station which will not be covered with a material that continually outgasses water. The mass release rate of other ionizable molecules could be scaled appropriately depending on their cross section for ionization. The sum total of all of these easily ionizable molecules would then have to be such that their emissions are below JSC 30237 specifications. This compares favorably with recommendations from the Space Station Payload Contamination Compatibility Workshop which recommended lower column densities of most species.

In January 1987 the OSSA contamination compatibility workshop recommended several changes in JSC 30426, which included lowering total acceptable column densities of O_2 , N_2 , and H_2 , as well as noble gases and other UV and non-IR active molecules. A further specification should be included which defines ionizable gases and the acceptable release rates for them. Furthermore, it is very important that we gain a detailed understanding of the chemistry and physics of reactions which occur between the ambient environment and the large shopping list of molecules which may be released during the non-operational periods to insure that experiments and the Space Station hardware are not subjected to effects described earlier.

Non-Quiescent Environment

JSC 30426 states that the Space Station be capable of supporting quiescent operation periods of up to 14 days. This period of minimum perturbation is essential for many science investigations and any disturbances during this period, however minor, must be noted. It is not clear that the requirement to record such disturbances is fully satisfied. Section 5.0 simply states that "...monitoring of the environment to a limited extent will be required." Since the IOC phase Space Station will not be gravity gradient stable, some fine tuning of attitude will be required. Whether it is accomplished with jets only or some combination of jets and gyros is unclear. It is clear, however, that during the long "quiescent" periods there will undoubtedly be some disturbances whether they be occasional jet firings, experiment vents, purges, or relief valve operations, EVA crew activity, etc. A clear requirement to monitor specific critical aspects of the environment must be in place. Space Station elements must have a way of "notifying the system" of an impending disturbance. Some monitoring can and should be real time and some may only be required after the fact. Whether PIMS or some other monitoring package is responsible is yet to be determined but the requirement must be a system responsibility with data accessible to all.

Non-quiescent periods, such as Shuttle docking, will provide significant disturbances. It is the consensus of a number of independent observations that the Shuttle orbiter carries with it a large amount of contaminant material, particularly water. Column densities near the orbiter of 10^{12} to

10^{13} should be expected. There is some disagreement over the decay time of the associated cloud. IECM observations (STS-2, STS-3, STS-4) indicated an initial decay time of ~10 hours. However, Narcisi et al. (1983) has observed wide variations in the water density cloud with some overall decrease in H_2O density with time, but a much stronger correlation between density and surface temperature. Raitt (private communication, 1987) reports that an ion signature, characteristic of H_2O^+ in his retarding potential analyzer, practically disappeared by the end of mission 51F. (51F spent a lot of time in a hot attitude due to a several day long solar observation cycle.)

The conclusion that may be reached from all of this is that the amount of contamination that will be carried into the space station environment by the orbiter may be reduced by simply waiting some minimum period of time (224 hours) in a relatively hot attitude behind the station, then going to a cool attitude for several hours before beginning the approach and docking. Clearly it will not be possible to operate some experiments while the orbiter is in rendezvous phase, both because of the outgassed cloud and thruster plume impingement. Docking procedures which minimize plume impingement and thruster activity will be preferred. Operation of experiments while the orbiter is present may be possible and is dependent on the type of experiment.

Other disturbances to the environment, such as EVA activity, should be scheduled as much as is practical for the non-quiet periods since gaseous products associated with the EVA suit can provide significant disturbances.

Summary

The developing requirements for Space Station must be responsive to the needs of the user and in line with the reality of Space Station logistics. They must also be internally consistent, be carried out to as full an extent as possible, and be "living documents" which can incorporate new knowledge as it becomes available. The PWG (Particle and Waves Working Group) has been responsive to the user's needs in writing requirements and assuring that the proper tools are in place to implement them. The definition and control of the particle, plasma, and wave environment has incorporated specific needs from a wide range of potential users. The Contamination Working Group has likewise been responsive and JSC 30426 reflects the panel's concern for the cleanliness of the Space Station environment for the user, the Station safety and longevity, and for the preservation of the delicate natural chemical balance of the ionosphere. It is not clear whether some oversight group such as the CWG will be responsible for continual evaluation and enforcement of the requirements. Some mechanism will be required to do this.

Only minor modifications to the documents may be required, but the importance of these modifications cannot be over emphasized. Let us first deal with recommendations to changes in JSC 30426:

(1) Incorporate specific requirements relating to easily ionizable molecules which contribute to the plasma environment. This should be stated in $g\ s^{-1}$ emission instead of column density; e.g. total water emission should be less than $\sim 1\ mg\ s^{-1}$ for adequate margin. Other common gases which contribute to this environment are N_2 , CO_2 , and H_2 , e.g.:



(2) Analysis of proposed vented products during non-operational periods must be performed to determine if the proposed contaminants are acceptable.

(3) More specific requirements for monitoring the environment should be in place. These should include real time or "warn" flags for certain releases which must be accounted for in data analysis or known about ahead of time.

JSC 30252, the Plasma Effects Control Process Requirements Document, must be consistent with the expected contamination levels and reflect the difference between operational and non-operational periods. Further recommendations in regards to operational considerations are the following:

(1) The orbiter should be allowed to outgas for ≥ 24 hours before docking with the Station (the orbiter should be behind the Station).

(2) Procedures minimizing thruster activity and plume impingement should be implemented for docking activity.

(3) Any plan which includes continuous thrusting for reboost should be eliminated for environmental considerations.

(4) Brief gaseous releases, either by Station hardware or other equipment, must be minimized, documented, and made available in a common data base.

(5) EVA activity should be confined to non-quiet periods whenever possible.

(6) It may be appropriate to include a section on operational guidelines in the JSC 30426 document.

Last of all, several recommendations regarding uncertainties about the physical processes involved are appropriate:

(1) The cross sections for charge exchange reactions of a broad range of molecules are not well known for O^+ at 5 eV.

(2) The susceptibility of certain molecules to CIV at Space Station altitudes is unknown. Laboratory and Shuttle experiments are appropriate.

(3) The precise cause of "Shuttle glow" must be determined.

(4) Models which predict line-of-sight emissions and absorption must take into account possible ionized species that are present. In order to do this, accurate models of cross sections for reactions are required.

(5) The mechanism for production of broadband instabilities must be better understood so scaling laws can be used with more assurance.

All of the above physical considerations may also be applied to co-orbiting platforms. The environmental constraints may be similar or tighter depending on experiment complements.

References

- Banks, P. M., P. R. Williamson, and W. J. Raitt, Space Shuttle glow observations, Geophys. Res. Lett., 10, 118, 1983.
- Bosley, J. and G. Curran, OSSA Space Station Waste Inventory, NASA/Ames Research Center, SS Projects Office, November 1986.
- Grebowsky, J. M., H. A. Taylor, Jr., M. U. Pharo, III, and N. Reese, Thermal ion perturbations observed in the vicinity of the Space Shuttle, Planet. Space Sci., in press, 1987.
- Hastings, D. E. and J. Wang, Induced emission of radiation from a large Space Station-like structure in the ionosphere, J. Spacecraft & Roc, submitted, 1987.
- Hastings, D. E., N. A. Gatsonis, and T. Mogstad, A simple model for the initial phase of a water plasma cloud about a large structure in space, J. Geophys. Res., in press, 1987a.
- Hastings, D. E., A. Barnett, and S. Olbert, Radiation from large space structures in low earth orbit with induced AC currents, J. Spacecraft & Roc, submitted, 1987b.
- Hunton, D. E. and J. M. Calo, Low energy ions in the Shuttle environment: Evidence for strong ambient-contaminant interactions, Planet. Space Sci., 33, 8, 1985.
- Koch, D. G., et al., Infrared observation of contamination from Shuttle flight 51F, Adv. Space Res., in press, 1987.
- McMahan, W., R. Salter, R. Hills, and D. Delorey, Measured electron contribution to Shuttle plasma environment, AIAA-83-2598, AIAA Shuttle Environment and Operations Meeting, October 31-November 3, 1983.
- Miller, E. R. (ed.), STS-2, -3, -4 Induced Environment Contamination Monitor (IECM) Summary Report, NASA TM-82524, 1983.
- Narcisi, R. S., R. E. Trzcinski, G. Federico, L. Wlodyka, and D. Delorey, The gaseous and plasma environment around the Space Shuttle, paper #83-2659 AIAA Conference on Shuttle Environment and Operations, Washington, D.C., 1983.
- Narcisi, R. S., Quantitative determination of the outgassing water vapor concentrations surrounding space vehicles from ion mass spectrometer measurements, Adv. Space Res., 2, 10, 1983.
- Papadopoulos, K., On the Shuttle glow (the plasma alternative), Radio Science, 19, 2, 1984.
- Paterson, W. R., Ion plasmas in the vicinity of the Orbiter: Observations and modeling, M.S. Thesis, University of Iowa, July 1987.
- Pickett, J. S., G. B. Murphy, W. S. Kurth, and C. K. Goertz, Effects of chemical releases by the STS-3 orbiter on the ionosphere, J. Geophys. Res., 90, 3487-3497, 1985.
- Reasoner, D. L., S. D. Shawhan, and G. B. Murphy, Plasma Diagnostics Package measurements of ionospheric ions and Shuttle-induced perturbations, J. Geophys. Res., 91, 13463-13471 1986.
- Shawhan, S. D., G. B. Murphy, and D. L. Fortna, Measurements of electromagnetic interference on OV102 Columbia using the Plasma Diagnostic Package, J. Spacecraft & Roc, 21, 4, 1984a.

- Shawhan, S. D., G. B. Murphy, and J. S. Pickett, Plasma Diagnostics Package initial assessment of the Shuttle orbiter plasma environment, J. Spacecraft & Roc, 21, 387, 1984b.
- Siskind, D. E., W. J. Raitt, P. M. Banks, and P. R. Williamson, Interactions between the orbiting Space Shuttle and the ionosphere, Planet. Space Sci., 32, 7, 1984.
- Space Station Payload Contamination Compatibility Workshop: Final Report, NASA, OSSA Washington, D.C., June 1987.
- Torr, M. R., Optical emissions induced by spacecraft-atmosphere interactions, Geophys. Res. Lett., 10, 114, 1983.
- Torr, M. R. and D. G. Torr, A preliminary spectroscopic assessment of the Spacelab 1/Shuttle optical environment, J. Geophys. Res., 90, 1683, 1985.
- Witteborn, F., L. J. Caroff, D. M. Rank, and G. Ashley, Nighttime spectroscopic and photometric observations of Spacelab-2 and other satellites, Geophys. Res. Lett., submitted, 1987.
- Wulf, E. and U. Von Zahn, The Shuttle Environment: Effects of thruster firings on gas density and composition in the payload bay, J. Geophys. Res., 91, 3270-3278, 1986.

Measurements of Plasma Density and Turbulence
Near the Shuttle Orbiter

by

A. TRIBBLE, N. D'ANGELO, G. MURPHY,
and J. PICKETT

Department of Physics and Astronomy
The University of Iowa
Iowa City, Iowa 52242

Internal Report

January 1987

ABSTRACT

In August 1985 the University of Iowa's Plasma Diagnostics Package was used in the Spacelab 2 mission to study the plasma environment near the shuttle orbiter. Measurements of the plasma density and the percentage density fluctuations yielded information about the structure of the orbiter's wake. These data appear to be in general agreement with previous shuttle results and with laboratory observations of plasma flow-body interactions.

The Spacelab 2 mission PDP (Plasma Diagnostics Package), designed and built at the University of Iowa to study the plasma and electromagnetic environment of the shuttle orbiter, was a satellite 53.3 cm in radius and 66 cm in height, which could be either positioned relative to the shuttle by the RMS (Remote Manipulator System) or ejected into free flight. One of the instruments on the PDP was a Langmuir probe, consisting of a 3 cm diameter gold-plated spherical sensor and associated electronics. The Langmuir probe was mounted on a moveable boom which was extended to a distance of about 60 cm from the cylindrical axis of the PDP during wake studies.

The Langmuir probe is a relatively simple instrument which has two operational modes, working either as an electron density/temperature measurement tool, or as a diagnostic for $\Delta N/N$ fluctuations in electron density over the frequency range 1 - 40 Hz. The electronics is alternated between the two modes by a timing signal generated by the PDP spacecraft encoder. The total cycle lasts for approximately 13 s and consists of a 12 s "lock" period during which the probe is held at +10 V relative to the PDP chassis, followed by a 1 s, 120-sample sweep from +10 V to -5 V (1).

During the lock period, the probe output current is sensed by a logarithmic sensor and sampled through three filters: 1 Hz low pass, 1 - 6 Hz bandpass, and 6 - 40 Hz bandpass. The 1 Hz filter provides a signal proportional to the plasma density, whereas the 6 - 40 Hz bandpass filter output is proportional to the percentage density fluctuation, $\Delta N/N$.

For almost one hour during the Spacelab 2 mission the PDP was positioned by the RMS at approximately 10 m directly above the orbiter cargo bay (Fig. 1). The orbiter then underwent a slow roll, at the rate of 1 degree per second, so that the PDP would pass alternately from the ram of the plasma flow into the orbiter's wake, nine times during the one-hour period. During this maneuver the orbiter's x-axis, as defined in Fig. 1, remained perpendicular to the plasma flow vector.

In Figs. 2, 3, and 4 we present samples of data obtained by the Langmuir probe during this period. Figs. 2a, 3a, and 4a show the plasma densities measured by the Langmuir probe as a function of time, while Figs. 2b, 3b, and 4b indicate, on the same time scale, the behavior of the percentage density fluctuation, $\Delta N/N$, measured by the 6 - 40 Hz bandpass filter. The data in Fig. 2 refer to daytime conditions, those in Fig. 3 are for daytime conditions until 0201:31 UT and for nighttime conditions after 0201:31 UT, while those in Fig. 4 are for nighttime conditions. During the one-hour roll period some of the thrusters on the orbiter had to be fired so that the proper attitude and roll rate were maintained. The times of thruster firing are indicated in Figs. 2, 3, and 4 by vertical arrows. Evidently, these thruster firings are responsible for some of the bursts seen in the density fluctuation data. The times at which the PDP is in the middle of the shuttle wake are indicated by asterisks.

These times are spaced one from the next by approximately 6 min, corresponding to a roll rate of 1 degree per second.

An examination of the wake transits indicates that the electron density in the wake of the orbiter is, typically, more than 2 orders of magnitude smaller than the density measured in the ram of the plasma flow, in general agreement with the results reported, e.g., by Murphy et al. (1). Density depressions are also observed when the Langmuir probe is located within the wake produced by the wrist joint of the RMS, these times being labeled by triangles (2). The arm wakes are, of course, of smaller depth and duration than the orbiter wakes.

As far as plasma density fluctuations are concerned, one notices that, in the frequency range 6 - 40 Hz, $\Delta N/N$ is, typically, on the order of 1-3% all around the shuttle orbiter. However, a special feature of this noise stands out, namely a substantial decrease of the noise within the shuttle wake, with enhancements occurring at its edges, when the Langmuir probe moves either into or out of the wake. This phenomenon has been reported and discussed previously by Murphy et al. (1). It appears also to be in line with recent laboratory observations by Merlino and D'Angelo (3) even though the laboratory scale size was much smaller. In studies of plasma flow-body interactions performed in a so-called DP (Double Plasma) device, an interesting complex noise structure in the wake of a metallic object was uncovered. The positions at which the noise amplitude is largest form an x-pattern downstream of the object. A scan of this noise pattern at just one fixed distance from the object would, of

course, have produced a result similar to the one obtained by the Langmuir probe on the PDP as it swept the ram-wake transition around the orbiter.

REFERENCES AND NOTES

1. G. Murphy, J. Pickett, N. D'Angelo, W. S. Kurth, Planet. Space Sci., Vol. 34, No. 10, pp. 993-1004, 1986.
2. Due to the rotation of the orbiter, it was necessary to rotate the PDP on the RMS in the opposite direction so that the orientation of the PDP, relative to the plasma flow, remained unchanged. As a consequence, the PDP periodically passed through the wake of the RMS.
3. R. L. Merlino, N. D'Angelo, J. Plasma Phys., in press.
4. We thank the crew of the Challenger for doing an outstanding job in performing the orbiter maneuvers and positioning the PDP on the RMS; the personnel at Johnson Space Center involved with the design and testing of RMS procedures, in particular Ann Austin; and the mission planners and Payload Operations Control Center cadre at Marshall Space Flight Center. This work was supported by grant NAG3-449 from the NASA Lewis Research Center and contract NAS8-32807 from the Marshall Space Flight Center.

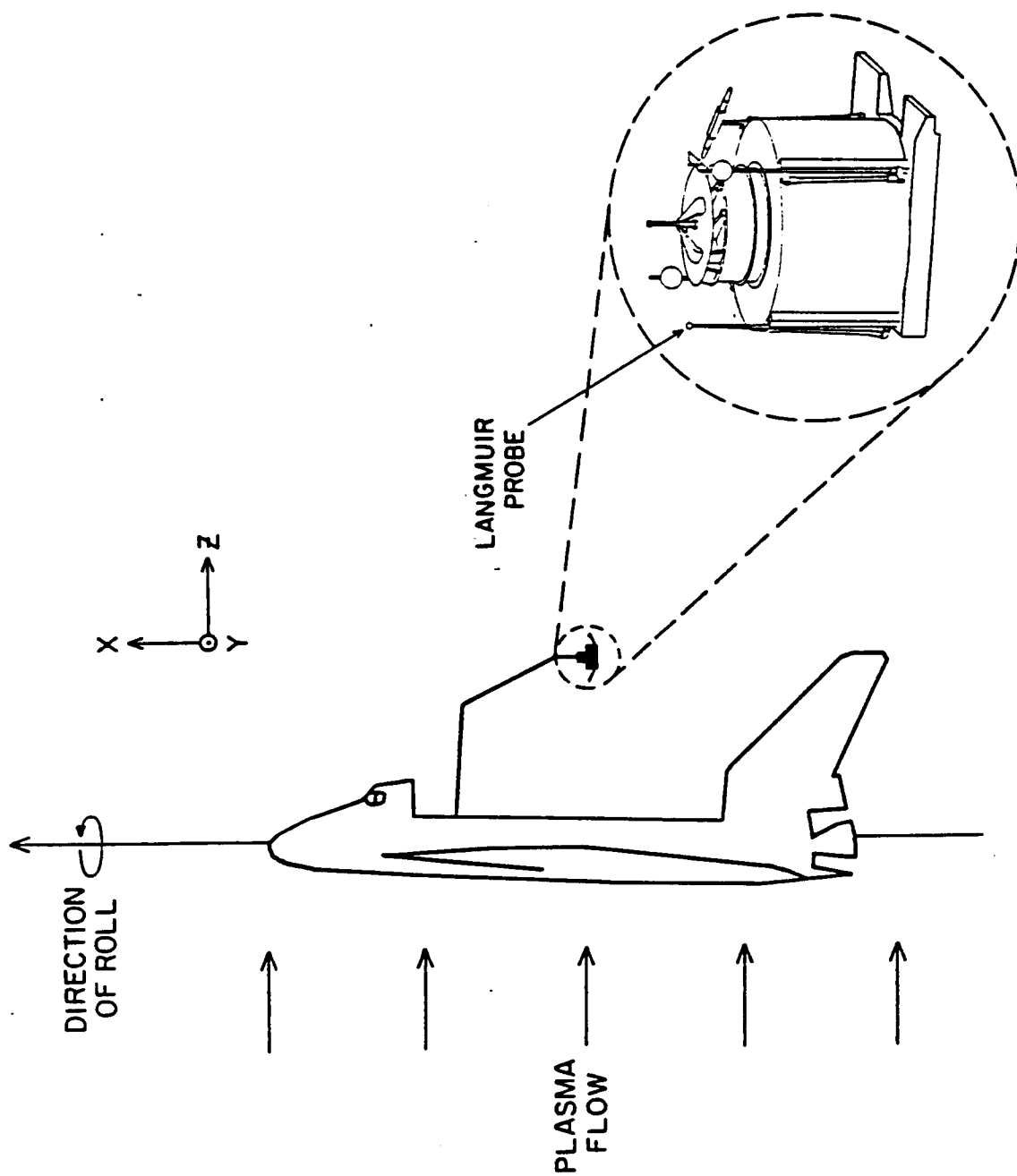
FIGURE CAPTIONS

Fig. 1. Location of the PDP on the RMS, relative to the shuttle orbiter, during plasma wake studies.

Fig. 2. Plasma density (a) and density fluctuation (b) data, 0152-0158 UT, day 212, 1985.

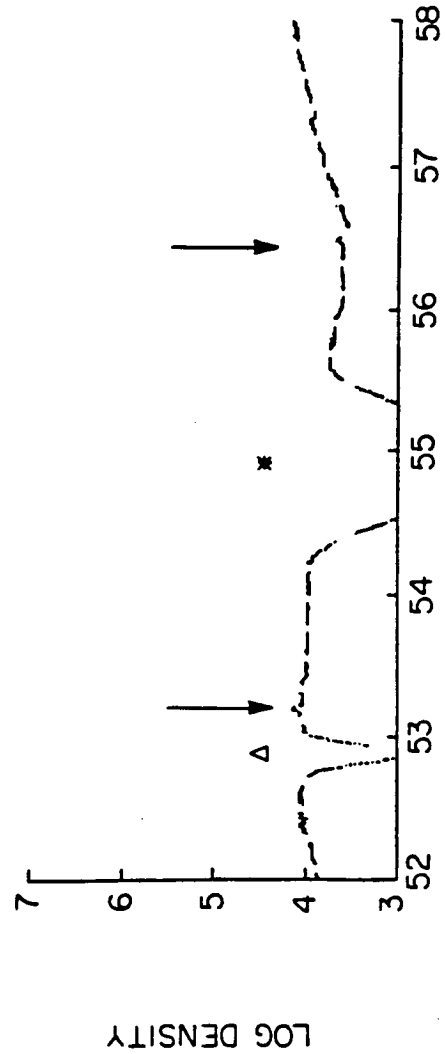
Fig. 3. Plasma density (a) and density fluctuation (b) data, 0158-0204 UT, day 212, 1985.

Fig. 4. Plasma density (a) and density fluctuation (b) data, 0204-0210 UT, day 212, 1985.

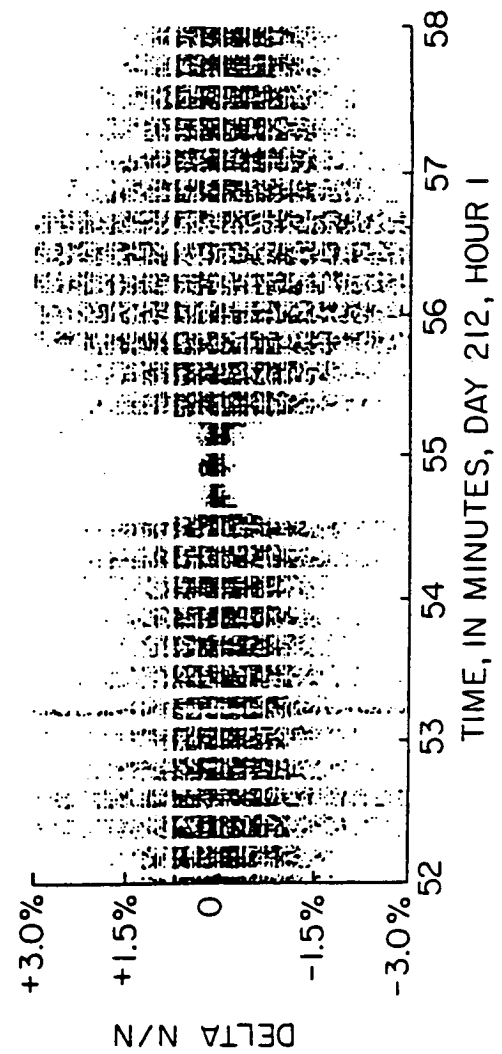


C-G87-30

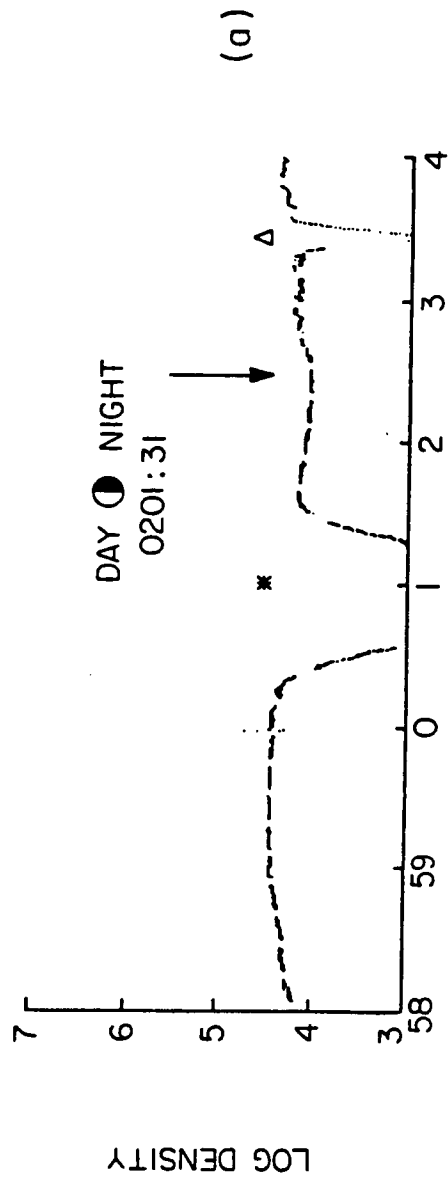
PLASMA DENSITY DATA



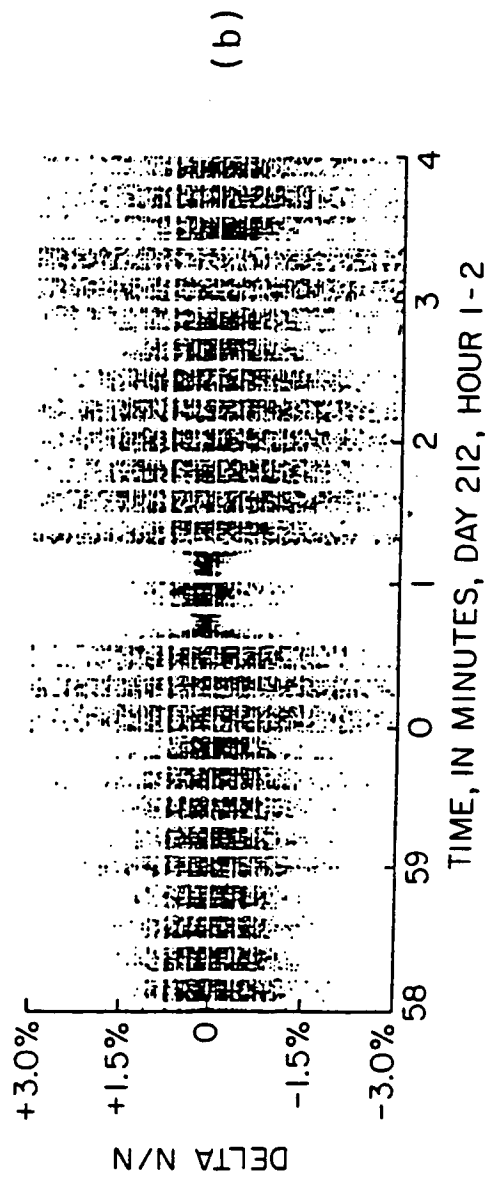
DENSITY FLUCTUATION DATA



PLASMA DENSITY DATA

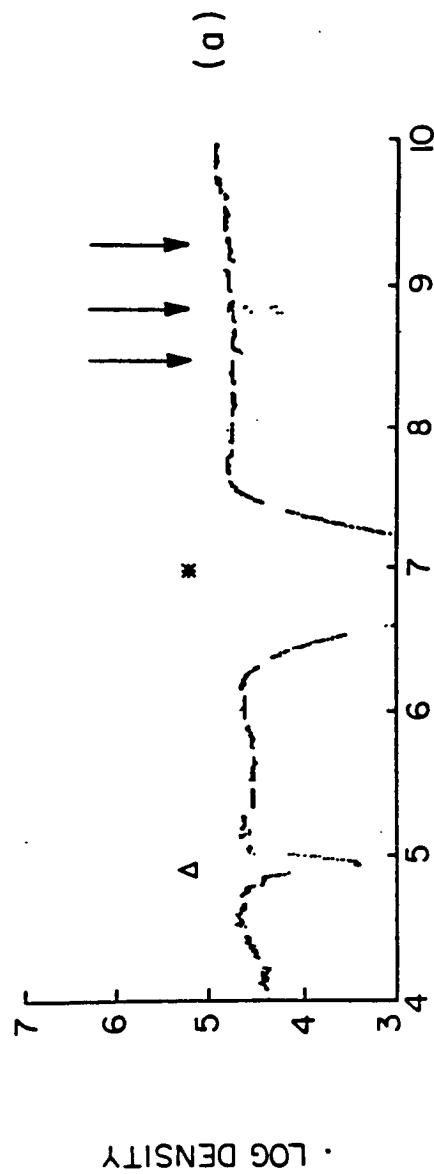


DENSITY FLUCTUATION DATA



C-687-29

PLASMA DENSITY DATA



DENSITY FLUCTUATION DATA

